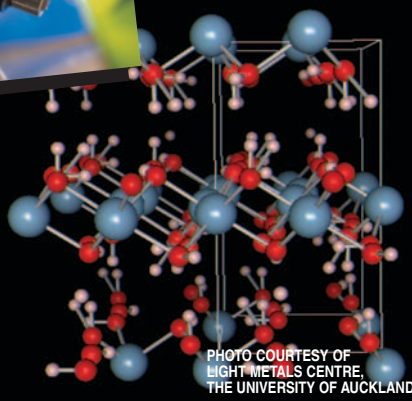


TMS2004

133rd Annual Meeting & Exhibition

The Minerals, Metals & Materials Society
welcomes you to the
TECHNICAL PROGRAM

for the 133rd TMS Annual Meeting & Exhibition,
to be held March 14–18, 2004, in Charlotte, North Carolina.



*For your convenience,
we have also included
details on*

- Meeting Activities and Registration
- Conference Proceedings
- Our Exhibition
- TMS Membership
- Additional On-line Resources that You May Utilize

*All designed to help
you prepare for—
and optimally benefit from—
one of the world's premier
metals and materials events.*

This document comprises

TUESDAY'S TECHNICAL PROGRAM

*Including fully text-searchable
paper titles, abstracts, and
author names with affiliations*

See you in Charlotte!

TMS



[http://www.tms.org/
AnnualMeeting.html](http://www.tms.org/AnnualMeeting.html)

*The Improved Web Resource
for Every TMS Publication...*

The New On-Line TMS Document Center

Customized to meet your unique needs and now upgraded to provide faster service and easier navigation, the On-Line TMS Document Center provides detailed information and on-line purchasing opportunities for TMS proceedings volumes, textbooks, journals, software programs, video series, and reports. If you need information, you've got to try the new TMS Document Center.

Check out these great new features:

Find, Select, and Check Out the Products You Want FAST

The new TMS Document Center provides easier navigation and faster service for an overall improved shopping experience.

Sample Articles Before You Buy

Not sure if a particular article is the one you need? Click on the PDF icon to view the first page of the article and know that you will be satisfied with your purchase.

TMS Members: View JOM On-Line Free of Charge

TMS members can view the journal for free through the new TMS Document Center. Simply log in and articles from past and current issues are instantly at your fingertips to browse, read, and print out, free of charge!

Purchase Download Suites

Purchase downloads in sets of 10, 25, 50, or 100, and use them to download any files in the TMS Document Center (for less than it would cost to download that many papers individually!). Download suites can be used all at once, over a series of visits to the site, or to create your own custom publication.

Create Your Own Custom Publication

Gather individual papers and articles from TMS proceedings volumes, *JOM*, *Journal of Electronic Materials*, and *Metallurgical and Materials Transactions A and B* to create a one-of-a-kind publication that meets your needs. TMS will compile them in either a softcover book or on a CD-ROM—it's your choice.

Coming in 2004: TMS Letters

TMS Letters is a peer-reviewed, on-line-only journal featuring technical updates of hitherto unpublished research presented at TMS meetings. Available free-of-charge to TMS members (and by subscription to nonmembers), the journal comprises two-page technical updates, including text and graphics. Visit the TMS Document Center for additional information about *TMS Letters*!



See it for yourself!

Visit the new TMS Document Center today.

<http://doc.tms.org>

AN INTERNATIONAL EVENT IN SCIENCE AND ENGINEERING

During the week of March 14–18, the 2004 TMS Annual Meeting & Exhibition will host approximately 4,000 science and engineering professionals, representing more than 70 different countries. They are convening at the Charlotte Convention Center to attend a field-spanning array of metals and materials symposia containing more than 200 sessions and 1,900 individual technical presentations.

This year's meeting will feature programming by

- TMS Electronic, Magnetic & Photonic Materials Division
- TMS Extraction & Processing Division
- TMS Light Metals Division
- TMS Materials Processing & Manufacturing Division
- TMS Structural Materials Division
- TMS Education Committee
- TMS Young Leaders Committee
- ASM International's Materials Science Critical Technologies Sector
- International Titanium Association
- International Magnesium Association
- National Science Foundation
- TMS Public & Governmental Affairs Committee

In addition to the technical programming featured on the following pages, attendees will have the opportunity to

- **Tour** the Exhibition of more than 160 Companies Displaying New Products and Services
- **Attend** Special Lectures and Tutorials
- **Participate** in Short Courses on Metal Matrix Composites, Introduction to Nanomanufacturing and Nanotechnology, Technology Transfer Seminar, Smelter Grade Alumina from the Smelting Perspective and Computational Modelling for the Materials Professional
- **Enjoy** Special Luncheons, Dinners, and Social Functions, including events honoring Didier de Fontaine, R.J. Arsenault, A.L. Roytburd and Roger D. Doherty
- **Network** Extensively
- **Experience** the Charm and Amenities of Charlotte

Extensive details about these and all conference-related activities can be found on the [2004 TMS Annual Meeting Web Site](#).

WANT TO BE PART OF THE ACTION?

Registration is easy.

Just complete and mail or fax the Annual Meeting Registration Form that appears in this document. Or, visit the meeting web site to register immediately (and securely) on-line.

To register in advance, your submission must reach TMS not later than **February 16, 2004**. After this date, it will be necessary to register at the meeting site.

The **Westin Charlotte Hotel** is the TMS headquarters hotel. Special conference rates have been contracted with this hotel and others in the area surrounding the **Charlotte Convention Center**. To receive special rates, use the TMS 2004 Housing Reservation Form that appears in this document and that can be found on the meeting web site.

Special Opportunity for TMS Nonmember Registrants: All nonmember registrants automatically receive a one-year introductory associate membership in TMS for 2004. Membership benefits include a subscription to *JOM* (print and on-line versions) and significant discounts on TMS products and services.

More on the benefits of membership appears on the [TMS Membership Web Pages](#).

INTERESTED IN BUSINESS OPPORTUNITIES?

The 2004 TMS Annual Meeting & Exhibition presents businesses, universities, institutions, agencies, consultants, and others with myriad opportunities to partner in effective marketing communication. Such opportunities to reach thousands of meeting attendees include:

- Placing a **Booth** in the Exhibition
- Placing an **Ad** in the Official Conference Publication and At-Meeting Program: *JOM*
- Sponsoring High-Profile **Attendee Services**, such as the CyberCenter, Coffee Breaks, Signage, and Prize Drawings.
- Hosting a **Hospitality Suite**

More information on these opportunities is available on the [2004 TMS Annual Meeting Sponsorship Web Pages](#).

CONFERENCE PROCEEDINGS: THE RECORDS OF EVENTS

The technical program of each TMS Annual Meeting yields numerous conference proceedings that document many presentations delivered in session rooms. Such publications can be ordered both before and after the meeting via the meeting registration form and/or the TMS Document Center.

The following symposium proceedings will be available in tandem with the meeting:

ADVANCED MATERIALS FOR ENERGY CONVERSION II

Dhanesh Chandra, Renato G. Bautista, and Louis Schlapbach, editors
ISBN 0-87339-574-3 • Approx. 560 pp., illus., index, softcover
Order No. 04-5743 • Weight 3 lbs
M \$112 + S \$89 + L \$160

ADVANCES IN SUPERPLASTICITY AND SUPERPLASTIC FORMING

Eric M. Taleff, Paul E. Krajewski, and Peter A. Friedman, editors
ISBN 0-87339-564-6 • Approx. 436 pp., illus., index, softcover
Order No. 04-5646 • Weight 2 lbs
M \$115 + S \$91 + L \$164

BULK METALLIC GLASSES

Peter K. Liaw and Raymond A. Buchanan, editors
ISBN 0-87339-573-5 • Approx. 256 pp., illus., index, softcover
Order No. 04-5735 • Weight 2 lbs
M \$125 + S \$99 + L \$179

EPD CONGRESS 2004

Mark Schlesinger, editor

Includes the proceedings from the following symposia: Electrochemical Measurements and Processing of Materials, General Pyrometallurgy, Materials Processing Fundamentals, Solid and Aqueous Wastes, Sustainable Development session of Recent Advances in Non-Ferrous Metals Processing, and General Recycling session of Recycling.

ISBN 0-87339-565-4 • Approx. 1,020 pp., CD-ROM
Order No. 04-5654-CD • Weight 1 lb
M \$71 + S \$56 + L \$101

LATERITE NICKEL SYMPOSIUM 2004

D.M. Lane and W.P. Imrie, editors

ISBN 0-87339-550-6 • Approx. 1,144 pp., illus., index, hardcover
Order No. 04-5506 • Weight 4 lbs
M \$119 + S \$94 + L \$170

LIGHT METALS 2004

A.T. Taberaux, editor

Includes the proceedings from the following symposia: Alumina & Bauxite, Aluminum Can Recycling, Aluminum Reduction Technology, Carbon Technology, Cast House Technology, Reactive Metals session of Recent Advances in Non-Ferrous Metals Processing, Aluminum and Aluminum Dross Processing sessions of Recycling.

ISBN 0-87339-567-0 • Approx. 1,150 pp., illus., hardcover & CD-ROM
Order No. 04-5670-G • Weight 7 lbs
M \$150 + S \$125 + L \$225

MAGNESIUM TECHNOLOGY 2004

Alan A. Luo, editor

ISBN 0-87339-568-9 • Approx. 436 pp., illus., hardcover & CD-ROM
Order No. 04-5689-G • Weight 3 lbs
M \$101 + S \$80 + L \$144

SOLIDIFICATION OF ALUMINUM ALLOYS

Men G. Chu, Douglas A. Granger, and Qingyou Han, editors

ISBN 0-87339-569-7 • Approx. 440 pp., illus., softcover
Order No. 04-5697 • Weight 2 lbs
M \$118 + S \$93 + L \$168

MULTIPHASE PHENOMENA AND CFD MODELING AND SIMULATION IN MATERIALS PROCESSES

L. Nastac and B. Li, editors

Includes the proceedings from the following symposia: Multiphase Phenomena in Materials Processing and CFD Modeling and Simulation of Engineering Processes.

ISBN 0-87339-570-0 • Approx. 760 pp., illus., softcover
Order No. 04-5700 • Weight 4 lbs
M \$132 + S \$105 + L \$189

SOLIDIFICATION PROCESSES AND MICROSTRUCTURES: A SYMPOSIUM IN HONOR OF PROF. W. KURZ

M. Rappaz, C. Beckermann, and R. Trivedi, editors

ISBN 0-87339-572-7 • Approx. 432 pp., softcover
Order No. 04-5727 • Weight 2 lbs
M \$112 + S \$88 + L \$159

THE FIFTH GLOBAL INNOVATIONS SYMPOSIUM ON MATERIALS PROCESSING AND MANUFACTURING: SURFACES AND INTERFACES IN NANOSTRUCTURED MATERIALS AND TRENDS IN LIGA, MINIATURIZATION, AND NANOSCALE MATERIALS

Sharmila M. Mukhopadhyay, John Smugeresky, Sudipta Seal, Narendra B. Dahotre, and Arvind Agarwal, editors

Includes the proceedings from the following symposia: Surfaces and Interfaces in Nanostructured Materials and the Fifth Global Innovations Symposium on Materials Processing and Manufacturing: Trends in LIGA, Miniaturization, and Nanoscale Materials

ISBN 0-87339-566-2 • Approx. 720 pp., illus., softcover
Order No. 04-5662 • Weight 4 lbs
M \$118 + S \$93 + L \$168

ULTRAFINE GRAINED MATERIALS III

Yuntian Theodore Zhu, Terence G. Langdon, and Ruslan Z. Valiev, editors

ISBN 0-87339-571-9 • Approx. 824 pp., illus., index, softcover
Order No. 04-5719 • Weight 4 lbs
M \$124 + S \$98 + L \$177

M /Member + S / Student + L / List

The following proceedings are planned for publication in TMS journals after the meeting:

In the Journal of Electronic Materials

Challenges in Advanced Thin Films: Microstructures, Interfaces, and Reactions

Lead-Free Solders and Processing Issues Relevant to Microelectronic Packaging

Phase Stability, Phase Transformation, and Reactive Phase Formation in Electronic Materials III

In Metallurgical and Materials Transactions

Beyond Nickel-Base Superalloys

Hume-Rothery Symposium: Structural and Diffusional Growth

Phase Transformations and Deformation in Magnesium Alloys

In TMS Letters

Processing and Properties of Powder-Based Materials

Other symposia eligible for *TMS Letters*:

Cost-Affordable Titanium

Dislocations

Educational Issues in Transport Phenomena in Materials Processing

General Abstracts

General Poster Session

Internal Stresses and Thermo-Mechanical Behavior in Multi-Component Materials Systems

Roytburd Symposium on Polydomain Structures

Symposium in Honor of Prof. Roger D. Doherty

The Didier de Fontaine Symposium on the Thermodynamics of Alloys

The Role of Grain Boundaries in Material Design

Detailed information about these publications, and many others, can be found in the [TMS Document Center](#).

ADDITIONAL RESOURCES

On-line answers to any of your 2003 TMS Annual Meeting & Exhibition questions can be found at

- **2003 TMS Annual Meeting & Exhibition Web Site:** Get up-to-the-minute meeting details and complete registration materials at <http://www.tms.org/AnnualMeeting.html>
- **TMS Personal Conference Scheduler:** Review the most-up-to-date version of the technical program, examine the calendar of events, and create your own personalized itinerary by visiting <http://pcs.tms.org>

- **TMS Document Center:** Review the complete tables of contents for conference proceedings and order publications by visiting <http://doc.tms.org>
- **TMS Membership:** Learn more about the benefits of membership by touring <http://www.tms.org/Society/membership.html>
- **TMS Business-to-Business Partnering:** Learn how TMS can help your organization maximize its impact by viewing <http://www.tms.org/Meetings/Annual-04/Exhibit2004/Annual04-exhibit-home.html>

If you want to contact a person, more details are available at

TMS Meetings Department
The Minerals, Metals & Materials Society
184 Thorn Hill Road, Warrendale, PA 15086 USA
Telephone: 1-800-759-4867 (in the U.S. and Canada) or
(724) 776-9000, ext. 243
Fax: (724) 776-3770

TMS LETTERS

A valuable new resource for members

A distinguished publication venue for authors



Timely, relevant, and rigorously reviewed, *TMS Letters* is a unique technical journal that presents cutting-edge research in succinct, informative technical updates.

The peer-reviewed journal will be available exclusively in on-line format through the TMS Document Center (doc.tms.org) and will be accessible free-of-charge to all TMS members as a benefit of membership. *TMS Letters* will be composed entirely of two-page technical updates, including text and graphics, of research presented at TMS meetings that are not published in any other book or journal.

The first issue of *TMS Letters* will consist exclusively of technical updates presented at the 2004 TMS Annual Meeting, to be held March 14–18, 2004. Presenters at the 2004 TMS Annual Meeting, whose work will not be published in any other book or journal, may submit their work for publication in the inaugural issue of *TMS Letters*.

To learn more about *TMS Letters* or to submit a technical update, contact:

Dan Thoma
Editor, *TMS Letters*
c/o TMS
184 Thorn Hill Road, Warrendale, PA 15086
E-mail: tmsletters@tms.org
Web: www.tms.org/tmsletters.html

www.tms.org/tmsletters.html

Visit this web site often, as more details will be made available throughout the year, including author instructions for submitting papers to the journal and non-member subscription information.

WEB <http://www.tms.org>
Web registration requires credit card payment.

FAX USA: 724-776-3770
Fax registration requires credit card payment.

MAIL Return with TMS, Meeting Services
payment to: 184 Thorn Hill Road
Warrendale, PA 15086

1. Member of: ☐ TMS ☐ AIST ☐ SME ☐ SPE Member Number: _____

☐ Dr. ☐ Prof. ☐ Mr. ☐ Mrs. ☐ Ms. Last Name First Name Middle Initial

Informal First Name to Appear on Badge: _____ Date of Birth: _____

Employer/Affiliation: _____ Title: _____

Address: ☐ Business ☐ Home _____

City: _____ State/Province: _____ Zip/Postal Code: _____ Country: _____

Telephone: _____ Fax: _____ E-Mail: _____

Guest/Spouse Name: _____

Guests do not receive admission to technical sessions.

2. Registration Fees:

	Advance Fees until February 16, 2004	On-Site Fees after February 16, 2004
<input type="checkbox"/> Member.....	\$400 M	\$500 ML
<input type="checkbox"/> Non-member Author.....	\$490 NMA	\$590 NMAL
<input type="checkbox"/> Non-member *.....	\$550 NM	\$650 NML
<input type="checkbox"/> Student Member ##.....	\$0 STU	\$0 STUL
<input type="checkbox"/> Student Non-member ## *.....	\$25 STUN	\$25 STUNL
<input type="checkbox"/> TMS Senior Member.....	\$250 RM	\$250 RML
<input type="checkbox"/> Exhibit Booth Personnel.....	\$0 E	\$0 EL
<input type="checkbox"/> Exhibit Only.....	\$35 EO	\$35 EOL

Registration TOTAL \$ _____

* Includes TMS membership for 2004

Students must attach a copy of their school's student identification card.

4. Tutorial Luncheon Tickets:

Monday 3/15/04

The Young Leader Tutorial Lecture is free.

You may purchase the optional box lunch for

Fee	Quantity	Total
\$25	_____	\$_____ EM

3. Social Function Tickets:

	Fee	Quantity	Total
Monday 3/15/04			
Didier de Fontaine Honorary Dinner	\$60	_____	\$_____ FD
R.J. Arsenalt Honorary Dinner	\$60	_____	\$_____ JD
Roger Doherty Honorary Dinner	\$60	_____	\$_____ DD
Tuesday 3/16/04			
TMS-AIME Banquet	\$60	_____	\$_____ AD
Tables of 8	\$480	_____	\$_____ AD8
Table Sign to Read			
Extraction & Processing Division Luncheon.....	\$35	_____	\$_____ EP
Tables of 8	\$280	_____	\$_____ EP8
Table Sign to Read			
Wednesday 3/17/04			
Light Metals Division Luncheon	\$35	_____	\$_____ LM
Tables of 8	\$280	_____	\$_____ LM8
Table Sign to Read			
A.L. Roytburd Honorary Dinner.....	\$60	_____	\$_____ RD
Social Function TOTAL \$			_____

5. Publication Orders: All orders that are not indicated for shipment on this form must be picked up at the meeting.

Order Number	Title	Shipping Weight	Quantity	Subtotal Weight	At-Meeting Price	List Price	Subtotal Price
04-5654-CD	EPD Congress 2004 (CD-ROM)	1	_____	_____	\$71	\$101	\$_____
04-5506	Laterite Nickel 2004	4	_____	_____	\$119	\$170	\$_____
04-5670-G	Light Metals 2004 (Book and CD-ROM Set)	7	_____	_____	\$150	\$225	\$_____
04-5689-G	Magnesium Technology 2004 (Book and CD-ROM Set)	3	_____	_____	\$101	\$144	\$_____
04-5743	Advanced Materials for Energy Conversion II	3	_____	_____	\$112	\$160	\$_____
04-5662	Fifth Global Symposium on Materials Processing and Manufacturing: Surfaces and Interfaces in Nanostructured Materials and Trends in LIGA, Miniaturization, and Nanoscale Materials	4	_____	_____	\$118	\$168	\$_____
04-5719	Ultrafine Grained Materials III	4	_____	_____	\$124	\$177	\$_____
04-5727	Solidification Processes and Microstructures (A Symposium in Honor of Prof. W. Kurz)	2	_____	_____	\$112	\$159	\$_____
04-5697	Solidification of Aluminum Alloys	2	_____	_____	\$118	\$168	\$_____
04-5735	Bulk Metallic Glasses	2	_____	_____	\$125	\$179	\$_____
04-5646	Advances in Superplasticity and Superplastic Forming	2	_____	_____	\$115	\$164	\$_____
04-5700	Multiphase Phenomena and CFD Modeling and Simulation in Materials Processes	4	_____	_____	\$132	\$189	\$_____
						Subtotal \$	_____

WEIGHT AND ZONE CHART

Weight	USA	Canada	Mexico	Western Europe	J.A. NZ	EE, C/S Am, Pac. Rim.	Middle East, Africa
1	\$4.50	\$4.00	\$5.00	\$4.50	\$5.00	\$5.50	\$7.50
2	\$5.00	\$7.50	\$9.50	\$8.50	\$9.50	\$10.50	\$14.50
3	\$5.50	\$11.00	\$14.00	\$12.50	\$14.00	\$15.50	\$21.50
4	\$6.00	\$14.50	\$18.50	\$16.50	\$18.50	\$20.50	\$28.50
5	\$6.50	\$18.00	\$23.00	\$20.50	\$23.00	\$25.50	\$35.50
6	\$7.00	\$21.50	\$27.50	\$24.50	\$27.50	\$30.50	\$42.50
7	\$7.50	\$25.00	\$32.00	\$28.50	\$32.00	\$35.50	\$49.50
8	\$8.00	\$28.50	\$36.50	\$32.50	\$36.50	\$40.50	\$56.50
9	\$8.50	\$32.00	\$41.00	\$36.50	\$41.00	\$45.50	\$63.50
10	\$9.00	\$35.50	\$45.50	\$40.50	\$45.50	\$50.50	\$70.50
11	\$9.50	\$39.00	\$50.00	\$44.50	\$50.00	\$55.50	\$77.50
12	\$10.00	\$42.50	\$54.50	\$48.50	\$54.50	\$60.50	\$84.50

If books are to be shipped, please complete the following.

Total Weight _____ Calculate shipping fees from the chart (at left) \$ _____

One-time \$5 handling fee per order shipped \$ _____

NOTE: If your order exceeds 12 pounds, add the amount that it is over from the chart (at the left) to reach the total weight of your order. [Example: 16 lbs. (delivered in U.S.A.) would be 12 lbs. (\$10.00) + 4 lbs (\$6.00) = 16 lbs. (\$16.00)]

Publications TOTAL \$ _____

6. Continuing Education Short Courses: Sunday, March 14, 2004

	Advance Fees until February 16, 2004		On-Site Fees after February 16, 2004	
	Member	Non-member	Member	Non-member
<input type="checkbox"/> 1. Metal Matrix Composites	\$475	\$560	\$525	\$610
<input type="checkbox"/> 2. Introduction to Nanomanufacturing and Nanotechnology	\$475	\$560	\$525	\$610
<input type="checkbox"/> 3. Technology Transfer Seminar	\$475	\$560	\$525	\$610
<input type="checkbox"/> 4. Smelter Grade Alumina from the Smelting Perspective.....	\$475	\$560	\$525	\$610
<input type="checkbox"/> 5. Computational Modeling for the Materials Professionals	\$475	\$560	\$525	\$610

Short Course TOTAL \$ _____ \$ _____

7. 2004 Membership Dues: For current TMS members only

<input type="checkbox"/> Full Member	\$90	FM
<input type="checkbox"/> Junior Member	\$55	JM
<input type="checkbox"/> ASM/TMS Joint Student Member	\$25	ST

8. Payment enclosed:

☐ Check, Bank Draft, Money Order

Make checks payable to TMS. Payment shall be made in USA dollars drawn on a USA bank.

☐ Credit Card Expiration Date: _____

Card No.: _____

☐ Visa ☐ MasterCard ☐ Diners Club ☐ American Express

Cardholder Name: _____

Signature: _____

9. TOTAL FEES PAID

Refund policy: Written requests must be mailed to TMS, post-marked no later than February 16, 2004. A \$50 processing fee will be charged for all cancellations. No refunds will be processed after February 16, 2004.

TMS2004

133rd Annual International Meeting & Exhibition
March 14-18, 2004 • Charlotte, North Carolina, USA

HOUSING RESERVATION FORM

Mail or fax this housing form to:
Travel Planners, Inc., 381 Park Ave. South, New York, NY 10016
FAX: 212-779-6128 • PHONE: 800-221-3531
(in 212, 718, 516, 914, 631 or international call 212-532-1660)
(CHOOSE ONLY ONE OPTION)

Making your reservation is easier than ever through Travel Planners' real-time Internet reservation system! Just log on to www.tms.org, and follow the link to Travel Planners. You will be able to view actual

availability, learn about your hotel's features and services, and obtain local city and sightseeing information. Most importantly, you will receive instant confirmation of your reservation!

Reservations must be received at Travel Planners by: Monday, February 16, 2004

Arrival Date _____ Departure Date _____
Last Name _____ First Name _____ MI _____
Company _____
Street _____ Address _____
City _____ State/County _____ Zip/Postal Code _____ Country _____
Daytime Phone _____ Fax _____
Additional Room Occupants _____
E-mail _____ (confirmation will be sent via e-mail if address is provided)
Non-Smoking Room Requested _____ Special Needs _____

Indicate 1st, 2nd, & 3rd hotel choice:

1. _____
2. _____
3. _____

Type of Accommodations: (check one)

- ☐ Single 1 person/1bed ☐ Double 2 people/1bed ☐ Twin 2 people/2 beds
☐ Triple 3 people/2 beds ☐ Quad 4 people/2 beds

If all three (3) requested hotels are unavailable, please process this reservation according to: (check one) ☐ ROOM RATE ☐ LOCATION

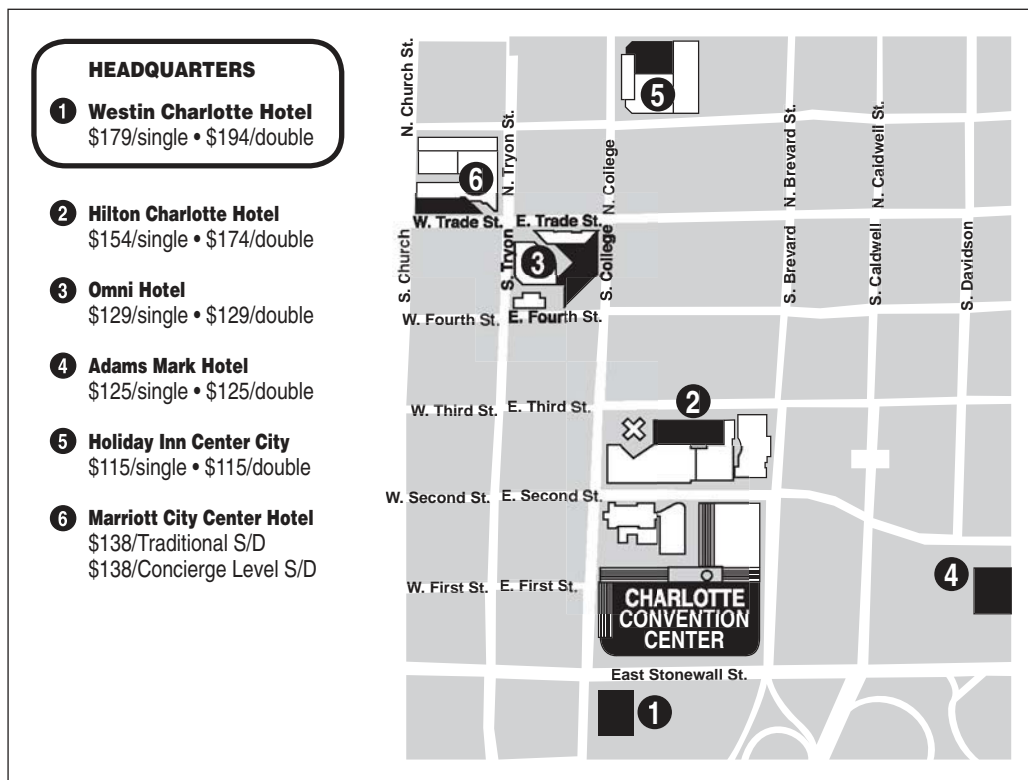
TMS has contracted a block of rooms at the headquarters hotel, Westin Charlotte Hotel, along with each of the hotels, and therefore has assumed a financial liability for any and all rooms in that block that are not reserved. You are strongly encouraged to reserve your room(s) at the hotels listed to limit our financial liability. Please help TMS achieve overall success with the 133rd TMS Annual Meeting & Exhibition by making your reservation at one of the listed hotels prior to the advance housing deadline. Thank you.

Confirmations: Confirmations will be e-mailed, faxed or mailed to you from Travel Planners, Inc. once your reservation has been secured with a deposit or credit card. You will not receive a confirmation from your hotel. If you do not receive a confirmation within 7 days, please call Travel Planners, Inc.

Changes/Cancellations: All changes and cancellations in hotel reservations must be made with Travel Planners, Inc. up until 3 business days prior to arrival and are subject to the individual hotel's cancellation policies. Cancellations and changes within 3 days of arrival MUST be made with your hotel directly. Many hotels are now imposing fees for early departure. This rate is set by each hotel and may vary accordingly. Please reconfirm your departure date at the time of check-in.

Reservations/Deposits: All reservations are being coordinated by Travel Planners, Inc. Arrangements for housing must be made through Travel Planners, Inc. and NOT with the hotel directly. Reservations via Internet, phone or fax will be accepted with a major credit card only. Housing forms and written requests will be accepted with a major credit card or deposit of one night's room and tax payable to Travel Planners, Inc. Check must be drawn in US funds on a US bank. No wire transfers will be accepted. Deposit policies are set by each hotel, and are outlined on your hotel confirmation.

Please read all hotel information prior to completing and submitting this form to Travel Planners, Inc. Keep a copy of this form. Use one form per room required. Make additional copies if needed.



HEADQUARTERS

- 1 **Westin Charlotte Hotel**
\$179/single • \$194/double
- 2 **Hilton Charlotte Hotel**
\$154/single • \$174/double
- 3 **Omni Hotel**
\$129/single • \$129/double
- 4 **Adams Mark Hotel**
\$125/single • \$125/double
- 5 **Holiday Inn Center City**
\$115/single • \$115/double
- 6 **Marriott City Center Hotel**
\$138/Traditional S/D
\$138/Concierge Level S/D

Deposit Payment: ☐ Check ☐ American Express ☐ MasterCard ☐ VISA ☐ Discover ☐ Diners

Account Number _____ Expiration Date _____

Card Holder Name _____ Authorized Signature _____

Monday-March 15		Tuesday-March 16		Wednesday-March 17		Thursday-March 18	
AM	PM	AM	PM	AM	PM	AM	
					Materials Analysis: Understanding the Columbia Disaster		Ballroom B
Dislocations: Modeling and Simulation Fundamentals	Dislocations: Simulation and Observation of Fundamental Mechanisms	Dislocations: Dislocation Structures and Patterning	Dislocations: Novel Experimental Methods	Dislocations: Plasticity, Voids, and Fracture	Dislocations: Dislocations in Complex Materials		201A
	Advances in Superplasticity and Superplastic Forming: Dvlp. of Advanced Superplastic Forming Processes	Advances in Superplasticity and Superplastic Forming: Advances in Superplastic Al-Mg Materials	Advances in Superplasticity and Superplastic Forming: Advances in Superplastic Forming of Light Alloys	Advances in Superplasticity and Superplastic Forming: Advd. Superplastic Matls. & the Sci. of Superplasticity	Advances in Superplasticity and Superplastic Forming: Modeling of Superplastic Forming Processes and Materials	General Abstracts: Session IX	201B
Computational Thermodynamics and Phase Transformations: Grain Growth and Particle Coarsening	Computational Thermodynamics and Phase Transformations: Interfaces and Grain Boundaries	Computational Thermodynamics and Phase Transformations: Phase Field Modeling I	Computational Thermodynamics and Phase Transformations: Phase Field Modeling II	Computational Thermodynamics and Phase Transformations: Phase Equilibria and Thermodynamic Assessments	Computational Thermodynamics and Phase Transformations: Thermodynamics and Phase Transformation		202A
General Pyrometallurgy: Session I	5th Global Innovations Symposium: Plenary: Trends: Past, Present, and Future	5th Global Innovations Symposium: Small Volume Deformation	5th Global Innovations Symposium: Properties & Characterization of Matls. for Microsys./LIGA Applications	5th Global Innovations Symposium: Properties, Processes, and Modeling	5th Global Innovations Symposium: Manufacturing and Evaluation of Layered Nano-Scale Materials		202B
Advanced Materials for Energy Conversion II: Energy Issues & Metal Hydrides I	Advanced Materials for Energy Conversion II: Metal Hydrides II	Advanced Materials for Energy Conversion II: Complex Hydrides I	Advanced Materials for Energy Conversion II: Complex Hydrides II	Advanced Materials for Energy Conversion II: Metal Hydrides III	Advanced Materials for Energy Conversion II: Metal Hydrides IV- Dynamics of Metal Hydrides & Tritium Gettering	Advanced Materials for Energy Conversion II: Thermoelectrics, Superconductors, and Piezoelectrics Materials	203A
Magnesium Technology 2004: Automotive Applications/Welding	Magnesium Technology 2004: Wrought Magnesium Alloys I	Magnesium Technology 2004: Wrought Magnesium Alloys II/Corrosion and Coatings	Magnesium Technology 2004: Primary Processing and Environmental Issues	Magnesium Technology 2004: Casting Processes and Properties	Magnesium Technology 2004: Fundamental Research	Magnesium Technology 2004: Alloy Development	203B
General Abstracts: Session I	General Abstracts: Session II	General Abstracts: Session IV	General Abstracts: Session V	Advanced Materials for Energy Conversion II: Thermodynamics, Superconductors & Batteries	Advanced Materials for Energy Conversion II: Magnetic Materials & Hydrogen Permeation	Advd. Matls. for Energy Conversion II: Metal Hydrides V- Thermal Energy Storage & Containment Matls.	204
Recent Advances in Non-Ferrous Metals Processing: Reactive Metals	Recent Advances in Non-Ferrous Metals Processing: Sustainable Development	Phase Transformations and Deformation in Mg Alloys: Solidification and Precipitation	Phase Transformations and Deformation in Mg Alloys: Plastic Deformation and Texture	Phase Transformations and Deformation in Mg Alloys: Creep Deformation	Phase Transformations and Deformation in Mg Alloys: Deformation and Strengthening		205
CFD Modeling and Simulation of Engineering Processes: Advanced Casting and Solidification Processes I	CFD Modeling and Simulation of Engineering Processes: Remelt Processes	CFD Modeling and Simulation of Engineering Processes: MEMS/ Microfluidics	CFD Modeling and Simulation of Engineering Processes: Advanced Casting and Solidification Processes II	CFD Modeling and Simulation of Engineering Processes: Process Modeling I	CFD Modeling and Simulation of Engineering Processes: Process Modeling II		206A
Cost-Affordable Titanium Symposium Dedicated to Prof. Harvey Flower: Overview and Innovative Processes	Cost-Affordable Titanium Symposium Dedicated to Prof. Harvey Flower: Break Through Technologies	Cost-Affordable Titanium Symposium Dedicated to Prof. Harvey Flower: Titanium Economics	Cost-Affordable Titanium Symposium Dedicated to Prof. Harvey Flower: Creative Processing	Cost-Affordable Titanium Symposium Dedicated to Prof. Harvey Flower: Creative Fabrication	Cost-Affordable Titanium Symposium Dedicated to Prof. Harvey Flower: Low Cost Titanium	Cost-Affordable Titanium Symposium Dedicated to Prof. Harvey Flower: Property Enhancement	206B
Third International Symposium on Ultrafine Grained Materials: Processing I: Fundamentals and Technology	Third International Symposium on Ultrafine Grained Materials: Processing II: Structural Evolution	Third International Symposium on Ultrafine Grained Materials: UFG Material Fundamentals	Third International Symposium on Ultrafine Grained Materials: Microstructure and Properties	Third International Symposium on Ultrafine Grained Materials: Mechanical Properties	Third International Symposium on Ultrafine Grained Materials: Superplasticity, Creep & Thermal Stability		207A
Materials Issues in Fuel Cells: State-of-the-Art	Materials Issues in Fuel Cells: Materials Challenges	Solidification of Aluminum Alloys: Microstructural Evolution I	Solidification of Aluminum Alloys: Microstructural Evolution II	Solidification of Aluminum Alloys: Solidification Cracking/ Mechanical Properties	Solidification of Aluminum Alloys: Gas Porosity/Micro-Macro Segregation	Solidification of Aluminum Alloys: Special Effects	207B/C

150

Monday-March 15		Tuesday-March 16		Wednesday-March 17		Thursday-March 18
AM	PM	AM	PM	AM	PM	AM
Aluminum Reduction - Potroom Improvements	Aluminum Reduction Technology: Cell Development and Operations	Aluminum Reduction Technology: Pot Control	Aluminum Reduction Technology: Modeling - Industry Trends	Aluminum Reduction Technology: Emerging Technologies	Aluminum Reduction Technology: Environmental	Aluminum Reduction Technology: Modeling
Phase Stability, Phase Transformation, and Reactive Phase Formation in Electronic Materials III Session I	Phase Stability, Phase Transformation, and Reactive Phase Formation in Electronic Materials III Session II	Phase Stability, Phase Transformation, and Reactive Phase Formation in Electronic Materials III Session III	Phase Stability, Phase Transformation, and Reactive Phase Formation in Electronic Materials III Session IV	Phase Stability, Phase Transformation, and Reactive Phase Formation in Electronic Materials III Session V	Solid and Aqueous Wastes from Non-Ferrous Metals Industry: Session I	Solid and Aqueous Wastes from Non-Ferrous Metals Industry: Session II
Nanostructured Magnetic Matls.: Recent Progress in Magnetic Nanostructures	Nanostructured Magnetic Matls.: Synthesis & Characterization of Nanostructured Magnetic Matls.	Nanostructured Magnetic Matls.: Magnetic Tunnel Junctions and Semiconductor Spintronics	Nanostructured Magnetic Matls.: Self Assembly and Patterned Nanostructures	Metals for the Future: Structural Materials	Metals for the Future: Functional Materials	Metals for the Future: Processing and Bio-Materials
Symp. on Microstructural Stability in Honor of Prof. Roger D. Doherty: Microstructural Stability: Recrystallization	Symp. on Microstructural Stability in Honor of Prof. Roger D. Doherty: Microstructural Stability: Texture Development	Symp. on Microstructural Stability in Honor of Prof. Roger D. Doherty: Microstructural Stability: Plastic Deformation	Symp. on Microstructural Stability in Honor of Prof. Roger D. Doherty: Microstructl. Stability: Precipitation & Other Topics	Roytburd Symposium on Polydomain Structures: Elastic Domains in Structural Materials	Roytburd Symposium on Polydomain Structures: Domains in Ferroelectrics and Magnetics	
The Didier de Fontaine Symp. on the Thermodynamics of Alloys: Fundamentals of Alloy Theory	The Didier de Fontaine Symp. on the Thermodynamics of Alloys: Experimental Techniques	The Didier de Fontaine Symp. on the Thermodynamics of Alloys: First Principle Calculations & Cluster Expansion Techniques	The Didier de Fontaine Symp. on the Thermodynamics of Alloys: Interatomic Potentials and Cluster Expansion Techniques	The Didier de Fontaine Symp. on the Thermodynamics of Alloys: Jt. Session w/Computatl. Thermodynamics & Phase Transformations I	The Didier de Fontaine Symp. on the Thermodynamics of Alloys: Jt. Session w/Computatl. Thermodynamics & Phase Transformations II	
		Surfaces & Interfaces in Nanostructured Matls.: General Phenomena & Processes	Surfaces & Interfaces in Nanostructured Matls.: Grain & Phase Boundaries	Surfaces & Interfaces in Nanostructured Matls.: Synthesis & Processing	Surfaces & Interfaces in Nanostructured Matls.: Coatings and Surface Modification	Surfaces & Interfaces in Nanostructured Matls.: Self-Organized & Biological Materials
International Laterite Nickel Symposium - 2004: Economics and Project Assessment	International Laterite Nickel Symposium - 2004: Mineralogy and Geometallurgy/Panel Discussion	International Laterite Nickel Symposium - 2004: Pressure Acid Leaching	International Laterite Nickel Symposium - 2004: Process Development for Prospective Projects	International Laterite Nickel Symposium - 2004: Process and Operational Lessons Learned - Part I	International Laterite Nickel Symposium - 2004: Process and Operational Lessons Learned - Part II	International Laterite Nickel Symposium - 2004: Atmospheric Leaching/Slurry Rheology, Solution Extraction and Other
Recycling: General Recycling	Recycling: Aluminum and Aluminum Dross Processing	Aluminum Can Recycling: Session I	International Laterite Nickel Symposium - 2004: Roasting and Smelting	Materials Education to Revitalize the Workforce: Session I	Materials Education to Revitalize the Workforce: Session II	
Alumina and Bauxite: Bayer Plant Operations: Red Side	Alumina and Bauxite: Process Modeling and Control	Alumina and Bauxite: Bayer Plant Operations: White Side	Alumina and Bauxite: Technology and Future Trends	The Role of Grain Boundaries in Material Design: Grain Boundary Character	The Role of Grain Boundaries in Material Design: Grain Boundary Segregation, Diffusion, Damage	The Role of Grain Boundaries in Material Design: Simulation of Grain Boundary Effects of Properties
Challenges in Advd. Thin Films: Microstructures, Interfaces & Reactions: Advances in Photonic & Optoelect. Matls. & Proc.	Challenges in Advd. Thin Films: Microstruct., Interfaces & Reactions: Microstruct., Prop. & Reliability of Microelec. Devices	Challenges in Advd. Thin Films: Microstructures, Interfaces and Reactions: Modification, Characterization, and Modeling	Challenges in Advd. Thin Films: Microstruct., Interfaces & Reactions: Design, Proc. & Property Control...	Multiphase Phenomena in Materials Processing: Session I	Multiphase Phenomena in Materials Processing: Session II	Multiphase Phenomena in Materials Processing: Session III
Nanostructured Materials for Biomedical Applications: Session I	Nanostructured Materials for Biomedical Applications: Session II	Nanostructured Materials for Biomedical Applications: Session III	Nanostructured Materials for Biomedical Applications: Session IV	Nanostructured Materials for Biomedical Applications: Session V	Nanostructured Materials for Biomedical Applications: Session VI	Nanostructured Materials for Biomedical Applications: Session VII
Lead-Free Solders & Procc. Issues Relevant to Microelectronic Pkgs.: Fundamentals, Phases, Wetting & Solidification	Lead-Free Solders & Procc. Issues Relevant to Microelect. Pkgs.: Environmental & Matls. Issues for Lead-Free	Lead-Free Solders & Procc. Issues Relevant to Microelect. Pkgs.: Mechanical Properties & Fatigue Behavior	Lead-Free Solders & Procc. Issues Relevant to Microelect. Pkgs.: Electromigration and Creep in Leadfree Solders	Lead-Free Solders & Procc. Issues Relevant to Microelect. Pkgs.: Interfacial Interactions, Intermetallics & Substrates	Lead-Free Solders & Procc. Issues Relevant to Microelect. Pkgs.: Microstructural Characterization & Evolution	

Table of Contents

(In Order By Technical Track)

SESSION TITLE	ROOM	DAY	PAGE
Hot-Topic Track: Building MSE Synergies			
High Risk Technologies in Metallurgy with Commercial Potential: Session I	210A	Wed-AM	369
High Risk Technologies in Metallurgy with Commercial Potential: Session II	210A	Wed-PM	414
Materials Analysis: Understanding the Columbia Disaster	Ballroom B	Wed-PM	418
Materials by Design: Atoms to Applications: Materials Chemistry and Alloy Design	210B	Mon-AM	192
Materials by Design: Atoms to Applications: Materials Characterization and Microstructural Modeling	210B	Mon-PM	234
Materials by Design: Atoms to Applications: Computational and Experimental Strategies	210B	Tues-AM	288
Materials by Design: Atoms to Applications: Designing Nanostructures	210B	Tues-PM	334
Materials by Design: Atoms to Applications: Design for Mechanical Functionality I	210B	Wed-AM	376
Materials by Design: Atoms to Applications: Design for Mechanical Functionality II	210B	Wed-PM	419
Materials Education to Revitalize the Workforce: Session I	217D	Wed-AM	377
Materials Education to Revitalize the Workforce: Session II	217D	Wed-PM	420
Materials Issues in Fuel Cells: State-of-the-Art	207B/C	Mon-AM	193
Materials Issues in Fuel Cell: Materials Challenges	207B/C	Mon-PM	235
Metals for the Future: Structural Materials	215	Wed-AM	379
Metals for the Future: Functional Materials	215	Wed-PM	422
Metals for the Future: Processing and Bio-Materials	215	Thurs-AM	445
Advanced Materials			
Advanced Materials for Energy Conversion II: Energy Issues & Metal Hydrides I	203A	Mon-AM	169
Advanced Materials for Energy Conversion II: Metal Hydrides II	203A	Mon-PM	210
Advanced Materials for Energy Conversion II: Complex Hydrides I	203A	Tues-AM	262
Advanced Materials for Energy Conversion II: Complex Hydrides II	203A	Tues-PM	309
Advanced Materials for Energy Conversion II: Metal Hydrides III	203A	Wed-AM	353
Advanced Materials for Energy Conversion II: Thermodynamics, Superconductors & Batteries	204	Wed-AM	354
Advanced Materials for Energy Conversion II: Metal Hydrides IV - Dynamics of Metal Hydrides, and Tritium Gettering	203A	Wed-PM	395
Advanced Materials for Energy Conversion II: Magnetic Materials & Hydrogen Permeation	204	Wed-PM	396
Advanced Materials for Energy Conversion II: Thermoelectrics, Superconductors, and Piezoelectric Materials	203A	Thurs-AM	435
Advanced Materials for Energy Conversion II: Metal Hydrides V, Thermal Energy Storage and Containment Materials	204	Thurs-AM	436
Beyond Nickel-Base Superalloys: Superalloys and Niobium Silicides	211B	Mon-AM	174
Beyond Nickel-Base Superalloys: Molybdenum Silicides I	211B	Mon-PM	215

SESSION TITLE	ROOM	DAY	PAGE
<i>Advanced Materials continued...</i>			
Beyond Nickel-Base Superalloys: Precious Metal Alloys	211B	Tues-AM	269
Beyond Nickel-Base Superalloys: Molybdenum Silicides II	211B	Tues-PM	315
Beyond Nickel-Base Superalloys: Niobium Silicides	211B	Wed-AM	357
Beyond Nickel-Base Superalloys: Other Systems and Physical Properties of Silicides	211B	Wed-PM	400
Bulk Metallic Glasses: Processing I	209A	Mon-AM	175
Bulk Metallic Glasses: Processing II	209A	Mon-PM	216
Bulk Metallic Glasses: Fatigue and Fracture	209A	Tues-AM	270
Bulk Metallic Glasses: Theoretical Modeling and Shear Bands	209A	Tues-PM	316
Bulk Metallic Glasses: Bio, Corrosion, and Fracture Behavior	209A	Wed-AM	359
Bulk Metallic Glasses: Phase Transformation and Alloy Design	209A	Wed-PM	402
Bulk Metallic Glasses: Mechanical Behavior	209A	Thurs-AM	438
Processing, Microstructure and Properties of Powder-Based Materials: Session I	208B	Mon-PM	242
Processing, Microstructure and Properties of Powder-Based Materials: Session II	208B	Tues-AM	295
Processing, Microstructure and Properties of Powder-Based Materials: Session III	208B	Tues-PM	340
Roytburd Symposium on Polydomain Structures: Elastic Domains in Structural Materials	216A	Wed-AM	384
Roytburd Symposium on Polydomain Structures: Domains in Ferroelectrics and Magnetics	216A	Wed-PM	425
Electronic Materials			
Challenges in Advanced Thin Films: Microstructures, Interfaces, and Reactions: Advances in Photonic and Optoelectronic Materials and Processes	218B	Mon-AM	179
Challenges in Advanced Thin Films: Microstructures, Interfaces, and Reactions: Microstructures, Properties, and Reliability of Microelectronic Devices	218B	Mon-PM	220
Challenges in Advanced Thin Films: Microstructures, Interfaces, and Reactions: Modification, Characterization, and Modeling	218B	Tues-AM	274
Challenges in Advanced Thin Films: Microstructures, Interfaces, and Reactions: Design, Process, and Property Control of Functional and Structural Thin-Films	218B	Tues-PM	320
Lead-Free Solders and Processing Issues Relevant to Microelectronic Packaging: Fundamentals, Phases, Wetting and Solidification	219B	Mon-AM	189
Lead-Free Solders and Processing Issues Relevant to Microelectronic Packaging: Environmental and Materials Issues for Lead-Free	219B	Mon-PM	231
Lead-Free Solders and Processing Issues Relevant to Microelectronic Packaging: Mechanical Properties and Fatigue Behavior	219B	Tues-AM	285
Lead-Free Solders and Processing Issues Relevant to Microelectronic Packaging: Electromigration and Creep in Leadfree Solders	219B	Tues-PM	331
Lead-Free Solders and Processing Issues Relevant to Microelectronic Packaging: Interfacial Interactions, Intermetallics and Substrates	219B	Wed-AM	373
Lead-Free Solders and Processing Issues Relevant to Microelectronic Packaging: Microstructural Characterization and Evolution	219B	Wed-PM	416
Phase Stability, Phase Transformation, and Reactive Phase Formation in Electronic Materials III: Session I	214	Mon-AM	198
Phase Stability, Phase Transformation, and Reactive Phase Formation in Electronic Materials III: Session II	214	Mon-PM	240

SESSION TITLE	ROOM	DAY	PAGE
<i>Electronic Materials continued...</i>			
Phase Stability, Phase Transformation, and Reactive Phase Formation in Electronic Materials III: Session III	214	Tues-AM	293
Phase Stability, Phase Transformation, and Reactive Phase Formation in Electronic Materials III: Session IV	214	Tues-PM	338
Phase Stability, Phase Transformation, and Reactive Phase Formation in Electronic Materials III: Session V	214	Wed-AM	382
Extraction and Processing			
Educational Issues in Transport Phenomena in Materials Processing: Presentations and Panel Discussion	209B	Wed-PM	408
General Pyrometallurgy: Session I	202B	Mon-AM	185
International Laterite Nickel Symposium - 2004: Economics and Project Assessment	217B/C	Mon-AM	188
International Laterite Nickel Symposium - 2004: Mineralogy and Geometallurgy	217B/C	Mon-PM	230
International Laterite Nickel Symposium - 2004: Panel Discussion	217B/C	Mon-PM	231
International Laterite Nickel Symposium - 2004: Pressure Acid Leaching	217B/C	Tues-AM	284
International Laterite Nickel Symposium - 2004: Process Development for Prospective Projects	217B/C	Tues-PM	328
International Laterite Nickel Symposium - 2004: Roasting and Smelting	217D	Tues-PM	330
International Laterite Nickel Symposium - 2004: Process and Operational Lessons Learned - Part I	217B/C	Wed-AM	372
International Laterite Nickel Symposium - 2004: Process and Operational Lessons Learned - Part II	217B/C	Wed-PM	415
International Laterite Nickel Symposium - 2004: Atmospheric Leaching	217B/C	Thurs-AM	443
International Laterite Nickel Symposium - 2004: Slurry Rheology, Solution Extraction and Other	217B/C	Thurs-AM	443
Materials Processing Fundamentals: Solidification and Casting	212B	Mon-AM	194
Materials Processing Fundamentals: Deformation Processing	212B	Mon-PM	236
Materials Processing Fundamentals: Liquid Metal Processing	212B	Tues-AM	289
Materials Processing Fundamentals: Smelting and Refining	212B	Tues-PM	335
Materials Processing Fundamentals: Aqueous Processing	212B	Wed-AM	378
Materials Processing Fundamentals: Powders, Composites, Coatings and Measurements	212B	Wed-PM	420
Recent Advances in Non-Ferrous Metals Processing: Reactive Metals	205	Mon-AM	199
Recent Advances in Non-Ferrous Metals Processing: Sustainable Development	205	Mon-PM	244
Recycling: General Recycling	217D	Mon-AM	200
Recycling: Aluminum and Aluminum Dross Processing	217D	Mon-PM	244
Solid and Aqueous Wastes from Non-Ferrous Metal Industry: Session I	214	Wed-PM	426
Solid and Aqueous Wastes from Non-Ferrous Metal Industry: Session II	214	Thurs-AM	448
Light Metals			
Alumina and Bauxite: Bayer Plant Operations: Red Side	218A	Mon-AM	170
Alumina and Bauxite: Process Modeling and Control	218A	Mon-PM	212

SESSION TITLE	ROOM	DAY	PAGE
<i>Light Metals continued...</i>			
Alumina and Bauxite: Bayer Plant Operations: White Side	218A	Tues-AM	265
Alumina and Bauxite: Technology and Future Trends	218A	Tues-PM	311
Aluminum Can Recycling: Session I	217D	Tues-AM	266
Aluminum Reduction - Potroom Improvements	213D	Mon-AM	171
Aluminum Reduction Technology: Cell Development and Operations	213D	Mon-PM	212
Aluminum Reduction Technology: Pot Control	213D	Tues-AM	267
Aluminum Reduction Technology: Modeling - Industry Trends	213D	Tues-PM	312
Aluminum Reduction Technology: Emerging Technologies	213D	Wed-AM	356
Aluminum Reduction Technology: Environmental	213D	Wed-PM	398
Aluminum Reduction Technology: Materials and Fundamentals	213A	Wed-PM	399
Aluminum Reduction Technology: Modeling	213D	Thurs-AM	437
Automotive Alloys 2004: Session I	210A	Mon-AM	172
Automotive Alloys 2004: Session II	210A	Mon-PM	213
Automotive Alloys 2004: Session III	210A	Tues-AM	268
Automotive Alloys 2004: Session IV	210A	Tues-PM	313
Carbon Technology: Cathode Material and Corrosion	213A	Mon-AM	176
Carbon Technology: Anode Raw Materials	213A	Mon-PM	217
Carbon Technology: Green Anodes and Soderberg Paste	213A	Tues-AM	272
Carbon Technology: Anode Baking	213A	Tues-PM	317
Carbon Technology: Anode Quality and Performance	213A	Wed-AM	360
Cast Shop Technology: Melting and Refractories	213B/C	Mon-AM	177
Cast Shop Technology: Modeling of Casting Processes	213B/C	Mon-PM	218
Cast Shop Technology: Casting	213B/C	Tues-AM	272
Cast Shop Technology: Metal Treatment	213B/C	Tues-PM	318
Cast Shop Technology: Alloying and Furnace Processing	213B/C	Wed-AM	361
Cast Shop Technology: Grain Refining	213B/C	Wed-PM	403
Cast Shop Technology: Foundry	213B/C	Thurs-AM	439
Cost-Affordable Titanium Symposium Dedicated to Prof. Harvey Flower: Overview and Innovative Processes.....	206B	Mon-AM	182
Cost-Affordable Titanium Symposium Dedicated to Prof. Harvey Flower: Break Through Technologies	206B	Mon-PM	223
Cost-Affordable Titanium Symposium Dedicated to Prof. Harvey Flower: Titanium Economics	206B	Tues-AM	278
Cost-Affordable Titanium Symposium Dedicated to Prof. Harvey Flower: Creative Processing	206B	Tues-PM	323
Cost-Affordable Titanium Symposium Dedicated to Prof. Harvey Flower: Creative Fabrication	206B	Wed-AM	364

SESSION TITLE	ROOM	DAY	PAGE
<i>Light Metals continued...</i>			
Cost-Affordable Titanium Symposium Dedicated to Prof. Harvey Flower: Low Cost Titanium	206B	Wed-PM	406
Cost-Affordable Titanium Symposium Dedicated to Prof. Harvey Flower: Property Enhancement	206B	Thurs-AM	440
Magnesium Technology 2004: Automotive Applications/Welding	203B	Mon-AM	191
Magnesium Technology 2004: Wrought Magnesium Alloys I	203B	Mon-PM	233
Magnesium Technology 2004: Wrought Magnesium Alloys II/Corrosion and Coatings	203B	Tues-AM	287
Magnesium Technology 2004: Primary Processing and Environmental Issues	203B	Tues-PM	332
Magnesium Technology 2004: Casting Processes and Properties	203B	Wed-AM	375
Magnesium Technology 2004: Fundamental Research	203B	Wed-PM	417
Magnesium Technology 2004: Alloy Development	203B	Thurs-AM	444
Phase Transformations and Deformation in Magnesium Alloys: Solidification and Precipitation	205	Tues-AM	294
Phase Transformations and Deformation in Magnesium Alloys: Plastic Deformation and Texture	205	Tues-PM	339
Phase Transformations and Deformation in Magnesium Alloys: Creep Deformation	205	Wed-AM	383
Phase Transformations and Deformation in Magnesium Alloys: Deformation and Strengthening	205	Wed-PM	425
Solidification of Aluminum Alloys: Microstructural Evolution I	207B/C	Tues-AM	298
Solidification of Aluminum Alloys: Microstructural Evolution II	207B/C	Tues-PM	343
Solidification of Aluminum Alloys: Solidification Cracking/Mechanical Properties	207B/C	Wed-AM	385
Solidification of Aluminum Alloys: Gas Porosity/Micro-Macro Segregation	207B/C	Wed-PM	427
Solidification of Aluminum Alloys: Special Effects	207B/C	Thurs-AM	449
Micro- and Nanoscale Technologies			
5th Global Innovations Symposium: Trends in LIGA, Miniaturization, and Nano-Scale Materials, Devices and Technologies: Plenary: Trends: Past, Present, and Future	202B	Mon-PM	209
5th Global Innovations Symposium: Trends in LIGA, Miniaturization, and Nano-Scale Materials, Devices and Technologies: Small Volume Deformation	202B	Tues-AM	261
5th Global Innovations Symposium: Trends in LIGA, Miniaturization, and Nano-Scale Materials, Devices and Technologies: Properties and Characterization of Materials for Microsystem/LIGA Applications	202B	Tues-PM	308
5th Global Innovations Symposium: Trends in LIGA, Miniaturization, and Nano-Scale Materials, Devices and Technologies: Properties, Processes, and Modeling	202B	Wed-AM	352
5th Global Innovations Symposium: Trends in LIGA, Miniaturization, and Nano-Scale Materials, Devices and Technologies: Manufacturing and Evaluation of Layered Nano-Scale Materials	202B	Wed-PM	394
Nanostructured Magnetic Materials: Recent Progress in Magnetic Nanostructures	215	Mon-AM	195
Nanostructured Magnetic Materials: Synthesis and Characterization of Nanostructured Magnetic Materials	215	Mon-PM	237
Nanostructured Magnetic Materials: Magnetic Tunnel Junctions and Semiconductor Spintronics	215	Tues-AM	290
Nanostructured Magnetic Materials: Self Assembly and Patterned Nanostructures	215	Tues-PM	336
Nanostructured Materials for Biomedical Applications: Session I	219A	Mon-AM	197

SESSION TITLE	ROOM	DAY	PAGE
<i>Micro- and Nanoscale Technologies continued...</i>			
Nanostructured Materials for Biomedical Applications: Session II	219A	Mon-PM	239
Nanostructured Materials for Biomedical Applications: Session III	219A	Tues-AM	291
Nanostructured Materials for Biomedical Applications: Session IV	219A	Tues-PM	337
Nanostructured Materials for Biomedical Applications: Session V	219A	Wed-AM	381
Nanostructured Materials for Biomedical Applications: Session VI	219A	Wed-PM	424
Nanostructured Materials for Biomedical Applications: Session VII	219A	Thurs-AM	447
Surfaces and Interfaces in Nanostructured Materials: General Phenomena & Processes ..	217A	Tues-AM	301
Surfaces and Interfaces in Nanostructured Materials: Grain & Phase Boundaries	217A	Tues-PM	346
Surfaces and Interfaces in Nanostructured Materials: Synthesis & Processing	217A	Wed-AM	388
Surfaces and Interfaces in Nanostructured Materials: Coatings and Surface Modification .	217A	Wed-PM	428
Surfaces and Interfaces in Nanostructured Materials: Self-Organized and Biological Materials	217A	Thurs-AM	450
Third International Symposium on Ultrafine Grained Materials: Processing I: Fundamentals and Technology	207A	Mon-AM	206
Third International Symposium on Ultrafine Grained Materials: Processing II: Structural Evolution	207A	Mon-PM	251
Third International Symposium on Ultrafine Grained Materials: Posters	207A	Mon-PM/Tue/Wed	253
Third International Symposium on Ultrafine Grained Materials: UFG Material Fundamentals	207A	Tues-AM	305
Third International Symposium on Ultrafine Grained Materials: Microstructure and Properties	207A	Tues-PM	349
Third International Symposium on Ultrafine Grained Materials: Mechanical Properties	207A	Wed-AM	391
Third International Symposium on Ultrafine Grained Materials: Superplasticity, Creep & Thermal Stability	207A	Wed-PM	432
Physical Metallurgy			
Advances in Superplasticity and Superplastic Forming: Development of Advanced Superplastic Forming Processes	201B	Mon-PM	211
Advances in Superplasticity and Superplastic Forming: Advances in Superplastic Al-Mg Materials	201B	Tues-AM	264
Advances in Superplasticity and Superplastic Forming: Advances in Superplastic Forming of Light Alloys	201B	Tues-PM	310
Advances in Superplasticity and Superplastic Forming: Advanced Superplastic Materials and the Science of Superplasticity	201B	Wed-AM	355
Advances in Superplasticity and Superplastic Forming: Modeling of Superplastic Forming Processes and Materials	201B	Wed-PM	397
CFD Modeling and Simulation of Engineering Processes: Advanced Casting and Solidification Processes I	206A	Mon-AM	178
CFD Modeling and Simulation of Engineering Processes: Remelt Processes	206A	Mon-PM	219
CFD Modeling and Simulation of Engineering Processes: MEMS/Microfluidics	206A	Tues-AM	273
CFD Modeling and Simulation of Engineering Processes: Advanced Casting and Solidification Processes II	206A	Tues-PM	319
CFD Modeling and Simulation of Engineering Processes: Process Modeling I	206A	Wed-AM	362
CFD Modeling and Simulation of Engineering Processes: Process Modeling II	206A	Wed-PM	404

SESSION TITLE	ROOM	DAY	PAGE
<i>Physical Metallurgy continued...</i>			
Computational Thermodynamics and Phase Transformations: Grain Growth and Particle Coarsening	202A	Mon-AM	180
Computational Thermodynamics and Phase Transformations: Interfaces and Grain Boundaries	202A	Mon-PM	222
Computational Thermodynamics and Phase Transformations: Phase Field Modeling I.....	202A	Tues-AM	276
Computational Thermodynamics and Phase Transformations: Phase Field Modeling II... ..	202A	Tues-PM	322
Computational Thermodynamics and Phase Transformations: Phase Equilibria and Thermodynamic Assessments.....	202A	Wed-AM	363
Computational Thermodynamics and Phase Transformations: Joint Session with The Didier de Fontaine Symposium on the Thermodynamics of Alloys I.....	216B	Wed-AM	389
Computational Thermodynamics and Phase Transformations: Thermodynamics and Phase Transformations.....	202A	Wed-PM	405
Computational Thermodynamics and Phase Transformations: Joint Session with The Didier de Fontaine Symposium on the Thermodynamics of Alloys II.....	216B	Wed-PM	430
Dislocations: Modeling and Simulation Fundamentals	201A	Mon-AM	182
Dislocations: Simulation and Observation of Fundamental Mechanisms	201A	Mon-PM	224
Dislocations: Dislocation Structures and Patterning	201A	Tues-AM	278
Dislocations: Novel Experimental Methods	201A	Tues-PM	324
Dislocations: Plasticity, Voids, and Fracture	201A	Wed-AM	365
Dislocations: Dislocations in Complex Materials	201A	Wed-PM	407
Electrochemical Measurements and Processing of Materials: Electrodeposition Processes	212A	Tues-AM	280
Electrochemical Measurements and Processing of Materials: Electrochemical Refining	212A	Tues-PM	325
Electrochemical Measurements and Processing of Materials: Electrochemical Metal Production	212A	Wed-AM	366
Electrochemical Measurements and Processing of Materials: Electrochemical Sensors and Measurements	212A	Wed-PM	409
Failure of Structural Materials: Fundamentals	211A	Wed-AM	367
Failure of Structural Materials: Fatigue	211A	Wed-PM	410
Failure of Structural Materials: General	211A	Thurs-AM	441
Hume Rothery Symposium: Structure and Diffusional Growth Mechanisms of Irrational Interphase Boundaries: Session I	208A	Mon-AM	186
Hume Rothery Symposium: Structure and Diffusional Growth Mechanisms of Irrational Interphase Boundaries: Session II	208A	Mon-PM	228
Hume Rothery Symposium: Structure and Diffusional Growth Mechanisms of Irrational Interphase Boundaries: Session III	208A	Tues-AM	282
Hume Rothery Symposium: Structure and Diffusional Growth Mechanisms of Irrational Interphase Boundaries: Session IV	208A	Tues-PM	327
Hume Rothery Symposium: Structure and Diffusional Growth Mechanisms of Irrational Interphase Boundaries: Session V	208A	Wed-AM	370
Hume Rothery Symposium: Structure and Diffusional Growth Mechanisms of Irrational Interphase Boundaries: Session VI	208A	Wed-PM	415

SESSION TITLE	ROOM	DAY	PAGE
<i>Physical Metallurgy continued...</i>			
Internal Stresses and Thermo-Mechanical Behavior in Multi-Component Materials Systems: Electronic Thin Films and Packaging Materials I	209B	Mon-AM	187
Internal Stresses and Thermo-Mechanical Behavior in Multi-Component Materials Systems: Electronic Thin Films and Packagaing Materials II	209B	Mon-PM	229
Internal Stresses and Thermo-Mechanical Behavior in Multi-Component Materials Systems: Creep and Plasticity I	209B	Tues-AM	283
Internal Stresses and Thermo-Mechanical Behavior in Multi-Component Materials Systems: Creep and Plasticity II	209B	Tues-PM	327
Internal Stresses and Thermo-Mechanical Behavior in Multi-Component Materials Systems: Anisotropy and Residual Stresses	209B	Wed-AM	371
Multiphase Phenomena in Materials Processing: Session I	218B	Wed-AM	379
Multiphase Phenomena in Materials Processing: Session II	218B	Wed-PM	423
Multiphase Phenomena in Materials Processing: Session III	218B	Thurs-AM	446
R.J. Arsenault Symposium on Materials Testing and Evaluation: Session I	211A	Mon-AM	201
R.J. Arsenault Symposium on Materials Testing and Evaluation: Session II	211A	Mon-PM	246
R.J. Arsenault Symposium on Materials Testing and Evaluation: Session III	211A	Tues-AM	296
R.J. Arsenault Symposium on Materials Testing and Evaluation: Session IV	211A	Tues-PM	342
Solidification Processes and Microstructures: A Symposium in Honor of Prof. W. Kurz: Processes	207D	Mon-AM	202
Solidification Processes and Microstructures: A Symposium in Honor of Prof. W. Kurz: Mushy Zone Dynamics	207D	Mon-PM	247
Solidification Processes and Microstructures: A Symposium in Honor of Prof. W. Kurz: Microstructures	207D	Tues-AM	299
Solidification Processes and Microstructures: A Symposium in Honor of Prof. W. Kurz: Rapid Solidification	207D	Tues-PM	344
Solidification Processes and Microstructures: A Symposium in Honor of Prof. W. Kurz: Phase Field	207D	Wed-AM	386
Symposium on Microstructural Stability in Honor of Prof. Roger D. Doherty: Microstructural Stability: Recrystallization	216A	Mon-AM	204
Symposium on Microstructural Stability in Honor of Prof. Roger D. Doherty: Microstructural Stability: Texture Development	216A	Mon-PM	249
Symposium on Microstructural Stability in Honor of Prof. Roger D. Doherty: Microstructural Stability: Plastic Deformation	216A	Tues-AM	302
Symposium on Microstructural Stability in Honor of Prof. Roger D. Doherty: Microstructural Stability: Precipitation and Other Topics	216A	Tues-PM	347
The Didier de Fontaine Symposium on the Thermodynamics of Alloys: Fundamentals of Alloy Theory	216B	Mon-AM	205
The Didier de Fontaine Symposium on the Thermodynamics of Alloys: Experimental Techniques	216B	Mon-PM	250
The Didier de Fontaine Symposium on the Thermodynamics of Alloys: First Principle Calculations and Cluster Expansion Techniques	216B	Tues-AM	304
The Didier de Fontaine Symposium on the Thermodynamics of Alloys: Interatomic Potentials and Cluster Expansion Techniques	216B	Tues-PM	348
The Didier de Fontaine Symposium on the Thermodynamics of Alloys: Joint Session with Computational Thermodynamics and Phase Transformations I	216B	Wed-AM	389

SESSION TITLE	ROOM	DAY	PAGE
<i>Physical Metallurgy continued...</i>			
The Didier de Fontaine Symposium on the Thermodynamics of Alloys: Joint Session with Computational Thermodynamics and Phase Transformations II	216B	Wed-PM	430
The Role of Grain Boundaries in Material Design: Grain Boundary Character	218A	Wed-AM	390
The Role of Grain Boundaries in Material Design: Grain Boundary Segregation, Diffusion, Damage	218A	Wed-PM	431
The Role of Grain Boundaries in Material Design: Simulation of Grain Boundary Effects of Properties	218A	Thurs-AM	451
General Abstracts			
General Abstracts: Session I	204	Mon-AM	184
General Abstracts: Session II	204	Mon-PM	225
General Abstracts: Session III	212A	Mon-PM	226
General Abstracts: Session IV	204	Tues-AM	281
General Abstracts: Session V	204	Tues-PM	326
General Abstracts: Session VI	208B	Wed-AM	368
General Abstracts: Session VII	208B	Wed-PM	411
General Abstracts: Session VIII	207D	Wed-PM	412
General Abstracts: Session IX	201B	Thurs-AM	441
General Poster Session			
General Poster Session	Ballroom Foyer	MonPM-WedPM	453

Table of Contents

(Alphabetical Order)

SESSION TITLE	ROOM	DAY	PAGE
5th Global Innovations Symposium: Trends in LIGA, Miniaturization, and Nano-Scale Materials, Devices and Technologies: Plenary: Trends: Past, Present, and Future	202B	Mon-PM	209
5th Global Innovations Symposium: Trends in LIGA, Miniaturization, and Nano-Scale Materials, Devices and Technologies: Small Volume Deformation	202B	Tues-AM	261
5th Global Innovations Symposium: Trends in LIGA, Miniaturization, and Nano-Scale Materials, Devices and Technologies: Properties and Characterization of Materials for Microsystem/LIGA Applications	202B	Tues-PM	308
5th Global Innovations Symposium: Trends in LIGA, Miniaturization, and Nano-Scale Materials, Devices and Technologies: Properties, Processes, and Modeling	202B	Wed-AM	352
5th Global Innovations Symposium: Trends in LIGA, Miniaturization, and Nano-Scale Materials, Devices and Technologies: Manufacturing and Evaluation of Layered Nano-Scale Materials	202B	Wed-PM	394
Advanced Materials for Energy Conversion II: Energy Issues & Metal Hydrides I	203A	Mon-AM	169
Advanced Materials for Energy Conversion II: Metal Hydrides II	203A	Mon-PM	210
Advanced Materials for Energy Conversion II: Complex Hydrides I	203A	Tues-AM	262
Advanced Materials for Energy Conversion II: Complex Hydrides II	203A	Tues-PM	309
Advanced Materials for Energy Conversion II: Metal Hydrides III	203A	Wed-AM	353
Advanced Materials for Energy Conversion II: Thermodynamics, Superconductors & Batteries	204	Wed-AM	354
Advanced Materials for Energy Conversion II: Metal Hydrides IV - Dynamics of Metal Hydrides, and Tritium Gettering	203A	Wed-PM	395
Advanced Materials for Energy Conversion II: Magnetic Materials & Hydrogen Permeation	204	Wed-PM	396
Advanced Materials for Energy Conversion II: Thermoelectrics, Superconductors, and Piezoelectric Materials	203A	Thurs-AM	435
Advanced Materials for Energy Conversion II: Metal Hydrides V, Thermal Energy Storage and Containment Materials	204	Thurs-AM	436
Advances in Superplasticity and Superplastic Forming: Development of Advanced Superplastic Forming Processes	201B	Mon-PM	211
Advances in Superplasticity and Superplastic Forming: Advances in Superplastic Al-Mg Materials	201B	Tues-AM	264
Advances in Superplasticity and Superplastic Forming: Advances in Superplastic Forming of Light Alloys	201B	Tues-PM	310
Advances in Superplasticity and Superplastic Forming: Advanced Superplastic Materials and the Science of Superplasticity	201B	Wed-AM	355
Advances in Superplasticity and Superplastic Forming: Modeling of Superplastic Forming Processes and Materials	201B	Wed-PM	397
Alumina and Bauxite: Bayer Plant Operations: Red Side	218A	Mon-AM	170
Alumina and Bauxite: Process Modeling and Control	218A	Mon-PM	212
Alumina and Bauxite: Bayer Plant Operations: White Side	218A	Tues-AM	265
Alumina and Bauxite: Technology and Future Trends	218A	Tues-PM	311

SESSION TITLE	ROOM	DAY	PAGE
Aluminum Can Recycling: Session I	217D	Tues-AM	266
Aluminum Reduction - Potroom Improvements	213D	Mon-AM	171
Aluminum Reduction Technology: Cell Development and Operations	213D	Mon-PM	212
Aluminum Reduction Technology: Pot Control	213D	Tues-AM	267
Aluminum Reduction Technology: Modeling - Industry Trends	213D	Tues-PM	312
Aluminum Reduction Technology: Emerging Technologies	213D	Wed-AM	356
Aluminum Reduction Technology: Environmental	213D	Wed-PM	398
Aluminum Reduction Technology: Materials and Fundamentals	213A	Wed-PM	399
Aluminum Reduction Technology: Modeling	213D	Thurs-AM	437
Automotive Alloys 2004: Session I	210A	Mon-AM	172
Automotive Alloys 2004: Session II	210A	Mon-PM	213
Automotive Alloys 2004: Session III	210A	Tues-AM	268
Automotive Alloys 2004: Session IV	210A	Tues-PM	313
Beyond Nickel-Base Superalloys: Superalloys and Niobium Silicides	211B	Mon-AM	174
Beyond Nickel-Base Superalloys: Molybdenum Silicides I	211B	Mon-PM	215
Beyond Nickel-Base Superalloys: Precious Metal Alloys	211B	Tues-AM	269
Beyond Nickel-Base Superalloys: Molybdenum Silicides II	211B	Tues-PM	315
Beyond Nickel-Base Superalloys: Niobium Silicides	211B	Wed-AM	357
Beyond Nickel-Base Superalloys: Other Systems and Physical Properties of Silicides	211B	Wed-PM	400
Bulk Metallic Glasses: Processing I	209A	Mon-AM	175
Bulk Metallic Glasses: Processing II	209A	Mon-PM	216
Bulk Metallic Glasses: Fatigue and Fracture	209A	Tues-AM	270
Bulk Metallic Glasses: Theoretical Modeling and Shear Bands	209A	Tues-PM	316
Bulk Metallic Glasses: Bio, Corrosion, and Fracture Behavior	209A	Wed-AM	359
Bulk Metallic Glasses: Phase Transformation and Alloy Design	209A	Wed-PM	402
Bulk Metallic Glasses: Mechanical Behavior	209A	Thurs-AM	438
Carbon Technology: Cathode Material and Corrosion	213A	Mon-AM	176
Carbon Technology: Anode Raw Materials	213A	Mon-PM	217
Carbon Technology: Green Anodes and Soderberg Paste	213A	Tues-AM	272
Carbon Technology: Anode Baking	213A	Tues-PM	317
Carbon Technology: Anode Quality and Performance	213A	Wed-AM	360
Cast Shop Technology: Melting and Refractories	213B/C	Mon-AM	177
Cast Shop Technology: Modeling of Casting Processes	213B/C	Mon-PM	218
Cast Shop Technology: Casting	213B/C	Tues-AM	272
Cast Shop Technology: Metal Treatment	213B/C	Tues-PM	318
Cast Shop Technology: Alloying and Furnace Processing	213B/C	Wed-AM	361

SESSION TITLE	ROOM	DAY	PAGE
Cast Shop Technology: Grain Refining	213B/C	Wed-PM	403
Cast Shop Technology: Foundry	213B/C	Thurs-AM	439
CFD Modeling and Simulation of Engineering Processes: Advanced Casting and Solidification Processes I	206A	Mon-AM	178
CFD Modeling and Simulation of Engineering Processes: Remelt Processes	206A	Mon-PM	219
CFD Modeling and Simulation of Engineering Processes: MEMS/Microfluidics	206A	Tues-AM	273
CFD Modeling and Simulation of Engineering Processes: Advanced Casting and Solidification Processes II	206A	Tues-PM	319
CFD Modeling and Simulation of Engineering Processes: Process Modeling I	206A	Wed-AM	362
CFD Modeling and Simulation of Engineering Processes: Process Modeling II	206A	Wed-PM	404
Challenges in Advanced Thin Films: Microstructures, Interfaces, and Reactions: Advances in Photonic and Optoelectronic Materials and Processes	218B	Mon-AM	179
Challenges in Advanced Thin Films: Microstructures, Interfaces, and Reactions: Microstructures, Properties, and Reliability of Microelectronic Devices	218B	Mon-PM	220
Challenges in Advanced Thin Films: Microstructures, Interfaces, and Reactions: Modification, Characterization, and Modeling	218B	Tues-AM	274
Challenges in Advanced Thin Films: Microstructures, Interfaces, and Reactions: Design, Process, and Property Control of Functional and Structural Thin-Films	218B	Tues-PM	320
Computational Thermodynamics and Phase Transformations: Grain Growth and Particle Coarsening	202A	Mon-AM	180
Computational Thermodynamics and Phase Transformations: Interfaces and Grain Boundaries	202A	Mon-PM	222
Computational Thermodynamics and Phase Transformations: Phase Field Modeling I	202A	Tues-AM	276
Computational Thermodynamics and Phase Transformations: Phase Field Modeling II... ..	202A	Tues-PM	322
Computational Thermodynamics and Phase Transformations: Phase Equilibria and Thermodynamic Assessments.....	202A	Wed-AM	363
Computational Thermodynamics and Phase Transformations: Joint Session with The Didier de Fontaine Symposium on the Thermodynamics of Alloys I.....	216B	Wed-AM	389
Computational Thermodynamics and Phase Transformations: Thermodynamics and Phase Transformations.....	202A	Wed-PM	405
Computational Thermodynamics and Phase Transformations: Joint Session with The Didier de Fontaine Symposium on the Thermodynamics of Alloys II.....	216B	Wed-PM	430
Cost-Affordable Titanium Symposium Dedicated to Prof. Harvey Flower: Overview and Innovative Processes.....	206B	Mon-AM	182
Cost-Affordable Titanium Symposium Dedicated to Prof. Harvey Flower: Break Through Technologies	206B	Mon-PM	223
Cost-Affordable Titanium Symposium Dedicated to Prof. Harvey Flower: Titanium Economics	206B	Tues-AM	278
Cost-Affordable Titanium Symposium Dedicated to Prof. Harvey Flower: Creative Processing	206B	Tues-PM	323
Cost-Affordable Titanium Symposium Dedicated to Prof. Harvey Flower: Creative Fabrication	206B	Wed-AM	364
Cost-Affordable Titanium Symposium Dedicated to Prof. Harvey Flower: Low Cost Titanium	206B	Wed-PM	406
Cost-Affordable Titanium Symposium Dedicated to Prof. Harvey Flower: Property Enhancement	206B	Thurs-AM	440

SESSION TITLE	ROOM	DAY	PAGE
Dislocations: Modeling and Simulation Fundamentals	201A	Mon-AM	182
Dislocations: Simulation and Observation of Fundamental Mechanisms	201A	Mon-PM	224
Dislocations: Dislocation Structures and Patterning	201A	Tues-AM	278
Dislocations: Novel Experimental Methods	201A	Tues-PM	324
Dislocations: Plasticity, Voids, and Fracture	201A	Wed-AM	365
Dislocations: Dislocations in Complex Materials	201A	Wed-PM	407
Educational Issues in Transport Phenomena in Materials Processing: Presentations and Panel Discussion	209B	Wed-PM	408
Electrochemical Measurements and Processing of Materials: Electrodeposition Processes	212A	Tues-AM	280
Electrochemical Measurements and Processing of Materials: Electrochemical Refining	212A	Tues-PM	325
Electrochemical Measurements and Processing of Materials: Electrochemical Metal Production	212A	Wed-AM	366
Electrochemical Measurements and Processing of Materials: Electrochemical Sensors and Measurements	212A	Wed-PM	409
Failure of Structural Materials: Fundamentals	211A	Wed-AM	367
Failure of Structural Materials: Fatigue	211A	Wed-PM	410
Failure of Structural Materials: General	211A	Thurs-AM	441
General Abstracts: Session I	204	Mon-AM	184
General Abstracts: Session II	204	Mon-PM	225
General Abstracts: Session III	212A	Mon-PM	226
General Abstracts: Session IV	204	Tues-AM	281
General Abstracts: Session V	204	Tues-PM	326
General Abstracts: Session VI	208B	Wed-AM	368
General Abstracts: Session VII	208B	Wed-PM	411
General Abstracts: Session VIII	207D	Wed-PM	412
General Abstracts: Session IX	201B	Thurs-AM	441
General Poster Session	Ballroom Foyer	MonPM-WedPM	453
General Pyrometallurgy: Session I	202B	Mon-AM	185
High Risk Technologies in Metallurgy with Commercial Potential: Session I	210A	Wed-AM	369
High Risk Technologies in Metallurgy with Commercial Potential: Session II	210A	Wed-PM	414
Hume Rothery Symposium: Structure and Diffusional Growth Mechanisms of Irrational Interphase Boundaries: Session I	208A	Mon-AM	186
Hume Rothery Symposium: Structure and Diffusional Growth Mechanisms of Irrational Interphase Boundaries: Session II	208A	Mon-PM	228
Hume Rothery Symposium: Structure and Diffusional Growth Mechanisms of Irrational Interphase Boundaries: Session III	208A	Tues-AM	282
Hume Rothery Symposium: Structure and Diffusional Growth Mechanisms of Irrational Interphase Boundaries: Session IV	208A	Tues-PM	327
Hume Rothery Symposium: Structure and Diffusional Growth Mechanisms of Irrational Interphase Boundaries: Session V	208A	Wed-AM	370

SESSION TITLE	ROOM	DAY	PAGE
Hume Rothery Symposium: Structure and Diffusional Growth Mechanisms of Irrational Interphase Boundaries: Session VI	208A	Wed-PM	415
Internal Stresses and Thermo-Mechanical Behavior in Multi-Component Materials Systems: Electronic Thin Films and Packaging Materials I	209B	Mon-AM	187
Internal Stresses and Thermo-Mechanical Behavior in Multi-Component Materials Systems: Electronic Thin Films and Packaging Materials II	209B	Mon-PM	229
Internal Stresses and Thermo-Mechanical Behavior in Multi-Component Materials Systems: Creep and Plasticity I	209B	Tues-AM	283
Internal Stresses and Thermo-Mechanical Behavior in Multi-Component Materials Systems: Creep and Plasticity II	209B	Tues-PM	327
Internal Stresses and Thermo-Mechanical Behavior in Multi-Component Materials Systems: Anisotropy and Residual Stresses	209B	Wed-AM	371
International Laterite Nickel Symposium - 2004: Economics and Project Assessment	217B/C	Mon-AM	188
International Laterite Nickel Symposium - 2004: Mineralogy and Geometallurgy	217B/C	Mon-PM	230
International Laterite Nickel Symposium - 2004: Panel Discussion	217B/C	Mon-PM	231
International Laterite Nickel Symposium - 2004: Pressure Acid Leaching	217B/C	Tues-AM	284
International Laterite Nickel Symposium - 2004: Process Development for Prospective Projects	217B/C	Tues-PM	328
International Laterite Nickel Symposium - 2004: Roasting and Smelting	217D	Tues-PM	330
International Laterite Nickel Symposium - 2004: Process and Operational Lessons Learned - Part I	217B/C	Wed-AM	372
International Laterite Nickel Symposium - 2004: Process and Operational Lessons Learned - Part II	217B/C	Wed-PM	415
International Laterite Nickel Symposium - 2004: Atmospheric Leaching	217B/C	Thurs-AM	443
International Laterite Nickel Symposium - 2004: Slurry Rheology, Solution Extraction and Other	217B/C	Thurs-AM	443
Lead-Free Solders and Processing Issues Relevant to Microelectronic Packaging: Fundamentals, Phases, Wetting and Solidification	219B	Mon-AM	189
Lead-Free Solders and Processing Issues Relevant to Microelectronic Packaging: Environmental and Materials Issues for Lead-Free	219B	Mon-PM	231
Lead-Free Solders and Processing Issues Relevant to Microelectronic Packaging: Mechanical Properties and Fatigue Behavior	219B	Tues-AM	285
Lead-Free Solders and Processing Issues Relevant to Microelectronic Packaging: Electromigration and Creep in Leadfree Solders	219B	Tues-PM	331
Lead-Free Solders and Processing Issues Relevant to Microelectronic Packaging: Interfacial Interactions, Intermetallics and Substrates	219B	Wed-AM	373
Lead-Free Solders and Processing Issues Relevant to Microelectronic Packaging: Microstructural Characterization and Evolution	219B	Wed-PM	416
Magnesium Technology 2004: Automotive Applications/Welding	203B	Mon-AM	191
Magnesium Technology 2004: Wrought Magnesium Alloys I	203B	Mon-PM	233
Magnesium Technology 2004: Wrought Magnesium Alloys II/Corrosion and Coatings	203B	Tues-AM	287
Magnesium Technology 2004: Primary Processing and Environmental Issues	203B	Tues-PM	332
Magnesium Technology 2004: Casting Processes and Properties	203B	Wed-AM	375
Magnesium Technology 2004: Fundamental Research	203B	Wed-PM	417
Magnesium Technology 2004: Alloy Development	203B	Thurs-AM	444

SESSION TITLE	ROOM	DAY	PAGE
Materials Analysis: Understanding the Columbia Disaster	Ballroom B	Wed-PM	418
Materials by Design: Atoms to Applications: Materials Chemistry and Alloy Design	210B	Mon-AM	192
Materials by Design: Atoms to Applications: Materials Characterization and Microstructural Modeling	210B	Mon-PM	234
Materials by Design: Atoms to Applications: Computational and Experimental Strategies	210B	Tues-AM	288
Materials by Design: Atoms to Applications: Designing Nanostructures	210B	Tues-PM	334
Materials by Design: Atoms to Applications: Design for Mechanical Functionality I	210B	Wed-AM	376
Materials by Design: Atoms to Applications: Design for Mechanical Functionality II	210B	Wed-PM	419
Materials Education to Revitalize the Workforce: Session I	217D	Wed-AM	377
Materials Education to Revitalize the Workforce: Session II	217D	Wed-PM	420
Materials Issues in Fuel Cells: State-of-the-Art	207B/C	Mon-AM	193
Materials Issues in Fuel Cell: Materials Challenges	207B/C	Mon-PM	235
Materials Processing Fundamentals: Solidification and Casting	212B	Mon-AM	194
Materials Processing Fundamentals: Deformation Processing	212B	Mon-PM	236
Materials Processing Fundamentals: Liquid Metal Processing	212B	Tues-AM	289
Materials Processing Fundamentals: Smelting and Refining	212B	Tues-PM	335
Materials Processing Fundamentals: Aqueous Processing	212B	Wed-AM	378
Materials Processing Fundamentals: Powders, Composites, Coatings and Measurements ..	212B	Wed-PM	420
Metals for the Future: Structural Materials	215	Wed-AM	379
Metals for the Future: Functional Materials	215	Wed-PM	422
Metals for the Future: Processing and Bio-Materials	215	Thurs-AM	445
Multiphase Phenomena in Materials Processing: Session I	218B	Wed-AM	379
Multiphase Phenomena in Materials Processing: Session II	218B	Wed-PM	423
Multiphase Phenomena in Materials Processing: Session III	218B	Thurs-AM	446
Nanostructured Magnetic Materials: Recent Progress in Magnetic Nanostructures	215	Mon-AM	195
Nanostructured Magnetic Materials: Synthesis and Characterization of Nanostructured Magnetic Materials	215	Mon-PM	237
Nanostructured Magnetic Materials: Magnetic Tunnel Junctions and Semiconductor Spintronics	215	Tues-AM	290
Nanostructured Magnetic Materials: Self Assembly and Patterned Nanostructures	215	Tues-PM	336
Nanostructured Materials for Biomedical Applications: Session I	219A	Mon-AM	197
Nanostructured Materials for Biomedical Applications: Session II	219A	Mon-PM	239
Nanostructured Materials for Biomedical Applications: Session III	219A	Tues-AM	291
Nanostructured Materials for Biomedical Applications: Session IV	219A	Tues-PM	337
Nanostructured Materials for Biomedical Applications: Session V	219A	Wed-AM	381
Nanostructured Materials for Biomedical Applications: Session VI	219A	Wed-PM	424
Nanostructured Materials for Biomedical Applications: Session VII	219A	Thurs-AM	447
Phase Stability, Phase Transformation, and Reactive Phase Formation in Electronic Materials III: Session I	214	Mon-AM	198

SESSION TITLE	ROOM	DAY	PAGE
Phase Stability, Phase Transformation, and Reactive Phase Formation in Electronic Materials III: Session II	214	Mon-PM	240
Phase Stability, Phase Transformation, and Reactive Phase Formation in Electronic Materials III: Session III	214	Tues-AM	293
Phase Stability, Phase Transformation, and Reactive Phase Formation in Electronic Materials III: Session IV	214	Tues-PM	338
Phase Stability, Phase Transformation, and Reactive Phase Formation in Electronic Materials III: Session V	214	Wed-AM	382
Phase Transformations and Deformation in Magnesium Alloys: Solidification and Precipitation	205	Tues-AM	294
Phase Transformations and Deformation in Magnesium Alloys: Plastic Deformation and Texture	205	Tues-PM	339
Phase Transformations and Deformation in Magnesium Alloys: Creep Deformation	205	Wed-AM	383
Phase Transformations and Deformation in Magnesium Alloys: Deformation and Strengthening	205	Wed-PM	425
Processing, Microstructure and Properties of Powder-Based Materials: Session I	208B	Mon-PM	242
Processing, Microstructure and Properties of Powder-Based Materials: Session II	208B	Tues-AM	295
Processing, Microstructure and Properties of Powder-Based Materials: Session III	208B	Tues-PM	340
Recent Advances in Non-Ferrous Metals Processing: Reactive Metals	205	Mon-AM	199
Recent Advances in Non-Ferrous Metals Processing: Sustainable Development	205	Mon-PM	244
Recycling: General Recycling	217D	Mon-AM	200
Recycling: Aluminum and Aluminum Dross Processing	217D	Mon-PM	244
Roytburd Symposium on Polydomain Structures: Elastic Domains in Structural Materials	216A	Wed-AM	384
Roytburd Symposium on Polydomain Structures: Domains in Ferroelectrics and Magnetics	216A	Wed-PM	425
R.J. Arsenault Symposium on Materials Testing and Evaluation: Session I	211A	Mon-AM	201
R.J. Arsenault Symposium on Materials Testing and Evaluation: Session II	211A	Mon-PM	246
R.J. Arsenault Symposium on Materials Testing and Evaluation: Session III	211A	Tues-AM	296
R.J. Arsenault Symposium on Materials Testing and Evaluation: Session IV	211A	Tues-PM	342
Solid and Aqueous Wastes from Non-Ferrous Metal Industry: Session I	214	Wed-PM	426
Solid and Aqueous Wastes from Non-Ferrous Metal Industry: Session II	214	Thurs-AM	448
Solidification of Aluminum Alloys: Microstructural Evolution I	207B/C	Tues-AM	298
Solidification of Aluminum Alloys: Microstructural Evolution II	207B/C	Tues-PM	343
Solidification of Aluminum Alloys: Solidification Cracking/Mechanical Properties	207B/C	Wed-AM	385
Solidification of Aluminum Alloys: Gas Porosity/Micro-Macro Segregation	207B/C	Wed-PM	427
Solidification of Aluminum Alloys: Special Effects	207B/C	Thurs-AM	449
Solidification Processes and Microstructures: A Symposium in Honor of Prof. W. Kurz: Processes	207D	Mon-AM	202
Solidification Processes and Microstructures: A Symposium in Honor of Prof. W. Kurz: Mushy Zone Dynamics	207D	Mon-PM	247
Solidification Processes and Microstructures: A Symposium in Honor of Prof. W. Kurz: Microstructures	207D	Tues-AM	299

SESSION TITLE	ROOM	DAY	PAGE
Solidification Processes and Microstructures: A Symposium in Honor of Prof. W. Kurz: Rapid Solidification	207D	Tues-PM	344
Solidification Processes and Microstructures: A Symposium in Honor of Prof. W. Kurz: Phase Field	207D	Wed-AM	386
Surfaces and Interfaces in Nanostructured Materials: General Phenomena & Processes ..	217A	Tues-AM	301
Surfaces and Interfaces in Nanostructured Materials: Grain & Phase Boundaries	217A	Tues-PM	346
Surfaces and Interfaces in Nanostructured Materials: Synthesis & Processing	217A	Wed-AM	388
Surfaces and Interfaces in Nanostructured Materials: Coatings and Surface Modification .	217A	Wed-PM	428
Surfaces and Interfaces in Nanostructured Materials: Self-Organized and Biological Materials	217A	Thurs-AM	450
Symposium on Microstructural Stability in Honor of Prof. Roger D. Doherty: Microstructural Stability: Recrystallization	216A	Mon-AM	204
Symposium on Microstructural Stability in Honor of Prof. Roger D. Doherty: Microstructural Stability: Texture Development	216A	Mon-PM	249
Symposium on Microstructural Stability in Honor of Prof. Roger D. Doherty: Microstructural Stability: Plastic Deformation	216A	Tues-AM	302
Symposium on Microstructural Stability in Honor of Prof. Roger D. Doherty: Microstructural Stability: Precipitation and Other Topics	216A	Tues-PM	347
The Didier de Fontaine Symposium on the Thermodynamics of Alloys: Fundamentals of Alloy Theory	216B	Mon-AM	205
The Didier de Fontaine Symposium on the Thermodynamics of Alloys: Experimental Techniques	216B	Mon-PM	250
The Didier de Fontaine Symposium on the Thermodynamics of Alloys: First Principle Calculations and Cluster Expansion Techniques	216B	Tues-AM	304
The Didier de Fontaine Symposium on the Thermodynamics of Alloys: Interatomic Potentials and Cluster Expansion Techniques	216B	Tues-PM	348
The Didier de Fontaine Symposium on the Thermodynamics of Alloys: Joint Session with Computational Thermodynamics and Phase Transformations I	216B	Wed-AM	389
The Didier de Fontaine Symposium on the Thermodynamics of Alloys: Joint Session with Computational Thermodynamics and Phase Transformations II	216B	Wed-PM	430
The Role of Grain Boundaries in Material Design: Grain Boundary Character	218A	Wed-AM	390
The Role of Grain Boundaries in Material Design: Grain Boundary Segregation, Diffusion, Damage	218A	Wed-PM	431
The Role of Grain Boundaries in Material Design: Simulation of Grain Boundary Effects of Properties	218A	Thurs-AM	451
Third International Symposium on Ultrafine Grained Materials: Processing I: Fundamentals and Technology	207A	Mon-AM	206
Third International Symposium on Ultrafine Grained Materials: Processing II: Structural Evolution	207A	Mon-PM	251
Third International Symposium on Ultrafine Grained Materials: Posters	207A	Mon-PM/Tue/Wed	253
Third International Symposium on Ultrafine Grained Materials: UFG Material Fundamentals	207A	Tues-AM	305
Third International Symposium on Ultrafine Grained Materials: Microstructure and Properties	207A	Tues-PM	349
Third International Symposium on Ultrafine Grained Materials: Mechanical Properties	207A	Wed-AM	391
Third International Symposium on Ultrafine Grained Materials: Superplasticity, Creep & Thermal Stability	207A	Wed-PM	432

5th Global Innovations Symposium: Trends in LIGA, Miniaturization, and Nano-Scale Materials, Devices and Technologies: Small Volume Deformation

Sponsored by: Materials Processing & Manufacturing Division, MPMD-Powder Materials Committee, MPMD-Phase Transformations Committee-(Jt. ASM-MSCTS), MPMD-Computational Materials Science & Engineering-(Jt. ASM-MSCTS), MPMD/EPD-Process Modeling Analysis & Control Committee, MPMD-Surface Engineering Committee, MPMD-Shaping and Forming Committee, MPMD-Solidification Committee

Program Organizers: John E. Smugeresky, Sandia National Laboratories, Department 8724, Livermore, CA 94551-0969 USA; Steven H. Goods, Sandia National Laboratories, Livermore, CA 94551-0969 USA; Sean J. Hearne, Sandia National Laboratories, Albuquerque, NM 87185-1415 USA; Neville R. Moody, Sandia National Laboratories, Livermore, CA 94551-0969 USA

Tuesday AM Room: 202B
March 16, 2004 Location: Charlotte Convention Center

Session Chairs: Erica T. Lilleodden, Lawrence Berkeley National Laboratory, Matls. Sci. Div., Berkeley, CA 94720 USA; Sean J. Hearne, Sandia National Laboratories, Nanostruct. & Semiconductor Physics Dept., Albuquerque, NM 87185-1415 USA

8:30 AM Keynote

Some Challenges in Understanding Mechanical Properties at the Nanometer and Micrometer Length Scales: *William D. Nix*¹; Feng Gang¹; Julia R. Greer¹; ¹Stanford University, Dept. of Matls. Sci. & Engrg., 416 Escondido Mall, Bldg. 550, Stanford, CA 94305-2205 USA

Nanomechanical devices are certain to play an important role in future technologies. Already sensors and actuators based on MEMS technologies are commonplace and new devices based on NEMS are just around the corner. These developments are part of a decades-long trend to build useful engineering devices and structures on a smaller and smaller scale. The creation of structures and devices calls for an understanding of the mechanical properties of materials at these small length scales. Size effects in plasticity are now well-known. Plastic deformation in small volumes requires higher stresses than are needed for plastic flow of bulk materials. The size dependence of the hardness of metals is described in terms of the geometrically necessary dislocations created in small indentations. This can be related to the continuum theory of strain gradient plasticity. It is equivalent to the effects of fine microstructures on strength, which can also be related to strain gradients. But such accounts break down when the size of the deformation volume begins to approach the spacing of individual dislocations. In this domain the nucleation of dislocations and plasticity under dislocation-starved conditions appears to be more important than strain gradients. In an effort to shed additional light on these topics, uniaxial compression experiments on tiny samples made by focused ion beam machining and integrated circuit fabrication methods are being conducted. These experiments involve by small deformation volumes and minimal strain gradients. They lead to some surprising results that are not yet understood.

9:00 AM

Indentation Size Effects in Face-Centered Cubic Thin Films: From Micro to Nano: Z. Zong¹; J. Lou¹; Y. Huang²; Y. Huang¹; D. Yang³; *W. O. Soboyejo*¹; ¹Princeton University, PMI/MAE Dept., D404 E. Quad., Princeton, NJ 08544 USA; ²University of Illinois, Dept. of Mech. & Industl. Engrg., 140 Mech. Engrg. Bldg., W. Green St., Urbana, IL 61801 USA; ³Hysitron Inc., 5721 W. 73rd St., Minneapolis, MN 55439 USA

This paper presents the effects of a combined experimental and computational study of indentation size effects in metallic produced using LIGA and single crystal growth techniques. These include Ni, Au and Ag single crystals with 001, 110 and 111 orientations and LIGA Ni MEMS structures. Indentation size effects are studied in these systems using a combination of Vickers, Berkovitch and cube cornered indenters. Strong indentation size effects are reported for indents with sizes between the micron- and nano-scales. Sharper indenters are also shown

to result in stronger size effects than blunter indenters. The measured trends in the indentation size effects are predicted using mechanism-based strain gradient plasticity theories. The limitations of strain gradient plasticity theory are also discussed before presenting some initial ideas for the modeling of indentation-induced plasticity at the nano-scale. The implications of the results are discussed for the modeling of contacts in micro- and nano-scale systems and devices.

9:20 AM

The Effect of Length Scale on the Plastic Stability of Nanolayered Metals: Amit Misra¹; *Richard G. Hoagland*¹; Duncan L. Hammon¹; Xinghang Zhang¹; Eric Vanderson¹; J. David Embury¹; John P. Hirth¹; ¹Los Alamos National Laboratory, Matls. Sci. & Tech. Div., MS G755, MST-8, Los Alamos, NM 87544 USA

Sputter deposited nanolayered metallic composites exhibit unusually high hardness when the bilayer periods approach nanometer dimensions. Self-supported Cu-Nb multilayered foils were room temperature rolled to study the deformation and fracture behavior at large plastic strains. At layer thickness of a few tens of nanometers, Cu-Nb multilayers exhibited extraordinary plastic stability undergoing uniform reduction in layer thickness to high levels of plastic strain. However, at layer thickness of a couple nanometers, fracture by shear localization was observed at rolling reductions of only a few percent. These observations are interpreted in terms of the effect of length scale on the dislocation mechanisms of deformation in nanolayered composites. The plastic stability of multilayers with alternating bilayer periods of tens of nanometers and few nanometers will also be discussed. This research is funded by DOE, Office of Science, Office of Basic Energy Sciences.

9:40 AM

Mechanical Performance of ALD Films for Microdevice Coatings: *Neville R. Moody*¹; Tom E. Buchheit²; Brad L. Boyce²; Tom M. Mayer²; Steve George³; ¹Sandia National Laboratories, Livermore, CA 94550 USA; ²Sandia National Laboratories, Albuquerque, NM 87185 USA; ³University of Colorado, Boulder, CO 80309 USA

Strength, friction, and wear are dominant factors in the performance and reliability of materials and devices fabricated using microsystem technologies. Applying coatings and films is one method to enhance device performance and reliability. This study characterizes films using Atomic Layer Deposition (ALD) as it is ideally suited for applying highly conformal, stress-free and well-adhered films necessary for coating microsystem devices. Results focus on the mechanical performance of tungsten and aluminum oxide ALD films. Nanoindentation and nanoscratch tests were used to assess properties and durability of both film systems. These tests showed that the properties varied with film thickness and composition. More importantly, they showed that the tungsten films exhibited pronounced susceptibility to delamination and spallation. These results will be discussed in terms of composition and structure of the ALD films and their impact on potential applications. This work supported by U.S. DOE Contract DE-AC04-94AL85000.

10:00 AM Break

10:20 AM

Using a Combined Modeling-Experiment Approach for Property Determination of Ultra-Thin ALD Films: *John Michael Jungk*¹; Thomas E. Buchheit²; James A. Knapp³; Thomas M. Mayer⁴; Neville R. Moody⁵; Joel W. Hoehn⁶; William W. Gerberich¹; ¹University of Minnesota, Chem. Engrg. & Matls. Sci., 421 Washington Ave., 151 Amundson Hall, Minneapolis, MN 55401 USA; ²Sandia National Laboratories, Microsys. Matls., Trib. & Tech., PO Box 5800, MS 0889, Albuquerque, NM 87185 USA; ³Sandia National Laboratories, Radiation-Solid Interactions, PO Box 5800, MS 1056, Albuquerque, NM 87185 USA; ⁴Sandia National Laboratories, Thin Film, Vacuum & Pkgg., PO Box 5800, MS 0959, Albuquerque, NM 87185 USA; ⁵Sandia National Laboratories, Microsys. & Matls. Mech., PO Box 969, MS 9404, Livermore, CA 94551 USA; ⁶Seagate Technology LLC, 7801 Computer Ave., Minneapolis, MN 55435 USA

Thin-film coatings are often applied to microelectronic or MEMS devices to improve their corrosion resistance and tribological properties. One technique that is ideally suited for producing hard, ultra-thin, conformal coatings is atomic layer deposition (ALD). Through multiple half-reaction cycles, an ALD film may be grown to a specific thickness, usually between 2-50 nm. Typical ALD thicknesses are at the limit of accurate properties determination via nanoindentation-based techniques. This study investigated the mechanical characteris-

tics of ALD films as a function of indentation depth and film thickness through nanoindentation-based methods coupled with ABAQUS finite element modeling to overcome the problem of characterizing these films. Details of this combined approach will be discussed. Hardness and modulus results were insensitive to film deposition at temperatures between 130°C–200°C. These properties increase slightly as the deposition temperature was increased above 200°C. Detailed results from 5 and 20 nm alumina-ALD films will be presented. This work is supported by Seagate Technology LLC through a MINT grant and a part of it was performed at Sandia National Laboratories. Sandia is a multiprogram laboratory operated by Sandia Corporation, a Lockheed Martin Company, for the United States DOE under Contract DE-ACO4-94-AL85000.

10:40 AM

Critical Thickness Theory and the Yield of Thin Beams: Andy Bushby¹; David Dunstan¹; ¹Queen Mary, University of London, Ctr. for Matls. Rsch., Mile End Rd., London E1 4NS UK

Although critical thickness theory was developed largely to understand the stability of strained epitaxial semiconductor layers, it is of much wider applicability to deformation in small volumes. It tells us that geometrically-necessary dislocations generated during yield should not lie within a certain depth h from a free surface. Implications for the observed yield point of a metal beam under a bending moment will be presented. In the size range below a few tens of microns thickness, the yield point is increased markedly. Experimental data on the bending of thin nickel beams will be reported and compared with the theory. Satisfactory agreement is obtained. We conclude that critical thickness theory may be sufficient to explain the observed size effects in the yield point, not only in beam-bending but in other geometries such as torsion and nano-indentation.

11:00 AM

Adhesion of Hard Coatings on Electroplated Metals for Micro-electronic Based Systems: D. F. Bahr¹; M. J. Cordill¹; N. R. Moody²; ¹Washington State University, Mech. & Matls. Engrg., PO Box 642920, Pullman, WA 99164-2920 USA; ²Sandia National Laboratories, PO Box 969, MS 940, Livermore, CA 94550 USA

Thin film mechanical behavior and adhesion properties can be determined using nanoindentation. For electroplated films (such as those used in LIGA based technologies), tungsten films can provide wear resistance and can be used as a seed layer for electroplating. The hardness of an electroplated copper film will be related to the interfacial fracture toughness of the tungsten overlayer. The hardness of the copper is inversely related to the practical work of adhesion of the overlayer, 50% changes in grain size to soften the film produce a more than doubling of the interfacial fracture energy. The copper surface after the removal of the buckled tungsten film shows a deformation induced plastic zone, and has been observed using both AFM and optical microscopy. The plastic zone is larger than the original buckle and exhibits a higher hardness than the bulk film when nanoindentation is carried out on the plastic zone.

11:20 AM

The Nanoindentation Response of Ultrathin Dendrimer-Mediated Soft Metallic Films: Xiao Li¹; Michael Curry¹; Shane C. Street¹; Mark L. Weaver¹; ¹The University of Alabama, Ctr. for Matls. for Info. Tech., Box 35487-0209, Tuscaloosa, AL 35487-0209 USA

Nanoindentation tests were conducted on dendrimer-free and dendrimer-mediated Cu, Al and Ti films deposited on Si substrates to investigate the influence of dendrimer underlayers on their mechanical and tribological properties. Ultrathin (10 nm) metal films were deposited via direct current (DC) magnetron sputtering onto (100) oriented Si substrates. Half of the substrates were coated with a commercial polyamido-amine (PAMAM) dendrimer monolayer, which measured 4.6 nm in thickness. In the dendrimer-containing samples, microstructural analysis revealed the presence of a 2 nm thick mixed nanocomposite region that formed between the dendrimer and the metallic overlayer, presumably during deposition. The results from nanoindentation experiments were analyzed to produce conventional load-displacement (P-d) plots and P-d² plots. Careful analysis revealed significant differences in the elastic and plastic responses of dendrimer-mediated specimens in comparison with dendrimer-free specimens, which could be correlated with the resultant hardness. The presence of a dendrimer interlayer was observed to reduce the amount of pileup around the indenter, as observed in AFM images. The composite hardness of samples was recalculated using the actual contact area, and the hardness of the samples with dendrimer was lower than that free of dendrimer at the low load range. The results for dendrimer-mediated and dendrimer free films are discussed relative to the indentation of bulk materials.

Advanced Materials for Energy Conversion II: Complex Hydrides I

Sponsored by: Light Metals Division, LMD-Reactive Metals Committee

Program Organizers: Dhanesh Chandra, University of Nevada, Metallurgical & Materials Engineering, Reno, NV 89557 USA; Renato G. Bautista, University of Nevada, Department of Chemical and Metal Engineering, Reno, NV 89557-0136 USA; Louis Schlapbach, EMPA Swiss Federal, Laboratory for Materials Testing and Research, Dübendorf CH-8600 Switzerland

Tuesday AM

March 16, 2004

Room: 203A

Location: Charlotte Convention Center

Session Chairs: Joseph R. Wermer, Los Alamos National Laboratory, Tritium Sci. & Engrg. Grp., Los Alamos, NM 87545 USA; Annik Percheron-Guegan, CRNS, Thais 94230 France; Jai-Young Lee, KAIST, Dept. of Matl. Sci. & Engrg., Dae-jeon 305-701 S. Korea

8:30 AM Plenary

The State-of-the-Art of Alanates Development for Hydrogen Storage: Karl J. Gross¹; ¹Hy-Energy Company, 33902 Juliet Cir., Fremont, CA 94555 USA

The discovery that hydrogen can be reversibly absorbed and desorbed from sodium-aluminum-hydrides (the Alanates) has created an entirely new prospect for light-weight hydrogen storage¹. These compounds release hydrogen through a series of decomposition / recombination reactions: $\text{NaAlH}_4 \rightarrow 1/3(\text{Na}_3\text{AlH}_6) + 2/3\text{Al} + \text{H}_2 \rightarrow \text{NaH} + \text{Al} + 3/2\text{H}_2$ Initial work demonstrated that the addition of Ti-containing additives resulted in dramatically improved sorption rates and improved hydrogen storage properties. Since that time a increasing efforts have focused on the development of advanced additives, better synthesis methods, and especially on gaining a fundamental understanding of the role of titanium in the enhanced hydrogen-sorption mechanisms. Ultimately however, the practical hydrogen storage capacity of this system is limited to the 5.6 wt.% hydrogen content of the two-step reactions. This has been the driving force for new studies on the reversibility of other similar complex hydrides. The results of these studies along with their implications on the viability of these materials for on-board hydrogen storage will be presented. ¹Bogdanovic and Schwickardi, J. Alloys and Compounds, Vol. 253 (1997) 1.

9:00 AM Keynote

Metal-Hydrogen Complex Compounds as Hydrogen Storage Materials: Seijirau Suda¹; ¹Kogakuin University, Dept. of Environml. & Chem. Engrg., 2665-1, Nakano-machi, Hachioji-shi, Tokyo 192-0015 Japan

The theoretical hydrogen storage capacity of numerous complex hydrides such as lithiumhydrides, alminohydrides, and borohydrides exceeds 10 mass% in general. Practically, Ti-doped LiAlH_4 releases 5.2 mass% H_2 at room temperature and Ti-doped NaAlH_4 decomposes thermally up to 5 mass% H_2 reversibly below 200°C, and alkaline solutions of NaBH_4 releases 10.8 mass% H_2 through catalytic hydrolysis at ambient temperature and pressure conditions. On the otherhand, conventional metal hydrides have been studied extensively over the past 30 years with the best available hydrogen content as a system of less than 2 wt% at reasonably lower temperature conditions. No further increase of H-capacity can be expected to the series of conventional metal hydrides as hydrogen storage materials. With respect to high capacity hydrogen storage materials, the presentation will be focused on the recent status and future scopes of metal-hydrogen complex compounds and their reversible processes under developing today. An important view scope on the existing state of hydrogen as diatomic (molecular), monatomic (protium), cationic (proton), and anionic (protide) will be discussed. As an illustration of the ionic bonding of hydrogen-rich anion of BH_4^- in sodium borohydride (NaBH_4), an electrochemical application of protide (H^-) will be introduced by DBFC (Direct Borohydride Fuel Cell).

9:25 AM Keynote

Electronic Structure of Hydrogen Storage Materials: Michèle Gupta¹; ¹Université Paris-Sud, EA3547, Bâtiment 415, Sci. des Matériaux, Orsay 91405 France

In this paper, we show that first principles electronic structure studies provide an understanding i) of the properties relevant to hydrogen storage applications such as the maximum hydrogen capacity, the preferred H sites occupancies, the stability of the materials. We

discuss the relative contributions of elastic and electronic effects on the thermodynamic behaviour of the materials. ii) of the modification of the most fundamental properties of the matrix such as metal-insulator transitions, magnetism and superconductivity on hydrogen absorption. To illustrate these points, several examples of intermetallic compounds of AB, AB₂ and AB₅ type (where A and B are transition or rare earth elements), as well as mono and polysubstituted compounds will be discussed. Our results will be analysed in light of available experimental photoemission, structural and thermodynamic data.

9:50 AM Keynote

Lithium-Based Aluminohydrides: From Basic Science to Future Energy Applications: *Vitalij K. Pecharsky*¹; *Viktor P. Balema*¹; *Jerzy Wiench*¹; *Marek Pruski*¹; ¹Iowa State University, Ames Lab. & Dept. of Matls. Sci. & Engrg., 242 Spedding, Ames, IA 5011-3020 USA

Hydrogen can be extracted from aluminohydrides in a number of different ways. The first group of methods involves controlled chemical decomposition with water or ammonia. The second technique - a thermochemical approach - is based on the thermal decomposition of sodium aluminohydride in the presence of transition metal catalysts. A third method involves the production of high purity hydrogen at ambient temperature during mechanical processing of lithium aluminohydride with inorganic transition metal catalysts. The mechanochemical approach combines the following attractive features: i) hydrogen is produced without heating; ii) the hydrogen gas is free of contaminants; iii) the input of mechanical energy can be easily managed, thus enabling easy control over the flow of hydrogen; iv) there is no fundamental barrier to the development of methods for dehydrogenated powder to be recharged with hydrogen, and v) mechanochemistry offers a unique pathway to direct synthesis of aluminohydrides from elements or from readily available precursors.

10:15 AM Break

10:30 AM Keynote

Hydrogen Storage Properties of Li-Based Complex Hydrides: *Shin-ichi Orimo*¹; *Yuko Nakamori*¹; ¹Tohoku University, Inst. for Matls. Rsch., 2-1-1, Katahira, Aoba-ku, Sendai, Miyagi 980-8577 Japan

Fundamental researches on complex hydrides are recently of great importance to develop applicable hydrogen storage materials with higher gravimetric hydrogen densities than those of conventional materials. First, we discuss the correlation between B-H atomistic vibrations in [BH₄]-clusters and melting temperatures of MBH₄ (M = Li, Na, and K), viewpoint from the charge densities at [BH₄]-cluster sites from counter-cations. This investigation provides a way for destabilizing the Li-based complex hydrides. Next, as an example, the hydrogen desorption properties of LiNH₂ and its partial substitution system are preliminarily examined. We found that the starting and ending temperatures for the hydrogen desorption reaction are lowered about 50 K by the partial elemental substitution of Li by Mg, due probably to the increase of the charge densities at [NH₂]-cluster site.

10:55 AM Keynote

Doped Sodium Aluminum Hydride: New Evidence for Bulk Dopant Substitution: *Craig M. Jensen*¹; *Mark Conradi*²; *Tetsu Kiyobayashi*²; *Dalin Sun*¹; *Walter Niemczura*¹; *Steve Brady*³; *Keeley Murphy*¹; *Sandra Eaton*¹; *S. Sairaman Srinivasan*¹; *Job Rijssenbeek*²; *Meredith Kuba*¹; ¹University of Hawaii, Dept. of Chmst., Honolulu, HI USA; ²National Institute for Advanced Industrial Science and Technology, Osaka Japan; ³Washington University, Dept. of Physics, St. Louis, MO USA; ⁴University of Denver, Dept. of Chmst., Denver, CO USA; ⁵GE Global Research Center, Niskayuna, NY USA

In 1997, Bogdanovic and Schwickardi reported that the elimination of hydrogen from solid NaAlH₄ is markedly accelerated and rendered reversible under moderate conditions upon mixing the hydride with a few mole percent of selected transition metal complexes. This was a revolutionary finding in the area of metal hydrides as hydrogen cycling at moderate temperatures was unprecedented for saline hydrides. We subsequently discovered an improved method of doping of NaAlH₄ that greatly promotes the kinetics of the reversible dehydrogenation of the hydride and stabilizes its hydrogen cycling capacity. It now appears that a variation of the doped hydride could possibly be developed as a viable means for the onboard storage of hydrogen. However, no dopant precursors have been found that give a greater kinetic enhancement than those cataloged in Bogdanovic's original 1995 patent. Similarly, only the sodium and mixed sodium, lithium salts of the alanates have been found undergo largely reversible dehydrogenation under moderate conditions upon doping. This lack of progress is surprising in view of the recent "gold rush" flurry of activity that has been direct towards the development of alanates as practi-

cal onboard hydrogen carriers. Clearly, these efforts have been handicapped by the dearth in the understanding of the nature and mechanism of action the dopants. We have therefore initiated efforts to elucidate the fundamental basis of the remarkable hydrogen storage properties of this material. In our early efforts, we obtained X-ray diffraction data that showed significant changes in the lattice parameters of the hydride occur upon doping. On the basis of these results, we proposed a model in which the dopants are substituted into the bulk hydride lattice. In order to verify this model, we have conducted solid state ¹H and ²H nuclear magnetic resonance, electron paramagnetic resonance, and time-of-flight selective ion mass spectroscopic, as well as kinetic studies of the doped hydride. The results of these studies will be presented and discussed in terms of their relationship to our "substitutional" model of the doped hydride.

11:20 AM

Studies of Ti Dopant in Single Crystal Sodium Aluminum Hydrides: *Eric H. Majzoub*¹; *David R. Tallant*²; *Vidvuds Ozolins*³; ¹Sandia National Laboratories, Analytical Matls. Sci. Dept., MS 9403, Livermore, CA 94550 USA; ²Sandia National Laboratories, Matls. Characterization Dept., MS 1411, Albuquerque, NM 87123 USA; ³University of California, Sch. of Engrg. & Applied Sci., Los Angeles, CA 90095-1595 USA

NaAlH₄ is an alanate compound at the forefront of hydrogen storage technology, with a capacity ideally around 5.4 wt.% H₂. The absorption and desorption rates for this material are known to be dramatically affected by the addition of a range of Ti-compounds such as TiCl₃, TiH₂, and nano-cluster Ti. The mechanism of enhanced kinetics in this system is still an open question, depending in part on the location of the Ti. Sample preparation techniques for pragmatic material often result in small coherence lengths making diffraction less effective as a tool due to large peak widths and the presence of multiple phases. In the present study, small single crystals of NaAlH₄ were grown both in pure form and also in the presence of Ti. The crystals were then gently ground for powder diffraction and analyzed for lattice expansion and structure factor changes, which may provide information about the Ti location. In addition, results of Raman spectroscopy from the Ti-exposed and unexposed single crystals will be presented.

11:40 AM

Kinetic Study and Determination of the Enthalpies of Activation of the Dehydrogenation of Titanium and Zirconium Doped NaAlH₄ and Na₃AlH₆: *Tetsu Kiyobayashi*¹; *Sesha S. Srinivasan*²; *Dalin Sun*²; *Nobuhiro Kuriyama*¹; *Craig M. Jensen*²; ¹National Institute of Advanced Industrial Science and Technology, Special Div. for Green Life Tech., 1-8-31 Midorigaoka, Ikeda, Osaka 563-8577 Japan; ²University of Hawaii, Dept. of Chmst., Honolulu, HI 96822 USA

The rates of the dehydrogenation of the sodium alanates, NaAlH₄ and Na₃AlH₆ doped with 2mol% Ti or Zr have been measured over the temperature range 363-423K. NaAlH₄ and Na₃AlH₆ undergo dehydrogenation at equal rates upon direct doping with titanium. However, Na₃AlH₆ arising from the dehydrogenation of Ti doped NaAlH₄ undergoes dehydrogenation at much slower rates. Rate constants were determined from the slopes of the dehydrogenation profiles. The enthalpies of activation for the dehydrogenation reactions were determined to be 100 kJ/mol for both Ti doped NaAlH₄ and Na₃AlH₆ and 135 kJ/mol for both Zr doped NaAlH₄ and Na₃AlH₆. These results suggest that the dehydrogenation reaction pathways are highly sensitive to the nature and distribution of the dopant but not to differences in the Al-H bonding interactions in the complex anions. Furthermore, we conclude that the kinetics are probably influenced by processes such as nucleation and growth, and/or range atomic transport phenomenon.

Advances in Superplasticity and Superplastic Forming: Advances in Superplastic Al-Mg Materials

Sponsored by: Materials Processing and Manufacturing Division, Structural Materials Division, MPMD-Shaping and Forming Committee, SMD-Mechanical Behavior of Materials-(Jt. ASM-MSCTS), SMD-Structural Materials Committee

Program Organizers: Eric M. Taleff, University of Texas, Mechanical Engineering Department, Austin, TX 78712-1063 USA; P. A. Friedman, Ford Motor Company, Dearborn, MI 48124 USA; Amit K. Ghosh, University of Michigan, Department of Materials Science and Engineering, Ann Arbor, MI 48109-2136 USA; P. E. Krajewski, General Motors R&D Center, Rajiv S. Mishra, University of Missouri, Metallurgical Engineering, Rolla, MO 65409-0340 USA; J. G. Schroth, General Motors, R&D Center, Materials and Processes Laboratory, Warren, MI 48090-9055 USA

Tuesday AM Room: 201B
March 16, 2004 Location: Charlotte Convention Center

Session Chairs: Amit K. Ghosh, University of Michigan, Dept. of Matls. Sci. & Engrg., Ann Arbor, MI 48109-2136 USA; James G. Schroth, General Motors, R&D Ctr., Warren, MI 48090-9055 USA

8:30 AM

Application of Superplastic Forming in the Transportation Industry: *Anthony J. Barnes*¹; ¹Superform USA, Inc., 6825 Jurupa Ave., Riverside, CA 92504 USA

Planes, trains and automobiles and a whole lot more?.. Over the past 30 years Superplastic Aluminum Forming has emerged as a unique industry of highly specialized material, equipment and people. Almost from the outset it has found interest and application in the business of transportation, where the combined attributes of aluminum and superplastic forming have offered advantages over other materials and processes. This presentation reviews the state-of-the-art of superplastic aluminum alloys and forming technology and highlights the technoeconomic factors that impact the viability of current and future applications.

8:55 AM

An Overview of Creep Deformation Behaviors in 5000-Series and Al-Mg Alloys: *Eric M. Taleff*¹; ¹University of Texas, Dept. of Mech. Engrg., 1 Univ. Sta., C2200, Austin, TX 78712-0292 USA

The 5000-series Al alloys have wide practical utility because they exhibit a number of desirable properties and behaviors, including reasonable strength, good resistance to corrosion and stress-corrosion cracking, and weldability. Of more recent interest is the rather high ductilities which 5000-series alloys can achieve at elevated temperatures and low strain rates. Under such conditions, many 5000-series alloys can achieve enhanced ductilities of 100 to over 300% as a result of deformation by solute-drag creep. Because solute-drag creep does not require a fine grain size, enhanced ductilities are achieved from standard commercial grades without additional processing for grain refinement. Experiments using Al-Mg alloys with ternary additions reveal the relationship between deformation behaviors of the much-studied Al-Mg binary alloys and their more complex commercial kin. Superplastic AA5083 alloys and their variants achieve superplasticity through significant grain refinement during sheet rolling and an increase in the content of intermetallic particles, which help retain a fine grain size by pinning grain boundaries. Despite the clearly demonstrated superplastic behavior of AA5083 materials, as temperature decreases and strain rate increases, they revert to the deformation behavior of less exotic 5000-series materials.

9:15 AM

Texture Development and Dynamic Recrystallization in AA5083 During Superplastic Forming at Various Strain Rates: *Paul E. Krajewski*¹; *Sumit Agarwal*²; *Clyde L. Briant*²; ¹General Motors, R&D Ctr., 30500 Mound Rd., MC 480-106-212, Warren, MI 48090 USA; ²Brown University, Div. of Engrg., Box D, Providence, RI 02912 USA

Texture development in AA5083 during superplastic forming has been studied at strain rates varying from 0.0005/sec to 0.3/sec. As shown previously in the literature, a random texture is maintained at slower strain rates (grain boundary sliding), while at the higher strain rates, a fiber texture develops (dislocation creep). At the higher strain rates (>0.03/sec), dynamic recrystallization is observed in the necked region of the sample prior to failure. This results in a dramatic transition from very fine grains (~10 nm) to large grains (>100 nm) at a critical strain. At strains above this critical level the grain size de-

creases. The effect temperature, strain rate, and constituent particle distribution on the extent and character of the recrystallized region is described. The results are explained in terms of critical strain recrystallization phenomena.

9:35 AM

Bulge Testing of Superplastic 5083 Aluminum Sheet: *John R. Bradley*¹; ¹General Motors, R&D Ctr., Matls. & Proc. Lab., MC 480-106-212, Warren, MI 48090-9055 USA

High temperature pneumatic bulge testing has been established as an effective means of assessing the superplastic ductility of 5083 aluminum sheet for production applications. The constant-pressure bulge test provides a faster, simpler and less expensive method for screening the quality of incoming material than conventional tensile testing. A correlation was demonstrated between total superplastic tensile elongation and bulge test dome height for 5083 aluminum sheet based on an evaluation of more than twenty five candidate materials. The ability of the bulge test to discriminate among high and low quality production alloys was demonstrated. The test was also shown to be useful in the evaluation of experimental alloys. A tendency for materials from different suppliers to deform at significantly different strain rates under the same conditions of forming temperature and pressure was investigated.

9:55 AM Break

10:10 AM

Deformation, Cavity Formation and Failure in Superplastic AA5083: *Keiichiro Oh-ishi*¹; *John F. Boydon*¹; *Terry R. McNelley*¹; ¹Naval Postgraduate School, Dept. of Mech. Engrg., 700 Dyer Rd., Monterey, CA 93943-5146 USA

The ductility of aluminum alloy AA5083 during superplastic forming is limited by cavity formation and linkage as well as by necking during elevated temperature deformation. Orientation Imaging Microscopy (OIM) methods have been used to assess the role of grain boundary disorientation in the processes of grain boundary sliding and separation that lead to the formation and growth of cavities. The contributions of dispersed intermetallic Al₆Mn and Al₃Fe particles have also been examined. Annealing of cold-rolled AA5083 at 450°C results in the formation of equiaxed grains 7 - 8 µm in size by particle-stimulated nucleation of recrystallization as well as a near-random microtexture and random grain-to-grain disorientation distributions. Cavities form in conjunction with sliding and separation of boundaries having disorientations = 10° during deformation under grain boundary sliding controlled conditions. Cavity formation appears to begin at dispersed intermetallic particles although many smaller cavities in the cavity size distribution are not associated with particles. Data for cavity formation during biaxial tension and plane strain deformation conditions will be compared to data for cavity formation under uniaxial tension.

10:35 AM

Superplastic Failure Mechanisms and Ductility of AA5083: *Mary-Anne Kulas*²; *W. Paul Green*¹; *Ellen C. Pettengill*¹; *Paul E. Krajewski*¹; *Eric M. Taleff*¹; ¹University of Texas, Mech. Engrg., 1 Univ. Sta., C2200, Austin, TX 78712-0292 USA; ²University of Texas, Matls. Sci. & Engrg., 1 Univ. Sta., C2201, Austin, TX 78712-0292 USA; ³General Motors Corp., R&D Ctr., 30500 Mound Rd., Warren, MI 48090-9056 USA

The aluminum alloy AA5083 is the most used aluminum material for superplastic forming operations. Advantages of AA5083, beyond its superplastic response, include moderate strength, good weldability, and corrosion resistance. Ductility of AA5083 during superplastic forming is limited by one of two failure mechanisms, necking and cavitation. Quantitative measurements of the contributions to failure from each mechanism are made using the newly developed Q parameter. This parameter provides insight into the deformation mechanisms active prior to failure in AA5083. AA5083 typically contains intermetallic particles of Al₆Mn and Al₃Fe, which can influence superplastic ductility. Particle size distributions are measured for several AA5083 materials and related to their ductilities and failure mechanisms.

10:55 AM

Microstructural Characterization of SPF AA5083 Aluminum Sheet: *SooHo Kim*¹; *Michael P. Balogh*²; *Richard A. Waldo*²; ¹General Motors, R&D Ctr., Matls. & Proc. Lab., MC 480-106-212, 30500 Mound Rd., Warren, MI 48090-9055 USA; ²General Motors R&D Center, Chem. & Environml. Scis. Lab., MC 480-106-320, 30500 Mound Rd., Warren, MI 48090-9055 USA

Two superplastic forming (SPF) AA5083 aluminum sheets, exhibiting different elevated temperature elongations (335% and 254%), were selected for detailed microstructural characterization. Neither X-

ray diffraction (XRD) nor metallography measurements could account for the differences in material behavior. Electron probe microanalysis (EPMA) and transmission electron microscopy (TEM) studies found differences in the composition and morphology of the constituent particles. The coarse constituent particles ($>2\mu\text{m}$) in the sample with the inferior elongation contain a lower concentration of silicon and are more angular with more internal cracks, which may create sources of cavitation during SPF. The fine dispersoid particles ($<2\mu\text{m}$) in the sample with the superior elongation are smaller, have a higher population density and are more uniformly distributed. These dispersoid particles are expected to effectively pin the grain-boundaries, thus limiting dynamic grain growth, producing better formability.

11:15 AM

Post-Form Properties of Superplastically Formed 5083 Aluminum Sheet: John R. Bradley¹; John E. Carsley¹; ¹General Motors, R&D Ctr., Matls. & Proc. Lab., MC 480-106-212, Warren, MI 48090-9055 USA

The tensile and fatigue behavior of two 5083 aluminum alloys following various degrees of superplastic deformation have been examined in order to correlate post-formed mechanical properties with initial microstructure and cavitation. The unformed materials were characterized in terms of both constituent particle size distribution and recrystallized grain size. A reduction in mechanical properties of both alloys with increasing superplastic strain was quantified. An abrupt increase in cavitation observed in both alloys at true thickness strains greater than about -0.6 was consistent with the threshold strain for rapid cavitation reported earlier. Marked decreases in yield strength, ultimate tensile strength, uniform elongation, and fatigue performance were correlated with the extent of cavitation damage as a function of superplastic thinning. Poorer performance of one alloy compared to the other was shown to be the result of accelerated cavitation, which was attributed to a significantly larger recrystallized grain size ($9.5\mu\text{m}$ vs. $6.5\mu\text{m}$).

11:35 AM

Rolling Process Optimization for Superplastic 5083 Aluminum Sheet: Ravi Verma¹; ¹General Motors, R&D, Matls. & Proc. Lab., 30500 Mound Rd., Warren, MI 48090 USA

The effect of sheet rolling process on superplasticity of 5083 aluminum alloy sheet has been investigated. A synergistic effect between hot rolling and cold rolling processes has been observed which helps optimize an efficient sheet rolling practice. A "skewed" cold rolling process, in which successive reduction levels are tailored to maximize the alloy's hardening response to cold work, was developed. The "skewed" cold rolling process further helps improve superplastic response of rolled 5083 sheet. Superplastic tensile elongations greater than 400% have been obtained.

Alumina and Bauxite: Bayer Plant Operations: White Side

Sponsored by: Light Metals Division, LMD-Aluminum Committee
Program Organizers: Travis Galloway, Century Aluminum, Hawesville, KY 42348 USA; David Kirkpatrick, Kaiser Aluminum & Chemical Group, Gramercy, LA 70052-3370 USA; Alton T. Tabereaux, Alcoa Inc., Process Technology, Muscle Shoals, AL 35661 USA

Tuesday AM Room: 218A
March 16, 2004 Location: Charlotte Convention Center

Session Chair: Milind V. Chaubal, Sherwin Alumina Company, Corpus Christi, TX 78469 USA

8:30 AM Cancelled

Effect of Total Soda on the Caustic Molar Ratio of the Agglomeration Zone in the Precipitation Circuit

8:55 AM

Kinetics of Crystallization in Sodium Aluminate Liquors: Qun Zhao¹; Yanli Xie¹; Shiwen Bi¹; Zijian Lu²; Yihong Yang¹; Bo Li¹; ¹Northeastern University, Sch. of Metall. & Matl., Shenyang, Liaoning 110004 China; ²Henan Branch of CHALCO, Dept. of Tech., Changqian Rd., Shangjie Dist., Zhengzhou 450041 China

The kinetics of crystallization of alumina trihydroxide from sodium aluminate liquors under industrial conditions was studied in a laboratory batch isothermal precipitator. The kinetic equation was deduced from the mechanism of crystallization. The parameters were

obtained by fitting experimental data to the equations. The kinetic equation of precipitation at low temperature is $dC/dt=2.59[\exp(-19.30\times 10^3/RT)](C-C_8)^2$, which is controlled by diffusion, while the equation at high temperature is $dC/dt=1.117\times 10^{-8}[\exp(-73.44\times 10^3/RT)](C-C_8)^2$, which is controlled by interfacial reaction. Furthermore, the formula for calculating the optimum temperature was derived, and the values from the experiment were calculated. These are 314.42°K (41.27°C) for low temperature and 346.24°K (73.09°C) for high temperature, respectively.

9:20 AM

The Application of Additives in the Precipitation of Bayer Sodium Aluminate Liquors: Zijian Lu¹; Qun Zhao²; Yanli Xie³; Shiwen Bi³; Yihong Yang³; ¹Henan Branch of CHALCO, Changqian Rd., Shangjie Dist., Zhengzhou, Henan 450041 China; ²Zhengzhou Light Metal Research Institute, No. 76 Jiyuan Rd., Shangjie Dist., Zhengzhou, Henan 450041 China; ³Northeastern University, Nonferrous Metall., No. 11, Ln. 3, Wenhua Rd., Heping Dist., Shenyang, Liaoning 110004 China

Additives used in the precipitation of sodium aluminate liquors can not only increase precipitation ratio and achieve coarser product but are also simple to operate and easy to control. The use of additives in the precipitation of sodium aluminate liquors is introduced, and its mechanism is analyzed as well in this paper.

9:45 AM Break

9:55 AM

Attrition Behaviour of Laboratory Calcined Alumina from Various Hydrates and its Influence on SG Alumina Quality and Calcination Design: Hans W. Schmidt¹; Alpaydin Saatci¹; Werner Stockhausen¹; Michael Stroeder¹; Peter Sturm¹; ¹Lurgi Metallurgie GmbH, Ludwig-Erhard-Strasse 21, D-61440 Oberursel Germany

Particle breakage and attrition in stationary calciners have been investigated since the introduction of this technology to the industry. Further to Outokumpu-Lurgi's experience of more than 40 calciners operating in the alumina industry with different hydrates new research work was undertaken to further improve the understanding of this important issue for smelter grade alumina quality. The attrition behaviour of various laboratory calcined aluminum hydrates was investigated in a special modified Forsythe-Hertwig apparatus at different temperatures. This modified test unit, which simulates certain sections of stationary calcination processes, is described. Various tests were carried out with different hydrates at a wide range of temperatures and other parameters. The fraction below $45\mu\text{m}$ was analysed before and after the attrition tests. If the fraction difference is chosen as a measure for attrition, it can be shown that there is a clear relationship between attrition and mechanical impulse of the air jet in the orifice of the test unit. The temperature during the attrition test does not seem to have a significant influence on attrition. An approach to specify the hydrate quality regarding the attrition behaviour is discussed. Conclusions from the results for the design of large calciners are described.

10:20 AM

A New Method for Smelting Grade Alumina (SGA) Characterization: Jean-Michel Lamérant¹; Sonia Favet¹; Valérie Martinet¹; Laurent Ferres¹; ¹Aluminium Pechiney, Direction de la Recherche et du Développement, BP. 54, Gardanne 13541 France

Pot operation efficiency in aluminium smelters is highly related to alumina quality. The properties currently measured (Specific Surface Area, Particle Size Distribution, Alpha Alumina content, Attrition Index, LOI, Chemical Analysis) are all relevant, but inadequate, to fully describe alumina behaviour in the pots, especially dissolution rate. The method under investigation analyses, by optical microscopy, SGA's diluted in a liquid having a Refractive Index of 1.73. The coloured pictures of samples reveal very significant differences between SGA's from different alumina refineries. As an example, it is possible to differentiate alumina from a fluid bed calciner and alumina from a rotary kiln, or to assess alpha alumina content and homogeneity of calcination. Quantification of differences is possible using Image Analysis software. Matching information from the new method with smelter data opens promising avenues. Potential for improved qualification of SGA's is under investigation.

10:45 AM

New Approaches to Phase Analysis of Smelter Grade Aluminas: Toshifumi Ashida²; James B. Metson¹; Margaret M. Hyland¹; ¹University of Auckland, Light Metals Rsch. Ctr., PB 92019, Auckland New Zealand; ²Kinki University, Dept. of Biotech. & Chmst., Sch. of Engrg. Japan

Specifications of smelter grade aluminas (SGA) represent a compromise between properties which are critical in performance and those which can be readily measured, but which provide only indirect

information on the quality and consistency of the alumina. For example, properties such as LOI (20-300°C) and LOI (300-1000), result from the relationship between the phase composition and the surface area required to meet the smelter specifications. Central to this is the problem that the phases which dominate SGA are largely poorly crystalline transition aluminas, and depend on calcining technology, but thus far a detailed phase analysis of SGA has proved intractable. Rietveld refinement of standard X-ray powder diffraction data and neutron diffraction studies have allowed us to explore a new model for the transition aluminas especially the gamma phase, optimized for SGA. In this model the structure of gamma alumina was assumed to consist of fcc lattice of oxygen, with 30% Al in the 4-fold site of a perfect spinel structure (filling 75% of the 4-fold sites), 45% Al in the 6-fold site of a perfect spinel structure (filling 56% of the 6-fold sites), 10% Al in a 4-fold interstitial site, 15% Al in 6-fold interstitial site, and 20% hydrogen substituted for Al. Thus the Al₂O₃ can be more accurately formulated as H₂(Al_{3.0})[Al_{4.5}]{Al_{1.0}, Al_{1.5}}O₁₆.

11:10 AM

Anti-Segregation of Alumina: Michael F. Barron¹; *Andreas Wolf*; ¹Claudius Peters (Americas) Inc., 4141 Blue Lake Cir., Dallas, TX 75244 USA

In the process cycle prior to the actual production of an ingot of aluminium, that key ingredient goes through many transition points. Following its initial manufacture, alumina powder is conveyed, bucket elevated, blown, loaded, sucked or screwed out, re-conveyed, stored, retrieved, blown again and finally distributed over a bank of cells at the smelter. These many transition points usually involve at least two countries, a minimum of two ports (one loading the other for unloading) hundreds or thousands of meters of various types of conveyors and elevating devices and a couple or more of storage (silos). Each transition can have an effect; good or bad on the quality of the alumina delivered to the production cells. This paper covers how Claudius Peters Technologies GMBH has applied its extensive knowledge on silo storage and pneumatic conveying to ensure that aluminium producers in all five continents get a uniform, non-segregated alumina feed.

Aluminum Can Recycling: Session I

Sponsored by: Extraction & Processing Division, Light Metals Division, LMD/EPD-Recycling Committee

Program Organizers: Donald L. Stewart, Jr., Alcoa Inc., Alcoa Technical Center, Alcoa Center, PA 15069-0001 USA; W. Bryan Stevenson, Alcoa Inc., Alcoa, TN 37701-3141 USA

Tuesday AM Room: 217D
March 16, 2004 Location: Charlotte Convention Center

Session Chairs: W. Bryan Stevenson, Alcoa Inc., Alcoa, TN 37701-3141 USA; Donald L. Stewart, Jr., Alcoa Inc., Alcoa Tech. Ctr., Alcoa Ctr., PA 15069 USA

8:30 AM Introduction

8:35 AM

Aluminum Can Recycling: That Was Then; This Is Now: *Craig Coverl*¹; ¹Alcoa Inc., Mkt. Dvlp. & Recycling, Alcoa Rigid Pkgg., 2300 N. Wright Rd., Alcoa, TN 37701 USA

Aluminum beverage can recycling began as a promotional vehicle to sell beer and soft drinks in aluminum cans to American consumers and has turned into a valuable source of metal to make more can sheet. Since its inception over 35 years ago, aluminum can recycling has captured the fancies of consumers across the U.S...and the world. Lately, there has been a decline in the aluminum beverage can recycling rate. What's in store for this American institution?

9:00 AM

A Model for Thermal Decoating of Aluminium Scrap: *Anne Kvithyld*¹; Jakub Kaczorowski²; Thorvald Abel Engh¹; ¹Norwegian University of Science and Technology, Dept. of Matls. Tech., Trondheim N-7491 Norway; ²Warsaw University of Technology, Fac. of Matls. Sci. & Engrg., Woloska 141, Warsaw, 02-507 Poland

A major problem in the recycling of aluminium is the presence of contaminants in the purchased scrap. This article attempts to give a fundamental description of thermal removal of lacquer in an industrial decoating unit. The material was aluminium sheet (420 µm in thickness) coil-coated with 5µm thick polyester. The coating was decomposed, the evolved gases were measured, the residues left on the alu-

minium sheet were characterised and other microscopic investigations performed. The degradation was also monitored visually using a hot stage light microscope. Previous work has shown that the mass loss curves show three (or two) peaks in oxidizing (or inert) atmospheres. The microscopic examinations here support that each peak is associated with a stage in the degradation process. It is also revealed that the coating has "weak points". The investigations resulted to two slightly different models for the degradation of the coating.

9:25 AM

Mathematical Modelling for Recycling Furnaces Optimisation: *Vincent Goutière*¹; Gaston Riverin¹; Bruno Gariepy¹; ¹Alcan International, ARDC- Ed 110 - 1955 Bd Mellon, Jonquiere G7S 4K8, Quebec Canada

Improvements achieved in the numerical modelling allowed obtaining new capacities in order to analyse the industrial remelt processes and find options aiming at decreasing the melting time or improving the thermal efficiency. Optimisation of the combustion furnaces becomes possible by changing the design, searching the best locations for the burners and their orientations, as well as choosing adequate types of burners. Following is presented the numerical methodology developed at Alcan International to improve the top charge furnaces. A two-step model is used: the first is dedicated to modelling the burner and its nearby region, and the second is to model the combustion chamber. After describing this model, different cases of improvements are shown.

9:50 AM Break

10:05 AM

The Impact of Hazardous Contaminants in Aluminum Used Beverage Containers During Processing: *D. L. Stewart*¹; W. B. Stevenson²; E. S. Martin³; ¹Alcoa Inc., 100 Technical Dr., Alcoa Ctr., PA 15069 USA; ²Alcoa Inc., 2300 N. Wright Rd., N290, Alcoa, TN 37701-3141 USA; ³Consultant, New Kensington, PA 15068 USA

Over 50 billion aluminum beverage cans (UBCs), approximately 700,000 metric tons, are recycled annually in the United States. The UBCs are collected at a large number of locations, where they are often baled or briquetted for convenient shipment to the ultimate processing location. These cans are recycled back into beverage can sheet and subsequent beverage containers in as little as 60 days. In a typical UBC recycling process, the baled material is subjected to sequential operations of shredding, magnetic material removal, delacquering to remove organic coatings, and melting. Potentially hazardous contaminants, such as aerosol cans containing flammable organics and live ammunition, have been found in the baled UBCs. The amount of energy, which will potentially be released by either of the hazardous contaminants during UBC processing, has been calculated and will be discussed, as well as steps to reduce the potential impact of the contaminants.

10:30 AM

Some of the Factors Affecting Dross Formation in Aluminum 5182 RSI: *Qingyou Han*¹; John Zeh²; Ray D. Peterson³; ¹Oak Ridge National Laboratory, Metals & Ceram. Div., One Bethel Valley Rd., PO Box 2008, Oak Ridge, TN 37831-6083 USA; ²Logan Aluminum Inc., US Hwy. 431 N., PO Box 3000, Russellville, KY 42276 USA; ³IMCO Recycling, Inc., 397 Black Hollow Rd., Rockwood, TN 37854 USA

Aluminum 5182 remelt secondary ingot (RSI) is prone to dross formation during the remelting processes. Recently we have found that dross formation in the center region of the RSI can be as high as 80% and is related to the cracking and porosity defect formation in that region. This article addresses dross formation in aluminum 5182 RSI under various processing conditions, such as the melting methods of the scrap materials, the composition of the alloy, the size of and the cooling rate in the RSI, and the casting temperature. Relationship between dross formation and the processing parameters are investigated and the mechanism of dross formation is discussed. It is suggested that the dross is formed during the solidification stage of the RSI processing. Dross formation increases with increasing magnesium concentration and decreasing cooling rate. Flux has little influence on dross formation.

Aluminum Reduction Technology: Pot Control

Sponsored by: Light Metals Division, LMD-Aluminum Committee
Program Organizers: Tom Alcorn, Noranda Aluminum Inc., New Madrid, MO 63869 USA; Jay Bruggeman, Alcoa Inc., Alcoa Center, PA 15069 USA; Alton T. Tabereaux, Alcoa Inc., Process Technology, Muscle Shoals, AL 35661 USA

Tuesday AM
March 16, 2004

Room: 213D
Location: Charlotte Convention Center

Session Chair: Ric Love, Century Aluminum Corporation, Ravenswood, WV 26164-0098 USA

8:30 AM

Metal Pad Temperatures in Aluminium Smelting Cells: *Daniel Simon Whitfield¹; Maria Skyllas-Kazacos¹; Barry Welch¹; Peter White²;* ¹University of New South Wales, Ctr. for Electrochem. & Minerals Proc., Sydney, NSW 2052 Australia; ²Heraeus Electro-Nite Intl. NV Belgium

Meaningful measurement of cell temperature is made difficult by a number of factors. Disturbances and errors are also introduced by the breaking and hole preparation for intermittent measurement, as well as errors associated with the depth of immersion. With the majority of the heat generated in a reduction cell originating in the electrolyte, with little heat generation in the metal pad, the thermal behaviour of the metal pad temperature is expected to be dependent on the electrolyte temperature. The large mass of liquid metal usually used in smelting cells gives a greater thermal inertia for the metal pad and it is partially isolated, or dampened, from the impact of frequent additions of cold alumina. Therefore it is expected that this will partially mitigate variation that occurs in the electrolyte when temperatures are measured in the metal pad. Investigation of the thermal behaviour of the metal pad and its relationship with the electrolyte indicated that the typical temperature difference between the two is 3-6°C. The metal pad temperature also showed a dampened response to variation in the electrolyte temperature. Measurement of the metal pad temperature may potentially allow inferential measurement and monitoring of the cell thermal state.

8:55 AM

Using Fume Duct Temperature for Minimizing Open Holes in Pot Cover: *Neal R. Dando¹;* ¹Alcoa Technology, 100 Techl. Dr., Alcoa Ctr., PA 15069 USA

The presence of open holes in pot ore cover has been identified as a major source of elevated fluoride emissions at aluminum smelters. Several commercially available technologies exist for providing real time monitoring of vapor-phase fluoride, however capital cost and maintenance issues preclude their implementation on an every-pot basis. This presentation will discuss the efficacy of monitoring individual pot exhaust duct temperatures as a means of providing low-cost, real-time indicators of pot crust cover integrity. This methodology also allows for in-plant best-practice benchmarking and enabling systematic documentation of process-effect improvements in pot-tending practices.

9:20 AM

Aspects of Alumina Control in Aluminium Reduction Cells: *Daniel Simon Whitfield¹; Maria Skyllas-Kazacos¹; Barry Welch¹; Fiona Stevens McFadden²;* ¹University of New South Wales, Ctr. for Electrochem. & Minerals Proc., Sydney, NSW 2052 Australia; ²Comalco Research and Technology, Thomastown, Victoria Australia

For all modern point fed aluminium-smelting cells, the alumina concentration is controlled within a band. This is achieved through inference indirectly by the general relationship between alumina concentration, inter-electrode distance and cell resistance. The standard strategy is to cycle the alumina feed rates, varying cell resistance and allowing inferential control of the alumina concentration. In this investigation, a magnetically compensated point fed cell, with four point feeders, was subjected to a typical feed cycle to test the response and quality of control. The variables measured in the response included the alumina concentration and its rate of change, temperature and pseudo-resistance. As a result of this investigation, several phenomena were observed that concur with the hypothesis of an alumina layer at the bath-metal interface. Significant differences between the theoretical and measured pseudo-resistance were observed during the underfed period, resulting in a flattening of the resistance curve. The net rate of alumina depletion was observed to correlate with temperature, possibly due to secondary feeding from a hypothesised alumina layer. It is

also hypothesised that the pseudo-resistance may have an added temperature dependence due to the alumina layer.

9:45 AM

Optimal Control System of Alumina Concentration in the Process of Aluminium Reduction when the Measuring Information is Incomplete: *Robert G. Lokshin¹; Mishel J. Fiterman¹;* ¹JSC VAMI, Sredny Str. 86, Saint-Petersburg Russia

Secondary losses of aluminium during its electrolytic production depend on anode-cathode distance, temperature and alumina concentration in the bath. When the anode-cathode distance and temperature are preset the minimum of secondary losses correspond to the minimum voltage of the pot. Therefore, the task of alumina concentration control refers to the class of extreme control tasks and couldn't be solved in analytical form. To get a solution the special conversion of measuring equations is applied, which allowed the reduction of the task to the classical problem of the control having a full measuring information. Algorithms of optimal concentration estimation and optimal control of estimation obtained take care of this problem. Respective search system of alumina concentration control has an optimal combination of searching and controlling actions. The structure and computational algorithms of optimal control system are proposed and its numeral simulation under conditions of real perturbations is carried out. The comparison of optimal control system with standard industrial systems shows that in the industrial systems the correlation of searching and controlling actions is far from being optimally arranged.

10:10 AM Break

10:20 AM

Criterial Parameters in Evaluation of Cell's Potentialities for Computerized Control: *Alexander I. Berezin¹; Peter V. Poliakov²;* *Oleg O. Rodnov¹; Pavel D. Stont¹; Tatyana V. Piskajova¹;* ¹RUSAL Engineering & Technology Center, Pogranichnikov st. 37, Krasnoyarsk 660111 Russia; ²STC "Light Metals", Vavilova st. 60, Krasnoyarsk 660025 Russia; ³Mayak PKF Ltd., Bograda st. 108, Krasnoyarsk 660021 Russia

In modern conditions to achieve high performance a cell has to operate at the limit of its functional potentials. The limit range of cell operation is determined by functional potentialities of its individual subsystems restricted by special process conditions. Criteria specifying performance of functions by major cell subsystems have been developed to evaluate cell conditions. The criteria employ controlled process parameters available in the plant process database. The criteria produced have been verified on a virtual model of a cell.

10:45 AM

Development of Aluminium Reduction Process Supervisory Control System: *Vladimir Victorovich Yurkov¹;* *Victor Cristianovich Mann¹;* *Konstantin Pheodorovich Nikandrov¹;* *Oleg Alexandrovich Trebuh¹;* ¹Engineering-Technological Centre Ltd, RUSAL, Automation Div., 37, Pogranichnikov St., Krasnoyarsk 660111 Russia

Simple algorithms for cell control have significant limitations when process behaviours are highly variable. At this location, the source of these variations are changes in raw materials, seasonal ambient temperature differences and changes in electrical power input. An effective process control system must adequately compensate for these effects. At this plant, a Computerized Process Control System, which controls cell voltage, alumina feed and fluoride additions has been in full operation for some time and has operated as designed. Work has now commenced to integrate compensation for changes in thermal condition and bath composition and the interactions of these factors. This objective will be achieved by means of supervisory control of the alumina feeding algorithm and the normalized voltage set-point as well as through the aluminium fluoride daily dosing calculation. To this end an analytical dynamic model was developed, based on physical-chemical mechanisms and laws of mass and energy conservation. The core of this work is focused on alumina concentration forecasting by means of an alumina solution mathematical model, which is a part of the full reduction dynamics model. The dual-mode control system based on this model sends control actions to the middle-level system and, additionally, "learns" through adapting model coefficients. Alumina concentration forecasting and model calibration is performed in real time, by comparing the voltage of the real cell and that of the math model where this voltage is determined according to calculated alumina concentration.

Automotive Alloys 2004: Session III

Sponsored by: Light Metals Division, LMD-Aluminum Committee
Program Organizer: Subodh K. Das, Secat, Inc., Coldstream Research Campus, Lexington, KY 40511 USA

Tuesday AM Room: 210A
 March 16, 2004 Location: Charlotte Convention Center

Session Chair: Subodh K. Das, Secat Inc., Coldstream Rsch. Campus, Lexington, KY 40511 USA

8:30 AM

Development of Continuous Cast Aluminum Alloy Sheets for Automotive Applications: *Zhong Li*¹; Steve Kirkland²; Paul Platek²; ¹Commonwealth Aluminum, 1505 Bull Lea Rd., Lexington, KY 40511 USA; ²Commonwealth Aluminum, 7319 Newport Rd., SE, Uhrichsville, OH 44683 USA

Commonwealth Aluminum has been developing continuous cast 5xxx series aluminum alloy sheet for automotive applications over the last several years. Continuous cast (CC) technology has the following advantages over conventional direct chill (DC) technology: (1) low capital investment; (2) high productivity; (3) low conversion cost and (4) short lead-time. The development work started by participating in the United States Automotive Materials Partnership (USAMP) CRADA. This research program ended in 1999 with auto parts (such as GM EV1 dash panel, Ford rear floor panel, etc) successfully stamped from CC sheet. Since then, Commonwealth Aluminum continued to carry on the development work with both domestic and foreign automobile manufacturers. The results showed that the continuous cast (twin belt casting technology) produced aluminum sheet can meet both the Aluminum Association and automobile manufacturer's mechanical property specifications. In addition to the mechanical property requirements, CC 5754 alloy sheet has met all the automotive requirements, such as, paint coating, spot welding, corrosion testing, phosphatability, adhesive compatibility, among others. So far, more than eighteen vehicle internal structural and heat shield parts have been successfully stamped from CC material manufactured by Commonwealth Aluminum. Additionally, some of these parts are now being commercially used by the automotive industry. Commonwealth Aluminum, Newport Rolling Mill, whose management systems are registered to QS9000: 1998 and ISO14001: 1996, has been approved as a raw material supplier for Ford Motor Company and General Motors Corporation. With the positive results of CC 5xxx aluminum alloy sheet, more automobile manufacturers are working with Commonwealth Aluminum in evaluating the benefits of using CC aluminum sheet in their automotive applications.

9:00 AM

Friction Stir Welded Tailor Welded Blanks for Automotive Applications: *Glenn J. Grant*¹; Richard W. Davies¹; Douglas J. Waldron²; ¹Pacific Northwest National Laboratory, Energy Matls., 902 Battelle Blvd. K2-03, Richland, WA 99352 USA; ²Advanced Joining Technologies, Inc., (A New Boeing Venture), 5222 Rancho Rd., Huntington Beach, CA 926417 USA

Tailor Welded Blanks (TWBs) are hybrid sheet products composed of either different materials or different thickness sheets that are joined together, then subjected to a forming or stamping operation to create a formed assembly. The strategy is employed generally to save weight and material costs in the formed assembly by placing higher strength or thicker sections only where needed. The forming or stamping process requires the joint to be severely deformed along with the parent sheets. Aluminum TWBs for automotive applications are particularly problematic because of the low formability of aluminum weld metal. This low formability is due to the fusion weld microstructure and the difficulty in making defect free aluminum fusion welds at the speeds appropriate for automotive applications. Friction Stir Joining is a process recently applied to Aluminum TWBs that has the potential to produce a higher quality weld at equivalent joining speeds to fusion welding. The current study presents data on the mechanical properties, formability, and FSJ weld process parameter development for Friction Stir Joined, Aluminum Tailor Welded Blanks. Data from microscopy, miniature tensile testing, and limited dome height formability tests will be presented on TWB joints in similar and dissimilar combinations of the following alloy types: 5182, 5052, and 6111.

9:30 AM

Characterization of Springback Stresses in Deep Drawn Cups for Automotive Alloys: *Thomas Gnäupel-Herold*¹; Timothy J.

Foecke²; Henry J. Prask¹; ¹National Institute of Standards and Technology, Matls. Sci. & Engrg. Lab., 100 Bureau Dr., Stop 8562, Gaithersburg, MD 20899 USA; ²National Institute of Standards and Technology, Metall. Div., 100 Bureau Dr, Stop 8553, Gaithersburg, MD 20899-8553 USA

Springback is the elastic shape change of a sheet metal part after forming and removal from the die. The need for a more accurate prediction of elastic springback in sheet metal forming is accompanied by a need for a standardizable test for measuring and characterizing springback. A test that has received considerable attention consists of a ring sample taken from the sidewall of a flat bottom, deep drawn cup. We have performed high resolution through-thickness stress measurements in the intact and split ring for different materials, wall thicknesses, and axial and circumferential locations. The results provide a comprehensive picture of springback stresses in deep drawn cups.

9:55 AM

In-Situ Synthesis of AlN Reinforced Magnesium Alloy Composites by Gas Bubbling Method: *Sumit Ashok Tyagi*¹; Qingjun Zheng¹; Ramana G. Reddy¹; ¹University of Alabama, Dept. of Metallurg. & Matl. Engrg., A129 Beville Bldg., 126 7th Ave., Tuscaloosa, AL 35487 USA

Magnesium Metal Matrix Composites (Mg-MMCs) have been gaining attention in recent years as a challenging choice for automotive and aerospace applications. In-situ formation of AlN-reinforced Mg alloy composites by gas-bubbling method was investigated in this paper. Feasibility and conditions for formation of the composites were analyzed based on Gibb's energy minimization method. Quasi-regular solution model was used for the activities of Mg and Al to calculate the species distribution in the melts. The calculated results showed that formation of undesirable phase Mg₃N₂ in the Mg melts can be prevented if the partial pressure of precursor gas nitrogen is not above the critical value, above which Mg₃N₂ phase appears in the melt. The thermodynamic results show that sufficient volume% of AlN particles can be formed in the Mg alloy in the temperature range of 700-1000°C. Preliminary results showed that in-situ gas bubbling route for production of Mg-AlN composites is technically feasible. Experiments are under way to confirm the thermodynamic predictions. The microstructure and phases of the composites formed in-situ are to be characterized using Scanning Electron Microscopy and X-Ray Diffraction.

10:20 AM

Modelling the Interaction Between Recovery, Recrystallization and Precipitation During Annealing of Cold Rolled AA6111: *Johnson Go*¹; Matthias Militzer¹; Warren J. Poole¹; Mary A. Wells¹; ¹University of British Columbia, The Ctr. for Metallurg. Process Engrg., Vancouver, BC V6T 1Z4 Canada

The recrystallization behaviour of commercial precipitation hardened alloys during annealing is complex as it may involve the simultaneous occurrence of recovery, recrystallization and precipitation. There are a number of possible interactions between precipitation and recrystallization. For example, the initial state of precipitation can affect the structure of the deformed state after cold rolling. In addition, it is well known that second phase particles may affect the kinetics of recrystallization significantly. In this study, a model framework is being developed to predict the recrystallization kinetics under the simultaneous occurrence of precipitation. Using the internal state variable approach an overall microstructure model is proposed where submodels for recovery, recrystallization and precipitation kinetics are coupled. Model predictions are validated with data obtained in isothermal annealing experiments which have been conducted on the cold rolled aluminum alloy AA6111 with systematically varied initial states of precipitation.

10:45 AM

The Effect of Iron Content on the Mechanical Properties of Continuous Cast AA5754 Aluminum Alloy: *Yansheng Liu*¹; David S. Wilkinson¹; ¹McMaster University, Dept. of Matls. Sci. & Engrg., 1280 Main St. W., Hamilton, Ontario L8S 4L7 Canada

The influence of iron content on mechanical properties of O-temper continuous cast (CC) AA5754 aluminum alloy was investigated. The variations of grain size, particles and texture distribution were examined. R-value was measured and the relationship between R-value and texture is discussed by computer simulation based on the Continuum Mechanics of Textured Polycrystals (CMTP) model. The result indicates that iron content has significant impact on grain size evolution during annealing. It is concluded that mechanical properties and texture distributions are alternated in some extent by the variation of iron content. The result is important for optimizing the industrial processing of CC AA5754 aluminum alloy.

11:10 AM

Abnormal Grain Growth and Texture Evolution in AA5754 Strip Cast Aluminum Alloy: *Hamid N. Azari*¹; David S. Wilkinson¹; ¹McMaster University, Dept. of Matls. Sci. & Engrg., 1280 Main St. W., Hamilton, Ontario L8S 4L7 Canada

The effect of abnormal grain growth on the microstructural evolution and texture development in a twin-belt strip cast AA5754 aluminum alloy was investigated. The results indicate that when homogenized at 560°C for 6 hours the alloy becomes particularly prone to abnormal grain growth when subsequently cold rolled to 90% reduction and isothermally annealed at 450°C for duration higher than one minute. It is shown that prior to the onset of abnormal grain growth, the recrystallization texture is characterized by Cube $\{001\}\langle 100 \rangle$ - and Q $\{013\}\langle 231 \rangle$ components. As abnormal grain growth proceeds with annealing time, the Cube component is gradually reduced in intensity, while the Q intensifies. However, the most striking effect of the abnormal grain growth is the emergence of CH $\{001\}\langle 120 \rangle$ - and H $\{001\}\langle 110 \rangle$ - as the main texture components. The results are discussed in terms of particle-assisted nucleation, the possible effect of homogenization treatment on the size and volume fraction of second phase particles and the preferential growth of CH oriented grains into the neighboring orientations arising from their special orientation relationship.

11:35 AM

The Influence of Severe Plastic Deformation on Mechanical Properties of AA6111 Sheet at Room Temperature: *Ki Ho Rhee*¹; Rimma Lapovok¹; Peter F. Thomson¹; ¹Monash University, CRC for Cast Metals Mfg. (CAST), Sch. of Physics & Matls. Engrg., PO Box 69M, Victoria 3800 Australia

AA6111 has been chosen in many countries for automotive outer body panels, but low ductility remains a major obstacle to competition with steel. Equal channel angular extrusion (ECAE) was used as a tool to enhance the ductility and to produce fine-grained structures. Conventional grain sizes in the range of 9–50 μm were investigated to determine the effect of grain size on tensile properties of AA6111 sheet at room temperature. It has been found that grain refinement through ECAE followed by heat treatment leads to an increase in both strength and ductility. This increase of tensile properties was also significantly influenced by heat treatment temperature at the final stage of sheet process.

Beyond Nickel-Base Superalloys: Precious Metal Alloys

Sponsored by: Structural Materials Division, SMD-Corrosion and Environmental Effects Committee-(Jt. ASM-MSCTS), SMD-High Temperature Alloys Committee, SMD-Mechanical Behavior of Materials-(Jt. ASM-MSCTS), SMD-Refractory Metals Committee
Program Organizers: Joachim H. Schneibel, Oak Ridge National Laboratory, Oak Ridge, TN 37831-6115 USA; David A. Alven, Lockheed Martin - KAPL, Inc., Schenectady, NY 12301-1072 USA; David U. Furrer, Ladish Company, Cudahy, WI 53110 USA; Dallis A. Hardwick, Air Force Research Laboratory, AFRL/MLLM, Wright-Patterson AFB, OH 45433 USA; Martin Janousek, Plansee AG Technology Center, Reutte, Tyrol A-6600 France; Yoshinao Mishima, Tokyo Institute of Technology, Precision and Intelligence Laboratory, Yokohama, Kanagawa 226 Japan; John A. Shields, HC Stark, Cleveland, OH 44117 USA; Peter F. Tortorelli, Oak Ridge National Laboratory, Oak Ridge, TN 37831-6156 USA

Tuesday AM
March 16, 2004

Room: 211B
Location: Charlotte Convention Center

Session Chairs: Dallis Hardwick, Air Force Research Laboratory/AFRL, Matls. & Mfg. Direct., Wright-Patterson AFB, OH 45433 USA; David R. Johnson, Purdue University, Sch. of Matl. Engrg., Lafayette, IN 47907-2044 USA

8:30 AM Invited

Iridium-Base Alloys for High-Temperature Structural Applications: *E. P. George*¹; C. G. McKamey¹; C. T. Liu¹; ¹Oak Ridge National Laboratory, Metals & Ceram. Div., Oak Ridge, TN 37831-6093 USA

Iridium is a platinum-group metal with the close-packed fcc crystal structure. Its high melting point (2443°C) and good oxidation/corrosion resistance make it an attractive candidate for high-temperature structural applications. A drawback of Ir-base alloys is low tensile ductility

when tested at conventional strain rates at ambient temperatures and at high strain rates at elevated temperatures. Another drawback is poor strength at high temperatures. Microalloying with ppm levels of Th and Ce has been shown to enhance grain-boundary cohesion and suppress brittle intergranular fracture in Ir alloys, whereas macroalloying with elements such as Hf and Zr increases high-temperature strength. In addition, harmful elements such as Si have also been identified that exacerbate brittle fracture in iridium. We will review the mechanisms of these effects and briefly discuss the successful use of iridium alloys aboard interplanetary spacecraft at temperatures to 1400°C. Research sponsored by the Office of Space and Defense Power Systems and the Division of Materials Sciences and Engineering, Office of Basic Energy Sciences, U. S. Department of Energy, under Contract DE-AC05-00OR22725 with UT-Battelle, LLC.

9:00 AM Invited

Creep Properties of Ir-Base Refractory Superalloys: *Yoko Yamabe-Mitarai*¹; Hiroshi Harada¹; Yuefeng Gu¹; Chen Huang¹; ¹National Institute for Materials Science, High Temp. Matls. Grp., Sengen 1-2-1, Tsukuba, Ibaraki 305-0047 Japan

The Ir-based alloys with the fcc and L1₂ two-phase structure has been developed as next-generation high-temperature materials. We found that cuboidal L1₂ precipitates aligned along $\langle 100 \rangle$ directions in the Ir-Nb binary alloy similar to Ni-base superalloys. The creep properties of the Ir-Nb, Ir-Nb-Zr, Ir-Nb-Ni alloys were investigated at temperatures between 1773 and 2073 K under 137 MPa. We found the addition of the third element was effective to improve the creep properties of the Ir-Nb alloy. For example, the minimum creep rate of Ir-Nb-Zr alloy at 2073 K was 10⁻⁶ /s, two order lower than that of the Ir-Nb alloy. The effect of Ni or Zr will be discussed in terms of microstructure, lattice misfit, deformation structure, and grain boundary strength. Then the way for alloy design of high-temperature materials will be pointed out.

9:30 AM

Experimental and Computational Investigations of the Al-Ni-Pt Ternary System: *Sara Natalia Prins*¹; Zi-Kui Liu¹; ¹Pennsylvania State University, Dept. of Matls. Sci. & Engrg., University Park, PA 16802 USA

A comprehensive understanding of the Al-Pt-Ni system is important from two perspectives. Firstly, the phases in the system form the basis of the phase equilibria and the phase transformation $\beta\text{-NiAl}$ to $\gamma\text{-Ni}_3\text{Al}$ in the environmentally protective aluminide coatings on Ni-base superalloys (NBSA). Pt additions to the NBSA substrate before aluminizing enhance the temperature and mechanical stability of the $\beta\text{-NiAl}$ coatings significantly. Secondly, although Ni additions to Pt-based alloys lower the solvus temperature of the Pt₃Al phase, these are beneficial to the mechanical properties and the unfavourable high density of Pt-based alloys. In the present work, the phase equilibria in the Al-Pt system, such as the structure and stability of the $\beta\text{-PtAl}$ phase and the phase boundaries of the γ / ($\gamma+\gamma'$) / γ' phases, are investigated as a base for the Al-Ni-Pt and other Pt-Al-X (X=Cr, Ti, Ta, Re) systems. The phase relations in the Al-Ni-Pt ternary system are also studied.

9:45 AM

Partial Phase Relationships in Ir-Nb-Ni-Al and Ir-Nb-Pt-Al Quaternary Systems and Mechanical Properties of their Alloys: *Huang Chen*¹; Yamabe-Mitarai Yoko¹; Yu Xihong¹; Nakazawa Shizuo¹; Harada Hiroshi¹; ¹National Institute for Materials Science (NIMS), High Temp. Matls. Grp., Refractory Superalloy Team, Sengen 1-2-1, Tsukuba, Ibaraki 305-0047 Japan

Two quaternary systems, Ir-Nb-Ni-Al, and Ir-Nb-Pt-Al were investigated successively to give assessments for ultra-high temperature applications. The phase relationships concentrated on fcc/L12 two-phase region were primarily established and mechanical properties were studied. Ir-Nb-Ni-Al quaternary alloys around Ir-rich or Ni-rich sides showed coherent fcc/L12 two-phase structure, analogous to Ni-base superalloys, however, most of the alloys presented three or four phases with two kinds of L12 phases. Although these alloys showed high compressive strain at high-temperature, they exhibited higher creep rate than Ir-base binary and ternary alloys. Another quaternary system Ir-Nb-Pt-Al showed promising results. Only fcc/L12 two-phase structure was found in all the alloys investigated with the compositions from Ir-rich to Pt-rich side, and the lattice misfit between fcc and L12 phases was small. The high-temperature strength at 1200 C of Ir-Nb-Pt-Al alloys was higher than that of Ir-Nb-Ni-Al alloys with the same Ir content (at.%). Moreover, Ir-Nb-Pt-Al alloys exhibited excellent creep-resistance.

TUESDAY AM

10:00 AM Break**10:30 AM**

Dislocation Structure and Mechanical Behavior of Ir-Based γ' Alloys: Oleg Y. Kontsevoi¹; Yuri N. Gornostyrev²; Andrey F. Maksyutov³; Arthur J. Freeman¹; ¹Northwestern University, Physics & Astron., 2145 N. Sheridan Rd., Evanston, IL 60208 USA; ²Institute of Metal Physics, Ekaterinburg 620219 Russia; ³Russian Science Center "Kurchatov Institute", Moscow 123182 Russia

A new approach for the development of high-temperature γ/γ' superalloys is based on using platinum group metals with higher melting temperatures and superior environmental properties. Indeed, refractory superalloys based on Ir are the strongest high-temperature materials developed to date. Unfortunately, there is no reliable information about dislocation properties and mechanisms driving the yield stress temperature dependence in Ir_3X alloys. We analyzed the structure and mobility of dislocations in Ir_3X (X = Nb, Ti, Zr, Ta) within the modified Peierls-Nabarro model with first-principles generalized stacking fault energetics calculated using the highly-precise FLAPW method. SISF-bound superdislocations (Kear splitting scheme) are found to be strongly preferred energetically in Ir_3Ta and Ir_3Nb , whereas APB-bound superdislocations (Shockley splitting scheme) are predicted in Ir_3Ti and Ir_3Zr . Because APB-bound superdislocations are considered responsible for the yield stress anomaly, our results predict that a positive yield stress temperature dependence should be expected in Ir_3Zr and Ir_3Ti , and a negative behavior in Ir_3Nb and Ir_3Ta . We discuss the connection of the mechanical behavior of the Ir_3X alloys with the $\text{L}_{12} \rightarrow \text{D}_{019}$ structural instability. Supported by the AFOSR (grant No. F49620-01-0166).

10:45 AM

Tensile Properties of Pt-Based Superalloys: Rainer Süß¹; Lesley Cornish¹; Lesley Heath Chown¹; Lizelle Glaner¹; ¹Mintek, Physl. Metall. Div., PB X3015, Randburg, Gauteng 2125 S. Africa

Since the Ni-based superalloys are reaching their temperature limit for operation in turbine engines, there is great interest in developing similar structured alloys based on a metal with higher melting point which can be used at temperatures of $\sim 1300^\circ\text{C}$. Platinum has a higher melting point than nickel. Although Pt-based alloys are unlikely to replace all Ni-based superalloys on account of both higher price and density, Pt-based alloys with microstructures analogous to that of nickel based superalloys are being developed for possible use in the highest application temperature components. The optimum alloys, based around the composition Pt84:Al11:Ru2:Cr3, have good mechanical properties and high temperature oxidation resistance. Previous work on hardness measurements and creep were very promising. Tensile tests are now being undertaken for selected alloys. The results are being compared to the hardness measurements to ascertain whether a relationship exists between these two quantities, as in steels.

11:00 AM

On the Development and Investigation of Quaternary Pt-Based Superalloys with Ni-Additions: Markus Wenderoth¹; Lesley Cornish²; Rainer Süß²; Stefan Vorberg³; Bernd Fischer³; Uwe Glatzel¹; Rainer Völkl¹; ¹University Bayreuth, Metals & Alloys, Ludwig-Thoma-Str. 36b, Bayreuth 95440 Germany; ²Council for Mineral Technology (MINTEK), Advd. Matls., 200 Hans Strijdom Dr., Randburg 2125 S. Africa; ³University of Applied Sciences Jena, Carl Zeiss Promenade 2, Jena 07745 Germany

Platinum group metals are of increasing interest for very high temperature application. The objective of this work is to produce an alloy showing a microstructure similar to Ni-based superalloys, but with a base metal having a higher melting point than Ni. Having a fcc crystal structure with a L_{12} coherent embedded phase, it can be expected to have high strength and temperature resistance beyond Ni-based superalloys. Our work concentrates on the development of a quaternary Pt-based superalloy. The elements Al, Cr and Ni were chosen as alloying components. In this stage we intend to vary the content of Ni between 0 and 10 at.%, the contents of the remaining components will be left in a fixed ratio. Additions of Ni may increase ductility and act also as solid solution strengthener. After arc-melting and heat treatment the alloys will be investigated, using SEM, calorimetric measurements and X-Ray diffraction.

11:15 AM

Ruthenium Aluminides as Structural Materials and Coatings: Brian Tryon¹; Fang Cao¹; Tapash Nandy¹; Qiang Feng¹; Tresa M. Pollock¹; ¹University of Michigan, Dept. of Matls. Sci. & Engrg., 2300 Hayward, Ann Arbor, MI 48109 USA

Systems based on RuAl are of potential interest for bulk structural applications as well as for bond coat interlayers in superalloy-TBC systems. The microstructure, mechanical properties and dislocation substructures observed in ternary and quaternary alloys based on this

system will be reviewed. Additions of Pt are of particular interest as Pt improves the oxidation characteristics of RuAl and changes the operative slip systems. To investigate the potential of this system to perform as a coating, a variety of interdiffusion studies have been conducted. A new ordered Ru-Al-Ta Heusler phase has been identified. Finally, microstructural evolution in Ru-containing coatings and the oxidation behavior of these coatings will be discussed.

11:30 AM

RuAl Eutectics: Todd Reynolds¹; David R. Johnson¹; ¹Purdue University, Sch. of Matls. Engrg., 501 Northwestern Ave., W. Lafayette, IN 47907-2036 USA

Intermetallics are often considered candidate materials for high temperature structural applications due to the high melting temperature and good oxidation resistance of many compounds. One promising high temperature aluminide ($\text{Tmp} > 2000^\circ\text{C}$) is ruthenium aluminide due to that it may also have a good room temperature fracture toughness. To lower the cost of RuAl alloys, the ruthenium must be substituted with a less expensive element. With the greater ease in processing of the eutectic alloys, bulk sized samples of controlled microstructure can be produced for fracture toughness testing. Ru-Al-Mo alloys with compositions near the RuAl-Mo (B2-hcp) eutectic compositions have shown to have fracture toughness near $37\text{MPa}\sqrt{\text{m}}$ and yield strength around 1100MPa. The oxidation resistance was low for the RuAl-Mo alloys, so the RuAl-Mo-Cr system was investigated. Mechanical property data from microhardness, compression, and four point bend tests will be reported for alloys of this system.

11:45 AM

Microstructure and Mechanical Properties of Cr-Ru Alloys: Yuefeng Gu¹; Y. Ro¹; T. Kobayashi¹; H. Harada¹; ¹National Institute for Materials Science, HTM21, Sengen 1-2-1, Tsukuba-shi, Ibaraki 305-0047 Japan

The metal chromium has been considered as a possible base for alloy systems since the last forties due to its higher melting points (1863°C), good oxidation resistance, low density and its high thermal conductivity. Major disadvantages that have held back its commercial exploitation are the high ductile-to-brittle transition temperature and further embrittlement resulting from nitrogen contamination during high-temperature air exposure. Since late of the last 1970s, chromium, as a practical alloy base, has remained virtually unstudied. Recently, a new look has been taken at chromium-base alloy systems. Analysis of rather scattered datum suggests that chromium-base alloys can be ductilized at ambient temperature and is quite capable of being strengthened to high levels at high temperature. New composition design and process would give high possibility to chromium-base alloys as structural materials in applications at temperatures up to 1300°C . This report will give our recent results on the microstructure and mechanical properties of Cr-Ru alloys.

Bulk Metallic Glasses: Fatigue and Fracture

Sponsored by: Structural Materials Division, ASM International; Materials Science Critical Technology Sector, SMD-Mechanical Behavior of Materials-(Jt. ASM-MSCTS)

Program Organizers: Peter K. Liaw, University of Tennessee, Department of Materials Science and Engineering, Knoxville, TN 37996-2200 USA; Raymond A. Buchanan, University of Tennessee, Department of Materials Science and Engineering, Knoxville, TN 37996-2200 USA

Tuesday AM
March 16, 2004

Room: 209A
Location: Charlotte Convention Center

Session Chairs: Reinhold H. Dauskardt, Stanford University, Matls. Sci. & Engrg., Stanford, CA 94305-2205 USA; Wole Soboyejo, Princeton University, Mech. & Aeros. Engrg., Princeton, NJ 08544 USA

8:30 AM Invited

Fatigue Behavior of Zr-Based Bulk Metallic Glass: Reinhold H. Dauskardt¹; Peter A. Hess¹; Brian Menzel¹; ¹Stanford University, Dept. of Matls. Sci. & Engrg., Stanford, CA 94305-2205 USA

The mechanisms of fatigue damage initiation and evolution in bulk metallic glasses (BMGs) are not well understood, limiting their use in safety-critical structural applications. We present recent studies of both the initiation of fatigue damage obtained from stress-life experiments on smooth specimens, and the growth of fatigue cracks mea-

sured under stable and transient cyclic loading conditions. The early stages of damage initiation and propagation resulting in the anomalously low reported fatigue endurance limits are discussed. In addition, both 'small' and 'long' fatigue crack growth rates were carefully characterized to elucidate the detailed mechanism of fatigue crack growth. High resolution characterization of fatigue specimen and fracture surfaces were used to provide the basis for micromechanical models of the resulting fatigue mechanisms. Unlike the meniscus instability mechanism that has been used to explain fracture processes, a new mechanism involving out-of-plane shearing processes is used to rationalize the observed fatigue behavior.

8:55 AM Invited

Nano Structured Bulk Glassy Alloys with High Fatigue Limit: *Yoshihiko Yokoyama*¹; Peter K. Liaw²; Akihisa Inoue³; ¹Himeji Institute of Technology, Mats. Sci. & Chmst., Shosha 2167, Himeji, Hyogo 671-2201 Japan; ²University of Tennessee, Mats. Sci. & Engrg., Rm. 427-B Dougherty Engrg. Bldg., Knoxville, TN 37996-2200 USA; ³Tohoku University, Inst. for Mats. Rsch., Katahira 2-1-1, Aobaku, Sendai, Miyagi 980-8577 Japan

We examined S-N curves of Zr50Cu40Al10, Zr50Cu30Ni10Al10 and Zr50Cu37Al10Pd3 bulk glassy alloys using a rotating-beam fatigue test to evaluate the effect of adding Ni and Pd elements on fatigue strength. As a result, we found that the fatigue limit was increased from 250 MPa to 500 MPa by adding 10 at% Ni instead of Cu to a Zr50Cu40Al10 bulk glassy alloy. Furthermore, fatigue limit significantly increased over 1000 MPa by adding a 3 at% Pd instead of Cu to a Zr50Cu40Al10 bulk glassy alloy. Zr50Cu37Al10Pd3 bulk glassy alloy shows nano-crystallized network structure, which is considered as the origin of fatigue crack stopping.

9:20 AM

Scattered Results and Premature Overload Fracture of Zirconium Based Bulk Metallic Glass Fatigue Specimens Tested in Vacuum: *William Hutchison Peter*¹; Bing Yang¹; Peter K. Liaw¹; C. T. Liu²; Ray A. Buchanan¹; Mark L. Morrison¹; G. Y. Wang¹; ¹University of Tennessee, Mats. Sci. & Engrg., 434 Dougherty Hall, Knoxville, TN 37996-2200 USA; ²Oak Ridge National Laboratory, Metals & Ceram. Div., PO Box 2008, MS 6115, Oak Ridge, TN 37831-6115 USA

After a decade of fabricating "bulk metallic glasses" (BMGs), some fundamental concepts and observations regarding the fracture mechanisms of these glasses have been made. However, a full understanding of the degradation process of BMGs has not been realized. Early fatigue studies in air and vacuum of a Zr-Based BMG, Zr52.5Cu17.9Ni14.6Ti5Al10 (at %), revealed a high fatigue limit in air comparable to other high strength alloys. BMG samples tested in vacuum experienced similar results to those tested in air at high stress ranges, but vacuum results were scattered close to the air fatigue limit. This research will revisit this comparison while also making an effort to understand the location, time, and mechanism of crack initiation. In-situ thermography, optical microscopy, and acoustic emission will be used in an attempt to determine the relative life span of crack initiation to crack propagation, and to understand any correlation with the scattered vacuum data. This research effort was made possible by the funding of the National Science Foundation Integrative Graduate Education and Research Training (IGERT) Program on 'Materials Lifetime Science and Engineering' (DGE 9987548), with Drs. W. Jennings and L. Goldberg as contact monitors, and by the Division of Materials Science and Engineering, Department of Energy under contract DE-AC-00OR22725 with Oak Ridge National Laboratory (ORNL) operated by UT-Battelle, LLC.

9:45 AM

Fatigue Behavior of Zr-Base Bulk Metallic Glasses: *Gongyao Wang*¹; P. K. Liaw¹; A. Peker²; Y. Yokoyama³; W. H. Peter¹; B. Yang¹; M. L. Benson¹; W. Yuan¹; L. Huang¹; M. Freels¹; R. A. Buchanan¹; C. T. Liu¹; C. R. Brooks¹; ¹University of Tennessee, Dept. of Mats. Sci. & Engrg., 323 Dougherty Blvd., Knoxville, TN 37996 USA; ²LiquidMetal Technologies Inc., Lake Forest, CA 92630 USA; ³Himeji Institute of Technology, Mats. Sci. & Engrg., Shosha 2167, Himeji City Japan; ⁴Oak Ridge National Laboratory, Metals & Ceram. Div., Oak Ridge, TN 37831 USA

High-cycle fatigue (HCF) experiments were conducted on zirconium (Zr)-based bulk metallic glasses (BMGs): Zr₅₀Al₁₀Cu₄₀, Zr₅₀Al₁₀Cu₃₀Ni₁₀, and Zr_{41.2}Ti_{13.8}Ni₁₀Cu_{12.5}Be_{22.5}, in atomic percent. The HCF tests were performed using an electrohydraulic machine at a frequency of 10 Hz with a R ratio of 0.1 and under tension-tension loading. Note that $R = \sigma_{min} / \sigma_{max}$, where σ_{min} and σ_{max} are the applied minimum and maximum stresses, respectively. The test environments were air and vacuum. A high-speed and high-sensitivity thermographic infrared (IR) imaging system has been used for nondestructive evalua-

tion of temperature evolution during fatigue testing of BMGs. Limited temperature evolution was observed during fatigue. However, a sparking phenomenon was observed at the final fracture moment of Zr₅₀Al₁₀Cu₃₀Ni₁₀. The effect of chemical composition on the fatigue behavior of the Zr-based BMGs was studied. The fatigue-endurance limit of Zr₅₀Al₁₀Cu₃₀Ni₁₀ (865 MPa) is somewhat greater than that of Zr₅₀Al₁₀Cu₄₀ (752 MPa) and Zr_{41.2}Ti_{13.8}Ni₁₀Cu_{12.5}Be_{22.5} (Batch 59: 703 MPa and Batch 94: 615 MPa) in air. The vein pattern and droplets with a melted appearance were observed in the apparent melting region. Fracture morphology indicates that fatigue cracks initiate from shear band or some defects. The fatigue lives in vacuum are generally comparable with those in air. The cracking shapes on the fatigue surfaces were analyzed and predicted. Fracture toughness was calculated from the measurement of the crack-propagation region of the fatigue-fractured surface. The present work is supported by the National Science Foundation (NSF), the Combined Research-Curriculum Development (CRCD) Program, under EEC-9527527 and EEC-0203415, the Integrative Graduate Education and Research Training (IGERT) Program, under DGE-9987548, and the International Materials Institutes (IMI) Program under DMR-0231320, with Ms. M. Poats, and Drs. P. W. Jennings, L. S. Goldberg, and C. Huber as contract monitors.

10:10 AM Invited

Contact-Induced Deformation and Fracture/Fatigue Behavior in Bulk Metallic Glasses: C. Mercer¹; R. Cirincione¹; C. Fenton¹; P. Anglin¹; M. Huang¹; *W. O. Soboyejo*¹; ¹Princeton University, PMI/Dept. of Mech. & Aeros., D404 E. Quad., Olden St., Princeton, NJ 08544 USA

This paper presents a combined experimental, analytical and computational study of contact-induced deformation in Zr-Be-based bulk metallic alloys. Contact-induced deformation is studied using Hertzian indentation techniques. The studies reveal the underlying surface and sub-surface shear bands, and the deformation patterns associated with Hertzian indentation. The deformation patterns are then correlated with stress components computed with finite element models. Subsequently, the fracture and toughening mechanisms are elucidated via resistance-curve experiments. The observed microcracks are shown to promote crack-tip shielding via microcrack shielding. The predicted shielding levels are consistent with the measured toughening levels. Finally, the paper examines the effects of stress ratio on the micromechanisms of fatigue crack growth. The crack growth rate data are shown to be consistent with a crack-tip opening displacement model. The implications of the results are then discussed for the design of amorphous bulk metallic alloys.

10:35 AM Invited

Deformation Behavior of Metallic Glasses and Metallic-Glass-Matrix Composites: *Todd C. Hufnagel*¹; ¹Johns Hopkins University, Mats. Sci. & Engrg., 102 Maryland Hall, 3400 N. Charles St., Baltimore, MD 21218-2681 USA

The disordered atomic-scale structure of amorphous alloys gives them mechanical behavior quite different from that of crystalline alloys. The most striking aspect of this behavior is the tendency for shear localization (at temperatures well below the glass transition) even at low strain rates. Although shear localization leads to fracture with relatively little macroscopic plastic deformation in single-phase metallic glasses, in two-phase materials a dramatic multiplication of shear bands can occur, making extensive macroscopic plastic deformation possible. In this talk, we will review the present understanding of fundamental aspects of plastic deformation of amorphous alloys, from both theoretical and experimental points of view. We will emphasize recent developments made possible by mechanical testing and structural characterization, including observations of dilatation associated with generation of excess free volume, and in situ x-ray diffraction observations of composite strain and microstructural evolution during deformation of metallic-glass matrix composites.

11:00 AM Invited

Deformation Mechanisms in Bulk Metallic Glass Matrix Composites: *Ersan Ustundag*¹; Bjoern Clausen²; Seung-Yub Lee¹; Gregory S. Welsh¹; ¹Caltech, Mats. Sci., MC 138-78, Pasadena, CA 91125 USA; ²Los Alamos National Laboratory, Neutron Sci. Ctr., Los Alamos, NM 87545 USA

Bulk metallic glasses (BMGs) have attractive mechanical properties: yield strength > 2 GPa, fracture toughness > 20 MPa.m^{1/2} and elastic strain limit ~ 2%. BMGs can also be processed into intricate shapes just like polymers. Unfortunately, monolithic BMGs fail catastrophically under unconstrained deformation by forming shear bands. To overcome this problem, BMG matrix composites with fiber and particulate reinforcements were proposed. We have recently investi-

gated the deformation behavior of various BMG composites. We performed loading measurements during neutron or high-energy X-ray diffraction to determine the lattice strains in the crystalline reinforcements. We then combined the diffraction data with finite element and self-consistent modeling to determine the behavior of the matrix. We show that usually the reinforcements yield first, then start transferring load to the matrix. The results will be presented with an aim to identify the 'ideal' reinforcement and its morphology.

11:25 AM

Deformation of In-Situ-Reinforced Bulk Metallic Glass Composites: *Seung-Yub Lee*¹; Gregory S. Welsh¹; Ersan Ustundag¹; Bjoern Clausen²; Mark A.M. Bourke²; Jonathan D. Almer³; Ulrich Lienert³; Dean R. Haefner³; ¹Caltech, Mats. Sci., MC 138-78, Pasadena, CA 91125 USA; ²Los Alamos National Laboratory, Neutron Sci. Ctr., Los Alamos, NM 87545 USA; ³Argonne National Laboratory, Advd. Photon Source, Argonne, IL 60439 USA

A promising bulk metallic glass (BMG) composite consists of crystalline dendrites that precipitate in situ during casting within an amorphous matrix. The reinforcements form an interpenetrating structure and enhance the ductility of the composite. To gain insight about the deformation mechanisms in these composites, a detailed neutron and high energy X-ray diffraction study was conducted. Specifically, the elastic deformation of the crystalline reinforcements was studied during mechanical loading of composites. In addition, self-consistent deformation models were employed to interpret the diffraction data and to deduce the evolution of load partitioning in the composites. The results suggest that the mechanical properties of the reinforcements, and hence the composite, are highly variable and quite sensitive to processing conditions.

Carbon Technology: Green Anodes and Soderberg Paste

Sponsored by: Light Metals Division, LMD-Aluminum Committee
Program Organizers: Markus Meier, R&D Carbon, Sierre CH 3960 Switzerland; Amir A. Mirchi, Alcan Inc., Arvida Research and Development Centre, Jonquiere, QC G7S 4K8 Canada; Alton T. Tabereaux, Alcoa Inc., Process Technology, Muscle Shoals, AL 35661 USA

Tuesday AM Room: 213A
March 16, 2004 Location: Charlotte Convention Center

Session Chair: Alberto Salvador Gomes, Albras Aluminio Brasileiro S.A., Carbon Plant, Barcarena, Para CEP 68.447-000 Brasil

8:30 AM

Anode Paste Preparation by Means of a Continuously Operated Intensive Mixing Cascade at Aostar Qimingxin Aluminium China: *Berthold Hohl*¹; André Pinoncelly²; Jean Claude Thomas³; ¹Maschinenfabrik Gustav Eirich, Hardheim 74732 Germany; ²Solios Carbone, Givors Cedex 69702 France; ³Aluminium Pechiney, Centr' Alp, Voreppe Cedex 38341 France

In 2002, Aostar Qimingxin Aluminium announced the construction of a new anode plant at their 250 000 t/y greenfield smelter in the Sichuan Province in Central China. Solios Carbone were awarded a contract for the supply of a 35 t/h paste plant. For the design, new principles and ideas led to the so called Intensive Mixing Cascade (IMC) which was jointly developed by Eirich, Solios Carbone and Aluminium Pechiney. This new technology reduces significantly both the investment and operating cost of the paste plant and allows for the production of up to 50 t/h of anode paste in one single line. The Intensive Mixing Cascade combines a conventional preheating screw with a continuously operated intensive hot mixer, followed by a continuously operated intensive remixer-cooler. This paper recalls the development of the Intensive Mixing Cascade technology, and describes the main characteristics and the operating philosophy of that new plant.

8:55 AM

Fuzzy Control in Green Anode Plant Mixers: *Edson Silva Cruz*¹; ¹Albras - Aluminio Brasileiro SA, Rodovia PA 483 Km 21 Vila Murucupi, Barcarena, PA 68447000 Brazil

This paper presents the results obtained by using "Fuzzy Logic" to improve the control system of continuous green paste mixers at the ALBRAS anode plants. Fuzzy Logic is used to convert heuristic control rules stated by a human operator into an automatic control strategy. Through Fuzzy Logic the system is able to track the mixer current

set point. A control strategy base was elaborated intuitively, observing how the operators commanded the mixer's damper. When the continuous mixer is being controlled adequately it produces a homogeneous green paste with the required qualities of mechanical rigidity, as well as a minimum standard deviation of the anode density. These paste characteristics depend directly on the damper control, and the previous system was unable to control this appropriately, causing variations in the mixture of the paste and consequently the amount of green scrap produced. Sometimes the operators needed to adjust the damper manually. The controller program was developed with ladder language and runs on programmable logical controller (PLC). The new system has been running since 2002 in the anode plants. The current used as the control varies around an established target. The results demonstrate the effectiveness and viability of the system that subsequently will be being implanted on other anode plant equipment.

9:20 AM

Laboratory and Full Scale Experiments to Improve Quality of the VS Soderberg Secondary Anode: *Turid Vidvei*¹; Roy Pedersen²; ¹Elkem Aluminium ANS Research, PO Box 8040 Vaagsbygd, N-4675 Kristiansand Norway; ²Elkem Aluminium ANS Lista, PO Box 128, N-4551 Farsund Norway

The secondary anode made of baked stud hole paste under each vertical Soderberg cell stud should have high density, low electrical resistivity and make a low contact resistance both to the stud and the primary anode. A poor secondary anode can give anode problems as points or hanging ends and a high anodic voltage drop. The procedures for the stud changing and time between adding stud hole paste until the stud was reset were important for an optimized secondary anode quality. This was found through experiments at the laboratory and at full-scale experiments at Elkem Aluminium Mosjøen (EAM). To implement the results in the potroom a new system was developed to visualize the resetting time to the operators.

9:45 AM

PAH Emissions from Soderberg Anodes with Standard and PAH-Reduced Binder Pitches: *Trygve Eidel*¹; Alf-Yngve Guldhav²; Atle Olsvik³; Morten Sørli¹; ¹Elkem Aluminium ANS Research, PO Box 8040 Vagsbygd, N-4675 Kristiansand Norway; ²Elkem Shared Services - Central Laboratory, PO Box 8040 Vagsbygd, N-4675 Kristiansand Norway; ³Elkem Aluminium ANS Lista, PO Box 128, N-4551 Farsund Norway

Elkem Aluminium Lista has a point fed vertical spike Soderberg line where all anode tops are hooded and the pitch binder fumes are collected and cleaned in a dry scrubber. This set-up makes it possible to sample anode emissions from individual pots without any interference from neighboring anodes. In order to obtain nonbiased results on possible reductions in polyaromatic hydrocarbon (PAH) emissions using PAH-reduced binders, a number of hooded anode cells at the Lista smelter have been charged with a PAH-reduced paste over a period of several months. Sampling of pitch fumes has been performed during stable operating conditions (anode top normally at its warmest), after briquetting (anode top at its coldest) and during spike pulling (top punctured and high temperature pitch fumes and baking gases released). These results are compared to similar measurements on hooded anodes charged with a Soderberg paste containing a standard coal tar pitch (CTP) binder.

Cast Shop Technology: Casting

Sponsored by: Light Metals Division, LMD-Aluminum Committee
Program Organizers: Corleen Chesonis, Alcoa Inc., Alcoa Technical Center, Alcoa Center, PA 15069 USA; Jean-Pierre Martin, Aluminum Technologies Centre, c/o Industrial Materials Institute, Boucherville, QC J4B 6Y4 Canada; Alton T. Tabereaux, Alcoa Inc., Process Technology, Muscle Shoals, AL 35661 USA

Tuesday AM Room: 213B/C
March 16, 2004 Location: Charlotte Convention Center

Session Chairs: J. Les Kirby, Alcoa Inc., Alcoa Tech. Ctr., Alcoa Ctr., PA 15069 USA; J. Martin Ekenes, Hydro Aluminium AS, Otis Orchards, WA 99027-0603 USA

8:30 AM

Surface Formation on VDC Casting: *Ian Bainbridge*¹; John A. Taylor¹; Arne K. Dahle¹; ¹University of Queensland, Cooperative Rsch. Ctr. for Cast Metals Mfg. (CAST), Brisbane, Queensland 4072 Australia

A range of surface defects commonly formed on vertical direct chill (VDC) cast product have been examined by various metallographic techniques. Whilst the presently accepted model for the formation of cold folds on the cast surface can be reconciled to the details obtained from these examined samples, the explanations for the formation of other common surface defects could not. This paper describes current research efforts aimed at measuring the strength of molten aluminium alloy oxide surfaces under various conditions. This data is used as the basis for a hypothesis of the behaviour of the melt in the meniscus region in a VDC mould during casting. The results obtained from the melt strength tests and the metallographic examination of the cast samples are discussed and possible mechanisms for the formation of various surface defects are proposed.

8:55 AM

Strontium Additions to Improve Ingot Surface Quality: *David H. DeYoung*¹; Douglas A. Weirauch, Jr.¹; ¹Alcoa Inc., Alcoa Tech. Ctr., 100 Tech. Dr., Alcoa Ctr., PA 15069 USA

The casting of rolling ingots is sometimes plagued by surface defects that can initiate cracking or hot tearing of the ingots. Vertical folds and oxide patches are examples of such surface defects. Because of the oxidation potential of high magnesium-containing 5xxx alloys, this alloy family is especially prone to surface defects. Recently it was found that small additions of strontium could markedly improve the surface of ingots and minimize cracking. This paper will review the development that is the subject of a recently issued U.S. patent.

9:20 AM

Safety and Performance Issues of Conventional Sheet DC Moulds Under Pulsed Water Conditions: Yves Caron¹; André Larouche¹; Joseph Langlais¹; *Denis Bernard*²; ¹Alcan International Ltd., Arvida R&D, 1955 Mellon Blvd., PO Box 1250, Jonquière, Québec G7S-4K8 Canada; ²Alcan Primary Metal Group: Laterrière Works, PO Box 6301, Laterrière, Québec G7N-1A2 Canada

In DC casting of molten aluminium, the liquid aluminium is poured into an open mould. At first, a thin ingot shell is formed by the mould cooling, but as the ingot exits the mould this shell is severely quenched by the water jet coming from below the mould. The cooling of the ingot body is thus mainly achieved by heat transport through water evaporation that causes steam generation below the mould. During DC casting of sheet ingots using a slot-generated continuous water curtain, water can move upwards through the mould-ingot interface and onto the surface of the liquid pool forming the ingot head. This poses a serious safety hazard. The conditions under which this phenomenon occurs are not fully understood but it is clearly driven by the steam pressure build-up between the ingot and the water curtain. The use of conventional water hole moulds solved this problem mainly because the water outlet is discontinuous and allows the steam to escape and avoid any water vapour pressure build-up. However, it was found that certain conventional hole mould technology designs, under pulsed water start-up conditions, led to poor start-up performances on certain alloys. This paper presents the solutions that were applied to mould design in order to increase casting performance and recovery while maintaining the absence of water getting onto the ingot head.

9:45 AM

Casting Metal Temperature Control by Launder Heating: *Jan Migchielsen*¹; Jan D. de Groot¹; ¹Thermcon Ovens B.V., Process Dept., PO Box 97, Geldermalsen 4190 CB The Netherlands

Launder preheating is an essential step in casting processes. Casting liquid aluminium through a launder that is not preheated is not feasible, even dangerous and would cause damage to the launder lining and contaminate metal with eroded material. For better process control launders, especially longer systems need to be equipped with permanently fitted and automated preheating systems. A casting launder can be provided with a continuous electrical heating system that offers full control to the metal temperature between the casting furnace and the casting machine. The paper makes a comparison between various methods of launder preheating and semi-continuous heating discussing the limitations and benefits of the methods and its implications for running cost and metal quality.

10:10 AM Break

10:45 AM

AutoPak - "Total Automation for D.C. Slab Casting": *John V. Griffin*¹; ¹Pechiney Aluminum Engineering, Inc., 333 Ludlow St., Stamford, CT 06902 USA

Pechiney Aluminium Engineering has built on 20 years of continual improvements and advancements in automatic slab casting technology to develop the "AutoPak". Technology Concept: The Pechiney "AutoPak" technology is a complete automotive casting package con-

sisting of "state-of-the-art" process equipment and a total integrated management and information system. The "AutoPak" process provides the cast house team with greater control over the operational casting station parameters; from the holding furnace(s) to the D.C. casting machine.

11:10 AM

FATA Hunter Optiflow® Variable Tip Width Adjustment System for Aluminum Sheet Casting: *Dennis Smith*¹; Özgül Keles²; Necmi Dogan²; ¹FATA Hunter, Inc., Tech. Dept., 1040 Iowa Ave., Riverside, CA 92507 USA; ²Assan Aluminium, Tuzla, Istanbul Turkey

FATA Hunter has recently developed and patented for the continuous twin roll casting lines an automated system which allows the end user to change the cast sheet width while casting in continuous operation. This system uses the new Optiflow boron nitride coated feed tip nozzle to ensure that the internal end dams glide with precise incremental movements. Typical cast house operations which would benefit the most from this system are continuous twin roll casting lines that frequently change the cast width for multiple end products. A program has been instituted to determine the effectiveness of this new design utilizing a range of the Fata Hunter twin roll casting lines from the old vintage casters to the new revolutionary SpeedCaster lines.

11:35 AM

Crystallographic Texture Development of Twin-Roll Cast Aluminum Strips: *Murat Dündar*¹; Özgül Keles¹; Bilal Kerty¹; Necmi Dogan¹; ¹Assan Aluminum, Tuzla, Istanbul Turkey

As compared to the traditional hot mill process, the relatively low capital cost of twin-roll casters, in combination with their lower energy and labor costs, have made twin-roll casting an increasingly popular method of producing a wide range of aluminum flat rolled products. In the highly competitive global market environment, the lower conversion cost advantages of twin-roll casting make it particularly attractive for the manufacturing of fin and foil products. Major challenge in this method is to reduce the casting gauge below 3 mm. Thin gauge casting provides significant improvement in the microstructure along with more isotropic mechanical properties in three different direction compared to the casting direction. Decrease in casting gauge is expected to result in higher load exerted on the cast sheet. This occurs in the "hot rolling" phase of the casting at the roll bite. Although there exists a limited plastic deformation, it would not be surprising to introduce a crystallographic texture to the sheet. Present study investigates the crystallographic texture development of as-cast aluminum strips, as the gauge is reduced from 5 to 1,80 mm. Pole figures are employed to characterize the dominant texture at different positions from the free surface of the strip. Casting width of the strips are 2200 mm for all the gauges. Macro and microstructural studies, along with the mechanical characterization, are also carried out on the samples. Texture analysis and mechanical characterization techniques are extended to 0,5 mm thick, "0" temper materials produced out of these strips.

CFD Modeling and Simulation of Engineering Processes: MEMS/Microfluidics

Sponsored by: Materials Processing & Manufacturing Division, ASM/MSCTS-Materials & Processing, MPMD/EPD-Process Modeling Analysis & Control Committee, MPMD-Solidification Committee, MPMD-Computational Materials Science & Engineering-(Jt. ASM-MSCTS)

Program Organizers: Laurentiu Nastac, Concurrent Technologies Corporation, Pittsburgh, PA 15219-1819 USA; Shekhar Bhansali, University of South Florida, Electrical Engineering, Tampa, FL 33620 USA; Adrian Vasile Catalina, BAE Systems, SD46 NASA-MSFC, Huntsville, AL 35812 USA

Tuesday AM

Room: 206A

March 16, 2004

Location: Charlotte Convention Center

Session Chairs: Shekhar Bhansali, University of South Florida, Elect. Engrg., Tampa, FL 33620 USA; Mario Castro, Concurrent Technologies Corporation, Largo, FL 33773 USA

8:30 AM Opening Remarks - Shekhar Bhansali

8:35 AM Invited

Design of an Asymmetric Waveform Spectrometer: *Mario H. Castro-Cedeno*¹; ¹Concurrent Technologies Corporation, 7995 114 Avenue, Largo, FL 33773 USA

TUESDAY AM

The goal of this project was to model, design and prototype a MEMS chip that would be the drift channel in a high-field asymmetric waveform ion mobility spectrometer or FAIMS. FAIMS uses and asymmetric RF voltage signal to separate the various ions in a stream of incoming air. The separation occurs in the drift channel when the RF voltage signal is used to charge the top or bottom channel walls. The potential between the top and bottom attracts and can separate ions of different mobility. Ions that have higher mobility reach the top or bottom first and are neutralized. The remaining ions can be detected at the exit of the drift channel. Asymmetric square waveforms at very high frequencies have been found effective in causing separation of chemicals where only one kind of ion reaches the channel exit. This effort was successful in building a CFD model of the drift channel and in simulating the separation of chemicals with different ion mobility by using square asymmetric voltage waveforms. In addition, a MEMS drift channel chip was fabricated. The spectrometer can be used to detect trace amounts of chemical compounds in air at room conditions. Some examples are drugs, toxic chemicals and explosives.

9:10 AM

Design and Simulation of a Piezoresistive MEMS Pressure Sensor for Marine Applications: *Shyam Aravamudan*¹; Shekhar Bhansali¹; ¹University of South Florida, Dept. of Electl. Engrg., 4202 E. Fowler Ave., ENB 118, Tampa, FL 33620 USA

The physical and biological processes in the ocean are critically influenced by ocean parameters (pressure, salinity and temperature). There is a need to design inexpensive and reliable sensors to continuously measure large volumes of sea-space over long time spans. This paper reports the design and simulation results of a micromachined diaphragm-type piezoresistive pressure sensor with temperature compensation capable of operating over a dynamic range (0-1000 meters) with 0.1% or better resolution. The sensor functions when the resistivity of the sensing resistor changes as the diaphragm deflects due to applied pressure. We report the simulation results (output voltage and sensitivity analysis) using coupled MemPZR-MemMech module of the CoventorWare2003 tool to help in optimizing the design and performance of the wheatstone bridge arrangement in the diaphragm pressure sensor. The relationship between the sensing parameters including diaphragm thickness, length, doping concentration and depth is characterized to increase the sensitivity and linearity of response.

9:40 AM

Influence of Materials and Processes on the Design of Micro Needles: *Kiran Potluri*¹; Shekhar Bhansali¹; ¹University of South Florida, Elect. Engrg., 4202 E. Fowler Ave., ENB 118, Tampa, FL 33620 USA

In this paper, we present the design and analysis of microneedles. We have designed and fabricated microneedles of different dimensions using various materials viz. SiO₂, Oxide-Nitride-Oxide and Gold. The design, modeling and analysis was done using the Finite Element Analysis (FEA) software ANSYSTM 6.1. Angular strength analysis of the microneedles was done using angular loading in ANSYSTM, with the corresponding material property settings. Using the force-displacement settings, forces of varying magnitude in the range of 10 mN - 20 mN were applied on needles of different lengths (10 - 100µm) and side wall thicknesses (1µm and 1.5µm). Eigen Buckling analysis was performed to study the buckling characteristics of the microneedles. The buckling and force-displacement analyses show that O-N-O micro needles are more strong and robust compared to needles of other materials.

10:10 AM Break

10:40 AM

Transient Analysis of Microchannel Heat Transfer With Volumetric Heat Generation in the Substrate: Shantanu S. Shevade¹; *Muhammad M. Rahman*¹; ¹University of South Florida, Mech. Engrg., Coll. of Engrg., 4202 E. Fowler Ave., Tampa, FL 33620 USA

Liquid flow and heat transfer in microchannels are critical to the design and process control of various Micro-Electric-Mechanical-Systems (MEMS) and biomedical lab-on-a-chip devices. Experimental and theoretical studies in the literature have showed that a very high rate of heat and mass transfer in microchannels is the key to the extreme efficiencies in the technologies being developed. This paper presents a systematic analysis of fluid flow and heat transfer processes during the magnetic heating of the substrate material. Heat is generated in the substrate material when a magnetic field is imposed due to change in orientation of the molecules. As a result, the substrate temperature rises. The study considered microchannels with rectangular and square cross section with heat generation in the substrate due to imposed magnetic field. The results computed were for Gadolinium substrate and water as a working fluid. Gadolinium is the magnetic

material that exhibits high temperature rise during adiabatic magnetization around its transition temperature of 295 K. It has been experimentally observed that adiabatic temperature rise increases with magnetic field strength and can be as high 20 K when a magnetic field of 10 T is applied. The purpose of this study is to explore the transient heat transfer coefficient when the fluid is circulated through the substrate via microchannels. Equations governing the conservation of mass, momentum, and energy were solved in the fluid region. In the solid region, heat conduction was solved. In both fluid and solid regions, all material properties were assumed to vary with temperature. This is particularly important for the magnetic material where there is usually a large variation of properties near the transition temperature. From the simulation results, plots of heat transfer coefficient and Nusselt number were obtained over the length of the channel. A thorough investigation for velocity and temperature distributions was performed by varying channel aspect ratio, Reynolds number, and heat generation rate in the channel. It was found that the peripheral average heat transfer coefficient and Nusselt number is larger near the entrance and decreases downstream because of the development of the thermal boundary layer. With the increase in Reynolds number, the outlet temperature decreased and the average heat transfer coefficient increased.

11:10 AM

Improved MEMS Thermal Actuator Design by Modification of Hot-Arm Topology: *Vandana Upadhyay*¹; Scott Samson²; Shekhar Bhansali¹; ¹University of South Florida, Electl. Engrg., 4202 E. Fowler Ave., Tampa, FL 33613 USA; ²University of South Florida, Coll. of Marine Sci., 140 7th Ave. S., St. Petersburg, FL 33701 USA

We present an improved design for a two-arm polysilicon thermal actuator. The classic thermal bimorph actuator design produces a localized hot spot at approximately the center of the thin actuator arm. This phenomenon limits the actuator efficiency, lifetime, and reliability. Since the deflection is based on thermal expansion of the material, advantage may be gained by making the temperature profile more uniform along the hot-arm length. In our design, the topology of the thin arm is modified by forming a nonlinear structure near the approximate location of the hot spot. Electromechanical simulations of this design show an increase in deflection and force, due to a flattening of the temperature profile along this hot arm. The solid model generation, finite element analysis and simulations are carried out using FEA software. Experimental devices are fabricated by using a polysilicon micromachining process. Finally, the simulation data is compared with the experimental results.

Challenges in Advanced Thin Films: Microstructures, Interfaces, and Reactions: Modification, Characterization, and Modeling

Sponsored by: Electronic, Magnetic & Photonic Materials Division, EMPMD-Thin Films & Interfaces Committee

Program Organizers: N. M. (Ravi) Ravindra, New Jersey Institute of Technology, Department of Physics, Newark, NJ 07102 USA; Seung H. Kang, Agere Systems, Device and Module R&D, Allentown, PA 18109 USA; Choong-Un Kim, University of Texas, Materials Science and Engineering, Arlington, TX 76019 USA; Jud Ready, Georgia Tech Research Institute - EOEM, Atlanta, GA 30332-0826 USA; Anis Zribi, General Electric, Global Research Center, Niskayuna, NY 12309 USA

Tuesday AM

Room: 218B

March 16, 2004

Location: Charlotte Convention Center

Session Chairs: N. M. (Ravi) Ravindra, New Jersey Institute of Technology, Dept. of Physics, Newark, NJ 07102 USA; Jud Ready, Georgia Tech Research Institute, Atlanta, GA 30332-0826 USA; Anis Zribi, General Electric, Global Rsch. Ctr., Niskayuna, NY 12309 USA

8:30 AM

A First-Principles Investigation of TiC and ZrC as Alternative Protective Coatings for Ferritic Steels: *Ashok Arya*¹; Emily A. Carter²; ¹Bhabha Atomic Research Center, Matls. Sci. Div., Mumbai India; ²University of California, Dept. of Chmst. & Biochmst., Los Angeles, CA USA

Given the wide use of steel in harsh operating environments, optimal protective coatings are desirable. The current chrome coating on ferritic steels contains inherent microcracks formed during the elec-

trodeposition process, which causes material degradation. As a result, alternative coatings that can withstand high amplitude thermal and mechanical fluctuations and can protect steel against reactive/corrosive gas environments are of considerable interest. The mechanical and thermodynamic properties of TiC and ZrC are commensurate with steels as required for strong adhesion. Here we present a pseudopotential-based density functional (DFT) investigation of TiC and ZrC coatings, wherein we predict the atomic structure, bonding, and the ideal work of adhesion of the interface between a TiC(ZrC)(100) coating and a bcc Fe(110) substrate.¹ Characterization of the low-index TiC, ZrC, and Fe surfaces revealed that all surfaces retain near bulk termination, in agreement with experiment. The TiC(ZrC)(100)/Fe(110) interfaces exhibited a lattice mismatch which is less than 3%, leading to a smooth interface with only a small structural relaxation, except for the ultrathin 1 monolayer (ML) coating. We will present results of interface relaxation, interfacial bonding and adhesion strength of this interface. Further, the potential of TiC (ZrC) as an alternative protective coating material for steels will also be discussed. ¹A. Arya and E.A. Carter, J. Chem. Phys., 118, (2003) 8982.

8:45 AM Invited

Surface Modification of Metals and Alloys with Boron: Roumiana S. Petrova¹; ¹New Jersey Institute of Technology, Dept. of Physics, Newark, NJ 07102 USA

Deterioration of metals and alloys in working conditions in most cases begins from their surface. Thermo-chemical treatment can be used to increase the operational life of parts subjected to wear, corrosion, and oxidation. This is a method by which nonmetals (C, N, B) or metals (Al, Cr, Zn) are penetrated by diffusion and subsequent chemical reaction into the surface. By thermo-chemical treatment, the surface layer changes its composition, structure, and properties. Thermo-chemical treatment is used to improve material surface properties of Ti, Mo, Nb, Ta, Zr, Co, Ni, Fe, and their alloys. Carburizing, nitriding, carbonitriding, chromizing, aluminizing are widely used methods in the industry. Boronizing is a method of surface diffusion treatment with Boron. It is a thermo-chemical surface hardening process that can be applied to variety of nonferrous, ferrous metals, alloys and cemented carbides. The process involves heating cleaned materials to high temperatures (800-1000°C), for a duration (2-8 h), in contact with a boroncontaining solid powder, paste, liquid, or gaseous medium. During boronizing, the diffusion and subsequent absorption of boron atoms into the ferrous alloy surface form boron compounds. The coating may consist of either a single phase boride (Fe₂B) or two phases boronized layer (Fe₂B+FeB) having a needle like structure, oriented perpendicular to the substrate grains. Boronized coating has a number of characteristic features compared with conventional casehardened layers. The extremely high hardness values of boronized layers produced on carbon steel (between 1450 and 2300 HV) illustrates that it exceeds the hardness of hardened tool steel, hard chrome electroplate, and is equivalent to that of tungsten carbide. Microstructure distribution, phase composition, interaction mechanisms with the substrate material, and effect on materials corrosion are experimentally studied and discussed.

9:10 AM

Microstructure and Mechanical Properties of Ceramic/SAM Bilayer Coatings: Kaustubh Chitre¹; Tolulope O. Salami²; Quan Yang¹; Scott R. Oliver²; Junghyun Cho¹; ¹State University of New York, Dept. of Mech. Engrg., Vestal Pkwy. E., PO Box 6000, Binghamton, NY 13902-6000 USA; ²State University of New York, Dept. of Chmst., Vestal Pkwy. E., Binghamton, NY 13902-6000 USA

Thin ceramic coatings find their applications in various electronic devices, sensors and MEMS as a protection/barrier layer as well as a dielectric layer. The coatings, however, suffer from inherent brittleness and defects formed during processing. In an attempt to compensate for the weakness of the ceramic coating, we have developed a low-temperature solution precursor process of creating strain-tolerant, protective bilayer coatings. The bilayer consists of an integrated ceramic-organic hybrid material. The top ceramic coating offers an inert, protective layer. At the same time, the underlying nanometer scale organic coating, fabricated by the self-assembly, provides compliance for the overlying hard coating upon mechanical and thermal stresses. In addition, this organic self-assembled monolayer (SAM) acts as a 'template' by forming a proper surface functionality for the subsequent growth of hard ceramic coatings. In this study, we will investigate the microstructure and mechanical properties of ZrO₂/SAM and YSZ/SAM bilayer coatings grown on Si. Molecular level understanding of the microstructure and micromechanics involved in the synthesis and processing of the coating is studied by a variety of characterization techniques, such as XRD, AFM, XPS, electron microscopes and nanoindentation.

9:25 AM Invited

Revealing Deformation Mechanisms Through In Situ Nanoindentation in a Transmission Electron Microscope: Andrew M. Minor¹; E. T. Lilleodden¹; M. Jin²; E. A. Stach³; J. W. Morris³; W. A. Soer⁴; J. Th.M. De Hosson⁴; ¹Lawrence Berkeley National Laboratory, Matls. Sci. Div., 1 Cyclotron Rd., MS 66, Berkeley, CA 94720 USA; ²University of California, Dept. of Matls. Sci. & Engrg., Berkeley, CA 94720 USA; ³Lawrence Berkeley National Laboratory, Natl. Ctr. for Electron Microscopy, 1 Cyclotron Rd., Berkeley, CA USA; ⁴University of Groningen, Netherlands Inst. for Metals Rsch., Dept. of Applied Physics, Groningen Netherlands

The deformation mechanisms of metals and ceramics have been investigated using the novel experimental technique of in situ nanoindentation in a transmission electron microscope. Al-Mg thin films were used to investigate the role of alloying constituents in the transmission of plasticity across grain boundaries. Al thin films with varying amounts of Mg were deposited onto silicon substrates, and the solutes at the grain boundaries will be shown to affect grain boundary mobility. Initial results suggest that in the Al-Mg alloys the solutes effectively pin the grain boundaries while in pure Al considerable grain boundary motion is observed. During in situ nanoindentation of single crystal silicon at room temperature, dislocation plasticity was observed in the absence of phase transformations. Typically, only phase transformation and fracture are thought to be relevant deformation mechanisms during room temperature indentation of silicon. In our experiments, the dislocation activity and absence of phase transformations is explained by our sample geometry. Finite element analysis reveals an increase in the near-surface shear stress, relative to conventional sample geometries, which leads to preferential surface nucleation of dislocations.

9:50 AM

Fracture, Adhesion, and Residual Stress in Piezoelectric Thin Films for MEMS: D. F. Bahr¹; M. S. Kennedy¹; M. C. Robinson¹; K. E. Shafer¹; C. D. Richards¹; R. F. Richards¹; ¹Washington State University, Mech. & Matls. Engrg., PO Box 642920, Pullman, WA 99164-2920 USA

Piezoelectric MEMS require a series of materials (metals, oxides, nitrides, and silicon) which have widely differing mechanical properties. This paper will demonstrate the effects of residual tensile stresses in lead zirconate titanate (PZT) on a platinized silicon substrate, and the subsequent control of the composite residual stress by the addition of thin metallic layers to provide a compressive stress to increase the mechanical compliance of micromachined membranes. Stresses between 200 and 400 MPa in 1000-2000 nm thick PZT films can be moderated by 100 nm thick metallic layers which have compressive stresses in the GPa range, producing a micromachined membrane with a 40% decrease in the compliance of the structure. The effects of thermal processing, control of plastic flow in the metallization layers, and the structure of the PZT film will be shown to impact the fracture and adhesion of these films with the application of mechanical strains over 0.1%.

10:05 AM Break

10:20 AM Invited

Interdiffusion Structures and Coefficients in Ternary Systems: Youngho Sohn¹; ¹University of Central Florida, Advanced Matls. Procg. & Analysis Ctr., Dept. of Mech., Matls. & Aeros. Engrg., Orlando, FL 32816-2455 USA

An overview of interdiffusion phenomena in ternary systems is presented with an emphasis on the development of diffusion structure and determination of interdiffusion coefficients. Selected diffusion phenomena such as uphill diffusion, zero flux planes, demixing of phases, and development of various types of boundaries are highlighted using diffusion couples in several ternary systems. Methods available for the determination of ternary interdiffusion coefficients based on Onsager's formalism are reviewed and discussed in terms of applications and uncertainties. Development of a new analytical method to determine composition-dependent interdiffusion coefficients is presented. Utilization of advanced characterization tools for structural observations and determination of concentrations is also highlighted.

10:45 AM

Interdiffusion in CdMnTe Thin Film Grown on CdTe Substrate: Sergej V. Kletsky¹; Yung Soop Yoon²; ¹Institute of Semiconductor Physics, Dept. No. 38, Prospekt Nauki, 45, Kiev 03650 Ukraine; ²Inha University, Rsch. Inst. of Semiconductor & Thin Film Tech., #253, Yonghyun-Dong, Nam-Ku, Incheon 402-751 Korea

Interdiffusion in II-VI solid solutions leads to the intensive degradation of initial abrupt profiles of concentration in semiconductor

microstructures and, as result, to the changes in device characteristics. The main goal of this note is the quantitative description of intermixing in the system "substrate - growing layer" during epitaxial growth of CdMnTe/CdTe and approximate evaluation of the interdiffusion coefficient D . The model gives the possibility to calculate the concentration of metallic components diffused from the growing film into substrate and in the opposite direction and to determine D as a function of a total amount of diffused substances, time and rate of growth. Concrete calculations are made in particular cases when boundary concentration is constant, exponential function of time, sum of time delta-functions (delta inclusions) and periodical time functions. The approach can be readily generalized for other pairs of components and other growth processes. Y.S. Yoon, S.V. Kletsky. Japan. J. Appl. Phys. v.42, No 4A, 2003, p.1709.

11:00 AM

Numerical Simulation of Thermal Wave Propagation During Laser Processing of Thin Films: Xin Ai¹; Ben Li¹; ¹Washington State University, Sch. of Mech. & Matls. Engrg., Pullman, WA 99164 USA

A numerical model is developed to represent the thermal wave propagation during ultra-short pulsing laser processing of thin films. The model development is based on the solution of non-Fourier heat conduction problem with temperature and thermal flux delays using the discontinuous finite element method. The thermal wave phenomena are studied for both 1-D, 2-D and 3-D geometries. The temperature distributions in both Fourier and non-Fourier regions are discussed. Computed results for various conditions of relevance to laser annealing of thin films are discussed.

11:15 AM Invited

Fluxon Pinning in the Nodeless Pairing State of Superconducting YBa₂Cu₃O₇: Anthony T. Fiory¹; Dale R. Harshman²; W. J. Kossler³; X. Wan⁴; A. J. Greer⁵; R. Noakes⁷; C. E. Stronach⁷; E. Koster⁸; A. Erb⁹; John D. Dow⁴; ¹New Jersey Institute of Technology, Dept. of Physics, Newark, NJ 07102 USA; ²Physikon Research Corporation, PO Box 1014, Lynden, WA 98264 USA; ³Arizona State University, Dept. of Physics, Tempe, AZ 85287 USA; ⁴College of William and Mary, Dept. of Physics, Williamsburg, VA 23187 USA; ⁵Gonzaga University, Dept. of Physics, Spokane, WA 99258 USA; ⁶Virginia State University, Dept. of Physics, Petersburg, VA 23806 USA; ⁷University of British Columbia, Dept. of Physics, Vancouver, BC V6T-1Z1 Canada

The width of the local magnetic field distribution ("linewidth") produced by fluxon (or vortex) lattices in a high-purity YBa₂Cu₃O₇ crystal in the superconducting mixed state was determined by the method of muon spin rotation (mSR) spectroscopy. Linewidth measurements in fluxon lattices convey information on the magnetic penetration depth, whose temperature dependence reveals the symmetry of the superconducting pairing state. Crystal lattice defects and thermal activation cause fluxon pinning, i.e., perturbations in the fluxon lattice formed by a superconductor in a magnetic field, and change the linewidth from its ideal value. The electronic anisotropy of YBa₂Cu₃O₇ and fluxon pinning allow transverse disorder along the length of the fluxons, which tends to decrease the linewidth. Pinning also induces fluctuations in the distance between fluxons, which tend to increase the linewidth. By taking into account the expected field-dependent and temperature-activated fluxon disorder, the experimental results are shown to be consistent with a nodeless (s-wave) superconducting order parameter. The temperature dependence of the magnetic penetration depth is best described by a strong-coupling two-fluid model of s-wave superconductivity. It is shown that the data are statistically inconsistent with order parameters possessing nodes, such as those having dx₂-y₂ symmetry (d-wave).

11:40 AM Invited

A Model on Thermoelectric Effect in Superconductivity: Eunjee Shin¹; ¹Pennsylvania State University, Dept. of Math., University Park, State College, PA 16802 USA

In this talk we investigate a model for non-isothermal, non-equilibrium superconductivity exhibiting energy losses, and examine how these losses lead to the suppression of superconductivity. The principal unknown fields explored in the model are the complex valued Ginzburg-Landau order parameter, the magnetic vector potential, and the temperature (T). This model accounts for the interchange of thermal and electro-magnetic energies through Joule heating. We first establish a conservation of energy law implying that the total energy for an insulated superconducting body (thermal and electro-magnetic) is conserved. Through this, we prove global existence and uniqueness of classical solutions provided that the thermoelectric constant is sufficiently small. In particular, for the case where a classical Ohm's law is applied, we analyze the large time behavior of the solution and

prove that the w-limit set as $t \rightarrow \infty$ consists of equilibrium solutions. We also prove that if the electro-magnetic energy of the superconductor is sufficiently large at time zero, T will then rise beyond the critical temperature. In contrast to the earlier analytic work based only on an isothermal model, this work produces markedly different results as a consequence of considering non-isothermal electro-magnetic effects in superconductivity.

12:00 PM

Study of Electromigration on Electronic Components: Xiaoxin Xia¹; John W. Denning¹; Richard Griesel¹; ¹Northrop Grumman Space Technology, One Space Park, Redondo Beach, CA 90278 USA

Electromigration induced short circuit was observed on a single four pin DC connector during electrical testing. Optical and scanning electron microscope (SEM) analyses exhibited surface contamination and dendritic growth between the connector pin and ground, which led to the electrical shortage and component failure. The conductors were soldered using Pb88Sn10Ag solder and no-clean flux. EDX analysis revealed that dendrites contained high Pb, O and C. It indicated that lead in the solder migrated and formed an electrical short from the connector pin to ground. The electromigration on the connector was probably related to the processing induced thermal stress. This stress can generate electrical potential and form electrical circuit, thus caused electromigration and mass transportation between the low and high stress concentration areas on the component. Temperature, stress distribution, chemical composition and microstructure of the electronic devices are main contributions to the electromigration. Moisture is known to be an accelerator. The mechanisms and effects of temperature, thermal stress and grain boundaries on electromigration are discussed in this paper.

Computational Thermodynamics and Phase Transformations: Phase Field Modeling I

Sponsored by: ASM International: Materials Science Critical Technology Sector, Electronic, Magnetic & Photonic Materials Division, Materials Processing & Manufacturing Division, Structural Materials Division, MPMD-Computational Materials Science & Engineering-(Jt. ASM-MSCTS), EMPMD/SMD-Chemistry & Physics of Materials Committee

Program Organizer: Jeffrey J. Hoyt, Sandia National Laboratories, Materials & Process Modeling, Albuquerque, NM 87122 USA

Tuesday AM
March 16, 2004

Room: 202A
Location: Charlotte Convention Center

Session Chair: TBA

8:30 AM Invited

Phase Field Modeling of Electrodeposition: Jonathan E. Guyer¹; William J. Boettinger¹; James A. Warren¹; Geoffrey B. McFadden²; ¹NIST, Metall. Div., 100 Bureau Dr., Gaithersburg, MD 20899 USA; ²NIST, Math. & Computational Scis. Div., 100 Bureau Dr., Gaithersburg, MD 20899 USA

We examine the kinetic behavior of a phase field model of the electrochemical interface in one dimension. We have previously shown that the equilibrium properties of this model (surface energy, surface charge, and differential capacitance) bear stronger resemblance to experimental measurements than to the predictions of existing sharp-interface models. For electrodeposition and electrodisolution conditions, using a single set of governing equations, we demonstrate ohmic conduction in the electrode and ionic conduction in the electrolyte. We find that, despite making simple, linear dynamic postulates, we obtain the nonlinear relationship between current and overpotential predicted by the classical "Butler-Volmer" equation and observed in electrochemical experiments. The charge distribution in the interfacial double layer is affected by the passage of current and, at sufficiently high currents, we find that the diffusion limited deposition of a more noble cation leads to alloy deposition with less noble species.

9:00 AM Invited

Influence of Mobile Dislocations on Phase Separation in Binary Alloys: Mikko Haataja¹; Francois Leonard²; ¹Princeton Materials Institute, Bowen Hall, 70 Prospect Ave., Princeton, NJ 08544 USA; ²Sandia National Laboratories, Livermore, CA 94551 USA

In this talk we address the role of mobile dislocations on the phase separation process of a binary alloy by employing a phase-field model, which explicitly incorporates the coupled dynamics of the composition and dislocation fields. In our approach, the kinetics of the local

composition and dislocation density are coupled through their elastic fields. We show both analytically and numerically that mobile dislocations modify the standard spinodal decomposition process, and lead to several regimes of growth. Depending on the dislocation mobility and observation time, the phase separation may be accelerated, decelerated or unaffected by mobile dislocations. At intermediate times, the dislocations segregate to interfaces, and their limited mobility creates a drag on the interfaces which decelerates the phase separation process. For any finite dislocation mobility, however, we show that the domain growth rate asymptotically becomes independent of the dislocation mobility, and is faster than the dislocation-free growth rate.

9:30 AM

A Phase-Field Model for θ' Precipitation in Al-Cu Alloys: *S. Y. Hu*¹; *D. J. Seol*¹; *C. Wolverton*²; *J. Murray*³; *H. Weiland*³; *Z. K. Liu*¹; *L. Q. Chen*¹; ¹Pennsylvania State University, Dept. of Matls. Sci. & Engrg. & the Matls. Rsch. Inst., Univ. Park, 106 Steidle Bldg., State College, PA 16802 USA; ²Ford Research Laboratory, MD3028/SRL, Dearborn, MI 48121-2053 USA; ³Alcoa Technical Center, 100 Tech. Dr., Alcoa Ctr., PA 15069 USA

A phase-field model of θ' (Al₂Cu) precipitation is developed by linking it to thermodynamic and kinetic databases for Al-Cu alloys. To describe the θ' precipitation, four field variables are employed, i.e. composition field describing Cu composition and three artificial fields describing three orientation variants of θ' precipitates. The chemical free energies of matrix phase (solid solution) and θ' phase from thermodynamic databases are directly used as the input to the phase-field model. The interface energy and interface mobility anisotropy as well as the elastic energy contribution are taken into account. We studied the growth of a single θ' precipitate in one, two and three dimensions. It is shown that the both interface-controlled and diffusion-controlled transformations can be modeled. The effect of interface energy and interface mobility anisotropy and the elastic energy contribution on the morphology and growth rate of θ' precipitates is studied using two- and three-dimensional simulations.

9:50 AM

Computational Simulation of θ' Precipitation During Stress Aging of Al-Cu Alloys: *D. J. Seol*¹; *S. Y. Hu*¹; *C. Wolverton*²; *J. Murray*³; *H. Weiland*³; *Z. K. Liu*¹; *L.-Q. Chen*¹; ¹Pennsylvania State University, Matls. Sci. & Engrg., Univ. Park, PA 16802 USA; ²Ford Research Laboratory, MD3028/SRL, Dearborn, MI 48121-2053 USA; ³Alcoa Technical Center, 100 Tech. Dr., Alcoa Ctr., PA 15069 USA

Stress aging is a combined thermal treatment in which an elastic stress is applied during aging of materials. The directionality of the applied stress during the aging of age-hardenable Al-Cu alloys is known to be responsible for the oriented distribution of θ' (Al₂Cu) precipitates, which strongly affects their mechanical properties. In this study we use a phase-field model to describe θ' precipitation under applied stress. The thermodynamic and kinetic parameters of the phase-field model have been obtained from databases for Al-Cu alloys with additional input from first-principles calculations. Four field variables are used, i.e. composition field, $c(x,t)$, describing Cu composition and three artificial fields, $\eta_i(x,t)$ ($i=1,2,3$), describing three orientation variants of θ' precipitates. We have simulated the effect of applied stress on the evolution of the θ' precipitates in the nucleation, growth, and coarsening stages, and analyzed the volume fraction and distribution of differently oriented θ' precipitates with respect to the applied stress at various aging temperatures. The threshold value of the applied stress that must be exceeded for the oriented alignment of precipitates are determined.

10:10 AM Break

10:20 AM Invited

Stability of Layered Phases in Thin Films: *Perry H. Leo*¹; ¹University of Minnesota, Aeros. Engrg., 107 Akerman Hall, 110 Union St. SE, Minneapolis, MN 55455 USA

The microstructural evolution of a layered, binary thin film is investigated by using a Cahn-Hilliard type equation. Evolution is triggered by elastic fields, which arise from composition dependence of the lattice parameter (compositional self-strain) and applied fields. Computations show that, depending on system parameters, the layered structure can persist through the evolution (one-dimensional evolution), or it can break down by a morphological instability at the interfaces between layers. We map the different behavior as a function of the elastic parameters of the system, and we discuss how an elastic substrate may be used to control the system's evolution.

10:50 AM Invited

Cyclical Phase Transformations and Dynamic Equilibrium in Mechanical Alloying: *William C. Johnson*¹; *Jong K. Lee*²; ¹Univer-

sity of Virginia, Dept. Matls. Sci. & Engrg., PO Box 400745, Charlottesville, VA 22904-4745 USA; ²Michigan Technological University, Dept. Matls. Sci. & Engrg., Houghton, MI 49931 USA

A mixture of equilibrium and nonequilibrium phases are often synthesized during mechanical attrition (MA). In some cases, the phase fraction becomes constant after a certain time and a steady-state (dynamic equilibrium) is reached. In other systems, or for different milling power, cyclical transformations are observed in which the phase fractions continue to vary with time in a quasi-periodic manner. Using energy balance equations, we derive sets of coupled ordinary differential equations which describe the evolution of the system during MA. We obtain analytic approximations to the equations near steady-state conditions and show that the number of steady-state solutions and their stability can change with milling power (bifurcations). The analytic approximations are compared with numerical solutions illustrating the conditions for which cyclical phase transformation is realized. This work is supported by the Department of Energy.

11:20 AM

Phase Transformations and Microstructure Evolutions Near Free Surfaces and in Thin Films: Phase Field Microelasticity Modeling: *Yongmei M. Jin*¹; *Yu U. Wang*¹; *Armen G. Khachaturyan*¹; ¹Rutgers University, Ceram. & Matls. Engrg., 607 Taylor Rd., Piscataway, NJ 08854 USA

The elastic strain generated by the coherent phase transformations plays critical role in the microstructure evolutions. This elastic strain is significantly modified by the image forces near free surfaces and in thin films. Phase transformations and microstructure evolutions near free surfaces and in thin films are considered by using computer simulations to investigate the different behaviors from that in bulk crystals. The simulation model, which is based on the recent advances of the Phase Field Microelasticity approach, numerically solves the exact elasticity equation for a heterogeneous multi-phase multi-domain system with free surfaces. No ad hoc assumptions are made on the morphology of microstructures along the evolution path. Various examples are considered, including multi-variant martensitic transformations in FeNi and AuCd alloys. It is shown that the microstructures near free surfaces and in thin films are affected by the crystallography and epitaxy of the films. The effects of image forces are discussed.

11:40 AM

Phase Field Microelasticity Modeling of Surface Roughening and Island Formation in Heteroepitaxial Films: *Yu U. Wang*¹; *Yongmei M. Jin*¹; *Armen G. Khachaturyan*¹; ¹Rutgers University, Ceram. & Matls. Engrg., 607 Taylor Rd., Piscataway, NJ 08854 USA

The stress relaxations in heteroepitaxial films are investigated by using computer simulations. Two main mechanisms, surface roughening and dislocations, are considered. To address this problem, a Phase Field Microelasticity approach has been used to simulate the processes of surface roughening and dislocation dynamics in a deposited film driven by the relaxation of the epitaxial stress. The model is based on a numerical solution of the exact elasticity equation for a heteroepitaxial system with arbitrary surfaces. No ad hoc assumptions are made on the morphology of roughening along the evolution path that leads to the formation of multi-island configuration. The nonlinear diffusional evolution of the grooved film surface driven by the strain energy relaxation is investigated. The simulation shows that an initial small random roughening of a deposited flat film develops to form a quasi-periodical array of islands. The surface morphology simultaneously grows and coarsens. The fully coarsened morphology exhibits a dominant wavelength that is significantly greater than the one that follows from the linear analysis of initial instability. The equilibrium morphology corresponding to a periodic array of islands is reached through self-assembling independent of the initial fluctuations of the surface profile. Phase Field Microelasticity approach has been also used to study a motion of threading dislocation and operation of Frank-Read source in epitaxial films. The effect of image forces generated on the free surface on dislocation motions is consistently taken into account.

Cost-Affordable Titanium Symposium Dedicated to Prof. Harvey Flower: Titanium Economics

Sponsored by: Structural Materials Division, SMD-Titanium Committee

Program Organizers: M. Ashraf Imam, Naval Research Laboratory, Washington, DC 20375-5343 USA; Derek J. Fray, University of Cambridge, Department of Materials Science and Metallurgy, Cambridge CB2 3Q2 UK; F. H. (Sam) Froes, University of Idaho, Institute of Materials and Advanced Processes, Moscow, ID 83844-3026 USA

Tuesday AM Room: 206B
March 16, 2004 Location: Charlotte Convention Center

Session Chair: M. Ashraf Imam, Naval Research Laboratory, Washington, DC 20375-5343 USA

8:30 AM

Near Net Shape Production Of Titanium: *J. C. Withers*¹; R. Storm¹; R. O. Loutfy¹; ¹MER Corporation, Tucson, AZ 85706 USA

Near net shape fabrication using rapid prototyping, also called solid free form fabrication, has grown into a mature manufacturing process for a variety of materials including titanium. Titanium powder is fed into a molten pool that is manipulated by 3D computer-aided processing to build fully dense components in complex geometries including receding angles, passages and blind holes without the necessity of tooling or operator attendance. Energy sources to melt the feed powder or wire into the molten pool have included lasers of various types, electron beams and plasma processes. The plasma transferred arc achieves over 90% power efficiency and powder utilization in contrast to less than one-third for lasers and is not restricted by reflectivity problems associated with lasers. A plasma transferred arc solid free form fabrication system capable of producing components up to five meters has been used to near net shape produce titanium components in several alloy systems. The strength properties of the as produced titanium is typically 30% above wrought and heat treatments can further enhance strengths. A four component feed system permits producing select alloy compositions as well as functionally grading compositions. Examples include grading the titanium composition, as well as grading titanium to other alloy systems such as steels and aluminum. Composites are also produced by feeding particulate with the titanium, which has provided excellent wear resistance, as well as reduced coefficient of friction. Processing information, example components and properties will be discussed.

9:00 AM

Development of Low Cost Titanium Alloy Sheets for Automotive Exhaust Applications: *Yoji Kosaka*¹; Stephen P. Fox¹; Kurt Faller²; Steven H. Reichman²; ¹TIMET, Henderson Tech. Lab., PO Box 2128, Henderson, NV 89009 USA; ²TIMET, TIMET Auto., 900 Hemlock Rd., Morgantown, PA 19543 USA

The application of titanium sheets to the exhaust system of automobiles and motorcycles has been growing in recent years. A weight reduction of exhaust system is a primary purpose of the use of titanium. More than 40% of weight saving was realized using titanium to replace stainless steel. Although titanium is attractive to exhaust applications, oxidation resistance and softening of titanium at elevated temperature limit the use of titanium to parts exposed to relatively low temperatures. Low cost manufacturing is a key factor to reduce material cost to be accepted for automotive applications. Electron beam cold hearth melting has an important role to decrease an overall production cost. In the present work, alloy development was performed to achieve improved environmental and mechanical properties over CP titanium sheets. Properties of the sheets will be introduced and discussed.

9:30 AM

Low Cost Processes for Automotive Titanium Materials: *Yoji Kosaka*¹; Kurt Faller²; Stephen P. Fox¹; Steven H. Reichman²; Daniel J. Tilly³; ¹TIMET, Henderson Tech. Lab., PO Box 2128, Henderson, NV 89009 USA; ²TIMET, TIMET Auto., 900 Hemlock Rd., Morgantown, PA 19543 USA; ³TIMET, Vallejo Plant, 403 Ryder St., Vallejo, CA 94590 USA

Automotive application has been a prime target of emerging markets for titanium and its alloys for last two decades. Alloy development work was one of the major activities performed primarily by titanium manufacturers aiming the reduction of formulation cost with a maximized use of recycles or less expensive raw materials. TIMETAL

LCB is one of good examples of alloys specifically designed for automotive applications. However, the reduction of the formulation cost alone will not be sufficient to reduce overall manufacturing cost of titanium parts for vehicles. In melting of titanium alloys, electron beam cold hearth melting is recognized as a versatile tool for the production of titanium and its alloys. A significant cost reduction is expected by combining effective operations with low cost alloys. This paper will introduce and discuss several examples that were aimed at automotive applications.

10:00 AM

Torch Efficiency in Plasma Arc Cold Hearth Melting: *Yuan Pang*¹; Chengming Wang²; Frank Spadafora³; Hao Dong¹; Kuang-O (Oscar) Yu³; Daniel L. Winterscheidt⁴; ¹Concurrent Technologies Corporation, Product & Proc. Analysis, 425 Sixth Ave., Regional Enterprise Tower, 28th Floor, Pittsburgh, PA 15219-1819 USA; ²The Procter & Gamble Company, Sharon Woods Tech. Ctr., 11450 Grooms Rd., SWTC Box C-21, GR-CNE72, Cincinnati, OH 45242 USA; ³RMI Titanium Company, R&D, 1000 Warren Ave., Niles, OH 44446-0269 USA; ⁴Concurrent Technologies Corporation, Mfg. Programs, 100 CTC Dr., Johnstown, PA 15904-1935 USA

During plasma arc cold hearth melting (PAM), multiple torches are used in the production of titanium ingots. Each torch generates a helium plasma jet, which transports heat to the titanium. If the amount of heat reaching the ingot is inadequate, a defect such as cold shuts can form on the surface that must be removed prior to forging. To cast PAM ingots of sufficient quality that no surface removal is necessary, an optimal combination of torch parameters must be considered for maximum thermal efficiency. This paper summarizes the experimental and computational results to illustrate the relationship between torch efficiency and parameters. Discussion is focused on experimentally measured power to the torch and numerically calculated energy to the metal using thermocouple data. The ratio of the prediction to the measurement yields estimated torch efficiency. How the present work will enhance a predictive model for ingot surface finish improvement is also addressed.

10:30 AM

Blended Elemental Powder Metallurgy Approach to Produce Gamma Titanium Aluminide and Composite Ti-6Al-4V/TiAl/Ti-6Al-4V Structures: *V. S. Moxson*¹; V. A. Duz¹; J. S. Montgomery²; F. H. (Sam) Froes³; F. Sun³; ¹ADMA Products, Inc., 8180 Boyle Pkwy., Twinsburg, OH 44087 USA; ²Army Research Laboratory, Aberdeen Proving Ground, MA 21005-5066 USA; ³University of Idaho, Inst. for Matls. & Adv. Proc. (IMAP), McClure Hall, Rm. 437, Moscow, ID 83844-3026 USA

Cost effective method of production of both chunky and flat components for potential military and terrestrial applications using a Blended Elemental (BE) powder metallurgy (P/M) approach will be discussed. This will include Gamma Titanium Aluminide and Ti-6Al-4V/TiAl/Ti-6Al-4V monolithic composites produced by innovative ADMATAL-23 processes. Detailed studies of the microstructures and interfaces developed in sintering and high temperature deformation will be presented.

Dislocations: Dislocation Structures and Patterning

Sponsored by: ASM International: Materials Science Critical Technology Sector, Electronic, Magnetic & Photonic Materials Division, Materials Processing & Manufacturing Division, Structural Materials Division, EMPMD/SMD-Chemistry & Physics of Materials Committee, MPMD-Computational Materials Science & Engineering-(Jt. ASM-MSCTS)

Program Organizers: Elizabeth A. Holm, Sandia National Laboratories, Albuquerque, NM 87185-1411 USA; Richard A. LeSar, Los Alamos National Laboratory, Theoretical Division, Los Alamos, NM 87545 USA; Yunzhi Wang, The Ohio State University, Department of Materials Science and Engineering, Columbus, OH 43210 USA

Tuesday AM Room: 201A
March 16, 2004 Location: Charlotte Convention Center

Session Chair: TBA

8:30 AM Invited

Dislocation-Based Multiscale Modeling of Plasticity: *L. Kubin*¹; B. Devincere¹; T. Hoc²; ¹LEM, CNRS-ONERA, 29 Av. de la Division Leclerc, BP 72, 92322 Chatillon, Cedex France; ²Ecole Centrale Paris,

Lab. MSSMat, Grande Voie des Vignes, 92295 Chatenay-Malabry, Cedex France

By combining 3-D mesoscopic modeling, simulations and continuum modeling, it is now possible to construct multiscale models for crystal plasticity which have a predictive value in the absence of adjustable parameters. The application presented deals with fcc crystals, where the basic mechanisms governing plastic flow are dislocation interactions and cross-slip. These mechanisms are incorporated into a dislocation-based model for the evolution of the stored dislocation density in each slip system, in which the relevant material parameters are deduced from simulations at various scales. The three-stage stress strain curves of fcc single crystals in monotonic deformation are fully recovered by inserting this constitutive formulation into a Finite Element code for the polycrystal, which accounts for the lattice rotation during plastic deformation. It appears that, in some situations to be discussed, it is more important to properly account for elementary dislocation mechanisms than to attempt describing patterning phenomena.

9:05 AM

Determination of Deformation Inhomogeneity in Polycrystalline Ni Under Uniaxial Tension With 3D X-Ray Microscope: Judy W. Pang¹; Rozaliya Barabash¹; Wenjun Liu¹; Gene E. Ice¹; ¹Oak Ridge National Laboratory, Metals & Ceram., PO Box 2008, MS 6118, Oak Ridge, TN 37831-6118 USA

Generation of deformation substructures has significant effects on materials development processes such as recrystallization. These substructures are caused by deformation inhomogeneities due to grain-to-grain interactions. Measurement of misorientations introduced due to the formation of substructures is essential to understand deformation mechanisms. In this paper, evolution of lattice rotations within sub-micron volume elements of neighboring grains in a polycrystalline Ni samples was studied by 3D x-ray microscope as a function of plastic strain using polychromatic Laue technique. Each individual grain exhibits its own rotation pattern due to grain-to-grain interactions. Variation in rotation as a function of depth was also found for all the grains measured. The Laue patterns were analyzed using strain gradient plasticity theory to deduce the possible dislocation activities. Different slip systems were activated within the same grain as depth increases.

9:25 AM

Observations and Modeling of Dislocation Structures in a Crept High Volume Fraction Superalloy: Shuwei Ma¹; Bhaskar S. Majumdar¹; ¹New Mexico Tech, Matls. & Metallurg. Engrg. Dept., 801 Leroy Place, Socorro, NM 87801 USA

Creep experiments were performed on a polycrystalline superalloy, CM-247 LC, that contained a high volume fraction (~65%) of gamma-prime phase. TEM observations revealed that while the gamma-prime phase remained largely undeformed, the narrow gamma channels were occupied by a network of dislocations. These are geometrically necessary dislocations that are accumulated in the narrow gamma channels to maintain strain compatibility. We then used the concept of Ashby's plastic strain gradient to estimate the density of geometrically necessary dislocations, where the plastic strain gradient was calculated using a finite element method. The resultant elastic strains in the phases, for grains whose [001] direction lay along the tensile axis of the specimen, are compared with strain data obtained from neutron diffraction measurements through insitu creep tests at the Los Alamos Neutron Science Center. In addition, the observed dislocation densities are compared with theoretical predictions based on the concept of geometrically necessary dislocations. Together, these results are anticipated to provide additional quantitative insight on microstructural instability and rafting that accompany creep of superalloys at high temperatures.

9:45 AM

Dislocation Structures and Their Relationship to {111} Microbands and Microtwins in Spherical and Plane Impact Deformed Nickel: Erika Vanessa Esquivel¹; L. E. Murr¹; ¹University of Texas, Metallurg. & Matls. Engrg., 500 W. Univ. Ave., El Paso, TX 79968 USA

Microstructural studies involving transmission electron microscopy (TEM) have revealed that there is a transition of dislocation structures when the geometry of the impact changes from plane, as in plane-wave shock loading, to spherical, as in impact cratering. Plane-wave shock loaded nickel has revealed microtwins, 0.02 micrometers thick lying on {111} traces, above a critical shock twinning pressure of ~30 GPa while microbands, also lying on traces of {111} with an approximate 2° misorientation, have been observed below craters produced by spherical projectile impact at pressures well above the plane-wave shock critical twinning pressure. In contrast to microtwins the microbands are roughly 10 times thicker (~0.2 micrometers). Both

types of impact have produced dislocation cells whose diameter increases with decreasing pressure, and the transition from the microband to microtwin formation is therefore believed to be strongly dependent on the shock wave geometry where a planar shock wave would promote microtwinning, while a spherical shock wave would facilitate cross-slip and allow microbanding. There is also a transition from microbands to dislocation cell structures in the spherical-shock impacted nickel and TEM observations have documented the details of the elongation of dislocation walls coincident with {111} to more randomly and equiaxed cell structures, and related dense dislocation wall structures.

10:05 AM Break

10:20 AM Invited

Atomistic Calculations of Shock Induced Phase Transformations and Microstructure Evolution: M. I. Baskes¹; S. G. Srinivasan¹; G. J. Wagner²; ¹Los Alamos National Laboratory, Los Alamos, NM USA; ²Sandia National Laboratory, Albuquerque, NM 87185 USA

Shock waves in materials produce a number of interesting phenomena including microstructure evolution and phase transformations. Underlying these phenomena is the generation and motion of dislocations. This presentation will discuss recent calculations of these phenomena at the atomic level using an embedded atom method (EAM) potential. Since the phenomena of interest involve subtle energy differences in the phase transformations and generation of grain boundaries, a realistic many-body EAM potential that represents the properties of nickel, a typical fcc material is used. Using a standard flyer-plate geometry of a single crystal, many calculations at different sample sizes and initial impact velocity were performed. In general the following observations about shock induced phase transformations at very high strain rates and stress may be made: (1) the fcc crystal transforms to a bcc-like crystal structure behind the shock wave; (2) after a period of time, the bcc structure transforms to domains of a highly faulted fcc structure; (3) the domains grow and form twin boundaries at the domain intersection; and (4) when the reflected shock wave traverses this material, the system mostly transforms back to polycrystalline fcc material containing a number of faults. These general observations appear to be insensitive to the in-plane sample periodicity, but the details, e.g., fault or twin spacing, appears to scale with this imposed periodicity. The role of dislocations in these processes will be discussed.

10:55 AM

Characterization of Dislocation Structure Evolution in High Purity Aluminum During Small Strain Compression: Pankaj B. Trivedi¹; David P. Field¹; ¹Washington State University, Sch. of Mech. & Matls. Engrg., PO Box 642920, Pullman, WA 99164-2920 USA

Dislocation structure evolution during small strain deformation (up to 20%) using channel die was studied in high purity aluminum. Samples from a coarse grained polycrystal and a single crystal were deformed to 15% and 20% strain and dislocation structure characterization was done using EBSD. Disorientation angle from an average orientation was studied for all the samples as a function of area and deformation. The distribution of disorientation angle as a function of area of the scanned region provides quantitative information about the average local variation of the crystal orientation and indirectly relates to dislocation cell structure. In an undeformed sample the distribution of disorientation angle remained same with increasing area. With increase in deformation in the case of single crystal the distribution of disorientation angle changed from mostly 2.1-2.2° at 0% deformation to 1.55-1.56° at 15% deformation and 2.05-2.2° after 20% deformation. In the case of single crystal after 15% deformation the distribution of disorientation angle remained same with increasing area but after 20% deformation the distribution increased from predominantly 1.55° to 2.1-2.2°. Dislocation cell size remained the same after 15% and 20% deformation for the single crystal whereas for the polycrystal there was a slight increase in cell size with increasing deformation. Grain orientation is shown to have an effect on the evolution of dislocation structure, and it appears that grains with lower Taylor factors form a well-organized cell structure.

11:15 AM

Dislocation Configurations and Long Range Internal Stresses: M. E. Kassner¹; M. A. Delos-Reyes¹; L. E. Levine²; ¹Oregon State University, Mech. Engrg., Rogers Hall, Corvallis, OR 97331 USA; ²NIST, Gaithersburg, MD 20899 USA

The concept of "long range internal stresses" (LRIS) is often utilized to explain various aspects of the mechanical behavior of materials, including cyclic deformation. These internal stresses are usually associated with the heterogeneous microstructure. Convergent beam

electron diffraction (CBED) and dislocation dipole separation measurements have been performed that indicate an absence of measurable LRIS. "X-ray diffraction line profile analysis" (XRD, LPA), specifically, the interpretation of asymmetry in strain broadened Bragg diffraction peaks, has been extensively used to support LRIS. The asymmetry literature has been surveyed and re-analyzed in this work. It is found that there is more than one reasonable explanation for x-ray line asymmetry, and that LRIS is not required for asymmetry to be present. Computer modeling of x-ray diffraction from dislocated crystals is being performed using standard and novel approaches, and these will be discussed.

11:35 AM

Static Recovery of Pure Copper at Low Homologous Temperature: *Chen-Ming Kuo*¹; Chin-Sheng Lin²; ¹I-Shou University, Dept. of Mech. Engrg., 1, Sec. 1, Hsueh-Cheng Rd., Kaohsiung 84008 Taiwan; ²I-Shou University, Dept. of Matls. Sci. & Engrg., 1, Sec. 1, Hsueh-Cheng Rd., Kaohsiung 84008 Taiwan

Static recovery experiments of pure copper near room temperature have been conducted via TEM, DSC, micro-hardness, and extensometer to explore the time and temperature dependent relationships. By using different applied strain rate, dislocation density is generated differently within specimens. Since strain hardening and dynamic recovery occur simultaneously during loading stage, for the lower applied strain rate specimens, dislocation density is less because it allows more time for dynamic recovery to occur. During static recovery experiments, the recovery phenomenon is more significantly as time and temperature increase, because dislocation annihilation occurs more considerably. Time dependent static recovery could be observed and measures by TEM, DSC, micro-hardness, and extensometer. On the other hand, extensometer measurement reveals temperature dependent static recovery. As temperature increases, static recovered strain is more appreciably. Activation energy of static recovery of pure copper is 53.29 kJ/mole measured by extensometer.

Electrochemical Measurements and Processing of Materials: Electrodeposition Processes

Sponsored by: Extraction & Processing Division, Materials Processing & Manufacturing Division, EPD-Aqueous Processing Committee, EPD-Process Fundamentals Committee, EPD-Pyrometallurgy Committee, ASM/MSCTS-Thermodynamics & Phase Equilibria Committee, EPD-Waste Treatment & Minimization Committee

Program Organizers: Uday B. Pal, Boston University, Department of Manufacturing Engineering, Brookline, MA 02446 USA; Akram M. Alfanzazi, University of British Columbia, Department of Metal & Materials Engineering, Vancouver, BC V6T 1Z4 Canada; Adam C. Powell, Massachusetts Institute of Technology, Department of Materials Science and Engineering, Cambridge, MA 02139-4307 USA

Tuesday AM Room: 212A
March 16, 2004 Location: Charlotte Convention Center

Session Chairs: Uday B. Pal, Boston University, Dept. of Mfg. Engrg., Brookline, MA 02446 USA; Seshadri Seetharaman, Royal Institute of Technology, Matls. Sci. & Engrg., Stockholm 10044 Sweden

8:30 AM Invited

Electrodeposition as a Means of Processing Semi-Conductor Industry Waste Streams Containing Copper: Ran Ding¹; *James William Evans*¹; Fiona M. Doyle¹; ¹University of California, Dept. of Matls. Sci. & Engrg., Berkeley, CA 94720 USA

Copper is becoming the material of choice for metallization in the semi-conductor industry. When the copper is electrodeposited, deposited by electroless techniques or subjected to CMP then aqueous waste streams containing copper and other species are created. The paper results from an ongoing investigation aimed at removing copper and recovering the water by a combination of ion-exchange and electrodeposition. The focus of the paper is on copper electrodeposition and a companion paper in another session reports on ion-exchange. Studies at the rotating disc electrode have shown that additives commonly occurring in these streams (e.g. citric acid and glycine) can inhibit electrodeposition. Results from cells using porous or particulate electrode for copper removal are described.

9:00 AM Invited

The Role of Surfactant Catalysts in Superfilling and Supersmoothing: *Daniel Josell*¹; Thomas P. Moffat¹; Daniel Wheeler¹; ¹NIST, Metall. Div., 100 Bureau Dr., MS 8555, Gaithersburg, MD 20899 USA

I will discuss the role of surfactant catalysts in achieving superconformal, bottom-up filling of fine features during metal electrodeposition. I will discuss the particular cases of copper and silver superfill for fabrication of sub-100 nm metallizations, including the electrolyte-additive systems and how the impact of the catalyst is quantified through the Curvature Enhanced Accelerator Coverage (CEAC) mechanism; this mechanism accounts for local change of catalyst coverage associated with change of the area upon which the catalyst is adsorbed during metal deposition on nonplanar surfaces. I will also discuss the significance of these results for stabilization of surfaces against concentration gradient induced roughening, as expressed in the CEAC brightening mechanism.

9:30 AM Invited

Electrolytic Preparation of Carbon Nanotubes in Molten Salts: *Derek J. Fray*¹; Carsten Schwandt¹; George Z. Chen¹; ¹University of Cambridge, Matls. Sci. & Metall., Pembroke St., Cambridge CB2 3QZ UK

It has been found that by making graphite the cathode in a bath of molten salts and applying a potential such that the salt decomposes, it is possible to create carbon nanotubes and nanoparticles. The production of carbon nanotubes in molten NaCl and LiCl was investigated as a function of applied voltage, current density and time of electrolysis. It was concluded that the mechanism for the production of nanotubes was due to the intercalation of the discharged cation into the graphite structure and this was investigated electrochemically. By careful control of the conditions it was possible to maximise the production of nanotubes. If a salt with a lower decomposition potential than the alkali chloride, such as SnCl₂, is introduced, the carbon nanotubes are full of tin. Possible applications for these materials are described.

10:00 AM Break

10:30 AM

A Substructurally Composite Chromium Electrochemical Coating Formed on a Canned-Food Steel Sheet from a Low-Concentration Solution of Hexavalent Chromium-Based Compounds: *Oleg B. Girin*¹; Igor D. Zakharov²; Volodymyr I. Ovcharenko¹; ¹Ukrainian State University of Chemical Engineering, Dept. of Matls. Sci., Pr. Gagarina, 8, Dnipropetrovsk 49005 Ukraine; ²Polimet Research and Technology Center, Lab. of Protective Coatings, Vul. Mandrykivska, 169, Dnipropetrovsk 49049 Ukraine

A composition of a low-concentration chrome-plating solution has been developed with the 100?20 g/l chromium anhydride content, and the process parameters have been tested for applying 0.01-0.03 mkm thick protective electrochemical coatings on canned-food steel sheet. The properties of the coatings have been studied taking into consideration their structure. There have been determined the optimum variants of applying on the steel sheet of composites comprised of chromium layers featuring different substructure anisotropy levels in the axial components of their texture that have improved protective properties. Based on the usage of the phenomenon of electrochemical deposition of metals via a supercooled metal liquid there has been developed a process of depositing on the canned-food steel sheet of a super-thin substructurally composite electrochemical chromium coating from a low-concentration solution based on hexavalent chromium compounds. This research project is financed by the Intergovernmental organization "Science & Technology Center in Ukraine", Project Agreement No.2520.

11:00 AM

The Nucleation and Growth Mechanism in Tin Electrodeposition: *Shixue Wen*¹; Sasha Omanovic²; Jerzy A. Szpunar¹; ¹McGill University, Dept. of Mining, Metals & Matls. Engrg., 3610 Univ., Montreal, Quebec H3A 2B2 Canada; ²McGill University, Dept. of Chem. Engrg., 3610 Univ., Montreal, Quebec H3A 2B2 Canada

Tin electrodeposition from sulfuric acid electrolytes was studied on a glassy carbon substrate by electrochemical techniques. The morphology of tin nuclei and crystallites was observed by scanning electron microscopy (SEM). The analysis of chronoamperometric experiments reveals that at the nucleation and growth mechanism of tin is dependent on the applied cathodic potentials. At a cathodic potential of -495mV, 3D progressive nucleation mechanism occurs. As potentials become more negative, the nucleation mechanism changes to 3D instantaneous nucleation mechanism. At potentials between -575mV and -680mV, 3D instantaneous nucleation and growth mechanism takes place. As potentials become more negative than -680mV, due to hy-

drogen evolution, the mechanism lies in between 3D progressive and 3D instantaneous nucleation mechanism. The morphology of tin nuclei varies with applied potentials. At the potential of -510mV, tetragonal nuclei and crystallites are dominant. As the potentials become more negative, clusters of tin needles increase. At -700mV, all grains are tin needles.

11:30 AM

The Texture and Microstructure of Electrodeposited Tin Coatings: *Shixue Wen*¹; Jerzy A. Szipunari¹; ¹McGill University, Dept. of Mining, Metals & Matls. Engrg., Montreal, Quebec H3A 2B2 Canada

Due to its good corrosion resistance, non-toxicity and solderability, tin is widely used in food packaging and electronic industries. Tin electrodeposition on copper substrates using stannous sulfate and sulfuric acid with organic additives was studied under different current densities and temperature. The macrotexture of the tin deposits was measured using an x-ray texture goniometer. The orientation imaging microscopy (OIM) was used to measure the orientations of individual grains along with the microstructure. It was found that tin coating with a (001) fiber texture can be produced by electrodeposition. If the coating is thin, tin grains grow epitaxially on copper substrate that has a strong (001) [-100] texture and the coating has a (001) fibre texture. In a thick coating, the texture was changed to (110) fibre texture, which indicates that at a thick deposit, the texture becomes independent of substrate orientation. The grain size distribution and misorientation between grains were also measured. It is demonstrated that the OIM is an ideal and powerful tool to measure texture at different depth of the coating and to analyze texture nucleation and growth.

General Abstracts: Session IV

Sponsored by: TMS

Program Organizers: Adrian C. Deneys, Praxair, Inc., Tarrytown, NY 10591-6717 USA; John J. Chen, University of Auckland, Department of Chemical & Materials Engineering, Auckland 00160 New Zealand; Eric M. Taleff, University of Texas, Mechanical Engineering Department, Austin, TX 78712-1063 USA

Tuesday AM
March 16, 2004

Room: 204
Location: Charlotte Convention Center

Session Chair: Ian Bainbridge, University of Queensland, CRC for Cast Metals Mfg., St. Lucia, QLD 4072 Australia

8:30 AM

An Investigation of the Factors Affecting the Occurrence of the Grain Boundary Serration: *Soo Woo Nam*¹; *Ki Jae Kim*¹; ¹Korea Advanced Institute of Science and Technology, Matl. Sci. & Engrg., 373-1 Guseong-dong, Yuseong-gu, Daejeon 305-701 Korea

The purpose of this study is to investigate the role of factors affecting the occurrence of the grain boundary serration in an AISI 316 stainless steel. Among the factors affecting the grain boundary serration, the effects of the grain boundary characteristics have been investigated by using the EBSD (Electron BackScattered Diffraction) technique. And the effect of the chemical compositions on the grain boundary serration has also been investigated. And the relationship between grain boundary serration and heat treatment conditions has been investigated. It might be expected that in case of high temperature aging conditions, the grain boundary serration does not occur, since the grain growth is easily occurred so that the total energy of the system is reduced, on the other hands, in case of low temperature aging conditions, the grain boundary serration is occurred to reduce the total energy of the system, since the grain growth is not easily occurred.

8:55 AM

Determination of Composition Dependent Ternary Interdiffusion Coefficients From a Single Diffusion Couple: *Abby Lee Elliott*¹; *Yongho Sohn*¹; ¹University of Central Florida, Advd. Matls. Procg. & Analysis Ctr., Box 162455, 4000 Central Florida Blvd., Orlando, FL 32816-2455 USA

A new method to extract composition dependent ternary interdiffusion coefficient from a single diffusion couple experiment is proposed. The calculations involve direct determination of interdiffusion fluxes from experimental concentration profiles and local integration and differentiation of Onsager's formalism. This new method was applied to concentration profiles obtained from selected diffusion couple experiments in the Cu-Ni-Al and Fe-Ni-Al systems. The calculated interdiffusion coefficients are consistent with those determined from

Boltzmann-Matano analysis and alternate analyses based on the concept of average ternary interdiffusion coefficients and square-root diffusivity. The concentration and interdiffusion flux profiles calculated from the ternary interdiffusion coefficients are in good agreement with the experimental profiles including those exhibiting uphill diffusion and zero-flux planes.

9:20 AM

Phase Transformation in a Nucleation and Growth Reaction: Application of Moments Methods: *David T. Wu*¹; *Lin Zhuo*¹; ¹Yale University, Dept. of Mech. Engrg., PO Box 208284, New Haven, CT 06520-8284 USA

For a first-order phase transformation, the expression for the isothermal fraction transformed as a function of time is well known for site saturation and for constant nucleation and growth conditions. In realistic situations such as in casting, however, the temperature can depend both on time and position; hence the nucleation and growth rates will be more general functions. While the Johnson-Mehl-Avrami-Kolmogorov formalism gives an expression for fraction transformed when the nucleation and growth rates are arbitrary, its direct evaluation is rather inefficient. We show that using the method of moments and the quadrature method of moments, the fraction transformed can be evaluated very efficiently.

9:45 AM Break

9:55 AM

Microstructural Evolution of AA-6061 Subjected to Severe Plastic Deformation: *Yogesh Bhambri*¹; *Shravan K. Indrakanti*¹; *Raghavan Srinivasan*¹; *Prabir Chaudhury*²; *Qingyou Han*³; ¹Wright State University, Dept. of Mech. & Matls. Engrg., 209 Russ Engrg. Ctr., 3640 Col. Glenn Hwy., Dayton, OH 45435 USA; ²Intercontinental Manufacturing Company USA; ³Oak Ridge National Laboratory, Metals & Ceram., Oak Ridge, TN USA

Grain size in metals can be substantially refined in bulk, to the sub-micrometer level, by imposing high strains through processes such as equal channel angular extrusion (ECAE). In this study, samples of annealed AA6061 with square cross-sections of 1/2-inch, 2-inch and 4-inch were subjected to severe plastic deformation at room temperature by ECAE by multiple passes through dies with channel angles of 120°, 90° and 105°, respectively. The changes in microstructure including grain refinement for these samples were studied. Additionally in this alloy, fracture and redistribution of precipitates were studied for samples processed through 120° die. Initial results indicate the precipitates break during the deformation process and are more uniformly distributed. The deformed specimens were heated to study the stability of microstructure to retain the fine grain size up to the forging temperatures for this alloy. The results show that after a small increase in size, grains remain stable in 300-400°C temperature range.

10:20 AM

Process Maps for Controlling Microstructure in Laser Deposited Ti-6Al-4V: *Srikanth Bontha*¹; *Nathan W. Klingbeil*¹; ¹Wright State University, Mech. & Matls. Engrg. Dept., 209 Russ Engrg. Ctr., 3640 Colonel Glenn Hwy., Dayton, OH 45435 USA

Laser deposition of titanium alloys is under consideration for aerospace applications, which require the consistent control of microstructure and resulting mechanical properties. The focus of this work is the development of process maps relating solidification cooling rate and thermal gradient (the key parameters controlling microstructure) to laser deposition process variables (e.g., laser power and velocity). General results are presented based on the Rosenthal solution for a moving point heat source traversing both thin-wall (2-D) and bulky (3-D) deposits, while the effects of finite geometry, temperature-dependent properties and latent heat of transformation are investigated through thermal finite element modeling. In addition, results are plotted on solidification maps for predicting grain morphology in laser deposited Ti-6Al-4V. The results of this work suggest that changes in process variables could result in a grading of the microstructure throughout the depth of the deposit, and that the size-scale of the laser deposition process is important.

10:45 AM

Directional Recrystallization of Polycrystalline Nickel Cold-Rolled at 77K: *H. Chang*¹; *Ian Baker*¹; ¹Dartmouth College, Thayer Sch. of Engrg., Hanover, NH 03755 USA

Polycrystalline nickel sheets cold rolled to 90% thickness reduction after cooling in liquid nitrogen were statically annealed at 350°C for 30 mins and then directionally annealed at 1000°C. A large temperature gradient of 1000° C/cm ahead of the hot zone was used during directional annealing and a wide range of hot zone velocities were examined. The as-rolled and directionally recrystallized microstruc-

tures were characterized using differentially scanning calorimetry, optical microscopy and electron back-scattered patterns from a scanning electron microscope. The results are contrasted with directional recrystallization of nickel rolled to 90% reduction at room temperature. Research supported by NSF grants DMI 9976509 and DMI 0217565.

11:10 AM

Experimental Observation of the Type III Boundary in a Two-Phase Ternary Diffusion Couple: *Abby Lee Elliott*¹; *Yongho Sohn*¹; ¹University of Central Florida, Advd. Matls. Procg. & Analysis Ctr., Box 162455, 4000 Central Florida Blvd., Orlando, FL 32816-2455 USA

Morral has classified the Type 0, I, and II phase boundaries according to the number of phases that are added/subtracted upon crossing the phase boundary during the annealing of two-phase diffusion couple. This classification system is based on a binary system and has been annexed to include the Type III and IV phase boundaries that may occur in a ternary system due to the existence of a three phase region on a ternary isotherm. The movement of each phase boundary type is discussed in terms of degrees of freedom via Gibbs phase rule. Type I and Type II boundaries have been frequently observed experimentally. In this work, experimental observation of the Type III ternary boundary is presented for an Fe-Ni-Al isothermal diffusion couple. This observation establishes the existence of a ternary phase boundary joining a two-phase region with a single-phase region, each region sharing no common phase. The diffusion path for this couple exits out the vertex of the equilibrium tie triangle resulting in a boundary joining a two-phase region with a single phase region.

Hume Rothery Symposium: Structure and Diffusional Growth Mechanisms of Irrational Interphase Boundaries: Session III

Sponsored by: Electronic, Magnetic & Photonic Materials Division, Structural Materials Division, EMPMD/SMD-Alloy Phases Committee, MPMD-Phase Transformation Committee-(Jt. ASM-MSCTS)

Program Organizer: H. I. Aaronson, Carnegie Mellon University, Department of Materials Science and Engineering, Pittsburgh, PA 15213 USA

Tuesday AM Room: 208A
March 16, 2004 Location: Charlotte Convention Center

Session Chair: W. T. Reynolds, Virginia Tech, Matls. Sci. Engrg. Dept., Blacksburg, VA 24061 USA

8:30 AM Invited

Atomistic Calculations of Incoherent Zr/ZrN Interfaces: *Michael I. Baskes*¹; *S. G. Srinivasan*¹; *Sven P. Rudin*²; ¹Los Alamos National Laboratory, Matls. Sci. & Tech. Div., MS G755, Los Alamos, NM 87545 USA; ²Los Alamos National Laboratory, Theoretical Div., MS B221, Los Alamos, NM 87545 USA

The interfaces between Zr and ZrN (B1) have been studied at the atomistic level using the Modified Embedded Atom Method (MEAM) interaction model. Literature MEAM potentials have been used for Zr and N and the Zr/N potential was developed using both experimental data and generalized gradient approximation calculations. The interfaces studied have the orientation relationship $[450]_{\text{Zr}} // [-10-1]_{\text{ZrN}}$ and $(002)_{\text{Zr}} // (-131)_{\text{ZrN}}$ as seen in experiment. A major complication in the calculations is that the Zr (hcp) contains ~ 25 at% N and the ZrN (B1) is not stoichiometric, containing ~45 at% N. Atomistic models have been created at these compositions for various interface planes. The relaxed interface structure and energy have been calculated and are compared to what is observed in experiment. The calculations will be used to explain the distribution of interface planes seen in experiment. This work was supported by the Office of Basic Energy Sciences, U.S. DOE.

9:10 AM Invited

EAM Modelling of Edge-to-Edge Interfaces: *W. T. Reynolds*¹; *Diana Farkas*¹; ¹Virginia Polytechnic Institute and State University, Matls. Sci. & Engrg. Dept., Holden Hall, MC 0237, Blacksburg, VA 24061 USA

The energies of high-index interphase boundaries are explored using molecular statics simulations with embedded atom potentials. We investigate planar boundaries between the α_2 and gamma phases in the Ti-Al system. The class of boundaries considered have a high-index boundary orientation, the orientation relationship between the

α_2 and gamma phases also is high-index, and a set of planes from each phase meet edge-to-edge at the boundary plane. The boundaries are commensurate in one direction and coincide with a moire plane given by the so-called "Ag" diffraction condition. The boundaries are not structurally singular, but they are energetically stable and do not appear to dissociate into other low energy configurations. Misfit compensating defects are not observed; misfit in directions other than the commensurate one appears to be distributed uniformly in the boundary. The relative boundary energy is evaluated as a function of the orientation relationship between the two phases.

9:50 AM Invited

Edge Matching at Grain Boundaries and the Five Macroscopic Degrees of Freedom: *Anthony D. Rollett*¹; ¹Carnegie Mellon University, Matls. Sci. & Engrg., 4315 Wean Hall, 5000 Forbes Ave., Pittsburgh, PA 15213 USA

The application of plane-edge-matching to grain boundaries is investigated. Phase transformations with heterophase interfaces exhibit edge matching only occur for certain specific orientation relationships. By contrast, there are many misorientations and boundary normals for which low index planes can satisfy edge matching criteria at homophase grain boundaries. Some simple mathematics that describes the situation for grain boundaries is described and its potential impact on grain boundary properties is explored.

10:30 AM Break

10:45 AM Invited

Observations of Interfaces Linking Proeutectoid Ferrite Allotriomorphs and Parent Austenite Crystals in an Fe-C-Mn-Si Alloy: *Malcolm G. Hall*¹; *Hui Guo*²; *Gary R. Purdy*²; ¹University of Birmingham, Dept. of Metall. & Matls., Edgbaston, Birmingham B15 2TT UK; ²McMaster University, Dept. of Matls. Sci. & Engrg., 1280 Main St. W., Hamilton, Ontario L8S 4L7 Canada

An alloy of Fe-0.38%C-3.0%Mn-1.85%Si was first homogenized, quenched, austenitized at 950°C to yield a grain size of approximately 50 microns and isothermally transformed at 650°C, a temperature at which Mn partition is expected (and observed). The specimens were then held for 12 hours at 350°C to stabilize the austenite immediately adjacent to the grain boundary ferrite precipitates, and prepared as thin foils for electron microscopic observation. We report on four aspects of the transformation products: the precipitate morphology; the orientation relationships among the ferrite and austenite crystals; the distribution of manganese in the region of the ferrite-austenite interfaces; and structural aspects of the ferrite-austenite interfaces. In most cases, growth of ferrite was apparently confined to one side of the precipitate, the other side remaining relatively planar and coincident with the original austenite grain boundary position.

11:25 AM Invited

Structure of Irrational Interphase Boundary Formed During Precipitation: *Tadashi Furuhashi*¹; *Tadashi Maki*¹; ¹Kyoto University, Dept. of Matls. Sci. & Engrg., Yoshida-honmachi, Sakyo-ku, Kyoto, Kyoto 606-8501 Japan

Three kinds of irrational interphase boundaries formed in precipitation are discussed; (1) (partly) coherent boundary satisfying a rational (or near-rational) orientation relationship with an irrational macroscopic habit plane, (2) boundary with an irrational orientation relationship and habit plane and (3) incoherent boundary with a rational orientation relationship and habit plane with large difference in atomic density between precipitate and matrix phases. A geometrical model (near coincidence site model) can explain the crystallographic feature of those boundaries reasonably well. Some problems in the extension of modeling are also pointed out.

Internal Stresses and Thermo-Mechanical Behavior in Multi-Component Materials Systems: Creep and Plasticity I

Sponsored by: Electronic, Magnetic & Photonic Materials Division, Structural Materials Division, EMPMD-Electronic Packaging and Interconnection Materials Committee, EMPMD-Thin Films & Interfaces Committee, SMD-Composite Materials Committee-Jt. ASM-MSCTS

Program Organizers: Indranath Dutta, Naval Postgraduate School, Department of Mechanical Engineering, Monterey, CA 93943 USA; Bhaskar S. Majumdar, New Mexico Tech, Department of Materials Science and Engineering, Socorro, NM 87801 USA; Mark A.M. Bourke, Los Alamos National Laboratory, Neutron Science Center, Los Alamos, NM 87545 USA; Darrel R. Frear, Motorola, Tempe, AZ 85284 USA; John E. Sanchez, Advanced Micro Devices, Sunnyvale, CA 94088 USA

Tuesday AM
March 16, 2004

Room: 209B
Location: Charlotte Convention Center

Session Chairs: J. W. Morris, University of California, Berkeley, CA 94720 USA; J. C.M. Li, University of Rochester, Rochester, NY 14627 USA

8:30 AM Keynote

Creep Resistance of the Directionally Solidified Ceramic Eutectic of Al₂O₃/C-ZrO₂ (Y₂O₃): Experiments and Models: *A. S. Argon*¹; *J. Yi*¹; ¹Massachusetts Institute of Technology, Cambridge, MA 02139 USA

The creep resistance of the directionally solidified (DS) ceramic eutectic of Al₂O₃/c-ZrO₂ (Y₂O₃) was studied in the temperature range of 1200-1520°C both experimentally and by mechanistic dislocation models. The topologically continuous majority phase of Al₂O₃, has a nearly perfect growth texture in the [0001] direction and encapsulates the minority c-ZrO₂ phase in a variety of morphologies. This encapsulated minority phase too has a <112> growth texture regardless of morphology. The two phases are separated by close to coherent and well structured interfaces. Upon growth, there are substantial levels of internal thermal misfit stresses present between the alumina and cubic-zirconia phases in the GPa range. The creep of the eutectic in its growth direction exhibits an initial transient that is attributed to stress relaxation in the c-ZrO₂ phase that also substantially eliminates the initial thermal misfit stresses. The steady state creep shows many of the same characteristics of creep in sapphire single crystals with c-axis orientation. The creep strain rate of the eutectic has stress exponents in the range of 4.5-5.0 and a temperature dependence suggesting a rate mechanism governed by oxygen ion diffusion in the Al₂O₃. Finite element analysis of stress distribution in the two phases under an applied tensile stress parallel to the axis, and a detailed dislocation model of the creep rate indicate that much of the nano-scale encapsulated c-ZrO₂ must be too small to deform by dislocation creep so that the major contribution to the recorded creep strain is derived from the diffusion-controlled climb of pyramidal edge dislocations in the Al₂O₃ phase. The evidence suggests that these climbing dislocations must repeatedly circumvent the nano-scale cubic zirconia domains acting as dispersoids. This is equivalent to the presence of a sinusoidally varying set of internal stresses through which the climbing dislocations must negotiate, resulting in the stress exponents larger than 3. The creep model is in very good agreement with the experiments, and demonstrates that the DS eutectics have creep resistance superior to that of sapphire. Work supported by AFOSR under Grant F49620-99-1-0276.

9:00 AM Invited

Development of Internal Stresses in Thermal Barrier Coatings as a Result of Bond Coat Plasticity and Phase Transformations: *Kevin J. Hemker*¹; ¹Johns Hopkins University, Depts. of Mech. Engrg. & Matls. Sci. & Engrg., 3400 N. Charles St., Baltimore, MD 21218 USA

Thermal barrier coatings (TBCs) are widely used in commercial gas turbine engines to insulate the metallic components from the hot gas stream. TBCs are complex multilayered systems with a ceramic top coat, thermally grown oxide (TGO), intermetallic bond coat and superalloy substrate. The top coat is the insulator, the TGO slows oxidation, the bond coat provides a reservoir for the formation of the TGO and improved adherence and the substrate carries the loads. During thermal cycling, the interaction of these chemically and mechanically disparate layers results in the development of internal stresses, which

lead to eventual spallation of the topcoat. Differences in thermal expansion, continued growth of the TGO, and deformation of the bond coat have been shown to result in interface rumpling. The elevated temperature bond coat properties have been measured with microsample tensile and creep testing. Moreover, observations of a martensitic transformation in the platinum modified nickel aluminide bond coat have been associated with inter-diffusion between the bond coat and the underlying superalloy substrate. TEM observations, differential thermal analysis and in situ X-ray diffraction experiments have been used to characterize the martensitic transformation, and results of FE simulations that incorporate these measurements point to the importance of this transformation in the generation of residual stresses in the TBC during thermal cycling.

9:25 AM

Measurement and Modeling of Internal Stresses During Creep of a Polycrystalline Superalloy: *S. Ma*¹; *P. Rangaswamy*²; *Don W. Brown*²; *B. S. Majumdar*¹; ¹New Mexico Tech, Matls. Dept., Socorro, NM 87801 USA; ²Los Alamos National Laboratory, Los Alamos, NM USA

The high temperature deformation and failure of superalloys containing a high volume fraction of gamma-prime phase are significantly influenced by the evolution of internal stresses in the gamma and gamma-prime phases. During most of the creep life, deformation is confined to the very narrow gamma channels. We have conducted insitu creep experiments using a pulsed neutron source to monitor elastic micro-strain evolution in a high-volume fraction superalloy. FEM modeling showed that the redistribution of stress of the individual phases are only modest, in slight disagreement with previous work. Neutron diffraction data showed that in the tertiary stage there was a rapid build up of stresses in the gamma-prime phase, but a substantial reduction in those of the gamma phase. We believe that the observed stress redistribution is caused by geometrically necessary dislocations, which induce stresses unaccounted for in FEM modeling. Results are complemented with TEM observations of interface dislocations.

9:50 AM

In Situ Oxide Growth Strains in a FeCrAlY Alloy: *Geoffrey A. Swift*¹; *Ersan Ustundag*¹; *Jonathan D. Almer*²; *David R. Clarke*³; ¹California Institute of Technology, Dept. of Matls. Sci., Pasadena, CA 91125 USA; ²Argonne National Laboratory, Advd. Photon Source, Argonne, IL 60439 USA; ³University of California, Matls. Dept., Santa Barbara, CA 93106 USA

FeCrAlY alloys are known to form a uniform, adherent scale of γ -Al₂O₃ when oxidized and are good model systems for the investigation of residual stresses due to the formation of thermally grown oxide (TGO) layers in a typical thermal barrier coating (TBC) system. In this study, high energy synchrotron X-rays were used to monitor in situ the oxidation of a cylindrical FeCrAlY sample around 800-1200°C. Oxide growth strains at constant temperature were seen to be small suggesting dynamic stress relaxation via creep. Upon cooling to room temperature, however, large compressive stresses (several GPa) were generated in the oxide due to the thermal contraction mismatch between the oxide and the FeCrAlY substrate. Strain data obtained from XRD will be compared to luminescence measurements and predictions of several models.

10:15 AM Invited

Constitutive Equations for High Temperature Deformation: *J. W. Morris*¹; *H. G. Song*¹; *W. H. Bang*²; *K. H. Oh*¹; ¹University of California, Dept. of Matls. Sci. & Engrg., Berkeley, CA 94720 USA; ²Seoul National University, Dept. of Matls. Sci. & Engrg., Seoul Korea

It has long been recognized that steady-state creep rates in the multiphase materials used for solders and other purposes are well described by simple constitutive equations of the Dorn (power law) or, alternatively, Garafalo (hyperbolic sign) forms. Recent research has led to the useful result that these same equations often provide equally good predictions of shear strength and stress relaxation rates at elevated temperature. The present talk will discuss data taken from work by a number of investigators that documents the similarity of the stress-strain rate-temperature relations that pertain to steady state creep, shear strength and stress relaxation and will show specifically how the parameters that appear in the Dorn equation govern the rate and temperature dependence of the shear strength and the rate of stress relaxation.

10:40 AM Invited

Stress Induced Phase Transformation in Uranium-Niobium Shape Memory Alloys: *Donald W. Brown*¹; *Mark A.M. Bourke*¹; *Robert D. Field*¹; *W. Larry Hults*¹; *David F. Teter*¹; *Daniel J. Thoma*¹; ¹Los Alamos National Laboratory, Matls. Sci. & Tech. Div., MS-H805, Bldg. 622, TA-53, Los Alamos, NM 87545 USA

TUESDAY AM

The shape memory effect (SME) has been reported in the uranium-niobium alloy system in the region of the phase diagram surrounding U_{6.5}wt%Nb. In this regime, the material may have either an α'' monoclinic (U₆Nb) or γ 0 tetragonal structure (U₇Nb) and is two phase near 6.5wt% niobium. In-situ neutron diffraction loading studies have revealed a stress induced phase transformation in U₇wt%Nb from the γ 0 to the α'' structure. The volume fraction of the γ 0 phase decreased nearly linearly with plastic strain from 100% initially to ~25% after 3% plastic deformation and some reversion is observed on release. The initial stress state of the stress induced α'' grains will be discussed as well as the load sharing between the two phases.

11:05 AM

Investigation of Silicon Nitride Creep Using Neutron Diffraction: *Geoffrey A. Swift*¹; Ersan Ustundag¹; Bjørn Clausen²; Mark A.M. Bourke²; ¹California Institute of Technology, Dept. of Matls. Sci., Pasadena, CA 91125 USA; ²Los Alamos National Laboratory, Neutron Sci. Ctr., Los Alamos, NM 87545 USA

The deep penetration of neutrons in most materials allows in-situ studies in extreme environments. This advantage of neutron diffraction was utilized in the investigation of strain and texture evolution during high temperature deformation of in-situ reinforced Si₃N₄. Tension experiments were performed in the 1100°C-1400°C temperature regime using the new SMARTS diffractometer at Los Alamos Neutron Science Center. In particular, the hkl-dependent strains were measured and the results were compared to literature data. Evidence of grain boundary sliding was observed when diffraction data (i.e., elastic lattice strains) were compared to macroscopic strains collected by an extensometer.

International Laterite Nickel Symposium - 2004: Pressure Acid Leaching

Sponsored by: Extraction & Processing Division, EPD-Aqueous Processing Committee, EPD-Copper, Nickel, Cobalt Committee, EPD-Process Fundamentals Committee, EPD-Process Mineralogy Committee, EPD-Pyrometallurgy Committee, EPD-Waste Treatment & Minimization Committee

Program Organizer: William P. Imrie, Bechtel Corporation, Mining and Metals, Englewood, CO 80111 USA

Tuesday AM Room: 217B/C
March 16, 2004 Location: Charlotte Convention Center

Session Chairs: Roman M. Berezowsky, Dynatec Corporation, Metallurgical Technologies, Ft. Saskatchewan, Alberta T8L 4K7 Canada; Ian G. Skepper, BHP-Billiton, Ravensthorpe Nickel Project, Perth, WA 6850 Australia

8:30 AM

Co-Treatment of Limonitic Laterites and Sulfur-Bearing Materials as an Alternative to the HPAL Process: *Cesar Joe Ferron*¹; Larry Seeley¹; Christopher A. Fleming¹; ¹SGS Lakefield Research Limited, Metallurg. Tech., 185 Concession St., PO Box 4300, Lakefield, Ontario K0L 2H0 Canada

High pressure acid leaching (HPAL) is used in four plants to treat limonitic laterites. Two major operating cost components are sulphuric acid and energy to heat the feed slurry. As an alternative to acid injection and steam heating, in-situ generation of sulphuric acid and heat from oxidation of sulfur-bearing materials blended with laterites, has been investigated at laboratory scale. Tested sulfur sources have included elemental sulfur, pyrrhotite, and nickel sulphide concentrates. At proper blend ratios, all sulfur sources generated sufficient acid to provide efficient dissolution of nickel and cobalt from both the host sulphide and the laterite. Significant improvement to the economics result from the use of sulfur sources containing valuable by-products, such as nickel/cobalt and/or precious metals (gold and PGMs). In the latter case, the HPAL must be operated under Platsol conditions (i.e. with the addition of 5-10 g/L of chloride) to ensure efficient recovery of the precious metals. Application examples for this concept are presented with discussion of its implication on autoclave design and downstream processes to recover values from leach solution.

8:55 AM

Effect of Process Water on High Pressure Sulphuric Acid Leaching of Laterite Ores: *Debbie Marshall*¹; Mohamed Buarzaiga¹; ¹Noranda Inc./Falconbridge Ltd., Metallurg. Tech. Grp., Falconbridge Tech. Ctr., Falconbridge, Ontario P0M 1S0 Canada

Process water is an important consideration in the development of a nickel lateritic project. Depending on the location of the ore body, sufficient fresh water may not be available and it may be necessary to use seawater (or saline groundwater) for ore preparation. This introduces various species, which have major effects on materials of construction and leaching chemistry. This paper summarizes batch testwork completed at the Falconbridge Technology Center. The leaching behavior of eleven different laterite ore samples was compared using seawater and fresh water. Each ore type was leached under identical conditions in both freshwater and seawater and the leaching chemistry was compared. The batch scale results were confirmed in a continuous pilot plant and leach kinetics for the two systems compared.

9:20 AM

Effect of Eh in the High Pressure Acid Leaching of Nickel Laterite Ores: *Julian Andrew Johnson*¹; Barry Ian Whittington¹; Robbie Gordon McDonald¹; David Michael Muir¹; ¹AJ Parker CRC for Hydrometallurgy, CSIRO Minerals, PO Box 90, Bentley, WA 6892 Australia

The effect of changing redox potential on the high temperature sulfuric acid leaching of Western Australian dry-land nickel laterite ores has been investigated. In particular, the effect of added reductant (sulfur, sodium sulfite) or oxidant (potassium chromate) on Eh, leaching kinetics, metal extractions, acid utilisation and leach residues has been determined. Three separate ores - nontronitic ores from Murrin Murrin and Bulong, and limonitic ore from Cawse - were used in the study. Sulfur addition varied from 0 to 7.8 kg/t ore. The total acid loading was kept constant at 430 kg/t (Murrin Murrin ore) and 330 kg/t (Cawse ore), whilst acid loading for Bulong ore was varied according to the presence of either reductant or oxidant. The extraction of both nickel and cobalt from limonite ore remained unaffected when small amounts of sulfur were added, but addition of even small amounts of reductant to nontronitic ore decreased both nickel and cobalt extraction. Increased manganese and iron dissolution were observed as the levels of reductant increased, accompanied by a decrease in chromium dissolution. As the iron dissolution increased, free acidity decreased, with a subsequent decrease in nickel extraction. In contrast, addition of oxidant lead to reduced iron and manganese dissolution and slower extraction of nickel and cobalt.

9:45 AM

Solution Chemistry and Reactor Modeling of the PAL Process: Successes and Challenges: *Vladimiro G. Papangelakis*¹; Haixia Liu¹; Dmitri Rubisov¹; ¹University of Toronto, Chem. Engrg. & Applied Chmst., 200 College St., Toronto, Ontario M5S 3E5 Canada

During the past five years, chemical modelling work at the University of Toronto has elucidated the role of soluble magnesium in the PAL process. It explained why feeds rich in magnesium, and other divalent metals, require more than the stoichiometric requirements for acid dissolution to ensure comparable Ni/Co leaching performance as with feeds low in magnesium and other divalents. This understanding has allowed the calculation of acid additions on a less empirical basis. Optimizing acid additions confers savings in neutralization costs, ensures high productivity and minimises unnecessary corrosion problems. Some theoretical concepts of chemical modelling of electrolyte systems at high temperature and software issues in support of this work are presented. Autoclave modelling based on better chemistry understanding and comparisons with pilot-plant data is also made. Finally, in spite of the above successes significant challenges lie ahead in theoretical data gaps and instrumentation, which are discussed.

10:10 AM Break

10:20 AM

Effect of Magnesium Content on Sulphuric Acid Consumption During High Pressure Acid Leaching of Laterite Ores: *Debbie Marshall*¹; Mohamed Buarzaiga¹; ¹Noranda Inc./Falconbridge Ltd., Metallurg. Tech. Grp., Falconbridge Tech. Ctr., Falconbridge, Ontario P0M 1S0 Canada

Nickel and cobalt in lateritic ores can be extracted by either a hydrometallurgical or a pyrometallurgical route. The high-iron limonitic fraction of a deposit is best processed hydrometallurgically while the magnesium-rich transitional and saprolitic fractions are more suited for pyrometallurgical processing. During hydrometallurgical processing, it may be attractive, for economic reasons, to blend the limonitic component with transitional and saprolitic ores, which contain higher nickel levels. However, blending increases the concentration of magnesium in the feed, leading to increased acid demands. The decision on how much ore to process then becomes an economic one. Ore samples with different magnesium contents were prepared for the leach test program by blending limonitic and transitional ores. The ore samples were slurried in seawater and tested in the Falconbridge Hydrometallurgical Pilot Plant. As expected, acid consumption increased with in-

creasing magnesium content of the ore. For target extractions of 95% nickel and 92% cobalt, the required residual free acid concentration increased from 30 g/L at 1.7% magnesium to 50 g/L at 2.7% magnesium. When the magnesium content was raised to 3.8% and 4.6% in subsequent pilot plant testing, the final free acid requirements did not increase beyond what was observed at 2.7% magnesium. Thus, the cut-off ore composition to maximize nickel units and minimize acid requirements is between 1.7- 2.7% magnesium.

10:45 AM

A Conceptual Design of PAL Using Tube-in-Tube Heat Exchangers: *Don J. Donaldson*¹; ¹APTEC, 2314 Quail Point Cir., Medford, OR 97504 USA

The PAL process for recovering nickel from laterite ore requires large volumes of thick abrasive slurry to be raised to high temperature (255°C +) and pressure (50 atm.+). Flow diagrams of the process typically result in facilities that have serious operating and reliability problems. Most of the problems can be attributed to using multiple pump stations to raise the slurry to autoclave pressure, large amounts of flash and live injection steam to heat the slurry to autoclave temperature, and several steps of flash cooling to lower the temperature and pressure of the abrasive autoclave slurry down to atmospheric conditions. It is proposed that operating and reliability problems of PAL facilities can be mitigated by using Tube-in-tube heat exchangers and "float type" positive displacement pumps. The subject paper describes an innovative application of such equipment in the facility design of the PAL process.

11:10 AM

Improvements to the Acid Pressure Leaching of Nickel Laterite Ores: *Walter Curlook*¹; ¹University of Toronto, Matls. Sci. & Engrg., 184 College St., Toronto, ON M5S 3E4 Canada

An improved process of hydrometallurgical treatment of laterite ores of the limonitic type for the recovery of nickel and cobalt using sulphuric acid has been developed and patented. The major improvement is brought about by recycling a significant portion of the "mother liquor" emanating from the pressure leaching reaction back to the feed preparation stage thereby substituting for all or at least a major proportion of the fresh water or de-ionized water that must be added. Concomitantly with the major savings in fresh water or de-ionized water requirements, a significant reduction in new sulphuric acid requirements is effected along with a corresponding saving in limestone and lime required for subsequent neutralizations.

11:35 AM

Cosimulation in Hydromet Process Design: *Lanre Oshinowo*¹; *Ida Fok*¹; ¹Hatch Associates Ltd., 2800 Speakman Dr., Mississauga, Ontario L6X 4R8 Canada

Computational Fluid Dynamics (CFD) is used in complement with process modelling at HATCH to achieve a superior level of confidence in the process design of hydromet process plants. The use of these tools to evaluate designs through virtual prototyping reduces the risks associated with making design decisions. This paper highlights the development of a cosimulation strategy at Hatch for the seamless integration of process modeling software addressing different scales (process time and space): flowsheet level models and equipment level models. With cosimulation, the process design engineers can improve design accuracy, troubleshoot and optimize the performance, and influence decisions impacting equipment operation by representing specific unit operations in the flowsheet model software with detailed CFD models. Specifically, this paper will focus on the co-simulation of a Ni/Co high-pressure acid leach (HPAL) process including heaters/heat exchangers and flash system, autoclave and quench/scrubber system. The knowledge developed can be transferable to other processes.

Lead-Free Solders and Processing Issues Relevant to Microelectronic Packaging: Mechanical Properties and Fatigue Behavior

Sponsored by: Electronic, Magnetic & Photonic Materials Division, EMPMD-Electronic Packaging and Interconnection Materials Committee

Program Organizers: Laura J. Turbini, University of Toronto, Center for Microelectronic Assembly & Packaging, Toronto, ON M5S 3E4 Canada; Srinivas Chada, Jabil Circuit, Inc., FAR Lab/Advanced Manufacturing Technology, St. Petersburg, FL 33716 USA; Sung K. Kang, IBM, T. J. Watson Research Center, Yorktown Heights, NY 10598 USA; Kwang-Lung Lin, National Cheng Kung University, Department of Materials Science and Engineering, Tainan 70101 Taiwan; Michael R. Notis, Lehigh University, Department of Materials Science and Engineering, Bethlehem, PA 18015 USA; Jin Yu, Korea Advanced Institute of Science and Technology, Center for Electronic Packaging Materials, Department of Materials Science & Engineering, Daejeon 305-701 Korea

Tuesday AM

March 16, 2004

Room: 219B

Location: Charlotte Convention Center

Session Chairs: James P. Lucas, Michigan State University, Dept. of Chem. Engrg. & Matls. Sci., E. Lansing, MI 48824-1226 USA; Kwang-Lung Lin, National Cheng Kung University, Dept. of Matls. Sci. & Engrg., Tainan 70101 Taiwan

8:30 AM Invited

Roles of Service and Material Parameters on TMF of Sn-Based Solder Joints: *H. Rhee*¹; *J. G. Lee*¹; *K. N. Subramanian*¹; ¹Michigan State University, Dept. of Chem. Engrg. & Matls. Sci., E. Lansing, MI 48824-1226 USA

Temperature extremes, differences in temperature, rates at which such temperature changes are imposed, and dwell times at the temperature extremes are service related parameters that can have significant effects on thermomechanical fatigue (TMF). Solder alloy, interfacial intermetallic layer and its thickness, and microstructural constituents within the solder joint, are material related parameters that contribute to TMF of a solder joint. This investigation examines the roles of these parameters and their relative importance on TMF by carrying out studies on Sn-based solder joints of realistic dimensions. Such studies include actual TMF cycling, and supporting studies under isothermal conditions. Work supported by the National Science Foundation under grant NSF DMR-0081796.

8:55 AM

The Interfacial Adhesion Strength of the Sn-9Zn-xAg Lead-Free Solders Wetted on Cu Substrate After Thermal Shock Testing: *Tao-Chih Chang*¹; ¹National Cheng Kung University, Dept. of Matls. Sci. & Engrg., 1 Ta-Hsueh Rd., Tainan 70101 Taiwan

In this study, the interfacial adhesion strength of the Sn-9Zn-xAg lead-free solders wetted on Cu substrate after thermal shock testing have been investigated by pull-off testing, scanning electron microscopy and energy dispersive spectrometry. The 63Sn-37Pb and Sn-3.5Ag solder alloys were tested for comparison. The Sn-3.5Ag solder alloy offers a more superior solder joint reliability than the others, the adhesion strength of the Sn-3.5Ag/Cu interface increases from 18.04 ± 1.03 to 21.75 ± 1.25 MPa after 5 times thermal shock. But it decrease slightly from 21.75 ± 1.25 to 18.47 ± 0.98 MPa with increasing the thermal shock times from 5 to 10. After 15 thermal shock testing, it increases again to 20.94 ± 1.12 MPa. The adhesion strength of the Sn-9Zn-xAg/Cu interface has a similar tendency to that of the Sn-3.5Ag/Cu interface. A maximum value of 14.60 ± 0.82 MPa is obtained for the Sn-9Zn-2.5Ag/Cu interface after 5 thermal shock testing. The 63Sn-37Pb solder alloy has a most inferior solder joint reliability in this test.

9:15 AM

Study of Pasty Zone and Latent Heat Release Mode for Sn-9Zn-xAg Lead-Free Solder Alloys: *Ying-Ling Tsai*¹; *Weng-Sing Hwang*¹; ¹National Cheng Kung University, Dept. of Matls. Sci. & Engrg., Tainan Taiwan

The pasty ranges and latent heat release modes of Sn-9Zn-xAg alloys, where x varies between 0.5 and 3.5, are measured in this study. The effects of alloy composition and cooling rate on the pasty range and latent heat release mode are also discussed. A Computer Aided-Cooling Curve Analysis (CA-CCA) technique is used to measure and

TUESDAY AM

calculate the pasty ranges and latent heat release modes for Sn-9Zn-xAg lead-free solder alloys. To comply with the requirements of CA-CCA, the experimental setup has to approach the heat transfer condition of a lumped system, where the alloy system is cooled down in a uniform fashion. Two thermocouples are inserted in a cylindrical crucible, where alloy is melted and subsequently cooled to solidify. The crucible is used with and without the wrappage of insulating material to obtain different cooling rates. The temperature readings show that the heat transfer condition in the experimental setup in this study indeed meets the requirement of a lumped system. The fraction of solid versus temperature relations; fs-T, for the various alloy compositions and cooling rates are then obtained from the temperature data analyzed by CA-CCA. The experimental results also shows that as silver content of the Sn-9Zn-xAg alloy increases, the pasty range also increases. As silver content is 0.5 wt%, silver has little effect on the microstructure, which is basically the Sn-9Zn eutectic phase. The fs-T relation is somewhat close to a vertical line. However, as silver content exceeds 1.5 wt%, the formation of intermetallic compound; Ag₃Zn₃, becomes obvious. It causes the alloy composition to deviate from the eutectic composition and leans towards the tin side of the Sn-Zn phase diagram. This in turn causes the content of primary tin phase to increase and that of zinc-tin eutectic phase to decrease. It reflects on the fs-T relation by two distinct vertical lines. One corresponds to the primary tin phase and the other to the eutectic phase. As silver content increases, the effects of the intermetallic compound formation become even more obvious. Cooling rate shows no significant effect on either pasty range or fs-T relation. However, smaller cooling rate results in lower solidus temperature as well as liquidus temperature.

9:35 AM

Effect of Cooling Rate on IMC and Mechanical Properties of Sn-Ag-Cu/Cu Pad: Sang Won Jeong¹; Jong Hoon Kim¹; Hyuck Mo Lee¹; ¹KAIST, Dept. of Matls. Sci. & Engrg., 373-1 Kusung-dong, Yusung-gu, Taejeon 305-701 Korea

Several solders of Sn-3.5Ag, Sn-3Ag-0.7Cu, Sn-3Ag-1.5Cu, Sn-3.9Ag-0.8Cu and Sn-6Ag-0.5Cu were cooled at different rates after reflow soldering on Cu pad above 250°C for 60s. Three different media of cooling were used to control cooling rates; water quenching, medium cooling on aluminum block and slow cooling in furnace. The resultant morphology of the interfacial intermetallic compound (IMC) of the samples was observed together with the lap shear strength of the joint measured. As content of Cu and Ag in solder alloys was increased, the thickness of the interfacial IMC increased and there was a change in phases of the IMC. With a slower cooling rate, the interfacial IMC became thicker and coarsened. At the same time, the lap shear joint showed lower shear strength and was fractured in a brittle mode between Cu₆Sn₅ and Cu₃Sn phases. The microstructural observation agreed well with mechanical properties and a variation in the fracture mode.

9:55 AM

Mechanical Properties of Near-Eutectic Sn-Ag-Cu Alloy Over a Wide Range of Temperatures and Strain Rates: Tia-Marje K. Korhonen¹; Pekka Turpeinen¹; Brian Bowman¹; Larry P. Lehman²; George H. Thiel³; Raymond C. Parkes³; Matt A. Korhonen¹; Donald W. Henderson³; Karl J. Puttlitz⁴; ¹Cornell University, Matls. Sci. & Engrg., 328T Bard Hall, Ithaca, NY 14853 USA; ²Binghamton University, Binghamton, NY 13902 USA; ³IBM Corporation, 1701 North St., Endicott, NY 13760 USA; ⁴IBM Corporation, Hopewell Junction, NY 12533 USA

Creep tests, constant strain rates tests, and stress relaxation tests were used to measure the deformation properties of Sn-Ag-Cu alloy in temperatures ranging from -40 to 125°C. The three testing methods complement each other, because the creep and constant strain rate tests give the steady state properties, while stress relaxation tests reflect the properties at constant structure. Several different strain rates were used, down to 10E-9. The measurements were done with dog-bone specimens that have a cross section of 1mm, which corresponds to a typical solder joint diameter in ball grid arrays. Cooling rates of the samples were selected to be comparable to ones used in BGA manufacturing. It was shown that the mechanical properties are very different from slowly cooled bulk solders. The strain rate sensitivity of the fast cooled samples was very low. The effect of temperature was also small, the activation energy was about 0.4 eV. Optical microscopy, SEM and electron back-scatter diffraction were used to study the microstructures of the test samples. The slower cooled samples had large Ag₃Sn platelets, but size of the platelets was significantly reduced with faster cooling rates. This was clearly reflected in the deformation behavior of the samples.

10:15 AM Break

10:25 AM Invited

Influence of Interfacial Intermetallic Compounds on Mechanical Properties of Thin Pb-Free Solder Joints: J. G. Lee¹; H. Rhee¹; J. P. Lucas¹; K. N. Subramanian¹; T. R. Bieler¹; ¹Michigan State University, Dept. of Chem. Engrg. & Matls. Sci., E. Lansing, MI 48824-1226 USA

Miniaturization of electronic packaging requires the same trends of the solder joints that electrically and mechanically connect components to particular substrates. As solder joints become thinner, concurrently, the extent of the substrate/solder interfacial intermetallic compound (IMC) layer increases in comparison to the overall solder volume of the joint. Moreover, as a result of isothermal or thermo-mechanical aging, the IMC layer can grow to such an extent that it may comprise 80-90% of the solder joint volume. Nanoindentation testing (NIT) will be used to investigate the mechanical properties of IMCs formed in thin (< 50 micron) solder joints. Various Sn-based eutectic and near-eutectic Pb-free solder alloys will be used. Creep studies will also be performed on as-reflow and aged solder joints to determine the influence of IMC layer thickness and evolving compositional change from predominately Cu₆Sn₅ to Cu₃Sn. This investigation reports on growth of the IMC layer in thin solder joints and the propensity of the IMC layer to affect subsequent mechanical properties.

10:50 AM

Advances in Producing Adaptive Lead-Free Solder Joints Via Shape-Memory Alloy Reinforcement of Solder Alloys: Deng Pan¹; W. Scott Horton¹; William Wright¹; Zhixiang Wang²; B. S. Majumdar²; Indranath Dutta¹; ¹Naval Postgraduate School, Mech. Engrg., 700 Dyer Rd., Monterey, CA 93943 USA; ²New Mexico Tech, Matls. Sci. & Engrg., Socorro, NM 87801 USA

Microelectronic solder joints are typically exposed to aggressive thermo-mechanical cycling (TMC) conditions during service. During TMC, strain localization occurs near solder/bond pad interfaces, where large inelastic shear strains accumulate, eventually causing low-cycle fatigue failure of the joint. In this study, a new methodology to mitigate the effects of strain localization within the joint are discussed, wherein the solder alloy is reinforced with Ni-Ti based shape memory alloy (SMA) powders are used to reinforce a Sn-4.7%Ag-1%Cu solder. Details of processing and characterization of the solder composite will be discussed, particularly with respect to the particle size and distribution, and interfacial structure and chemistry. Ball-shaped solder joints between copper rods simulating flip chip (FC) or ball-grid array (BGA) joints were tested in shear under thermal mechanical cycling conditions. The behavior of the composite is compared with that of unreinforced solder and solder reinforced by copper particles to elucidate the impact of the shape-memory effect on the overall joint behavior. Experiments on model single-fiber NiTi-solder composites to provide insight into the mechanics of deformation of smart solders are also reported.

11:10 AM

Comparison of 95.5Sn-3.8Ag-0.7Cu Solder Joint and Bulk Solder Properties: John H.L. Pang¹; ¹Nanyang Technological University, Sch. of Mech. & Production Engrg., 50 Nanyang Ave. 639798 Singapore

Mechanical properties for lead-free 95.5Sn-3.8Ag-0.7Cu solder joint and bulk solder will be presented. A soldered lap shear joint specimen was used for characterizing the microstructure and mechanical properties of the solder joint. The specimens were soldered using 95.5Sn-3.8Ag-0.7Cu solder sphere with no-clean flux on FR-4 substrates by solder reflow process. Three solder reflow peak temperatures at 235°C, 240°C and 250°C were investigated. The average solder joint shear force were 4.1N, 4.8N and 5.0N respectively. Shear tests were carried out at three temperatures (25°C, 75°C and 125°C) and at three constant strain rate (2.6 x 10E-2, 2.6 x 10E-3 and 2.6 x 10E-4) conditions. The stress strain properties in shear were converted to equivalent tensile stress strain values for comparison to tensile test results on 95.5Sn-3.8Ag-0.7Cu bulk solder. The apparent tensile modulus, yield stress and ultimate tensile stress will be presented as a function of temperature and strain rate.

11:30 AM

Analysis of Deformation and Damage in Solder Joints During Lap Shear Tests: E. S. Ege¹; X. Deng²; Y.-L. Shen¹; N. Chawla²; ¹University of New Mexico, Mech. Engrg., MSC01 1150, Albuquerque, NM 87131 USA; ²Arizona State University, Chem. & Matls. Engrg., Tempe, AZ 85287 USA

Thermomechanical testing of solder using the lap shear technique is commonly employed to quantify the shear stress-strain and fatigue

behavior. In this study the effects of geometric and material parameters on the monotonic and cyclic mechanical response are evaluated in detail using numerical finite element analyses. Lap shear experimental results are compared with the modeling. The commonly observed cracking in solder near, but not at, the interface between solder and intermetallic can be explained by the development of plastic flow pattern during cyclic loading. It is also found that the conventional method for determining the nominal shear strain in solder is prone to large errors. The solder joint carries a smaller strain than that based on the far-field value, as confirmed by experiments. This is largely due to the delayed transmission of deformation from the substrate to the solder before solder fully yields plastically. Thicker, shorter, and stiffer substrates are shown to generate more accurate results. Other implications to practical characterizations and evaluations of solder properties are discussed.

11:50 AM

Segregation and Coarsening Effects on Mechanical Properties in Aged Tin-Silver-Copper Solder Joints: *Iver Eric Anderson*¹; Joel L. Harringa²; Bruce A. Cook³; ¹Ames Laboratory (USDOE), Metal & Ceram. Scis. Prog., 222 Metals Dvlp. Bldg., Ames, IA 50011 USA; ²Ames Lab (USDOE), Metal & Ceram. Scis. Prog., 252 Spedding Hall, Ames, IA 50011 USA; ³Ames Lab (USDOE), Metal & Ceram. Scis. Prog., 47 Wilhelm Hall, Ames, IA 50011 USA

Since many new electronic assembly applications involve service at high temperature and stress levels a thorough investigation of promising Sn-Ag-Cu solder alloys is required to relate microstructural changes on high temperature aging to mechanical properties and fracture behavior. This effort has involved detailed characterization of solder joint microstructures, resistivity, and shear strength after isothermal aging at 150°C for time intervals out to 1,000 hrs. Elemental Cu substrates were joined with near eutectic Sn-Ag-Cu and Sn-Ag-Cu-X (X = Co, Fe) solder alloys for the study. Microanalytical electron probes were used to track phase coarsening and to determine the role of local segregation on embrittlement and partial debonding after extensive aging of joints, especially those lacking Co and Fe additions. Project funding received from Iowa State University Research Foundation with additional support from USDOE-BES through contract no.W-7405-Eng-82.

Magnesium Technology 2004: Wrought Magnesium Alloys II/Corrosion and Coatings

Sponsored by: Light Metals Division, LMD-Magnesium Committee
Program Organizer: Alan A. Luo, General Motors, Materials and Processes Laboratory, Warren, MI 48090-9055 USA

Tuesday AM
March 16, 2004

Room: 203B
Location: Charlotte Convention Center

Session Chairs: Xin Wu, Wayne State University, Detroit, MI 48202 USA; Eric Nyberg, Pacific Northwest National Laboratory, Richland, WA 99352 USA

8:30 AM

Infrared Processing of Magnesium Wrought Alloys: *Joe A. Horton*¹; Sean R. Agnew²; Craig A. Blue³; ¹Oak Ridge National Laboratory, Metals & Ceram. Div., Bldg. 4500S, MS6115, PO Box 2008, Oak Ridge, TN 37831-6115 USA; ²University of Virginia, Matls. Sci. & Engrg., 116 Engineer's Way, Charlottesville, VA 22904-4745 USA; ³Oak Ridge National Laboratory, Metals & Ceram. Div., Bldg. 4508, MS6083, PO Box 2008, Oak Ridge, TN 37831-6083 USA

It is of interest to produce magnesium wrought products more efficiently in order to make them more attractive for application. Previous studies have shown that heat treatments performed using radiant heating by plasma arc lamp can produce the same result in seconds as one hour anneals at 400°C in a convection furnace. The influence of infrared radiant heating on the deformation processing of magnesium will be presented. Metallurgical structure and mechanical property measurements are used to compare with traditional processing. (Research sponsored by the U.S. Dept. of Energy, Assistant Secretary for Energy Efficiency and Renewable Energy, Office of Transportation Technology, Office of Heavy Vehicle Technology, at Oak Ridge National Laboratory, operated by UT-Battelle, LLC, under contract DE-AC04-00OR22725.)

8:50 AM

Superplasticity in Fine-Grained Mg-Zn-Y-(Zr) Alloy Sheets In-Situ Reinforced by Icosahedral Quasicrystalline Particles: *D. H. Bae*¹; Y. Kim¹; D. S. Kim¹; I. J. Kim¹; ¹Yonsei University, Dept. Metallurg. Engrg., 134 Shinchondong Seodaemungu, Seoul 120-749 Korea

Superplastic deformation behavior of fine-grained Mg-rich Mg-Zn-Y-(Zr) alloy sheets, consisting of in-situ icosahedral quasicrystalline particles in the volume fraction up to 0.1, have been investigated in the temperature range of 300°C to 425°C (and constant strain-rate: 5x10⁻⁴s⁻¹ ~ 5x10⁻¹s⁻¹). Fine-grained microstructure of the alloys in the range of 2 to 6 micrometer has been developed via particle-induced dynamic recrystallization processes by conventional thermomechanical processes. The alloys provide large elongation to failure up to 600%, increasing with increasing temperature and decreasing strain-rate. A sigmoidal relationship between log(stress) and log(strain-rate) is observed for each test condition. In the superplastic deformation regime, grain mantle creep is believed to be controlled by dislocation glide and climb processes by evaluation stress exponent (~2) and activation energy (~115kJ/mol) in the creep equation. Interestingly, although the alloys contain large number of particles, they do not provide cavitation significantly during superplastic deformation due to relatively low interfacial energy between the icosahedral quasicrystalline particle and the matrix.

9:10 AM

Development of Wrought Mg Alloys Via Strip Casting: *Sung S. Park*¹; Jung G. Lee¹; Hak C. Lee¹; Kwang S. Shin²; Nack J. Kim¹; ¹POSTECH, Matls. Sci. & Engrg., San 31, Hyoja-dong, Nam-gu, Pohang, Kyungbuk Korea; ²Seoul National University, Sch. of Matls. Sci. & Engrg., Seoul Korea

Mg alloys are the lightest commercial structural alloys and have the excellent specific strength and stiffness. They also have high damping capacity and good fatigue resistance. These characteristics of Mg alloys have made them quite attractive for automotive applications. However, the majority of Mg alloys currently in use are cast products and only a limited number of Mg alloys is available as wrought products. The development of wrought Mg alloys, particularly sheet alloys, would greatly expand the application areas of Mg alloys. Up to now, direct chill (DC) casting has been the most important casting technique for producing rolling slabs and extrusion billets of Mg alloys. It is believed that the strip casting process can be an alternative for the production of Mg alloys sheets. Strip casting process combines casting and hot rolling into a single step, having an advantage of one-step processing of flat rolled products. Besides being such a cost-effective process, strip casting also has beneficial effects on microstructure such as reducing segregation, improving inclusion size distribution and refining microstructural and textural homogeneity. The present research is aimed at studying the structure and properties of strip cast Mg alloys to establish the feasibility of strip casting for the production of wrought Mg alloys. Several alloy systems, including AZ and the experimental alloys, are strip cast and their structure-property relationships are established. Microstructure and mechanical properties of strip cast Mg alloys will be discussed with particular emphasis on the solidification behavior during strip casting. The effects of alloying additions and thermo-mechanical treatment will also be discussed.

9:30 AM

Dynamic Mechanical Analysis of Pure Mg and Mg AZ31 Alloy: *Abraham Munitz*¹; David Dayan²; David Pitchure¹; R. Ricker¹; ¹National Institute of Standards and Technology-NIST, Metall. Div., Gaithersburg, MD 20899 USA; ²NRCN, PO Box 9001, Beer-Sheva 841900 Israel

Dynamic mechanical analyses were performed on pure Mg and Mg AZ31 alloy to study the impact of thermo-mechanical state and grain structure on the complex modulus, creep, stress relaxation and springback. It was found that the storage and loss moduli of pure Mg depend on grain size and grain morphology. Large grain size has storage modulus of about 42 GPa and the grain boundary loss modulus peak is at about 210°C. Decreasing the grain size decreased the storage modulus to 40 GPa and moved the grain boundary peak to about 235°C. It was found that the activation energy for grain relaxation is 1.386 eV, which is very close to the activation energy of the self-diffusion of Mg (1.408 eV). The storage and loss moduli of AZ31 depend on grain size and on solute distribution of Al and Zn in the grains. Cold work, which was achieved via rolling or biaxial strain at temperatures up to 350°C, decreases the storage modulus to about 34.5 GPa while the loss modulus remains almost the same (between 180 and 200°C). On the other hand solute distribution has an impact on the internal friction (loss modulus) while the storage modulus remains almost unaffected.

9:50 AM Break

10:20 AM

Corrosion Protection of a Die Cast Magnesium Automotive Door: *G. T. Bretz*¹; K. A. Lazarz¹; D. J. Hill¹; P. J. Blanchard¹; ¹Ford Research & Advanced Engineering Staff, Dearborn, MI USA

TUESDAY AM

It is well known that magnesium alloys, in close proximity to other alloys, are susceptible to galvanic corrosion. Combined with this fact, in automotive applications, it is rare that magnesium will be present in the absence of other alloys such as steel or aluminum. Therefore, in wet applications where the galvanic cell is completed by the formation of an electrolyte, it is necessary to isolate the magnesium in order to prevent accelerated corrosion. There are numerous commercial pretreatments available for magnesium, however this paper will focus on conversion coatings in conjunction with a spray powder coat. By means of example, results for a hem flange joint on an AM50 die cast magnesium door structure will be presented. The outer door skin is an aluminum alloy hemmed around a cast magnesium flange. An adhesive is used between the inner and outer to help with stiffness and NVH (Noise Vibration and Harshness). Results from bonded coupon tests that have been exposed to accelerated corrosion cycles are presented. A second phase of this work considered a surrogate hem flange coupon, which was similarly exposed to the same accelerated corrosion cycle. Results from both of these tests are presented within this paper along with a discussion as to their suitability for use within automotive applications.

10:40 AM

Chemical Conversion Coating on AZ91D and its Corrosion Resistance: *En-Hou Han*¹; *Wanqiu Zhou*¹; *Dayong Shan*¹; *Wei Ke*¹; ¹Chinese Academy of Sciences, Inst. of Metal Rsch., 72 Wenhua Rd., Shenyang, Liaoning 110016 China

The chromium-free conversion coating could be obtained when AZ91D magnesium alloy was immersed in a solution containing a manganese salt, phosphate and an inhibitor. Corrosion resistance of the chemical conversion coating was evaluated by anodizing polarization curve and salt immersion. The passivation region is quite large for more than 200mv. XRD analysis showed that the conversion coating was mainly composed of Mn₃(PO₄)₂ with amorphous structure. The morphology of the coating in different time is observed by SEM. The corrosion rate is lower than that of Dow 7 conversion coating and Shadan conversion coating, and the conversion coating with manganese oxide and MgF from KMnO₄ and HF, although there exist microcracks on surface.

11:00 AM

Pretreatment Schemes for Magnesium/E-Coat Automotive Applications: *William C. Gorman*¹; ¹Technology Applications Group, Inc., 4957 10th Ave. S., Grand Forks, ND 58201 USA

The use of magnesium in exterior applications in the automotive industry is rapidly increasing and with this trend comes the need for a robust corrosion protection scheme. A properly designed protection scheme must allow for the convenient installation of the magnesium component without compromising the coating, thereby minimizing the risk of galvanic corrosion, and provide a high level of corrosion resistance throughout the lifetime of the part. This paper will look at the cyclic corrosion rate and galvanic corrosion of popular magnesium pretreatments coupled with E-coat as well as an anodized coating/E-coat system. The pretreatments to be investigated are iron phosphate, NH₃5 and Alodine® along with the anodized coating, Tagnite. These pretreatment schemes will be applied to popular magnesium die cast alloys followed by E-coat paint for this evaluation.

11:20 AM

The Application of Power Ultrasound to the Preparation of Anodizing Coatings Formed on Magnesium Alloys: *Xingwu Guo*¹; *Wen Jiang Ding*¹; *Chen Lu*¹; *Chunquan Zhai*¹; ¹Shanghai Jiao Tong University, Matl. Sci. & Engrg., Huashan Rd. 1954, Shanghai 200030 China

This paper reports the application of power ultrasound to the anodizing of magnesium alloys. The influence of power ultrasound at a constant frequency of 25kHz on the structure and composition of anodizing coatings formed on magnesium alloy AZ31 was investigated. Results clearly show that ultrasound enhances the growth rate of anodic coatings and plays a very important role in the formation of coating structure and the distribution of coating composition. The anodic coatings consist of only one layer if the ultrasound field was not applied in the solution used in this paper. However, the anodic coatings will consist of two layers when the ultrasound field was applied and the acoustic power value increases to 400W. The inner layer is compact and enriched in aluminum and fluorine. In contrast, the contents of aluminum and fluorine in the external layer are very low and its thickness is non-uniform.

11:40 AM

Corrosion Performance Evaluation of Magnesium Alloys by Electrochemical Polarization Technique: *B. Rajagopalan*¹; *P. S. Mohanty*²; *P. K. Mallick*¹; *R. C. McCune*²; *M. S. Rickkets*²; ¹University

of Michigan, 4901 Evergreen Rd., Dearborn, MI 48128 USA; ²Ford Motor Company, Scientific Rsch. Lab., 2101 Village Rd., Dearborn, MI 48121 USA

The repeatability of electrochemical polarization tests for magnesium alloys in aqueous solutions has been investigated in this study. The investigation includes pure Mg and two magnesium alloys (AM60 and AZ91D), various pH's (both buffered and unbuffered) and chloride concentrations. In unbuffered solutions AM60 showed extreme scatter in corrosion rate relative to AZ91D, especially at pH 4 and pH 10. In general, as the salt concentration increased the relative corrosion rate of AM60 with respect to AZ91D dropped, though at all times it was greater than AZ91D. At pH 4, the greatest spread in corrosion rates of AM60 was observed at all chloride concentrations. In buffered solutions the extreme scatter found in the case of unbuffered solutions was absent, thus suggesting that use of buffered solutions offered a more reproducible analysis by reducing the local pH change that occurs near the working electrode during polarization. In a buffered solution of pH 6 and 0.1% NaCl concentration, pure Mg, AM60 and AZ91D showed the greatest spread in relative corrosion rates, suggesting this regime to be optimal for further evaluations.

Materials by Design: Atoms to Applications: Computational and Experimental Strategies

Sponsored by: Electronic, Magnetic & Photonic Materials Division, EMPMD/SMD-Chemistry & Physics of Materials Committee

Program Organizers: Krishna Rajan, Rensselaer Polytechnic Institute, Department of Materials Science and Engineering, Troy, NY 12180-3590 USA; Krishnan K. Sankaran, The Boeing Company, Phantom Works, St. Louis, MO 63166-0516 USA

Tuesday AM

March 16, 2004

Room: 210B

Location: Charlotte Convention Center

Session Chairs: Surendra Saxena, Florida International University, Miami, FL 33199 USA; Craig S. Hartley, Air Force Office of Scientific Research, Arlington, VA USA

8:30 AM

Inverse Problems and Optimization in Solidification Using Electric, Magnetic and Thermal Fields: *George S. Dulikravich*¹; ¹Florida International University, Mech. & Matls. Engrg., 10555 W. Flagler St., Miami, FL 33714 USA

When growing a large single crystal from a melt, such as a semiconductor crystal, it is desirable to achieve a distribution of the dopant in the solid crystal that is as uniform as possible. This is easier to realize under pure heat conduction with no convection. Since semiconductor melts are highly electrically conducting, it should be possible to use magnetic and electric fields to suppress the buoyancy induced flows. This presentation outlines numerical simulations that can be used together with optimization to determine the distributions of the magnets and electrodes that will control the convective flow throughout the melt. The computational results suggests the possibility of developing smart manufacturing protocols for creating objects that will have functionally graded physical properties.

9:00 AM

Inverse Methods for Construction of Microstructures for Simulation and Modeling of Nanoscale Crystalline Materials: *Mo Li*¹; ¹Georgia Institute of Technology, Sch. of Matls. Sci. & Engrg., Atlanta, GA 30332 USA

Similar to polycrystalline materials, nanocrystalline materials are characterized by the same microstructure attributes such as grain size, grain boundaries, and various crystallographic and atomic structures. Extracting those detailed microstructure properties experimentally proves to be a difficult endeavor because of the small characteristic scales of the material. Very often it is the mean values of grain size, limited number of characterization of grain boundaries and crystallographic properties are available. As a consequence, computer modeling and simulation of nanocrystalline materials in the past resort to various ad hoc approaches. In this talk, I shall present several approaches we developed that are intended to represent microstructures, which can be justified physically. Among these methods are (1) Inverse Monte Carlo method, (2) kinetic grain growth methods, and (3) geometric models which are both computationally efficient and accurate in generating microstructures. Topological and atomic structural properties of the microstructures from these different methods will be compared

and analyzed. Examples of atomistic and continuum modeling of mechanical and magnetic properties using these microstructures will also be presented.

9:30 AM

Informatics and Combinatorial Based Strategies for Materials Design and Selection: *K. Rajan*¹; ¹Rensselaer Polytechnic Institute, 110 Matls. Rsch. Ctr., 110 8th St., Troy, NY 12180 USA

In this presentation we discuss a materials by design methodology which use a combination of data mining and computational materials science tools with combinatorial methods in experimental techniques. The impetus for this approach is that usually only incremental progress is made in specific technological areas of interest. On the other hand we need to have a means of exploring vast combinations of structure-property relationships. If new significant advances in materials science are to be made, we need to have search tools that can accelerate the discovery process. Data mining is envisaged as a tool to exploit the masses of available data to accelerate the discovery of these relationships and possible new associations. We provide examples of how we are integrating the informatics tools with high throughput materials synthesis and characterization of multicomponent alloys to aid in the rapid selection and design of materials.

10:00 AM Break

10:15 AM

High Throughput Ab-Initio Computing: Phase Stability Prediction: *Stefano Curtarolo*¹; *Dane Morgan*¹; *Gerbrand Ceder*¹; ¹Massachusetts Institute of Technology, Dept. Matls. Sci. & Engrg., Rm. 13-4069, 77 Mass. Ave., Cambridge, MA 02139 USA

High throughput ab-initio computational materials science is a new and powerful tool to describe and analyze similarities between different systems. We have used such an approach to calculate the stable crystal structures in nearly 80 systems, thereby creating a library of ~15,000 ab-initio structural energies. From this library it is possible to extract rules that generalize well known phenomenological approaches such as the one by Miedema or Pettifor. In our case, these rules are formulated as mathematical correlations between structural energies so that they can be used to make predictions in completely new systems. In this work we describe the method we have implemented, and list the results of new crystal structure predictions. This large study also benchmarks the accuracy of LDA ultra-soft pseudopotentials approaches.

10:45 AM

Computer Aided Engineering and Design: *Farrokh Mistree*¹; *David L. McDowell*¹; ¹Georgia Institute of Technology, Mech. Engrg., Atlanta, GA 30332-0405 USA

Abstract not available.

11:15 AM

Combinatorial Exploration of Magnetic Materials Using Thin-film Techniques: *Ichiro Takeuchi*¹; ¹University of Maryland, MD USA

We have developed a methodology for performing combinatorial investigation of a variety of magnetic materials. Combinatorial pulsed laser deposition systems and an ultra high vacuum magnetron co-sputtering system are used to investigate metal oxide systems and metallic systems, respectively. Thin-film combinatorial libraries and composition spreads of different designs are utilized to effectively map large compositional landscapes on individual chips. High-throughput characterization of magnetic properties is performed using room temperature scanning SQUID microscopes. Systems studied to date include ferromagnetic shape memory alloys, exchanged coupled magnetic bilayers and artificial magnetoelectric materials. Scanning x-ray diffractometry is used to map the phase distribution of entire combinatorial samples in order to rapidly establish composition-structure-property relationships across compositional phase diagrams.

Materials Processing Fundamentals: Liquid Metal Processing

Sponsored by: Extraction & Processing Division, Materials Processing & Manufacturing Division, EPD-Process Fundamentals Committee, MPMD/EPD-Process Modeling Analysis & Control Committee

Program Organizers: Adam C. Powell, Massachusetts Institute of Technology, Department of Materials Science and Engineering, Cambridge, MA 02139-4307 USA; Princewill N. Anyalebechi, Grand Valley State University, L. V. Eberhard Center, Grand Rapids, MI 49504-6495 USA

Tuesday AM
March 16, 2004

Room: 212B
Location: Charlotte Convention Center

Session Chair: TBA

8:30 AM Invited

Control of Convection in Containerless Processing: *Robert W. Hyers*¹; *Douglas M. Matson*²; *Kenneth F. Kelton*³; *Jan R. Rogers*⁴; ¹University of Massachusetts, Dept. of Mech. & Industrial Engrg., 160 Governors Dr., Amherst, MA 01003 USA; ²Tufts University, Dept. of Mech. Engrg., Medford, MA 02155 USA; ³Washington University, Dept. of Physics, St. Louis, MO 63130 USA; ⁴NASA Marshall Space Flight Center, MC SD46, Huntsville, AL 35812 USA

Many different containerless processing techniques are employed in materials research, with the common goals of eliminating chemical reactions with the crucible and reducing heterogeneous nucleation sites. Each containerless method has different driving forces for flow in a liquid sample, and each has different relations between the flow variables and the process parameters. Often more than one technique is required to achieve the objectives of an experimental program. For example, one project requires solidification experiments over a range of almost two orders of magnitude in flow velocity, in both laminar and turbulent flow, while another requires a particular combination of shear rate and cooling rate, leading to a different processing strategy. The results of a modeling effort to determine the best combination of methods to meet the requirements of these two different experimental programs are presented.

9:00 AM

The Influence of Internal and External Convection in the Transformation Behavior of Fe-Cr-Ni Alloys: *Rakesh Venkatesh*¹; *Robert W. Hyers*²; *Douglas M. Matson*¹; ¹Tufts University, Mech. Engrg., 200 College Ave., 025 Anderson, Medford, MA 02155 USA; ²University of Massachusetts, Dept. of Mech. & Industrial Engrg., 160 Governors Dr., Engrg. Lab Bldg., Amherst, MA 01003 USA

A difference in the transformation delay times was observed between electromagnetic levitation (EML) and electrostatic levitation (ESL) experiments on steel alloys. This deviation is due to the difference in convection. Using high speed imaging, we can observe the frequency of nucleation as a function of declination angle measured from the equatorial plane and we can observe the delay between nucleation events. These measurements show no preference for location in ESL testing. For EML tests, primary recrystallization preferentially occurs on the top hemisphere where cooling gas impinges on the surface. Delay times did not vary significantly between top and bottom hemispheres and thus external convection does not explain the deviation observed. For EML tests, the frequency of secondary nucleation appears to disfavor positions along the equator and both poles, where internal flows are minimized, indicating that internal convection is responsible for the observed deviation.

9:20 AM

Experimental Measurement of Melt Flow With and Without an Applied Magnetic Field: *X. Bing*¹; *Ben Li*¹; ¹Washington State University, Sch. of Mech. & Matls. Engrg., Pullman, WA 99164 USA

This paper discusses the measurement of melt flows induced by thermal gradients with and without an applied magnetic field. An experimental system has been setup when low melting point melt flow is driven by buoyancy forces. The melt velocity is measured by a hot wire probe. The measurements are conducted with and without an externally applied magnetic field. The measured data are compared with numerical predictions and a reasonably good comparison is obtained.

TUESDAY AM

9:40 AM

Study on the Motion States of Impurity Particles in Static Magnetic Field: *L. Zhang*¹; G. C. Yao¹; W. L. Jiao¹; ¹Northeastern University, Sch. of Matl. & Metall., Liaoning, Shenyang 110004 China

The physical property differences between impurity particles and mother metal including conductivity and magnetic susceptibility were used for electromagnetic separation, which would bring different motion rules in magnetic field to make the mother metal more purified. The motion states of impurity particles (metallic particles magnetized) imposed by magnetic force in static magnetic field were studied mainly. After analyzing of force imposed and theoretic calculation, the final motion velocities of impurity particles imposed by magnetic force were confirmed. The separating efficiencies of impurity particles were made out adopting the models of piston and trajectory according to the different fluxion states of molten metal, respectively. From the results, it was found that the influence factors of separating efficiency were different obviously when the melt was in the different fluxion states. This conclusion was applicable to weak magnetism melt, especially to molten aluminum.

10:00 AM Break

10:20 AM Invited

Metallurgical Processes and Non-Equilibrium Thermodynamics: *Ji He Wei*¹; ¹Shanghai University, Coll. of Matls. Sci. & Engrg., Dept. of Metallic Matls., Rm. 301, No. 1, 669 Long, Ping Xing Guan Rd., Shanghai City China

Taking the vacuum circulation (RH) refining of clean steel (ultralow-carbon and ultralow-sulphur steel) as an example, the non-linear and non-equilibrium features of metallurgical processes have been illustrated. The similarities and differences between metallurgical reaction engineering and non-equilibrium thermodynamics have been analyzed. The necessity and feasibility investigating and dealing with practical metallurgical processes from the viewpoints, fundamentals and methods of non-equilibrium thermodynamics with metallurgical reaction engineering have been discussed. It is pointed out that non-equilibrium thermodynamics should and can play its role in the metallurgical area.

10:40 AM

The Dissolved Element and Nucleant Influence on the Aluminum Alloys Grain Refining Degree: *Petru Moldovan*¹; Gabriela Popescu¹; Mihai Butu¹; Ioana Apostolescu¹; ¹Polytechnic University Bucharest, Matls. Sci. & Engrg., Spaiul Independentei 313, Sect. 6, Bucharest 77206 Romania

The aim of this paper is to study the titanium and boron, introduced in the melt as AlTi10 and AlTiB master alloy, influence on the grain refining of AlMgSi alloy. The laboratory research underlined the role of free Ti and borides on the cast alloys grain dimensions. Microstructure analyzes realized by optical (Buehler OMNIMET EXPRESS) and electronic (SEM with EDAX) microscopy highlighted the titanium and boride role during the nucleation and grain growth processes in cast bars. The paradigms of dissolved elements and nucleant were verified during the grain refining process of deformable alloys.

11:00 AM

Precipitation of Inclusions in Iron Melts Treated with Ti and Mn: *Sukru Talas*¹; Ayhan Erol¹; ¹A. Kocatepe University, Techl. Educ. Faculty, A.N.S. Campus, B Block, Afyon, Afyon 03200 Turkey

Precipitation of inclusions in steelmaking process is of prime importance since it affects the mechanical properties during its service life. The nucleation and formation of inclusions especially in weld metals occurs as a result of complex reactions and sequence of nucleation is not well understood when it forms in non-equilibrium conditions. In this work, the sequence of inclusion formation in melts produced using copper chilled substrate has been documented and the effect of each inclusion forming alloying elements on the solidification behavior is also presented.

11:20 AM

A Method to Study the Effect of Alloying Elements at Low O Levels: *Ayhan Erol*¹; Sukru Talas¹; ¹A. Kocatepe University, Tech. Educ. Fac., A.N.S. Campus, B Block, Afyon 03200 Turkey

A method developed to study the effect of each alloying elements at very low level of O is to be presented. With this method, laboratory size melts can be obtained with very low O contents as low as 58 ppm without the addition of Al or Si deoxidizing elements. Method involves the use of high purity powders and a sequence of various processing routes ensuring low O content and free of impurities. This method was used to study the effect of C, Mn, and Ti on the morphology of iron and similar microstructures of steels can also be obtained.

11:40 AM

Effects of Impurities in Aluminum Alloys Processing: *Shengjun Zhang*¹; ¹Pennsylvania State University, Dept. Matl. Sci. & Tech., 107 Steidle Bldg., State College, PA 16801 USA

Calcium, lithium and sodium are impurity elements in aluminum-based alloys. They increase the hydrogen solubility in the melt and promote the formation of porosity in aluminum castings. During fabrication of aluminum alloys, these three elements cause the hot-shortness and embrittlement owing to cracking. In the present work, the thermodynamic description of the Al-Ca-Li-Na quaternary system is studied using the Calphad modeling approach to understand the effects of Ca, Li and Na on phase stability of aluminum alloys. Combining proper models and thermodynamic databases, the surface tension and viscosity of Al-base alloys are calculated. This work is beneficial to better understand and resolve some industry problems, such as viscosity decreasing and blistering during Al-alloy processing.

Nanostructured Magnetic Materials: Magnetic Tunnel Junctions and Semiconductor Spintronics

Sponsored by: Electronic, Magnetic & Photonic Materials Division, EMPMD-Superconducting and Magnetic Materials Committee, EMPMD-Nanomaterials Committee

Program Organizers: Ashutosh Tiwari, North Carolina State University, Department of Materials Science & Engineering, Raleigh, NC 27695-7916 USA; Rasmi R. Das, University of Wisconsin, Applied Superconductivity Center, Materials Science and Engineering Department, Madison, WI 53706-1609 USA; Ramamoorthy Ramesh, University of Maryland, Department of Materials and Nuclear Engineering, College Park, MD 20742 USA

Tuesday AM
March 16, 2004

Room: 215
Location: Charlotte Convention Center

Session Chair: TBA

8:30 AM Invited

Tunnel Junction Spin Injectors for Semiconductor Spintronics: *Stuart Parkin*¹; ¹IBM Almaden Research Center, K11-D2, 650 Harry Rd., K11-D1, San Jose, CA 95120-6099 USA

Using a combination of spin-dependent tunneling in magnetic tunneling junctions (MTJ) and spin filtering effects in ultra-thin ferromagnetic layers we have created a source of highly spin polarized electrical current, a magnetic tunneling transistor. This three-terminal hot-electron device marries a magnetic tunneling junction with a GaAs or Si semiconducting collector.¹ For GaAs based devices thirty-fold collector current changes are observed in small magnetic fields consistent with about 95% spin-polarized current. Using a quantum-well light emitting diode as a detector we have demonstrated that the collector current injected into GaAs is more than 10% spin-polarized.² Recent results showing evidence for much higher spin polarized currents using tunnel junction injectors will also be discussed. ¹"Non-monotonic bias voltage dependence of magnetocurrent in GaAs-based magnetic tunnel transistors", S. van Dijken, X. Jiang and S.S.P. Parkin, Phys. Rev. Lett. 90, 197203 (2003). ²"Optical detection of hot electron spin injection into GaAs from a Magnetic Tunnel Transistor Source"?, X. Jiang, R. Wang, S. van Dijken, R. Shelby, R. Macfarlane, G. Solomon, J. Harris and S.S.P. Parkin, Phys. Rev. Lett. 90, 256603 (2003).

9:00 AM Invited

Recent Development in Magnetic Tunnel Junctions: *John Q. Xiao*¹; Xiaohai Xiang¹; Tao Zhu²; F. Shen³; Z. Zhang³; ¹University of Delaware, Dept. of Physics & Astron., Newark, DE 19716 USA; ²Chinese Academy of Science, Inst. of Physics, State Key Lab. for Magnetism, Beijing 100080 China; ³Chinese Academy of Science, Institute of Physics, Beijing Lab. of Electron Microscopy, Beijing 100080 China

Recent developments in magnetic tunnel junctions (MTJs) will be discussed. First, we will present results of possibly using electron holography technique to directly probe the energy profile of tunnel barrier. Barriers with different oxidation conditions (over, optimum, and over-oxidized) have been investigated. One important finding is that there is always slight oxidation of the top electrode. Second, we will discuss an alternative barrier material which leads to the observation of an inversed tunneling magnetoresistance (TMR) at a high bias. A model is proposed to explain the behavior. The finding leads to the possibilities of achieving better signals at high bias in real applications. Finally, we will discuss the TMR dependence on both magnetic and nonmagnetic

electrode thicknesses. The results indicate the existence of bulk-like contribution to TMR.

9:30 AM Invited

Spin Dependent Transport in Magnetic Oxide Junctions: *Yuri Suzuki*¹; ¹University of California, Dept. of Matls. Sci. & Engrg., 380 Hearst Memorial Mining Bldg., MC 1760, Berkeley, CA 94720-1760 USA

Highly spin polarized ferromagnetic materials have been the focus of recent fundamental and technological studies. In particular, half metallic materials with nominally 100% spin polarization at the Fermi level are of interest. The degree and sign of spin polarization of the carriers in these materials have been probed in a variety of spin polarized tunnel junctions. The spin polarization of the material is positive if the majority spin at the Fermi level is parallel to the bulk magnetization and negative if the minority spin at the Fermi level is parallel to the bulk magnetization. Negative spin polarization, however, has rarely been observed. Magnetite (Fe_3O_4) is unique in that it is predicted not only to have negative spin polarization but also to be a half-metallic ferromagnet. We have fabricated epitaxial oxide trilayer junctions composed of Fe_3O_4 and doped manganite ($\text{La}_{0.7}\text{Sr}_{0.3}\text{MnO}_3$). The junctions exhibit inverse magnetoresistance as large as -25% in fields of 4kOe. The inverse magnetoresistance confirms the theoretically predicted negative spin polarization of Fe_3O_4 . Transport through the barrier can be understood in terms of hopping transport through localized states that preserves electron spin information. The junction magnetoresistance versus temperature curve exhibits a peak around 60K that is explained in terms of the paramagnetic to ferrimagnetic transition of the CoCr_2O_4 barrier. In collaboration with Guohan Hu and Rajesh Chopdekar.

10:00 AM Invited

Computational Design of New Spintronic Materials: *Nicola Spaldin*¹; ¹University of California, Matls. Dept., Santa Barbara, CA 93106 USA

Spin-polarized electronics is a rapidly expanding research area, both because of the fascinating fundamental physics observed in new spintronic materials, and because of their potentially far-reaching technological applications. In this talk we illustrate the utility of theoretical and computational methods in the design and optimization of three new spintronic systems. First we explore the influence of the interface on the spin transport in cobalt-contacted carbon nanotube transistors. Second we investigate the effects of doping and clustering on the magnetic properties of diluted magnetic semiconductors. And third we describe the successful prediction and subsequent synthesis of a new "multiferroic" material (which is simultaneously ferromagnetic and ferroelectric). Finally we mention some recent advances in computational methods that have allowed us both to understand the novel phenomena observed in spintronic materials, and to design improved materials for specific technological applications.

10:30 AM Invited

High-Temperature Ferromagnetism in Co-Doped Semiconductors: *Samuel E. Lofland*¹; ¹Rowan University, Ctr. for Matls. Rsch. & Educ., 201 Mullica Hill Rd., Glassboro, NJ 08028-1701 USA

We have completed a thorough study of Co-doped anatase TiO_2 and TiN in thin-film and bulk forms by a variety of techniques, including magnetization, Hall effect, transmission electron microscopy, electron energy loss spectroscopy. While bulk material and highly substituted thin films (> 5% Co substitution) are either nonmagnetic or show signs of clustering of elemental Co, thin films with smaller Co doping are semiconducting with a Curie temperature of about 600 K. We discuss these results and our work on Co-doped SnO_2 , which we have recently shown to be a ferromagnetic semiconductor but is optically transparent and has an anomalously large Co moment (~ 8 mB). This work was supported in part by NSF MRSEC Grant DMR 00-80008 and the New Jersey Commission on Higher Education.

11:00 AM

Rectifying Electrical Characteristics of ZnO/LSMO Heterostructure: *A. Tiwari*¹; C. Jin¹; J. Narayan¹; ¹North Carolina State University, Matls. Sci. & Engrg., Raleigh, NC 27695 USA

We have fabricated a p-n junction, consisting of hole-doped (p-type) manganite and electron-doped (n-type) ZnO layers grown on sapphire substrate. These junctions exhibit good electrical rectifying behavior over the temperature range 20-300K. Electrical characteristics of $\text{La}_{0.7}\text{Sr}_{0.3}\text{MnO}_3$ (LSMO) film in this heterostructure is found to be strongly modified by the built-in electric field of the junction. It has been shown that by applying the external bias voltage, the thickness of the depletion layer and hence the electrical and magnetic characteristics of LSMO film can be modified.

11:20 AM

Structural and Magnetic Properties of Fe Doped Zn1-xMgxO Thin Films: *Rasmi R. Das*¹; Pijush Bhattacharya¹; Gyana R. Pattanaik²; Jose Nieves¹; Yuri I. Yuzyuk¹; Ram S. Katiyar¹; ¹University of Wisconsin, Applied Superconductivity Ctr., Matls. Sci. & Engrg. Dept., 2163 ECB, 1550 Engrg. Dr., Madison, WI 53706-1609 USA; ²Indian Institute of Technology, Dept. of Physics, Hauz Khas, New Delhi 110016 India

ZnO is a versatile wide band gap material for optoelectronic devices due to its higher excitonic energy (~60 meV). The band gap of ZnO is often enhanced with increase in Mg concentrations within the solid solubility limit. Recently, there is an increasing interest to use ZnO host with doped 3d transition elements or cations having magnetic moment in order to manipulate the spin that will be useful for spintronic applications. We have prepared high quality ZnO and (ZnMg)O alloy with different concentrations of Fe using pulsed-laser deposition technique on sapphire substrates. It was observed that Fe starts segregating after certain concentrations (> 10%) in ZnO as observed from the x-ray diffraction and Raman scattering. Micro Raman spectra of ceramics as well as thin films showed disorder induced Raman bands besides standard wurtzite ZnO modes. Optical absorption data showed an additional absorption band towards lower bandgap energy (3 eV) with the increase in Fe content and was believed to be due to the secondary phase. The influence of Fe on magnetic properties of ZnO was studied using a vibration sample magnetometer. The remanence and coercivity of the ZnO films was found to be maximum for the sample with 10% Fe contents. The detailed results of structural and magnetic properties will be correlated with intrinsic properties of the doped cations.

Nanostructured Materials for Biomedical Applications: Session III

Sponsored by: Electronic, Magnetic & Photonic Materials Division, EMPMD-Thin Films & Interfaces Committee

Program Organizers: Roger J. Narayan, Georgia Tech, School of Materials Science and Engineering, Atlanta, GA 30332-0245 USA; J. Michael Rigsbee, North Carolina State University, Department of Materials Science and Engineering, Raleigh, NC 27695-7907 USA; Xinghang Zhang, Los Alamos National Laboratory, Los Alamos, NM 87545 USA

Tuesday AM
March 16, 2004

Room: 219A
Location: Charlotte Convention Center

Session Chairs: Jackie Y. Ying, Institute of Bioengineering and Nanotechnology, Singapore 117586 Singapore; Andres J. Garcia, Georgia Institute of Technology, Sch. of Mech. Engrg., Atlanta, GA 30332 USA; Yadong Wang, Georgia Institute of Technology, Coulter Dept. of Biomed. Engrg., Atlanta, GA 30332-0535 USA

8:30 AM Invited

Growth, Structure and Mechanical Properties of Abalone Shell: *Marc Andre Meyers*¹; Albert Lin¹; ¹University of California, Dept. of Mech. & Aeros. Engrg., MC 0411, La Jolla 92093-0411 USA

The self-assembly of aragonitic calcium carbonate found in the shell of abalone (*Haliotis*) is studied through examination of laboratory-grown flat pearl samples and slices of the nacreous shell. The growth occurs by the successive nucleation of crystals and their arrest by means of a protein-mediated mechanism, forming terraced cones. The protein layer is virtually absent where plates on a same plane abut (along lateral surfaces of tiles). A mechanism is proposed through c-axis aragonite growth arrest by the deposition of a protein layer of approximately 10-30 nm, periodically activated. This determines the thickness of the aragonite platelets, which are remarkably constant (0.5 μm). This platelet size was found to be independent of shell size. The overall growth process is expressed in terms of parameters incorporating the anisotropy of growth velocity in aragonite (V_c , the velocity along c axis, and V_{ab} , the velocity in basal plane). Naturally-developed abalone exhibits mesolayers ~0.3 mm apart; these mesolayers result from seasonal interruptions in feeding patterns, creating thicker (~10-20 μm) layers of protein. These mesolayers play a critical role in the mechanical properties, and are powerful crack deflectors. The mechanisms of deformation are discussed and a novel mode of compressive failure is described. The role of the organic intertile layer is modeled.

9:00 AM Invited

3-D Nanoparticle Structures with Self-Replicating Shapes and Synthetically-Tailored Compositions: *Ken H. Sandhage*¹; Chris-

topher S. Gaddis¹; Matthew B. Dickerson¹; Samuel Shian¹; Rajesh R. Naik²; Morley O. Stone²; Mark M. Hildebrand³; Brian P. Palenik³; ¹Georgia Institute of Technology, Sch. of Matls. Sci. & Engrg., 771 Ferst Dr., Atlanta, GA 30332-0245 USA; ²Air Force Research Laboratory, MLPJ Hardened Matls. Branch, Biotech. Grp., Wright-Patterson AFB, Dayton, OH 45433-7702 USA; ³University of California, Scripps Oceanographic Inst., Marine Bio. Rsch. Div., 9500 Gilman Dr., La Jolla, CA 92093-0202 USA

Widespread use of nanostructured materials in biomedical and other applications has been hampered by conflicting requirements for precise control over fine features and for mass production. Nature provides numerous examples of mineralized (bioclastic) structures with precise 3-D shapes that are mass-produced under ambient conditions. Particularly striking examples are the microshells of diatoms (single-celled algae). Each of the 10₅ diatom species assembles a uniquely-shaped 3-D microshell of silica nanoparticles. Sustained diatom reproduction can yield enormous numbers of identical microshells. A revolutionary processing paradigm that utilizes such precise (genetically-controlled) and massively-parallel biological replication to generate nanoparticle structures with tailored shapes and chemistries will be presented: the BaSIC (Bioclastic and Shape-preserving Inorganic Conversion) process. The BaSIC process has been used to convert bioclastic or biosculpted structures into MgO, CaO, TiO₂, ZrO₂, SiC, and polymeric materials for biomedical or other applications. Various biogenic preforms and conversion methods will be discussed.

9:30 AM Invited

Designing Biomimetic Nano-Structured Scaffolds for Tissue Engineering: *Peter X. Ma*¹; ¹University of Michigan, Dept. of Biologic & Matls. Scis., 1011 N. Univ. Ave., 2211 Dental Sch., Ann Arbor, MI 48109-1078 USA

Our group focuses on biomimetic design and fabrication of polymer scaffolds for tissue engineering. The scaffolds mimic certain advantageous aspects of natural extracellular matrix, and impart certain controllable structural features and properties from the synthetic materials design. These scaffolds serve as 3D templates to guide tissue regeneration, and eventually degrade and resorb, leaving nothing foreign in the body. To mimic bone matrix, biodegradable polymer/nanobioceramic composite scaffolds have been developed. To mimic the nano fibrous architecture and to overcome the concerns of immunorejection and disease transmission associated with collagen from a natural source, synthetic nano fibrous scaffolds have been developed in our laboratory. To optimize scaffolding function, a variety of macropore networks have been designed in the nanofibrous material. These novel nano-structured scaffolds selectively adsorb certain proteins, and enhance cell adhesion and function. Our experimental data demonstrate that the biomimetic design of nano-structured scaffolds is a powerful approach in tissue engineering.

10:00 AM Invited

Bio-Inspired Nanostructured Materials: *Jun Liu*¹; ¹Sandia National Laboratories, Chem. Synthesis & Nanomatls., PO Box 5800, MS 1411, Albuquerque, NM 87185 USA

The formation and functions of biomaterials and organisms are fundamentally different from those of synthetic materials and devices. Synthetic materials tend to have static structures that are not compatible with biomaterials, and are not capable of adapting to the functional needs of changing environments. In contrast, living systems have hierarchical structural ordering on multiple length scales, and are capable of responding to internal and external stimuli to heal and reconfigure in a dynamic fashion. In this talk, we will first discuss strategies to develop self-assembled nanostructures based on lessons from biomineralization. By controlling the surface chemistry and the crystallization behavior, we are able to produce complex two dimensional and three dimensional microstructures showing remarkable resemblance to those observed in biominerals. These novel materials showed great potential for enhancing the activities of biomaterials (proteins) and demonstrated the possibility for ultrasensitive sensing. We are also investigating strategies to use active proteins such as motor proteins and microtubules to assemble dynamic materials. This strategy is used by biomaterials to form complex shells of diatoms and responsive pigment arrays in chameleons and other organisms to change their color. We hope our approach will lead to new concepts and new materials for controlled release, tissue engineering and healing.

10:30 AM Invited

Proteomic Understanding of Novel Cellular Factors for Controlling Growth of Nanocrystals: *Xian Chen*¹; ¹Los Alamos National Laboratory, Biosci. Div., M888, Los Alamos, NM 87545 USA

Certain microorganisms such as *Candida glabrata* and *Schizosaccharomyces pombe* in nature are able to mediate the deposi-

tion of metal nanocrystals in vivo with high accuracy and efficiency. It is of tremendous interest to understand the cellular machinery of these microorganisms at molecular level by which nanocrystalline particles are synthesized as well as the regulatory mechanism(s) by which their sizes and morphologies are strictly controlled. We have used the state-of-the-art mass spectrometry-based technology to analyze the composition and spatial organization of cellular machinery of certain microorganisms that are able to produce nanocrystals. We have systematically identified the cellular factors involved in the biologically mediated synthesis of CdS nanocrystals. For example, yeast cells were cultured in exposure to different Cd(II) concentrations, and subjected to MS-based proteome analysis at certain intervals of time. We have established an in vitro system in which formation of nanocrystals is mediated by the identified proteins.

11:00 AM Invited

Molecular Biomimetics Approach to Engineered Polypeptides for Nanobiotechnology: *Mehmet Sarikaya*¹; ¹University of Washington, Matls. Sci. & Engrg., Roberts Hall, Box 352120, Seattle, WA 98195 USA

Structures and, therefore, functions of all biological hard and soft tissues in organisms are controlled by proteins based on their unique and specific interactions with other macromolecules (lipids, DNA, polysaccharides, and other proteins) and inorganics. Taking lessons from biology and using the tools of molecular biology, polypeptides can be genetically engineered to bind specifically to selected inorganics for use in nano- and biotechnology, a new field we call molecular biomimetics. Using bacterial cell surface and phage coat and coat proteins, we combinatorially select short (7-14 amino acid) polypeptide sequences with affinity to bind to (noble) metals and semiconducting oxides (Cu-, Zn-, Cd-, Al-, etc.). These genetically engineered polypeptides for inorganics (GEPIs) can be used as molecular erector sets for assembly of functional nanostructures. Based on the three fundamental principles of molecular recognition, self-assembly and DNA manipulation, I will demonstrate successful uses of GEPI in nanotechnology (molecular electronics) and nanobiotechnology (biosensors) applications.

11:30 AM Invited

Synthetic Biology and Nanobiotechnology: *Glen A. Evans*¹; ¹Egea Biosciences, Inc., 6759 Mesa Ridge Rd., Ste. 100, San Diego, CA 92069 USA

The information accumulated by genome sequencing projects provides raw materials for the creation new generations of industrial proteins, protein drugs, biomaterials and ultimately nanomachines and synthetic life. Synthetic Biology is a new way of developing proteins and protein devices through large scale DNA synthesis where DNA is "programmed" to produce novel substances and regulatory mechanisms. One aspect of synthetic biology is protein design where realm of possible protein sequences, and variations around naturally occurring protein sequences, defines an astronomically large sequence space that must be evaluated in developing new protein structures. A second challenge is the development and construction of synthetic pathways and genetic systems, designed to recapitulate the systems biology inherent in living organisms. Egea Biosciences is utilizing automated large scale DNA synthesis to develop new protein drugs and genetic pathways by producing libraries of protein variants and systematic screening them for enhanced properties. This approach provides basic information representing "rules" or design specifications for protein engineering and allows development of a common language for rational protein design.

Phase Stability, Phase Transformation, and Reactive Phase Formation in Electronic Materials III: Session III

Sponsored by: Electronic, Magnetic & Photonic Materials Division, Structural Materials Division, EMPMD/SMD-Alloy Phases Committee

Program Organizers: C. Robert Kao, National Central University, Department of Chemical and Materials Engineering, Chungli City 32054 Taiwan; Sinn-Wen Chen, National Tsing-Hua University, Department of Chemical Engineering, Hsinchu 300 Taiwan; Hyuck Mo Lee, Korea Advanced Institute of Science & Technology, Department of Materials Science & Engineering, Taejon 305-701 Korea; Suzanne E. Mohny, Pennsylvania State University, Department of Materials Science & Engineering, University Park, PA 16802 USA; Michael R. Notis, Lehigh University, Department of Materials Science and Engineering, Bethlehem, PA 18015 USA; Douglas J. Swenson, Michigan Technological University, Department of Materials Science & Engineering, Houghton, MI 49931 USA

Tuesday AM
March 16, 2004

Room: 214
Location: Charlotte Convention Center

Session Chairs: H. M. Lee, Korea Advanced Institute of Science and Technology, Dept. of Matls. Sci. & Engrg., Taejon 305-701 Korea; K. N. Subramanian, Michigan State University, Dept. of Chem. Engrg. & Matls. Sci., E. Lansing, MI 48824-1226 USA

8:30 AM Invited

Multiphase Field Simulations of the Evolution of Intermetallic Layer During Soldering Reactions: *Joo-Youl Huh*¹; Kyung-Kuk Hong¹; ¹Korea University, Div. of Matls. Sci. & Engrg., 5-1, Anam-Dong, Sungbuk-Ku, Seoul 136-701 Korea

Intermetallic compounds form at the interface between a liquid solder and a metallic substrate during soldering reaction and are indicative of joint adhesion. As the dimension of the solder joint continues to decrease in electronic packaging technology, the morphology and thickness of the intermetallic layer formed during soldering reaction become ever important for the mechanical properties of solder joints and thus for the integrity of electronic packaging. In this study, two-dimensional simulations of the microstructural evolution of intermetallic (Cu₆Sn₅) layer during soldering reactions between liquid Sn-Cu solder and Cu substrate were carried out using a multiphase field method. The intermetallic layer consists of grains which coarsen simultaneously as the intermetallic layer grows. The simulation results will be presented with the emphasis on the effects of intermetallic grain boundary diffusion on the morphology and growth kinetics of the intermetallic layer, and will be discussed in comparison with experimental observations.

8:50 AM Invited

Solder Reaction of Bare Cu and Kirkendall Void Formation During Solid State Ageing: *Kejun Zeng*¹; Roger Stierman¹; ¹Texas Instruments Inc., Semiconductor Pkgs. Dvlp., 13536 N. Central Expressway, MS 940, Dallas, TX 75265 USA

Reaction of bare Cu with lightly-alloyed SnPb solders and Pb-free SnAgCu has been studied. After reflow, samples were annealed at different temperatures up to 80 days, then cross sectioned for microanalysis. Focused ion beam was used to polish the cross sections after mechanical grinding to reveal the Kirkendall voids. While the number and size of Kirkendall voids after reflow are so small that they can be ignored from the reliability perspective, the voiding of interface after high temperature thermal ageing is so extensive that its impact on solder joint reliability should not be ignored in extreme temperature applications or tests. Although the IMC layers were flattening and growing during ageing, this effect on joint reliability is expected to be much less than that of the interfacial voids. Thermodynamically calculated phase diagrams of the SnPbCu and SnAgCu systems are used to rationalize the formation of IMCs. The growth of IMC layers and formation of voids are also discussed.

9:10 AM Invited

Microstructural Features Contributing to Enhanced Behavior of Sn-Ag Based Solder Joints: *J. G. Lee*¹; *K. N. Subramanian*¹; ¹Michigan State University, Dept. of Chem. Engrg. & Matls. Sci., E. Lansing, MI 48824-1226 USA

This study investigated the role of microstructure of solder joints made with eutectic Sn-Ag solder and Sn-Ag solder with Cu and/or Ni additions on the creep and thermomechanical fatigue (TMF) properties. Quaternary alloys containing small amounts of Cu and Ni exhibited better creep resistance at higher temperatures, and also better TMF resistance with longer dwell times at high temperature extreme, than eutectic Sn-Ag, and Sn-Ag-Cu ternary alloy solder joints. Microstructural studies of the quaternary solder alloys revealed the presence of ternary Cu-Ni-Sn intermetallic compound (IMC) at Sn grain boundaries. These precipitates can retard grain boundary sliding that can occur during TMF with longer dwell times at high temperature extreme, and high temperature creep. Acknowledgement: Work supported by the National Science Foundation under grant NSF DMR-0081796.

9:30 AM

The Influence of Dissolved Element on the Nanoindentation Characteristics of Cu₆Sn₅ and Ni₃Sn₄ Intermetallic Compound in the Solder Bump: *Guh Yaw Jang*¹; Jenq Gong Duh¹; Jyh Wei Lee²; ¹National Tsing Hua University, Dept. of Matls. Sci. & Engrg., 101, Kuang Fu Rd., Sec. 2, Hsinchu 300 Taiwan; ²Tung Nan Institute of Technology, Mech. Engrg., No. 152, Sec. 3, PeiShen Rd., ShenKeng, Taipei 222 Taiwan

The interfacial reactions between solders and under bump metallization (UBM) are the focused issue in flip chip technology. Two kinds of intermetallic compound (IMC), i.e. (Cu, Ni)₆Sn₅ and (Ni, Cu)₃Sn₄, formed between Sn-37Pb solder and Ni/Cu UBM. In this study, nanoindentation technique was employed to investigate the nanohardness and elastic modulus of (Cu, Ni)₆Sn₅ and (Ni, Cu)₃Sn₄ IMCs. Alloys of Cu-5wt%Ni and Ni-5wt%Cu were immersed in the molten Sn at 240°C for 0.5, 1, 4, 9 hours. (Cu_{1-x}, Ni_x)₆Sn₅ and (Ni_{1-y}, Cu_y)₃Sn₄ IMCs were revealed. The concentration variation in the IMC was carefully measured with the aid of an electron probe microanalyzer. As compared with the property of (Cu, Ni)₆Sn₅ with Cu₆Sn₅, the hardness and elastic modulus of (Cu, Ni)₆Sn₅ IMC was enhanced by the dissolved Ni. In contrast, the dissolved Cu slightly decreased the hardness and elastic modulus of (Ni, Cu)₃Sn₄ IMC. In addition, the strain rate sensitivity of (Cu, Ni)₆Sn₅ and (Ni, Cu)₃Sn₄ IMCs was also evaluated.

9:45 AM

Nanoindentation of Intermetallics Formed in Pb-Free Solder Joints: Experiments and Simulation: *X. Deng*¹; M. C. Koopman²; N. Chawla¹; K. K. Chawla²; ¹Arizona State University, Dept. of Chem. & Matls. Engrg., Tempe, AZ 85287 USA; ²University of Alabama, Dept. of Matls. Sci. & Engrg., Birmingham, AL 35294 USA

A knowledge of the elastic properties of Cu and Ag-based intermetallics, formed during reflow of Sn-rich solder joints on Cu, is extremely important in understanding and predicting the mechanical behavior of the joint. Bulk testing of these intermetallics is problematic because of the difficulty in achieving fully-dense materials, and because the microstructure in bulk form is often quite different from that observed in the joint. In this study, we have used nanoindentation to probe the mechanical properties of intermetallics in the joint in situ. The Continuous Stiffness Measurement (CSM) method was used during indentation to obtain the instantaneous Young's modulus as a function of depth. The Young's moduli of Cu₆Sn₅, Cu₃Sn, Ag₃Sn, Sn-Ag solder, pure Sn, and Cu, were measured by nanoindentation. After indentation, the surface characteristics of each phase were examined using atomic force microscopy (AFM). Significant pile-up due to dislocations was observed in Sn, Sn-Ag solder, and Cu. Finite element analysis was conducted to investigate and predict the deformation behavior during indentation and correlated very well with the experimental results.

10:00 AM

Electromigration Characteristics of SnPb and SnAgCu Thin Stripe Lines: *Min-Seung Yoon*¹; Shin-Bok Lee¹; Young-Chang Joo¹; ¹Seoul National University, Sch. of Matls. Sci. & Engrg., 30-503, Seoul 151-742 S. Korea

Rapidly decreasing size of electronic packages has brought about drastic increase in the current density through the flip chip bumps, and this caused a failure due to electromigration at the bumps. We have investigated the electromigration characteristics of eutectic SnPb and SnAgCu. Thin stripe-type test structures were fabricated and tested at 80-120°C with the current densities of 4-8*10⁴ A/cm². Scanning electron microscope and energy-dispersive X-ray spectroscopy were used to investigate the damaged morphology and the compositional changes. Hillocks were formed near the anode of the stripe pattern, and voids were observed at the cathode of the line. In eutectic SnPb, the content of Pb increased monotonically with the distance from the cathode to

the anode, and the activation energy for electromigration was 0.77eV. Accumulation of Ag atoms at the anode of line was observed in SnAgCu. The electromigration parameters and effects of compositional change on electromigration in solders are discussed.

10:15 AM Break

10:30 AM Invited

Impact Reliability of Solder Joint: *Masayoshi Date*¹; Tatsuya Shoji²; Masaru Fujiyoshi²; Koji Sato³; King-Ning Tu¹; ¹University of California, Dept. of Matls. Sci. & Engrg., 405 Hilgard Ave., Los Angeles, CA 90095-1595 USA; ²Hitachi Metals, Ltd., Metallurg. Rsch. Lab., Yasugi, Shimane 692-8601 Japan; ³Hitachi Metals, Ltd., Yasugi Works, Yasugi, Shimane 692-8601 Japan

When a portable electronic device drops to the ground, it may fail due to solder joint fracture. Owing to reliability concern of consumer electronic products, the measurement of impact toughness of solder joints is required. We conducted the measurement by using a small size Charpy test. Four kinds of solder balls (eutectic Sn-Pb, near-eutectic Sn-Ag-Cu, eutectic Sn-Zn and Sn-Zn-Bi) bonded to either Cu or Au/Ni(P) pad were tested with and without aging. Among them, the Sn-Zn-Bi on the Au/Ni(P) showed the best impact toughness. Interestingly, the Sn-Zn-Bi on the Cu showed a significant loss of the toughness with aging. We also compared the impact test to the conventional shear test. They are similar in shear deformation except that the shear rate of the former is three orders higher than the latter. The results of these tests were different. The impact test revealed more failure due to interfacial fracture.

10:55 AM Invited

Phase Stability and Interfacial Reaction in Palladium/Solder Diffusion Couples: *Gautam Ghosh*¹; ¹Northwestern University, Dept. of Matls. Sci. & Engrg., 2225 N. Campus Dr., Evanston, IL 60208-3108 USA

Palladium and palladium-containing alloys are commonly used as metallizations in electronic packaging. Due to high thermodynamic driving forces and also due to kinetic reasons, Pd reacts fairly rapidly with Sn-base solders. This is of particular interest due to use of Pb-free solders which are very Sn-rich. We have carried out a systematic study of interfacial reaction between Pd and solders (both Pb-Sn and Pb-free). The results show that the interfacial microstructure is time dependent. These results will be discussed in terms of phase stability of the Pd-Sn system, and also diffusion paths in Pd-Sn-X systems.

11:15 AM Invited

Self-Assembled Metallic Nanodots: *L. J. Chen*¹; ¹National Tsing Hua University, Matls. Sci. & Engrg., 101, Sect. 2, Kung-Fu Rd., Hsinchu Taiwan

The fabrication of self-assembled metallic nanodots is of both fundamental interest and technological importance. Highly regular self-assembled 2-D and 3-D Au and Ag nanodots were formed using two-phase reaction with a phase transfer catalyst. Honeycomb structure of metal nanoparticles on silicon was drop-cast from the metal nanoparticle solution under appropriate conditions. Hexagonal networks with discrete metal particles were generated in samples annealed in N₂ ambient. NiSi, TiSi₂ and CoSi₂ nanodots were formed on Si_{0.7}Ge_{0.3} on (001)Si with a sacrificial amorphous Si (a-Si) interlayer. The formation of the one-dimensional ordered structure is attributed to the nucleation of NiSi, TiSi₂ and CoSi₂ nanodots on the surface undulations induced by step bunching on the surface of SiGe film owing to the miscut of the wafers from normal to the (001)Si direction. The two-dimensional, pseudo-hexagonal structure was achieved under the influence of repulsive stress between nanodots.

11:35 AM

Electromigration-Induced Cu Dissolution Rate in Sn(Cu) Flip-Chip Solder Joints: *Ling Ke*¹; C. Y. Liu¹; ¹National Central University, Dept. of Chem. & Matls. Engrg., No. 300 Jung-Da Rd., Jung-Li City Taiwan

Electromigration-induced Cu dissolution has been observed by Kao. Yet, it is of important to know the rate of Cu dissolution due to the current stressing. In this study, flip-chip solder joint of Cu/Sn/Cu structure were stressed by a current density of 105 A/cm² at three elevated temperature, which are 150°C, 180°C, 200°C. We found that the consumption of Cu foil at the current-entering interface was faster than that at the current-existing interface. By estimating the amount of Cu consumption at the current-entering interface, the Cu dissolution rates due to the current stressing were determined. Also, the activation energy of EM-induced Cu dissolution will be estimated and reported in this talk. In this talk, we will also present the effect of Cu additive on the EM-induced Cu dissolution rate. Two Sn(Cu) alloys will be studied, which are Sn_{0.7}Cu, and Sn_{3.0}Cu.

11:50 AM

Electromigration in Flip Chip Solder Bump of 97Pb-3Sn/37Pb-63Sn Combination Structure: *Jae Woong Nah*¹; *Jong Hoon Kim*¹; *Kyung Wook Paik*¹; *Hyuck Mo Lee*¹; ¹KAIST, Dept. of Matls. Sci. & Engrg., Kusong-Dong 373-1, Yusong-Gu, Taejeon 305-701 Korea

Electromigration damage in the flip chip solder bump of 97wt%Pb-3wt%Sn/37wt%Pb-63wt%Sn combination structure was studied after current stressing up to 20 hr. The UBM for 97wt%Pb-3wt%Sn solder on the chip side was TiW/Cu/electroplated Cu while the bond-pad for 37wt%Pb-63wt%Sn solder on the PCB side was electroless Ni/Au. We observed in the thermo-electromigration test that failure occurred at the top of the bump with a downward electrical current flow while there was no failure in the opposite current polarity. The Pb atoms were found to move in the same direction as with the electron current flow. Therefore, in the case of downward electron flow, the composition of the upper solder bump changed from 97wt%Pb-3wt%Sn to 83wt%Pb-17wt%Sn and it enabled the Cu₆Sn₅ phase to precipitate at on chip side. Due to precipitation and growth of the Cu₆Sn₅ IMC, the Cu UBM was quickly consumed and the subsequent void formation induced failure.

12:05 PM

Effects of Ni and Cu Additive on Electromigration in Sn Solder Lines: *S. C. Hsu*¹; *H. T. Chiew*¹; *C. C. Lu*¹; *C. Y. Liu*¹; *Fay Hua*²; ¹National Central University, Dept. of Chem. & Matls. Engrg., No. 300 Jung-Da Rd., Jung-Li City Taiwan; ²Intel Corporation, Matls. Tech. Operation, Santa Clara, CA 95054 USA

The Cu and Ni alloying effects on Electromigration (EM) in Sn solder lines have been studied under different ambient temperatures. Small Cu additive was found to enhance EM rate. However, we found that the Ni additives retarded EM rate. The possible mechanism will be proposed during this talk and the important effective charge number of Sn(Cu) and Sn(Ni) alloys will be estimated and reported. Under elevated ambient temperature, a faster EM rate was observed. Hillock and void formation are very different from that in the room temperature. Also, the Cu and Ni additives have distinct effects on the interfacial compound morphologies under EM tests.

Phase Transformations and Deformation in Magnesium Alloys: Solidification and Precipitation

Sponsored by: Materials Processing and Manufacturing Division, MPMD-Phase Transformations Committee-(Jt. ASM-MSCTS)

Program Organizer: Jian-Feng Nie, Monash University, School of Physics and Materials Engineering, Victoria 3800 Australia

Tuesday AM
March 16, 2004

Room: 205
Location: Charlotte Convention Center

Session Chairs: Jian-Feng Nie, Monash University, Sch. of Physics & Matls. Engrg., Victoria 3800 Australia; Gordon W. Lorimer, University of Manchester/UMIST, Manchester Matls. Sci. Ctr., Manchester M1 7HS UK

8:30 AM Invited

Mechanisms of Grain Refinement of Magnesium Alloys: *David H. StJohn*¹; *Ma Qian*¹; ¹University of Queensland, CAST CRC, Div. of Matls. Engrg., St Lucia, Brisbane, Queensland 4072 Australia

Unlike most other alloy systems a fine grain size is required for good creep resistance for most magnesium alloys so that a thin intermetallic phase forms along the boundaries preventing grain boundary sliding. For magnesium alloys that do not contain aluminium, zirconium is the best grain refiner. To minimise cost and thus the amount of zirconium added it is important to understand the mechanism by which zirconium refines these alloys. The mechanism revealed by recent work and the resultant improved refiner addition that was developed is described. In contrast, magnesium alloys that contain aluminium do not have a reliable and easy to use grain refiner addition. This paper describes the range of grain refining technologies that have been developed. These are considered in the light of the current theory of grain refinement. Directions for research are suggested that could lead to a commercially viable refiner for magnesium-aluminium based alloys.

9:05 AM Invited

Simulations of Continuous and Discontinuous Precipitations in Mg-Al Alloys: *Zi-Kui Liu*¹; *Jingzhi Zhu*¹; *Long-Qing Chen*¹; ¹Pennsylvania State University, Matls. Sci. & Engrg., 209 Steidle, Univ. Park, PA 16802 USA

In Mg-Al alloys, when an α -Mg phase homogenized at high temperatures is quenched to low temperatures, the $Mg_{17}Al_{12}$ intermetallic phase precipitates from the α -Mg matrix. Experimental observations reported in the literature showed that continuous precipitation, i.e. the direct precipitation of $Mg_{17}Al_{12}$ particles from the matrix, is favored at high and low temperatures, while discontinuous precipitation, i.e. the cellular type of cooperative growth of α -Mg and $Mg_{17}Al_{12}$ into the α -Mg matrix, dominates at intermediate temperatures. In the present work, the thermodynamic and atomic mobility databases of the Mg-Al system are integrated into the phase-field simulation to understand the transition between the continuous and discontinuous precipitations.

9:40 AM Invited

Precipitation in Magnesium Rare Earth Alloys: *G. W. Lorimer*¹; ¹University of Manchester/UMIST, Manchester Matls. Sci. Ctr., Grosvenor St., Manchester M1 7HS UK

The precipitation sequence in binary magnesium alloys with rare earth metals of the cerium subgroup, including Mg-Nd and Mg-La, is: Mg(ssss) \rightarrow GP zones \rightarrow β'' (DO19) \rightarrow β' \rightarrow β . The crystal structures of the β' and β phases are system specific. In the binary magnesium alloys with rare earth metals of the yttrium group (except Yb) the precipitation sequence has been reported as: Mg(ssss) \rightarrow β'' \rightarrow β' \rightarrow β . No GP zones have been observed and there is still considerable debate concerning the crystal structure of the phases in different alloy systems. In alloys such as WE43 and WE54, that contain rare earth metals of both the cerium and yttrium groups, the precipitation sequence can involve several intermediate precipitates: Mg(ssss) \rightarrow plates \rightarrow β' (BCO) \rightarrow β_1 (FCC) \rightarrow β (FCC). Extremely complicated precipitation sequences have been reported, and the nucleation of one phase can involve pre-existing precipitates.

10:15 AM Break

10:30 AM Invited

Characterisation of Precipitate Phases in Mg-Zn-Al Casting Alloys: *Jian-Feng Nie*¹; *Xiao-Ling Xiao*¹; *Laure Bourgeois*¹; ¹Monash University, Sch. of Physics & Matls. Engrg., Victoria 3800 Australia

It has recently been demonstrated that Mg-Zn-Al casting alloys are age-hardenable and exhibit creep resistance superior to that of binary Mg-Al alloys. Despite the engineering importance of this group of alloys, there is currently a lack of understanding of the structure, orientation, morphology, composition, and distribution of strengthening precipitate phases in these Mg-Zn-Al alloys and the factors that control the age hardening and creep behaviours of these alloys. The present work involves detailed characterisation using transmission electron microscopy of precipitate microstructures in Mg-8wt%Zn-(4-8)wt%Al casting alloys. It will be shown that the microstructure of peak-aged samples of the Mg-Zn-Al alloys contains predominantly a fine-scale distribution of precipitates of a ternary phase that appears to have a quasicrystalline structure. The creep resistance of these alloys will also be briefly discussed in the context of the microstructural observations.

11:05 AM Invited

Interfacial Structure and Orientation Relationship Between $Mg_{17}Al_{12}$ and Matrix: *Wenzheng Zhang*¹; *Min Zhang*¹; *Fei Ye*¹; ¹Tsinghua University, Matls. Sci. & Engrg., Beijing 100084 China

A small angular deviation from the Burgers orientation relationship (OR) between $Mg_{17}Al_{12}$ and matrix was found and confirmed repeatedly in previous investigations. The deviation angle was first explained with a Δg parallelism criterion, a method originally used for calculating the primary O-lines. However, the criterion of the primary O-line structure in a habit plane is only valid for small misfit systems. For large misfit systems, such as $Mg_{17}Al_{12}$ /Mg, the relationship between the interfacial structure and Δg parallelism criterion is different. This paper presents a comparison of simulated interfacial structures between $Mg_{17}Al_{12}$ and matrix for the Burgers OR and for the OR that obeys a Δg parallelism rule. The result shows that a small rotation from the Burgers OR ($\sim 0.5^\circ$) can lead to singular interfacial structures in both habit plane and major side facet, so that the lattice point matching is optimized.

11:40 AM Invited

Novel Structure in Rapidly Solidified Mg-Zn-RE Alloys: *Yoshihito Kawamura*¹; *Eiji Abe*²; ¹Kumamoto University, Matls. Sci. & Engrg., 2-39-1 Kuro-kami, Kumamoto 860-8555 Japan; ²National Institute for Materials Science, 1-2-1 Sen-gen, Tsukuba 305-0047 Japan

High strength Mg-Zn-Y alloys have been developed by rapidly solidified powder metallurgy (RS P/M) processing. RS P/M $Mg_{97}Zn_1Y_2$ alloy exhibits high tensile yield strength of 610 MPa and elongation of 5%. We employ a unique atomic-resolution high-angle annular dark-field scanning transmission electron microscopy to investigate the

microstructure of recently developed nanocrystalline Mg alloys with small additions of Zn and rare earth metals. A novel long-period ordered structure was observed in the RS P/M $Mg_{97}Zn_1Y_2$ alloy, which had a unit cell composed of six close-packed planes of the magnesium crystal, with a stacking sequence of ABCBCB' where A and B' layers are significantly enriched in Zn and Y. This result demonstrates that the additional elements of a few atomic percent to Mg can lead to formation of a long-period, chemically-ordered as well as stacking-ordered structure. Results of other RS Mg-Zn-RE alloys will also be presented.

Processing, Microstructure and Properties of Powder-Based Materials: Session II

Sponsored by: Materials Processing and Manufacturing Division, MPMD-Powder Materials Committee

Program Organizers: K. B. Morsi, San Diego State University, Department of Mechanical Engineering, San Diego, CA 92182 USA; James C. Foley, Los Alamos National Laboratory, Los Alamos, NM 87545 USA; Karl P. Staudhammer, Los Alamos National Laboratory, Nuclear Materials Technology Division, Los Alamos, NM 87545 USA

Tuesday AM
March 16, 2004

Room: 208B
Location: Charlotte Convention Center

Session Chair: Karl P. Staudhammer, Los Alamos National Laboratory, Nucl. Matls. Tech. Div., Los Alamos, NM 87545 USA

8:30 AM Invited

Powder Processing of Metallic Hot Gas Filters: *Iver E. Anderson*¹; *Robert L. Terpstra*¹; *Brian Gleeson*¹; ¹Ames Laboratory, Metal & Ceram. Scis., 222 Metals Dvlp., Ames, IA 50011 USA

Successful development of metallic filters with high temperature oxidation/corrosion resistance and high mechanical reliability for fly-ash capture is a key to enabling advanced coal combustion and power generation technologies. A beneficial metallic filter structure, composed of a thin wall (0.5mm) tube with uniform porosity (about 30 to 40%), is being developed using spherical powder processing and partial sintering, combined with porous sheet rolling and resistance welding. Modified superalloys, e.g., Ni-16Cr-9.0Al-3Fe (wt.%), are being tested in porous and bulk samples for oxide scale stability in simulated oxidizing/sulfidizing atmospheres found in combustion systems at temperatures up to 850°C. Analysis of "hanging o-ring" samples from coal-fired combustion exposure testing enabled study of combined corrosion effects from particulate deposits and hot exhaust gases. Additional studies have explored the correlation between sintered microstructure, tensile strength, and permeability of porous sheet samples. Support is gratefully acknowledged from DOE-FE (ARTD) through Ames Lab contract No. W-7405-Eng-82.

8:50 AM

Processing, Microstructure and Uses of Borated Aluminum Metal Matrix Composites: *Monte D. Hart*¹; *Ann M. Hagni*¹; ¹EaglePicher Technologies, LLC, Boron Dept., PO Box 798, 798 Hwy. 69A, Quapaw, OK 74363 USA

Borated aluminum has been utilized in the nuclear industry for twenty years providing criticality control in spent fuel storage systems. The matrix is a precipitation hardened 6000 series aluminum alloy where strength is required and 1100 alloy for non-structural use. The process involves the reaction of a proprietary salt with molten aluminum forming secondary boride phases (either AlB₂ or TiB₂). The proprietary salt contains boron enriched in the B-10 isotope (> 95 wt%) for enhanced thermal neutron absorption. The borides range in size from 1-5 μ m for TiB₂ and 5-10 μ m for AlB₂. Semi-continuous direct chill casting is used to produce ingots for subsequent extrusion or rolling. Neutron transmittance measurement and real-time neutron radiographic inspection techniques are used to determine the concentration and dispersion of 10B. A process for the manufacture of a MMC by co-injection of B₄C powder with atomized Al is currently being evaluated.

9:10 AM

A Model to Predict the Damping Characteristics of Piezoelectric-Reinforced Metal Matrix Composites: *A. Goff*¹; *A. O. Aning*¹; *S. L. Kampe*¹; ¹Virginia Tech, Matls. Sci. & Engrg., 213 Holden Hall, Blacksburg, VA 24061 USA

A numerical model based on the Eshelby equivalent inclusion method has been developed as a means to gauge the energy absorption (damping) capability of piezoelectric-reinforced metal matrix composites.

The model computes the joule heating generated within a variety of metallic matrices as a consequence of the mechanical excitation of various randomly dispersed piezoelectric reinforcement formulations. The model predicts that enhanced damping performance by such a mechanism would, in general, be realized for highly conductive metallic matrices containing reinforcements with high piezoelectric capability.

9:30 AM

Synthesis of In Situ Piezoelectric-Reinforced Metal Matrix Composites: *J. S. Franklin*¹; A. O. Aning¹; S. L. Kampe¹; ¹Virginia Tech, Matls. Sci. & Engrg., 213 Holden Hall, Blacksburg, VA 24061 USA

A series of in situ metal matrix composites containing dispersed piezoelectric-capable ceramic reinforcements have been synthesized using mechanical alloying or reaction synthesis techniques. Specifically, copper matrices containing 20, 30, and/or 40 volume percent of BaTiO₃, PbTiO₃, or ZnO have been produced and microstructurally characterized using metallographic and x-ray diffraction techniques. The results indicate that the successful in situ synthesis of a complex piezoelectric ceramic composition within a metal matrix relies on process approach, percentage of reinforcement within the formulation, and formulation chemistry.

9:50 AM

Centrifugal Infiltration of Particulate Metal Matrix Composites: *Jessada Wannasin*¹; Merton C. Flemings¹; ¹Massachusetts Institute of Technology, Dept. of Matls. Sci. & Engrg., 77 Mass. Ave., Rm. 8-402, Cambridge, MA 02139 USA

A novel high pressure liquid infiltration process utilizing centrifugal force is described. The high pressure obtained in this process can be used to fabricate metal matrix composites containing high volume fractions of very fine reinforcements. This paper will discuss the design and development of the process. Experimental results are presented of infiltration of Sn-Pb alloy into performs of different particle types ranging in size from 25 to 0.3 microns, and of resulting microstructures.

10:10 AM Break

10:20 AM

Synthesis of Ni-CaO Material from Selective Reduction of Oxide Precursors: *Benjamin C. Church*¹; Thomas H. Sanders¹; Robert F. Speyer¹; ¹Georgia Institute of Technology, Matls. Sci. & Engrg., 771 Ferst Dr., Atlanta, GA 30332-0245 USA

Oxide dispersion strengthened (ODS) alloys are known for having excellent mechanical properties at elevated temperatures. Traditionally, nickel base ODS alloys have been made via mechanical alloying of metal powders. An alternative processing technique of selective reduction is used to create a dispersion of CaO in a nickel matrix. This technique is well suited for the production of Ni-ODS metal honeycomb structures made by the extrusion and subsequent reduction of metal oxide pastes. A series of Ni-CaO materials have been produced from solid solution oxide powder precursors. The reduction and sintering of the materials have been studied using x-ray diffraction and dilatometry. The structure has been observed using a combination of optical, scanning electron, and transmission electron microscopy. Processing-structure relationships are determined and issues relating to the fabrication of more complex Ni-ODS alloys (ex. Ni-Fe-Cr-CaO) using this technique are discussed.

10:40 AM

Influence of Composition on Fracture Mechanism in Al-Al4C3 Materials: *Michal Besterci*¹; Jozef Ivan²; Oksana Velgosova³; ¹Slovak Academy of Science, Inst. of Matls. Rsch., Watsonova 47, Kosice 04353 Slovakia; ²Slovak Academy of Sciences, Inst. of Matls. & Machine Mech., Račianska 75, Bratislava 838 12 Slovakia; ³Technical University, Faculty of Metall., Dept. of Non-Ferrous Matls. & Waste Treatment, Letná 9/A, Kosice 04200 Slovakia

Method of "in-situ tensile test in SEM" is suitable for investigation of fracture mechanism because it enables to document deformation processes, by which the initiation and development of plastic deformation and fracture can be reliably described. The aim of the present study is to evaluate the influence of volume fraction of Al4C3 particles (8 and 12 vol.%) on the fracture mechanism. Detailed study of the deformation changes showed that the crack initiation is caused by decohesion, and occasionally also by rupture of the large particles. Decohesion is a result of different physical properties of different phases of the system. The Al matrix has significantly higher thermal expansion coefficient and lower elastic modulus than both Al4C3 and Al2O3 particles. Based on the microstructure changes observed in the process of deformation, the following model of fracture mechanism has been proposed.

11:00 AM

Mixed Rare Earth Iron Boride Powders for Bonded Isotropic Permanent Magnets: *Nick Buelow*¹; Iver E. Anderson²; William McCallum²; Matthew J. Kramer²; Kevin Dennis²; Wei Tang²; ¹Iowa State University, Matls. Sci. & Engrg., 221 Metals Dvlp., Ames, IA 50011 USA; ²Ames Laboratory, Metals & Ceram. Sci., Ames, IA 50011 USA

Bonded isotropic permanent magnets (BPMs) formed by injection or compression molding offer good corrosion resistance and net shape manufacturing. Substituting Y and Dy for Nd in Nd₂Fe₁₄B results in a mixed rare earth iron boride (MRE-Fe-B) for use in BPMs. MRE-Fe-B exhibits stabilization of the remanence and coercivity loss up to the Curie temperature. Extrinsicly, maximum energy product (BH_{max}) is improved by increasing the fill factor (f) of BPMs due to the reduction in BH_{max} proportional to f². Spherical powders, which exhibit high fill factors, made by gas atomization are being explored. Gas atomization offers rapid solidification effects that promote glass formation or uniform fine microsegregation to the particulate. Microstructures of MRE-Fe-B powders directly affect the magnetic properties of the BPMs. A review of recent activities in this area will be presented. Support from USDOE-EE is acknowledged through contract no. W-7405-Eng-82.

11:20 AM

Preparation of Pyroelectric Material by Spark Plasma Sintering: *Kazuyuki Kakegawa*¹; Shinnosuke Yoshida¹; Naofumi Uekawa¹; ¹Chiba University, Fac. of Engrg., 1-33 Yayoi-cho, Inage-ku, Chiba-shi, Chiba 263-8522 Japan

Pyroelectric material, Pb{Zr,Ti,(Zn_{1/3}Nb_{2/3})}O₃, was prepared using spark plasma sintering technique (SPS). This material has a transition point between ferroelectric-ferroelectric phases, and exhibits a peak of Pyroelectric constant. The peak is too sharp, so that this cannot be used as an infrared sensor for the normal wide temperature region. A pyroelectric material that exhibits high pyroelectric coefficient over a wide temperature region was successfully prepared by a combination of different compositions and partial diffusion technique. Initially, starting material that has a desired compositional distribution was prepared. This was sintered by SPS technique. SPS technique produced a sintered material without changing the compositional distribution.

R.J. Arsenault Symposium on Materials Testing and Evaluation: Session III

Sponsored by: Structural Materials Division, SMD-Mechanical Behavior of Materials-(Jt. ASM-MSCTS), SMD-Nuclear Materials Committee-(Jt. ASM-MSCTS)

Program Organizers: Raj Vaidyanathan, University of Central Florida, AMPAC MMAE, Orlando, FL 32816-2455 USA; Peter K. Liaw, University of Tennessee, Department of Materials Science and Engineering, Knoxville, TN 37996-2200 USA; K. Linga Murty, North Carolina State University, Raleigh, NC 27695-7909 USA

Tuesday AM
March 16, 2004

Room: 211A
Location: Charlotte Convention Center

Session Chairs: Raj Vaidyanathan, University of Central Florida, AMPAC/MMAE, Orlando, FL 32816-2455 USA; Hahn Choo, University of Tennessee, Matls. Sci. & Engrg., Knoxville, TN 37996-2200 USA

8:30 AM Invited

Insights on Polycrystalline Deformation from Neutron Diffraction and In Situ Deformation: *Mark A.M. Bourke*¹; D. W. Brown¹; B. Clausen¹; S. C. Vogel¹; T. Sisneros¹; ¹Los Alamos National Laboratory, MS H805, Los Alamos, NM 87545 USA

By making neutron diffraction measurements during deformation of a polycrystalline material unique physical insights can be achieved that complement other techniques. The inherently bulk sampling of a neutron measurement ensures a representative average response, whereas the diffraction physics probes deformation at the microstructural level. The SMARTS spectrometer at Los Alamos is instrumented with a 230 kN tension or compression loading capability with simultaneous temperature control from +1800 K to 77 K. Over the last two years it has been used to study a broad range of metals, ceramics and in a few cases bulk metallic glasses. Areas of study have included; composite codeformation, twinning, stress induced phase transformations, creep, and validation of polycrystalline plasticity models. This talk will illustrate, by example, the range of insights that can be achieved by making in situ neutron diffraction measurements.

9:00 AM Invited

Neutron Diffraction Study of Residual Stresses in Fe-Mn-Si Based Shape Memory Alloys With and Without VN Precipitates: *Edward C. Oliver*¹; Tsutomu Mori²; Mark R. Daymond¹; Philip J. Withers²; ¹Rutherford Appleton Laboratory, ISIS Facility, Chilton, Didcot, Oxon OX11 0QX UK; ²Manchester Materials Science Centre, Grosvenor St., Manchester M1 7HS UK

The role of residual stresses in the reported improvement of shape memory behaviour in Fe-Mn-Si based alloys due to the addition of carbide or nitride precipitates has been investigated using neutron diffraction. This method provides information on the evolution of lattice strains, volume fractions and preferred orientation in both the parent and product phases. Diffraction spectra were recorded in situ during tensile loading and subsequent shape recovery heat treatment of two alloys: one a standard composition alloy, the other containing 0.2% VN precipitates. Texture changes demonstrate the preferential transformation of parent grains having $\langle 110 \rangle$ parallel to the tensile axis. This is close to that grain orientation having the greatest Schmid factor for the transformation shear. The precipitate-containing alloy in the virgin state exhibits as good a shape recovery as that of the standard alloy after training treatment. We associate this with back stresses caused by the presence of the non-transforming precipitates.

9:30 AM

Lattice Strain Evolution During Creep Deformation of an Austenitic Stainless Steel: *Hahn Choo*¹; Wanchuck Woo¹; ¹University of Tennessee, Matls. Sci. & Engrg., 434 Dougherty Hall, Knoxville, TN 37996-2200 USA

Intergranular strain evolution was studied during high-temperature creep deformation of an austenitic 316L stainless steel using in-situ time-resolved neutron diffraction. In this study, changes in the elastic/plastic anisotropy were investigated as a function of time to understand the effects of accumulation of creep-induced plastic strains on the hkl-specific lattice strain evolution. A series of tensile-creep measurements were carried out between 723 and 823K under stresses corresponding to the elastic regime, power-law creep regime, and plastic regime. The relationship between the creep-induced lattice strain behavior and plastic anisotropy obtained from a tension test is discussed. In particular, the crystallographic anisotropy (e.g., behavior of plastically-deforming and load-bearing orientations) and geometrical anisotropy (i.e., axial and transverse behavior) are discussed as well as the signs and magnitudes of the lattice strains accumulated with time during the creep deformation. These observations provide a fundamental understanding of creep-induced elastic-lattice strain evolution in a single-phase, polycrystalline fcc alloy.

9:50 AM

A Neutron Diffraction Investigation of Linear Superelasticity in NiTi: *C. R. Rathod*¹; B. Clausen²; M. A.M. Bourke²; Raj Vaidyanathan¹; ¹University of Central Florida, AMPAC/MMAE, Engr-I Rm. 381, 4000 Central Florida Blvd., Orlando, FL 32816-2455 USA; ²Los Alamos National Laboratory, Los Alamos, NM 87545 USA

The superelastic effect in NiTi occurs due to a reversible stress-induced phase transformation from a cubic austenite phase to a monoclinic martensite phase. There is usually a hysteresis associated with the forward and reverse transformations which translates to a hysteresis in the stress-strain curve during loading and unloading. This hysteresis is reduced in cold-worked NiTi and the macroscopic stress-strain response is more linear, a phenomenon called linear superelasticity. Here we report on in situ neutron diffraction measurements during loading and unloading in plastically deformed (up to 11%) NiTi. The experiments relate the macroscopic stress-strain behavior (from an extensometer) with the texture, phase volume fraction and strain evolution (from neutron diffraction spectra) in linear superelastic NiTi. This work is supported by NASA and NSF (CAREER DMR-0239512).

10:10 AM Break**10:30 AM**

Nuclear Spin Relaxation for In-Situ Characterization of Dynamical Behavior of Line and Point Defects During Deformation of Materials: *K. Linga Murthy*¹; Otmar Kanert²; ¹North Carolina State University, Coll. of Engrg., Burlington Engrg. Labs., Box 7909, Raleigh, NC 27695-7909 USA; ²Universitat Dortmund, 44221 Dortmund Germany

Nuclear spin relaxation rates (NSR) were determined using NMR pulse techniques to characterize the dynamical behavior of vacancies (atomic motion/diffusion) and dislocations (jump distances) during deformation of pure and doped alkali halide single crystals (NaCl and NaF) and thin (25 mm thick) pure (99.999%) Al foils. Spin-lattice relaxation times in rotating frame (T_{1ρ}) enabled an evaluation of the

dislocation jump distances in NaCl during constant strain-rate deformation and creep at temperatures below about 500K, while atomic motion dominated at higher temperatures. Effects of impurities are considered by examining NaCl single crystals doped with Ca⁺⁺ and K⁺. The mean jump distance of the mobile dislocations, evaluated from the NSR without deformation and during creep, decreased (from around 200b) with time/strain reaching a constant value (around 20b) during the steady-state creep regime. These jump distances are orders of magnitude smaller than the subgrain size and dislocation-dislocation spacing while are in good agreement with the climb distances predicted by Weertman's pill-box model (60b) and Arsenault's computer simulations involving climb of dislocations in the subgrain boundaries (10b-30b). At higher temperatures, the relaxation was seen to be due to point defect diffusion that was enhanced by excess vacancies produced during deformation. CUT-sequence pulse technique allowed an evaluation of the strain-induced vacancy concentration as a function of strain-rate, strain and temperature in NaCl, NaF and Al. Experimental results correlated with models based on vacancy production through mechanical work (versus thermal jogs) while in-situ annealing of excess vacancies becomes important at higher temperatures. The investigations clearly reveal the utility of NMR in non-evanescently characterizing the dynamical behavior of defects in materials during deformation.

10:50 AM

In Situ Neutron Diffraction Studies on the Fatigue of Haynes® 230® Nickel Based Superalloy: *Tarik A. Saleh*¹; Michael L. Benson¹; Hahn Choo¹; Peter K. Liaw¹; Raymond A. Buchanan¹; Mark A.M. Bourke²; Bjorn Clausen²; Donald W. Brown²; Thomas Sisneros²; Dwaine L. Klarstrom³; ¹University of Tennessee, Dept. of Matls. Sci., 434 Dougherty, Knoxville, TN 37996-2200 USA; ²Los Alamos National Laboratory, Manuel Lujan Jr. Neutron Scattering Ctr., Los Alamos, NM 87545 USA; ³Haynes International, Inc., Kokomo, IN 46904-9013 USA

Haynes 230, a single phase FCC, Ni based superalloy, shows anomalous fatigue behavior: the fatigue life is shorter at high strains at 816°C than at 927°C. Previous work with neutron diffraction in fatigue has shown the development and disappearance of residual strains as fatigue progresses. To explore this effect in Haynes 230 we have performed neutron diffraction at the Spectrometer for Materials Research at Temperature and Stress (SMARTS) facility at the Los Alamos Neutron Science Center (LANSCE). Specimens of Haynes 230 alloy were subjected to hold time fatigue tests under load control conditions with a 15 minute hold time, an R ratio of 0.1, a $\sigma_{\max} = 1.75 * \sigma_{\text{yield}}$ at 3 separate temperatures: 23°C, 816°C and 923°C. The sample was held for 15 minutes at the σ_{\max} of each cycle, during which a diffraction pattern was taken. The hkl and lattice strains were monitored in both the transverse and loading direction for each cycle for approximately 100 cycles. The evolution of residual elastic strains in the polycrystalline matrix is discussed in the context of constitutive behavior and fatigue lifetime.

11:10 AM

Texture and Strain Measurements During Tensile-Compressive Loading of Shape-Memory NiTi: *A. L. Little*¹; C. R. Rathod¹; D. W. Brown²; M. A.M. Bourke²; Raj Vaidyanathan¹; ¹University of Central Florida, AMPAC/MMAE, Engr-I Rm. 381, 4000 Central Florida Blvd., Orlando, FL 32816-2455 USA; ²Los Alamos National Laboratory, Los Alamos, NM 87545 USA

Shape-Memory NiTi differs in its mechanical response under tension and compression. Neutron diffraction measurements during loading offer a way to obtain in situ texture and strain measurements from bulk, polycrystalline samples. Here we report on in situ neutron diffraction measurements during tensile and compressive loading of polycrystalline shape-memory martensitic NiTi with no starting texture. The diffraction spectra are analyzed to follow the texture and strain evolution due to twinning and elastic deformation in martensitic NiTi. Both single peak fits and Rietveld refinement of diffraction spectra are used to link the macromechanical and micromechanical behaviors in tension and compression and examine reasons for the differences. This work is supported by NASA and NSF (CAREER DMR-0239512).

11:30 AM

Non-Destructive Evaluation of Micro-Strains in High-Cycle Fatigue by Neutron Time-of-Flight Diffraction: *Alexandru Dan Stoica*¹; Xun-Li Wang¹; Derek J. Horton²; Yan Dong Wang¹; Hongbo Tian²; Peter K. Liaw²; James W. Richardson³; Even Maxey³; ¹Oak Ridge National Laboratory, Spallation Neutron Source, 701 Scarboro Rd., Oak Ridge, TN 37830 USA; ²University of Tennessee, Dept. of Matls. Sci. & Engrg., Rm. 427-B Dougherty Engrg. Bldg., Knoxville, TN 37996-2200 USA; ³Argonne National Laboratory, Intense Pulsed Neutron Source, Argonne, IL 60439 USA

Neutron time-of-flight diffraction was used to study 316 stainless steel under high-cyclic fatigue. The experimental data show that in early stage of fatigue testing, the grain-orientation-dependent intergranular strain oscillates between two extreme states with identical symmetry but a sign reversal, as the cyclic deformation includes successive loadings in tension and compression. In late stage, the intergranular strain vanishes for tests ending in tension and remains the same for tests ending in compression. The different behaviours in tension and compression are related to the crack initiation and growth characteristics of fatigue tests. As the diffraction contrast is sensible to the dislocations type and distribution, the elastic intra-granular strain developed around immobile dislocations (mainly of edge type) can be evaluated, as well as the energy stored into the distorted lattice. The intra-granular strain evolution is a fingerprint of the material hardening process and can be related with the successive stages of deformation.

Solidification of Aluminum Alloys: Microstructural Evolution I

Sponsored by: Materials Processing & Manufacturing Division, MPMD-Solidification Committee

Program Organizers: Men Glenn Chu, Alcoa Inc., Alcoa Technical Center, Alcoa Center, PA 15069 USA; Douglas A. Granger, GRAS, Inc., Murrysville, PA 15668-1332 USA; Qingyou Han, Oak Ridge National Laboratory, Oak Ridge, TN 37831-6083 USA

Tuesday AM Room: 207B/C
March 16, 2004 Location: Charlotte Convention Center

Session Chairs: Men G. Chu, Alcoa Inc., Alcoa Technical Center, Alcoa Ctr., PA 15069 USA; Qingyou Han, Oak Ridge National Laboratory, Metals & Ceram. Div., Oak Ridge, TN 37831-6083 USA

8:30 AM Opening Remarks

8:35 AM Keynote

Phase Formation and Solidification Path Analysis of Multi-component Aluminum Alloys: *Austin Chang*¹; Fanyou Xie²; Xinyan Yan³; Shuanglin Chen²; ¹University of Wisconsin, Dept. of Matls. Sci. & Engrg., 1509 Univ. Ave., Madison, WI 53706 USA; ²CompuTherm, LLC, Madison, WI USA; ³Alcoa Technical Center, PMD, 100 Tech. Dr., Alcoa Ctr., PA 15069 USA

A metallurgist can, in many cases, forecast the phase formation sequence or solidification path of a ternary alloy when its liquidus projection is known. However, the task becomes more challenging for a higher order system even when the liquidus projection is available. In actuality, these projections are rarely available for these systems. However, recent advancement achieved in phase diagram calculations resolves this dilemma. In the presentation we will show that the predicted solidification paths of multicomponent aluminum alloys using a simple Scheil model coupled with phase diagram calculation are in reasonable agreement with experiments. An example will be also presented to demonstrate its utility in welding research and practice. On the other hand, the calculated microsegregations within the dendrites using the Scheil model is not satisfactory. However, when coarsening, back diffusion and undercooling are incorporated with the basic Scheil model, the calculated microsegregations are in accord with results obtained from directional solidification.

9:05 AM

Conduction and Radiation Parameters for Analytical Models of Differential Scanning Calorimetry Instruments: *Adrian S. Sabau*¹; Wallace D. Porter²; Jay I. Frankel³; ¹Oak Ridge National Laboratory, Metals & Ceram. Div., Bldg. 4508, MS 6083, Oak Ridge, TN 37831-6083 USA; ²Oak Ridge National Laboratory, High Temp. Matls. Lab., Bldg. 4515, MS 6064, Oak Ridge, TN 37831 USA; ³University of Tennessee, Mech. & Aero. Engrg. & Engrg. Sci. Dept., 402 Dougherty Hall, Knoxville, TN 37996-2210 USA

The Differential Scanning Calorimetry (DSC) measurements are routinely used to determine enthalpies of phase change, phase transition temperatures, and heat capacities. DSC data has also been used to estimate the fractional latent heat release during phase changes. To date, DSC measurements are plagued by temperature lags due to the use of thermocouples that are placed at different location than that of the sample. In this study, the temperature lags, which are inherent to the measurement process, are estimated through a computational analysis of the raw DSC data. An analytical model is presented that accounts for different heat transfer mechanisms among instrument components. Through a direct analysis of an experimental data set, it is

shown that the proposed analytical model can accurately describe the experimental data. The direct analysis presented is to be complemented by inverse process analysis in order to determine more accurate values for the model parameters.

9:25 AM Keynote

Nucleation and Growth Temperature and the Formation of Microstructure in Steady State Solidification of Aluminum-Based Alloys: *Howard Jones*¹; ¹University of Sheffield, Dept. of Engrg. Matls., Sir Robert Hadfield Bldg., Mappin St., Sheffield S1 3JD UK

Recent work (primarily by the author and his collaborators) on measurement of formation temperature of constituents of Al-based alloys under Bridgman solidification conditions is reviewed. Together with associated microstructural observations, the results indicate control by heterogeneous nucleation in the case of polygonal primary silicon in Al-18.3wt % Si alloy, while competitive growth is controlling in the case of aluminide dendrites in Al-Fe, Al-Ni and Al-Ce or La alloys, for which measured tip undercoolings are in good agreement with values calculated from dendrite growth models. Extrapolation to zero growth velocity of measured growth temperatures of eutectics in such systems agree closely with reliable values by other methods and values of kinetic constants A and BEU for dendrites and eutectic derived from measured velocities for extinction of the dendritic constituent are shown to be in accord with direct measurements. The sometimes dramatic effects of ternary alloy or trace additions remain to be fully explored.

9:55 AM

Modelling of Microstructural Evolution in Bridgman Specimens: *T. E. Quedt*¹; A. L. Greer¹; ¹University of Cambridge, Dept. of Matls. Sci. & Metall., Pembroke St., Cambridge CB2 3QZ UK

A Bridgman furnace is used to investigate fundamental issues associated with solidification during DC casting (e.g. primary microstructure and secondary-phase selection). Thin, cylindrical specimens held in alumina sheaths are directionally solidified by their controlled removal from the furnace into a quenching water bath. Modelling and experiment has been carried out to determine the microstructural evolution of Al-Mg alloys inoculated with TiB₂ within the Bridgman furnace. Two approaches to modelling were used: (a) cellular-automaton finite-element (CAFE) software Calcosoft2D® to create graphic representations of the predicted primary microstructures; (b) simulations which calculate the evolution of volume fraction of solid given laws governing dendritic growth rates and grain initiation events; grain initiation is assumed to be determined by the free-growth criterion, rather than by nucleation itself. This allows prediction of grain size and the steady-state conditions for the columnar-to-equiaxed transition.

10:15 AM Break

10:35 AM

Directional Solidification of Type AA3003 Alloys with Additions of Zn and Si: *Majed Jaradeh*¹; *Torbjörn Carlberg*¹; ¹Mid Sweden University, Engrg., Physics & Math., Holmgatan 10, Sundsvall 85170 Sweden

To improve alloys of the AA3003 type for heat exchanger applications it is important to increase the basic knowledge of structure formation during solidification. A technique, to study the effect of different alloy additions and solidification parameters on the structure formation, is Bridgman directional solidification with quenching. In the first phase of this work parameters, such as growth rate and temperature gradient, have been adjusted to simulate the solidification in DC cast ingots, and a comparison has been made between Bridgman grown and DC cast structures. Modifications of the alloy by Zn additions improve the strength of the matrix of the material through solid solution hardening. At a level of 5% the hardness is improved by about 50%, but the solidification structure becomes less promising. The DAS and the secondary phases become coarse, and the solidification range increases significantly as the Zn content increases from 2.5 to 5%.

10:55 AM

Characterization by the p* Method of Eutectic Aggregates Spatial Distribution in As-Cast 3xxx and 5xxx Aluminum Alloys Cast in Wedge Molds and Comparison with SDAS Measurements: *Philippe P. Jarry*¹; ¹Pechiney CRV, BP27, Voreppe F-38341 France

In order to quantitatively compare the microsegregation patterns of as cast aluminum alloys, and in the future, to objectively compare computed microstructures with real ones, a quantitative metallography index named p* for as cast microstructures based on an image analysis algorithm has been developed within Pechiney and shared among the participants of the European project VIRCAST. The present paper presents the results of a benchmark study done by all participants within the project on the use of the p* measurement, on two families of alloys (3xxx and 5xxx) cast in Corus laboratories in a

wedge shaped mold in order to scan various solidification rates. It is shown that the p^* algorithm provides a quantitative and reliable assessment of the average size of particle free zones in as cast microstructures as long as proper parameters are used in terms of sampling vs resolution compromise. The p^* values have been shown to correlate with the main alloy and solidification parameters (cooling rate, grain refinement, eutectic fraction) inasmuch as these parameters exert interactive influences on the morphological or topological patterns of the solidification structure.

11:15 AM

Solidification of Aluminum Alloy A356 Under Ultrasonic Vibration: *X. Jian*¹; *Q. Han*²; *H. Xu*¹; *T. T. Meek*¹; *S. Viswanathan*³; ¹University of Tennessee, Matl. Sci. & Engrg., 434 Dougherty Bldg., Knoxville, TN 37996 USA; ²Oak Ridge National Laboratory, Metals & Ceram. Div., Bethel Valley Rd., PO Box 2008, Oak Ridge, TN 37831-6083 USA; ³Sandia National Laboratories, Albuquerque, NM 87185-1134 USA

Ultrasonic vibration has been shown to be an effective way of obtaining globular grains, but its influence on the nucleation and growth grains is unclear. In the present study, thermodynamic simulations were carried out to determine the temperature versus solid fraction curve of AA 3004 alloy. The alloy was then treated at various temperatures using ultrasonic vibrations. Color metallography was employed to reveal grain size of the specimens. Initial results indicate that it's difficult to obtain globular grains if the specimens are treated at temperatures in the mushy zone. This means that dendrite fragmentation may play a less important role in producing globular grains. Applying ultrasonic vibrations to the alloy close to its liquidus temperatures resulted in fine globular grains if the treated specimens were cooled quickly. The experimental results suggest that nucleation plays a key role in the formation of globular grains when the specimens are under ultrasonic vibrations.

11:35 AM

Formation of Iron-Rich Intermetallic Phases During Solidification of Aluminum Casting Alloys: *Liming Lu*¹; *Arne K. Dahle*¹; *Mal J. Couper*²; ¹The University of Queensland, CRC for Cast Metals Mfg. (CAST), Div. of Matls., Sch. of Engrg., Brisbane, Queensland 4072 Australia; ²Comalco Research and Technical Support, 15 Edgars Rd., Thomastown, Vic 3074 Australia

Iron is the most common and detrimental impurity in aluminum casting alloys and has long been associated with impaired properties and often an increase in casting defects. While the negative effects of iron are clear, the mechanism involved is not fully understood. It has generally been associated with the formation of iron-rich intermetallic phases. However, the conditions that control the formation of these phases are not well understood. Many factors, including solute elements, melt treatment, iron level and cooling rate, could play a role. In the present study, the interactions between iron and other common alloying elements in aluminum casting alloys were investigated. The iron-rich intermetallic phases were characterized using the electron probe microanalysis technique (EPMA) and compared with the results predicted from Thermocalc. The implications of these iron-effects on eutectic solidification and casting defect formation are also outlined.

Solidification Processes and Microstructures: A Symposium in Honor of Prof. W. Kurz: Microstructures

Sponsored by: Materials Processing & Manufacturing Division, MPMD-Solidification Committee

Program Organizers: Michel Rappaz, Ecole Polytechnique Fédérale de Lausanne, MXG, Lausanne Switzerland; Christoph Beckermann, University of Iowa, Department of Mechanical Engineering, Iowa City, IA 52242 USA; R. K. Trivedi, Iowa State University, Ames, IA 50011 USA

Tuesday AM
March 16, 2004

Room: 207D
Location: Charlotte Convention Center

Session Chair: Rohit Trivedi, Iowa State University, Ames, IA 50011 USA

8:30 AM **Invited**

Dendritic Scaling Laws: Application to Microstructure Prediction: *Martin E. Glicksman*¹; ¹Rensselaer Polytechnic Institute, Matls. Sci. & Engrg., 110 8th St., CII-9111, Troy, NY 12180-3590 USA

Understanding the kinetics of dendritic growth is essential for controlling solidification processes and microstructures, and for improving modeling at small scales. The Isothermal Dendritic Growth Experiments (IDGE) is a series of microgravity experiments designed to study dendrites in ultra-pure materials. Data resulting from these space-flight experiments reveal fundamental aspects of the solidification process: 1) thermal transport occurring at mesoscopic scales, 2) microstructural scaling laws, 3) dynamic shapes of dendrites, and 4) the possible presence of eigenfrequencies during growth. It was found that once convection phenomena in the melt are suppressed adequately, diffusion-limited models become reliable. Scaling laws connecting microstructure length scales and growth rates were found to be robust and independent of convection in the melt, permitting applications of the theories to many metallic systems, including alloys. The author and Professor Kurz have collaborated on these topics, and it is with considerable pleasure to recount this activity in his honor.

9:00 AM **Invited**

Selection of Eutectic Carbides in Multi-Component High Speed Steel Type Cast Irons: *Takateru Umeda*¹; *Toshimitsu Okane*²; ¹Chulalongkorn University, Fac. of Engrg., Dept. of Metallurg. Engrg., Phayathai Rd., Phatumwan, Bangkok 10330 Thailand; ²National Institute of Advanced Industrial Science and Technology, Digital Mfg. Rsch. Ctr., 1-2-1 Namiki, Tsukuba-shi, Ibaraki 305-8564 Japan

High speed steel type cast iron to maintain high fracture toughness and wearing resistance is necessary to control eutectic carbides, M_7C_3 , M_7C_3 , M_6C , M_2C and MC. To predict carbide formation under certain solidification conditions of multi-component cast iron, interface temperature analysis and quantitative maximum temperature criterion are needed. Interface undercooling, ΔT , for eutectic growth was given as a function of growth rate, V ; $\Delta T = kv^{1/2}$. Interface temperature of each eutectic carbide formed in Fe-M-C (M: Cr, V, Mo) systems; $g + M_7C_3$ and $g + M_7C_3$ eutectics in the Fe-C-C system, $g + VC$ eutectics in Fe-V-C system and $g + M_7C_3$ and $g + M_2C$ eutectics in Fe-Mo-C system, was measured during unidirectional solidification process. The k values of eutectic carbides were then estimated. Relationships between k , carbide spacing and growth rate were discussed. Application of k values obtained in ternary systems to more multi-component systems was also discussed.

9:30 AM

Extending the Lipton-Kurz-Trivedi Dendrite Growth Model into the Two-Phase Regime: *Douglas M. Matson*¹; *Joan E. Kertz Yurko*²; *Robert W. Hyers*³; ¹Tufts University, Mech. Engrg., 200 College Ave., 025 Anderson, Medford, MA 02155 USA; ²Massachusetts Institute of Technology, Dept. of Matls. Sci. & Engrg., 77 Mass Ave., Cambridge, MA 02139 USA; ³University of Massachusetts, Dept. of Mech. & Industrial Engrg., 160 Governors Dr., Engrg. Lab Bldg., Amherst, MA 01003 USA

The rapid solidification transformation behavior of Fe-Cr-Ni steel alloys was examined using electromagnetic levitation and high-speed imaging. A revision of the Lipton-Kurz-Trivedi growth model is proposed to explain the observed acceleration of growth rates for the stable austenite phase following primary solidification of metastable ferrite. This model is based on an effective mushy zone heat capacity where an additional heat rejection mechanism exists involving isothermal melting of the pre-existing metastable solid to promote enhanced dendritic growth.

9:45 AM

The Effect of Dimensionality on Microstructures in Directionally Solidified SCN-Salol Alloys: *Shan Liu*¹; *Myung-Jin Suk*¹; *Rohit K. Trivedi*¹; ¹Iowa State University, Ames Lab.-USDOE, Ames, IA 50011 USA

Directional solidification has been conducted in SCN-Salol system with an emphasis on morphological evolution and pattern formation under different geometrical conditions. There are two sample configurations used in this study: traditional thin sandwiched glass cell and capillary tube. For thin sample cells, five different thicknesses were used: 12, 25, 50, 100 and 200 μm . While keeping alloy composition, temperature gradient and growth velocity the same, we found that the growth morphology is significantly dependent on the sample thickness. For example, in a 12 μm thick sample, cells cannot form even at a velocity $<1.0 \mu m/s$; while for a sample larger than 100 μm , smooth cells have been observed across solid/liquid interface. For capillary samples, three diameters-45, 75 and 100 μm -have been employed and the cellular patterns in these capillaries will be presented to disclose the scaling relationship among the different length scales describing cellular growth morphology.

TUESDAY AM

10:00 AM

Characteristic Substructure in Directionally Solidified Dilute Al-Cu Alloys: *Oswaldo Fornaro*¹; Hugo A. Palacio²; Heraldo Biloni³; ¹University Nacional del Centro de la Provincia de Buenos Aires, IFIMAT-Fac. Cs. Exactas & CONICET, Pinto 399, Tandil B7000GHG Argentina; ²University Nacional del Centro de la Provincia de Buenos Aires, IFIMAT-Fac. Cs. Exactas & CICPBA, Pinto 399, Tandil B7000GHG Argentina; ³CICPBA

Al-0.2 wt.% Cu alloy samples were directionally solidified under similar thermal gradient conditions. As the growth velocity was increased, the transition among successive stages from planar, nodes, bidimensional, regular and irregular cells, was characterized through careful metallographic analysis of the microsegregation. During the different transitions, a nodal precipitation mechanism seems to be responsible for the evolution of the substructure, where the eutectic precipitation at the nodes plays a fundamental role in the fixation of the substructure. During planar to bands transition, the nodes slow down the interface in certain critical points of it, and the primary spacing can be well defined. This phenomenon seems to be similar during the transition of all the substructure stages under study. The primary spacing fits the order of magnitude of maximum rate wavelength predicted by Morphological stability theory. In several cases, a second order microsegregation pattern at cellular wall level has been observed, that seems to be due to small variation in the microsegregation during the lateral growth of the cells in an enriched intercellular liquid. The secondary microsegregation pattern detected has a rugosity close to the minimum unstable wavelength.

10:15 AM Break**10:45 AM**

Effect of Lead and Antimony on the Grain Structure of Directionally Solidified Zn-Al Alloys: *M. Rappaz*¹; A. S. Quiroga¹; A. Sémoroz²; ¹EPFL, Inst. of Matls., Computational Matls. Lab., MXG, Lausanne CH-1015 Switzerland; ²Alstom (Switzerland) Ltd., TGTT-D, Pav. 4, Baden CH-5400 Switzerland

Zinc alloys with 0.2% Al are widely used to protect steel sheets against corrosion. The thin coatings (typically 20-30 µm), deposited by hot dipping, exhibit fine grains (typically 1 mm in diameter), but with small additions of lead or antimony, the grains become much larger (typically 1 cm). In order to investigate this phenomenon, bulk specimens have been solidified in a standard Bridgman (SB) furnace and in a water-cooled directional solidification (DS) experiment. In this last device, a pre-coated steel sheet was immersed in the melt parallel to the solidification direction in order to induce a competition between regular columnar grains and grains nucleated on the substrate and growing in a transverse direction. In the SB specimens, it was found that the structure changed from columnar to equiaxed when the Al content was increased from 0.2 wt% to 3 wt%. However, with 0.11 wt% Pb addition, the Zn - 3 wt%Al exhibited again a fully columnar structure. In Zn-0.2%Al DS alloys, the structure was columnar almost up to the top of the specimen, but transverse grains could form at the surface of the sheet. Their extension was analyzed using a model similar to that of Hunt for the columnar-to-equiaxed transition. With small additions of Sb, these transverse grains totally disappeared. From microstructure observations and EBSD analyses, it is concluded from both experiments that Pb and Sb most likely poison the nucleation sites.

11:00 AM

Peritectic Reaction in Fe-Co Alloys: *Neill John McDonald*¹; Sridhar Seetharaman¹; ¹Carnegie Mellon University, Matls. Sci. & Engrg., 5000 Forbes Ave., Pittsburgh, PA 15213 USA

Recent work by Professor Kurz along with Dr. Sumida studied the directional solidification of Fe-Co peritectic alloys in order to re-evaluate the Fe-rich part of the phase diagram. Comparing the results of Thermocalc modeling to those of Harris and Hume-Rothery Kurz and Sumida found that there was a significant difference and a new phase diagram, based on experiments completed with a Bridgmann apparatus, was suggested. Using the Confocal Scanning Laser Microscope (CSLM) at Carnegie Mellon University, an investigation of the solidus and liquidus temperatures for hypo- and hyperperitectic Fe-Co samples was performed and the results compared with those of Kurz and Sumida. Also, the rate of austenite formation and growth along the delta-ferrite/liquid boundary was measured and compared to available plate-growth models and past CSLM observations for Fe-Ni. Finally, wavelength dispersive spectroscopy was used to measure the cobalt concentration through the various phases present.

11:15 AM

On Crystallographic Effects in Thin and Bulk Lamellar Eutectic Growth: *Gabriel Paul Faivre*¹; ¹CNRS, GPS (Groupe de Physique

des Solides, GPS - Campus Boucaut -140 Rue de Lourmel -F-75015, Paris 75015 France

We study the effects of a weak surface tension anisotropy on lamellar eutectic microstructures. We report in situ observations made in 10-µm and 300-µm thick, single-grain samples of the transparent alloy CBr₄-C₂Cl₆, and calculations performed in a planar-front approximation. We find that a stationary lamellar pattern actually travels laterally at a definite rate v_d , which is of the order of $10^{-2}xV$ (V : solidification rate), depends on the orientation of the two solid phases, and thus changes from a eutectic grain to another. Therefore, lamella terminations, lamella creations and other dynamical defects occur repetitively along eutectic grain boundaries, preventing the pattern from reaching a stationary state in multigrain samples. This may explain the permanent dispersion of the lamellar spacing observed in long-lasting solidification runs, and the fact that lamellar mismatches ("faults") are observed in transverse cross-sections along subgrain boundaries.

11:30 AM

Mechanisms of Morphological Selection in Al-Si Eutectics: *Ralph E. Napolitano*¹; Luke G. England¹; Choonho Jung¹; Halim Meco¹; ¹Iowa State University, Dept. of Matls. Sci. & Engrg., 204A Wilhelm Hall, Ames, IA 50011 USA

Morphological transitions in Al-Si eutectic solidification are investigated experimentally at both high and low growth rates. Si growth morphology, branching mechanisms, and the selection of overall eutectic structure are examined at directional solidification rates ranging from 5×10^{-7} to 2×10^{-3} m/s. Time evolution of Si particle morphology, interface structure, phase distribution, and crystallographic orientation are measured. Mechanisms of spacing adjustment and crystallographic competition are examined, and the role of interfacial properties is discussed.

11:45 AM

3D Observation of Eutectic Structure of Al₂O₃-YAG System: *Hideyuki Yasuda*¹; Itsuo Ohnaka¹; Akira Sugiyama¹; Yoshiki Mizutani¹; Yishiharu Waku²; Akira Tsuchiyama³; Tsukasa Nakano⁴; Kentaro Uesugi⁵; ¹Osaka University, Dept. of Adaptive Machine Sys., Yamadaoka 2-1, Suita, Osaka 5650871 Japan; ²UBE Industries, Ube Rsch. Lab., Ube, Yamaguchi 7558633 Japan; ³Osaka University, Dept. of Earth & Space Sci., Toyonaka, Osaka 560-0043 Japan; ⁴National Institute of Advanced Industrial Science and Technology, Geological Survey of Japan, Tsukuba, Ibaragi 3058567 Japan; ⁵Japan Synchrotron Radiation Research Institute, Mikazuki, Hyogo 6795198 Japan

The unidirectionally solidified Al₂O₃-YAG(Y₃Al₅O₁₂) eutectic composites have excellent mechanical properties at high temperatures and their mechanical properties are closely related to the characteristic eutectic structure. 3D observation will be useful to understand the structure development, since unidirectionally solidified specimens remain time-evolution of the eutectic structures in the growth direction. This paper presents 3D observation of eutectic structures of Al₂O₃-YAG oxide system and metallic systems (Sn-Pb and Sn-Bi alloys). The micro X-ray computer tomography using monochromatized X-ray of a synchrotron radiation source and a high-resolution detector (0.5mm/pixel) was performed for 3D observation. In the Al₂O₃-YAG composite, both phases were continuous and the sequential branching of Al₂O₃ and YAG in the growth direction resulted in the characteristic eutectic structure in which the constituent phases were entangled each other. The branching sequence was significantly different from the metallic alloys exhibiting the regular and the irregular eutectic structure.

12:00 PM

Lamellar/Rod Transition in Al-Cu Alloys: *Shan Liu*¹; *Jehyun Lee*²; Rohit K. Trivedi¹; ¹Iowa State University, Ames Lab.-USDOE, Ames, IA 50011 USA; ²Changwon National University, Dept. of Metall., Changwon S. Korea

It is generally accepted that binary eutectic either takes lamellar or rod-like form and the transition between them depends on the volume fraction of the minor constituent in the eutectic structure. Through detailed experimental studies in Al-Cu system, we have examined the regimes of the stability of these two morphologies and characterized the dynamics of the transition. We found that the transition is not sharp and the two morphologies can co-exist over a range of volume fraction of the minor phase. Experiments in hyper-eutectic alloys showed that the inter-dendritic or inter-cellular eutectic would always be lamellar. However with the disappearance of the primary phase, the eutectic first becomes rod-like; and then rod and lamellar eutectic coexist over the cross-section of the sample with the rod eutectic region located in the center of the sample. A modified criterion for the regimes of their stability is developed.

12:15 PM

Phase Selection in Unidirectional Growth of Sn-Ag₃Sn Eutectic Alloy: *Hisao Esaka*¹; Kei Shinozuka¹; Manabu Tamura¹; ¹National Defense Academy, Mats. Sci. & Engrg., 1-10-20 Hashirimizu, Yokosuka 239-8686 Japan

The Sn-Ag₃Sn eutectic alloy is one of the candidates for lead-free solders. The solidified structure of this eutectic system is complex. To understand the coupled zone of this alloy, the unidirectional solidification experiments have been carried out. At lower growth velocity, eutectic interface appears. On the other hand, Sn-dendrite appears as a primary phase at higher growth velocity. The distance between the dendrite tip and following eutectic interface (L) are measured with varying the growth velocity (V). L increases rapidly near the transition velocity from eutectic to Sn-dendrite interface with increasing V. L remains constant at higher growth velocity, which indicates that the temperature difference between Sn-dendrite tip and eutectic interface is almost constant, even though the both interface temperatures are the function of V.

12:30 PM

Formation and Effects of Al₂Si₂Ce-Type Phase in Hypereutectic Al-Si Alloy Castings Containing Additions of Phosphide Inoculant and Rare Earths: *Howard Jones*¹; ¹University of Sheffield, Dept. of Engrg. Matls., Sir Robert Hadfield Bldg., Mappin St., Sheffield S1 3JD UK

The effect of 2, 4 and 7wt% cerium mischmetal (RE) additions on constitution and microstructure of Al-20wt%Si-100 ppm P sand shell mould castings is reported. Increasing amounts of primary Al₂Si₂Ce phase are produced together with the primary silicon with the number of primary silicon particles per unit area of section showing a maximum at 2wt%RE while size distribution of the longest silicon particle dimension showed a peak at a value which decreased with increasing RE addition. The XRD data from the Al₂Si₂Ce phase is consistent with the P m1 space group of La₂O₃ and lattice parameters a = 421.5 pm and c = 689.7 pm with the cerium in one of the oxygen positions in the La₂O₃ unit cell. Positioning of RE atoms on silicon attachment sites provides one possible explanation for the growth restricting effects on primary silicon of RE additions.

Surfaces and Interfaces in Nanostructured Materials: General Phenomena & Processes

Sponsored by: Materials Processing and Manufacturing Division, MPMD-Surface Engineering Committee

Program Organizers: Sharmila M. Mukhopadhyay, Wright State University, Department of Mechanical and Materials Engineering, Dayton, OH 45435 USA; Arvind Agarwal, Florida International University, Department of Mechanical and Materials Engineering, Miami, FL 33174 USA; Narendra B. Dahotre, University of Tennessee, Department of Materials Science & Engineering, Knoxville, TN 37932 USA; Sudipta Seal, University of Central Florida, Advanced Materials Processing and Analysis Center and Mechanical, Materials and Aerospace Engineering, Oviedo, FL 32765-7962 USA

Tuesday AM
March 16, 2004

Room: 217A
Location: Charlotte Convention Center

Session Chair: Sharmila M. Mukhopadhyay, Wright State University, Dept. of Mech. & Matls. Engrg., Dayton, OH 45435 USA

8:30 AM **Invited**

Commercialization Programs in Nanostructured Materials: *T. James Rudd*¹; ¹Industrial Innovation, National Science Foundation

The Small Business Innovation Research (SBIR) and Small Business Technology Transfer (STTR) Programs of the National Science Foundation (NSF) provide grants to small companies who are pursuing commercialization of new products based on nanostructured materials. This paper will describe NSF's strategy for nanotechnology development through the SBIR/STTR program. Examples of nanostructured materials will be given that are being commercialized by the small business community and will demonstrate how features of the surfaces and interfaces are being engineered to provide uniquely differentiated products for advanced nanocomposites in chemical, structural, electronic, and biotechnology products.

8:55 AM

Nanoscale Morphology Control Using Ion Beams: *Michael J. Aziz*¹; ¹Harvard University, Div. of Engrg. & Appl. Scis., 29 Oxford St., Cambridge, MA 02138 USA

Low energy ion irradiation of a solid surface can be used to control surface morphology on length scales from 1 micron to 1 nanometer. Focused or unfocused ion irradiation induces a spontaneous self-organization of the surface into nanometer-sized ripples. Dots, or holes; it also induces diameter increases and decreases in a pre-existing nanopore by a tradeoff between sputter removal of material and stimulated surface mass transport. Here we report experiments that illuminate the kinetics of evolution of the surface morphological instability; the influence of initial and boundary conditions on guiding the self-organization; and the kinetics governing the fabrication of nanopores for single-molecule detectors.

9:15 AM

Impurity Effects on the Fracture of Nanocrystalline Fe Using Atomistic Simulations: *Diana Farkas*¹; Brian Hyde¹; Antoine Latapie¹; ¹Virginia Polytechnic Institute and State University, Matls. Sci. & Engrg., 201-A Holden Hall, Blacksburg, VA 24061 USA

Crack propagation studies in nanocrystalline alpha-iron samples with grain sizes ranging from 6 to 12 nm are reported at temperatures ranging from 100K to 600K using atomistic simulations and empirical many body potentials. The mechanisms of plastic deformation energy release are studied in detail. Intergranular fracture is shown to proceed by the coalescence of nano-voids formed at the grain boundaries ahead of the crack. The simulations also show that at an atomistic scale the fracture resistance and plastic deformation energy release mechanisms increase with increasing temperature. The influence of carbon impurities present on the grain boundaries is studied and our results show that the presence of C impurities increases fracture resistance.

9:35 AM

Transformation Behavior in Nanoscale Powders of Binary Aluminum Alloys: *Jixiong Han*¹; Martin J. Pluth¹; Kazuo Furuya²; Jai A. Sekhar¹; Vijay K. Vasudevan¹; ¹University of Cincinnati, Chem. & Matls. Engrg., Cincinnati, OH 45221-0012 USA; ²National Institute of Materials Science, Nanomatls. Lab., Sakura 3-13, Tsukuba 305-0003 Japan

Nanoparticles of Al-Cu and Al-Zn were synthesized by plasma ablation of precursor ingots and the structure of these particles as well structural changes in these on aging at temperatures between 65-190°C for times to 100h studied by electron diffraction, nanoprobe energy dispersive x-ray spectroscopy and HRTEM. The particles were super-saturated fcc state in both cases, but displayed a variation in the individual particle composition when compared with the precursor bulk alloys. A 3-5 nm thick oxide layer was present around all the particles. On aging the Al-Cu nanoparticles, a precipitation sequence consisting of nearly pure Cu precipitates to θ' to the equilibrium θ was observed, with all three forming only along the outer oxide-particle interior interface. The structure of θ' and its interface with the Al matrix was characterized in detail. In the Al-Zn alloy, a spinodal structure was noted in the as-synthesized nanoparticles, which coarsened on aging into a fine scale structure composed of f.c.c twin-related platelets within which were contained platelets with a hcp structure. This morphology led to relatively complicated diffraction effects, which were analyzed in detail. Nearly-pure Zn precipitates, with an hcp structure, also formed along the oxide-particle interface and consumed the spinodal structure with time. Details of the precipitation sequence, nature and structure of second phase precipitates and interphase interfaces and formation mechanisms will be reported. Finally, if time permits results on the precipitation behavior in ultrafine (5-25 nm) Al-Cu nanoparticles will also be presented. Support for this research from AFOSR under grant no. F49620-01-1-0127, Dr. Craig S. Hartley, Program Monitor, is deeply appreciated.

9:55 AM

In-Situ TEM Observation of Crystalline-to-Liquid Phase Change in Nanometer-Sized Alloy Particles: *Jung-Goo Lee*¹; Hiroto Mori¹; ¹Osaka University, Rsch. Ctr. for Ultra High Voltage Electron Microscopy, Yamadaoka 2-1, Suita, Osaka 565-0871 Japan

Alloy phase formation in nanometer-sized particles has been studied using particles in the Sn-Bi system at elevated temperatures. In the tin-rich side, with increasing bismuth concentration, an approximately 8-nm-sized particle of the terminal tin solid solution directly changed into a liquid phase, without taking a stage of solid-liquid coexistence. In the bismuth-rich side, an approximately 8-nm-sized particle of the terminal bismuth solid solution changed first to a particle with a crystal/liquid two-phase microstructure and eventually to a liquid phase, with increasing tin concentration. An approximately 5-nm-sized par-

TUESDAY AM

ticle of the terminal bismuth solid solution, however, directly changed into a liquid phase with increasing tin concentration. From these results, it is expected that the contribution of solid/liquid interface to the total Gibbs free energy is so large with decreasing system size that the behavior of crystalline-to-liquid phase change in nanometer-sized alloy particles is significantly different from that of the corresponding bulk materials.

10:15 AM Invited

Superconducting and Mechanical Aspects of Nanocrystalline Systems: *Chandra Shekhar Pande*¹; Robert A. Masumura¹; ¹Naval Research Laboratory, Code 6325, Washington, DC USA

Critical current (J_c) of superconductors and mechanical strength of normal materials depend sensitively on grain size, leading to a potentially high J_c in fine grained superconductors and the mechanical softening (Inverse Hall Petch) in normal nanocrystalline systems. This paper will discuss the physical mechanisms leading to these results and present analytical expressions describing these properties.

10:40 AM

Critical Factors That Determine FCC to BCC Phase Transformation in Sputter Deposited Austenitic Stainless Steel Films: *Xinghang Zhang*¹; Amit Misra¹; Haiyan Wang¹; C. J. Wetland¹; Roland K. Schulze¹; John D. Embury¹; R. G. Hoagland¹; M. Nastasi¹; ¹Los Alamos National Laboratory, Matls. Sci. & Tech. Div., MS G755, Los Alamos, NM 87545 USA

Bulk austenitic stainless steels (such as 304 SS and 316 SS) have face centered cubic (fcc) structure. However, sputter deposited films synthesized using 304 austenitic stainless steel targets usually exhibit body centered cubic (bcc) structure, while 330 SS films showed fcc structure. The effect of processing parameters on the phase stability of 304 and 330 SS thin films are studied. 304 SS thin films with in-plane, biaxial residual stresses in the range of ~1 GPa (tensile) to ~300 MPa (compressive) exhibited only bcc structure. The retention of bcc 304 SS after high temperature annealing followed by slow furnace cooling is consistent with a depletion of Ni in the as-sputtered 304 SS films. Rutherford backscattering spectroscopy and Auger depth profiling also indicated slight decrease in the Ni content below the ~8% needed to stabilize fcc structure at room temperature. The concentration of Ni, substrate temperature and energy of deposited atoms are considered crucial factors in determining the phase transformations in sputter deposited austenitic SS films.

11:00 AM

Surface Damage Mechanisms in Clay-Filled Polymer Nanocomposites: *Aravind Dasari*¹; Pankaj Nerikar¹; Santosh D. Wanjale²; Jyoti P. Jog²; Devesh K. Misra¹; ¹University of Louisiana, Dept. of Chem. Engrg., PO Box 44130, Lafayette, LA 70504-4130 USA; ²National Chemical Laboratory, Pashan, Pune, Maharashtra 411008 India

Resistance to surface damage introduced by scratching or mechanical deformation process is important to many engineering applications. The paper describes micromechanisms of surface deformation and subsequent propagation into the bulk in clay-filled polymer nanocomposites. The potential of atomic force microscopy is combined with high resolution scanning electron microscopy to examine micro- and nanoscale deformation processes.

Symposium on Microstructural Stability in Honor of Prof. Roger D. Doherty: Microstructural Stability: Plastic Deformation

Sponsored by: Aluminum Association, Materials Processing and Manufacturing Division, Structural Materials Division, MPMD-Solidification Committee, SMD-Physical Metallurgy Committee
Program Organizer: Anthony D. Rollett, Carnegie Mellon University, Department of Materials Science & Engineering, Pittsburgh, PA 15213-3918 USA

Tuesday AM Room: 216A
March 16, 2004 Location: Charlotte Convention Center

Session Chair: Roger D. Doherty, Drexel University, Matls. Engrg. Dept., Philadelphia, PA 19104 USA

8:30 AM

Deformation and Annealing Structures in Cold-Rolled Aluminium (AA1200): *Niels Hansen*¹; Xiaoxu Huang¹; Grethe Winther¹; Qingfeng Xing¹; ¹Risø National Laboratory, Matls. Rsch. Dept., Ctr.

for Fundamental Rsch., Metal Structures in 4-D, Roskilde DK-4000 Denmark

TEM investigations of metals deformed to low and medium strains have shown a correlation between the crystallographic orientation and the deformation microstructure, which is characterized by a number of structural parameters, e.g., morphology, spacing between and misorientation angle across dislocation boundaries and high angle grain boundaries. To examine if such a correlation also exists after deformation to large strains, aluminium of commercial purity (AA1200) was cold rolled to a strain of 2 and characterized by TEM and Kikuchi pattern analysis. The examination of longitudinal sections showed elongated volumes on a relatively large scale belonging to different texture components and within each of these a fine lamellar structure composed of extended boundaries and short interconnecting boundaries. The deformation was followed by annealing at 200 and 220°C for 2 hours, which gave rise to a structural coarsening and a change in morphology from a lamellar structure towards a more equiaxed microstructure. The observations were discussed, especially the correlations between crystallographic orientation and microstructural parameters both in the deformed state and after annealing.

9:00 AM

Orientation Changes of Individual Bulk Grains During Deformation: *Grethe Winther*¹; Lawrence Margulies¹; Henning Friis Poulsen¹; ¹Risø National Laboratory, Matls. Rsch. Dept., Ctr. for Fundamental Rsch., Metal Structures in 4-D, DK-4000 Roskilde Denmark

Modelling deformation textures has mainly been based on experimental bulk textures. An essential question is the relative effects of the initial orientation of a grain and its local environment, i.e. grain interaction. To effectively address this question, data on individual grains is needed. Studies of surface grains provide such data but surface conditions may deviate strongly from bulk. To mimic bulk conditions, split samples have been used. Recently, three dimensional X-ray diffraction has proven capable of measuring the behaviour of individual grains deeply embedded in the bulk of the sample. About 100 individual grains in the bulk of AA 1050 during tension has been investigated. The grain size was 75 micrometer and the elongation 6%. The data are analysed for the relative effects of initial grain orientation and grain interaction. Comparison with the Taylor model is made, revealing that it works well in some cases but not in others.

9:25 AM

Definition Elaboration for Recrystallization Either Dynamic or Static: *Hugh J. McQueen*¹; ¹Concordia University, Mech. Engrg., 1455 Maisonneuve Blvd. W, Montreal, Quebec H3G 1M 8 Canada

Currently there are controversial descriptions of hot strain induced microstructures in aluminum or ferrite: either as dynamic recovery (DRV) or as continuous dynamic recrystallization (DRX). For steady state creep, DRV adequately explains the substructure remaining constant in character and axial ratio in elongating grains; however in warm working, some random subboundary segments (other than transition boundaries between deformation bands) attain misorientations above 8°. While DRV theory predicts these would be subject to rearrangement, continuous DRX theory claims they constitute recrystallization. The controversy would end if the definition of recrystallized grains required the formation of regions surrounded by relaxed high angle boundaries that (i) are not responsive to stress and (ii) can migrate without dislocation participation. With this definitional requirement, polygonized misoriented regions in warm working, like layer bands after heavy cold rolling, are not recrystallized until annealed.

9:50 AM

Twinning and Stages of Deformation in Low Stacking Fault Energy Austenitic Steel Single Crystals: *Ibrahim Karaman*¹; Huseyin Sehitoglu²; Hans J. Maier³; Yuriy I. Chumlyakov⁴; ¹Texas A&M University, Dept. of Mech. Engrg., MS 3123, College Sta., TX 77843 USA; ²University of Illinois, Dept. of Mech. & Industrial Engrg., 1206 W. Green St., Urbana, IL 61801 USA; ³University of Paderborn, Lehrstuhl f. Werkstoffkunde, Paderborn 33095 Germany; ⁴Siberian Physical-Technical Institute, Revolution Sq. 1, Tomsk 634050 Russia

The works of Prof. Roger D. Doherty on fcc materials have helped understanding of the mechanisms of the work-hardening stages in these materials. The present authors have been often inspired by his works on their study on the deformation of low stacking fault energy austenitic steels, in particular on the stainless steel and Hadfield manganese steel single crystals. In the present talk, our recent findings on these materials will be summarized in regards to the competition between slip and twinning, texture evolution, interstitial atom content and precipitation. Twinning was observed as a primary deformation mechanism at the onset of deformation in certain orientations. The

volume fraction of twinning was increased with increasing carbon concentration but first decreased and then increased by increasing nitrogen concentration. Incoherent precipitates did not suppress twinning but increased the flow stress level. In the orientations where twinning theoretically is impossible, extrinsic stacking faults and very thin twins were observed. In the conditions in which twinning is the case, an upward stress-strain response was evident. The single crystal data has provided insight into the operating microstructural mechanisms and the orientation relationships, and the micromechanisms behind the aforementioned observations are explained. We have used the data obtained on polycrystals for the mesoscopic and macroscopic model development and for verification purposes. The vehicle for the quantitative bridge between single and polycrystal results is crystallographic texture measurements. Major thrust of the modeling studies have been the treatment of the competing effects of several deformation mechanisms (cell structure, twinning, coherent and incoherent precipitates). These effects are being incorporated into single crystal hardening laws with a sound mechanism-based internal state variable theory and validated through the stress-strain response, and microstructural and texture evolution of several single crystal orientations. The part of the research conducted at Texas A&M University was supported by the National Science Foundation contract CMS 01-34554, Solid Mechanics and Materials Engineering Program, Directorate of Engineering, Arlington, Virginia. The part of the work conducted at The University of Illinois was supported by the National Science Foundation contract CMS 99-00090, Mechanics of Materials Program, Directorate of Engineering, Arlington, Virginia.

10:10 AM

The Effect of Twinning on the Work Hardening Behavior of Hafnium: *E. K. Cerreta*¹; C. A. Yablinsky²; G. T. Gray¹; ¹Los Alamos National Laboratory, MST-8, MS G755, Los Alamos, NM 87545 USA; ²Carnegie Mellon University, Matls. Sci. Dept., 5000 Forbes Ave., Pittsburgh, PA 15213 USA

In many HCP metals, both twinning and slip are known to be important modes of deformation. However, the interaction of the two mechanisms and their effect on work hardening is not well understood. In hafnium, twinning and work hardening rates increase with increasing strain, increasing strain rate, and decreasing temperature. At low strains and strain rates and at higher temperatures, slip dominates deformation and rates of work hardening are relatively lower. To characterize the interaction of slip and twinning, Hf specimens were prestrained quasi-statically in compression at 77K, creating specimens that were heavily twinned. These specimens were subsequently reloaded at room temperature. Twinning within the microstructures was characterized optically and using transmission electron microscopy. The interaction of slip with the twins was investigated as a function of prestrain and correlated with the observed rates of work hardening.

10:30 AM

Evaluation of Path Dependency in Shock Wave Damage Through Electron Backscatter Diffraction: *Benjamin L. Henrie*¹; Thomas A. Mason¹; George (Rusty) T. Gray¹; David B. Holtkamp²; ¹Los Alamos National Laboratory, MST-8, PO Box 1663, MS G755, Los Alamos, NM 87545 USA; ²Los Alamos National Laboratory, P-22, PO Box 1663, MS D410, Los Alamos 87545 USA

A number of plate impact experiments using an 80-mm launcher and direct high explosive (HE) experiments were performed to study dynamic damage in high-purity copper and tantalum. Real time free surface velocity (VISAR) measurements were captured and specimens were recovered for subsequent postmortem characterization using optical metallography and electron backscatter diffraction (EBSD). Analysis of the intensity and quality of the EBSD patterns yields greater insight into the characterization of strain localization. This analysis will be used to compare the damage arising in samples shocked with square and Taylor waves.

10:50 AM

Effect of Deformation Twinning on the Strain Hardening of hcp Titanium: *A. A. Salem*¹; S. R. Kalidindi²; R. D. Doherty²; S. L. Semiatin³; ¹Universal Technology Corporation, 1270 N. Fairfield Rd., Dayton, OH 45432 USA; ²Drexel University, Matls. Engrg. Dept., Philadelphia, PA 19104 USA; ³Air Force Research Laboratory, Matls. & Mfg. Direct., AFRL/MLLM, Wright-Patterson AFB, OH 45433 USA

The stress-strain behavior of two grades of textured alpha-titanium was established using quasi-static simple compression tests at ambient-temperature. Compression samples cut from the specimen reference directions (RD, TD, and ND) were used to evaluate the effect of crystallographic texture on the stress-strain response. Plots of the strain-hardening rate versus stress revealed three distinct stages for the material that had the basal pole close to the compression axis or

perpendicular to it. The sudden increase in the strain-hardening rate was correlated to the onset deformation twinning. Microhardness measurements revealed that the deformation twins were harder (immediately after being formed) than the matrix. This observation supported the Basinski model for the hardening associated with twinning. As a result, deformation twinning leads to two competing effect on the overall strain hardening response: (1) strain hardening via the Hall-Petch and Basinski hardening mechanisms and (2) texture softening due to reorientation of the twinned areas.

11:10 AM

The Effect of Surface Shear From Rolling on Surface Texture, Recrystallization, and Functional Properties in Pure Cu and Pure Nb: *Hairong Jiang*¹; *Alireza Fallahi*¹; *Thomas R. Bieler*¹; *Chris C. Compton*²; *Terry L. Grimm*²; ¹Michigan State University, Dept. Chem. Engrg. Matl. Sci., 2527 Engrg. Bldg., E. Lansing, MI 48824 USA; ²Michigan State University, Natl. Superconducting Cyclotron Lab., E. Lansing, MI 48824 USA

Pure Cu and pure Nb are used to make RF (radio frequency) cavities used in particle accelerators. The performance of RF cavities is degraded by electron emission, which is strongly dependent on crystal orientation and surface roughness. Analyses of texture gradients from the surface to the interior in rolled and recrystallized pure Nb shows strong $\langle 111 \rangle // ND$ (normal direction) fiber texture in the center, similar to IF (interstitial free) steels, but the surface has a high population of grains with $\langle 100 \rangle // ND$, unlike IF steels. The work function for electron emission of $\langle 100 \rangle$ grains is much smaller than for $\langle 111 \rangle$ grains, making $\langle 100 \rangle$ grains undesirable for Nb RF cavities. Using tapered specimens of pure Nb and pure Cu, the effect of the amount of reduction and the rolling path are examined to determine how they affect recrystallization textures on the surface as compared to the interior. The recrystallization phenomena and mechanisms of surface grains are discussed and compared to existing studies in other FCC and BCC metals.

11:35 AM

The Relationship Between the Shearable/Non-Shearable Transition and the Mechanical Response of 6000 Series Alloys: *Warren J. Poole*¹; *John David Embury*²; *David J. Lloyd*³; ¹University of British Columbia, Dept. of Metals & Matls. Engrg., 309-6350 Stores Rd., Vancouver, BC V6T 1Z4 Canada; ²McMaster University, Dept. of Matls. Sci. & Engrg., 1280 Main St. W., Hamilton, ON L8S 4L7 Canada; ³Alcan International, Kingston R&D Ctr., 945 Princess St., Kingston, ON Canada

Currently, there is a particular interest in the application of 6000 series alloys in the automotive sector. This has led to the desire for the development of process models to predict mechanical properties for a variety of multi-step ageing treatments. This work focuses on the dependence of the yield strength, work hardening rate and strain rate sensitivity on the precipitate size, volume fraction and the size distribution. A yield strength model has been developed which explicitly includes the effect of the precipitate size distribution which was quantified by detailed transmission electron microscope (TEM) studies. The work hardening behaviour have been understood in the Kocks-Mecking framework after suitable modifications to include an appropriate flow stress superposition law and a geometric dislocation storage term when precipitates are non-shearable. It was observed that there were significant changes in the material behaviour at the shearable/non-shearable transition, i.e. after the transition, slip lines cannot be observed on the surface and there is a characteristic increase in the rate of dynamic recovery. Detailed TEM and high resolution TEM studies were conducted to examine the details dislocation/precipitate interactions for the cases of shearable and non-shearable precipitates. It was found that the work hardening behaviour, slip line and TEM observations are consistent.

12:00 PM

Deformation Twinning in FCC and HCP Metals: New Insights from Collaborations with Roger Doherty: *Surya R. Kalidindi*¹; ¹Drexel University, Matls. Sci. & Engrg., Philadelphia, PA 19104 USA

Deformation twinning has been known to play a significant role in the mechanical response of hcp metals (e.g. Ti alloys) and low stacking fault energy fcc metals (e.g. Brass). This has been a major area of research collaboration between the author and Professor Roger D. Doherty for the last ten years. This collaboration has provided tremendous new insight into the physics of how deformation twins influence the mechanical behavior of these metals. Although there are major differences in the driving factors for the formation of deformation twins in these two distinctly different classes of materials, the consequence on the mechanical behavior shows remarkable similarity in several aspects. The main results of this collaborative effort will be

highlighted, and the implications of these results on the modeling effort will be discussed.

The Didier de Fontaine Symposium on the Thermodynamics of Alloys: First Principle Calculations and Cluster Expansion Techniques

Sponsored by: Materials Processing and Manufacturing Division, MPMD-Computational Materials Science & Engineering-(Jt. ASM-MSCTS)

Program Organizers: Diana Farkas, Virginia Polytechnic Institute and State University, Department of Materials Science and Engineering, Blacksburg, VA 24061 USA; Mark D. Asta, Northwestern University, Department of Materials Science and Engineering, Evanston, IL 60208-3108 USA; Gerbrand Ceder, Massachusetts Institute of Technology, Department of Materials Science and Engineering, Cambridge, MA 02139 USA; Christopher Mark Wolverton, Ford Motor Company, Scientific Research Laboratory, Dearborn, MI 48121-2053 USA

Tuesday AM Room: 216B
March 16, 2004 Location: Charlotte Convention Center

Session Chair: TBA

8:30 AM Invited

Electronic Structure, Stability, and Order in V-X (X=Ru,Rh,Pd) Alloys: *Patrice E.A. Turchi*¹; Vaclav Drchal²; Josef Kudrnovsky²; Richard M. Waterstrat³; ¹Lawrence Livermore National Laboratory, PO Box 808 (L-353), Livermore, CA 94551 USA; ²Academy of Sciences of the Czech Republic, Inst. of Physics, Na Slovance 2, Prague 8, CZ 182-21 Czech Republic; ³National Institute of Science and Technology, Matls. Sci. & Engrg. Lab., 100 Bureau Dr., Gaithersburg, MD 20899-8551 USA

Using a first-principles methodology, electronic structure, ordering trends and stability properties of V-X alloys, where X=Ru, Rh, and Pd, are presented. The methodology is based on the Generalized Perturbation Method (GPM) applied to the fully relativistic Tight-Binding Linear Muffin-Tin Orbital (TB-LMTO) description of the electronic structure of the chemically random configuration of the alloy within the Coherent Potential Approximation (CPA). Density of states at the Fermi energy and γ of specific heat measurements are compared as functions of composition for the three alloys. Finally ordering trends and stability properties are rationalized as functions of simple electronic parameters. Work performed under the auspices of the U. S. Department of Energy by the University of California Lawrence Livermore National Laboratory under Contract W-7405-ENG-48. This work has benefited from the experimental results of the late R. Kuentzler.

9:00 AM

Prediction of Complex Binary Ground State Structures in bcc-Based Refractory Alloys: *Volker Blum*¹; Alex Zunger¹; ¹National Renewable Energy Laboratory, 1617 Cole Blvd., Golden, CO 80401 USA

The stability of bcc-based binary ground state configurations is often discussed in terms of simple interatomic interactions, which stabilize simple usual-suspect structures. Using realistic interactions from the LDA-based mixed-basis cluster expansion method, we find unexpectedly complex ground states in the bcc-based refractory alloy systems Ta-Mo and Nb-W. In Ta-Mo (Ref. 1), a quasi-continuous series of Mo-rich (100) superlattices (including C11b and B2) coexists with Ta-rich large-cell ground states (13 and 16 atoms per unit cell). Surprisingly, the ground states of Nb-W are quite different from Ta-Mo, with (111) superlattices as the dominant motif. We then predict order-disorder transition temperatures and the mixing enthalpy and short-range order of the solid solution phase at $ST > 0$ for both systems from canonical Monte Carlo simulations. ¹Volker Blum and Alex Zunger, "Are binary bcc ground states more complex than we knew: The case of bcc Mo-Ta", submitted to Phys. Rev. B (2003).

9:20 AM

First-Principles Thermodynamic Calculations of Phase Equilibria of Fe-Based Alloy Systems: *Ying Chen*¹; Shuichi Iwata¹; Tetsuo Mohri²; ¹University of Tokyo, Dept. of Quantum Engrg. & Sys. Sci., Hongo 7-3-1, Bunkyo-ku, Tokyo 113-8655 Japan; ²Hokkaido University, Grad. Sch. of Engrg., Div. of Matls. Sci. & Engrg., Kita-13 Nishi-8, Kita-ku, Sapporo, Hokkaido 060-8628 Japan

By combining FLAPW total energy calculations with the Cluster Variation Method via Cluster Expansion Method, first-principles investigation of phase equilibria on three kinds of Fe-based alloy systems has been attempted. The particular emphasis is placed on the L10-disorder phase equilibria. With the effective cluster interaction energies extracted based on the total energies of stable ordered phases, the transition temperature is well reproduced with high accuracy for each system. Two major modifications are attempted. The first one is the incorporation of lattice vibration effects through quasi harmonic approximation, and the resultant transition temperature is further improved. The second modification is to introduce the information of hypothetical ordered phases to include long distant or larger cluster interactions. For this, additional total energy calculations are performed for L11 and D022 ordered phases. The resultant phase equilibria is critically examined.

9:40 AM

Phase Stability of Al-Ti-Zn System: Integration of Ab Initio Results and Computational Thermodynamics: *Gautam Ghosh*¹; Zhe Liu¹; Axel van de Walle¹; Mark D. Asta¹; ¹Northwestern University, Dept. of Matls. Sci. & Engrg., 2225 N. Campus Dr., Evanston, IL 60208-3108 USA

As a part of our research effort to design precipitation strengthened Al-base alloys, we present two major results concerning the phase stability modeling of the Al-Ti-Zn system. First, the results of ab initio phase stability of the Ti-Zn system where a part of the phase diagram is known but there is no measured thermodynamic data. Second, ab initio results of vibrational entropy contributions to the phase stability of selected intermetallic compounds. To facilitate calculation of binary and ternary phase diagrams, ab initio results are successfully integrated within computational thermodynamics formalism. We also present the application of phase stability modeling and computational thermodynamics to design new Al-base alloys.

10:00 AM Invited

Structure, Dynamics and Thermodynamics of Metal Surfaces from First-Principles: *Nicola Marzari*¹; ¹Massachusetts Institute of Technology, Dept. of Matls. Sci. & Engrg., 77 Mass. Ave., Cambridge, MA 02139 USA

The thermodynamical stability of metal surfaces has been investigated using ab-initio molecular dynamics and linear-response techniques. Several systems exhibited unexpected characteristics, and were strongly influenced by temperature and crystallographic orientation. The reasons for this variety lie in the subtle balance between energetic and entropic effects, and in the wide range of environments that surface atoms experience. First-principles calculations provide an unbiased description of such bonding, while the small barriers involved allow for affordable thermalization timescales. (a) Clean Al(110) is shown to be strongly anharmonic, where the first interlayer distance contracts with increasing temperature. The atoms in the second layer show large mean square displacements that are preliminary to the ejection of adatoms onto the surface. (b) The diffusion of adatoms on Al(100) becomes increasingly complex with temperature, switching from direct exchanges to long, concerted exchanges, and leading to a reversible, local melting around the adsorption sites. (c) Al(111) and Ag(111) surfaces have small barriers between stable and metastable stackings, allowing the vibrational entropy to become the driving force tuning the stability of small islands.

10:30 AM Break

10:40 AM Invited

Large Scale Simulations of the Relaxor Ferroelectric Pb(Sc_{1/2}Nb_{1/2})O₃: *Benjamin P. Burton*¹; Umesh Waghmare²; Eric Cockayne¹; ¹National Institute for Science and Technology, Ceram., 1 Bureau Dr., A226/223, Gaithersburg, MD 20899 USA; ²J. Nehru Center for Advanced Scientific Research, Bangalore 560 064 India

Experiments indicate that both chemical order-disorder and Pb-vacancies strongly affect the dielectric properties of relaxor ferroelectrics such as Pb(Sc_{1/2}Nb_{1/2})O₃ (PSN) and Pb(Mg_{1/3}Nb_{2/3})O₃ (PMN). Of particular interest are microstructures with 4-10 nm short-range ordered (SRO) domains in a disordered matrix. We use a first-principles based effective Hamiltonian to investigate the effects of ordered microdomains on temperature-dependent properties of PSN. Our model is based on Pb-centered polar variables and includes the local random fields at Pb-sites which are caused by: 1) B-site chemical disorder; 2) Randomly placed Pb-O vacancy pairs. We create supercells (40x40x40-primitive cells) that contain a variety of ordered and partially ordered states: Fully ordered; Random; ~4 nm ordered PSN domains in a disordered matrix; a short-range ordered state and some long-range ordered states with various degrees of disorder, that were calculated from first-principles via the cluster expansion approach.

11:10 AM

The Calculated Thermodynamic Properties of Al, Ni, NiAl, and Ni₃Al: *Yi Wang*¹; Zikui Liu¹; Longqing Chen¹; ¹Pennsylvania State University, Matls. Sci. & Engrg., 106 Steidle Bldg., State College, PA 16802-5006 USA

The thermodynamic properties of Al, Ni, NiAl, and Ni₃Al have been studied through the first-principles approach. The 0-K total energies are calculated using the ab initio plane wave pseudopotential method within the generalized gradient approximation. The contribution to the free-energy from the lattice is calculated using the phonon densities of state derived by means of the ab initio linear-response theory. The thermal electronic contribution to the free-energy is calculated from the one-dimensional numerical integration over the electronic density-of-state. With the deduced Helmholtz free energy thereafter, the thermal expansion and enthalpy as a function of temperature between 0 K and melting temperatures are calculated and compared with the experimental data.

11:30 AM

First Principles Calculation of Diffusion in Binary Alloys: *Anton Van der Ven*¹; Gerbrand Ceder¹; ¹Massachusetts Institute of Technology, Dept. of Matls. Sci. & Engrg., Rm. 13-4053, 77 Mass. Ave., Cambridge, MA 02139 USA

Diffusion in multicomponent solids plays an important role in battery and fuel cell applications as well as during the synthesis of a material as this is often accompanied by phase transformations involving atomic redistribution. We have extended the mathematical tools of alloy theory (theory of first principles phase-diagram calculations) for the study of diffusion in solids with configurational disorder. We have applied this formalism to study diffusion in Al-Li alloys as a function of alloy composition and temperature from first principles. We predict that the vacancy concentration in this alloy has a strong dependence on the short-range order among lithium and aluminum atoms with the vacancy preferring aluminum over lithium in its first nearest neighbor shell. Furthermore, the vacancy concentration is predicted to depend strongly on alloy composition within the ordered Al₃Li L1₂ phase. While the vacancy prefers aluminum rich environments, first principles calculations of activation barriers predict that Li has a lower activation barrier than Al for exchange with a neighboring vacant site. With the cluster expansion formalism combined with kinetic Monte Carlo simulations, we have calculated the alloy diffusion coefficients using Green-Kubo relations. These can be used in phase-field models to predict the kinetics of precipitation transformations in this alloy.

11:50 AM

Hydrogen in Aluminum: *Chris Wolverton*¹; Mark D. Asta²; Vidvuds Ozolins³; ¹Ford Motor Company, MD 3083/SRL, PO Box 2053, Dearborn, MI 48121 USA; ²Northwestern University, Dept. of Matls. Sci., Evanston, IL 60208 USA; ³University of California, Dept. of Matls. Sci. & Engrg., Los Angeles, CA 90095-1595 USA

Despite decades of study, several key aspects of the Al-H system remain the subject of considerable debate. We perform a thorough study of this system using first-principles density functional calculations. We show that generalized gradient calculations provide an accurate picture of energetics, phase stability and structure, diffusion, and defect binding in the Al-H system. A series of calculations for hydrides in the M-H systems (M = Al, Ba, Ca, K, Mg, La, Li, Na, Ni, Pd, Sc, Sr, Ti, V, and Y) also shows that the GGA calculations are a quantitatively accurate predictor of hydride formation energies. For Al-H, we find: 1) Atomic relaxation and anharmonic vibrational effects play important roles in the interstitial site preference. 2) The calculated heat of solution and hydride energetics are both consistent with experimental measurements. 3) Interstitial H interacts strongly with Al vacancies, with vacancies strongly influencing the migration energy of H diffusion.

Third International Symposium on Ultrafine Grained Materials: UFG Material Fundamentals

Sponsored by: Materials Processing & Manufacturing Division, MPMD-Shaping and Forming Committee

Program Organizers: Yuntian Ted Zhu, Los Alamos National Laboratory, Materials Science and Technology Division, Los Alamos, NM 87545 USA; Terence G. Langdon, University of Southern California, Departments of Aerospace & Mechanical Engineering and Materials Engineering, Los Angeles, CA 90089-1453 USA; Terry C. Lowe, Metallum, Santa Fe, NM 87501 USA; S. Lee Semiatin, Air Force Research Laboratory, Materials & Manufacturing Directorate, Wright Patterson AFB, OH 45433 USA; Dong H. Shin, Hanyang University, Department of Metallurgy and Material Science, Ansan, Kyunggi-Do 425-791 Korea; Ruslan Z. Valiev, Institute of Physics of Advanced Material, Ufa State Aviation Technology University, Ufa 450000 Russia

Tuesday AM

Room: 207A

March 16, 2004

Location: Charlotte Convention Center

Session Chairs: Yuntian T. Zhu, Los Alamos National Laboratory, Matls. Sci. Tech. Div., Los Alamos, NM 87545 USA; Dieter Wolf, Argonne National Laboratory, Matls. Sci. Div., Argonne, IL 60516 USA; Minoru Umemoto, Toyohashi University of Technology, Toyohashi, Aichi 441-8580 Japan

8:30 AM **Invited**

Deformation Mechanisms in Nanocrystalline Materials by Molecular Dynamics Simulation: *Dieter Wolf*¹; ¹Argonne National Laboratory, Matls. Sci. Div., 9700 S. Cass Ave., Bldg. 212, Argonne, IL 60516 USA

We describe large-scale molecular-dynamics simulations of nanocrystalline-Al and Pd model microstructures to demonstrate how and why the conventional dislocation-slip mechanism shuts down with decreasing grain size, in favor of a grain-boundary based deformation mechanism. Our simulations of textured and fully three-dimensional Al polycrystals reveal that, instead of from the usual Frank-Read sources, dislocations nucleate from the grain boundaries and grain junctions. As the grain size decreases, the magnitude of the stress-dependent splitting distance of these dissociated dislocations eventually becomes comparable to the grain size, preventing their complete nucleation and hence contributing ever less to the total strain. Our simulations also reveal that, in the absence of grain growth and any dislocation activity, nanocrystalline fcc metals deform via a mechanism involving an intricate interplay between grain-boundary sliding and grain-boundary diffusion.

8:50 AM **Invited**

What Simulations Suggest on Deformation Mechanism in nc-Metals: *Helena Van Swygenhoven*¹; P. M. Derlet¹; A. Hasnaoui¹; ¹Paul Scherrer Institute, NUM-ASQ, CH-5232, Villigen Switzerland

Large-scale molecular dynamics simulations of fully 3D-nanocrystalline (nc) Ni samples provide intriguing insights into the effects of grain size and grain boundary (GB) structure on nc structural and mechanical properties. The simulations suggest a deformation mechanism intrinsic to the nanosized GB network where the GB structure plays a central role consisting of an interplay between (1) GB sliding accommodated by GB and Triple Junction migration and (2) dislocation emission and absorption in GBs, both of which are at the origin of the formation of local shear planes that facilitates plastic deformation explaining the dimple-like features seen on experimental fracture surfaces. The proposed mechanisms are interpreted in terms of recent experimental results such as work hardening, activation volume and in-situ rms strain measurements in the Swiss Light Source.

9:10 AM **Invited**

Mechanical Behavior of Nanostructured Metals: New Mechanisms and Applications: *Evan Ma*¹; ¹Johns Hopkins University, Matls. Sci. & Engrg., 3400 N. Charles, Baltimore, MD 21218 USA

The mechanical properties of nanostructured materials are of considerable interest at present. New phenomena and opportunities are expected to emerge when the grain sizes of the metals are brought down to the ultrafine-grained or nanocrystalline regime. For example, at the high stresses needed for the nanostructured metals to plastically deform, the formation of stacking faults and deformation twins can become prevalent, as the role of the partial dislocations becomes important.¹ Also, with nanoscale grains, one has now extra room to manipulate the grain structure in favor of high strength, ductility, or a

TUESDAY AM

combination of both.² The altered mechanical responses, in terms of the strain rate/temperature dependences and the tendency for shear localization^{3,4} for example, may be desirable in certain applications. Examples will be presented in this talk to discuss the various aspects outlined in the preceding paragraph. ¹M.W. Chen et al., Science 300 (2003) 1275. ²Y.M. Wang et al., Nature 419 (2002) 912. ³D. Jia et al., Acta mater. 51 (2003) 3495. ⁴Q.M. Wei et al., unpublished data.

9:30 AM Invited

Compact and Dissociated Dislocations in Al: Implications for Deformation in fcc Metals: *S. G. Srinivasan*¹; M. I. Baskes¹; X. Z. Liao¹; R. J. McCabe¹; Y. H. Zhao¹; Y. T. Zhu¹; ¹Los Alamos National Laboratory, Matls. Sci. & Tech., Los Alamos, NM 87545 USA

Recently, our high-resolution electron-microscopy studies revealed the existence of both compact and dissociated dislocations in ultrafine-grained aluminum. We examine the consequences of this dual core state using atomistic simulations, employing two state of the art embedded atom method Al potentials. The calculated minimum stress (Sp) required moving an edge dislocation is approximately 20 times smaller for dissociated than for equivalent compact dislocations. The well-accepted generalized stacking fault energy paradigm, however, predicts similar Sp values for both configurations. Additionally, Frank's rule and Schmid law are also disobeyed. We examine the implications of these results in addressing the long-standing problem of the magnitude of Sp in face-centered-cubic metals.

9:50 AM Invited

Stacking Fault and Twinning in Ultrafine-Grained Al: *Xiaozhou Liao*¹; Yonghao Zhao¹; Srivilliputhur G. Srinivasan¹; Fei Zhou²; Enrique J. Lavernia²; Michael I. Baskes¹; Yuntian T. Zhu¹; ¹Los Alamos National Laboratory, Matl. Sci. & Tech. Div., MS G755, Los Alamos, NM 87545 USA; ²University of California, Dept. Chem. Engrg. & Matl. Sci., Davis, CA 95616 USA

Ultrafine-grained (UFG) materials with grain sizes ranging from 10-1000 nm are believed to deform by different mechanisms from their coarse-grained counterparts. Here we report the experimental observations of stacking faults (SF) ribbons and deformation twinning in UFG Al processed by severe plastic deformation. The SF ribbons are 1.4-8.6 nm in width, which is 3-17 times the width of SFs in coarse-grained Al. The deformation twinning was formed by new mechanisms different from conventional pole mechanism. Partial dislocations emitted from grain boundaries played a critical role in the formation of SFs and twinning. These results are surprising because 1) partial dislocation emission from grain boundaries has never been experimentally observed and 2) deformation twinning have never been reported in Al due to its high SF energy. These observations directly validate some recent molecular dynamics simulations and provide further insights on deformation mechanisms in UFG materials.

10:10 AM

Formation Mechanisms of Colossal Stacking Fault in Ultrafine-Grained Al: *Yuntian T. Zhu*¹; Xiaozhou Liao¹; Yonghao Zhao¹; Srivilliputhur G. Srinivasan¹; Michael I. Baskes¹; ¹Los Alamos National Laboratory, Matl. Sci. & Tech. Div., MS G755, Los Alamos, NM 87545 USA

Colossal stacking fault ribbons have been observed in UFG Al processed by severe plastic deformation (SPD). The stacking fault ribbons are 1.4-8.6 nm in width, which is 3-17 times the width of stacking faults in coarse-grained Al. This observation are really surprising considering the high stacking fault energy. Our analytical modelling indicates that these colossal stacking faults were formed due to the size effect in ultrafine-grained Al and the high density of stacking faults and full dislocations. They present a new critical piece to the puzzle of deformation mechanisms in ultrafine-grained materials and provide a good explanation for the good ductility in ultrafine-grained materials.

10:25 AM

3D Atom Probe Investigation of a Pearlitic Steel Deformed by High Pressure and Torsion: *Xavier Sauvage*¹; Ruslan Z. Valiev²; ¹Université de Rouen, Groupe de Physique des Matériaux, CNRS - UMR 6634, Ave. de l'université, BP 12, Saint-Etienne du Rouvray 76801 France; ²Ufa State Aviation Technical University, Inst. of Physics of Advd. Matls., 12, K. Marx St., Ufa 450000 Russia

The nanostructure and the phase composition of a pearlitic steel deformed by high pressure and torsion (HPT) were investigated by field ion microscopy (FIM) and 3D atom probe (3D-AP). In spite of the extremely high level of plastic deformation, the original lamellar structure of pearlite remains in the deformed material. The inter-lamellar spacing is however strongly reduced and 3D reconstructions at the atomic scale show that cementite (Fe₃C) lamellae are dissolved. The lamellar nanostructure is made of ferrite lamellae almost carbon free and of carbon rich region (former Fe₃C) with a carbon amount in

a range of 4 to 14 at%. These data are compared with previous investigations of the same pearlitic steel processed by cold drawing.

10:40 AM Break

10:50 AM Invited

Plasticity of Ultrafine Grained Materials: *Horst W. Hahn*¹; ¹TU Darmstadt, Inst. of Matls. Sci., Petersenstr. 23, Darmstadt, Hesse 64287 Germany

From the beginning of research on nanocrystalline metals and ceramics the mechanical properties and in particular the plasticity of this novel class of materials have attracted much attention. This is due to the fact, that the strong grain size dependence of mechanical properties can lead to plastic behavior in brittle materials. There are many reports on mechanical properties of nanocrystalline metals, ceramics and composites. Some surprising results, i.e. the inverse Hall-Petch relationship observed in nanocrystalline metals and alloys, have led to the development of new theoretical models of the deformation processes of materials with nanometer sized grains. In addition, computer simulations have been employed substantially in the last few years to analyze the atomistic processes during deformation. In the talk the experimental results, the phenomenological models and the results of computer simulations will be presented and compared critically.

11:10 AM Invited

X-Ray Analysis of SPD Metals: *Igor V. Alexandrov*¹; Ascar R. Kilmametov¹; ¹Ufa State Aviation Technical University, Inst. of Physics of Advd. Matls., 12 K. Marx St., Ufa, Bashkortostan 450000 Russia

The results of recent experimental x-ray investigations of bulk ultrafine-grained (UFG) metals, processed with the help of various severe plastic deformation (SPD) techniques are summarized in the given report. At the same time a special attention is paid to the analysis of the processes of preferred orientations as a result of SPD. Metals having different types of the crystal lattice, different SPD schemes (high pressure torsion and equal-channel angular pressing), routes and accumulation strain degrees are considered. The results of low-temperature investigations of metals having different structure, formed at different SPD stages are represented. Regularities in the formation of enhanced atomic displacements depending on the structure state of SPD metals have been established and analyzed.

11:30 AM Invited

Grain Boundary Structure of Nanocrystalline Cu Processed by Cryomilling: *J. Y. Huang*¹; X. Z. Liao²; Y. T. Zhu²; F. Zhou³; E. J. Lavernia³; ¹Boston College, Dept. Physics, Chestnut Hill, MA 02467 USA; ²Los Alamos National Laboratory, Matls. Sci. & Tech, Los Alamos, NM 87545 USA; ³University of California, Dept. Chem. Engrg. & Matl. Sci., Davis, CA 95616 USA

The microstructures of cryogenically ball-milled Cu was investigated by high-resolution electron microscopy. It was found that the grain-size reduction is a dislocation-controlled continuous process, consists of the formation of small-angle grain boundaries, a gradual increase of misorientations as a result of accumulation of more dislocations, and finally, the formation of large-angle grain boundaries (GBs). The grain boundaries were generally curved, wavy or faceted, and heavily strained, which are typical characteristics of nanostructured materials. In addition, extrinsic dislocations were found in many GBs, indicating that most are in a high-energy, non-equilibrium configuration, which is consistent with observations in equal-channel angular pressing processed Cu, Ni, and Al-Mg, repetitive corrugation and straightening processed Cu and room-temperature ball-milled Cu. These results support a still-disputed concept that GBs in nanostructured metals processed by severe plastic deformation are mostly in non-equilibrium states.

11:50 AM Invited

Grain Boundary Diffusion and Plasticity of Polycrystalline and Nanostructured Metals and Alloys: *Yuri Romanovich Kolobov*¹; ¹SB Russian Academy of Science, Inst. of Strength Physics & Matls. Sci., Lab. Phys. Matls. Sci., Akademicheskii 2/1, Tomsk 634021 Russia

The regular features of grain boundary diffusion in polycrystalline and nanostructured metals and alloys produced by electrodeposition and severe plastic deformation, as well as in the corresponding coarse-grain counterparts are considered. It has been found that the grain-boundary diffusivities obtained for nanocrystalline and nanostructured metals far exceeds (by one to four orders) those of the coarse-grain counterparts. The probable physical causes for the above distinguishing features manifested by the diffusion in nanostructured materials are addressed. An investigation was performed for a range of polycrystalline, fine-grained and nanostructured metals, which allowed to reveal a hitherto unknown creep activation effect, i.e. initiation of

grain boundary sliding by diffusion impurity fluxes from the environment. Using the Mo(Ni) and Fe(Ni) systems by way of an example, it was shown that the action of grain boundary sliding by diffusant fluxes from an external source might cause superplastic state to be realized in the material.

12:10 PM

Work Hardening Behaviour of Fine Grained Materials: *Chad S. Sinclair*¹; Warren J. Poole¹; Yves Brechet²; ¹University of British Columbia, Metals & Matls. Engrg., 309-6350 Stores Rd., Vancouver, BC V6T 1Z4 Canada; ²Institut National Polytechnique de Grenoble, LTPCM, 1130 rue de la Piscine, Domaine Universitaire, BP 75, Grenoble France

The plastic deformation of fine grained copper and an Al-3.5Mg alloys has been characterized by tensile tests over the temperature range from 77 K to ambient temperature. The temperature dependence of the yield stress and the work hardening behaviour has been examined with particular attention to the influence of grain size. Work hardening behaviour has been characterized by plots of the work hardening rate vs flow stress and energy storage rate vs. flow stress. The results of these experiments are critically evaluated against the classic Kocks-Mecking formulation.

12:25 PM

HRTEM and EFTEM Investigation of the Eutectoid Steel After Severe Plastic Deformation: *Yulia Ivanisenko*¹; Ian MacLaren²; Harald Rösner¹; Ruslan Z. Valiev³; Hans-Jörg Fecht¹; ¹Forschungszentrum Karlsruhe, INT, PO Box 3640, Karlsruhe D-76021 Germany; ²Darmstadt University of Technology, Inst. for Matls. Sci., Darmstadt 64287 Germany; ³Ufa State Aviation Technical University, Inst. of Phys. of Advd. Matls., Ufa 450000 Russia

The nanocrystalline structure of a eutectoid steel after severe plastic deformation by High Pressure Torsion (HPT) was studied by means of High Resolution TEM (HRTEM) and Energy Filtered TEM (EFTEM). In an as-processed specimen nano-sized areas of modulated fringe contrast were revealed. It was shown, that in most cases the observed fringes can be explained as Moiré patterns resulting from the overlapping of two lattices: normal iron and a highly distorted lattice with a structure similar to BCC iron. It seemed most likely that these distorted regions were transitional carbon-containing phases. Distortions due to dislocation networks were shown to be unlikely in this case. EFTEM investigation revealed a fairly uniform distribution of carbon in the HPT steel that corresponds well with our previous results about total cementite dissolution as a result of HPT, although some small carbon enrichments were seen, which correspond to the distorted phases observed by HRTEM.

5th Global Innovations Symposium: Trends in LIGA, Miniaturization, and Nano-Scale Materials, Devices and Technologies: Properties and Characterization of Materials for Microsystem/LIGA Applications

Sponsored by: Materials Processing & Manufacturing Division, MPMD-Powder Materials Committee, MPMD-Phase Transformations Committee-(Jt. ASM-MSCTS), MPMD-Computational Materials Science & Engineering-(Jt. ASM-MSCTS), MPMD/EPD-Process Modeling Analysis & Control Committee, MPMD-Surface Engineering Committee, MPMD-Shaping and Forming Committee, MPMD-Solidification Committee

Program Organizers: John E. Smugeresky, Sandia National Laboratories, Department 8724, Livermore, CA 94551-0969 USA; Steven H. Goods, Sandia National Laboratories, Livermore, CA 94551-0969 USA; Sean J. Hearne, Sandia National Laboratories, Albuquerque, NM 87185-1415 USA; Neville R. Moody, Sandia National Laboratories, Livermore, CA 94551-0969 USA

Tuesday PM Room: 202B
March 16, 2004 Location: Charlotte Convention Center

Session Chairs: James P. Lucas, Michigan State University, Chem. Engrg. & Matls. Sci., E. Lansing, MI 48824-1226 USA; John Jungk, University of Minnesota, Chem. Engrg. & Matls. Sci., Minneapolis, MN 55401 USA

2:00 PM

New Nanoindentation and Scanning Probe Tools and Techniques: *Warren C. Oliver*¹; ¹MTS Nano Instruments Innovation Center, 1001 Larson Dr., Oak Ridge, TN 37931 USA

Recent developments in the tools and techniques associated with Nanoindentation and probe scanning techniques will be presented. New calibration techniques provide simpler verification of system performance and accuracy. Quantitative sample scanning equipment and techniques provide the user with new tools for the mechanical characterization of miniature structures (MEMS) and allow for new types of mechanical properties testing of films. Indentation, uniaxial and biaxial tensile testing of thin films will be described.

2:20 PM

Fatigue of LIGA Ni MEMS Structures: *J. Lou*¹; S. Allameh¹; R. Rabeeh¹; B. L. Boyce²; T. E. Buchheit¹; W. O. Soboyejo¹; ¹Princeton University, PMI/MAE Dept., D404 Engr. Quad., Olden St., Princeton, NJ 08544 USA; ²Sandia National Laboratories, PO Box 5800, Albuquerque, NM 87185-5800 USA

This paper presents the results of recent studies of fatigue in LIGA Ni MEMS structures. Following a brief review of microstructures and micro-textures, the micromechanisms of fatigue are elucidated for cyclic deformation under uniaxial tension and bending conditions. Stress-life and strain-life are also presented, along with Coffin-Manson approaches to the modeling of low- and high-cycle fatigue. Finally, the results from recent fatigue crack growth experiments are described before discussing the implications of the current work for the design and assessment of reliable LIGA Ni MEMS devices.

2:40 PM

High Temperature Tensile and Creep Properties of LIGA Materials: *Thomas E. Buchheit*¹; Steven H. Goods²; Brad L. Boyce¹; Joseph R. Michael³; James J. Kelly⁴; ¹Sandia National Laboratories, Dept. 1851, MS 0889, PO Box 5800, Albuquerque, NM 87185 USA; ²Sandia National Laboratories, Dept. 8725, MS 9404, PO Box 969, Livermore, CA 94551 USA; ³Sandia National Laboratories, Dept. 1822, MS 0886, PO Box 5800, Albuquerque, NM 87185 USA; ⁴Sandia National Laboratories, Dept. 8729, MS 9401, PO Box 969, Livermore, CA 94551 USA

Specific applications utilizing the LIGA (Lithography, Electroforming, Molding) technology require materials with reasonable strength and creep resistance up to ~600°C. The primary processing method utilized within the LIGA technology is electrodeposition, thus pure metals with a successful electroplating history, such as Ni and Cu, remain the favored LIGA structural materials. However, pure metals anneal soften readily and have poor strength and creep resistance at even modest elevated temperatures. To meet specified properties criteria necessary for high temperature applications, new material systems must be developed within the electroplating constraints imposed by LIGA technology. This presentation focuses on high temperature and creep testing results from one promising LIGA alloy, pulse plated

Ni- (0.5-1.0at%) Mn. LIGA Ni-Mn results will be compared baseline pure LIGA Ni results and results from a previously reported study on LIGA fabricated oxide dispersion strengthened nickel (ODS-Ni). When appropriate, commensurate microstructure analysis was performed. Results indicate that improved elevated temperature strength and creep resistance can be realized through appropriate choice of the electrodeposited material. Sandia is a multiprogram laboratory operated by Sandia Corporation, a Lockheed Martin company, for the United States Department of Energy under Contract DE-AC04-94AL85000.

3:00 PM

Characterization of Twinning in Electrodeposited Ni-Mn for Microsystems Applications: *Gene A. Lucadamo*¹; Nancy Y.C. Yang¹; James J. Kelly²; Alec Talin³; Douglas L. Medlin⁴; ¹Sandia National Laboratories, Analytical Matls. Sci., MS 9161, PO Box 969, Livermore, CA 94551-0969 USA; ²Sandia National Laboratories, Microsys. Procg., MS 9410, PO Box 969, Livermore, CA 94551-0969 USA; ³Sandia National Laboratories, Nanolithography, MS 9409, PO Box 969, Livermore, CA 94551-0969 USA; ⁴Sandia National Laboratories, Thin Film & Interface Sci., MS 9161, PO Box 969, Livermore, CA 94551-0969 USA

Twinning is ubiquitous in electrodeposited metals. We have investigated twinning in Ni-Mn alloys developed for use in the LIGA process. In this material, twins are present at high densities with widths on the order of nanometers. The presence of many twin boundaries combined with an overall refinement in grain size enhances the mechanical strength in the alloy electrodeposits. Transmission electron microscopy (TEM) was used to characterize twinning in as-plated microstructures. In general, the orientation of the twin planes with respect to the plating direction depends directly on the crystallographic texture. For instance, in {110} textured deposits twinning can occur on {111} planes perpendicular and oblique to the substrate. However, planview TEM images of Ni-Mn show that twins are formed primarily on those planes parallel to the plating direction. Consequently, repeated twinning on equivalent planes results in multiply-twinned particles and grains enclosed by twin boundaries. Measurements of twin density in Ni-sulfamate with and without Mn indicate that while the addition of <1 wt.% Mn clearly refines the microstructure, it also dramatically increases the incidence of twin formation. Another consequence of this high twinning density is the formation of a large number of junctions where the twin boundaries intersect. Our measurements show that the junction density is comparable to the density of dislocations in a cold-worked metal. The strain fields associated with these junctions can interact with dislocations and act as pinning sites. A comparison shows that the twin microstructure in direct and pulsed-current deposits are qualitatively similar. Sandia is a multiprogram laboratory operated by Sandia Corporation, a Lockheed Martin Company, for the United States Department of Energy's National Nuclear Security Administration under contract DE-AC04-94AL85000.

3:20 PM Break

3:40 PM

Nanostructured Metals for Enhanced Performance of LIGA Components: *Mohammadreza Baghbanan*¹; Uwe Erb¹; Gino Palumbo²; ¹University of Toronto, Matls. Sci. & Engrg., Rm. 140, 184 College St., Toronto, Ontario M5S 3E4 Canada; ²Integran Technologies Inc., #1 Meridian Rd., Toronto, Ontario M9W 4Z6 Canada

This paper addresses the issues of performance variability and reliability concerns frequently encountered with metallic microsystem components produced by electrodeposition methods such as LIGA. Experimental results will be presented which demonstrate that microsystem components produced by conventional electrodeposition approaches show relatively low overall hardness and considerable variations in Young's modulus and hardness throughout the cross section of the components. These undesirable properties are traced back to i) the microstructure of the deposits which is characterized by grain size gradients resulting from the fine grained to columnar structure transition and ii) the relatively large grain size in comparison to the overall component size. In past efforts both post deposition recrystallization annealing and texture control during the electroplating process have been used to alleviate these concerns, with some limited success. In this paper we present a new approach which essentially involves the modification of the electrodeposition process to produce fully dense nanostructured deposits throughout the entire cross section of the component without transition from fine to large grained columnar structure. Results will be presented for such components which show i) uniform hardness and Young's modulus in cross section and ii) significant enhancements in hardness and other important performance indicators such as specific strength, elastic energy storage capacity and wear resistance.

4:00 PM

Combining On-Chip Testing and Electron Microscopy to Obtain a Mechanistic Understanding of Fatigue and Wear in Microelectromechanical Systems: *Daan Hein Alsem*¹; Eric A. Stach²; Christopher L. Muhlstein³; Michael T. Dugger⁴; Robert O. Ritchie¹; ¹University of California, Dept. of Matls. Sci. & Engrg., 1 Cyclotron Rd., MS 72/150, Berkeley, CA 94720 USA; ²Lawrence Berkeley National Laboratory, Natl. Ctr. for Electron Microscopy, 1 Cyclotron Rd., MS 72/150, Berkeley, CA 94703 USA; ³Pennsylvania State University, Dept. of Matls. Sci. & Engrg., 310 Steidle Bldg., Univ. Park, PA 16802 USA; ⁴Sandia National Laboratory, Matls. & Process Scis. Ctr., PO Box 5800, Albuquerque, NM 87185-0889 USA

Wear and fatigue are important factors in determining the reliability of microelectromechanical systems (MEMS). While the reliability of MEMS has received extensive attention, the physical mechanisms responsible for these failure modes have yet to be conclusively determined. In our work, we use a combination of on-chip testing methodologies and electron microscopy observations to investigate these mechanisms. Our previous studies have shown that fatigue in polysilicon thin films is a result of a "reaction-layer" process, whereby high stresses induce a room-temperature mechanical thickening of the native oxide, which subsequently undergoes environmentally-assisted cracking. In this presentation, we discuss how the initial native oxide thickness affects the fatigue life and report on new in vacuo observations, which exploit a phase-lock loop control system to drive the test system at resonance. This allows us to characterize both the changes in fatigue behavior and development of reaction layers in a relatively oxygen-free environment. Additionally, we have used polysilicon MEMS sidewall friction test specimens to study active mechanisms in sliding wear, including the role of the surface roughness and the presence of lubricants (such as an oxide layer or a thin film of water). In particular, we have performed in vacuo and in-situ experiments in the scanning electron microscope, with the objective of determining the mechanisms causing both wear development and debris.

4:20 PM

Fabrication and Testing of Ultra Small-Scale Samples: *S. J. Polasik*¹; H. L. Fraser¹; M. J. Mills¹; M. D. Uchic²; D. M. Dimiduk²; ¹Ohio State University, Matls. Sci. & Engrg. Dept., Columbus, OH 43210 USA; ²Air Force Research Laboratory, Matls. & Mfg. Direct., Wright-Patterson AFB, OH 4533-7817 USA

In this talk we describe an ultra small-scale mechanical testing methodology capable of investigating the mechanical behavior of small volumes of material with dimensions of tens of micrometers. This method alleviates the need to fabricate macroscopic specimens that may differ in chemistry, microstructure, scale, and impurity content from the manufactured component. Dual Beam Focused Ion Beam (DB-FIB) microscopes provide the capability to site specifically machine micron-scale three dimensional structures that function as test specimens. DB-FIB machined cylindrical compression specimens, with diameters ranging from 5µm to 40µm, are tested in uniaxial compression at room temperature using a nanoindenter equipped with a flat-ended tip. Presently, single crystal Ti-6Al is under investigation as a model for the α-phase of commercial Ti alloys. The comparison of this data with the bulk sample response will be discussed. Additionally, this talk will also discuss the development of a tensile testing methodology capable of characterizing samples at this size scale.

4:40 PM

Mechanical Property Measurements of Pure Ni, Ni₃Al, and Ni-Base Superalloys at the Micron-Size Scale: *Michael D. Uchic*¹; Dennis M. Dimiduk¹; Michael J. Seekely¹; Jeff N. Florando²; William D. Nix³; ¹Air Force Research Laboratory, Matls. & Mfg. Direct., AFRL/MLLMD, 2230 Tenth St., WPAFB, OH 45433-7817 USA; ²Lawrence Livermore National Laboratory, Livermore, CA USA; ³Stanford University, Dept. of Matls. Sci. & Engrg., Stanford, CA 94305-2205 USA

In order to measure the critical resolved shear stress from individual grains of a fully-processed polycrystalline engineering alloy, we have developed a test methodology to extract mechanical test samples from the bulk that have micron-size dimensions. The test methodology consists of using both a Focused Ion Beam microscope to fabricate compression specimens from the bulk, and a nanoindenter fitted with a flat tip to perform uniaxial compression tests. Using this methodology, we have performed microsample compression experiments on three different metallic bulk single crystals-pure Ni, Ni₃(Al, Ta), and a Ni-base superalloy (gas turbine blade alloy composition)-and a polycrystalline Ni-base superalloy (gas turbine disk alloy composition). The fabrication of microsamples from bulk single crystals has allowed us to compare the effect of microsample specimen size on the resultant mechanical properties, and we have tested samples ranging in size from tens of microns to sub-micron in diameter in order to find the

size limit where the microsamples deviate from bulk behavior. Of note, we have measured a significant size effect for Ni₃Al (where the yield strength increases dramatically with decreasing sample size), whereas more subtle size effects are observed for the pure Ni and Ni-base superalloy. We also show measurements of the single crystal mechanical properties for specimens isolated within single grains of a polycrystalline superalloy using this test methodology.

Advanced Materials for Energy Conversion II: Complex Hydrides II

Sponsored by: Light Metals Division, LMD-Reactive Metals Committee

Program Organizers: Dhanesh Chandra, University of Nevada, Metallurgical & Materials Engineering, Reno, NV 89557 USA; Renato G. Bautista, University of Nevada, Department of Chemical and Metal Engineering, Reno, NV 89557-0136 USA; Louis Schlapbach, EMPA Swiss Federal, Laboratory for Materials Testing and Research, Duebendorf CH-8600 Switzerland

Tuesday PM
March 16, 2004

Room: 203A
Location: Charlotte Convention Center

Session Chairs: Klaus Yvon, Université de Genève, Lab. de Cristallographie, Geneva Switzerland; Reiner Kirchheim, Universitaet Goettingen, Inst. fuer Materialphysik, Goettingen D-37077 Germany; Hiroyuki T. Takeshita, Kansai University, Fac. of Engrg., Suita, Osaka 564-8680 Japan

2:00 PM Keynote

Complex Metal Hydrides for Hydrogen Storage: What Are Their Limits of Performance?: *Klaus Yvon*¹; ¹Université de Genève, Lab. de Cristallographie, Geneva Switzerland

In principle, solid-state metal hydrides provide the safest and most energy efficient means of storing reversibly hydrogen at ambient conditions. However, in spite of considerable R&D efforts the materials presently available do not meet performance targets for a great variety of applications, both stationary and mobile, such as fuel cells. Critical issues are weight efficiency, reversibility, kinetics and cost. Some thousand binary, ternary and quaternary metal hydrides are known and more are about to be discovered. Those considered to have greatest potential at present are the so-called "complex" metal hydrides that derive their name from the presence of discrete metal-hydrogen complexes in their structures (for reviews see refs.1 and 2). The complexes are centred by either p-elements such as B and Al or d-elements such as Mn, Fe, Co, Ni, Cu and Zn. In this contribution an attempt is made to evaluate the potential of complex metal hydrides to meet performance targets such as those recently reformulated for the transportation sector by various national research funding agencies. At first sight p-metal hydrides appear to be favoured over d-metal hydrides because of weight and cost considerations. However, the situation is far from being clear-cut. While the performance limits with respect to weight, reversibility and cost are relatively well known for p-elements such limits are less apparent for d-elements. The hydrogen-to-metal ratio, for example is limited to H/M~3 for current p-metal hydrides while it may exceed H/M=4 for d-metal hydrides. Thus the door for new discoveries among d-metal hydrides remains wide open. Finally, it is argued that performance targets for hydrogen storage should not be based exclusively on present-day technology, consumer habit and profit seeking. Additional aspects such as sustainability, energy saving and environment must be taken into account in order to avoid over-ambitious performance targets, unrealistic expectations and undesirable side effects such as blocking of promising research fields that are wrongly considered unapt to meet preset performance targets. ¹K. Yvon : Solid state transition metal complexes, in *Encycl. Inorg. Chem.* (Ed. R.B. King) 3, 1401 John Wiley (1994); see also *Chimia* 52, 613. (1998). ²G. Sandrock and B. Bogdanovic, *MRS bulletin*.

2:25 PM Invited

Electrochemical Insertion of Lithium into Si-C Composite Prepared by Mechanical Ball Milling: *Jai-Young Lee*¹; Ki-Tae Kim¹; Yong-Ju Lee¹; Yong-Mook Kang¹; You-Min Kim²; Seo-Jae Lee²; Ki-Young Lee²; ¹KAIST, Dept. of Matl. Sci. & Engrg., 373-1, Guseong-dong, Yuseong-gu, Daejeon 305-701 Korea; ²Battery Research Institute, LG Chem. Ltd. Rsch. Park, 104-1, Yuseong-gu, Daejeon 305-380 Korea

In recent years, graphite materials have been an anode in lithium secondary battery. In spite of their successful commercialization, however, various new anode materials have been investigated to overcome

the limited theoretical capacity of graphite (372 mAh/g). Intermetallic compounds such as Sn, Sb, and Si have been extensively investigated because of high capacity. Among them, tin or silicon based intermetallic compounds appear to be promising anode materials. However, large irreversible capacity at the first charge-discharge cycle and poor cyclability are still serious problems. These problems are caused by a large volume change of particles or grains during Li insertion and extraction. Therefore, modified micro or nano structure which can accommodate the volume expansion is required for practical use. In this study, we report the electrochemical properties of Si-C composite prepared by mechanical ball milling. Micro or nano structure of Si-C composite can be controlled by mechanical ball milling because it can apply high energy to material. Further, lithium insertion/extraction behavior into/from Si-C composite was investigated. Si-C composite showed 3 distinct peaks at the first cycle in CV measurement. The two peaks at about 1.7 V and 0.7 V correspond to the electrolyte decomposition and SEI formation respectively. After 2nd cycle, 1.7 V peak and 0.7 V peak were hardly observable. Constant current (0.2 C rate) was performed between 1.5 and 0.005 V (versus Li/Li+) at 1st cycle, and between 1.5 and 0.01 V (versus Li/Li+) from 2nd cycle. The discharge capacity of 1st cycle was about 1020 mAh/g, and after 2nd cycle it was decreased to about 680 mAh/g. Coulombic efficiency was higher than 98.7% after 3rd cycle. It is conformed by XRD data that Li was intercalated to the C first, and then reacted with Si during Li insertion at 1st cycle. Further, Li was deintercalated from C first, and then extracted from Si during Li extraction at 1st cycle. It is expected that strong bonding, observed by XPS and FTIR should increase the contact between Si and C. We think that Si-C electrical connection will be maintained because of their strong bonding. From the charge/discharge capacity analysis, it was conformed that Si and C were partially participated in the reaction. After 50th cycle, capacity was maintained about 678 mAh/g, which is remarkable result. We can summarize the reasons for good cyclability of Si-C composite. First reason is the partial participation of Si and C in the reaction with Li. Second reason is the strong bonding between Si and C, which will maintain the electrical contact. And the final reason is the stored stress in carbon layer due to the earlier reaction with Li than that of Si. The Si-C composite prepared by high energy ball milling can be suggested as a new anode active material with high capacity and good cyclability for Li ion batteries.

2:50 PM Invited

Structural and Thermodynamic Aspects of Alanates for Hydrogen Storage: *Karl J. Gross*¹; ¹Hy-Energy LLC, 33902 Juliet Cir., Fremont, CA 94555 USA

The discovery that hydrogen can be reversibly absorbed and desorbed from NaAlH₄ by doping with Ti and other transition metals has created an entirely new prospect for lightweight hydrogen storage¹. NaAlH₄ releases hydrogen through the following set of decomposition reactions. NaAlH₄ → 1/3(Na₃AlH₆) + 2/3Al + H₂ → NaH + Al + 3/2H₂. An overview is presented of recent advances in the development of new and improved alanates for hydrogen storage applications and in the fundamental understanding of how Ti-doping enhances hydrogen absorption. New methods of preparing and doping the alanates, absorption/desorption performance, safety aspects, cycle-life studies, and results on other complex hydrides will be discussed. ¹Bogdanovic and Schwickardi, J. Alloys and Compounds Vol. 253,1 (1997).

3:15 PM Break

3:30 PM Cancelled

Hydrogen Storage in Graphitic Nanofibres

3:55 PM

Alkaline-Earth Metals and Alloys for Energy Storage: *Hiroyuki T. Takeshita*¹; ¹Kansai University, Fac. of Engrg., Dept. of Matls. Sci. & Engrg., 3-3-35, Yamate-chou, Suita, Osaka 564-8680 Japan

Alkaline Earth Metals and Alloys are one of the promising candidates for hydrogen storage system of hydrogen energy system. Mg and Mg₂Ni-based alloys are attractive as hydrogen fuel storage tank of fuel cell electric vehicles because of their high gravimetric hydrogen storage capacities, while some Ca-Mg-Ni based alloys such as (Ca,Mg)Ni₃, which have been recently developed, exhibit reversible hydrogenation/dehydrogenation properties at ambient temperatures and pressures, accompanied by very flat plateau, and are expected to be applied to hydrogen stations as inexpensive hydrogen absorbers. In this talk, some recent topics will be introduced on Mg and Mg₂Ni based alloys, (Ca,Mg)Ni₂ and (Ca,Mg)Ni₃ alloys and metastable MgNi and CaNi based hydrides which can be obtained by mechanical alloying.

4:15 PM Cancelled

A Mechanism for Sodium Alanate Decomposition

4:35 PM

Outgassing in the LiD/LiOH System: *Long N. Dinh*¹; William McLean¹; Marcus A. Schildbach¹; James D. LeMay¹; Wigbert J. Siekhaus¹; Mehdi Balooch¹; ¹Lawrence Livermore National Laboratory, Chmst. & Matls. Sci., 7000 East Ave., PO Box 808, L-356, Livermore, CA 94551 USA

Temperature programmed decomposition and complimentary microscopy from the surface inward. The energy barriers measured for the decomposition of surface and near-surface lithium hydroxide are noticeably smaller than the values associated with bulk counterpart. The conversion of Li₂O grains back to lithium hydroxide during moisture exposure was also found to proceed from the surface inw/spectroscopy techniques were performed on micrometer-grain lithium hydroxide. The results reveal that lithium hydroxide grains are thermally decomposed into Li₂O, releasing H₂O, following a three dimensional phase boundary movement such that surface states are filled before bulk states. In a different set of experiments, nanometer composite grains composed of LiD inner cores and LiOH outer layers were observed to form on top of pressed polycrystalline LiD upon moisture exposure. A diffusion coefficient on the order of 10-23 m²/sec was measured for the diffusion controlled reaction of LiOH with LiD in the nanopowder at room temperature in a dry environment. The measured kinetics in this work were used to construct the evolution steps in the LiD/LiOH composite system in a dry environment.

Advances in Superplasticity and Superplastic Forming: Advances in Superplastic Forming of Light Alloys

Sponsored by: Materials Processing and Manufacturing Division, Structural Materials Division, MPMD-Shaping and Forming Committee, SMD-Mechanical Behavior of Materials-(Jt. ASM-MSCTS), SMD-Structural Materials Committee

Program Organizers: Eric M. Taleff, University of Texas, Mechanical Engineering Department, Austin, TX 78712-1063 USA; P. A. Friedman, Ford Motor Company, Dearborn, MI 48124 USA; Amit K. Ghosh, University of Michigan, Department of Materials Science and Engineering, Ann Arbor, MI 48109-2136 USA; P. E. Krajewski, General Motors R&D Center, Rajiv S. Mishra, University of Missouri, Metallurgical Engineering, Rolla, MO 65409-0340 USA; J. G. Schroth, General Motors, R&D Center, Materials and Processes Laboratory, Warren, MI 48090-9055 USA

Tuesday PM

March 16, 2004

Room: 201B

Location: Charlotte Convention Center

Session Chairs: Peter A. Friedman, Ford Motor Company, Dearborn, MI 48121 USA; Eric M. Taleff, University of Texas, Dept. of Mech. Engrg., Austin, TX 78712-0292 USA

2:00 PM

Research Opportunities for Automotive SPF Alloys: *Paul E. Krajewski*¹; ¹General Motors, R&D Ctr., 30500 Mound Rd., MC 480-106-212, Warren, MI 48090 USA

General Motor's extensive experience with superplastic forming has resulted in a unique opportunity to produce, characterize, and understand superplastic materials capable of high volume automotive production. This work has included investigations into the effects of composition, second phase particles, and thermomechanical processing on elevated temperature behavior as well as understanding deformation mechanisms, elevated temperature fracture, and surface phenomena. The goal of this paper is to identify opportunities for research to improve the performance of superplastic materials, which could ultimately result in wider use of superplastic forming in the automobile industry.

2:25 PM

Particle Interface Damage Effect on Cavitation Control in Superplastic Aluminum Sheet: *Amit K. Ghosh*¹; Ruth Cleveland¹; ¹University of Michigan, Matls. Sci. & Engrg., 2300 Hayward St., Ann Arbor, MI 49109-2136 USA

Recent studies have confirmed that cavitation in commercial alloys used in superplastic forming application start primarily at the interface of hard second phase particles and inclusions. Analysis of preexisting damage on particle surface has demonstrated that the nuclei for cavities typically undergo plasticity growth to become eventually visible under the optical microscope. In this work, we obtained evidence that damage is produced at particle-matrix interface during

cold rolling of the alloy, which is generally not fully recovered during annealing or recrystallization practice. In this regard, prior sintering models appear to be inconsistent with the times required for void closure. However, the application of high hydrostatic pressure at elevated temperature has been found to improve the integrity of the particle-matrix interface, and significantly reduce the cavitation tendencies of these alloys. The experimental results will be viewed in relation to theoretical considerations and discussed in this paper.

2:45 PM

Superplasticity in a 15% Vol. Al₂O₃ Particulate-Reinforced 6061Al Alloy Composite: *Lihong Han*¹; Henry Hu¹; Derek Northwood¹; ¹University of Windsor, Dept. of Mech., Auto. & Matl. Engrg., Windsor, Ontario N9B 3P4 Canada

The superplastic characteristics of a 15% vol.% Al₂O₃ particulate-reinforced 6061Al alloy composite have been studied. The composite was fabricated by Powder Metallurgy techniques and hot-extruded with two different extrusion ratios. The grain size after extrusion is approximately 3 μ m and is stable at high temperatures. The composite exhibits superplasticity (with an elongation to failure of 200%) at lower strain rates (approximately 10⁻⁴). The superplastic properties of the composite, including elongation, strain rate sensitivity, and activation energy, were characterized. Differential Thermal Analysis (DTA) was used to ascertain the possibility of any partial melting in the vicinity of the optimum superplastic temperature. Scanning Electron Microscopy (SEM) was used to observe the distribution of reinforcement in matrix and the failure characteristics of the surface of the specimen, and Transmission Electronic Microscopy (TEM) was used to characterize for the interfacial behaviors (grain-grain and grain-reinforcement) and the configuration of dislocations in the matrix.

3:05 PM

Analysis of Superplastic Deformation of Al-Al₄C₃ Composites: *Michal Besterčí*¹; Oksana Velgosa²; ¹Slovak Academy of Science, Inst. of Matls. Rsch., Watsonova 47, Kosice 04353 Slovakia; ²Technical University, Fac. of Metall., Dept. of Non-Ferrous Matls. & Waste Treatment, Letna 9/A, Kosice 04200 Slovakia

Mechanical alloying technique, such as dry, high energy ball milling process, is suitable for producing composite metal powders with a fine controlled microstructure. This method is crucial for obtaining a homogeneous distribution of nano-sized dispersoids in a more ductile matrix (e.g. aluminium- or copper based alloys). Dispersoids can be formed in a solid state reaction of materials that react with the matrix during milling or during subsequent heat treatment. Superplastic deformation is a combination of parallel processes such as slip on grain boundaries, dislocation creep, and recrystallisation. The aim of this work is to investigate deformation process in the Al-Al₄C₃ systems with different second phase particle content under different temperatures and strain rates, and analyse the corresponding deformation processes.

3:25 PM Break

3:45 PM

Achieving Superplasticity in Light Alloys Through the Application of Severe Plastic Deformation: *Cheng Xu*¹; Minoru Furukawa²; Zenji Horita³; *Terence G. Langdon*¹; ¹University of Southern California, Aeros. & Mech. Engrg. & Matls. Sci., Los Angeles, CA 90089-1453 USA; ²Fukuoka University of Education, Dept. of Tech., Munakata, Fukuoka 811-4192 Japan; ³Kyushu University, Matls. Sci. & Engrg., Faculty of Engrg., Fukuoka 812-8581 Japan

The light alloys, such as aluminum and magnesium, have considerable potential for use in the automotive industry. However, the superplastic forming of conventional alloys, where the grain sizes are often ~5 μ m or larger, tends to occur at strain rates which are generally too slow for use in the processing of high volumes of components. This limitation may be removed, and the superplastic forming operation achieved at a faster rate, by reducing the grain size of the alloy to the submicrometer or even the nanometer level. This paper describes the process of achieving grain refinement and superplastic properties in representative Al and Mg alloys using a procedure in which the alloys are subjected to severe plastic deformation. The results show that this processing technique is capable of producing excellent superplastic properties in alloys that are nominally not superplastic.

4:10 PM

High Strain Rate Superplasticity in Friction Stir Processed Aluminum Alloys: *Rajiv S. Mishra*¹; Zong Yi Ma¹; Indrajit Charit¹; ¹University of Missouri, Dept. of Metallurg. Engrg., 1870 Miner Cir., Rolla, MO 65409 USA

Friction stir processed aluminum alloys exhibit enhanced superplasticity. In addition, friction stir processing can enable several new

concepts, such as, selective superplasticity, thick plate superplasticity and superplasticity of contoured plates. A brief review of the state-of-the-art will be presented. The constitutive relation for friction stir processed aluminum alloys show an enhancement of more than 20 times. Friction stir processing is an enabling concept that can extend the use of superplastic forming for new applications. The support of the National Science Foundation through grants DMI-0085044 and DMI-0323725 is gratefully acknowledged.

4:30 PM

High Strain Rate Superplasticity in a Commercial Al-Mg-Li-Sc-Zr Alloy Subjected to Hot Intense Plastic Straining: *Fanil Musin*¹; Rustam O. Kaibyshev¹; Ksenia Saytaeva¹; ¹Institute for Metals Superplasticity Problems, Khalturina 39, Ufa 450001 Russia

The superplastic properties of an Al-4.1%Mg-2.0%Li-0.16%Sc-0.07%Zr alloy subjected to intense plastic straining by equal-channel angular extrusion (ECAE) at 400°C was studied in the temperature interval 250-500°C at strain rates ranging from 1.4x10⁻⁵ to 1.4 s⁻¹. The grain size after ECAE was about 3 μ m and the fraction of high angle boundaries was about 90%. The highest elongation to failure of about 3000% appeared at a temperature of 450°C and initial strain rate of 1.4x10⁻² s⁻¹ with the strain rate sensitivity coefficient of about 0.65. It was shown that the ECAE processed alloy exhibits high strain rate superplasticity properties in the temperature range 350-500°C with ductility higher than 1000%. Microstructural evolution and cavitation during high strain rate deformation were examined in detail.

Alumina and Bauxite: Technology and Future Trends

Sponsored by: Light Metals Division, LMD-Aluminum Committee
Program Organizers: Travis Galloway, Century Aluminum, Hawesville, KY 42348 USA; David Kirkpatrick, Kaiser Aluminum & Chemical Group, Gramercy, LA 70052-3370 USA; Alton T. Tabereaux, Alcoa Inc., Process Technology, Muscle Shoals, AL 35661 USA

Tuesday PM

March 16, 2004

Room: 218A

Location: Charlotte Convention Center

Session Chair: Lester A.D. Chin, McDonough, GA 30252-3917 USA

2:00 PM

Solubility of Calcium in Bayer Liquor: *Marie Raty*¹; Kenneth T. Stanton¹; B. K. Hodnett¹; M. Loan¹; ¹University of Limerick, Matl. Sci. & Tech. Dept., Plassey Technological Park, Limerick Ireland

There is empirical evidence which suggests that calcium inhibits precipitation of gibbsite (Al₂O₃·3H₂O) in the Bayer process. This phenomenon may be used in the mud circuit as a means of preventing loss of product or scale reduction. Here, we present a comprehensive study of calcium solubility in water, caustic soda, synthetic Bayer liquor and also in a liquor obtained from an alumina refinery. Experiments were based on Ca added as CaCO₃ and solubility was determined in each case as a function of time and temperature. In addition, solubilities in NaOH and Bayer liquors were determined as a function of causticity and concentration of aluminate respectively. Surprisingly, results show little difference in Ca solubility in water as a function of temperature. Solubility increases with caustic concentration up to 1 M NaOH and decreases thereafter. Also, greater concentration of aluminate in synthetic liquors decrease the solubility.

2:25 PM

Organic Control Technologies in Bayer Process: *Gervais Soucy*¹; Jacques E. Larocque²; Guy Forté³; ¹Université de Sherbrooke, Chem. Engrg. Dept., 2500 Blvd. Université, Sherbrooke, Québec J1K 2R1 Canada; ²Consultant, Asbestos, Québec J1T 1W6 Canada; ³Alcan International Ltd., Arvida R&D Ctr., 1955 Blvd. Mellon, CP 1250, Jonquière, Québec G7S 4K8 Canada

Many Bayer plant problems originate from organics contamination of the Bayer liquor. Organics can decrease liquor productivity either by increasing alumina solubility or by covering active sites on alumina hydrate seeds. Organics also induce coloration of the liquor, cause excessive foaming, and increase liquor viscosity, density and boiling point. All these examples have deleterious effects on the Bayer process. This paper describes a full survey of patent literature including more than 60 patents filed between 1953 and 2001. Most patents in use today were issued in the early 80's. Apart from sodium oxalate control, very few patents are still in use with the sole objective of controlling organic carbon species in Bayer liquor. The most likely

explanation is the poor economic viability of organics control in general. Most of the recent patents combine several different methods to reach the objective of organics control. A new innovative technology will be presented. It involves treatment of Bayer spent liquor by direct contact with thermal submerged plasma. The multi-forms of energy provided by the plasma are efficiently used. Preliminary results will be given.

2:50 PM

Alumina Refinery Brownfield Expansion - Hindalco Experience: R. P. Shah¹; Sheo Nandan Gararia¹; R. J. Singh¹; ¹Hindalco Industries Ltd., PO Renukoot 231 217, Sonbhadra, UP India

Recently Hindalco Alumina Refinery has created a landmark by enhancing its production capacity by 210,000 TPY with benchmark capital cost of US \$271 per annual tonne through radical modernization and up-gradation schemes. The innovative approach involves Introduction of Sweetening Process, Modernization of Digestion Units and Up-gradation of Precipitation Circuit. The addition of sweetening slurry to digestion units substantially increased 'equilibrium alumina to caustic ratio'. The Free Caustic Threat was adequately addressed by converting the units to single stream flows incorporating innovative Mixing Tube concept. The schemes achieved an increase in caustic concentration by 30-35 gpl and A/C ratio by about 60 units. To minimize capital expenditure, maximum use of existing equipment was ensured. The state-of-the-art Alusuisse Precipitation Technology was successfully incorporated to increase liquor productivity from 58 to 77.3 gpl. The entire project, in addition to increasing production and productivity, has started yielding reduction of operating cost by 10-12%.

3:15 PM

The Third Generation of Autoclave Feed Pumps: Berry van den Broek¹; ¹Weir Netherlands b.v., Business Dvlp., PO Box, Venlo 5900 AE The Netherlands

Piston Diaphragm Pumps have been in use for the feed of autoclaves since the mid 1980's. Heat Barrier Pumps have been designed to effectively handle abrasive and hot slurries. The first generation of these pumps was developed for the refractory gold ore autoclaves in Nevada/USA. The second generation of Heat Barrier Pumps was supplied in the mid 1990's and handles slurry temperatures of up to 200°C and capacities of approximately 400 m³/h at the lateritic nickel processing plants in Western Australia. This paper describes the optimisations and enhancements of the Third Generation of Heat Barrier Pumps. These pumps will be supplied to the Rio Tuba Laterite Nickel Processing Plant in the Philippines. These enhancements allow reduction in investment as well as operating cost, whilst improving the reliability of the equipment. In alumina refineries, Heat Barrier Pumps can be an attractive proposition for the feed of high pressure digesters with hot bauxite slurries.

3:40 PM Break

3:50 PM

The Trends of China Alumina Production with Combined Process: Qingjie Zhao¹; Qiyuan Chen²; Qiaofang Yang³; ¹Central South University and Zhengzhou Research Institute of Aluminum Corporation, China, Ltd. China; ²Central South University China; ³Zhengzhou Research Institute of Aluminum Corporation, China, Ltd. China

Most of Chinese bauxite is diasporic bauxite, which has the characteristics of high alumina, high silicon and low iron. Furthermore, the impurity minerals of this bauxite are complex, so most of Chinese alumina is produced by the combined process or the sintering process with high energy consumption. To save energy and reduce costs, it is suggested that the present combined process be reconstructed with a parallel-combined process. Then the bauxite with Al₂O₃/SiO₂ (A/S) weight ratio higher than 10 is dealt with by the Bayer process and the bauxite with A/S 5-8 by the sintering process. The concentration of green liquor in the sintering system is almost the same as that in the Bayer process, and the productivity of both present Bayer and sintering parts can be improved. An economic analysis shows that economic benefit can obviously be obtained. Therefore, the parallel-combined process is a suitable new way for reconstruction of present Chinese alumina production.

4:15 PM

A Study of the New Technology Combined with Bayer Process in Manufacture of Calcium Aluminate Cements: Jinyong Zhu¹; ¹Aluminum Corporation of China, Ltd., Zhengzhou Rsch. Inst., Shangjie Dist., Zhengzhou City, Henan 450041 China

A new technology combined with the Bayer process in manufacture of calcium aluminate cements (CAC) is proposed. Al₂O₃ in the Bayer spent liquor is precipitated by adding lime, and the washed sediment

(calcium aluminate hydrate) has a major phase of 3CaO·Al₂O₃·6H₂O with very fine particle size and large specific surface, which becomes 12CaO·7 Al₂O₃ and CaO when dehydrated by heating. The sediments mixed with certain amounts of alumina and/or aluminum trihydrate can be sintered into CAC containing 70 to 80% Al₂O₃ content. The major phases of the CAC are CaO·Al₂O₃ and CaO·2Al₂O₃, and the impurities of Fe₂O₃ and Na₂O in the CAC are low. The spent liquor with very low Al₂O₃ concentration returns to the Bayer digestion step, after concentration by evaporation, with a 95% increase in digestion capability.

4:40 PM

Tube Digesters: Protection of Heating Surfaces and Scale Removal: A. G. Suss¹; I. V. Paromova¹; T. N. Gabrielyan¹; S. S. Snurnitsyn¹; A. V. Panov¹; I. V. Lukyanov¹; ¹Russian National Aluminium & Magnesium Institute (VAMI), Dept. of Alumina Tech., 86, Sredny pr, St. Petersburg 199106 Russian Federation

Tube digesters have recently found wide application for alumina extraction from bauxite in the Bayer process. In spite of many advantages in construction and operation, tube digesting has the problem of incrustation scales formation on heating surfaces that affects hydraulic resistance of the tube digester and impairs heat transfer, thus sharply decreasing productivity. There are several ways of protecting heating surfaces and removing scale- including use of magnetic and electric fields, ultrasound, thermal treatment, mechanical cleaning, and mainly hydro-monitoring (high pressure water "jetting") and chemical cleaning, used before hydro-monitoring to soften and loosen scale. In VAMI we have performed a number of tests for selection of the most efficient mixtures of acids and inhibitors for chemical cleaning of heating surfaces. It was shown that sulfuric acid (used at present at many alumina plants) has low effectiveness since the majority of high-temperature scales contain calcium oxide. As a result of the investigations, an effective technique of chemical cleaning of tube digester heating surfaces was developed allowing neutralization and disposal of the spent solutions.

5:05 PM

Alumina Surface Material with High Thermal Stability: Wangxing Li¹; Donghong Li¹; Qingwei Wang¹; ¹Zhengzhou Research Institute of Light Metals, Special Alumina Dept., No. 82 Jiyuan Rd., Shangjie, Zhengzhou 450041 China

A new preparation method of high-purity and superfine alumina is introduced in this paper. By molecule- structure-designing, the organic space resistance factors are imported in the aluminate molecular structure and forming organic envelope around aluminum ions. After thermal decomposition, high-purity (4N) alumina surface material which original particle sizes 20~30nm and apparent particle sizes less than 80nm was obtained. By leading mould-guiding and thermal stability agents into aluminate molecular structure, ultimately the high-purity and active alumina with high thermal stability was attained. Which specific surface area more than 148m²/g, and original particle sizes is 0.1~0.2µm. The size and morphology of the apparent particle can be controlled. This alumina product is very suitable for application in automotive exhaust catalysts and luminescent and optical coating materials.

Aluminum Reduction Technology: Modeling - Industry Trends

Sponsored by: Light Metals Division, LMD-Aluminum Committee
Program Organizers: Tom Alcorn, Noranda Aluminum Inc., New Madrid, MO 63869 USA; Jay Bruggeman, Alcoa Inc., Alcoa Center, PA 15069 USA; Alton T. Tabereaux, Alcoa Inc., Process Technology, Muscle Shoals, AL 35661 USA

Tuesday PM
March 16, 2004

Room: 213D
Location: Charlotte Convention Center

Session Chair: Mike Barber, Arvida Research and Development Centre, Jonquiere, Quebec G7S 4K8 Canada

2:00 PM

Using System Dynamic Modelling for Scenario Simulations in Electrolysis Plants: Ole-Jacob Siljan¹; ¹Norsk Hydro ASA, Matls. Dvlp., Rsch. Ctr. HPI, Hydro Porsgrunn, N3907 Porsgrunn 3907 Norway

This paper presents the development of a scenario simulation model in Hydro Aluminium based on system dynamics. The purpose of the model was to perform high-level analysis to support discussions on a

common "best practice" operational philosophy in the new Hydro Aluminium. The model is based on technical, organisational and financial relationships, and the simulations are performed through defined scenarios and what/if analysis. The model has proved to be a useful tool, and the simulation results give firm indications on consequences of technological and organisational changes. Simulating effects of changes more reliable and construction improved mental models, allows the model to be used to carve out strategies for reducing the impact of changes on operating results, through pointing out preventive actions prior to and during the changes.

2:25 PM

Lowering Energy Intensity and Emissions in the Aluminum Industry with Government/Industry Partnerships: *Thomas P. Robinson*¹; William T. Choate²; ¹US Department of Energy, Energy Efficiency & Renewable Energy, Industrial Tech. Prog. EE-2F, 1000 Independence Ave., SW, Washington, DC 20585-0121 USA; ²BCS, Inc., 5550 Sterrett Pl. #306, Columbia, MD 21044 USA

The US Department of Energy, Energy Efficiency and Renewable Energy (EERE) Office's Industrial Technologies Program (ITP) seeks to lower the energy intensity of the U.S. aluminum industry through a coordinated program of research and development, validation, and dissemination of energy efficiency technologies and operating practices. Science fundamentals show a direct correlation between energy efficiency improvements and CO₂ emission reductions. ITP's Aluminum Industries of the Future (IOF) has partnered with more than 70 firms in over 35 R&D projects. These projects have focused on wetted cathodes, inert anodes, magnetohydrodynamic stability, process control systems, dross reduction and many other topics. This paper presents an overview of ITP's Aluminum IOF partnerships and their impact on energy intensity and emissions. It covers the technical progress, expected benefits, demonstration status and market projections for the portfolio's projects, emphasizing the energy savings and environmental impact reductions. The authors also describe new opportunities for R&D projects, BestPractice programs and other EERE R&D for lowering energy intensity and emissions.

2:50 PM

Inert Anodes: An Update: *Rudolf P. Pawlek*¹; ¹Technical Info Services & Consulting, Le Forum des Alpes, Ave. du Rothorn 14, CH - 3960 Siere Switzerland

To reduce the emission of greenhouse gases the primary aluminium industry is under increasing pressure to replace carbon anodes with inert anodes. During the last few years much effort has gone into developing inert anodes for the aluminium industry. Besides further developments of Alcoa's cermet anodes, interest also focussed on Moltech's metal anodes. Alcoa fine-tuned its recipes for the manufacture of inert anodes and for their introduction into conventional aluminium reduction cells. On the other hand Moltech reported about special efforts to prevent dissolution of metal anodes into the bath and, reported about tests in a 20 kA pilot cell, as well as about wear rates of only 3.5 mm per year from 1000 A cell tests. Other research teams have performed laboratory tests with inert anodes with other compositions than the Alcoa cermets and metal oxides. Laboratory scale tests determined dissolution rates of oxides into the electrolyte, how these contaminate the aluminium, and their dissolution mechanisms.

3:15 PM

Aluminum Versus Steel: Production Trends - Past, Present and Future: *Torstein Arnfinn Utigard*¹; ¹University of Toronto, Matls. Sci. & Engrg., 184 College St., Toronto, Ontario M5S 3E4 Canada

The evolution of production technologies of aluminum and steel are compared both for primary as well as secondary metals production. Steel got a head start on aluminum since it was easier and cheaper to produce on a large scale. Over the last 100 years, steel production technologies have changed frequently while for aluminum the basic technology has prevailed with gradual and continuous improvements. For steel there has already been a dramatic shift from primary to secondary scrap production. This has lead to a significant drop in primary steelmaking with no new integrated plant built in North-America for 40 years. Secondary aluminum production is also increasing, but since there still is good growth and since the "inventory" of old aluminum scrap is limited, the primary aluminum industry has until very recently, been shielded from these structural changes. The differences in cost and energy requirements between primary and secondary processing, are much greater for aluminum than for steel, suggesting that future changes for aluminum may be equally significant.

3:40 PM Break

3:50 PM

Analytical System of Long-Term Forecasting of Base Metals World Prices: *Boris Arlyuk*¹; ¹Alumconsult Ltd., 2, Shkiperski protok, St. Petersburg 199106 Russia

The complex system has been developed for long-term assessment of world prices and sale volume of base metals or commodities when using the analytical model of the market and market supply forecasts as well as economy development in the Western countries characterized by the industrial production indices. As example of developed approach is used the market of primary aluminium. The model has been developed for forecasting of the degree of capacities utilization rate of smelters depending on the aluminium price level in the world. The model contains a statistic part corresponding to the capacities distribution by the production cost, and a dynamic part determining the deviation from the static depending on the price variation dynamics. The developed complex model has been identified by the actual data of conservation and reactivation of aluminium production in the Western countries within the period from 1985 to 2002 and it is characterized by the average error of assessment of the part of idled capacities of 2.4%, this value variation being 3.3%. The error of long-term forecasting of average annual prices is 7% of the average price value, provided at the forecasting of new capacities commissioning and industrial production indices are correct. Similar models can be used for the world market and long term price forecast of base metals and commodities.

4:15 PM

The Development of 65kA Three-Layer Electrolysis Cell for Refining of Aluminum: *Huimin Lu*¹; Ruixin Ma¹; Zongren Liu²; Bin Wu²; Yingqian Zhang²; ¹University of Science and Technology, Metall. Engrg. Sch., Light Metal Rsch. Inst., 30 Xueyuan Rd., Beijing, Beijing 100083 China; ²Xinjiang Join-world Co., Ltd., 18 Kashidong Rd., Wulumuqi, Xinjiang 830013 China

Xinjiang Join-world Co., Ltd. is the largest refined aluminum producer in China. It had 64 32kA three-layer electrolysis cells for refining of aluminum with the Gadeau process electrolyte system and capacity of 5,000t/y before October 2002. To reach the target capacity of 20,000t/y, it was proposed to build 65kA three-layer electrolysis cells with the SAIA process electrolyte system. A pilot plant of 64 65kA three-layer electrolysis cells (XJ-65) was commissioned in October 2002. Advanced design and new materials were applied for the cell shell and lining to get better stability of magnetic hydrodynamics and heat balance. The two process electrolyte systems were tested in four 65kA three-layer electrolysis cells. At last, the Gadeau process electrolyte system with solid refined aluminum cathode was selected for the pilot plant. With eight months test production, the cathodic current efficiency is up to 99%, DC power consumption 15000kWh/t aluminium.

Automotive Alloys 2004: Session IV

Sponsored by: Light Metals Division, LMD-Aluminum Committee
Program Organizer: Subodh K. Das, Secat, Inc., Coldstream Research Campus, Lexington, KY 40511 USA

Tuesday PM

March 16, 2004

Room: 210A

Location: Charlotte Convention Center

Session Chair: Subodh K. Das, Secat Inc., Coldstream Rsch. Campus, Lexington, KY 40511 USA

2:00 PM

Comparison of the Auto Aluminum Sheets Blanked with Laser and Traditional Mechanical Processes: *Frank Feng*¹; ¹Alcan International Ltd., Kingston R&D Ctr.

1 mm thick 6111 aluminum sheets cut with three different processes were compared in this study. They are high-speed laser cutting, traditional punch shearing and mill machining. The stretch ability of these cut edges was evaluated based on the hoop strain limits of the specimens with 2" diameter holes on a 4" diameter dome tester. It was found that the stretch ability of the laser cut edges, even though not as good as milling machined, are superior to the punch sheared edges. The cut edges were also characterized with a 3D WYKO non-contact profilometer, optical and scanning electron microscopy and micro-hardness survey.

2:30 PM

Dynamic Side Impact Simulation of Aluminum Road Wheels Incorporating Material Property Variations: *Robert Shang*¹; Naiyi

Li²; William Altenhof¹; Henry Hu¹; ¹University of Windsor, Dept. of Mech., Autom. & Matls. Engrg., 401 Sunset Ave., Windsor, Ontario N9B 3P4 Canada; ²Ford Motor Company, Ford Rsch. Lab., 2101 Village Rd., Dearborn, MI 48124 USA

The performance of road wheel impact resistance is a major concern related to new designs of automotive road wheels and their optimization. In this study, nonlinear dynamic finite element analysis has been employed to numerically investigate side impact of an aluminum road wheel. Based upon the experimental side impact testing device and method described in SAE J175, a numerical model incorporating the aluminum road wheel and a steel loading striker was developed using the parametric mesh generating software TrueGrid. The road wheel was mounted at an incline of 13° to the horizontal and the loading block was prescribed an initial velocity to simulate a 230mm vertical drop. Different simulated impacts at radial locations on the wheel spoke and in between spokes were conducted to investigate the structural performance of the road wheel. The material structural inhomogeneity was taken into consideration by assigning different material properties (including yield stress, ultimate tensile strength, and material elongation) to specific sections of the road wheel, which were evaluated by conducting standardized tensile tests on specimens extracted from various regions of the road wheel. Consideration of material variation throughout the road wheel within the numerical model better represents its actual mechanical behavior.

3:00 PM

Optical Technique to Measure Distortion on Heat Treated Parts In Situ: *Federico Mariano Sciammarella*¹; Phillip Nash¹; Calvin Tszeng¹; ¹Illinois Institute of Technology, Thermal Procg. Tech. Ctr., 10 W. 32nd St., Chicago, IL 60616 USA

The automotive industry continually seeks to improve and extend the use of aluminum. The heat treatments of these parts are very vital in providing the properties needed for their particular applications. Moreover understanding the effects of heat treatments that may cause distortion to a part is critical. Most of the work carried out in this field is a pre and post measurement after part has experienced its treatment. In this study, we carry out in-situ measurements of the distortions that a heat-treated part undergoes when subjected to temperatures near melting followed by a slow cooling. In order to confirm the experimental measurements HOTPOINT a modeling package was used to simulate the experiment and compare results. This study will provide much needed insight to the complex occurrences that aluminum parts undergo during heat treatment.

3:30 PM

Surface Modification of Titanium by Adding SiC, WC and BN2 to the Surface of Ti 6-4 Alloy: *Glen A. Stone*¹; William J. Arbogast¹; Glenn J. Grant²; Stanley M. Howard¹; ¹South Dakota School of Mines and Technology, Matls. & Metall. Engrg., 501 E. St. Joseph St., Rapid City, SD 57701-3995 USA; ²Pacific Northwest National Laboratory, Matls. Procg. & Performance/Energy Matls., 902 Battelle Blvd. K2-03, Richland, WA 99356 USA

The Advanced Materials Processing Center (AMP) at the South Dakota School of Mines and Technology in conjunction with the Pacific Northwest National Lab is developing methods to stir micron size particles into the surface of titanium and other metals to create surface regions enriched in ceramic particulate for enhancement of wear, hardness, or thermal barrier properties. Hard particle reinforcement of the surface of titanium may have numerous industrial applications in rotating or reciprocating assemblies, engines, or other situations where bulk strength, light weight, and surface wear resistance is needed over conventional monolithic materials. Studies of tool geometry, Friction Stir Processing (FSP) parameters as a function of carbide and nitride particle distribution are presented. Tool materials currently being explored are Tungsten-Rhenium and Ferro-TiC HT-6A.

4:00 PM

Method for Testing Tension/Compression of Sheet Alloys: *R. K. Boger*¹; R. H. Wagoner¹; M. G. Lee²; K. Chung²; ¹Ohio State University, Dept. of Matls. Sci. & Engrg., 477 Watts Hall, 2041 College Rd., Columbus, OH 43210 USA; ²Seoul National University, Sch. of Matls. Sci. & Engrg., 56-1 Shinlim-dong, Kwanak-gu, Seoul 151-742 Korea

The mechanical behavior of sheet alloys under reversed loading and other non-proportional paths is important for simulating forming and springback behavior. A new method for obtaining large-strain compression/tension has been developed and optimized for use with a standard tensile testing machine. Compressive strains greater than 15% have been obtained and have revealed new behavior. Interpretation of the test requires simple analysis to compensate for frictional and off-axis loading effects. The development, optimization, and capabilities of the new method will be presented, along with preliminary

results of its application to the Bauschinger effect, to room-temperature creep, and to anelasticity.

4:30 PM

The Effects of Mg and Mn Precipitation on Serrated Yielding and on Texture Evolution During Cold Rolling and Subsequent Annealing: *Wei Wen*¹; James G. Morris¹; ¹University of Kentucky, Chem. & Matls. Engrg., 177 F. Paul Anderson Hall, Secat Inc., 1505 Bull Lea Rd., Lexington, KY 40506 USA

Continuous Cast (CC) AA5182 aluminum alloy was subjected to a high temperature heat-treatment of 482°C for 48hr and a low temperature heat-treatment of 182°C for 100hr. In the first case, fine MnAl₆ dispersoids were precipitated out of solid solution while in the latter case, large and dense Mg₂Al₃ particles were formed mainly along the grain boundaries. Tensile results show that the intensity of serrated yielding was greatly reduced for the material with the low temperature heat-treatment (182°C) while that with the high temperature treatment the serrated yielding was significantly increased. This is understandable, since it is well known that Mg atoms in solid solution interact with mobile dislocations and cause serrated yielding. The more Mg atoms in solid solution, the more intense is the serrated yielding. On the other hand, Mn atoms, due to their much slower diffusion rate and a higher binding energy with vacancies, do not interact significantly with mobile dislocations and at the same time block the path for the diffusion of Mg atoms. To investigate the effects of Mg and Mn precipitation on the texture evolution during cold rolling and subsequent annealing, the hotband was first annealed at 399°C for 4hr to obtain a completely recrystallized condition before the aforementioned high- and low-temperature heat-treatments. After the heat-treatments, the materials were cold rolled from 0% to 90% reduction in thickness to investigate the texture evolution during cold rolling. For the material cold rolled to 70% reduction, further salt bath annealing was carried out to investigate the texture evolution during annealing. During cold rolling, the material with Mg precipitation (182°C treatment) has a lower rate of "disappearance" of the Cube+*r*-Cube component, a higher rate of "disappearance" of the random component and a higher rate of "formation" of the β fiber component than the material heat-treated at 482°C. During subsequent annealing, due to the large Mg₂Al₃ particles formed during low temperature annealing, new grains are nucleated and grow much faster. On the other hand, the fine MnAl₆ dispersoids formed during high temperature heat-treatment have a retarding effect on recrystallization.

5:00 PM

Fabrication of P/M Processed Super High Strength Aluminum Alloy: *Kozo Osamura*¹; Hiroki Adachi¹; Jun Kusu²; Ken Kikuchi²; ¹Kyoto University, Dept. MSE, Sakyo-ku, Yoshida-honmachi, Kyoto 606-8501 Japan; ²Toyo Aluminium, R&D Lab., Shiga 529-16 Japan

Recently our group developed extremely high strength AlZnMgCu alloys (MesoaliteTM) by means of powder metallurgy. The air-atomized powder was canned into the aluminum container and then pressed under hydrostatic pressure of 392 MPa. After degassing, the compact piece was hot-extruded at 773K. The extrusion ratio was selected as 10 or 20. Several kinds of alloys including alloy elements of Zn, Mg, Cu, Mn and Ag were investigated. The present technique can provide a large scale product, for instance, the rod with dimension of 60 mm dia and 1000 mm length. As a standard procedure of heat treatment, the solution treatment was carried out at 763 K for 7.2ks and followed by water quenching. The standard condition of aging treatment as T6 was 393 K and 86.4 ks. A selected alloy (MESO20) with composition of Al-9.5%Zn- 3.0%Mg- 1.5%Cu- 4.0%Mn- 0.04%Ag in mass% recorded tensile strength of 910 MPa and compressive strength of 1032MPa. The present super-high strength aluminum alloys could be achieved by the combination of several strengthening mechanisms; (1) fibre reinforcing, (2) fine grain strengthening and (3) precipitation hardening. Especially nano-scale coherent particles are very effective to achieve the high strength materials.

Beyond Nickel-Base Superalloys: Molybdenum Silicides II

Sponsored by: Structural Materials Division, SMD-Corrosion and Environmental Effects Committee-(Jt. ASM-MSCTS), SMD-High Temperature Alloys Committee, SMD-Mechanical Behavior of Materials-(Jt. ASM-MSCTS), SMD-Refractory Metals Committee
Program Organizers: Joachim H. Schneibel, Oak Ridge National Laboratory, Oak Ridge, TN 37831-6115 USA; David A. Alven, Lockheed Martin - KAPL, Inc., Schenectady, NY 12301-1072 USA; David U. Furrer, Ladish Company, Cudahy, WI 53110 USA; Dallis A. Hardwick, Air Force Research Laboratory, AFTL/MLLM, Wright-Patterson AFB, OH 45433 USA; Martin Janousek, Plansee AG Technology Center, Reutte, Tyrol A-6600 France; Yoshinao Mishima, Tokyo Institute of Technology, Precision and Intelligence Laboratory, Yokohama, Kanagawa 226 Japan; John A. Shields, HC Stark, Cleveland, OH 44117 USA; Peter F. Tortorelli, Oak Ridge National Laboratory, Oak Ridge, TN 37831-6156 USA

Tuesday PM Room: 211B
March 16, 2004 Location: Charlotte Convention Center

Session Chairs: S. G. Fishman, US Navy, Office of Naval Rsch., Arlington, VA 22217 USA; Martin Janousek, Plansee AG, Tech. Ctr., A-6600 Reutte/Tyrol Austria

2:00 PM Invited

Characterization of a Primary Deformed Moss-Mo₅SiB₂-Mo₃Si Composite Material: *Pascal Jéhanno*¹; Dirk Handtrack²; Martin Heilmair³; Heinrich Kestler¹; Andreas Venskutonis¹; Michael Schaper²; ¹Plansee AG, Tech. Ctr., Reutte in Tirol 6600 Austria; ²Technische Universität Dresden, Inst. für Werkstoffwissenschaft, Helmholtzstraße 7, Berndt-Bau, Dresden 01069 Germany; ³Otto von Guericke Universität Magdeburg, Inst. für Werkstofftechnik und Werkstoffprüfung, Ernst Schiebold Gebäude, Große Steinernischstraße, Magdeburg 39016 Germany

A ternary Molybdenum-Silicon-Boron alloy with the composition Mo - 8.9 % Si - 7.7 % B (at.%) was manufactured using an industrial powder metallurgical processing route, comprising gas atomization and hot isostatic pressing. Subsequently, the material was primary deformed via high temperature extrusion in order to obtain a microstructure consisting of a molybdenum solid solution matrix surrounding intermetallic particles. The microstructure was characterized by SEM, EDX and X-ray diffraction including Rietveld analysis. Mechanical properties were investigated using tensile tests at temperatures ranging from 1000°F (538°C) to 2000°F (1093°C). The primary deformation of the material resulted in a revolutionary increase of the strength in comparison with as-HIPed prematerial, reaching values equivalent to TZM. Additionally, the ductile to brittle transition temperature decreased by 200°C and the strain to failure increase to 25-30% at temperatures as low as 2000°F (1093°C).

2:30 PM

Effect of Al Addition on Ultra-High Temperature Performance of Mo/Mo₅SiB₂ In-Situ Composites: *Kyosuke Yoshimi*¹; Akira Yamauchi¹; Masafumi Tsunekane²; Shuji Hanada¹; ¹Tohoku University, Inst. for Matls. Rsch., 2-1-1 Katahira, Aoba-ku, Sendai, Miyagi 980-8577 Japan; ²Tohoku University, Dept. of Matls. Proc., 2-1-1 Katahira, Aoba-ku, Sendai, Miyagi 980-8577 Japan

Mo/Mo₅SiB₂ in-situ composites are one of promising candidates for ultra-high temperature structural applications. In this work, the effect of Al addition on the ultra-high temperature performance of Mo/Mo₅SiB₂ in-situ composites is investigated. (Mo-8.7Si-17.4B)_{1-x}Al_x (x = 0, 1, 3 and 5%) alloys were prepared by arc-melting, and homogenized at 2073 K for 24 h in an Ar gas atmosphere. In binary Mo-8.7Si-17.4B, fine two-phase microstructure is developed by the heat treatment, suggesting eutectic or eutectoid reaction occurs at this composition. It is identified by XRD that the matrix is Mo₅SiB₂ and fine precipitates are Mo solid solution. The binary Mo/Mo₅SiB₂ in-situ composite exhibits excellent high temperature strength, for instance about 1 GPa even at 1773 K. The melting point, microstructure, and high temperature oxidation resistance and strength are varied with Al concentration. Therefore, it is found that the Al addition affects the ultra-high temperature performance of the Mo/Mo₅SiB₂ in-situ composites.

2:45 PM

Mechanical Properties of the T₂ Phase in the Mo-Si-B System and Related Mo Based Alloys: *Kazuhiro Ito*¹; Taisuke Hayashi¹; Masakuni Fujikura²; Masaharu Yamaguchi¹; ¹Kyoto University, Matls.

Sci. & Engrg., Sakyo-ku, Kyoto 606-8501 Japan; ²Japan Ultra-high Temperature Materials Research Center Ltd., Tajimi, Gifu 507-0801 Japan

Plastic deformation was observed only for [021] and [443] oriented single crystals of the T₂ phase with the D8₁ structure in the Mo-Si-B system at 1773 K at a strain rate of 1x10⁻⁵ s⁻¹. Slip on [001](010) was observed in the [021] oriented crystals, but other slip systems were not observed. While, [0001], [13⁻40], [22⁻49] oriented single crystals of the Mo₅Si₃C with the D8₈ structure can be plastically deformed at temperatures higher than 1573 K. Slip occurs on {0001}<11⁻20> and an unidentified non-basal system. This is similar case of Mo₅Si₃ with the D8_m structure. The creep strength at elevated temperature of single crystalline and polycrystalline Mo₅SiB₂ is superior to those of MoSi₂, Mo₅Si₃ and Si₃N₄ based structural ceramics. The directionally solidified T₂/Mo_{ss} eutectic alloy has the room temperature fracture toughness of about 11 MPa√m. It is substantially improved from that of the monolithic T₂.

3:00 PM

The Fracture Toughness and Toughening Mechanisms of Wrought LCAC, TZM, and ODS Molybdenum Plate Stock: *Brian V. Cockeram*¹; ¹Bechtel Bettis Laboratory, PO Box 79, W. Mifflin, PA 15122-0079 USA

The high-temperature strength and creep resistance of Low Carbon Arc Cast (LCAC) pure molybdenum, Oxide Dispersion Strengthened (ODS) molybdenum, and TZM molybdenum make these alloys of interest for various high-temperature structural applications. However, these same alloys have been poorly characterized as to fracture toughness (K_{IC}) and transition temperatures from brittle to ductile behavior. This work reports K_{IC} testing performed in accordance with ASTM E399 methods over a temperature range of -150C to 1000C using LCAC, ODS, and TZM molybdenum plate stock. The use of bend specimens and compact tension specimens of varying sizes showed that the results obtained with sub-sized bend and disc-CT specimens were comparable to values obtained with conventional specimens. Based on the fracture toughness data and failure mode, the transition temperature to brittle behavior was defined to occur in a range of toughness values between 26 to 34 MPa m^{1/2}. The ductile to brittle transition temperature (DBTT) for ODS molybdenum was below room-temperature for both the transverse and longitudinal orientations. The DBTT for LCAC and TZM molybdenum in the longitudinal direction was between 100C and 150C, while the transition temperature for the transverse orientation was 150C to 200C. It has been postulated that the refined microstructure of ODS molybdenum produces the significantly lower DBTT. Thin sheet toughening is shown to be the dominant toughening mechanism for all molybdenum alloys.

3:15 PM

Role of Microstructure in Creating High Toughness Mo-Si-B Alloys: *Jamie J. Kruzic*¹; Joachim H. Schneibel²; *Robert O. Ritchie*¹; ¹Lawrence Berkeley National Laboratory, Matls. Scis. Div., 1 Cyclotron Rd., Bldg. 62R0100-8255, Berkeley, CA 94720-8139 USA; ²Oak Ridge National Laboratory, Metals & Ceram. Div., PO Box 2008, Oak Ridge, TN 37831-6115 USA

Mo-Si-B based alloys containing α-Mo, Mo₅Si, and Mo₅SiB₂ (T₂) phases have been targeted for high temperature turbine engine applications. However, to achieve adequate resistance to oxidation, creep, fracture and fatigue, microstructural optimization is necessary. To further this goal, an understanding of how microstructural features affect the fracture and fatigue properties at ambient to high temperature is presented. Specifically, the fracture toughness and fatigue-crack growth resistance have been investigated from 25°-1300°C for several Mo-Si-B alloys with both α-Mo and intermetallic matrix microstructures. These alloys were produced by both ingot and powder metallurgy processing routes with compositions nominally as Mo (bal.), 12-20 at.% Si, 8-10at.% B. The role of microstructural variables including volume fraction of α-Mo, its ductility, and the morphology and coarseness of the microstructure are considered in terms of how each variable affects the observed toughening mechanisms. Such mechanisms have been identified as crack trapping, crack bridging, and microcrack toughening. Work supported by the Department of Energy, through the Office of Science (Basic Energy Sciences) under Contract No. DE-AC03-76SF00098 (for JJK and ROR), and the Office of Fossil Energy (Advanced Research Materials) under Contract No. DE-AC05-00OR22725 (for JHS).

3:30 PM Break

4:00 PM

Fracture Toughness and Hardness of Multiphase Mo-Si-B Alloys: *Zeynep Kasapoglu*¹; David R. Johnson¹; Mysore A. Dayananda¹;

¹Purdue University, Sch. of Matls. Engrg., 501 Northwestern Ave., W. Lafayette, IN 47907-2044 USA

In this study multiphase Mo-Mo₅SiB₂(T₂)-Mo₅Si alloys with different compositions were examined for microstructure and fracture toughness. The alloys were prepared by using the arc zone-melting technique. For the reduction of grain boundary embrittlement, 0.8%Yttrium was added to selected compositions. In addition, for alloys with near-eutectic compositions Mo was substituted with Nb to explore equilibrium among the Mo, T₂ and Mo₅Si₃ phases. The alloys were characterized by SEM, optical microscopy and XRD techniques. Four-point bending tests and Vickers hardness tests were performed with alloy specimens to determine their fracture toughness and hardness.

4:15 PM

Cyclic Deformation of Mo-Si-B Alloys: Amruthavalli P. Alur¹; Ping Wang¹; Sharvan Kumar¹; ¹Brown University, Div. of Engrg., 182 Hope St., Box D, Providence, RI 02912 USA

The cyclic deformation behavior of two Mo-Si-B alloys (Mo-2Si-1B and Mo-3Si-1B) in the isothermally forged condition has been characterized in terms of their room-temperature S-N response and crack growth behavior using precracked compact tension specimens. Crack growth studies were conducted in air in the temperature range 20°C-600°C and compared to T₂M subjected to similar loading history. Additionally, fatigue crack growth experiments were also performed in vacuum at 600°C to delineate the effects of environment on fatigue crack growth resistance. The interaction of the advancing crack tip with the microstructure on the specimen surface was examined to obtain an appreciation of the role of the matrix and intermetallic phases in contributing to fatigue resistance. Fracture surfaces were characterized in all instances to help understand the measured properties.

4:30 PM

High-Temperature Compression Response of T₂M and Mo-Si-B Alloys: Amruthavalli P. Alur¹; Ping Wang¹; Molly Curran¹; Sharvan Kumar¹; ¹Brown University, Div. of Engrg., 182 Hope St., Box D, Providence, RI 02912 USA

The 1000°C-1400°C compression response of a powder-metal-lurgy processed T₂M alloy (MT 104) and two Mo-Si-B alloys (a two-phase alloy, Mo-2Si-1B and a three-phase alloy, Mo-3Si-1B) was evaluated. At 1000°C, the flow stress at 4% strain of T₂M varies between 300 MPa and 250 MPa for nominal strain rates ranging from 10⁻⁴s⁻¹ to 10⁻⁶s⁻¹ respectively. In contrast, for a two-phase Mo-Si-B alloy, the corresponding flow stress values are ~1150 MPa and ~800 MPa; however, when the strain rate is decreased to 10⁻⁷s⁻¹, the flow stress for the two-phase Mo-Si-B alloy drops to ~400 MPa. At 1400°C and a strain rate of 10⁻⁴s⁻¹, a flow stress of ~250 MPa is obtained for the MoSiB alloy. The initial and deformed microstructures were examined in a transmission electron microscope and microstructural observations will be discussed in the context of measured properties.

4:45 PM

Optimization of Mo-Si-B Intermetallics: Joachim H. Schneibel¹; Robert R. Ritchie²; Jamie J. Kruzic²; Peter F. Tortorelli¹; ¹Oak Ridge National Laboratory, Metals & Ceram., PO Box 2008, Oak Ridge, TN 37831 USA; ²Lawrence Berkeley National Laboratory and University of California, Matls. Scis. Div. & Dept. of Matls. Sci. & Engrg., Berkeley, CA 94720 USA

Mo-Si-B intermetallics based on the phases Mo₃Si, Mo₅SiB₂, and Mo solid solution offer promise as ultra-high temperature structural materials. By varying the composition, microstructural scale, and microstructural topology, the oxidation resistance, creep resistance, or fracture toughness properties of these alloys can be improved. Experiments illustrating the ways in which the various properties can be enhanced will be described. Work on improving the fracture toughness of Mo-Si-B alloys by additions of Zr and the ductility of the Mo solid solution phase by adding MgAl₂O₄ spinel particles is in progress. This work was sponsored by the Office of Fossil Energy, Advanced Research Materials (ARM) Program, and the Division of Materials Sciences and Engineering, U.S. Department of Energy, under contract DE-AC05-00OR22725 with Oak Ridge National Laboratory managed by UT-Battelle, LLC.

Bulk Metallic Glasses: Theoretical Modeling and Shear Bands

Sponsored by: Structural Materials Division, ASM International: Materials Science Critical Technology Sector, SMD-Mechanical Behavior of Materials-(Jt. ASM-MSCTS)

Program Organizers: Peter K. Liaw, University of Tennessee, Department of Materials Science and Engineering, Knoxville, TN 37996-2200 USA; Raymond A. Buchanan, University of Tennessee, Department of Materials Science and Engineering, Knoxville, TN 37996-2200 USA

Tuesday PM
March 16, 2004

Room: 209A
Location: Charlotte Convention Center

Session Chairs: James R. Morris, Ames Laboratory, Physics, Ames, IA 50011-3020 USA; Katharine H. Flores, Ohio State University, Matls. Sci. & Engrg., Columbus, OH 43210-1178 USA

2:00 PM Invited

Shear Banding in the Self-Consistent Dynamic Free Volume Model: Sven Bossuyt¹; A. Lindsay Greer¹; William L. Johnson²; ¹University of Cambridge, Dept. of Matls. Sci. & Metall., Pembroke St., Cambridge CB2 3QZ UK; ²California Institute of Technology, Engrg. & Appl. Sci., MC 138-78, Pasadena, CA 91125 USA

Recently, a self-consistent free volume model was proposed to analyze the Newtonian and non-Newtonian uniform flow data for bulk glass forming liquids such as those of the Zr-Ti-Cu-Ni-Be Vitreloy family. The model is based on the traditional free volume model of the glass transition, the Vogel-Fulcher-Tamman equation, and a simple treatment of free volume production and annihilation during flow. In this paper, we consider the implications of this model regarding flow localization into shear bands, by applying linear stability analysis and numerical finite element methods within the self-consistent dynamic free volume framework.

2:25 PM Invited

Mechanisms of Deformation-Assisted Decomposition in a Metallic Glass: Michael Atzmon¹; Wenhui Jiang¹; ¹University of Michigan, NERS/MSE, Cooley Bldg./N. Campus, Ann Arbor, MI 48109-2104 USA

Nanocrystallites have been observed to form at shear bands resulting from deformation in several metallic glass alloy types. Although there is a driving force for crystallization below the melting point, the kinetics are typically too sluggish at room temperature. There is both fundamental and practical interest in the effect of plastic deformation on the stability of a metallic glass. We have used transmission electron microscopy (TEM) to study the nanocrystallization mechanisms in amorphous Al₉₀Fe₅Gd₅ deformed by bending and nanoindentation. In bent samples, nanocrystallites are observed in the predominantly compressive region only. Using high-resolution TEM and image filtering, we observe nanovoids within the shear bands in the predominantly tensile region only. During nanoindentation, the nucleation rate is sensitive to the applied loading rate. The results are consistent with free-volume annihilation kinetics of order higher than one. Ruling out a temperature effect, we interpret the results in terms of diffusion enhancement by free-volume production. This work was funded by the US National Science Foundation, Grant DMR-9902435.

2:50 PM Invited

Deformation Induced Structural Changes in Bulk Metallic Glasses: Katharine M. Flores¹; ¹Ohio State University, Dept. of Matls. Sci. & Engrg., 2041 College Rd., Columbus, OH 43210-1178 USA

The magnitude and distribution of free volume is thought to play a central role in shear band formation and the resulting flow behavior in metallic glasses. To elucidate the influence of free volume, structural changes after plastic deformation and thermal relaxation have been investigated. Positron annihilation spectroscopy studies on a Zr-Ti-Cu-Ni-Be alloy suggest that most of the free volume is associated with the larger solvent atoms (Zr and Ti) and that plastic deformation results in a net free volume increase and redistribution. Similar investigations of Cu-based alloys have been undertaken and will be discussed. Shear band formation in the vicinity of a sharp crack tip has also been investigated. Previous investigations of crack tip deformation under tensile loading reveal significant increases in fracture toughness to more than 80 MPa√m, 4-5 times the inherent toughness of the alloy, due to the formation of a large damage zone. Controlling the formation of such a damage zone is integral to the optimization of bulk metallic glass composites.

3:15 PM

Fundamental Mechanisms of Deformation in Simulations of Metallic Glass Nanoindentation: *S. B. Biner*¹; J. R. Morris¹; ¹Iowa State University, Ames Lab., Metal & Ceram. Scis., Ames, IA 50011 USA

The localized plastic deformation behavior of amorphous solids were examined by molecular dynamic simulations of nanoindentation. The model system was two-dimensional and composed of a binary alloy with a two-body Lennard-Jones potential. It will be shown that the mechanism of shear localization and the formation of shear bands is a dynamic process balancing transient events of dilatation and contraction in regions involving a limited number of atoms. These shear localization regions were characterized in terms of the initial stress state, stiffness and free volume. A connection is also established with the serrated plastic flow that is seen during the nanoindentation experiments on metallic glasses. This work was performed for the United States Department of Energy by Iowa State University under contract W-7405-Eng-82. This research was supported by the Director of Energy Research, Office of Basic Sciences.

3:40 PM

Modeling the Propagation of Shear Bands in Bulk Metallic Glasses: *Brian J. Edwards*¹; Kathleen Feigl²; Peter K. Liaw³; ¹University of Tennessee, Chem. Engrg., 419 Dougherty Hall, Knoxville, TN 37996-2200 USA; ²Michigan Technological University, Applied Math., 311 Fisher Hall, Houghton, MI 49931 USA; ³University of Tennessee, Matls. Sci. & Engrg., Knoxville, TN 37996-2200 USA

Recent observations have indicated that shear bands originate and propagate in bulk metallic glasses (BMGs) under tensile loading once plastic deformation has begun. These shear bands propagate and dissipate on the order of milliseconds, as witnessed with high-speed and high-sensitivity infrared thermography. In this presentation, we present results of a study aimed at understanding the onset, propagation, and eventual dissipation of these shear bands under tensile loading in BMGs. Initial results are discussed, based on the application of a non-equilibrium thermodynamics approach to this problem, which results in a system of equations that couples the applied stress distribution within the sample with temperature and an additional vector field associated with the free volume in BMGs. This set of equations describes the shear-band formation, propagation, and dissipation within the BMGs, and gives hints concerning the origination of shear bands, their speeds of propagation, and the magnitude of any permanent plastic deformation that occurs across them.

4:05 PM

Interaction of Shear Bands with Inclusions in Metallic Glasses: *Alan C. Lund*¹; Christopher A. Schuh¹; ¹Massachusetts Institute of Technology, Matls. Sci. & Engrg., 77 Mass. Ave., Cambridge, MA 02139 USA

Shear bands represent the only mechanism for plastic accommodation in metallic glasses at low temperature, so the physics of shear strain development are therefore central to the international effort in metallic glass development. Recent works have shown that shear bands interact with inclusions at both the nano- and macro-scales, and load sharing with such inclusions may be a viable means of increasing glass ductility. Here we explore the development of shear strain in simulated metallic glasses with and without nano-scale crystalline inclusions. In particular, we examine the effect of these particles on the strength of the glass as well as the tendency for shear localization. Preliminary results are presented for inclusions of different sizes, and compared with existing experimental literature.

4:30 PM

Shear Band Formation and Ductility of Metallic Glasses: *Alla V. Sergueeva*¹; Nathan A. Mara¹; Amiya K. Mukherjee¹; ¹University of California, Chem. Engrg. & Matls. Sci. Dept., 1220 Bainer Hall, Davis, CA 95616 USA

Variations in microstructure and chemical compositions of the metallic glasses found in the literature, as well as an overall lack of experimental data on inhomogeneous behavior of metallic glass makes the formulation of a conclusion on the shear band/fracture behavior effects on mechanical properties of metallic glasses difficult. Investigating the effect of strain localization alone on inhomogeneous flow seems to be a first step in approaching this problem. Mechanical behavior of metallic glasses at room temperature and various strain rates in tension and compression was investigated. Formation of multiple shear bands was observed at high strain rates. An increase in strain rate leads to enhance ductility in tension, whereas, the ductility of the material in compression decreases with increasing strain rate. Differences in deformation processes in tension and compression were compared. This work is supported by ONR Grant N00014-03-1-0149.

4:55 PM

In-Situ Observations of the Evolution of Plasticity in Metallic Glasses: *A. Bastawros*²; A. Antoniou²; C. C.H. Lo¹; *S. B. Biner*¹; ¹Iowa State University, Ames Lab., Metal & Ceram. Scis., Ames, IA 50011 USA; ²Iowa State University, Dept. of Aeros. Engrg. & Engrg. Mech., Ames, IA 50011 USA

The onset and evolution of plastic deformation under a cylindrical indenter in a metallic glass (Zr41.2-Ti13.8-Cu12.5-Ni10-Be22.5, atomic %) on a micro scale was continuously monitored by using a microscopic digital image correlation system. The plastic zone beneath the indenter is comprised of near orthogonal sets of shear band traces. They almost follow the α and β characteristic lines of the Prandtl slip line field for a cylindrical indenter, and the whole field evolves essentially in a self-similar way. By matching the experimentally observed load-displacement curves with finite element predictions, a general constitutive behavior that describes the shear band evolution was developed. Also, detailed examinations of shear bands by atomic force microscopy and transmission electron microscopy will be presented. This work partially funded by USDOE to Iowa State University under contract W-7405-Eng-82. This research was also partially supported by the Director of Energy Research, Office of Basic Sciences.

Carbon Technology: Anode Baking

Sponsored by: Light Metals Division, LMD-Aluminum Committee
Program Organizers: Markus Meier, R&D Carbon, Sierre CH 3960 Switzerland; Amir A. Mirchi, Alcan Inc., Arvida Research and Development Centre, Jonquiere, QC G7S 4K8 Canada; Alton T. Tabereaux, Alcoa Inc., Process Technology, Muscle Shoals, AL 35661 USA

Tuesday PM

March 16, 2004

Room: 213A

Location: Charlotte Convention Center

Session Chair: Masood T. Al Ali, Dubal Aluminum Company Ltd., Dubai United Arab Emirates

2:00 PM

Performance Enhancement of Anode Baking Furnaces at Hindalco's Aluminium Smelter: *S. C. Tandon*¹; ¹Hindalco Industries Ltd., Renukoot, Sonbhadra, UP India

Hindalco is India's largest integrated aluminium complex and one of the lowest cost producers in the world with primary aluminium smelting capacity of 342 KT/Y, besides having its own captive power plant, alumina refinery and down stream fabrication facilities. With increased aluminium smelting capacity, enhancement of anode baking capacity became necessary. A performance enhancement plan of anode baking furnaces was undertaken to optimize fuel oil consumption, increase production capacity, reduce fire cycle time, improve baked anode quality and enhance refractory life. Based on Hindalco's long experience in bake furnace operation, a strategic plan was worked out for regulating the heat distribution in furnaces through introduction of microprocessor based firing and draft control system. There is substantial gain in anode baking capacity and quality besides reduction in fuel oil consumption. This paper describes the technology and strategy and presents the improvement in plant performance based on actual plant data.

2:25 PM

Expansion of an Albras Bake Furnace in Continuous Operation: *Alexandre Manuel Aquino*¹; *Ronaldo Raposo Moura*²; *Jorge Magalhães Mello*¹; ¹ALBRAS Albras Alumínio Brasileiro SA, Carbon Process Engrg., Rodovia Pa 483, Km21, Vila Murucupi, Barcarena, Para 68447-000 Brazil

In order to support the growing anode demand it was needed to increase the total anode baking capacity by around 10%. As the increase of anode demand took place before we were able to increase our anode baking capacity, was needed to reduce the anode baking cycle to build-up sufficient anode inventory to permit us to stop a furnace. This article shows how the expansion work of an Open Ring Baking Furnace with 36 sections was done to add 18 more sections without shut down it - increasing the anode production capacity by 2160 blocks per month. In this article are explained aspects about logistic of the physical construction, as well as planning and operational aspects that made it possible the continuous operation of the furnace during the construction work. Then, the production gains obtained with this procedure were evaluated and showed that the anode quality was not affected.

TUESDAY PM

2:50 PM

A Simplified Baking Furnace Model for Improving Flue Wall Design: John A. Johnson¹; Alexander V. Rozin²; Alexander P. Skibin³; ¹RUSAL Engineering & Technical Center, Head, Anode Tech. & Carbon Matls., Pogranichnikov St. 37, Krasnoyarsk, Krasnoyarsk Krai 660111 Russia; ²Lomonosov Moscow State University, Inst. of Mech., 1 Michurinsky Pr., Moscow 119899 Russia; ³Lomonosov Moscow State University, 1 Michurinsky Pr., Moscow 119899 Russia

A simplified mathematical model for solving the conjugate heat transfer problem in the anode baking furnace is developed. The air motion in the flue induced by the exhaust draft is described by the system of differential equations for the viscous compressible multi-component gas taking into account heat and mass transfer. The flow is turbulent and the k- ϵ model is used. Turbulence-controlled eddy break-up model governs the combustion. The diffuse method is used for calculating the radiation flux. It is shown that the problem can be simplified if we treat the processes in the flue as stationary and solve the transient thermal conductivity equation only in the pit. The fields of pressure, velocity, temperature and concentrations are obtained in the flue and time dependent temperature distributions for each of the baking anodes evaluated.

3:15 PM

A Unique Refractory Solution for Anode Baking Furnace Flues: James R. Uhrig¹; ¹RESCO Products Inc., Penn Ctr. W. Two, Ste. 430, Pittsburgh, PA 15276 USA

Large quantities of refractories continue to be used for initial construction and replacement of flue walls in anode baking furnaces operated by primary aluminum producers. Refractory industry consolidation has led to a reduction in the number of acceptable product offerings available for this critical application, a continuing increase in costs, and concerns about on-going product availability. Failure mechanisms of flue walls are well known. Stresses caused by thermal expansion, reactions from intrusion of aluminum and sodium fluorides that cause varying chemical and physical alteration across the width of the wall, along with thermal cycling, are generally manifested by subsidence, cracking, and bowing. In addition, graphite rich deposits on the pit side of the walls can lead to high maintenance costs for cleaning or premature replacement due to reduced pit capacity, and less efficient thermal transfer. Although there has been a gradual and almost universal upgrading in refractory selection for flue walls to fired brick of about 50% alumina content, flue failures ultimately occur for the same reasons cited above. Considerable past experience showed that extruded shapes of about 42% alumina content based on a unique domestic pyrophyllite/andalusite raw material, characterized by low impurity oxide content, provided excellent service in this application. In addition to improved resistance to chemical and physical destructive mechanisms, pit side build-up was dramatically reduced. Since thicker shapes can be made, flue construction is faster, reducing labor costs. This non-traditional approach for flue wall construction has the potential to be a superior and cost effective alternative to current refractory practice. This paper discusses the properties and unique features, benefits and performance characteristics of this product.

Cast Shop Technology: Metal Treatment

Sponsored by: Light Metals Division, LMD-Aluminum Committee
Program Organizers: Corleen Chesonis, Alcoa Inc., Alcoa Technical Center, Alcoa Center, PA 15069 USA; Jean-Pierre Martin, Aluminum Technologies Centre, c/o Industrial Materials Institute, Boucherville, QC J4B 6Y4 Canada; Alton T. Tabereaux, Alcoa Inc., Process Technology, Muscle Shoals, AL 35661 USA

Tuesday PM
March 16, 2004

Room: 213B/C
Location: Charlotte Convention Center

Session Chairs: Pierre Le Brun, Pechiney, Ctr. de Recherches de Voreppe, Voreppe, Cedex 38341 France; Lawrence D. Ray, Alcoa Inc., Global Pkgg. & Consumer Grp., Richmond, VA 23237 USA

2:00 PM

Investigation of Ultrasonic Degassing in Molten Aluminum A356 Alloy: Hanbing Xu¹; Xiaogang Jian¹; Thomas T. Meek¹; Qingyou Han²; ¹University of Tennessee, Dept. of Matls. Sci. & Engrg., 434 Dougherty Hall, Knoxville, TN 37996 USA; ²Oak Ridge National Laboratory, Metals & Ceram. Div., PO Box 2008, MS6083, Oak Ridge, TN 37831-6083 USA

This article addresses ultrasonic degassing in aluminum A356 alloy. An experimental setup has been built for the degassing of aluminum using ultrasonic vibration at a frequency of 20 kHz and vibration intensities up to 1500 W. Ultrasonic degassing has been tested in a small volume of aluminum melt at various processing temperatures and durations. The efficiency of degassing is evaluated by density measurement of the reduced pressure samples. Initial experimental results indicate that a steady-state hydrogen concentration can be obtained within a few minutes of ultrasonic vibration, regardless of the initial hydrogen concentration in the melt. The dynamics of hydrogen evolution as a function of processing time, melt temperature, and initial hydrogen concentration have been investigated. The mechanism of ultrasonic degassing is discussed. It is suggested that ultrasonic vibration can be used to reduce porosity formation in aluminum alloys.

2:25 PM

Evaluation of Relative Efficiency of Various Degassing Lances for Molten Aluminum Treatment Applications: Q. T. Fang¹; Marshall A. Klingensmith¹; Ronald E. Boylstein¹; Larry Podey²; ¹Alcoa Inc., Alcoa Tech. Ctr., 100 Tech. Dr., Alcoa Ctr., PA 15069 USA; ²Alcoa Kentucky Casting Center, 1660 State Rte. 271N, Hawesville, KY 42348 USA

A water model was used to compare the relative efficiency of three selected types of degassing lances for molten aluminum treatment applications using the oxygen decay method. The selected lances were then tested in molten aluminum in a continuous operation with metal flow rates in the range of 400 to 1200 lbs per hour. Satisfactory results were obtained in terms of maintaining metal vacuum density consistently above 2.60 for 8 to 10 weeks. It was found that with the selected lance replacing a previous rotary degassing unit, the dross generated inside the hot zone in the adjacent holding furnace was decreased by an average of 69%, due to significantly less churning of metal. In addition, the argon consumption was reduced by 50~60%. The implementation of the lance degassing unit in place of the previous rotary degassing unit in a production line has resulted in a cost savings of 85% per unit, or \$9,200 per unit per year, due to less capital, less maintenance, reduced argon consumption, and reduced metal loss associated with dross formation.

2:50 PM

Study of Molten Aluminium Cleaning Process Using Physical Modelling and CFD: Jin Long Song¹; Mark R. Jolly¹; Waldemar Bujalski²; Alvin W. Nienow²; Fabio Chiti³; ¹University of Birmingham, IRC in Sch. of Engrg., Birmingham, W. Midlands B15 2TT UK; ²University of Birmingham, Dept. of Chem. Engrg., Birmingham, W. Midlands B15 2TT UK; ³Dipartimento di Ingegneria Chimica, Via Diotisalvi 2, Pisa 56126 Italy

With the increasing demand for high quality aluminium alloys, there is a growing need for improved cleanliness of molten aluminium. Generally alkalis, non-metallic inclusions and dissolved hydrogen have to be reduced to a minimum before casting. Traditionally a chlorine/inert gas mixture was injected into the liquid aluminium. In recent years the fluxing process has been modified through the introduction of impellers and injection of particulate salts. In this paper, through laboratory physical modelling and CFD simulation, both lance bubbling and mechanical agitation processes have been investigated to study the underlying science. Particle image velocimetry (PIV) was used to obtain instantaneous liquid velocities. Mixing times have been calculated using CFD models and compared with decolourization experiments. It was found that, at the same mean specific energy dissipation rate, mechanical agitation with an impeller will lead to much more efficient and controlled fluxing than the lance bubbling process.

3:15 PM

The Pick-Up of Micro Bubbles During LiMCA II Measurements Post an Inline Gas Fluxing Unit: Arild Hakonsen¹; Geir Maland¹; Terje Haugen¹; Erling Myrbostad¹; Ann Oygard²; ¹Hydro Aluminium, Hycast a.s., PO Box 225, Sunndalsøra 6601 Norway; ²Hydro Aluminium, R&D Matl. Tech., PO Box 219, Sunndalsøra 6601 Norway

The most common and reliable method of documenting the removal efficiency of a particle filter is to use the LiMCA apparatus. This method measures the electrical resistance through a 300im opening of an insulating aluminosilicate probe as melt is sucked into the probe. As particles are passing the orifice the resistance is continuously changing. The resistance versus time information is used to calculate the number and size of particle. All gas fluxing units produces various amounts of micro bubbles which stays in the melt for a long time. These small bubbles are to some extent measured as particles in the LiMCA measurements. This work has focused on determine the pick-up of micro bubbles in the LiMCA apparatus after the I-60 SIR melt refining unit. After this unit an probe with an extension tube were

used to minimize the micro bubble pick-up. Only micro bubbles smaller than diameter 40-50 μ m were found to be picked up in the LiMCA measurements. The measurements in the 15-20 μ m range were largely influenced by the micro bubbles. Finally the removal efficiency of the SIR unit was calculated accounting for the micro bubble pick-up. The removal efficiency was estimated to be 50% for particles of diameter 20 μ m, 98% for particles of diameter 40 μ m and close to 100% for particles with diameter larger than 50 μ m.

3:40 PM Break

4:15 PM

Laboratory and Full Scale Measurements of Bubble Behavior in Gas Fluxing Units: Autumn Fjeld¹; James W. Evans¹; D. Corleen Chesonis²; ¹University of California, Matls. Sci. & Engrg., Berkeley, CA 94720 USA; ²Alcoa Inc., Alcoa Tech. Ctr., 100 Tech. Dr., Alcoa Ctr., PA 15069 USA

The performance of gas-fluxing units, as reflected in removal of impurities and throughput of metal, is dependent on the behavior of the bubbles formed as gas is injected into the aluminum. For example, unless the bubbles are dispersed throughout the volume of the metal, a fraction of the capacity of the unit may be wasted. The surface area of the bubbles, and therefore the bubble size, can influence the rate at which impurities are removed. Circulation of the metal, which in some units is promoted by the rising gas bubbles, plays a role in homogenizing the melt. A potential problem arising from bubble behavior is the disturbance of the metal surface as the bubbles burst, causing splashing and ejection of droplets at high gas flow rates. This paper describes measurements at Berkeley and Alcoa Technical Center on bubbles and bubble phenomena in molten aluminum. A "capacitance probe" has been used to measure the frequency of occurrence of bubbles in both laboratory and full-scale melts to determine the distribution of bubbles and what factors affect that distribution. Results of the calculation of bubble-driven flow using the computational fluid-dynamics software FLUENT® are given. In another aspect of the investigation, a high-speed digital camera has been used to study the bubble breaking phenomena at the surface of a low melting point alloy to discover how splashing and droplet formation might be controlled.

4:40 PM

Ceramic Rotary Degassers - Designing for Optimum Material Performance: David P. Bacchi¹; Ted L. Collins¹; Michael J. Hanagan¹; ¹Blasch Precision Ceramics, 580 Broadway, Albany, NY 12204 USA

The use of ceramic as a replacement for traditional graphite material used for rotary degassers has the potential for overall economic savings. In order to maximize the performance of the ceramic material some rotor design modifications are generally needed. A traditional graphite rotor design and several rotors re-designed to optimize the material properties of the ceramic were compared. Thermomechanical evaluations of the various rotor designs were conducted using finite element analysis. The degassing efficiency for each design was measured using a flowing water test trough to simulate an inline degassing system.

5:05 PM

A 2D Lattice-Boltzmann Model of Aluminium Depth Filtration: Carlos Rivière²; Hervé Duval¹; Jean-Bernard Guillot¹; ¹Ecole Centrale Paris, L.E.M., Grande Voie des Vignes, Châtenay-Malabry F-92295 France; ²Pechiney, Ctr. de Recherches de Voreppe, 725, rue Aristide Bergès, BP 27, Voreppe F-38341 France

A two-dimensional mathematical model of the initial stage of depth filtration has been developed. This model describes the fluid flow and the inclusion transport and capture in a two-dimensional representative section of the filter. A typical simulation can be sketched as follows: in a first step, the flow field is computed in the whole complex void space of the two-dimensional filter using the lattice-Boltzmann method. Indeed, this method is particularly suitable to investigate fluid flow at low values of the Reynolds number and in complex geometry. In a second step, the trajectory analysis is derived by applying Newton's second law to suspended inclusions in the flowing fluid. This approach is applied to the liquid aluminium filtration within a ceramic foam

filter. The effects of the interception number, the gravitational number and the adhesive-surface forces on the filter coefficient are studied.

CFD Modeling and Simulation of Engineering Processes: Advanced Casting and Solidification Processes II

Sponsored by: Materials Processing & Manufacturing Division, ASM/MSCTS-Materials & Processing, MPMD/EPD-Process Modeling Analysis & Control Committee, MPMD-Solidification Committee, MPMD-Computational Materials Science & Engineering-(Jt. ASM-MSCTS)

Program Organizers: Laurentiu Nastac, Concurrent Technologies Corporation, Pittsburgh, PA 15219-1819 USA; Shekhar Bhansali, University of South Florida, Electrical Engineering, Tampa, FL 33620 USA; Adrian Vasile Catalina, BAE Systems, SD46 NASA-MSFC, Huntsville, AL 35812 USA

Tuesday PM
March 16, 2004

Room: 206A
Location: Charlotte Convention Center

Session Chairs: Adrian V. Catalina, BAE Systems, Huntsville, AL 35812 USA; Dilip K. Banerjee, National Institute of Standards and Technology, Advd. Tech. Prog., Gaithersburg, MD 20899-4730 USA; Robert F. Dax, Concurrent Technologies Corporation, Pittsburgh, PA 15219 USA

2:00 PM Opening Remarks - Adrian Catalina

2:05 PM

Numerical Simulation of Solidification and Microstructure Evolution of Single Crystal Investment Castings: Zuoqian Liang¹; Qingyan Xu¹; Jiarong Li²; Hailong Yuan²; Shizhong Liu²; Baicheng Liu¹; ¹Tsinghua University, Dept. of Mech. Engrg., Qinghua Garden, Beijing 100084 China; ²Beijing Institute of Aeronautical Materials, Lab. of Advd. High Temp. Structural Matls., Beijing 100095 China

The solidification process of single crystal investment castings causes a number of problems that have to be solved such as casting defects and complexity of production process. In the paper, a mathematical model for the three dimensional simulation of solidification of single crystal growth of investment castings was developed based on the crystal growth mechanism and the basic transfer equations such as heat, mass and momentum transfer equations. Many factors including constitutional undercooling, curvature undercooling and anisotropy, which had vital influences on the microstructure evolution, were considered in the model. Temperature, velocity and solute distributions, dendritic morphologies, crystal orientations and stray crystal of single crystal superalloy investment castings were investigated at different withdrawal rates. The study indicates three dimensional solidification simulation is a powerful tool for understanding the formation of grain defects in the single crystal investment castings.

2:40 PM Cancelled

3D Modeling of Porosity Formation in Aluminum Alloys: A Comparison Between Two Numerical Models and With Experimental Results for an A356 Alloy Plate Casting

3:10 PM

Solidification of Aluminum Alloys on Uneven Surfaces: Deep Samanta¹; Nicholas Zabaras¹; ¹Cornell University, Sibley Sch. of Mech. & Aeros. Engrg., Matls. Process Design & Control Lab., 188 Frank H. T. Rhodes Hall, Ithaca, NY 14853-3801 USA

Solidification of aluminum on uneven surfaces modeled in the form of sinusoidal curves is simulated. Wavelength and amplitude effects of these sinusoidal surfaces on heat transfer, fluid flow and solid-liquid front morphology in the early stages of solidification will be reported. Interfacial heat transfer between the solid shell and mold will be modeled in terms of empirical correlations to highlight the variable nature of heat flux on the boundary. The same analysis will be extended to aluminum alloys. A recently developed stabilized finite element formulation for simulating flow in binary alloy solidification and porous media will be used to simulate the macrosegregation and growth of the solid shell. Sensitivity analysis to demonstrate the importance of wavelengths on the heat transfer, fluid flow and front morphology will be discussed. The analysis will then be expanded to include meniscus formation and their role in surface segregation.

3:40 PM Break

TUESDAY PM

4:00 PM Cancelled**Simulation and Real-Time X-Ray Observation of Foam Pattern Permeability Effects on the Lost Foam Casting Process****4:30 PM**

Validation and Improvement of Computer Modeling of Lost Foam Casting Process Via Real Time X-Ray Technology: *Wanliang Sun*¹; Preston Scarber¹; Harry E. Littleton¹; ¹University of Alabama, Matls. Sci. & Engrg., 917 Bldg., 1530 3rd. Ave. S., Birmingham, AL 35294 USA

Lost Foam Casting (LFC) process is relatively immature when comparing other casting processes. To make the process more robust, computer modeling is needed in lead time and casting defects deduction. In this study, metal filling of lost foam aluminum castings was visualized using the state-of-art real time X-Ray technology. Meanwhile, the metal filling of the lost foam casting was simulated using a commercial software package. The result of the computer simulation was validated with the results of the real time X-Ray visualization. Some of the computer simulation agreed well with the results from the real time X-Ray visualization, but some did not. Based on other studies using real time X-Ray technology, new input variables, such as foam density field and gas permeability field were developed for the computer modeling. With the new variables, the modeling of the lost foam casting process becomes more realistic.

5:00 PM

Mathematical Modeling of a Liquid Metal Feeding System for Single Belt Casters: *Roberto Parreiras Tavares*¹; Frederico da Costa Fernandes¹; Guilherme Antonio Defendi¹; Júlio César Sousa Pena¹; Vangleik Ferreira da Cruz¹; ¹Federal University of Minas Gerais, Metallurg. & Matls. Engrg., Rua Espírito Santo, 35-Sala 229, Metalurgia - Centro, Belo Horizonte, Minas Gerais 30160-030 Brazil

Near-net-shape casting is an important area of research in the iron and steel industry today. Among the "Near-Net-Shape" casting processes, the single-belt caster seems to be the most promising, since it is the only one that can achieve levels of productivity similar to those obtained with conventional continuous casting machines. One of the most important aspects in the single-belt casting is the feeding system used to deliver liquid metal over the belt. This system determines the velocity distribution and the levels of turbulence of the liquid metal and affects the quality of the strips. In the present work, a metal delivery system having a simple geometry was proposed. Using the CFD codes CFX4.4 and CFX 5.5, a mathematical model to simulate three-dimensional turbulent fluid flow and heat transfer in that system has been developed. This model was used to analyze different configurations of the metal delivery system and the free surface shape of the fluid was also determined. A physical model of the feeding system was built and used to validate the predictions of the mathematical model. The fluid flow calculations have been validated by dye injection experiments and laser doppler anemometry. Measurements of the free surface levels have also been performed. These experiments provided supporting evidence for the predictions of the mathematical model.

Challenges in Advanced Thin Films: Microstructures, Interfaces, and Reactions: Design, Process, and Property Control of Functional and Structural Thin-Films

Sponsored by: Electronic, Magnetic & Photonic Materials Division, EMPMD-Thin Films & Interfaces Committee

Program Organizers: N. M. (Ravi) Ravindra, New Jersey Institute of Technology, Department of Physics, Newark, NJ 07102 USA; Seung H. Kang, Agere Systems, Device and Module R&D, Allentown, PA 18109 USA; Choong-Un Kim, University of Texas, Materials Science and Engineering, Arlington, TX 76019 USA; Jud Ready, Georgia Tech Research Institute - EOEM, Atlanta, GA 30332-0826 USA; Anis Zribi, General Electric Global Research Center, Niskayuna, NY 12309 USA

Tuesday PM
March 16, 2004

Room: 218B
Location: Charlotte Convention Center

Session Chairs: Choong-Un Kim, University of Texas, Matls. Sci. & Engrg., Arlington, TX 76019 USA; Jud Ready, Georgia Tech Research Institute, Atlanta, GA 30332-0826 USA; David P. Field, Washington State University, Sch. of Mech. & Matls. Engrg., Pullman, WA 99164-2920 USA

2:00 PM Invited

Dielectric Films for Silicon Solar Cell Applications: *Bhushan Sopori*¹; ¹National Renewable Energy Laboratory, 1617 Cole Blvd., Golden, CO 80401 USA

Silicon solar cells use thin films of a variety of dielectrics, primarily for the purposes of enhancing antireflection (AR) or reflection characteristics of various interfaces and for surface passivation. Typically, different materials are required to meet different demands of optical and electronic properties. For example, although SiO₂ layers can give excellent surface passivation, they are not well suited for AR purposes because of a low refractive index. Typical AR coating materials for solar cells consist of TiO₂ and SiN, which have a refractive index of > 2. However, to minimize the cost of solar cell fabrication, it is desirable to use only one coating that can accomplish both electronic and optical demands. Recently, it was determined that hydrogenated SiN (SiN:H) can satisfy these needs, and now this material has become a very popular dielectric. The advantages of SiN:H are that: (i) it has a dielectric constant that matches well for AR effects, and (ii) it has capability to accumulate a positive charge at the interface to give a high degree of surface passivation. Recently, additional advantages of SiN:H have been discovered. It has been determined that a silk-screened metal pattern on a thin layer of SiN:H can be directly fired through it to yield excellent ohmic contacts to solar cells. Use of a nitride, deposited by plasma-enhanced chemical vapor deposition, offers yet other advantage by creating a source of H, which can diffuse into Si to passivate impurities and defects. This mechanism can improve the performance of a low-cost solar cell by about 4 absolute percentage points to about 16%. However, as the number of functions that a dielectric has to perform increases, the complexity of understanding and controlling various functions become more crucial. This paper will review various properties of dielectric films needed for solar cell applications, discuss processing requirements, and discuss methods of optimizing cell performance.

2:25 PM Invited

Progress in Crystalline Multijunction and Thin-Film Photovoltaics: *Donna Cowell Senft*¹; ¹Air Force Research Laboratory, Space Vehicles Direct, USA

Photovoltaics are important for power generation in terrestrial applications such as remote power and renewable energy but are the primary source of electrical power for space systems. Development of solar cells for space, where priorities are high conversion efficiency and resistance to degradation from ionizing radiation, is driving research into crystalline III-V multijunction solar cells and lower efficiency but flexible, lightweight polycrystalline or amorphous thin-film solar cells. Crystalline triple junction III-V solar cells have reached conversion efficiencies of 30% at Air Mass Zero (AM0), but identifying and growing additional junction materials with the appropriate bandgap and lattice constant are creating challenges to higher efficiency cells. New lattice mismatch techniques and new classes of nitride materials hold promise for increasing the efficiency of these cells. Thin-film solar cells, on the other hand, generally have efficiencies of <15%, but provide the benefits of greater radiation resistance,

lower cost, flexibility, and lower mass. Development work in thin-film solar cells centers on increasing efficiency in polycrystalline materials such as Cu(In,Ga)Se₂ or CdTe and amorphous silicon.

2:50 PM

A Novel Process for the Synthesis of Multinary Thin Films: *Billy J. Stanbery*¹; ¹HelioVolt Corporation, Ste. 100F, 1101 S. Capital of Texas Hwy., Austin, TX 78746 USA

A novel method is described for the rapid reactive formation of (I-III)-VI thin films suitable for applications as photovoltaic absorbers. This technique circumvents the limitations of prior approaches by a combination of (1) reduced thermal budget and volatile reactant loss, (2) facilitating optimal precursor deposition while avoiding deleterious pre-reactions, (3) direct control of pressure during synthesis, and (4) application of an electrostatic field during synthesis to athermally modify ionic transport. This is a two-stage process, wherein reaction precursors are first separately deposited onto two surfaces, one the film substrate, and the other a reusable tool that has been coated with a dielectric release layer. In the second stage, the tool and substrate are brought together and pressure applied, in this case by electrostatic compression resulting from an electrical bias between the two, and heated in a rapid thermal processor. Application of the method to CIGS photovoltaic devices will be described.

3:05 PM Invited

Ion Beam Mixing of Silicon-Germanium for Solar Cell Applications: *Sufian Abedrabbo*¹; *D. Arafah*¹; *Anthony Fiory*²; *Bhushan Sopori*³; *N. M. Ravindra*²; ¹University of Jordan, Dept. of Physics, Amman 11942 Jordan; ²New Jersey Institute of Technology, Dept. of Physics, Newark, NJ 07102 USA; ³National Renewable Energy Laboratory, Golden, CO 80401 USA

A brief overview of silicon-germanium alloys for solar cell and light emitting diode applications is presented here. The overview considers factors such as methods of formation, and device performance. In particular, results of preliminary experiments of ion-beam mixing of silicon germanium multi-layers deposited by physical vapor deposition and subsequently ion-implanted with varying doses of argon are described.

3:30 PM

Magnetic and Transport Properties of Magnetic Semiconductors CdCr₂Se₄ Thin Films Diluted by In: *L. J. Maksymowicz*¹; *M. Lubecka*¹; *B. T. Ciecwa*¹; *Z. St. Sobkow*¹; *R. Szymczak*²; *M. Sikora*³; *Cz. Kapusta*³; ¹AGH University of Science and Technology, Dept. of Elect., Al. Mickiewicza 30, Krakow 30-059 Poland; ²Polish Academy of Sciences, Inst. of Physics, Al. Lotnikow 32/46, Warszawa 02-668 Poland; ³AGH University of Science and Technology, Dept. of Solid State Physics, Fac. of Physics & Nucl. Techniques, Al. Mickiewicza 30, Krakow 30-059 Poland

The spinel structure for compound A[B₂]X₄ was realized by thin films of magnetic semiconductor (Cd_{1-y}In_y)[Cr_{2-2x}In_{2x}]Se₄. The increase in the lattice parameter with increasing dilution level was detected. The field-cooled and zero field-cooled DC magnetization measurements, carried out with a SQUID magnetometer, show that magnetic ordering changes with increasing In concentration. For CdCr₂Se₄ the magnetic state with reentrant transition is obtained, while we have the SG state when x=0 and y>0 or y=0 and x>0. The randomly canted state was found for x>0 and y>0. Changes of the local atomic environments around Cr and Se ions were observed by EXAFS with the increase of dilution level. Spectral voltage responsivity of the films was found using a lock-in technique. It was found that the voltage sensitivity of the investigated films is altered with the amount of indium and temperature. The maximum of voltage sensitivity is shifted toward the infrared region with reduced dilution level. The largest voltage sensitivity was obtained for the lightly diluted samples, below Curie temp.

3:45 PM Break

4:00 PM

Dynamic Nonlinear Response of Semiconducting Oxides to the Ambient Atmosphere: *T. Pisarkiewicz*¹; *W. Maziarz*¹; ¹AGH University of Science and Technology, Dept. of Elect., Al. Mickiewicza 30, Krakow 30-059 Poland

LTCC and micromachined structures were developed as substrates for deposited metal oxide SnO₂, In₂O₃ or ZnO semiconductors interacting with ambient reducing or oxidizing atmospheres. The dynamic response of a single sensor with modulated temperature, where pulse or sinusoidal voltage is applied to the sensor heater, was analysed. The time dependent interaction of semiconductor surface with the ambient gas is related to both the kinetics of gas molecules at the surface (adsorption, desorption, diffusion and oxidation) and the chemical

structure and concentration of the gas species. The authors performed a series of experiments by varying the temperature and modulation frequency range for selected sensitive oxides and gas species. The oxidation process caused by ionosorbed oxygen was particularly investigated during interaction of semiconductor surface with ambient air of varying humidity.

4:15 PM

Novel PLD- VO₂ Thin Film for Ultrafast Applications: *Huimin Liu*¹; *Omar Vasquez*²; *Victor R. Santiago*¹; *Luz Diaz*¹; *Felix E. Fernandez*¹; ¹UPRM, Physics, PO BOX 5023, Mayaguez, PR 00681-5023 USA

VO₂ thin films deposited on fused quartz substrate were successfully fabricated by pulsed laser deposition (PLD) technique using excimer laser and metallic vanadium target for ablation. Microscopic examination and X-ray diffraction scans of all samples show a very broad diffraction peak under 2θ = 25°, corresponding to amorphous material. The film shows fast, passive thermochromic effect of insulator-to-metal or semiconductor-to-metal phase transition (PT) with a characteristic hysteresis at the temperature near 68°C. Thermochromic effect was measured as resistivity or optical transmission and reflectance versus temperature. Ultrafast PT from monoclinic semiconductor phase to a metallic tetragonal rutile structure could also be induced optically by laser excitation. Nd:YAG pulsed laser operating at 532 nm with pulse duration of 30 psec was used to drive the PT. Degenerate-four-wave-mixing technique was used to detect the ultrafast PT. In this paper we report correlation between the ultrafast PT and the dynamical process of the excited states. It is also the first time, to our knowledge, to report the extremely large polarizability and the potential photonic applications.

4:30 PM

Pulsed Laser Deposited Coatings for Hydrogen and Hydrogen Isotope Permeation Resistance: *Thad Matthew Adams*¹; *James Fitzgerald*²; ¹Savannah River Technology Center, Bldg. 773-41A/151, Aiken, SC 29808 USA; ²University of Virginia, Matls. Sci. & Engrg., 116 Engineer's Way, Charlottesville, VA 22904 USA

To date several coating materials and materials systems have been investigated to reduce the permeation of hydrogen and hydrogen isotopes through common structural materials such as stainless steels. These materials include oxide ceramics, thermally grown oxides, metals, intermetallics, and amorphous systems. Permeation response for these coatings system has also been shown to be highly dependent on application techniques-thermal spray, CVD, EBPVD. The current research is focused on three coatings systems applied using pulsed laser deposition on 304L stainless steel substrates. The stainless steel substrates have been coated with aluminum oxide, chromium oxide, titanium carbide and an Al-Ni-Gd amorphous alloy using PLD. Characterization of the coating-substrate system adhesion has been performed using scratch adhesion testing and microindentation. Coating stability and environmental susceptibility has also been evaluated for two conditions-air at 350°C and Ar-H₂ at 350°C for up to 100 hours. Lastly, thermal cycling and hydrogen charging-5,000-10,000psi—testing has been performed to evaluate overall coating performance.

4:45 PM

Microstructural Characterizations of (11-20)a-Plane ZnO Thin Films Grown on (1-102)r-Plane Sapphire: *Jin-Serk Hong*¹; *Won-Yong Kim*²; *Sung-Hwan Lim*¹; ¹Kangwon National University, Dept. of Advd. Matls. Sci. & Engrg., Chuncheon 200-701 Korea; ²Korea Institute of Industrial Technology, Advd. Matls. R&D Div., Incheon 404-254 Korea

There has been considerable interest in the development of ZnO films for optoelectronic devices.¹ Nakamura et al. succeeded in the growth of ZnO films on (1-102) r-plane sapphire via ECR-assisted MBE. However, a critical problem is a high concentration of various defects in the growth of ZnO films. These defects can act as traps and recombination centers. Thus, understanding of the characteristics of structural defects was a major emphasis of the present ZnO research. In this presentation we describe the structural characteristics of non-polar (11-20) a-plane ZnO films grown on r-plane sapphire. The structural analyses were carried out using electron diffraction, weak beam microscopy, and HREM. The in-plane orientation of the ZnO with respect to the sapphire was confirmed to be [0001]ZnO||[0-111]sapphire and (11-20)ZnO||[01-12]sapphire. Threading dislocations and stacking faults, observed in plan-view and cross-sectional TEM images, dominated the a-ZnO microstructure with densities of about 10¹¹ cm⁻² and 10⁶ cm⁻¹, respectively. ¹S.-H. Lim and D. Shindo, Phys. Rev. Lett. 86. 3795 (2001).

5:00 PM Invited

SAM-Ceramic Protective Bilayers for MEMS Device Packaging: *Tolulope O. Salami*¹; *Sergei Zarembo*¹; *Quan Yang*²; *Kaustubh*

Chitre²; Junghyun Cho²; *Scott R.J. Oliver*¹; ¹SUNY, Dept. of Chmst., Vestal Pkwy. E., Binghamton, NY 13902 USA; ²SUNY, Dept. of Mech. Engrg., Vestal Pkwy. E., Binghamton, NY 13902 USA

Structures and devices in microelectromechanical systems (MEMS) require hermetic packaging for protection, reliability and proper function. The recent reduction in the size of MEMS structures creates several problems, such as an increase in resistive forces, leading to increased friction/stiction and wear. We are developing a protective bilayer thin film coating to solve these problems. The bilayer is an inorganic-organic hybrid material, consisting of a hard inorganic ceramic coating (ZrO₂, YSZ) and a compliant underlying organic buffer layer. Nanoscale ultrathin organic coatings, fabricated by self-assembly, are used as a 'template' for the subsequent growth of the hard ceramic coating. We chemically tune the organic terminal groups, as well as vary ceramic synthetic conditions, in order to promote growth of the top inorganic layer. Molecular level understanding of the microstructure and micromechanics involved in the synthetic process are studied by a variety of characterization techniques, such as electron microscopy, XRD, AFM and nanoindentation. Our presentation will overview some of our results.

5:15 PM

Study on Deposition Procession, Structure and Properties of Super Hard Protective TiB₂ Coatings by Cathode Arc Ion Reactive Method: *Jiansheng Zhao*¹; *Kwang-Leng Choy*²; ¹Huazhong University of Science and Technology, Dept. of Matls., Wuhan, Hubei 430074 China; ²Nottingham University, Dept. of Matls., Nottingham UK

Using pure metal titanium as a target, diborane as the reactive gas, the super hard protective TiB₂ coatings were deposited by cathode arc ion reactive plating method. The structures and properties of the deposited coatings were analyzed by means of XPS, XRD and scratch test. The results show that the coatings have very high hardness of above HV30Gpa. The structures of the coatings related to the deposition procession. While the flow rate of diborane changed from 20 sccm to 160 sccm, the structures of the coatings changed from Ti + TiB₂ ? TiB + TiB₂ ? TiB₂. The pure TiB₂ coatings could be obtained in the flow rate of diborane 160sccm. The adhesion stresses between the coatings and the substrates decreased from 913MPa to 770.7MPa along with the increasing of flow rate of diborane. The possible reason of this decreasing was related to the residual stresses existing in the coatings.

Computational Thermodynamics and Phase Transformations: Phase Field Modeling II

Sponsored by: ASM International: Materials Science Critical Technology Sector, Electronic, Magnetic & Photonic Materials Division, Materials Processing & Manufacturing Division, Structural Materials Division, MPMD-Computational Materials Science & Engineering-(Jt. ASM-MSCTS), EMPMD/SMD-Chemistry & Physics of Materials Committee

Program Organizer: Jeffrey J. Hoyt, Sandia National Laboratories, Materials & Process Modeling, Albuquerque, NM 87122 USA

Tuesday PM
March 16, 2004

Room: 202A
Location: Charlotte Convention Center

Session Chair: TBA

2:00 PM Invited

Phase Field Simulations of Coarsening in Three-Dimensional Topologically Complex Structures: I. Savin¹; R. Mendoza¹; *P. W. Voorhees*¹; ¹Northwestern University, Matls. Sci. & Engrg., 2225 N. Campus Dr., Cook Hall, Evanston, IL 60208 USA

The coarsening process in systems consisting of spherical particles in a matrix has been studied extensively. In contrast, coarsening in systems that possess both positive and negative curvatures have received less study. We employ three-dimensional phase field calculations to follow the evolution of such a topologically complex dendritic solid-liquid mixture during coarsening. We use the phase field method to determine the instantaneous interfacial velocities for a given experimental microstructure. Using this information we compute the average time rate of change of a given pair of principle interfacial curvatures. We show that this information can be used to predict qualitatively the evolution of the interface shape distribution, the probability of finding a patch of interface with a given pair of principle curvatures, and to understand the mechanisms responsible

for coarsening in these topologically complex systems. A comparison between the predictions of the calculations and experiments will be given.

2:30 PM Invited

Modeling Solidification, Elasticity and Structural Stability Using Phase Field Crystals: *Ken R. Elder*¹; ¹Oakland University, Physics, Rochester, MI 48309-4401 USA

Elastic and plastic deformations often play a significant role in determining the microstructures that emerge during non-equilibrium processing. The microstructures produced in these phenomena are important since they can significantly alter the structural properties of the material. In this talk I would like to discuss a phase field technique that can predict both the creation and structural properties of non-equilibrium microstructures. The technique will be applied to a number of phenomena including, liquid phase epitaxial growth, spinodal decomposition, eutectic solidification and dendritic growth.

3:00 PM

Phase-Field Modeling of Solidification Under Stress: *Julia Slutsker*¹; Geoffrey B. McFadden²; Alexander L. Roytburd³; William J. Boettinger¹; James A. Warren¹; ¹NIST, MSEL, 100 Bureau Dr., Gaithersburg, MD 20899 USA; ²NIST, Math & Computer Sci., 100 Bureau Dr., Gaithersburg, MD 20899 USA; ³University of Maryland, Matls. Sci. & Engrg., College Park, MD 20742 USA

The phase field model of the non-isothermal solidification taking into account the stress field is developed. This model has been applied to the kinetics of melting and solidification in confined sphere. The complete numerical solutions taking into account the time-space evolution of temperature, order parameter and stress field has been obtained. It has been shown that at some boundary and initial conditions the evolution results in steady states corresponding time-independent distribution of order parameter and uniform temperature. The value of interface energy has been estimated by comparing the phase fraction in the steady states with the equilibrium following from the sharp-interface model. It has been shown that at small radii of sphere the equilibrium two-phase states significantly shifted and their unstability appears due to effect of interface energy. This effect is particularly significant if the radius of sphere on the nano-scale level is considered.

3:20 PM Cancelled

A Phase-Field Approach to the Nanocrystallization of Metallic Glasses

3:40 PM Break

3:50 PM Invited

Modeling Thermodynamics and Microstructure Evolution of Ni-Base Superalloys: J. Zhu¹; S. Zhou¹; Yi Wang¹; T. Wang¹; Z. K. Liu¹; C. Woodward²; R. A. MacKay³; A. J. Ardell⁴; *Long-Qing Chen*¹; ¹Pennsylvania State University, Matls. Sci. & Engrg., Univ. Park, PA 16802 USA; ²UES Inc., Dayton, OH USA; ³NASA Glenn Research Center; ⁴University of California, Matls. Sci. & Engrg., Los Angeles, CA USA

Ni-based superalloys consist of ordered intermetallic gamma-prime precipitates embedded in a disordered face-centered cubic (fcc) gamma matrix. The control of the gamma+gamma-prime two-phase microstructure and its high-temperature stability is the key to the success for the design of superalloys with desired high temperature properties. This presentation will discuss our recent work to integrate various computational tools ranging from first-principles calculations, thermodynamic and materials property database development, to microstructure prediction using the phase-field approach. The initial effort is on the Ni-Al-Mo-Ta quaternary system and its binary and ternary subsystems. It will be demonstrated that it is possible to predict quantitatively, both in time and spatial scales, the microstructure evolution in Ni-base superalloys through first-principles assisted database development and phase-field simulations. The focus will be on the validation of the computational results by comparing with analytical theories for simple model systems and with existing experimental measurements in Ni-base alloys. The work is supported by NASA.

4:20 PM Invited

Quantitative Phase Field Modeling of Interdiffusion Microstructures in Multi-Phase and Multi-Component Alloys: Kaisheng Wu¹; John E. Morral¹; *Yunzhi Wang*¹; ¹Ohio State University, Matls. Sci. & Engrg., 2041 College Rd., Columbus, OH 43210 USA

Most earlier simulation work on diffusion couples containing dispersed phases was limited to one-dimensional (1D) models. The models assumed that all diffusion occurs in the matrix phase and that precipitates are point sources or sinks of solute. Microstructural evolution in the interdiffusion zone and its effect on diffusion kinetics were ignored. There has been an increasing interest recently in apply-

ing the phase field method to study explicitly microstructural evolution in the interdiffusion zone and its effect on diffusion path. So far the work has been limited to prototype model systems without material-specific inputs. In this presentation we will discuss quantitative phase field modeling of interdiffusion microstructures by linking directly the free energies and mobility data to available databases developed by the CALPHAD method. Its applications are demonstrated for microstructural evolution in single-phase/two-phase and two-phase/two-phase diffusion couples of Ni-Al-Cr alloys. The simulated microstructural features and kinetics of boundary migration agree well with experimental observations at the same length and time scales. The diffusion paths calculated from the phase field simulations are compared with analytical predictions and 1D diffusion calculations. The work is supported by the National Science Foundation.

4:50 PM

Phase Decomposition in Polymeric Membrane Formation by Immersion Precipitation: *Bo Zhou*¹; Adam C. Powell¹; ¹Massachusetts Institute of Technology, Dept. of Matls. Sci. & Engrg., 77 Mass. Ave., 4-117, Cambridge, MA 02139 USA; ¹Massachusetts Institute of Technology, Dept. of Matls. Sci. & Engrg., 77 Mass. Ave., 4-043, Cambridge, MA 02139 USA

Abstract Most commercial microporous membranes, which enjoy widespread use in filtration and purification, are made by the immersion precipitation process. This process begins with liquid-liquid demixing of a non-solvent/solvent/polymer ternary system into polymer-rich and polymer-lean phases; this demixing step determines much of the final morphology. In this work, a ternary Cahn-Hilliard formulation incorporating a Flory-Huggins homogeneous free energy function and coupled with variable-viscosity interface-driven fluid flow is used to simulate phase separation during liquid-liquid demixing. Simulations begin with uniform initial condition with a small random fluctuation to simulate spinodal decomposition, and also with a two-layer polymer-solvent/nonsolvent initial condition to simulate actual membrane fabrication conditions. 2-D and 3-D simulation results are presented which demonstrate the effects of K_{ij} (gradient penalty coefficients) and composition change in the coagulation bath and polymer solution on phase separation behavior.

5:10 PM

On Some Computational Issues of Allen-Cahn Equation in the Phase Field Modeling: *Qiang Du*¹; *Wenxiang Zhu*¹; ¹Pennsylvania State University, Math., 307 McAllister Bldg., Univ. Park, PA 16802 USA

In this paper, first we study the exponential time differencing (ETD) schemes and demonstrate the effectiveness of the ETD type schemes through the numerical solution of Allen-Cahn equation in phase field modeling and through the comparisons with other existing methods. Secondly, we demonstrate benchmarking test results on the comparisons of the numerical solutions of the Allen-Cahn equation by finite difference method and spectral method as the interfacial width ϵ goes to 0.

Cost-Affordable Titanium Symposium Dedicated to Prof. Harvey Flower: Creative Processing

Sponsored by: Structural Materials Division, SMD-Titanium Committee

Program Organizers: M. Ashraf Imam, Naval Research Laboratory, Washington, DC 20375-5000 USA; Derek J. Fray, University of Cambridge, Department of Materials Science and Metallurgy, Cambridge CB2 3Q2 UK; F. H. (Sam) Froes, University of Idaho, Institute of Materials and Advanced Processes, Moscow, ID 83844-3026 USA

Tuesday PM Room: 206B
March 16, 2004 Location: Charlotte Convention Center

Session Chair: David Rugg, Rolls Royce, Derby DE248BJ UK

2:00 PM

Electrochemical Deoxidation Mechanisms of Titanium Oxides in Molten Calcium Chloride: *Kevin Frederick Dring*¹; Martin Jackson¹; Richard J. Dashwood¹; Harvey M. Flower¹; Douglas Inman¹; ¹Imperial College London, Matls., Royal Sch. of Mines, Prince Consort Rd., London SW7 2AZ England

Titanium oxides were successfully deoxygenated to below 1500ppm oxygen levels by electrochemical reduction in molten calcium chloride via the Fray-Farthing-Chen (FFC) process. Electrolysis was performed

below the standard decomposition potential of CaCl_2 at 950°C and using an yttria stabilised zirconia counter electrode. Oxide preforms of near-bulk density were prepared by sintering precursor powders, under vacuum as necessary. Material was characterised pre- and post-reduction by scanning electron microscopy, x-ray energy dispersive spectrometry, and secondary ion mass spectrometry. Cyclic voltammetry and chronopotentiometry studies were conducted at various stages of reduction to ascertain the characteristics of the oxygen ionisation reaction at the cathode-electrolyte interface.

2:30 PM

Properties of Cost-Affordable High-Performance Titanium Alloy Series "Super-TiX™": *Akira Kawakami*¹; Hideki Fujii²; Kazuhiro Takahashi³; Yoshito Yamashita¹; Takeshi Hirata¹; Takashi Oda¹; ¹Nippon Steel Corporation, Titanium Div., Otemachi 2-6-3, Chiyoda, Tokyo 100-8071 Japan; ²Nippon Steel Corporation, Steel R&D Labs., Shintomi 20-1, Futtsu, Chiba Japan; ³Nippon Steel Corporation, Hikari R&D Lab., Shimada 3434, Hikari, Yamaguchi Japan

Super-TiX™ series were originally developed in order to enlarge titanium use in new application fields, such as automobiles, sports and utility goods, etc by featuring their cost-affordability and high-performance. Although they contain only inexpensive alloying elements, Fe, O, N and Al, they possess unique properties such as a wide range of tensile strength from 700 to 1100MPa, good ductility, excellent hot & cold workability and high-fatigue properties, depending on compositions. Ti-5%Al-1%Fe (Super-TiX51AF) and Ti-1%Fe-0.35%O-0.01%N (Super-TiX800) are defined as the core alloys. The former shows mechanical properties similar to that of Ti-6Al-4V with hot workability higher than that of Ti-6Al-4V. The latter has tensile strength between that of Ti-3Al-2.5V and Ti-6Al-4V with hot workability as high as that of CP. Alloy design concept and performances of the alloys are introduced. Moreover, some attentions to be paid when the alloys are actually used are also discussed.

3:00 PM

Affordable Ti-6Al-4V Castings: *Kevin L. Klug*¹; Mehmet N. Gungor¹; Ibrahim Ucok¹; Christopher Hatch²; Robert Spencer³; Ronald Lomas⁴; ¹Concurrent Technologies Corporation, MTF, 100 CTC Dr., Johnston, PA 15904 USA; ²United States Marine Corps, PEO-Ground Combat & Support Systems, SFAE-GCSS-JLW, Bldg. 151, Picatinny Arsenal, NJ 07806 USA; ³PCC Structural, Inc., 4600 S.E. Harney Dr., Portland, OR 97206 USA; ⁴BAE Systems - RO Defence, HIP - Bldg. B40, Barrow-in-Furness, Cumbria LA14 1AF UK

To extend the application of structural titanium alloy components beyond aerospace systems, the affordability of such parts must be addressed through reduced raw material, manufacturing and inspection costs. One example of a titanium-intensive land-based system is the XM777 Lightweight Howitzer (LWH), which is being developed to meet the U.S. Marines' and U.S. Army's increased operational thresholds for mobility, survivability and deployability. In an on-going Navy MANTECH program, investment casting was selected over machining and welding titanium plate to reduce part count and associated manufacturing expense for several LWH components. A study was also undertaken to reduce raw material costs through the utilization of scrap titanium that conforms to chemical constraints that are broader than aerospace standards. The microstructures and mechanical properties of experimental investment cast Ti-6Al-4V alloy sample plates were evaluated and compared to investment cast aerospace grade Ti-6Al-4V. Test results for the investigated materials will be presented and compared. This work was conducted by the National Center for Excellence in Metalworking Technology, operated by Concurrent Technologies Corporation under contract No. N00014-00-C-0544 to the U.S. Navy as part of the U.S. Navy Manufacturing Technology Program.

3:30 PM

Development of a New Process for Producing Low Cost TiAl and Ti3Al/TiAl Powders: *Deliang Zhang*¹; Gorgees Adam¹; Jing Liang¹; Guangsi Guo¹; ¹University of Waikato, Dept. of Matl. & Proc. Engrg., Private Bag 3105, Hamilton 2001 New Zealand

With the increasing potential of using gamma titanium aluminides in mass production of automotive parts and aerospace components and structures, TiAl based powders will likely become a valuable commodity. The cost of the TiAl based powders produced by the traditional method of alloying Ti and Al and then atomising the melt still proves to be too expensive to be used in large scale. Being able to produce high quality TiAl based powders at a significantly lower cost is essential for the use of TiAl based materials for mass production of components and sheets. At Waikato University, we have developed a new process which can be used to produce TiAl based powders with a strong potential of lowering the cost of this type of powders. The

process uses TiO_2 and other oxides and Al metal powders as raw materials, and it combines solid state reactions between TiO_2 and Al, sintering, mechanical milling, and other physical and chemical processes. Through reaction between TiO_2 and Al, mechanical milling and a physical process, a $\text{Ti}(\text{Al}_2\text{O}_3)/\text{Al}_2\text{O}_3$ or $\text{Ti}_3\text{Al}/\text{Al}_2\text{O}_3$ based powder with a low volume fraction of Al_2O_3 can be produced and then this powder can be used as a raw material to produce TiAl based powders using a chemical process. This paper will use production of TiAl and $\text{Ti}_3\text{Al}/\text{TiAl}$ alloy powders as an example to introduce the scientific principles underlying the process, and discuss the implications of the research results.

4:00 PM

Cold Formability Response to Solution Treatment Temperature of Low Cost Beta Ti Alloys for Welfare Goods: *Masahiko Ikeda*¹; Shinya Komatsu¹; Mitsuhide Ueda²; Akihiro Suzuki³; ¹Kansai University, Matls. Sci. & Engrg., 3-3-35, Yamate-cho, Suita, Osaka 564-8680 Japan; ²Kansai University, Suita, Osaka 564-8680 Japan; ³Daido Steel Co., LTD

Ti-4.3Fe-7.1Cr and 3.0Al alloys were developed as low cost beta Ti alloys for welfare goods. These alloys have good tensile properties in solution treated state, and compares well to the developed beta Ti alloys. In general beta Ti alloys have better cold formability than those of alpha and alpha+beta Ti alloys. It is important to investigate cold formability of these alloys for welfare goods, e.g. wheel chair. In this study, cold formability of these alloys was evaluated by cold compression test. In solution treated condition below the beta transus temperature, partially re-crystallized structure was observed, whereas only re-crystallized structure was observed in specimens solution-treated at or above the beta transus temperature. In these alloys quenched from a temperature above the beta transus temperature, true strain exceeded value of one. Details of results will be presented.

4:30 PM

The Way to Reduce the Cost of Titanium Alloys: *Y. Q. Zhao*¹; H. Chang¹; Y. L. Li¹; ¹Northwest Institute for Nonferrous Metal Research, PO Box 51, Xi'an, Shaanxi 710016 China

Titanium alloys possess excellent properties and have been widely put into practical applications. However, their high cost limits their extensive applications in civil field. There are several ways to reduce Ti cost. This paper mainly discusses three ways. One is low cost Ti alloys developed with cheap alloying element, such as Fe. Using this way, Ti12LC and Ti8LC low cost alloy were developed by using cheap Fe-Mo master alloy. These two alloys have good mechanical properties. The second way is to use large deformation to process Ti12LC and Ti8LC alloys and P/M method to produce typical parts from Ti12LC alloy. The third way is semi-solid deformation.

Dislocations: Novel Experimental Methods

Sponsored by: ASM International: Materials Science Critical Technology Sector, Electronic, Magnetic & Photonic Materials Division, Materials Processing & Manufacturing Division, Structural Materials Division, EMPMD/SMD-Chemistry & Physics of Materials Committee, MPMD-Computational Materials Science & Engineering-(Jt. ASM-MSCTS)

Program Organizers: Elizabeth A. Holm, Sandia National Laboratories, Albuquerque, NM 87185-1411 USA; Richard A. LeSar, Los Alamos National Laboratory, Theoretical Division, Los Alamos, NM 87545 USA; Yunzhi Wang, The Ohio State University, Department of Materials Science and Engineering, Columbus, OH 43210 USA

Tuesday PM
March 16, 2004

Room: 201A
Location: Charlotte Convention Center

Session Chair: TBA

2:00 PM Invited

Internal Structure of Geometrically Necessary Dislocation Boundaries in fcc Metals: *Rodney J. McCabe*¹; S. G. Srinivasan²; Amit Misra²; Michael I. Baskes²; Terence E. Mitchell²; ¹Los Alamos National Laboratory, MST/MST-6, MS G770, Los Alamos, NM 87545 USA; ²Los Alamos National Laboratory, MST/MST-8, MS G755, Los Alamos, NM 87545 USA

Experiments and modeling were used to study the structure within geometrically necessary dislocation boundaries (GNB) in fcc metals. Using weak beam and stereo transmission electron microscopy, a crystallographic GNB in rolled copper was found to be composed primarily

of dislocations from the three highest stressed slip systems. The boundary also contained a large number of dislocation nodes and Lomer locks. The general boundary minimum energy solution to Frank's formula does not agree well with the experimentally observed configuration. Alternate forms of Frank's formula were considered, some resulting in much better agreement. Dislocation simulations were used to provide insight into the formation of the observed structure.

2:35 PM

Dislocations and the Distortion of Materials: *Craig S. Hartley*¹; ¹AFOSR, Direct. of Aeros. & Matls. Scis., 4015 Wilson Blvd., Rm. 713, Arlington, VA 22203 USA

The scale of experimental measurements of the distortion of a material subjected the changes in its thermo-mechanical environment has dramatically decreased in recent years. It is now possible to measure the distortion of grids or other surface features over distances corresponding to several thousand atoms. Parallel advances in techniques for measuring the distortion of crystal lattices by diffraction techniques employing synchrotron x-radiation, electron backscattered diffraction (EBSD) and neutron scattering provide an unparalleled opportunity for verifying the validity of relationships between lattice distortion, total shape distortion and dislocation distortion. This paper reviews these relationships in an effort to clarify the physical nature of quantities measured by the two types of techniques and to describe experiments that would assist in revealing the role of dislocations in deformation at the nano- and micro-scale.

2:55 PM

Characterization of the Dislocation Density Tensor With White Beam Diffraction: *Rozaliya Barabash*¹; Gene E. Ice¹; Judy W. Pang¹; Wenjun Liu¹; ¹Oak Ridge National Laboratory, Metals & Ceram., MS 6118, One Bethel Valley Rd., Oak Ridge, TN 37831 USA

The white beam intensity distribution is sensitive to the organization of the dislocations, which occurs at several structural levels. Near a Bragg reflection the intensity distribution in reciprocal space exhibits characteristic features due to dislocations. At the lowest level individual dislocations can exist within a crystal. At a higher structural level dislocations can organize into strongly correlated arrangements including walls and sub-boundaries. The distribution of scattered intensity in reciprocal space is sensitive to these dislocation ensembles. After some kinds of plastic deformation unpaired dislocations of one sign n^+ (geometrically necessary dislocations) as well as geometrically necessary boundaries may be formed in the crystal. These cause not only random deformation, but also strongly correlated local rotations within the crystal, grain, or subgrain. Such correlated deformation changes the conditions for x-ray (or neutron) scattering in the transverse plane of each reflection. In the framework of strain gradient plasticity we describe the plastic deformation by a dislocation density tensor ρ_{ij} and strain gradient tensor of the third rank. A primary set of geometrically necessary dislocations or dislocation walls and subboundaries results in elongated streaks in the Laue image. The direction of the streak depends on the mutual orientation of all activated dislocation slip systems and on the components of dislocation density tensor. Laue images collected using synchrotron x-ray microbeams can reveal nano/meso-scale distribution of the primary paired and unpaired dislocations and dislocation walls. White beam diffraction analysis of several examples of deformation inhomogeneities in poly- and single crystals are discussed.

3:15 PM

Dislocation Density Measurements in CP Titanium Using Electron Channeling Contrast Imaging: *Martin A. Crimp*¹; John T. Hile¹; Thomas R. Bieler¹; Michael G. Glavicic²; ¹Michigan State University, Dept. Chem. Engrg. & Matls. Sci., E. Lansing, MI 48824-1226 USA; ²UES Inc., (AFRL/MLLM), 4401 Dayton-Xenia Rd., Dayton, OH 45432-1894 USA

Dislocation densities have been measured in warm rolled commercially pure Ti using electron channeling contrast imaging (ECCI) and compared to values determined from x-ray line broadening analysis. Samples were rolled to reductions of 1.08%, 2.16%, 5.17% and 15.05% at 366 K. The samples were mechanically prepared and electropolished to remove surface contamination and superficial damage. ECCI, a scanning electron microscopy technique that allows imaging of near surface dislocations in bulk samples, was carried out on the polished samples. Dislocation densities were determined by measuring the number of dislocation/surface intersections per unit area. Electron backscattered diffraction (EBSD) patterns were used to determine the orientation of individual grains, facilitating identification of the active slip planes through trace analysis. Comparison of the results from ECCI and x-ray line broadening studies demonstrates the two techniques are effective at measuring dislocation densities at significantly

different plastic strain levels. This work has been supported by Air Force Research Laboratory, Materials and Manufacturing Directorate, and the Air Force Office of Scientific Research, Grant # F49620-01-1-0116.

Electrochemical Measurements and Processing of Materials: Electrochemical Refining

Sponsored by: Extraction & Processing Division, Materials Processing & Manufacturing Division, EPD-Aqueous Processing Committee, EPD-Process Fundamentals Committee, EPD-Pyrometallurgy Committee, ASM/MSCTS-Thermodynamics & Phase Equilibria Committee, EPD-Waste Treatment & Minimization Committee

Program Organizers: Uday B. Pal, Boston University, Department of Manufacturing Engineering, Brookline, MA 02446 USA; Akram M. Alfantazi, University of British Columbia, Department of Metal & Materials Engineering, Vancouver, BC V6T 1Z4 Canada; Adam C. Powell, Massachusetts Institute of Technology, Department of Materials Science and Engineering, Cambridge, MA 02139-4307 USA

Tuesday PM Room: 212A
March 16, 2004 Location: Charlotte Convention Center

Session Chairs: Donald R. Sadoway, Massachusetts Institute of Technology, Matls. Sci. & Engrg., Cambridge, MA 02139-4307 USA; Ramana G. Reddy, University of Alabama, Metallurgl. & Matls. Engrg., Tuscaloosa, AL 35487-0202 USA

2:30 PM Invited

Electrochemical Measurement of Dissolved Gases in Molten Metals: *Jeffrey W. Fergus*¹; ¹Auburn University, Matls. Rsch. & Educ. Ctr., 201 Ross Hall, Auburn, AL 36849 USA

Gases dissolved in molten metals during processing can lead to defects, such as porosity and inclusions, and thus must be carefully controlled. Optimization of processes for such control requires on-line measurement of dissolved gas content. Solid-electrolyte-based electrochemical sensors are well-suited for such measurements and have been used for many years to measure the oxygen content in molten iron and steel. Other electrochemical sensors, such as those for measuring the amount of hydrogen in molten aluminum, are less fully developed, but offer potential improvements in process control. The high temperatures and low oxygen partial pressures present in molten metals can lead to significant concentrations of undesired electronic or ionic defects, which creates challenges in sensor development. In this paper, this and other issues in the development of sensors for measuring oxygen and hydrogen in molten metals will be discussed.

3:00 PM Invited

The Refining Effect of Cold Plasma on Liquid Metal: *Weizhong Ding*¹; *Xionggang Lu*¹; ¹Shanghai University, Sch. of Matls. Sci. & Engrg., No. 149, Yanchang Rd., Shanghai 200072 China

An interesting phenomenon has been observed in this investigation: the refining effect of cold plasma on liquid metal. The impurity elements in metal may be removed by distillation and gas evolution process. The purification of metal can be enhanced if ionic gas exists in a reaction chamber of the process. In the above case nitrogen, sulfur and phosphorus as impurities in liquid metal are converted into volatile compounds and distilled off. This refining process could not be done under normal atmosphere. The refining effect of cold plasma has made it possible to develop a new technology, which can be used to produce very clean metal. According to the experimental result, the refining mechanism of the cold plasma has been discussed.

3:30 PM

Recycling of Al-Metal Matrix Composites in Ionic Liquids Via Low Temperature Electrolysis: *Venkat Kamavaram*¹; *Ramana G. Reddy*²; ¹University of Alabama, Metallurgl. & Matls. Engrg., A129 Bevell Bldg., PO Box 870202, Tuscaloosa, AL 35487 USA; ²University of Alabama, Dept. of Metallurgl. & Matls. Engrg. & Ctr. for Green Mfg., A129 Bevell Bldg., PO Box 870202, Tuscaloosa, AL 35487 USA

Recycling of aluminum metal matrix composites via electrolysis in ionic liquids at low temperatures was investigated. The electrolytic melt comprised of 1-butyl-3-methylimidazolium chloride (BMIC) and anhydrous AlCl₃. Impure aluminum composite (Duralcan MMC Al-380, 20 vol% SiC) was electrochemically dissolved at the anode and pure aluminum (99.9%) was deposited on a copper cathode. The de-

posits were characterized by scanning electron microscope, X-ray diffraction, and mass spectrometer. The recycling process yielded current densities in the range of 200-500 A/m², and average current efficiency of about 90% in all the cases. The results indicated that impurities such as Si, Cu, Ni, Fe, Mg, Mn, and SiC particles were removed as anode residue. Energy consumption of about 3.0 kWh/kg-Al was obtained at a cell voltage of 1.0V and cell temperature of 105°C. Low energy consumption and no emission of pollutants are the two main advantages of this process compared to present industrial processes.

4:00 PM Break

4:30 PM

Deoxidation of Molten Steel with Application of Electrochemical Technique: *Hyun-Woo Koo*¹; *Hae-Geon Lee*¹; ¹Pohang University of Science and Technology (POSTECH), Dept. of Matls. Sci. & Engrg., San31, Hyoja-Dong, Namgu, Pohang, Kyungbuk 790-784 S. Korea

Deoxidation of molten steel was studied by employing an electrochemical cell principle using a solid oxide electrolyte. This technique enabled to deoxidize liquid steels without leaving deoxidation products in the steel. A number of different combinations and arrangements of solid electrolytes and deoxidizers were designed and tested. Among various solid electrolytes Y₂O₃-stabilized ZrO₂ (YSZ) and Gd₂O₃-doped CeO₂ (GDC) were found to exhibit a good oxygen ion conduction. Various deoxidants including C(s)/CO mixture, metallic Ti, and Al were examined and compared of their efficiency in reacting with oxygen ion transported through an electrolyte. In order to improve electronic as well as ionic conductivity of the electrolytes, several different materials were mixed to or coated on the electrolytes. All experimental works were carried out at 1873K under an inert atmosphere by flowing purified argon gas. It was found that the rate of deoxidation was dependent to a large extent on the electronic and ionic conductivities of the electrolyte. The rate of deoxidation was also dependent on the deoxidant used. Solid deoxidants such as Al and Ti performed poorly in taking oxygen due to chemical interaction with the electrolyte material and also due to the formation of oxidation product layer between the electrolyte and deoxidant. The deoxidant of C/CO mixture, although its equilibrium oxygen potential was much higher than that of either Al or Ti, exhibited much faster deoxidation. Based on the present study, the possibility of industrial application of this technique for production of ultra-clean steels was discussed.

5:00 PM

A New Unpolluted Deoxidation Way: *Xionggang Lu*¹; *Guozhi Zhou*¹; *Weizhong Ding*¹; ¹Shanghai University, Sch. of Matls. Sci. & Engrg., No. 149, Yanchang Rd., Shanghai 200072 China

Using a deoxidizer placed into a magnesia-stabilized zirconia (MSZ) tube and an electronic conductor sealed the open of the MSZ tube, the deoxidization units are prepared. According to the principle of the short-circuited deoxidization of solid electrolyte cell, oxygen atoms in the melt obtain electrons and transform into oxygen ions at the melt/electrolyte interface, oxygen ions diffused through the electrolyte to the electrolyte/deoxidizer interface react with the deoxidizer and produce deoxidization product. The electrons produced transfer through the electronic conductor to the melt/electrolyte interface and neutralize the positive charges accumulated, the electronic field stopping the diffusion of oxygen ions is destroyed. So the deoxidization process will go on until the deoxidization equilibrium. Deoxidization product remained inside deoxidization unit is removed together, so this deoxidized way will not pollute the melt and is a novel method which is experimentally verified to be effective. The rate and limit of deoxidization are got, and a model is established and simplified.

5:30 PM

Measurement of Conductivity and Electronic Conduction of Cryolite Alumina Melts: *Ye Ya Ping*¹; *Zheng Yunyou*¹; *Li Fushen*²; *Li Lifeng*²; *Zhou Guozhi*²; ¹University of Science & Technology, Applied Sci. Sch., Beijing 100083 China; ²University of Science & Technology, Lab. on Solid Electrolytes & Metallurgl. Testing Techniques, Beijing 100083 China

The conductivity of molten Na₃AlF₆ with Al₂O₃ was measured using AC impedance spectrum. The dependence of the conductivity of cryolite alumina upon temperature and concentration of alumina in the molten were studied. According to these data, a rule of conductivity vs. composition and temperature for molten cryolite could be found under 1010?°. The electronic conductivity measurements were also performed using the Wagner measurement technique under inverse polarization conditions.

General Abstracts: Session V

Sponsored by: TMS

Program Organizers: Adrian C. Deneys, Praxair, Inc., Tarrytown, NY 10591-6717 USA; John J. Chen, University of Auckland, Department of Chemical & Materials Engineering, Auckland 00160 New Zealand; Eric M. Taleff, University of Texas, Mechanical Engineering Department, Austin, TX 78712-1063 USA

Tuesday PM Room: 204
March 16, 2004 Location: Charlotte Convention Center

Session Chair: Anis Zribi, General Electric, Global Rsch. Ctr., Niskayuna, NY 12309 USA

2:00 PM

Characteristics of Ti5Si3 Dispersed Titanium Alloy Prepared by Powder Metallurgy: Toshiyuki Nishio¹; Keizo Kobayashi¹; Akihiro Matsumoto¹; Kimihiro Ozaki¹; ¹Aist chubu, Aichi, Nagoya 463-8560 Japan

Titanium silicide Ti5Si3 is expected as a high temperature structural material for aerospace use because of its own low density and a high melting temperature. Therefore, Ti5Si3 is potentially a one of effective dispersoid in titanium matrix to improve mechanical properties. Ti-Ti5Si3 composite has been prepared by powder metallurgy and also the properties of the composite has been investigated. Elemental titanium(30mm), silicon(20mm) and a fine silicon (<1mm) powders were used in this work. The fine silicon powder was mechanically ground for 45ks. Ti5Si3 was synthesized in a vacuum furnace. When using a fine silicon powder, Ti5Si3 was successfully synthesized at a relatively lower temperature. The synthesized Ti5Si3 was milled into fine powder by ball milling. The powder mixture of the composition of Ti-10mass%Ti5Si3 was consolidated by pulsed current sintering equipment. Microstructural observation of the composite revealed Ti5Si3 particles were homogeneously dispersed in the titanium matrix without pores.

2:25 PM

Microstructure Effects of Shear Localization Evaluated With Electron Backscatter Diffraction: Benjamin L. Henrie¹; Qing Xue¹; George (Rusty) T. Gray¹; ¹Los Alamos National Laboratory, PO Box 1663, MS G755, Los Alamos, NM 87545 USA

Adiabatic shear localization was studied in 316L stainless steel and tantalum. A force shear technique was utilized under high-strain-rate loading using a compression split-Hopkinson pressure bar and hat-shaped specimens. Electron backscatter diffraction (EBSD) was used to understand how the microstructure changed as a function of position relative to the shear band. Using EBSD, spatially coordinated crystallographic information was achieved immediately adjacent to the shear band. For the 316L stainless steel significant grain deformation occurred within a few grains of the shear band. In the tantalum case no shear band formed and some grains experienced ~250% strain while only experiencing a 10 degree grain misorientation.

2:50 PM Cancelled

Castability and Microstructure Characterization of Reduced and Lead Free Brasses for Sanitary Applications

3:15 PM

Microstructure and Mechanical Properties of a Dispersion Strengthened Al-Nano Al₂O₃ Composite: Jixiong Han¹; Yong-Ching Chen²; Vijay K. Vasudevan¹; ¹University of Cincinnati, Chem. & Matls. Engrg., Cincinnati, OH 45221-0012 USA; ²Cummins Inc., Metallurg. Engrg., MC 50183, Columbus, IN 47201 USA

The microstructure, thermal stability and mechanical properties of a novel aluminum matrix composite reinforced with a high volume fraction nanoscale Al₂O₃ particles was studied. This material was produced by a casting route by Chesapeake Composites. The as-received dispersion strengthened composite (DSC) material was observed to possess an unusual microstructure composed of clusters of nanoscale (30-100 nm diameter) Al₂O₃ particles surrounded by the Al matrix. Annealing at high temperatures lead to coalescence of these particles to larger size entities, giving rise to an interesting Al-Al₂O₃ composite that is otherwise thermally stable and retains impressively high hardness (~170HV). The tensile strength of the DSC material decreased nearly linearly from ~40 ksi at room temperature to ~20 ksi at 400°C, the latter value being impressively high for an Al alloy. The fracture morphology correspondingly changed from brittle to ductile/dimpled rupture with presence of microvoids containing oxide particles in their interior. Thermal soaking at high temperatures for times to 500h led

to no degradation of the tensile properties. Although the macroscopic ductility remained low over the entire temperature range in both the unsoaked and soaked materials, there was substantial evidence for high localized plasticity as manifested by stretching, tearing and void formation in the Al matrix around the oxide particles. These results will be presented and discussed.

3:40 PM Break

3:50 PM

Study of Solid Solution Strengthening by Ternary Elements Additions on Mo₃Si Matrix: I. Rosales¹; H. Martinez²; ¹Centro de Investigación en Ingeniería y Ciencias Aplicadas-FCQ e Ing. UAEM., Av Univ. 1001 Col. Chamilpa, Cuernavaca, Mor. 62210 Mexico; ²Centro de Ciencias Físicas, UNAM, Av Univ. s/n Col. Chamilpa, Cuernavaca, Mor. 62210 Mexico

Ternary element addition on a Mo₃Si matrix resulted in mechanical variation properties. Solid solution additions in the alloys, were evaluated by Microhardness test, Lattice parameter measurements by Xray diffraction method and Young's Modulus determination by indentation technique. Microhardness test shown in the case of the alloys with Cr no disparity for the different concentrations is observed. However samples with V and Nb addition shown a remarkable variation on the properties for the different Nb concentrations. High temperature compression test at 1300 and 1400°C at 10⁻⁵ s⁻¹ shown a strong temperature and composition dependence, the calculated stress exponent from compressive analysis resulted to be n= 6.

4:15 PM

Syntheses and Studies on BST: MgTiO₃ Ceramic Composites and Sputtered Thin Films: Tai-Nan Lin¹; Jinn P. Chu¹; Sea-Fue Wang²; J. Michael Riggsbee³; Wen-Rong Wu²; C. C. Lin¹; C. H. Lin¹; ¹National Taiwan Ocean University, Inst. of Matls. Engrg., No. 2, Pei-Ning Rd., Keelung 202 Taiwan; ²National Taipei University of Technology, Dept. of Matls. & Mineral Resources, 1, Sec. 3, Chung-Hsiao E. Rd., Taipei 106 Taiwan; ³North Carolina State University, Dept. of Matls. Sci. & Engrg., 229 Riddick Engrg. Labs, Box 7907, Raleigh, NC 27695 USA

The (Ba,Sr)TiO₃ (BST) system is well known for its high response of the dielectric constant to an applied electric field. However, the large dielectric constants found in this system limit its usefulness at microwave frequencies. Some research groups have used composite structures to dilute the dielectric constant and to minimize the dielectric loss of BST for microwave applications. (1-x) BST(Ba_{0.3}Sr_{0.7}TiO₃) : x MT(MgTiO₃) [BSMT(x)] composites were fabricated by conventional solid state reaction process. Thin films were thus prepared from the corresponding targets, i.e., pure BST, BSMT(0.05), BSMT(0.1), BSMT(0.2), BSMT(0.4), BSMT(0.6), BSMT(0.8) and pure MT (x is mole fraction). The decrease in the dielectric constants of BSMT(x) composites with increasing x is observed. The microwave quality factor Q and Q x f values exhibit a decreasing trend at x < 0.6. At x = 0.1, the dielectric constant is 154 and the Q x f value is 1883 GHz. As for the composite thin films, the dielectric constants also exhibit a decreasing trend between 0 < x < 0.2.

4:40 PM

Manufacture and Performance of Bi-Layer Tetrahedral Truss Core Sandwich Panels: Gregory William Kooistra¹; Haydn N.G. Wadley¹; ¹University of Virginia, Matls. Sci. & Engrg. Dept., 116 Engineer's Way, Charlottesville, VA 22904 USA

Sandwich panels with cores made of period cellular metals are produced by a variety of techniques. This presentation gives a method for the manufacture bi-layer tetrahedral truss cores from a single sheet of patterned and stamped 6061 aluminum alloy. The cores are joined to facesheets of the same alloy via the brazing process creating an open architecture sandwich panel suitable for multifunctional applications. The performance of these panels is compared with honeycomb, truss, textile, and foam structures. Analytical models are developed to describe the relative mechanical properties of the core material. Experimental results demonstrate a strong performance dependent relationship to the condition of the parent alloy in both the elastic and plastic deformation regimes.

5:05 PM

Instrumentation for Determining the Local Damping Capacity in Honeycomb Sandwich Composites: John D. Lincoln¹; L. E. Rieger¹; J. C. Earthman¹; ¹University of California, Matls. Sci. & Engrg., Engrg. Tower 644F, Henry Samueli Sch. of Engrg., Irvine, CA 92697 USA

A mechanical tapping probe originally designed for determining the damping capacity of dental implants has been adapted to assess the local damping capacity of honeycomb sandwich composites without inflicting damage on the structure. The new instrumentation is light,

portable, and inexpensive when compared with other testing techniques. Furthermore, it allows quick access to areas not easily accessible by ultra-sonic methods. The damping capacity of honeycomb sandwich composite structures is of interest to engineers as it reflects the ability of a material to absorb and isolate vibration, both acoustic and mechanical. Honeycomb sandwich structures with various damping treatments were constructed and accurately evaluated with the instrumentation.

Hume Rothery Symposium: Structure and Diffusional Growth Mechanisms of Irrational Interphase Boundaries: Session IV

Sponsored by: Electronic, Magnetic & Photonic Materials Division, Structural Materials Division, EMPMD/SMD-Alloy Phases Committee, MPMD-Phase Transformation Committee-(Jt. ASM-MSCTS)

Program Organizer: H. I. Aaronson, Carnegie Mellon University, Department of Materials Science and Engineering, Pittsburgh, PA 15213 USA

Tuesday PM Room: 208A
March 16, 2004 Location: Charlotte Convention Center

Session Chair: T. Furuhashi, Kyoto University, Dept. of Matls. Sci. & Engrg., Kyoto 606-8501 Japan

2:00 PM Invited

Interfacial Structure of Cementite Dendrites Formed at Austenite Grain Boundaries: Milo V. Kral¹; George Spanos²; ¹University of Canterbury, Mech. Engrg., PO Box 4800, Christchurch New Zealand; ²US Naval Research Laboratory, Phys. Metall. Brch., 4555 Overlook Ave., SW, Washington DC 20375 USA

A Fe-13Mn-1.3%C alloy has been studied extensively using three-dimensional analysis techniques and electron diffraction techniques. The 3D work showed that grain boundary cementite assumes a dendritic or fern-like morphology with dendrite arms growing along the grain boundary plane. Electron backscatter diffraction pattern analysis showed that many of these precipitates obtain a (near) rational orientation relationship with one of the adjacent austenite grains and an irrational orientation with the other austenite grain. The interfacial structure of cementite/austenite interfaces on both sides of cementite grain boundary precipitates will be studied using high-resolution transmission electron microscopy.

2:40 PM Invited

Interphase Boundaries in the Massive Transformation: Vijay K. Vasudevan¹; James E. Wittig²; ¹University of Cincinnati, Chem. & Matls. Engrg., Cincinnati, OH 45221-0012 USA; ²Vanderbilt University, Elect. Engrg. & Compu. Sci., Nashville, TN 37235-1683 USA

The massive-matrix interphase interfaces associated with the α to γ_M massive transformation in Ti-(46-48)Al alloys were studied. The transformation was arrested at an early stage utilizing either special heat treatments or by rapid solidification. Orientation relations between the γ_M and parent α (retained α_2) phases were determined using EBSD in an SEM and by electron diffraction, and the interphase interfaces and defect structures in the γ_M phase characterized by two-beam bright-field/weak-beam dark-field TEM and HRTEM. The results reveal that the γ_M forms at grain boundaries generally with a low-index orientation relation and coherent interface with one parent grain, but grows into the adjacent grain with a high-index/irrational orientation relation. In the case of γ_M formed at grain edges and corners, no low-index orientation relations were found with any of the surrounding parent grains. The growth interphase boundaries between the two phases are generally free of misfit dislocations or other defects and consist of curved parts as well as planar facets whose macroscopic habit planes are of generally high-index/irrational orientation and deviate substantially from the close-packed planes. On an atomic scale the growth interphase boundaries are sometimes found to be faceted along {111} planes, as well as along other planes, with closely spaced steps, but are concluded to be incoherent with respect to the parent grain into which growth occurs. The results obtained will be compared with those in other alloy systems and their implications on the nucleation and growth mechanisms associated with the massive transformation will be discussed.

3:20 PM Invited

Structure of Irrational Interfaces Operative During the Pearlite Reaction: Gary J. Shiflet¹; ¹University of Virginia, Matls. Sci. &

Engrg., PO Box 400745, 116 Engineers Way, Charlottesville, VA 22904-4745 USA

This presentation will examine the microstructural consequences associated with crystallographic constraints associated with irrational interphase boundaries at the pearlite growth front. A generalization of the calculations by Lee and Aaronson concerning grain boundary precipitate embryo equilibrium morphologies to interphase boundaries will be developed. These results will then be applied to Fe-C-V pearlite growing with concomitant interphase boundary precipitation of VC. A critical and quantitative comparison between growth interphase boundaries that are irrational, but have a deference to crystallographic constraints, and disordered growth fronts that do not will be made. Support by the National Science Foundation, DMR is acknowledged.

4:00 PM Break

4:15 PM Invited

Structure of Irrational Interphases Operative During the Cellular Transformation: Gary J. Shiflet¹; Max W.H. Braun²; Jan H. van der Merwe³; ¹University of Virginia, Matls. Sci. & Engrg., PO Box 400745, 116 Engrs. Way, Charlottesville, VA 22904-4745 USA; ²University of Pretoria, Dept. of Physics, Pretoria S. Africa; ³University of South Africa, Dept. of Physics, Pretoria S. Africa

The cellular, or discontinuous precipitation, reaction occurs widely in alloys. Although it is often modeled possessing a disordered growth front, extensive experimental work in binary Cu-Ti alloys has shown that even though the individual lamellae interphase boundary growth fronts are indeed irrational, deference to crystallography still occurs, which includes periodic misfit compensating defects. This paper will provide a theoretical framework illustrating the energetics associated with irrational orientation relationships that still have energies lowered by matching at the advancing phase boundary. The Embedded Atom Method (EAM), coupled with van der Merwe's mathematical approach, is applied to examine specific irrational interphase boundary structures and energies for this system. Support by the National Science Foundation, DMR is acknowledged.

Internal Stresses and Thermo-Mechanical Behavior in Multi-Component Materials Systems: Creep and Plasticity II

Sponsored by: Electronic, Magnetic & Photonic Materials Division, Structural Materials Division, EMPMD-Electronic Packaging and Interconnection Materials Committee, EMPMD-Thin Films & Interfaces Committee, SMD-Composite Materials Committee-Jt. ASM-MSCTS

Program Organizers: Indranath Dutta, Naval Postgraduate School, Department of Mechanical Engineering, Monterey, CA 93943 USA; Bhaskar S. Majumdar, New Mexico Tech, Department of Materials Science and Engineering, Socorro, NM 87801 USA; Mark A.M. Bourke, Los Alamos National Laboratory, Neutron Science Center, Los Alamos, NM 87545 USA; Darrel R. Frear, Motorola, Tempe, AZ 85284 USA; John E. Sanchez, Advanced Micro Devices, Sunnyvale, CA 94088 USA

Tuesday PM Room: 209B
March 16, 2004 Location: Charlotte Convention Center

Session Chairs: David C. Dunand, Northwestern University, Evanston, IL 60208 USA; Bhaskar S. Majumdar, New Mexico Tech, Socorro, NM 87801 USA

2:00 PM Invited

Internal Stress in Plasticity and Microplasticity: James C.M. Li¹; ¹University of Rochester, Dept. of Mech. Engrg., Matls. Sci. Prog., Rochester, NY 14627 USA

While the yield stress is the minimum stress to start plastic deformation, internal stress is that to sustain plastic deformation. After yielding, the applied stress needed to continue deformation may be lower than the yield stress so the internal stress must be measured during deformation such as by stress relaxation. Obviously the internal stress relates to the microstructure developed during deformation and hence it can be altered by further deformation, reverse deformation, deformation in another direction as well as by annealing. The role of internal stress played in work hardening, latent hardening, ductility and fracture is reviewed. Internal stress development in micro and nanoindentation will be reported also. Work supported by the N.Y. State Infotonics Center of Excellence and by NSF through DMR9623808 monitored by Dr. Bruce MacDonald.

2:25 PM Invited

Internal Stresses and Constitutive Behavior of Ferroelectrics: Ersan Ustundag¹; Robert Rogan¹; S. Maziar Motahari¹; Bjørn Clausen²; Chad Landis³; ¹California Institute of Technology, Dept. of Matls. Sci., Pasadena, CA 91125 USA; ²Los Alamos National Laboratory, Neutron Sci. Ctr., Los Alamos, NM 87545 USA; ³Rice University, Dept. of Mech. Engrg. & Matls. Sci., Houston, TX 77251 USA

Ferroelectric materials exhibit a unique response to electromechanical loading and can be used as both sensors and actuators. This presentation will first review recent studies that employed diffraction to investigate strain and texture evolution in various ferroelectrics under electromechanical loading. In addition, our recent work on the multiscale internal stress characterization of Pb(Zr,Ti)O₃ and BaTiO₃ materials will be discussed. Then a new self-consistent micromechanics model will be presented. This model considers different domain variants and attempts to estimate strain and texture (or domain switching) evolution during the loading of ferroelectrics. Finally, the diffraction data will be compared to the predictions of this model.

2:50 PM Invited

In Situ Study of Cyclic Mechanical and Thermal Loading in a Two Phase System Using Diffraction: Mark R. Daymond¹; ¹Rutherford Appleton Laboratory, ISIS Fac., Chilton, Didcot, Oxfordshire OX11 0QX UK

Neutron and synchrotron x-ray diffraction allow the monitoring of the bulk internal stress state of polycrystalline materials during in situ loading. In multi-phase materials the stress partitioning between the two phases can be monitored. In both multi-phase and single phase materials the redistribution of load between differently oriented grain families within the polycrystal material can be monitored. By comparing diffraction results with predictions from micromechanical models (both finite element and self-consistent) we can obtain an insight into the deformation mechanisms occurring in the material. Recent studies of cyclic mechanical and thermo-mechanical loading of two phase systems will be described, in particular Al/SiC and two phase steels. As well as illustrating the interplay between continuum and grain level assumptions, these results bring an insight into slip system cross hardening and Bauschinger effects.

3:15 PM Invited

A Methodology for Determining Internal Stresses in Multi-Component Materials: Bjorn Clausen¹; Mark A.M. Bourke²; Donald W. Brown²; Ersan Ustundag³; ¹Los Alamos National Laboratory, LANSCE-12, PO Box 1663, MS H805, Los Alamos, NM 87545 USA; ²Los Alamos National Laboratory, MST-8, PO Box 1663, MS H805, Los Alamos, NM 87545 USA; ³California Institute of Technology, Matls. Sci. Dept., Keck Lab., MC 138-78, 1200 E. Calif. Blvd., Pasadena, CA 91125 USA

In most cases, determining the constitutive behavior of a composite is not as simple as using the rule of mixtures, especially for the inelastic properties such as phase yield stress and hardening. Furthermore, the processing conditions will most likely alter the properties of the constituents compared to their monolithic properties due to changes in the microstructure and introduction of thermal residual stresses. A methodology for determining the internal stresses in multi-phase materials based on neutron diffraction measurements and finite element modeling (FEM) will be presented. The diffraction technique is inherently phase specific, and it yields information about internal elastic lattice strains in bulk crystalline materials. The combination of the experimental results and FEM enables us to indirectly determine the in-situ properties of the constituent phases. As an example, the constitutive performance of fiber reinforced composites will be presented for tungsten fiber composites with either Kanthal or bulk metallic glass matrix.

3:40 PM Invited

Internal-Stress Plasticity in Iron Wires by Rapid Thermal Cycling Through the Allotropic Transformation: John Marvin¹; David C. Dunand¹; ¹Northwestern University, Matls. Sci., 2220 Campus Dr., 2043 Cook Hall, Evanston, IL 60208 USA

Iron and eutectoid steel wires, ca. 0.5 mm in diameter, were rapidly cycled through the alpha-gamma phase transformation range by direct current Joule heating while being subjected to a tensile stress. The wires deform plastically after each crossing of the phase transformation, as reported in the literature for bulk iron and steel samples subjected to slow thermal cycling. The mechanism responsible for this phenomenon is called internal-stress plasticity, and relies on the biasing by the external stress of the internal mismatch stresses due to the co-existence of both alpha and gamma phases with different density. The present experiments demonstrate that internal-stress plasticity can be achieved under very rapid cycling (2.5-second cycles, or 0.4 Hz),

which is two order of magnitude faster that has been achieved so far with bulk samples (4-minute cycles or 0.004 Hz).

4:05 PM Invited

The Relationship Between Microstructure and Ductility in Cast Aluminum: Stephen J. Harris¹; James Boileau¹; Wen Yang¹; Bhaskar S. Majumdar²; Somnath Ghosh³; ¹Ford Research and Advanced Engineering, Dept. of Matls. Sci., Dearborn, MI 48121 USA; ²Ford Research and Advanced Engineering, PES Dept., MD #3083, SRL Bldg., 2101 Village Rd., Dearborn, MI 48121 USA; ³New Mexico Institute of Technology, NM USA; ⁴Ohio State University, Mech. Engrg., OH USA

The increased use of cast aluminum for automotive applications highlights the need to develop a better database of mechanical and physical properties for cast Al alloys. In general, improvements in all mechanical properties are often desired. However, in practice, the difficulty in increasing both strength and ductility simultaneously can lead to undesirable tradeoffs. Because of this, a study was undertaken to correlate microstructure with ductility and strength in cast 319 and 356 Al alloys. 3-point bending tests were performed on a set of specimens with similar strengths but different ductilities and on a set of specimens with similar ductilities but different strengths. The tests were done in-situ in an SEM. The resulting images were analyzed to yield local displacement and strain fields. Complementary micro-Raman experiments were carried out under an optical microscope and yielded direct measurements of strain in selected Si particles. The results will be discussed in terms of the particular microstructural features (e.g., Si particles, intermetallics) that are responsible for ductile fracture in these alloys and how their actions are controlled by local stresses and strains.

4:30 PM

Constitutive Behavior of Pb(Zr,Ti)O₃ Ferroelectrics: Robert Rogan¹; Ersan Ustundag¹; S. Maziar Motahari¹; Bjørn Clausen²; Ulrich Lienert³; Mark R. Daymond⁴; ¹California Institute of Technology, Dept. of Matls. Sci., Pasadena, CA 91125 USA; ²Los Alamos National Laboratory, Neutron Sci. Ctr., Los Alamos, NM 87545 USA; ³Argonne National Laboratory, Advd. Photon Source, Argonne, IL 60439 USA; ⁴Rutherford-Appleton Laboratory, ISIS Neutron Scattering Facility, Chilton, Didcot OX11 0QX

Electromechanical loading was applied to monitor strain and texture (domain switching) evolution in various Pb(Zr,Ti)O₃ or PZT ceramics using neutron and high energy X-ray diffraction. In-situ uniaxial compression experiments were performed on various PZTs using neutron diffraction to determine their ferroelastic behavior. PZTs near the edge of the morphotropic phase boundary as well as single phase (tetragonal and rhombohedral) specimens were investigated. Analysis of the diffraction patterns allowed for observation of the onset and culmination of domain switching through modeling of the sample texture using the March-Dollase model. In a separate experiment, high energy XRD with an area detector provided information about the ferroelectric response of a La-doped PZT to cyclic electrical loading. Diffraction data suggested a high degree of anisotropy and a complicated internal stress state in all specimens. The data were also compared to the predictions of a new self-consistent model to describe the constitutive behavior of PZTs.

International Laterite Nickel Symposium - 2004: Process Development for Prospective Projects

Sponsored by: Extraction & Processing Division, EPD-Aqueous Processing Committee, EPD-Copper, Nickel, Cobalt Committee, EPD-Process Fundamentals Committee, EPD-Process Mineralogy Committee, EPD-Pyrometallurgy Committee, EPD-Waste Treatment & Minimization Committee

Program Organizer: William P. Imrie, Bechtel Corporation, Mining and Metals, Englewood, CO 80111 USA

Tuesday PM

March 16, 2004

Room: 217B/C

Location: Charlotte Convention Center

Session Chairs: Peter G. Mason, Principle Consultant, Hydrometallurgy, Falconbridge, Queensland Australia; Larry Seeley, President & CEO, SGS Lakefield Research Limited, Lakefield, Ontario K0L 2H0 Canada

2:30 PM

Development of Process Design in Coral Bay Nickel Project: Naoyuki Tsuchida¹; ¹Sumitomo Metal Mining Co., Ltd., Non-Ferrous

Metals Div. Coral Bay Project Dept., 11-3, Shinbashi 5-Chome, Minato-ku, Tokyo 105-8716 Japan

Sumitomo Metal Mining Co. Ltd. (SMMC) is currently developing the flowsheet to treat stockpiled limonite, a type of laterite ore, at Rio Tuba on southern Palawan Island, Philippines. The new plant will be commissioned at the end of 2004. Rio Tuba Nickel Mining Corporation (RTNMC) has been mining saprolite since 1977, and the limonite ore located above the saprolite ore body has been stockpiled separately according to nickel and magnesium content. Ore from these stockpiles will be blended and used for the operation. The annual production of nickel will be 10,000 metric tons for the next twenty years. The proposed process consists of ore preparation, high pressure acid leach (HPAL), counter-current decantation wash, impurity removal and sulfide precipitation. Precipitated mixed sulfide will be processed to electrolytic nickel by the Matte Chlorine Leach Electrowinning (MCLE) process at Niihama, Japan. SMMC has established new technologies during the process development, such as zinc removal and sulfide precipitation. Applying this technology, preferential removal of zinc can be achieved by hydrogen sulfide gas with negligible loss of nickel. Precipitation of nickel by hydrogen sulfide gas is carried out at low temperature. Slow kinetics is selected for control of the particle size of the precipitated mixed sulfide

2:55 PM

A Complete Approach to Complex Flowsheet Development—Niquel do Vermelho (CVRD) Case Study: *Michael Adams*¹; Dwight van der Meulen¹; John Ernest Angove¹; ¹SGS, Lakefield Orestest Pty Ltd, 431 Victoria Rd., Malaga, Perth, Western Australia 6090 Australia

A comprehensive pre-feasibility study has been conducted on CVRD's Niquel do Vermelho nickel laterite deposit. Five integrated flowsheet options were developed, via batch and pilot campaigns at Lakefield Orestest over an intensive five-month period, from ore receipt to final reporting. Key objectives included demonstrating the technical viability of the beneficiation of several ore types, processing through integrated PAL/MHP and PAL/MSP circuits and treatment of barren liquors to meet stringent environmental requirements. Refining of the MHP was by ammonia re-leach and solvent extraction to produce LME-grade nickel cathodes, NiCO₃, NiO and CoS. LME grade nickel and cobalt was also produced by oxidation of the MSP and hydrogen reduction on the leachate. The database and acquisition system, along with web-based reporting, enabled rapid turnaround on both daily and comprehensive run reports, with speedy and confident setpoint decisions on complex flowsheets. The high value of such data is thus given due recognition and will play a pivotal role in the successful progression of laterite projects through to sustainable commercial viability.

3:20 PM

Development of a Fluid-Bed Pyrohydrolysis Process for Inco's Goro Nickel Project: *Ahmed Vahed*¹; Fred Colton¹; Jean-Paul Duterque²; Wilhelm Karner³; Frank Baerhold³; ¹Inco Technical Services Limited, 2060 Flavelle Blvd., Sheridan Park, Mississauga, Ontario L5K 1Z9 Canada; ²Goro Nickel S.A., Imm. Le Kariba, 7 Bis, Rue Suffren, B.P. 218-98845, Noumea New Caledonia; ³Ruthner Surface Technologies, Eibesbrunnengasse 20, Vienna A-1121 Austria

The Goro Nickel Project is situated in the Southern Province of New Caledonia. Inco Limited and Goro Nickel S.A. have developed a process that features the use of pyrohydrolysis to produce nickel oxide. The process treats a blend of laterites by Pressure Acid Leaching followed by solvent extraction of nickel and cobalt using Cyanex 301®. Purified nickel chloride solution is converted to high purity NiO product and 6M hydrochloric acid, which is recycled back to the SX circuit. In co-operation with Andritz AG, spray roaster and fluid-bed pyrohydrolysis technologies were examined for this purpose. Tests were conducted at the Andritz AG pilot plant in Vienna, Austria, and at Goro in larger scale installations. The latter served to establish process engineering design parameters for scale-up. Several process variables were investigated in both technologies and the off-gas characteristics were established. Fluid-bed pyrohydrolysis was selected for the Goro commercial plant, primarily because it produced a granular nickel oxide. The main focus of this paper is to outline the results obtained in a 0.8 m diameter fluid-bed pyrohydrolysis circuit.

3:45 PM Break

3:55 PM

Piloting of the Beneficiation and EPAL® Circuits for Ravensthorpe Nickel Operations: *Mike Adams*¹; Dwight van der Meulen¹; Chad Czerny¹; Peter Adamini¹; John Turner¹; Sunil Jayasekera¹; Jason Amaranti¹; John Mosher²; Mike Miller³; David White³; Geoff Miller³; ¹SGS Lakefield Orestest, 431 Victoria Rd., Malaga, Western Australia 6090 Australia; ²AR McPherson Consultants Ltd; ³Ravensthorpe Nickel Operations

Comprehensive pilot testwork has been conducted on BHP Billiton's Ravensthorpe nickel laterite deposit over a fifteen-month period at Lakefield Orestest. Some 228 tonnes of ore were processed in a beneficiation pilot-plant comprising scrubbing, attrition scrubbing, screening and thickening over sixteen pilot runs with an average mass closure of 99.2%. This produced a suitable feed for hydrometallurgical piloting over seven runs covering 1,680 hours of operation. The integrated EPAL® (enhanced pressure acid leach) circuit comprised a limonite pressure acid leach front end discharging into a saprolite atmospheric leach circuit and subsequently to induced jarosite precipitation, counter-current decantation, iron removal, mixed hydroxide precipitation, and manganese removal. The pilot plant met its key objectives in demonstrating the flowsheet's technical viability, and generating raw data inputs for the project feasibility study. Rapid, intensive data capture, collation and reporting helped solve key flowsheet issues. The pilot plant also demonstrated its value as a risk management tool in the resolution of numerous engineering, metallurgical and materials selection issues at a manageable scale. A disciplined approach to experimental planning, operation and management was a significant contributor to the overall success of the campaign.

4:20 PM

Niquel do Vermelho Project—Prefeasibility Study: *Vanessa de Macedo Torres*¹; Marcelo Lopes Costa¹; Omar Antunes Carmo¹; Ruy Lacourt Rodrigues¹; Salomao Solino Evelin¹; ¹Companhia Vale do Rio Doce, Base Metals Projects Dept., BR 262-Km 296, Santa Luzia, MG 33030-970 Brazil

Cia. Vale do Rio Doce is currently developing Niquel do Vermelho Project. The laterite deposit is located at Carajas Mineral Province at less than 15 km from Sossego Copper Project, scheduled for start-up on 2004. The available infrastructure, includes paved roads, large capacity railroad and port complex owned by CVRD, power supply and good quality water. The project was evaluated in the past for ferronickel production. In the late 1990s, CVRD switched its attention to investigating the usage of pressure acid leaching. The combination of good metallurgical behaviour for pressure acid leach (PAL) process route with reasonable mineable grades, and existing infrastructure justified the start of engineering studies in 2002. The project approach at the engineering phase is based on the dual objective of minimizing risks while maximizing project profitability and value. CVRD is currently completing the Niquel do Vermelho prefeasibility study. This paper outlines the main outcomes of the study and future perspectives for the project.

4:45 PM

The Jaguar Nickel Inc. Sechol Laterite Project Atmospheric Chloride Leach Process: G. B. Harris¹; T. J. Magee¹; *V. I. Lakshmanan*²; R. Sridhar²; ¹Jaguar Nickel Inc., 55 Univ. Ave., Ste. 910, Toronto, ON M5J 2H7 Canada; ²Process Research ORTECH Inc., 2395 Speakman Dr., Mississauga, ON L5K 1B3 Canada

Jaguar Nickel Inc. is developing the Sechol Nickel-Cobalt Laterite Project in Guatemala, Central America. Recognizing the potential advantages offered by chloride brine chemistry, Jaguar, at the facilities of Process Research ORTECH Inc, Mississauga, has developed an Atmospheric Chloride Leaching Process using a mixed chloride lixiviant to recover the nickel and cobalt, whilst leaving the majority of the iron and magnesium in the leach residue. Subsequent solution purification and mixed nickel/cobalt hydroxide product recovery is by standard precipitation methods, using recycled caustic magnesia, with a final stage of pyrohydrolysis of a portion of the concentrated magnesium chloride brine for recycling both the caustic magnesia and chloride lixiviant. The flowsheet that has been developed also offers opportunities for by-product recovery and efficient, environmentally clean process effluent management. The paper discusses some of the early leaching results in the context of strong chloride brine chemistry, with emphasis on how the controlling of water activity, hydrogen ion activity and chloride concentration permits the selective leaching of nickel and cobalt from an iron-magnesium matrix.

International Laterite Nickel Symposium - 2004: Roasting and Smelting

Sponsored by: Extraction & Processing Division, EPD-Aqueous Processing Committee, EPD-Copper, Nickel, Cobalt Committee, EPD-Process Fundamentals Committee, EPD-Process Mineralogy Committee, EPD-Pyrometallurgy Committee, EPD-Waste Treatment & Minimization Committee

Program Organizer: William P. Imrie, Bechtel Corporation, Mining and Metals, Englewood, CO 80111 USA

Tuesday PM
March 16, 2004

Room: 217D
Location: Charlotte Convention Center

Session Chairs: John G. Schofield, Pyrometallurgical Consultant, Nanoose Bay, BC V9P 9G5 Canada; Egil J.M. Jahnsen, Pyrometallurgical Consultant, Hagan, 4480 Kvinesdal Norway

2:30 PM

Contribution to the Recycling of Rotary Kiln Dust in Nickeliferous Laterite Reduction: Reduction Behavior of the Dust: *Elias Rigopoulos*¹; Ismene-Polyxeni Kostika²; Emmanuel N. Zevgolits²; Iliana Halikia²; ¹Silver and Baryte Ores Mining Co. S.A, Milos Island, Milos Greece; ²National Technical University of Athens (NTUA), Sch. of Mining & Metallurg. Engrg., Zografou Campus, 5780, Athens Greece

In the present study the reductive behavior of dust from the rotary kilns (R/K) in ferronickel production from nickeliferous Greek laterites is investigated. The study concerns dust of various origins (washing towers, electrostatic filters, polycyclones) and pellets made from the dust. Reducibility was studied in the temperature range of 700°C to 850°C in a laboratory tube furnace. Experimental results showed that reduction degree increases with temperature up to about 800°C. The rate of reduction is great during the first minutes, giving a reduction degree R% equal to about 25%, in only a few minutes. After this, the rate is decreasing until it diminishes to zero after about 10-20 minutes of reaction. Maximum reduction degree, at reaction equilibrium, is 26 to 28%. The rate and the reduction degrees at various temperatures are higher for the dust samples than those of the respective pellet samples.

2:50 PM

Calcination and Reduction of Laterite Nickel Ores: *Andreas Orth*¹; Bernd Kerstiens¹; ¹Outokumpu Lurgi Metallurgie GmbH, Ferrous Tech., Ludwig-Erhard-Str. 21, Oberursel 61440 Germany

Outokumpu Lurgi Metallurgie has developed a process for the calcination and reduction of laterite nickel ores where the reduction of iron and nickel to the wuestite/metallic states respectively, is performed in a fluidized bed reactor using reduction gas generated very cost effectively from natural gas in an auto thermal catalytic reactor. As an option coal can be used as reductant as well as additional fuel. The process of reduction and calcination is very energy-optimized. It uses the off gas from the fluidized bed reduction reactor, which still contains sufficient energy to dry and calcine the nickel ore fines, in a primary stage circulating fluidized bed (CFB) reactor. The product shows high metallization of nickel and reduced iron oxides to the wuestite state. This results in considerable energy savings in smelting to ferronickel from the pre-reduced product. Alternatively the product can be leached to produce nickel. Laboratory tests showed a very high recovery of nickel and cobalt.

3:10 PM

Liquidus Temperatures of Ferro-Nickel Smelting Slags: Shengqi Chen¹; Lourens Erasmus²; Steve C.C. Barnett³; Evgueni Jak¹; *Peter Charles Hayes*¹; ¹University of Queensland, Pyrometall. Rsch. Ctr., Frank White Bldg., Brisbane, Qld 4072 Australia; ²Samancor Chromium, Simmons St., Johannesburg S. Africa; ³BHPBilliton, Stainless Steel Matls., Neathouse Place, London SW1V 1BH England

The reduction smelting of nickel laterites produces slag, consisting principally of the chemical components MgO, "FeO", SiO₂, and Al₂O₃, and ferro-nickel alloy. Despite the fact that the phase equilibria for the ternary MgO-"FeO"-SiO₂ up to 1500°C is well established limited experimental data are available in the MgO-"FeO"-SiO₂-Al₂O₃ system, which is relevant to commercial operation of the process. A methodology has been developed for the experimental investigation of the liquidus temperatures for the multi-component system MgO-"FeO" - SiO₂-Al₂O₃-Cr₂O₃ in equilibrium with metallic iron. Experiments have been carried out using high temperature equilibration, quenching, followed by electron probe X-ray microanalysis (EPMA). Liquidus temperatures have been determined in the silica primary phase field in the composition ranges directly relevant to the Cerro Matoso S.A. ferro-

nickel smelting slag. Liquidus isotherms have been determined for temperatures between 1450 to 1600°C. The study enables the liquidus to be described for a range of MgO/FeO ratios. It was found that liquidus temperatures in the silica primary phase field decrease significantly with the addition of Al₂O₃.

3:30 PM

Dust Issues from Rotary Devices: Causes and Cures: *Ronald K. Riddle*¹; ¹FFE Minerals, Pyro Tech. Grp., 3235 Schoenersville Rd., Bethlehem, PA 18016-0810 USA

The processing of lateritic ores in rotary drying and preheating/pre-reduction systems has historically been plagued by problems associated with significant dust generation. These problems include handling issues, kiln capacity limitations, negative impacts on furnace stability, a reduction in nickel recovery and higher operating costs. The dust is formed in the rotary devices during heating and tumbling due to the following three mechanisms: (1) mechanical decrepitation of the ore as a result of tumbling and attrition, (2) thermal decrepitation during rapid vaporization of internal free and bound water, and the (3) loss of free moisture which functions as a binder. This paper investigates the causes of dust formation, provides methods to reduce dust carryover from the rotary devices, describes systems for the handling and transportation of dust, and finally offers methods to recover the dust in the existing pyrometallurgical process.

3:50 PM Break

4:00 PM

Nickel Ore Treatment in Rotary Kilns and Cyclone Reactors: *Norbert Patzelt*¹; Thomas Schmitz¹; Guido Grund¹; ¹Polysius AG, Dept. Minerals, Graf-Galen-Strasse 17, Beckum D-59269 Germany

The demand for nickel is growing and will continue to do so for the foreseeable future. This will make the construction of new leaching and smelting plants necessary. This paper described a number of possible alternative processes. The first projects with new technology are currently undergoing trials and feasibility studies. Experience from other industrial sectors and from existing plants is being incorporated into these investigations. The question is, to what extent the old nickel producing concepts will continue to be applied in the future

4:20 PM

Developments in Integrated Furnace Controls to Enhance Furnace Operation and Crucible Integrity in Shielded-Arc Laterite Smelting: *Frank Allan Stober*¹; Terry Gerritsen¹; Jakob Janzen¹; Andre Kepes¹; ¹Hatch, Tech., 2800 Speakman Dr., Sheridan Sci. & Tech. Park, Mississauga, Ontario L5K 2R7 Canada

The paper describes the development of components in an Integrated Furnace Control system for shielded-arc smelting focusing on operation and crucible integrity enhancement. The paper reviews the mechanisms of power, feed and energy input and losses into the shielded-arc smelting process and describes the furnace control system module development and integration to tailor the process. The ultimate success of a furnace control system application is transfer of knowledge, training, and operational support during furnace start-up and ramp-up phases and model for how this has been achieved is discussed. The control modules of a shielded-arc laterite smelting furnace are described in detail including measured results and screen captures from application in laterite smelting furnaces. This paper focuses on developments in Integrated Furnace Controls tailored to shielded-arc laterite smelting but development of common furnace control modules for improved crucible and tapping operation integrity applied to other furnace processes including immersed-arc smelting are covered.

4:40 PM

Furnace Technology for Ferro-Nickel Production – An Update: *N. Voermann*¹; T. Gerritsen¹; I. Candy¹; F. Stober¹; A. Matyas¹; ¹HATCH, 2800 Speakman Dr., Mississauga, Ontario L5K 2R7 Canada

This paper describes developments in ferro-nickel furnace technology, specifically improvements to cooling methods, furnace controls, and high voltage furnace operating regime. The evolution of these technologies is briefly presented, as context for describing the current state of the art that has enabled ferro-nickel furnace operation at over 75 MW and specific energy consumption of less than 400 kWh/t dry ore. Examples from existing operations are used to illustrate present best practices, and potential future trends are discussed. The paper begins with an overview of the fundamental aspects of pyrometallurgical treatment of lateritic ores that drive ferro-nickel furnace design. Furnace wall cooling methods are related to the requirements resulting from specific furnace process conditions, including slag and metal compositions, as well as arc and bath power. The benefits of high productivity and low specific energy consumption resulting from high voltage (shielded-arc) operating practice are dis-

cussed, along with the furnace controls and electrical power train that enable such operation even with captive power generation. This paper is an update to that which the authors prepared for the Infacon X ferro-alloys conference.

5:00 PM

SPLC - A Power Supply for Smelting Furnaces: *Terry Gerritsen¹; Tom Ma¹; Mohammed Sedighy¹; Jakob Janzen¹; Frank A. Stober¹; Nils Voermann¹; ¹Hatch Associates, 2800 Speakman Dr., Mississauga, Ontario L5K 2R7 Canada*

Electrode control systems regulate power by physically positioning electrodes. Due to the size and weight of the electrodes, this is a slow process where power fluctuations of less than a few seconds are not fully corrected. Nickel laterite AC furnaces operating in high voltage, shielded arc mode typically incur frequent power variations of approximately +/- 20% around the power set point. To provide enhanced power control, Hatch has recently supplied, at commercial scale, a thyristor-switched reactance system called an SPLC. The SPLC incorporates predictive control software to operate furnaces at the maximum transformer rating by reducing the large power swings experienced without the SPLC. The resulting higher average power enables higher production, without increasing transformer or power plant capacity. A 60 MW production version of the SPLC has been commissioned on Falconbridge Dominicana's laterite nickel furnace, yielding excellent results with a 3 to 1 reduction in power fluctuations.

Lead-Free Solders and Processing Issues Relevant to Microelectronic Packaging: Electromigration and Creep in Leadfree Solders

Sponsored by: Electronic, Magnetic & Photonic Materials Division, EMPMD-Electronic Packaging and Interconnection Materials Committee

Program Organizers: Laura J. Turbini, University of Toronto, Center for Microelectronic Assembly & Packaging, Toronto, ON M5S 3E4 Canada; Srinivas Chada, Jabil Circuit, Inc., FAR Lab/Advanced Manufacturing Technology, St. Petersburg, FL 33716 USA; Sung K. Kang, IBM, T. J. Watson Research Center, Yorktown Heights, NY 10598 USA; Kwang-Lung Lin, National Cheng Kung University, Department of Materials Science and Engineering, Tainan 70101 Taiwan; Michael R. Notis, Lehigh University, Department of Materials Science and Engineering, Bethlehem, PA 18015 USA; Jin Yu, Korea Advanced Institute of Science and Technology, Center for Electronic Packaging Materials, Department of Materials Science & Engineering, Daejeon 305-701 Korea

Tuesday PM Room: 219B
March 16, 2004 Location: Charlotte Convention Center

Session Chairs: Jin Yu, Korea Advanced Institute of Science and Technology, Ctr. for Elect. Pkgt. Matls., Dept. of Matls. Sci. & Engrg., Daejeon 305-701 Korea; Paul T. Vianco, Sandia National Laboratories, MS0889, Albuquerque, NM 87185-0889 USA

2:00 PM

Creep of Pb-Free Solder Joints at Small Length Scales: *Matthew Kerr¹; Nik Chawla¹; Fay Hua²; ¹Arizona State University, Dept. of Chem. & Matls. Engrg., PO Box 876006, Tempe, AZ 85287-6006 USA; ²Intel Corporation, Santa Clara, CA USA*

The differences in the thermal expansion coefficient between components in an electronic package generate shear stresses in the solder. In particular, the behavior of the solder under creep conditions is quite important because of the long-term nature of the applied stress. The microstructure of bulk solder may be quite different from that of the solder sphere, because of differences in cooling rate that arise from the differences in surface-to-volume ratio. Thus, the correlation of bulk creep data to the creep behavior at smaller length scales may be misleading. In this talk, we report on the creep behavior of individual solder spheres. Sn-3.5wt% Ag solder spheres, 1 mm in diameter, were reflowed onto copper substrates to form lap shear specimens and creep tests were performed. The specimens were tested over a temperatures range between 25 to 130°C. Microstructure of the joints upon reflow and the evolution of damage during creep were characterized. The stress exponents and activation energies for creep were determined, and these will be described in terms of the underlying mechanisms for creep deformation in these materials.

2:20 PM

Role of Grain Boundary Sliding in Creep of Pb-Free Solders: *Felipe A. Ochoa¹; Rajen Sidhu¹; Xin Deng¹; Nikhilesh Chawla¹; ¹Arizona State University, Dept. of Chem. & Matls. Engrg., PO Box 876006, Tempe, AZ 85287-6006 USA*

While the creep behavior of Pb-free solders has been studied extensively, there appears to be a lack of consensus on the underlying creep deformation mechanisms. Two major creep mechanisms have been proposed in the literature: (a) Thermally-induced climb of dislocations over fine intermetallic particles (such as Ag₃Sn) and (b) grain boundary sliding (GBS). In this talk, we report on a systematic study on the role of GBS in creep of bulk Sn-3.5 wt% Ag solder alloys at 60°C and 120°C. The solder microstructure was varied by cooling at two different rates: 24°C/s (finer microstructure) and 0.08°C/s (coarser microstructure). Fiducial lines were inscribed on the solder surface and creep tests were interrupted to quantify the evolution of microstructure and strain due to GBS. The microstructure evolution due to creep deformation was characterized using atomic force microscopy (AFM) and scanning electron microscopy (SEM). Measurements of the transverse offset in the fiducial marks were carried out and the strain due to GBS was quantified. It will be shown that, in general, the strain due to GBS is quite inhomogeneous and is a small fraction of the total creep strain (in the primary and steady-state creep regimes), although the contribution of GBS varies with temperature and microstructure.

2:40 PM Invited

The Compression Creep Behavior of Sn-Ag-0.6Cu Solder: *Paul T. Vianco¹; Jerome A. Rejent¹; J. Mark Grazier¹; ¹Sandia National Laboratories, PO Box 5800, MS0889, Albuquerque, NM 87185-0889 USA*

Unified creep-plasticity models, which predict the reliability of Pb-free solder interconnections, incorporate time independent (stress-strain) and time dependent (creep) deformation in the constitutive equation. The creep behavior of the 95.5Sn-3.9Ag-0.6Cu (wt.%) solder was studied with the constant load compression technique. Samples were evaluated in the as-fabricated condition and following aging treatments for 24 hours at 125C or 150C. Test temperatures ranged from -25C to 160C and true stresses of 2 to 40 MPa. The steady-state strain rate kinetics were temperature dependent, indicating a fast diffusion process at T<75C and bulk diffusion process at T>75C. The stress magnitude caused only a subtle power law breakdown effect. The aging treatments impacted creep behavior, albeit, there was no noticeable change to solder microstructure. Sandia is a multi-program laboratory operated by Sandia Corporation, a Lockheed Martin Company, for the United States Department of Energy under Contract DE-AC04-94AL85000.

3:05 PM

Accelerated Thermal Fatigue of Lead-Free Solder Joints as a Function of Reflow Cooling Rate: *Yan Qi¹; Mike Agia²; Hamid Raza Ghorbani¹; Polina Snugovsky³; Jan K. Spelt¹; ¹University of Toronto, Mech. & Industrial Engrg., 5 King's College Rd., Toronto, ON M5S 3G8 Canada; ²Digital Security Controls Ltd., 3301 Langstaff Rd., Concord, ON L4K 4L2 Canada; ³Celestica, 20/429, 844 Kon Mills Rd., Toronto, ON M3C 1V7 Canada*

The introduction of lead-free solders has focused the need to better understand their thermomechanical behavior. In this paper we examine lead-free solder joints reliability as a function of reflow cooling rate. The test vehicle was a Leadless Chip Resistor assembly, manufactured using both traditional SnPb and lead-free (Sn3.8Ag0.7Cu) solders. The lead-free LCR test vehicles were assembled using three different cooling rates. They were then exposed to an accelerated thermal cycling (ATC). The test results indicated that lead-free solder joints have better creep-fatigue performance compared with the SnPb solder joints while the lead-free LCR built with medium cooling rate showed the longest fatigue life. The number of cycles to failure was significantly correlated to the void defect rate and interface microstructures. Failure analyses were done using cross-sectioning methods and SEM.

3:25 PM

The Creep Properties of Sn Joints: *Ho Geon Song¹; John William Morris¹; Fay Hua²; ¹University of California, Matls. Sci., One Cyclotron Rd., Bldg. 66R0200-8254, Berkeley, CA 94720 USA; ²Intel Corp., Matls. Tech. Operation, 3065 Bowers Ave., Santa Clara, CA 95054 USA*

Creep tests on solder joints of Sn-rich, Pb-free solders show anomalies in creep behavior at temperatures near room temperature. The anomalies include a strong temperature dependence of both the stress exponent and the apparent activation energy. The anomalies appear to have their source in the behavior of the Sn constituent itself. The

microstructures of these solders are, primarily, Sn, and test joints of pure Sn show the same anomalies. The present paper discusses this anomalous behavior in terms of the creep behavior of pure Sn and the microstructures of the solder joints.

3:45 PM Break

3:55 PM Invited

The Effect of IMC Morphology on Cu Diffusion in Sn-Ag and Sn-Pb Solder Bump on Ni/Cu UBM: *Chien Sheng Huang¹; Guh Yaw Jang¹; Jeng Gong Duh¹*; ¹National Tsing Hua University, Dept. of Matls. Sci. & Engrg., 101, Sect. 2 Kuang Fu Rd., Hsinchu 300 Taiwan

The eutectic Sn-Ag solder alloy is one of strong candidates to replace the conventional Sn-Pb solder. In this study, diffusion behaviors of Cu in eutectic Sn-Ag and Sn-Pb solder with Ni/Cu under bump metallization (UBM) were investigated with a joint assembly of solder/Ni/Cu/Ti/Si₃N₄/Si multiplayer structure. The atomic flux of Cu diffused through Ni was evaluated by detailed quantitative analysis in an electron probe microanalyzer. The atomic flux of Cu diffusion in the Sn-Pb system was rather larger than that in the Sn-Ag system. With regard to the amounts of Cu diffusion, they increased dramatically during reflow in the Sn-Pb system. However, they remained identical in the Sn-Ag case. The distinct diffusion behaviors between these two systems could be related to the microstructure evolution and grain size of intermetallic compound (IMC). The role played by the IMC in the Cu diffusion from the UBM toward the solder bump was probed and discussed.

4:20 PM

Ultra Fast Cu Dissolution Induced by Electric Current in Flip Chip Solder Joints: *C. M. Tsai¹; Y. H. Lin¹; Y. C. Hu¹; Y. L. Lin¹; C. Robert Kao¹*; ¹National Central University, Dept. of Chem. & Matls. Engrg., Chungli City 320 Taiwan

The effect of electric current on the failure mechanism of flip chip solder joints was studied. The solder used was Pb-Sn eutectic, and the joints had a diameter of 100 micron. The soldering pad on the chip-side had a Cu metallurgy, and that on the board-side had an Au/Ni/Cu metallurgy. The flip chip packages were placed in an oven set at 100°C, with 2x10⁴ A/cm² electric current passing through some of the joints in the packages. The rest of the solder joints, which were in the same package but without current passing through, were used as control. A new failure mode induced by the electric current was found. The joints failed by very extensive Cu dissolution on the chip-side. Not only part of the Cu soldering pad was dissolved, but also part of the internal Cu conducting trace within the chip. The dissolved region was back-filled with solder. Large amount of Cu₆Sn₅ intermetallic was present inside the solder joint. The source of Cu in Cu₆Sn₅ was from the dissolved Cu pad and trace. The site of failure was at the conducting trace that had been back-filled with solder, where a much greater current density was present due to a smaller cross-section.

4:40 PM

Behavior of Eutectic Sn-Zn, Sn-Ag and Sn-Pb Solders Under High Current Stressing Conditions: *Jenn-Ming Song¹*; Dong-Yuan Tsai¹; Truan-Sheng Lui¹; Li-Hui Chen¹; ¹National Cheng Kung University, Dept. of Matls. Sci. & Engrg., Tainan 701 Taiwan

Due to the trend of miniaturization and subsequent high interconnect density, solder joints may suffer a high density current. This study aims to explore the behavior of some two-phase eutectic solder alloys, Sn-Pb, Sn-Zn and Sn-Ag, under high current-stressing. Results show that when the current is raised constantly, there exists a critical current for the solder strip to break off. It can be also found that the critical current varies directly with the electrical conductivity. Sn-Zn with the lowest electrical resistance possesses a higher critical current to failure than Sn-Ag, and also higher than Sn-Pb. This is closely related to the microstructural characteristics.

5:00 PM

Electromigration Studies on Lead-Free Sn(Cu) and Sn(Ni) Solder Stripes: *C. C. Wei¹; C. Y. Liu¹*; ¹National Central University, Chem. Engrg. & Matls. Engrg., No. 300 Jung-Da Rd., Chung-Li Taiwan

Blech structure of Sn-based alloys stripes were fabricated by lithography method on Si substrate. The thickness of solder stripes were about 2 micrometers and the lengths of Sn alloys stripes are ranging from 50 µm to 1 cm. Under the EM (Electromigration) tests with 104 A/cm² current stressing, the voiding area and hillocks were observed at the cathode and anode side, respectively. Since EM rate could be determined by the depletion area at the cathode side, the important Cu and Ni alloying effects on EM rate were observed. Besides, our preliminary results imply that the length of solder stripe show no significant influence on the EM rate. The possible mechanism of alloying and length effects will be proposed and discussed in this talk. Also, we will report

the effect of current gradient by using the so-called hang-over structure at the cathode side.

5:20 PM

Electromigration on Electronic Components: *(Susan) Xiaoxin Xia¹; John W. Denning¹; Richard Griese¹*; ¹Northrop Grumman Space Technology, Elect. Production Tech. Ctr., One Space Park, M573, R6/1587, Redondo Beach, CA 90287 USA

Electromigration induced short circuit was observed on a single four pin DC connector during electrical testing. Optical and scanning electron microscope (SEM) analyses exhibited surface contamination and dendritic growth between the connector pin and ground, which led to the electrical shortage and component failure. The conductors were soldered using Pb88Sn10Ag02 solder and no-clean flux. EDX analysis revealed that dendrites contained high Pb, O and C. It indicated that lead in the solder migrated and formed an electrical short from the connector pin to ground. The electromigration on the connector was probably related to the processing induced thermal stress. This stress can generate electrical potential and form electrical circuit, thus caused electromigration and mass transportation between the low and high stress concentration areas on the component. Temperature, stress distribution, chemical composition and microstructure of the electronic devices are main contributions to the electromigration. Moisture is known to be an accelerator. The mechanisms and effects of temperature, thermal stress and grain boundaries on electromigration are discussed in this paper.

5:40 PM

Electromigration in SnAg3.8Cu0.7 Lead-Free Solder Thin Film Lines: *Ying Chao Hsu¹; Chih Chen¹*; ¹National Chao Tung University, Dept. of Matls. Sci. & Engrg., 1001 Ta Hsueh Rd., Hin Chu 300 Taiwan

A novel method for preparing thin film solder lines has been developed. Electromigration of lead-free SnAg3.8Cu0.7 solder thin film lines was studied under high current densities and various temperature. To measure the activation energy for electromigration, samples has been stressed at 50°C, 100°C, and 150°C. Electromigration rate is obtained by measuring the void volume near the cathode end. Effective charge numbers, Z*, is also measured from the depletion near the cathode. By applying various current density from 1 x 10⁴ A/cm² to 1 x 10⁵ A/cm², threshold current density has been obtained.

Magnesium Technology 2004: Primary Processing and Environmental Issues

Sponsored by: Light Metals Division, LMD-Magnesium Committee
Program Organizer: Alan A. Luo, General Motors, Materials and Processes Laboratory, Warren, MI 48090-9055 USA

Tuesday PM

March 16, 2004

Room: 203B

Location: Charlotte Convention Center

Session Chairs: Howard Kaplan, US Magnesium LLC, Salt Lake City, UT 84116 USA; Ramaswami Neelameggham, US Magnesium LLC, Salt Lake City, UT 84116 USA

2:00 PM

A New Technique of Magnesium Electrolysis With Bischofite From Qinghai Salt Lakes in China: *Huimin Lu¹; Lanlan Yu¹; Ruixin Ma¹; Yitian Liang²; Bei Liang²; Youkun Yang²*; ¹University of Science and Technology, Metall. Engrg. Sch., Light Metal Inst., 30 Xueyuan Rd., Beijing 100083 China; ²Qinghai University, Non-Ferrous Metal Metallurg. Rsch. Inst., 97 Ningzhang Rd., Xining, Qinghai 810016 China

Qinghai salt lakes in China have plenty of magnesium and potassium resources. Every year, Potassium fertilizer is produced with the by-product of bischofite. At present, bischofite cannot be used and is discarded. This cause not only the waste of resources, but also the formation of magnesium harm to the ecological environment. Therefore, comprehensive utilization of bischofite is emergent. This paper presents a combined process of comprehensive using bischofite: preparation of magnesia with ammonia and direct electrolysis of magnesia with the RECl₃-MgCl₂ system as support electrolyte. This process produces magnesium with the by-product of magnesia with 99.5% of purity, the current efficiency is 90%, the energy consumption is 11.5kWh/kg Mg and carbon dioxide is discharged on carbon anode. This new technique has low energy consumption, high current efficiency and less pollution for the environment.

2:20 PM

Experimental Observations on the Use of a Hydrogen Anode in the Production of Electrolytic Magnesium: *Gus Van Weert*¹; Mazi Rejaee²; ¹ORETOME Limited, Caledon, ON Canada; ²CELLMAG Inc., Montreal, QC Canada

Most electrolytic magnesium metal production utilizes a magnesium oxide feed material. One process route requires hydrochloric acid for feed dissolution, which in turn requires cleaning, drying, compression and combustion of the chlorine gas produced in the electrowinning process. An alternative route utilizes the chlorine in the anhydrous reduction of MgO to MgCl₂. Either operation constitutes a significant part of the capital investment and operating cost of an electrolytic magnesium facility. This work explores the concept of producing hydrogen chloride gas on the anode in molten salt electrowinning of magnesium metal, which in addition to offering capital savings can also lower the cell voltage by one (1) Volt compared to chlorine gas evolution. The experimental cell used in the testwork is described and results are presented.

2:40 PM

Production of Dense Rod from Magnesium Swarf for Re-Melting: *Rimma Lapovok*¹; P. F. Thomson¹; ¹Monash University, CAST CRC, SPME, Clayton, Vic, 3800, Melbourne Australia

This work was aimed on investigation of swarf compaction technique leading to increase recovery rate of Mg in re-melting due to eliminating melting losses at the surfaces and decrease hazards of transportation of swarf. The new method to enhance compaction to the density of bulk magnesium is developed, namely Equal Channel Angular Extrusion (ECAE) with back-pressure. It was found that ECAE promotes compaction very effectively. Parameters affecting the compaction process were investigated. This technique still has a disadvantage of high surface to volume ratio leading to melt losses, high oxide content and hazards during transportation. The role of grease and other contaminants, lubricants, oxide films and the need to remove them, were also considered. It was shown by re-melting experiments that recovery of magnesium increased significantly to 77% for swarf uncleaned from machining oil and to 92-96% for a cleaned swarf. The comparison with conventional technology of briquetting of swarf has been done. The briquetting technique allows to produce batches with density of 1.4-1.5 g/cm³ and has shown the recovery rate of 46 and 68% for cleaned and uncleaned swarf respectively.

3:00 PM

Study of Electrolyte Impurities Effect on the Magnesium Oxides Speciation Techniques: *Sina Kashani-Nejad*¹; Ka Wing Ng¹; Ralph Harris¹; ¹McGill University, Mining, Metals & Matls. Engrg., 3610 Univ. St., Wong Bldg., Montreal, Quebec H3A 2B2 Canada

Oxide containing compounds in the electrolytic magnesium production processes can be present either in the form of MgO or as "hydroxychlorides". The physical and chemical properties of MgO as an insoluble specie in the electrolyte are different from those of the soluble hydroxychlorides such that they have differing effects on the magnesium production process. As a result, oxide speciation techniques have been developed for process control and optimization. Industrial electrolytes also contain minor element impurities in the form of oxides, chlorides and fluorides as well as metallic particles. These impurities can interfere with the speciation procedure and considerably degrade the accuracy of the speciation measurements. In this work, different electrolyte impurities and their effect on currently available speciation techniques were studied. Also the distribution of the impurities based on their solubility in the electrolyte, is presented.

3:20 PM

Qualitative Characterization of MgOHCl/MgO Mixture with Infrared Spectroscopy (IR): *Sina Kashani-Nejad*¹; Ka Wing Ng¹; Ralph Harris¹; ¹McGill University, Mining, Metals & Matls. Engrg., 3610 Univ. St., Wong Bldg., Montreal, Quebec H2W 1S7 Canada

Oxide species are detrimental to the electrolytic magnesium production processes and severely lower the efficiency of electrolytic cells. These oxides are either in the form of MgO or Hydroxychlorides. As the result, it is possible to use infrared spectrometry for the characterization of hydroxyl ion bounded to the magnesium chloride in an isolated mixture of magnesium oxides. This paper describes an analytical procedure for the IR spectrometry of magnesium oxides. It was found essential to eliminate water interference by using methanol leaching prior to the IR analysis. It was also found that MgOHCl characteristic absorption peak is located at 3550 cm⁻¹ and change in the composition and crystal structure of the hydroxychlorides shifts the characteristic hydroxyl absorption peak from 3550 cm⁻¹ to 3720 cm⁻¹.

3:40 PM Break**3:50 PM**

The Environmental Impact of New Magnesium Alloys on the Transportation Industry: *Eli Aghion*¹; Boris Bronfin¹; Zeev Rubinovich¹; ¹Dead Sea Magnesium Ltd., Rsch., POB 1195, Beer-Sheva 84111 Israel

The increased environmental demand from the transportation industry to reduce CO₂ emissions by 30% till 2010 generated various actions aiming at addressing this demand. One of the most important solutions is weight reduction, which can be implemented by using light structural materials and Mg alloys particular. Currently the properties of the existing Mg alloys are limited. Many applications that require an adequate combination of cost competitiveness and properties such as increased creep, ductility and corrosion resistance are difficult to address. The present paper aims at evaluating the transportation's industry requirements in terms of combined properties and processing technologies. The major focus will be directed to new Mg alloys and the prospects that they may introduce. This will be related to casting and wrought magnesium alloys for practical applications such as engine blocks, gearbox housings, oil pumps, instrumental panels, thin wall body parts, seat frames and road wheels. Special attention will be given to the affordability of new alloys in terms cost of raw material and process technologies. The paper will also try to identify the main stream of alloys development programs and their compatibility with the 21st century transportation requirements. This will relate to particular examples such as presented by electric cars and secondary structures and systems in aerospace applications.

4:10 PM Cancelled

Protective System for Magnesium Melt

4:30 PM

A Comparison of the Greenhouse Impact of Magnesium Produced by Pidgeon and Electrolytic Processes: *Subramania Ramakrishnan*¹; Paul Koltun¹; ¹CSIRO, Mfg. & Infrastruct. Tech., Locked Bag No. 9, Preston, Vic 3072 Australia

The growing use of lightweight magnesium components in automobiles to reduce greenhouse emission requires a clear understanding of the life cycle greenhouse impact of producing magnesium. There are two practical methods for producing magnesium: (i) electrolysis of magnesium chloride; and (ii) reduction of magnesium oxide with ferrosilicon by a thermal process, known as the Pidgeon process. The Pidgeon process is used mainly in China, which now supplies approximately 40% of the world demand for magnesium. This paper compares the results of the life cycle greenhouse impact of the magnesium or magnesium alloy ingots produced by these two methods, by using realistic life cycle inventory data for the two routes. The paper considers the following two cradle-to-gate product systems: (i) Magnesite entering the system is processed using the Australian Magnesium process to deliver magnesium alloy ingots; and (ii) Dolomite ore is calcined and reduced in China using the Pidgeon process to produce metal ingots. The cradle-to-gate impacts of the ingots produced by the two product systems are estimated in terms of kg of carbon dioxide equivalent (kg CO₂-e) for a product functional unit of 1 kg of magnesium alloy ingot. The study shows that the cradle-to-gate GHG impact of Chinese magnesium ingots is ~ 42 kg CO₂-e/kg Mg ingot. This value is based on the current usage of sulphur powder for blanketing molten magnesium while casting. The GHG emission of the ingots produced by the Australian Magnesium process is approximately 24 kg CO₂-e/kg of Mg ingot. The Australian Magnesium process is assumed to use HFC-134a as the cover gas, and electricity is generated using Australian black coal. The sensitivity of the results to the cover gas used for melt protection, and to the geographical location of alloying plants are discussed in the paper.

4:50 PM

Collaborative Study of Protective Cover Gas Reaction Products: *Scott Charles Bartos*¹; ¹U.S. Environmental Protection Agency, Climate Protection Partnerships Div., 1200 Penn. Ave. NW 6202J, Washington, DC 20460 USA

Historically, the magnesium industry has primarily used sulfur hexafluoride (SF₆) as a cover gas to inhibit surface oxidation, which can result in fires if not controlled. Modern science has determined SF₆ to be an extremely potent and long-lived greenhouse gas. The magnesium industry, working in cooperation with national governments, is making great strides towards implementing more environmentally friendly cover gases. Some of the cover gases identified are strong greenhouse gases themselves or the gas may generate potent global warming byproducts (e.g., PFCs) in a magnesium furnace environment. This measurement study builds upon EPA's previous investigation of SF₆ cover gas reactions with molten magnesium to deter-

mine the level of input gas destruction and identify emissions of concern to human health and the environment.

Materials by Design: Atoms to Applications: Designing Nanostructures

Sponsored by: Electronic, Magnetic & Photonic Materials Division, EMPMD/SMD-Chemistry & Physics of Materials Committee

Program Organizers: Krishna Rajan, Rensselaer Polytechnic Institute, Department of Materials Science and Engineering, Troy, NY 12180-3590 USA; Krishnan K. Sankaran, The Boeing Company, Phantom Works, St. Louis, MO 63166-0516 USA

Tuesday PM Room: 210B
March 16, 2004 Location: Charlotte Convention Center

Session Chair: B. B. Rath, Naval Research Laboratory, Washington, DC USA

2:00 PM

Films, Lines and Dots: Dimensional Effects on the Strength of Nanoscale Structures: *Krystyn J. Van Vliet*¹; Yoonjoon Choi¹; Ju Li²; Subra Suresh¹; ¹Massachusetts Institute of Technology, Matls. Sci. & Engrg., 77 Mass. Ave., Rm. 8-309, Cambridge, MA 02139 USA; ²Ohio State University, Matls. Sci. & Engrg., Columbus, OH 12345 USA

When the physical and microstructural dimensions of electronic/photonic structures are reduced to the nanometer scale, feature dimensions approach those typical of atomistic deformation processes. Thus, there is considerable interest in whether and how the mechanical integrity of critical components will be affected in this length scale regime. Here, we employ systematic experiments and computations to investigate the effects of dimensional constraint on the elastic and yielding characteristics of metallic thin films, lines and dots. We find that the resistance to plastic deformation is a strong function of dimensional constraint in nanoscale structures, and that these effects are modeled most accurately by atomistic simulations. From this synthesis of experiments and computations in a model system, we develop criteria to predict the mechanical behavior of nanoscale structures in current applications.

2:30 PM

Novel Nanostructured Materials by Design: *Jagdish Narayan*¹; ¹North Carolina State University, Matls. Sci. & Engrg., Raleigh, NC 27695 USA

We have developed a novel method based upon pulsed laser deposition to produce nanocrystalline metal, semiconductor and magnetic material thin films and composites. The size of nanocrystals was controlled by interfacial energy, number of monolayers and substrate temperature. By incorporating a few monolayers of W during PLD, the grain size of copper nanocrystals was reduced from 160nm (Cu on Si (100)) to 4nm for a multilayer (Cu/W/Cu/W/Si (100)) thin film. The hardness increased with decreasing grain size up to a certain value (7nm in the case of copper) and then decreased below this value. While the former is consistent with Hall-Petch model, the latter involves a new model based upon grain boundary shear and deformation. We have used the same PLD approach to the form nanocrystalline metal (Ni, Co, Fe embedded in -Al₂O₃ and MgO) and semiconductor (Si, Ge, ZnO, GaN embedded in AlN and -Al₂O₃) thin films. These nanocrystalline composites exhibit novel magnetic properties and novel optoelectronic properties with quantum confinement of electrons, holes and excitons in semiconductors. We review advanced PLD processing, detailed characterization, structure property correlations and potential applications of these materials.

3:00 PM

Nanostructured Magnetic Materials: *Mutsuhiro Shima*¹; ¹Rensselaer Polytechnic Institute, Dept. of Matls. Sci. & Engrg., Troy, NY 12180 USA

Finely structured magnetic materials attract a great deal of interest driven by emerging needs for nanotechnology applications.¹ Recently extensive efforts have been made to gain comprehensive and systematic understanding of synthesis-structure-property correlation in this class of materials, so that they can be predictably tailored as functional materials for specific applications. Knowledge available in the field until now clearly indicates that nanomagnets are useful for a range of applications including data storage and sensor devices as well as biomedical applications. Nanosized magnetic objects often exhibit a drastic change in the magnetic properties, depending on the fabrication

process and geometric factors such as size, shapes² and interfaces³ of the magnetic objects, where the thermal instability of magnetization becomes more significant.⁴ In the finite size regime materials can exhibit multiple phases depending on the size. For instance, it is well known that iron exists in different allotropic forms, where at ambient conditions the most stable phase is ferromagnetic body-centered cubic α -Fe and the face centered cubic γ -Fe is thermodynamically unstable and not ferromagnetic. We have found that iron catalyst nanoparticles trapped in carbon nanotubes form are indeed ferromagnetic γ -Fe at room temperature. The unusual magnetic moment observed for γ -Fe nanoparticles is explained by a lattice expansion due to insertion of carbon atoms into the interstitial sites. We have also recently demonstrated that magnetic nanoparticles can be grown onto sequenced peptide molecular nanotubes. Such a nano-scale magnetic structure can provide an excellent building block that permits engineering to design novel device architectures for future technological applications. In this paper our recent works on magnetic nanoparticles assembly with nanotubes will be presented. ¹S. D. Bader, *Surf. Sci.* 500, 172 (2002). ²M. Shima, M. Hwang and C. A. Ross, *J. Appl. Phys.* 93, 3440 (2003). ³R. M. Bhatkal and K. Rajan, *J. Electronic Mater.* 23, 907 (1994). ⁴X. Batlle and A. Labarta, *J. Phys. D* 35, R15 (2002).

3:30 PM Break

3:45 PM

Chemical Design of Inorganic Nanowires and Nanowire-Networks: *M. K. Sunkara*¹; ¹University of Louisville, Dept. of Chem. Engrg., Louisville, KY 40292 USA

Inorganic nanowires and nanotubes, if available in large quantities, could enable bottom-up assembly of next generation devices, sensors, thin films, composites and systems. In addition, the availability of several types of materials in nanowire format will speed up our studies on the physical and chemical behavior of low-dimensional solids. The progress in the synthesis of nanowires has been rapid but requires further innovation to be useful. In this regard, our group has focused on developing new concepts for bulk synthesis of nanowires for a variety of systems, i.e., metals, elemental semiconductors, oxides and nitrides. For example, we illustrated that multiple nucleation and growth of one-dimensional structures could occur out of immiscible molten metals. In addition to bulk synthesis of nanowires, we illustrated the formation of nanowire networks (nanowebs) by coalescence of nanowires during growth parallel to substrate. We acknowledge National Science Foundation and US AFOSR for financial support.

4:15 PM

First Principles Study of Spin Assisted Transport in Nanoscale Systems: *Saroj Nayak*¹; ¹Rensselaer Polytechnic Institute, Dept. of Physics, Troy, NY 12180-3590 USA

Electron transport through a single molecule attached to electrodes forms the core of molecular electronics. The coupling between a molecule and magnetic electrodes gives rise to new transport phenomena, such as spin-polarized electron transport. The use of an externally applied local magnetic field to obtain the anti-parallel spin alignment between two contacts separated by molecules of sub-nanometer length has been a daunting task and has hindered experimental investigation of spin transport behavior at the molecular level. Here, using parameter free first-principles density functional theory and the Landauer-Büttiker formalism, we study the spin-polarized transport in atomic and molecular wires. Quantum conductance calculations reveal that for the parallel alignment (ON) of spins at the opposite ends of the molecular wire, the conductance is significantly higher than that in the anti-parallel alignment (OFF). We also find, for the first time, that the ground state of such a system has the anti-parallel alignment suggesting that experiments could be performed in such a structure (with magnetic cluster contacts) where an external magnetic field would be needed only for the ferromagnetic alignment to turn from the OFF state to the ON state. This information will be critical to our understanding of the basic phenomena underlying the application of molecular systems to spintronics.

4:45 PM Invited

Modeling of Composites with Self-Assembling Micro- and Nanostructures: *Alexander L. Roytburd*¹; Julia Slutsker²; Andrei Artemev³; ¹University of Maryland, Matls. Sci. & Engrg., College Park, MD 20742 USA; ²National Institute of Standards and Technology, MSEL, Gaithersburg, MD 20899 USA; ³Carleton University, Mech. & Aeros. Engrg., Ottawa, ON Canada

The theory and phase-field modeling of formation and deformation of adaptive nano-composites containing polydomain martensitic layers are developed. It has been shown that superplastic and superelastic deformation of heterophase and polydomain martensite structures are reversible in the composites to the contrary to bulk shape memory

materials. The stress-strain constitutive equations are obtained for an adaptive composite. By the engineering of constraint controlled polydomain structures can be designed and characteristics of the superelastic and superplastic deformation can be optimized. This work is supported by AFOSR.

Materials Processing Fundamentals: Smelting and Refining

Sponsored by: Extraction & Processing Division, Materials Processing & Manufacturing Division, EPD-Process Fundamentals Committee, MPMD/EPD-Process Modeling Analysis & Control Committee

Program Organizers: Adam C. Powell, Massachusetts Institute of Technology, Department of Materials Science and Engineering, Cambridge, MA 02139-4307 USA; Princewill N. Anyalebechi, Grand Valley State University, L. V. Eberhard Center, Grand Rapids, MI 49504-6495 USA

Tuesday PM Room: 212B
March 16, 2004 Location: Charlotte Convention Center

Session Chair: TBA

2:30 PM

Method for Computation and Investigation of Thermal Performance of Flash Smelting Processes: *V. M. Paretsky*¹; ¹State Research Center of Russian Federation, State Rsch. Inst. of Nonferrous Metals, 13, Acad. Korolyov St., 129515 Moscow Russia

A method has been developed for definition of mathematical three-dimensional zonal models of heat exchange in autogenous smelting furnaces oxygen-flame furnace (KFP). The paper presents the results of studies into the thermal performance of an operating KFP-1 furnace at the Almalyk copper smelter in case of smelting of standard-grade concentrate and demonstrates the feasibility of the smelting process with burners located in the furnace roof without any furnace design modification. A full-scale KFP furnace with vertical arrangement of the flame has lining temperature lower by 110-175°C as compared with a similar furnace with horizontal burners and a similar cooling system; the offgas temperature at the furnace outlet decreases also by 52°C, while the temperatures of matte and slag at the furnace outlet virtually do not change. An analysis of the thermal efficiency of two design modifications of a planned KFP-2 furnace has been made for the second stage of the Almalyk copper smelter extension. Optimal cooling conditions for the furnace lining have been determined depending on the length of sulfide flame, feed charge supply rate and the heat generation by the feed charge.

2:55 PM

Distribution of Metals Between Highly Basic Slag and Nickel Matte in CaO-FeOx-FeS-Ni3S2 System: *V. M. Paretsky*¹; *A. V. Tarasov*¹; *S. D. Klushin*¹; ¹State Research Center of Russian Federation, State Rsch. Inst. of Nonferrous Metals, 13, Acad. Korolyov St., 129515 Moscow Russia

The experimental results demonstrated that, in the process of contacting of matte and ferrite-calcium slag, redistribution of nickel, cobalt, sulfur and iron between the phases took place and, at the same time, the number of phases changed. In tests with feed mattes containing from 15.0% to 57.9% Ni, the concentrations of non-ferrous metals in the bottom phase (sulfide-metal alloy) increased, while the iron and sulfur concentrations decreased. This fact was also confirmed by changes in the ferrite-calcium slag composition, i.e., increasing concentrations of sulfur and ferrous iron (along with a simultaneous decrease in the content of ferric iron). When converter matte (75.4% Ni) was used as feed sulfide material, then iron was transferred from slag to matte, probably. The new equilibrium state reached by the matte-slag system was to a substantial degree dependent on the oxidizing ability of the initial slag, i.e., the ratio of ferric to ferrous iron ions and the iron content in relation to the matte. The data obtained indicates that nickel losses can be reduced in the process of upgrading of matte with respect to non-ferrous metals by decreasing the degree of sulfidization (by increasing the metallization) of matte and by increasing the concentrations of calcium and aluminum oxides in the slag.

3:20 PM

Distribution of Metals Between Combined Slag and Nickel Converter Matte in CaO - FeOx - SiO2 - Ni3S2 System: *A. V. Tarasov*¹; *S. D. Klushin*¹; *V. M. Paretsky*¹; ¹State Research Center of

Russian Federation, State Rsch. Inst. of Nonferrous Metals, 13, Acad. Korolyov St., 129515 Moscow Russia

When studying the compositions of the mattes produced and equilibrium slags it was found that in case of contacting of molten converter matte with iron-containing slag saturated with Fe²⁺ a new equilibrium state was established and the concentrations of nickel and sulfur in the sulfide melt decreased, while that in the slag increased. In slags in equilibrium with mattes containing 67.1-71.3% Ni and 0.08-0.15% Ni the concentrations of nickel and cobalt were from 1.7% to 2.8% and from 0.03% to 0.06%, respectively. A change in the basicity (CaO / SiO₂) of the slag had an effect on the concentrations of non-ferrous metals in matte and slag, as well as on the distribution coefficients of $\frac{[Ni]}{[Ni]_{slag}}$ and $\frac{[S]}{[S]_{slag}}$ and sulfur. High nickel and cobalt distribution coefficients were obtained when using slags containing over 16% CaO. Factors have been identified which permit control of the metals distribution (Ni and Co) between matte and slag in the FeOx - CaO - SiO₂ - Ni₃S₂ system. By changing the degree of matte sulfidization and the basicity of slag, it is possible to transfer the bulk of cobalt into slag, minimizing thereby the loss of nickel.

3:45 PM

Behavior of Zinc in Oxide-Sulfide Melts: *A. V. Tarasov*¹; ¹State Research Center of Russian Federation, State Rsch. Inst. of Nonferrous Metals, 13, Acad. Korolyov St., 129515 Moscow Russia

Studies into the effect of temperature (1200-1300°C), oxygen content of the gaseous phase (50% to 70% by vol.) and the composition of the sulfide melt of Cu - Fe - Zn - S system (40% to 60% Cu and 3% to 8% Zn by weight) on the degree of transfer of zinc to oxide melt under conditions of complete desulfurization have been carried out using methods of integrated thermal analysis and chemical analysis of smelting products. It has been found that depending on the smelting conditions the degree of zinc transfer into oxide melt varies from 61% to 100%. Investigations of zinc sulfide behavior under a layer of slag containing magnetite have shown that zinc sulfide dissolved in the slag is oxidized by magnetite to form zinc oxide and sulfur dioxide. Zinc oxide is reduced by ferrous iron contained in the slag resulting in zinc vapor formation. The constant of zinc evaporation rate from the melt is virtually dependent on the smelting temperature. The experimental results obtained in the process of investigations have been used for selection of process conditions for pilot-scale tests of smelting of copper-zinc sulfide concentrates in molten bath.

4:10 PM Break

4:20 PM

NiModel - A Thermodynamic Model and Computer Program of Nickel Smelting and Converting Processes: *Pengfu Tan*¹; ¹Portovesme Nonferrous Metallurgy Company, S. P. n. 2 - Carbonia/Portoscuso - km. 16.5, Portoscuso, CA I-09010 Italy

NiModel, a thermodynamic model, database and computer program, has been developed to predict the distribution behavior of Ni, Cu, Co, Fe, S, O, As, Sb and Bi, and heat balance in the nickel pyrometallurgical processes such as Outokumpu flash smelting, Outokumpu direct high-grade matte smelting, INCO flash smelting, and Peirce-Smith converting processes. In this model, as much as 16 elements (Ni, Cu, Co, Fe, As, Sb, Bi, S, O, Al, Ca, Mg, Si, N, C and H) are considered. The model predictions were compared with the known industrial data from Kalgoorlie Nickel Smelter in Australia, Outokumpu Harjavalta Nickel Smelter in Finland and INCO Metals Company in Canada, and an excellent agreement was obtained. In this paper, the applications of NiModel in the nickel pyro-metallurgical industries have been presented. NiModel has been used by Jinchuan Group Limited in China plant.

4:45 PM

CuModel - A Thermodynamic Model of Copper Smelting and Converting Processes and its Applications in the Industry: *Pengfu Tan*¹; ¹Portovesme Nonferrous Metallurgical Company, S. P. n. 2 - Carbonia/Portoscuso - km. 16.5, Portoscuso, CA I-09010 Italy

A thermodynamic model, database and software, CuModel, has been developed to simulate the element distribution behaviors, and heat balance in copper smelting process, matte converting process and copper continuous smelting process. In this model, 21 elements (Cu, S, Fe, Ni, Co, Sn, As, Sb, Bi, Pb, Zn, Au, Ag, O, N, C, H, Ca, Mg, Al and Si) are considered. It can be predicted for any set of controllable process parameters such as feed composition, smelting temperature, degree of oxygen enrichment and volume of oxygen enriched air. This model accounts for physical entrainment in the melts. The predictions by the present computer model are compared with the known commercial data from several companies, good agreements are obtained. The model has been used to optimize the actual industrial operating condi-

TUESDAY PM

tions of flash furnace at Guixi Smelter in China and PASAR in Philippines, and Noranda furnace at Daiye Smelter in China.

5:10 PM

Comparison of Two Control Strategies of the Vanadium Roast Process: *Bernhard Voglauer*¹; Wolfgang Geyrhofer¹; Hanns Peter Jörgl¹; ¹Vienna University of Technology, Inst. for Machine & Proc. Automation, Gusshausstraße 27-29, E 328, Vienna 1040 Austria

A well known routine for the production of vanadium is alkaline roasting of steel slag in a multiple hearth furnace or rotary kiln. Previous work concerning this process was carried out by the authors and contains the design of a dynamic model capable of calculating mass flow, temperature and concentrations of major components in a multiple hearth furnace, an empirically obtained model of the chemical reaction kinetics and a controller design mainly based on operational knowledge of an industry scale plant. The current work compares the performance of a model based control system to the previously published knowledge based control system. The knowledge based control system represents a robust system due to the implementation of expert knowledge gained in many years of manual control. The comparison shall show expected advances of process efficiency by the use of advanced control strategies.

Nanostructured Magnetic Materials: Self Assembly and Patterned Nanostructures

Sponsored by: Electronic, Magnetic & Photonic Materials Division, EMPMD-Superconducting and Magnetic Materials Committee, EMPMD-Nanomaterials Committee

Program Organizers: Ashutosh Tiwari, North Carolina State University, Department of Materials Science & Engineering, Raleigh, NC 27695-7916 USA; Rasmi R. Das, University of Wisconsin, Applied Superconductivity Center, Materials Science and Engineering Department, Madison, WI 53706-1609 USA; Ramamoorthy Ramesh, University of Maryland, Department of Materials and Nuclear Engineering, College Park, MD 20742 USA

Tuesday PM Room: 215
March 16, 2004 Location: Charlotte Convention Center

Session Chair: TBA

2:00 PM Invited

Novel Nanostructured Magnetic Materials: *J. Narayan*¹; A. Tiwari¹; H. Zhou¹; ¹North Carolina State University, Dept. of Matls. Sci. & Engrg., Raleigh, NC 27695-7916 USA

We synthesized novel nanostructured materials using a self-assembly processing in a controlled way. The orientation and size of nanoparticles were controlled by providing a template for epitaxial growth and controlling the flux of depositing species. The structures were characterized with a resolution of 0.16 nm using STEM-Z contrast imaging for atomic structure, chemical composition and bonding characteristics. The primary goal was to establish correlation of these parameters with magnetic properties. Modeling of magnetic properties was found to be consistent with experimental observations. Role of the strain in the fabrication of novel magnetic structures will be discussed.

2:30 PM Invited

2D and 3D Arrays of Magnetic Nanoparticles: *Sara Majetich*¹; ¹Carnegie Mellon University, Physics Dept., 5000 Forbes Ave., Pittsburgh, PA 15213-3890 USA

Self-assembled arrays of monodisperse Fe nanoparticles are ideal for studying magnetic interaction effects. Here the arrays are formed from surfactant-coated monodisperse iron nanoparticles. These particles are up to 9 nm in diameter and have specific magnetizations over 170 emu/g. The strength and nature of the magnetic coupling can be adjusted by varying the particle size and interparticle spacing, and by altering the self-assembly conditions to form monolayers, multilayers, or three-dimensional nanoparticle crystals. As the particle interactions are increased, the zero field cooled (ZFC) magnetization curve broadens, indicating a range of magnetic environments. The coercivity and remanence increase somewhat, and magnetic relaxation is slower. The existence of magnetic domains is suggested by small angle neutron scattering. 3D nanoparticle crystals have large structural coherence lengths in all directions. Their ZFC magnetization curve is nearly flat, and they have faster magnetic relaxation than the 2D arrays.

3:00 PM Invited

Self-Assembled Epitaxial Magnetic Nanostructures Via MBE Growth: *Dongqi Li*¹; ¹Argonne National Laboratory, Matls. Sci. Div., Bldg. 223, Argonne, IL 60439 USA

We have fabricated self-assembled magnetic nanostructures with molecular beam epitaxy (MBE) on single-crystal substrates. For example, epitaxial Co dots, antidots, and dot-chains, each dot ~100nm wide and several nm thick, were grown on flat and patterned Ru(0001) as driven by strain and diffusion during epitaxial growth. Fe nanowires (1 atomic layer thick, several nm wide) were grown along the step edges of vicinal Pd(110) via step-flow growth mode. The high degree of crystalline ordering of these structures allows us to observe intrinsic new magnetic properties due to confinement, which are understood with micromagnetic modeling and in terms of low dimensional physics in general, such as 2D-to-1D finite size scaling and 1D Ising chains. Work supported by the US DOE BES-Materials Sciences under contract # W-31-109-ENG-38.

3:30 PM Invited

Synthesis and Characterization of Self-Assembled Magnetic Nanoparticles: *D. Kumar*¹; ¹North Carolina A&T State University, Dept. of Mech. & Chem. Engrg., Greensboro, NC 27411 USA

A novel thin film processing method is reported based on pulsed laser deposition to process nanocrystalline materials with accurate size and interface control with improved magnetic properties. Using this method, single domain nanocrystalline Fe and Ni particles in the 5-10 nm size range embedded in amorphous alumina as well as in crystalline TiN have been produced. By controlling the size distribution in confined layers, it was possible to tune the magnetic properties from superparamagnetic to ferromagnetic behavior. Magnetic hysteresis characteristics below the blocking temperature are consistent with single-domain behavior. The paper also presents our results from investigations in which scanning transmission electron microscopy with atomic number contrast (STEM-Z) and electron energy loss spectroscopy (EELS) were used to understand the atomic structure of Ni nanoparticles and interface between the nanoparticles and the surrounding matrices. It was interesting to learn from EELS measurements at interfaces of individual grains that Ni in alumina matrix does not form an ionic bond indicating the absence of metal-oxygen bond at the interface. The absence of metal-oxygen bond, in turn, suggests the absence of any dead layer on Ni nanoparticles even in an oxide matrix.

4:00 PM Invited

Magnetic Nanostructures from Diblock Copolymer Templates: *Mark T. Tuominen*¹; ¹University of Massachusetts, Physics Dept., 411 Hasbrouck Lab, Amherst, MA 01003 USA

Many future applications of magnetic technology require nanoscale magnetic elements configured into system architectures that provide useful functionalities. This talk will focus on highly dense arrays of magnetic and superconducting nanoscale elements made by new integrated nanofabrication techniques that utilize the guided microphase separation of diblock copolymers together with electrochemical deposition. First the magnetization properties of cobalt and permalloy nanowire arrays will be discussed as a model patterned magnetic system. We analyze the behavior these arrays with regards to magnetocrystalline anisotropy, shape anisotropy, and magnetostatic interactions. Secondly research will be presented on integrated magnetotransport nanowire devices in lateral and vertical transport geometries. Fabrication is achieved by combining nanoporous polymer templates with electron beam lithography. Measurements include spin-dependent electron transport GMR and AMR behavior, and Andreev-coupled superconducting behavior in nanoscale device geometries. This work is supported by NSF grants DMI-0103024, DMR-0071756, and MRSEC.

4:30 PM Invited

Metastable Cation Distribution in Nano-Size Mn-Zn Ferrites: *Naresh C. Mishra*¹; Chandana Rath¹; S. Anand²; R. P. Das²; C. Upadhyaya³; H. C. Verma³; ¹Utkal University, Physics Dept., Bhubaneswar, Orissa India; ²Regional Research Laboratory, Bhubaneswar, Orissa India; ³Indian Institute of Technology, Physics Dept., Kanpur, UP 208016 India

Mn_{1-x}Zn_xFe₂O₄ (x = 0 to 1) nanosize particles prepared through hydrothermal route has been studied by X-ray diffraction, magnetization measurements, Mossbauer spectroscopy, transmission electron microscopy and differential scanning calorimetry. The particle size was found to decrease from 13 to 4 nanometers with increasing Zn concentration from 0 to 1. The chemical composition is thus shown to influence the physical size of the nanoparticles. The as prepared samples are largely ferimagnetic with ferri- to paramagnetic transition temperature increasing from 175C to 500C with decreasing Zn content. These Curie temperatures were much higher than the corre-

sponding bulk values. At compositions within $x = 0.35$ and 0.5 , the temperature dependence of the magnetization exhibits a cusp like behavior below the Curie temperature. The cusps irreversibly disappear on annealing at 550°C , which indicate a redistribution of cations from a metastable state to a stabler state. The cationic redistribution occurs between the two chemically inequivalent sites in the cubic lattice of the ferrite. In contrast to general expectations, annealing of the nanoparticles is shown to convert the ferrimagnetic particles to superparamagnetic ones. Such a conversion is shown to be a consequence of the cation redistribution also.

5:00 PM

Self Assembled Magnetic Nanomaterials: *Mircea Chipara*¹; Jagannathan Sankar²; Septimiu Balascul¹; ¹Indiana University, Cyclotron Facility, 2401 Milo B Sampson Ln., Bloomington, IN 47403 USA; ²North Carolina A&T State University, Dept. of Mech. Engrg., Greensboro, NC 27411 USA

Barium ferrite (BaFe) magnetic nanoparticles have been obtained by energetic mechanical milling. The average size of magnetic nanoparticles was estimated from the line width of Wide Angle X Ray Scattering spectra. The nanoparticles have been introduced into dilute solutions of polystyrene-polyisoprene-polystyrene copolymer (SIS) and sonicated for 50 hours at room temperature. Thin films of BaFe-SIS have been obtained by spin coating the solution onto Si substrates. The solvent has been removed by heating the samples in vacuum at 50°C for 24 hours. The magnetic features of the films were investigated by SQUID, in the temperature range 4 K to 300 K , and by ferromagnetic resonance spectroscopy (X Band). The angular dependence of ferromagnetic spectra is consistent with an anisotropic distribution of magnetic nanoparticles. Atomic Force Microscopy investigations revealed that the introduction of a small amount of magnetic nanoparticles into SIS is not disturbing its self-assembled structure.

Nanostructured Materials for Biomedical Applications: Session IV

Sponsored by: Electronic, Magnetic & Photonic Materials Division, EMPMD-Thin Films & Interfaces Committee

Program Organizers: Roger J. Narayan, Georgia Tech, School of Materials Science and Engineering, Atlanta, GA 30332-0245 USA; J. Michael Rigsbee, North Carolina State University, Department of Materials Science and Engineering, Raleigh, NC 27695-7907 USA; Xinghang Zhang, Los Alamos National Laboratory, Los Alamos, NM 87545 USA

Tuesday PM Room: 219A
March 16, 2004 Location: Charlotte Convention Center

Session Chairs: Mehmet Sarikaya, University of Washington, Matls. Scis. & Engrg., Seattle, WA 98195 USA; Kenneth H. Sandhage, Georgia Institute of Technology, Sch. of Matls. Scis. & Engrg., Atlanta, GA 30332-0245 USA

2:00 PM Invited

Orthopaedic Implants and Biomaterials - Clinical Problems and the Development of Current Implants: *William G. Ward*¹; ¹Wake Forest University School of Medicine, Med. Ctr. Blvd., Winston-Salem, NC 27157 USA

Orthopaedic uses of metals and biomaterials have expanded greatly over the past few decades, especially in the internal fixation of fractures and in joint replacement. The materials utilized for internal fixation of fractures have evolved from stainless steel implants into the super alloys of titanium and other materials. The greatest developments however, have been in the materials used for total joint replacements (arthroplasty). The problems of frictional wear and the biologic response to the wear-generated debris have led to an evolution of bearing surface materials. Chrome cobalt bearing surfaces articulating with ultra high molecular weight polyethylene have been utilized for approximately forty years. However, late loosening of such implants due to wear debris-induced osteolysis has led to the development of newer articulations, including metal on metal, ceramic on metal, ceramic on polyethylene and ceramic on ceramic. These developments and the associated products will be demonstrated, along with clinical examples.

2:45 PM Invited

Nanostructured Ti-Base Alloys for Biomedical Applications: *Guo He*¹; Satoshi Emura¹; Masuo Hagiwara¹; ¹National Institute for

Materials Science, Light Matls. Grp., 1-2-1 Sengen, Tsukuba, Ibaraki 305-0047 Japan

Ti-base alloys for biomedical applications have received much attention due to their excellent biocompatibility, low density, excellent corrosion resistance and good balance of mechanical properties. However, some problems are difficult to solve. For example, the Young's modulus of the available biomedicine-used Ti-base alloys is too high compared to that of bone. This is harmful for bone healing and remodeling. When attempts were made to reduce the Young's modulus, the strength was also severely degraded. Recently, we found that the nanostructured Ti-base alloys exhibit very low elastic modulus and very high strength. This just meets the demands of the biomaterials. By delicate composition design we can directly obtain bulk nanostructured Ti-base alloys. Using in situ composite techniques, we can overcome the shortcomings of low ductility of the nanostructured metallic materials and achieve the high performance of the Ti-base alloys for the biomedical applications.

3:30 PM Invited

Nanostructured Titanium Oxide Based Surface for Enhanced Bone Growth: *Sungho Jin*¹; Brian Oh¹; ¹University of California, Dept. of Mech. & Aeros. Engrg., 9500 Gilman Dr., La Jolla, CA 92093-0411 USA

Titanium and its alloys are widely utilized in orthopedic and dental implants by virtue of their load-bearing capability, light weight and bio-compatibility. As Ti can not directly bond to bone, the addition of bio-active surface coatings are desirable. The anatase phase of titanium oxide is known to promote the formation of hydroxyapatite and bone growth. We have studied the dependence of anatase vs rutile phase formation on microstructural and processing parameters in titanium oxide coating, and evaluated the effect of nano- vs micro-scale dimensional and morphological control on hydroxyapatite and bone growth. Various processing techniques including anodic oxidation have been employed to produce a variety of shapes and sizes of nano features, and their behavior and properties have been compared.

4:15 PM Invited

Plasma-Sprayed ZrO₂ Bond Coat as an Intermediate Layer for Porcelain Veneered on Commercially Pure Titanium: *Tsung-Nan Lo*¹; Truan-Sheng Lui¹; Tai-Nan Lin²; ¹National Cheng Kung University, Dept. Matls. Sci. & Engrg., No. 1, Univ. Rd., Tainan 701 Taiwan; ²National Taiwan Ocean University, Inst. of Matls. Engrg., No. 2, Pei-Ning Rd., Keelung 202 Taiwan

This investigation was to study the strength of the ZrO₂ bond coat introduced as an intermediate layer between porcelain and titanium. Four-point bending test was used to measure the bond strength of single-layer porcelain coating and two-layer porcelain/ZrO₂ coating on titanium. Experimental results indicate that an improved bond strength of porcelain/ZrO₂ composite coating on titanium was found. The bond strength increases from 23.0 ± 2.1 Mpa of porcelain coating to 35.8 ± 5.7 Mpa of porcelain/ZrO₂ composite coating. The fracture regions between the ceramic coatings and titanium were analyzed by using scanning electron microscopy (SEM) and thin-film X-ray diffraction techniques. Elemental diffusion was found at porcelain/ZrO₂ interface. It promotes the chemical bonding between porcelain/ZrO₂ interface to strengthen the bonding of porcelain veneered on titanium. The surface roughness of the plasma-sprayed ZrO₂ coating were investigated by surfacoder. It also indicated that the ZrO₂ bond coat provided rougher surface morphology to aid in the bonding for porcelain veneered on titanium.

Phase Stability, Phase Transformation, and Reactive Phase Formation in Electronic Materials III: Session IV

Sponsored by: Electronic, Magnetic & Photonic Materials Division, Structural Materials Division, EMPMD/SMD-Alloy Phases Committee

Program Organizers: C. Robert Kao, National Central University, Department of Chemical and Materials Engineering, Chungli City 32054 Taiwan; Sinn-Wen Chen, National Tsing-Hua University, Department of Chemical Engineering, Hsinchu 300 Taiwan; Hyuck Mo Lee, Korea Advanced Institute of Science & Technology, Department of Materials Science & Engineering, Taejeon 305-701 Korea; Suzanne E. Mohny, Pennsylvania State University, Department of Materials Science & Engineering, University Park, PA 16802 USA; Michael R. Notis, Lehigh University, Department of Materials Science and Engineering, Bethlehem, PA 18015 USA; Douglas J. Swenson, Michigan Technological University, Department of Materials Science & Engineering, Houghton, MI 49931 USA

Tuesday PM Room: 214
March 16, 2004 Location: Charlotte Convention Center

Session Chairs: John H.L. Pang, Nanyang Technological University, Sch. of Mech. & Production Engrg., Singapore 639798 Singapore; Paul T. Vianco, Sandia National Laboratories, Albuquerque, NM 87185-0889 USA

2:00 PM Invited

Interfacial Reactions Between Sn-Ag-0.6Cu Solder and Silver (Ag) Substrates: Paul T. Vianco¹; Joseph J. Martin¹; Robert D. Wright²; ¹Sandia National Laboratories, PO Box 5800, MS0889, Albuquerque, NM 87185-0889 USA; ²Sandia National Laboratories, PO Box 5800, MS 0886, Albuquerque, NM 87185-0886 USA

Silver (Ag) is an important surface finish in electronic packaging, more so with the advent of immersion Ag coatings for the conductive features on printed circuit boards. A study was performed which examined the physical metallurgy and rate kinetics of reactions between the 95.5Sn-3.9Ag-0.6Cu (wt.%) solder and Ag. The first task examined the consumption rate and intermetallic compound layer growth between molten Sn-Ag-0.6Cu solder and Ag under temperatures of 240 to 350°C and time periods of 5 to 240 s. The second task investigated the solid-state intermetallic compound layer development between the Pb-free solder and Ag under aging temperatures of 55 to 205°C and time periods of 1 to 400 days. Concurrent experiments were performed with 63Sn-37Pb solder to provide baseline data. Sandia is a multi-program laboratory operated by Sandia Corporation, a Lockheed Martin Company, for the United States Department of Energy under Contract DE-AC04-94AL85000.

2:20 PM Invited

IMC Formation on BGA Package with Sn-Ag-Cu and Sn-Ag-Cu-Ni-Ge Solder Balls: Kwang-Lung Lin¹; Po-Cheng Shih¹; ¹National Cheng Kung University, Matls. Sci. & Engrg., 1 Ta-Hsuey Rd., Tainan, Taiwan 701 China

The BGA substrate with Cu/Ni-P/Au metallization was attached with solder balls. The compositions of the solder ball are Sn-3.2Ag-0.5Cu and Sn-3.0Ag-0.5Cu-0.07Ni-0.01Ge. The package was subjected to thermal aging at 240°C from 100 to 1000 hours for investigating the IMC formation behavior. Cross section of IMC layer as well as top view, revealed by etching off the unreacted solder, was inspected and analyzed with SEM and EDX. The IMC mainly consists of two types of morphology, hexagonal and whisker. The hexagonal crystal was identified to be (Cu, Ni)₆Sn₅ and the whisker crystal is (Ni, Cu)₃Sn₄. The dissolution of Ni in the Cu₆Sn₅ compound results in a synergistic effect on enhancing the growth of the compound, while similar effect was not observed for the dissolved Cu in Ni₃Sn₄ compound. This phenomenon was explained through the vacant energy band of the 3d-orbital of Ni. Ag₃Sn compound was also detected in the solder region near the interfacial IMC. The Ag₃Sn compound was not in direct contact with BGA substrate.

2:40 PM Invited

Differences in Formation and Growth of Interface Between Sn-Ag and Sn-Ag-Cu Lead-Free Solder with Ni-P/Au Plating: Chi-Won Hwang¹; Katsuyuki Suganuma¹; Masayuki Kiso²; Shigeo Hashimoto²; ¹ISIR, Osaka University, Mihogaoka 8-1, Ibaraki, Osaka

567-0047 Japan; ²C. Uyemura & Co., Ltd., Deguchi 1-5-1, Hirakata, Osaka 573-0065 Japan

The formation and growth mechanism of the interfaces of Sn-Ag(-Cu) lead-free solder with Au/Ni-6wt%P plating were studied. During the soldering at 230°C, Au dissolved into molten solder, and double reaction layers of Ni₃Sn₄/Ni₃SnP formed between Sn-3.5Ag solder and Ni-6P. P content increases in the surface region of the Ni-6P layer due to the depletion of Ni diffused into molten solder, resulting in the formation of Ni₃P+Ni layer. For Sn-3.5Ag-0.7Cu solder, an (Ni,Cu)₃Sn₂ single layer, containing Cu of about 50 at%, formed as a reaction layer. With increasing of reaction time, both interface of Sn-Ag and Sn-Ag-Cu reaction systems repeatedly undergo thickening and thinning in their thickness, while the mechanisms are different. This fluctuation of the reaction layer thickness affects joint strength, which also exhibits repeated strengthening and degrading.

3:00 PM

Interfacial Reactions and Shear Strengths Between Sn-Ag Based Pb-Free Solder Balls and Au/EN/Cu Metallization: Sang-Won Kim¹; Jeong-Won Yoon¹; Seung-Boo Jung¹; ¹Sungkyunkwan University, Dept. of Advd. Matls. Engrg., 300 Chunchun-dong, Changan-gu, Suwon, Kyounggi-do 440-746 Korea

Several Sn-Ag system Pb-free solders have been identified to replace Sn-Pb eutectic solder in reflow process applications. Also, electroless Ni-P (EN) has been adopted and used as a diffusion barrier in the under-bump metallurgy (UBM) for flip-chip application. In this study, the alloy compositions of solder balls included Sn-3.5Ag, Sn-3.5Ag-0.75Cu, and Sn-3Ag-6Bi-2In. And, the solder ball pads were a copper substrate with an Au/electroless Ni-P surface finish. The formation and growth of the intermetallic phases at the solder joints were investigated. Also, ball shear strength was measured to investigate the effect of the microstructures and interfacial reactions on the reliability of solder bumps.

3:15 PM

Multi-Component Base Metal Dissolution and Inter-Metallic Compound Formation in Porous Noble Metal Thick Films: Kenneth L. Erickson²; Polly L. Hopkins²; Paul T. Vianco¹; Joseph J. Martin¹; Gary A. Zender³; ¹Sandia National Laboratories, PO Box 5800, MS0889, Albuquerque, NM 87185-0889 USA; ²Sandia National Laboratories, PO Box 5800, MS 0834, Albuquerque, NM 87185-0834 USA; ³Sandia National Laboratories, PO Box 5800, MS0886, Albuquerque, NM 87185-0886 USA

Previous studies showed that preferential dissolution of base metal constituents influenced short-term, base metal erosion and long-term inter-metallic compound (IMC) growth. Experiments with 76Au-21Pt-3Pd (wt%) alloy sheet and molten 63Sn-37Pb (wt.) solder indicated that preferential Au dissolution produced Pt-rich IMC layers that caused induction periods during subsequent IMC growth. Induction periods were a significant concern in previous work to develop models for IMC growth in 76Au-21Pt-3Pd porous thick films contacted with 63Sn-37Pb solder. Results are described which come from recent experiments which examined dissolution and simultaneous IMC growth in 76Au-21Pt-3Pd porous thick films contacted with 63Sn-37Pb solder. The analysis uses a previously reported model for multi-component dissolution and IMC growth based upon diffusion coefficients derived from Sn-Pb couples with 76Au-21Pt-3Pd alloy sheet. Sandia is a multi-program laboratory operated by Sandia Corporation, a Lockheed Martin Company, for the United States Department of Energy under Contract DE-AC04-94AL85000.

3:30 PM

The Effect of Gold Thickness on Solder/UBM Interfacial Reaction in Flip Chip Package: Y. L. Lin¹; C. M. Tsai¹; Y. C. Hu¹; Y. H. Lin¹; C. Robert Kao¹; ¹National Central University, Dept. of Chem. & Matls. Engrg., Chungli City 320 Taiwan

Flip-chip technology provides a solution for smaller, thinner, and more powerful IC package. As the package size continues to shrink, the bump size becomes smaller as well. Consequently, the effect of gold thickness of Ni/Au surface finish will become more important. In this research, the effect of gold thickness of Ni/Au surface finish during long-term thermal aging in flip chip package was studied. The solder used was eutectic lead-tin. The under bump metallization (UBM) on the chip side was Cu/Ni(V)/Al, and the surface finish on the substrate side was Ni/Au. Two different gold thickness, 0.045 μm and 0.85 μm, were used. After thermal aging, the results showed that thick gold caused the formation of (Au_xNi_{1-x})Sn₄ compounds at the interface, and had a higher Ni consumption rate.

3:45 PM Break

4:00 PM Invited

Intermetallic Growth Studies on Sn-Ag-Cu Lead-Free Solder Joints: *John H.L. Pang¹; X. Q. Shi²; W. Zhou¹; S. L. Ngho¹;* ¹Nanyang Technological University, Sch. of Mech. & Production Engrg., 50 Nanyang Ave., Singapore 639798 Singapore; ²Singapore Institute of Manufacturing Technology, Joining Tech. Grp., 71 Nanyang Dr., Singapore 638075 Singapore

Intermetallic growth studies on 95.8Sn-3.5Ag-0.7Cu lead-free solder joint subjected to iso-thermal aging exposure will be presented. The motivation for this study is to characterize the solid-state diffusion mechanism for intermetallic growth behavior with respect to iso-thermal aging test parameters of temperature and time. Solder joint reliability qualification process often employ accelerated temperature cycling tests where the temperature profile effects of cycle time, ramp rate and dwell time are important parameters. Intermetallic growth studies on 95.5Sn-3.8Ag-0.7Cu lead-free solder joint subjected to thermal cycling (TC) aging and thermal shock (TS) aging will be reported. Iso-thermal aging studies on intermetallic growth behavior for lap shear soldered specimens were investigated. The lap shear specimens were soldered using 95.8Sn-3.5Ag-0.7Cu solder paste on copper specimen parts coated with Ni and Au surface finish at the wetted area. Iso-thermal aging tests for three aging temperatures (125°C, 150°C, and 175°C) and four aging time exposures (24, 72, 144 and 336 hours) were conducted. Digital imaging techniques were employed in the measurement of the average intermetallic growth thickness. Details of the intermetallic growth behavior will be discussed with respect to the aging test parameters and curve-fitted to solid-state diffusion mechanisms. Intermetallic growth studies on 95.5Sn-3.8Ag-0.7Cu solder joint specimens subject to temperature cycling aging were investigated. The specimen consist of a 0.5mm solder sphere (of 95.5Sn-3.8Ag-0.7Cu composition) soldered between two FR-4 substrates at the copper pad terminals. The copper pads were coated with Ni and Au surface finish. The thermal cycling (TC) aging test, cycles between -40°C to 125°C, with a cycle time of 56 minutes and a dwell time of 15 minutes at the upper and lower temperature limits. The thermal shock (TS) aging test, alternates between -55°C to 125°C, with a cycle time of 17 minutes, and a dwell time of 5 minutes at each temperature limit. Similar intermetallic growth measurement technique was employed as in iso-thermal aging experiments. Comparison between intermetallic growth behavior for TC and TS exposure for 0, 500, 1000 and 2000 cycles of aging exposure will be reported. A framework for correlating intermetallic growth behavior subjected to TC, TS and Iso-thermal aging conditions will be proposed.

4:20 PM Invited

Mechanism of Interfacial Reaction for SnPb Solder Bump with Ni/Cu UBM in Flip Chip Technology: *Chien Sheng Huang¹;* Jenq Gong Duh¹; ¹National Tsing Hua University, Dept. of Matls. Sci. & Engrg., 101, Sect. 2 Kuang Fu Rd., Hsinchu 300 Taiwan

Ni-based under bump metallization has been widely used in flip chip technology due to the slow reaction rate with Sn. In this study, solder joints after reflow were employed to investigate the mechanism of interfacial reaction between Ni/Cu UBM and eutectic Sn-Pb solder. After deliberately quantitative analysis with an electron probe microanalyzer, the effect of Cu content in solder near the interface of solder/IMC on interfacial reaction could be probed. After the first cycle of reflow, only one layered (Ni_{1-x}, Cu)₃Sn₄ with homogeneous composition was found between the solder bump and UBM. However, after multiple reflows, another type of intermetallic compound (Cu_{1-y}, Ni)₆Sn₅ formed between solder and (Ni_{1-x}, Cu)₃Sn₄. It was observed that the concentration of Cu in solder near solder/IMC interface increased to a specific value. When (Cu_{1-y}, Ni)₆Sn₅ IMC formed, the Cu contents in (Ni_{1-x}, Cu)₃Sn₄ were not uniform anymore. The values of x varied from 0.09 to 0.35. With the aid of microstructure evolution, quantitative analysis, and related phase equilibrium data of Sn-Ni-Cu, the reaction mechanism of interfacial phase transformation between Sn-Pb solder and Ni/Cu UBM could be revealed.

4:40 PM Invited

Control of Interface Reaction Mechanism Between Cu and Sn-Based Solder Alloys: *Choong-Un Kim¹;* Jaeyong Park¹; Rajendra Kobade¹; Viswanadham Puligandla²; Ted Carper²; ¹University of Texas, Matls. Sci. & Engrg., Arlington, TX 76019 USA; ²Nokia Mobile Phones, Inc., Rsch. & Tech. Access, 6000 Connection Dr., Irving, TX 75039 USA

Interface reaction between Cu and molten solder is one of the most extensively studied subjects in metallurgy. It is the key reaction for solder joint formation yet is a reliability concern because, if excessive, it can weaken the mechanical properties of the joint. While several theories on the interface reaction mechanism exist, they provide only limited understanding. Recently, we found that the interface reaction

mechanism can be altered by the addition of minor additives to solder alloys. These additives are elements having a strong affinity to Cu, such as Au and Ni, and induce the formation of ternary Cu-Sn intermetallic phases. The interplay between 1) the migration of these elements in molten solder and 2) the change in the thermodynamic potential for reaction results in a change in the reaction mechanism and produces a unique interface microstructure consisting of an intermetallic phase and Sn islands. While the composite microstructure is proven to be effective in enhancing solder reliability, the study of its formation provides new insights into the reaction mechanism between Cu and solder alloys. This paper presents a self-consistent reaction mechanism explaining the formation of intermetallic phases and their subsequent morphology and property changes.

5:00 PM

Interfacial Metallurgical Reaction Kinetics During Lead-Free Soldering: *Jin Liang¹;* Nader Dariavach¹; Paul Callahan¹; Stuart Downes¹; ¹EMC, 176 South St., Hopkinton, MA 01748 USA

Intermetallic growth and substrate dissolution take place rather rapidly during a normal soldering operation. Since lead-free soldering requires substantially higher temperatures (around 250°C), the rates for intermetallic growth and substrate dissolution are expected to increase significantly compared to the current Sn-Pb eutectic soldering. This study attempts to investigate and to model the intermetallic growth kinetics for three lead-free solders (SnAg eutectic, SnCu eutectic and SnAgCu eutectic) with copper substrates, and other metal finishes, such as Ni/Au, OSP, and Pd. A thorough understanding of lead-free solder/substrate interfacial metallurgical reactions would lead to optimum lead-free soldering processes and optimum lead-free coating thickness for component and PCB terminal finishes, as well as USM for flip-chip and BGAs.

5:15 PM

Effects of Pd Addition on Au Stud Bumps/Al Pads Interfacial Reactions and Bond Reliability: *Hyoung-Joon Kim¹;* Jong-Soo Cho²; Yong-Jin Park²; Jin Lee²; Kyung-Wook Paik¹; ¹Korea Advanced Institute of Science and Technology (KAIST), Matls. Sci. & Engrg., Rm. 2423, Appl. Engrg. Bldg., 373-1, Guseong-Dong, Yuseong-Gu, Daejeon 305-701 Korea; ²MK Electron Co., Ltd., R&D Ctr., 316-2, Kumeu-ri, Pogok-myun, Yongin, Kyunggi-do 449-812 Korea

Pd has been used as one of the important alloying elements in Au bonding wire manufacturing processes. Therefore, in this study, Au-1wt%Pd wire was used to make Au stud bumps on Al pads. To investigate the effects of Pd on Au/Al interfacial reactions, thermal aging was performed at 150, 175, and 200°C for 0 to 1200 hours, respectively. Cross-sectional SEM, EDS, and EPMA were performed to identify the IMC (Intermetallic Compound) phase and Pd behavior at Au/Al bonding interface. According to the experimental results, the dominant IMC was Au₅Al₂ and Pd-rich layers were formed in front of the Au-Al IMC. Furthermore, TEM study has been performed as a supplement. Finally, ball shear tests were performed to know the effects of Pd-rich layers on bond reliability. Therefore, after ball shear tests, fractured pads and balls were investigated with SEM and EDS, and failure analysis was executed.

Phase Transformations and Deformation in Magnesium Alloys: Plastic Deformation and Texture

Sponsored by: Materials Processing and Manufacturing Division, MPMD-Phase Transformations Committee-(Jt. ASM-MSCTS)
Program Organizer: Jian-Feng Nie, Monash University, School of Physics and Materials Engineering, Victoria 3800 Australia

Tuesday PM

Room: 205

March 16, 2004

Location: Charlotte Convention Center

Session Chairs: David Embury, McMaster University, Dept. of Matls. Sci. & Engrg., Hamilton, Ontario L8S 4M1 Canada; Sean R. Agnew, University of Virginia, Dept. of Matls. Sci. & Engrg., Charlottesville, VA 22904-4745 USA

2:00 PM Invited

The Effect of Texture on the Deformation Mechanisms of AZ31B: *Sean R. Agnew¹;* Carlos N. Tome²; Donald W. Brown²; ¹University of Virginia, Matls. Sci. & Engrg., 116 Engineer's Way, Charlottesville, VA 22904-4745 USA; ²Los Alamos National Laboratory, MST-8, Los Alamos, NM USA

In-situ neutron diffraction measurements of internal stress and texture development have been employed to elucidate the roles of

various deformation mechanisms with magnesium alloy AZ31B. Three different wrought forms of the alloy have been studied due to the striking differences in crystallographic texture and mechanical behavior. 1) Hot-rolled plate with a basal fiber texture oriented parallel to the plate normal direction, 2) Extruded bar with basal poles oriented perpendicular to the extrusion axis, and 3) Equal Channel Angular (ECA) processed bar with a strong basal fiber inclined 45° from the bar axis. Each sample was tested in tension and compression along the prior working directions. Rolled and extruded samples exhibited strong tension/compression asymmetry associated with twinning, while the ECA processed sample did not. A viscoplastic self-consistent polycrystal model elucidated the aspects of the twinning mechanism, while an elastoplastic self-consistent model provided insights regarding slip-dominated deformation and corresponding internal stress development.

2:35 PM Invited

Plastic Anisotropy and its Effects on Mechanical Parameters in Mg Alloys at RT: *Junichi Koike*¹; ¹Tohoku University, Dept. of Matls. Sci., 02 Aoba, Aramaki, Aoba-ku, Sendai, Miyagi 980-8579 Japan

Mg alloys exhibit substantial plastic anisotropy at ambient temperature. The plastic anisotropy complicates the interpretation of various mechanical parameters, such as, elastic modulus, yield stress, r -value, homogeneous strain, and fracture. Physical basis of plastic anisotropy and its effects on the mechanical parameters can be delineated based on dominant deformation mechanisms under given conditions. The present paper deals with various possibilities of deformation mechanisms, including dislocation glide on basal and nonbasal planes, twinning, and grain-boundary sliding. The necessary conditions to activate each mechanism are discussed in relation to grain size and crystallographic texture. The effects of each mechanism on the mechanical parameters are also discussed with an aim to help improve shape forming capabilities of Mg alloy sheets.

3:10 PM Invited

Grain Size of Wrought Magnesium: Manipulation and Mechanical Effects: *Matthew R. Barnett*¹; ¹Deakin University, Sch. of Engrg., Pigdons Rd., Geelong, VIC 3217 Australia

Controlling the grain size is one of the key tools used in engineering mechanical properties. The present paper reviews the main approaches used to achieve this in the manufacture of wrought magnesium. It also briefly examines the current knowledge of the influence of the grain size on mechanical response. Results of a series of deformation experiments are examined to reveal the influence of processing conditions on the grain size. The mechanisms considered include continuous dynamic recrystallization, discontinuous dynamic recrystallization, static recrystallization and meta-dynamic recrystallization. The influence of grain size on the mechanisms activated in subsequent deformation treatments is also reported. It is shown that the grain size exerts a significant influence on the activation of twinning. A subset of the possible grain sizes and stresses is defined within which {10-12} twinning will not occur, irrespective of the crystallographic texture. The results of both of these avenues of investigation, i.e. the control of grain size and the effects of grain size on mechanical behaviour, are summarized in a single deformation map in strain rate-grain size space.

3:45 PM Break

4:00 PM Invited

Processing of Magnesium Alloys Using Severe Plastic Deformation: *Zenji Horita*¹; Yuichi Miyahara¹; Terence G. Langdon²; ¹Kyushu University, Matls. Sci. & Engrg., Fac. of Engrg., Fukuoka 812-8581 Japan; ²University of Southern California, Aeros. & Mech. Engrg. & Matls. Sci., Los Angeles, CA 90089-1453 USA

Magnesium alloys are potentially attractive for use in structural applications because of their low density and good machinability. Nevertheless, their use tends to be restricted because of the inherent difficulties in forming structural components. It appears in principle that it may be possible to overcome this difficulty by refining the grain size to the submicrometer level through the application of severe plastic deformation. This paper describes recent attempts to achieve a superplastic forming capability in Mg-based alloys through the use of a two-step process, termed EX-ECAP, in which the Mg alloys are initially extruded and then processed using equal-channel angular pressing. It is demonstrated that this two-step procedure leads to excellent superplastic properties with elongations to failure up to >500%.

4:35 PM Invited

Deformation and Plasticity of Magnesium Alloys - Materials Design by Understanding from Ab Initio Calculation: *Kenji Higashi*¹; ¹Osaka Prefecture University, Dept. of Metall. & Matls. Sci., 1-1 Gakuen-cho, Sakai, Osaka 599-8531 Japan

Recently magnesium alloys have been expected to be one of the most promising structural materials. However, it is a large problem that magnesium alloys have low plastic formability at room temperature and less resistance to creep at elevated temperatures. Investigations to develop correct ideas for understanding the deformation mechanism are very much in order. In the present paper, two problems in the deformation mechanism are discussed using ab initio calculation that gives a reliable and accurate description of structural properties and of the distribution of electrons that accompanies the atomic bond for the magnesium-based materials. First, the effect of the substitutional-alloying-elements on the generalized stacking fault (GSF) energy is investigated for the inclusive understanding of the dominant diffusion-creep process at elevated temperatures. It is precisely determined that both Y and Ca among the elements investigated in the present paper are the promising elements to improve the resistance to creep controlled by dislocation-climb in the Mg-based alloys. Second, the misfit strain for some substitutional-alloying-elements, which is obtained from the distortion of atomic positions by ab initio calculation, is calculated as a first step of searching most effective solute element for the solid-solution strengthening in Mg-based substitutional solid solution. Additionally, based on the results of ab initio calculation, materials design for the optimum chemical compositions will be applied to developing new Mg-based alloys exhibiting high strength with reasonable high ductility.

Processing, Microstructure and Properties of Powder-Based Materials: Session III

Sponsored by: Materials Processing and Manufacturing Division, MPMD-Powder Materials Committee

Program Organizers: K. B. Morsi, San Diego State University, Department of Mechanical Engineering, San Diego, CA 92182 USA; James C. Foley, Los Alamos National Laboratory, Los Alamos, NM 87545 USA; Karl P. Staudhammer, Los Alamos National Laboratory, Nuclear Materials Technology Division, Los Alamos, NM 87545 USA

Tuesday PM
March 16, 2004

Room: 208B
Location: Charlotte Convention Center

Session Chair: James C. Foley, Los Alamos National Laboratory, Matls. Tech., Los Alamos, NM 87545 USA

2:00 PM Invited

Processing of High-Porosity NiTi by Powder Densification and Subsequent Gas Bubble Expansion: Scott M. Oppenheimer¹; *David C. Dunand*²; ¹Northwestern University, Dept. of Matls. Sci. & Engrg., Evanston, IL 60201 USA

Powders of nickel-rich NiTi (Ni-49 wt.%Ti, with superelastic composition) were densified by hot-isostatic pressing in the presence of argon, resulting in a continuous NiTi preform containing a large number of isolated, pressurized argon bubbles with volume fraction below ca. 1%. Annealing this preform above 1000°C resulted in the expansion of these gas-filled bubbles due creep of the surrounding NiTi matrix. The resulting NiTi "foams" exhibit porosity in excess of 30 vol. % with pore size above 100 micrometers. Foaming kinetics, maximum porosity and pore connectivity to the surface are explored as a function of annealing temperature and initial argon pressure.

2:20 PM

Stress Relaxation of Powder Metallurgy Disk Superalloys: *Timothy P. Gabb*¹; Jack Telesman¹; Peter T. Kantzos²; Peter J. Bonacuse³; Robert L. Barrie³; Paul Prevey⁴; ¹NASA Glenn Research Center, 21000 Brookpark Rd., Cleveland, OH 44135 USA; ²Ohio Aerospace Institute, 22800 Cedar Point Rd., Cleveland, OH 44142 USA; ³Army Research Laboratories, 21000 Brookpark Rd., Cleveland, OH 44135 USA; ⁴Lambda Research, 5521 Fair Ln., Cincinnati, OH 45227 USA

Modern powder metallurgy (PM) processed disk superalloys have improved mechanical properties and temperature capabilities over previous cast and wrought disk alloys, due to improved microstructural uniformity and higher refractory element contents. However, these PM improvements have been accompanied by increased sensitivities to notches and defects at disk surfaces. These surface sensitivities can be addressed by applying beneficial compressive residual stresses at disk surfaces. The compressive residual stresses are produced with surface enhancement processes such as shot peening which plastically deform the near-surface material, usually performed after final disk machining. Such compressive residual stresses act to preclude or delay

surface cracking during service due to loading, defects, handling or foreign object damage, and environmental attack. An issue of general concern is the potential relaxation of beneficial compressive surface residual stresses as engine temperatures increase. The objective of this study was to assess the relaxation of stresses at increasing temperatures in several PM disk superalloys. The effects of temperature, time, and plasticity were examined, and potential approaches to minimize stress relaxation will be discussed.

2:40 PM

Consolidation of Powders by Severe Plastic Deformation: *K. Ted Hartwig¹; Ibrahim Karaman¹; Suveen N. Mathaudhu¹; Jae-Taek Im¹; ¹Texas A&M University, Mech. Engrg., 319 Engrg. Phys. Bldg., College Sta., TX 77843-3123 USA*

Advances in the production of nanostructured powders over the past decade have given materials engineers new opportunities for the creation of high strength bulk materials. Mechanical alloying, gas atomization, electro-explosion and other novel synthesis methods coupled with better alloy composition selections have enabled the production of a wide variety of metastable extremely fine structured powders. Bulk material with extraordinary properties should result if such powders can be consolidated without significant changes to the microstructure. In the work reported here, one method of severe plastic deformation (equal channel angular extrusion - ECAE) is evaluated for effective consolidation of several different nanostructured materials including copper, Ti, stainless steel and Bi₂Te₃ alloy. The effects of particle size, starting microstructure, and several extrusion conditions are investigated by metallographic examination and mechanical testing. The results show that ECAE possesses interesting benefits for consolidation of particulate and is a viable method for fabrication of bulk nanostructured materials.

3:00 PM

Fabrication of Bulk Nanocrystalline Metals by the Consolidation of Nanoparticles Using Equal Channel Angular Extrusion: *Ibrahim Karaman¹; Mohammed Haouaoui¹; G. Guven Yapiçi¹; Hans J. Maier²; ¹Texas A&M University, Dept. of Mech. Engrg., MS 3123, College Sta., TX 77843 USA; ²University of Paderborn, Lehrstuhl für Werkstoffkunde, Paderborn 33095 Germany*

Materials with ultrafine grains and nanostructures (< 100 nm) have attracted considerable interest because of their unique properties as compared with conventional materials. Although this class of materials seems to offer new opportunities for small scale applications, utilizing them in large scale structural applications is still a challenge due to the difficulty of fabricating nanocrystalline materials in bulk. The present work is focussed on fabrication of near full density bulk nanocrystalline copper and stainless steel from powder precursors using equal channel angular extrusion (ECAE). The initial powder sizes were 50 nm, 150 nm and 45 micron for copper and 100 nm for stainless steel. Different processing routes were selected for comparison purposes and to determine the best processing route for specific end microstructures. The microstructure is characterized for different ECAE routes and number of passes. The stress-strain responses are determined by tension and compression tests at room temperature. The effect of initial powder size and resulting consolidate grain size on the mechanical properties are discussed in view of the Hall-Petch relationship. In this talk, some of these experimental observations will be presented in comparison with microcrystalline consolidates and with severely deformed pure copper and stainless steel. This study helps to clarify the relationship between different ECAE processing parameters, mechanical properties and the microstructure of nanocrystalline metals with low and medium stacking fault energies. This work was supported by the National Science Foundation contract CMS 01-34554, Solid Mechanics and Materials Engineering Program, Directorate of Engineering, Arlington, Virginia and Deutsche Forschungsgemeinschaft.

3:20 PM

Corrosion Resistance of Laser Deposited 316L Stainless Steels: *Eswar R. Yarrapareddy¹; Alan J. Anderson¹; James W. Sears¹; ¹South Dakota School of Mines & Technology, Advd. Matls. Procg. Ctr., 501 E. St. Joseph St., Rapid City, SD 57701 USA*

Laser Powder Deposition (LPD) involves injecting particles (metallic and/or ceramic) into a molten pool produced by a focused laser beam. A computer-controlled robot controls the position of the molten pool. The process allows for sequential layering to produce solid free form shapes directly from a CAD/CAM interface. The Process parameters were implemented to control the molten pool size by modulating laser power and process speed. In the current study, the corrosion behavior of laser deposited 316L stainless steels were investigated in 3.5% NaCl solution at 23°C by cyclic potentiodynamic

polarization method. From this, the corrosion potential, pitting potential, protection potential and current density were calculated and polarization curves were generated. The susceptibility of intergranular corrosion (IGC) was studied by hot boiling sulphuric sensitization test. The pit morphology after polarization test was also examined by optical microscopy.

3:40 PM Break

3:50 PM

High Density Infrared Processing of α -TiAl Sheet: *John D.K. Rivard¹; ¹Oak Ridge National Laboratory, Metals & Ceram., 1 Bethel Valley Rd., MS 6083, Oak Ridge, TN 37831 USA*

Gamma titanium aluminide (g-TiAl) alloys are of interest for engineering solutions in the aerospace and the automotive industry because of a unique combination of low density, oxidation resistance, burn resistance and high temperature strength. Current productions methods limit the implementation of α -TiAl in regular use due to high cost and long cycle times of production. A difficulty is that engineers have a talent for making existing technology work by trading off other parameters at a reduced cost. But, a recently developed method for the fabrication of sheet materials has made the regular use of α -TiAl one step closer to reality. This novel method utilizes high-density infrared (HDI) radiant heating from a plasma arc lamp to rapidly heat and liquid phase sinter powder metal precursors. In this study, α -TiAl sheet was produced from tape cast Ti-48Al-2Cr-2Nb. Predictive finite volume modeling was used to determine appropriate processing parameters. A complete database of the appropriate thermophysical properties was also compiled. Thin gage α -TiAl sheet was produced in panels measuring up to 10cm x 10cm. Resultant microstructures will be presented as well as mechanical properties. Comparisons of conventional and HDI processed α -TiAl will be presented.

4:10 PM

The Influence of Heterogeneous Microstructure on Fatigue Crack Growth in Powder Metallurgy Steels: *George B. Piotrowski¹; Xin Deng¹; Nikhilesh Chawla¹; ¹Arizona State University, Dept. Chem. & Matls. Engrg., PO Box 876006, Tempe, AZ 85287-6006 USA*

Powder metallurgy steels processed by pressing and sintering generally exhibit a highly heterogeneous microstructure. In Ni-containing steels, it is not uncommon for Ni-rich retained austenite, pearlite, and bainite to all be present in the microstructure (in addition to porosity). Thus, fatigue crack growth is directly dependent on the local character of the microstructure. In this study, we have correlated the local microstructure with fatigue crack growth in a Fe-2Ni-0.85Mo-0.6C steel at three different densities: 7.0, 7.4, 7.6 g/cm³. The microstructure at each density was characterized by optical microscopy, scanning electron microscopy, and indentation to identify the phases present and quantify the fractions of each phase. The microstructure consisted of Ni-rich austenite regions, pearlite, and bainite. Fatigue crack growth tests were conducted at several R-ratios, ranging from -1 to 0.8. Increasing density and decreasing R-ratio resulted in an increase in ΔK_{th} . The interaction between fatigue cracks and the local microstructure was conducted by in situ crack growth measurements through a traveling microscope. The crack growth resistance of each of the phases was quantified and will be discussed in terms of strategies for developing sintered steels with enhanced fatigue crack growth resistance.

4:30 PM

Aluminium and Aluminium Alloy Powders for P/M Applications: *Ray Cook¹; Henry S. Meeks²; Isaac T.H. Chang³; Lucian C. Falticeanu³; ¹The Aluminium Powder Company Ltd., Forge Ln., Minworth, Sutton Coldfield, W. Midlands B76 1AH UK; ²Ceracon Inc., 5150 Fair Oaks Blvd. #101-330, Carmichael, CA 95608 USA; ³University of Birmingham, Sch. of Metall. & Matls., Edgbaston, Birmingham B15 2TT UK*

Aluminium is becoming of more interest in various P/M industries due to the possibilities of lightweighting components. There are many processes for manufacturing from powder feedstocks that are either in production, becoming commercialised or still undergoing development. The nature of these processes and the required properties of the end products mean that powders of different particle size, shape, composition and microstructure must be produced. The requirements of various processes requiring aluminium and aluminium alloy powders for metal matrix composites, laser sintering, powder forging and metal injection moulding are discussed in relation to powder particle size and structure. The key requirement of the powder manufacturer is to supply cost effective materials for these different processes. This may require compromises to be made by the supplier and consumer while the techniques evolve from development to large scale production.

4:50 PM

Processing and Properties of Porous Structures Made from Filamentary Nickel Powders: *David S. Wilkinson*¹; Valery Chani¹; Alex Zaitsev²; ¹McMaster University, Matl. Sci. & Engrg., 1280 Main St. W., Hamilton, ON L8S 4L7 Canada; ²INCO Technical Services, Sheridan Park, Mississauga, ON L5K 1Z9 Canada

INCO Ltd. manufactures a range of filamentary nickel powders that have high aspect ratios and irregular shapes. Such powders pack rather poorly making them ideal for the manufacture of low density structures (typical porosity levels are about 15 vol%). We have recently shown that the application of colloidal processing methodologies can be used to significantly increase the strength of such materials without increasing relative density. In the application of these materials in batteries adhesion to a rigid substrate is also important. We will discuss how this can be achieved through careful control of additives and the sintering process.

R.J. Arsenault Symposium on Materials Testing and Evaluation: Session IV

Sponsored by: Structural Materials Division, SMD-Mechanical Behavior of Materials-(Jt. ASM-MSCTS), SMD-Nuclear Materials Committee-(Jt. ASM-MSCTS)

Program Organizers: Raj Vaidyanathan, University of Central Florida, AMPAC MMAE, Orlando, FL 32816-2455 USA; Peter K. Liaw, University of Tennessee, Department of Materials Science and Engineering, Knoxville, TN 37996-2200 USA; K. Linga Murty, North Carolina State University, Raleigh, NC 27695-7909 USA

Tuesday PM
March 16, 2004

Room: 211A
Location: Charlotte Convention Center

Session Chairs: Raj Vaidyanathan, University of Central Florida, AMPAC/MMAE, Orlando, FL 32816-2455 USA; Nik Chawla, Arizona State University, Dept. of Chem. & Matls. Engrg., Tempe, AZ 6006 USA

2:00 PM Invited

Adhesion Test Using Cylindrical Indenters: *James C.M. Li*¹; ¹University of Rochester, Dept. of Mech. Engrg., Rochester, NY 14627 USA

The JKR (K. L. Johnson, K. Kendall and A. D. Roberts, Proc. Roy. Soc. London, A324, 301-313, 1971) theory of adhesion test between two spheres or a sphere and a plate has a hysteresis problem between the experimental loading curve and that of unloading. Most likely it is due to the change of interfacial energy with time or load or both. Such hysteresis prevents accurate calculation of adhesion energy at the time of pull-off from the JKR theory. A cylindrical indenter with a flat end avoids such problem and provides a more precise way of measuring adhesion energy at the instant of separation. This technique on thin films coated over a rigid substrate as well as the effect of moisture which may cause the formation of a thin layer of water between contact surfaces are reported. Work supported by N.Y. State Infotonics Center of Excellence and by NSF through DMR9623808 monitored by Dr. Bruce MacDonald.

2:30 PM

Evaluation of Ambient and Elevated Temperature Mechanical Behavior of Silicon Microdevices: *Brad L. Boyce*¹; Justin J. Van Den Avyle¹; Thomas E. Buchheit¹; ¹Sandia National Laboratories, Matls. & Proc. Scis. Ctr., PO Box 5800, MS 0889, Albuquerque, NM 87185-0889 USA

The emergence of microelectromechanical systems (MEMS) has required the concurrent development of techniques to determine their mechanical reliability. Testing at the relevant size scale is paramount due to the potential size-scale effects. Specifically, in brittle materials such as polycrystalline silicon, failure is thought to be size dependent due to the statistical sampling of flaws: smaller gage volumes have a lower likelihood of containing a large flaw. However, at the microsystem scale, non-standardized test techniques have led to ambiguous interpretations of size effects. In the current study, refined test methodology capable of testing at temperatures up to 800°C is coupled with self-aligning 2 micron wide micro-tensile specimens that span over two orders of magnitude in sampling volume. The results clearly show the size-dependence of strength on sampling volume, and are consistent with Weibull strength distributions. Discussion will focus on the implications with respect to the underlying material flaw distribution and reliable design. Sandia is a multiprogram laboratory operated by

Sandia Corporation, A Lockheed Martin Company, for the United States Department of Energy's National Nuclear Security Administration under contract DE-AC04-94AL85000.

2:50 PM

Micromechanical Testing at Small Length Scales: *Nik Chawla*¹; ¹Arizona State University, Dept. of Chem. & Matls. Engrg., Ira A. Fulton Sch. of Engrg., PO Box 876006, Tempe, AZ 85287 USA

With increasing interest in materials at nanometer and micrometer length scales, new innovative techniques are required to conduct mechanical testing. In this talk, we report on a micromechanical testing system with ultra-low force and high resolution capability for materials at small volumes. Mechanical testing of three types of materials will be cited as examples: (a) creep of Pb-free solder microspheres, (b) tensile and fatigue testing of high performance ceramic fibers, and (c) tensile testing of Al/SiC multilayered nanolaminates. The advantages and challenges associated with micromechanical testing at small length scales will be discussed.

3:10 PM

Measures of Plasticity in Single Crystals from Surface Deformation and Lattice Rotation Measurements Around Indents: *Pedro D. Peralta*¹; Robert Dickerson²; Majid Al Maharbi³; Mehdi Hakik¹; ¹Arizona State University, Dept. of Mech. & Aeros. Engrg., Engrg. Ctr., G Wing, Rm. 346, Tempe, AZ 85287-6106 USA; ²Los Alamos National Laboratory, Matls. Sci. & Tech. Div., MST-8, MS G755, Los Alamos, NM 87545 USA; ³Arizona State University, Sci. & Engrg. of Matls. Prog., Tempe, AZ 85287 USA

Vickers and Spherical indents on several monocrystalline substrates have been characterized using optical, electron and scanning probe microscopy as well as profilometry. Orientation Imaging Microscopy was used to map changes on the local crystallographic orientation of the surface surrounding one indent on copper to obtain maps of the lattice rotation due to plastic deformation. The results indicate that sink-in and pile-up behavior depend strongly on the in-plane crystallographic orientation of the diagonals of the indent and is related to local multiplicity of slip. Regions with multiple slip show larger lattice rotations and sink-in, whereas regions with lower slip density had lower lattice rotations and show pile-ups. Strains surrounding the indents were obtained from OIM data using kinematical relations for single crystal plasticity. An average strain of 29% next to a Vickers indent was deduced from the analysis, which agrees quite well with the characteristic strain reported for Vickers indents.

3:30 PM Break**3:50 PM**

An Instrumented Indentation Study of Deformation in Shape-Memory NiTi: *S. Rajagopalan*¹; Raj Vaidyanathan¹; ¹University of Central Florida, AMPAC/MMAE, Eng-I Rm. 381, 4000 Central Florida Blvd., Orlando, FL 32816-2455 USA

Shape-memory alloys (SMAs) are of theoretical and commercial interest for the deformation phenomena they exhibit - twinning and stress-induced/temperature-induced phase transformation. Here we report on the use of instrumented indentation to capture the formation of stress-induced martensite and twinning from load-depth indentation responses in NiTi and assess the effect of geometrical and microstructural length scales on deformation behavior. Load-depth curves from indentation were correlated with macroscopic stress-strain curves. Applications of SMAs usually call for specific thermomechanical properties and a variety of compositions and thermomechanical treatments can thus be empirically attempted in centimeter scaled buttons and indented prior to large scale production, resulting in substantial cost savings. This work is supported by NASA and NSF (CAREER DMR-0239512).

4:10 PM

Miniaturized Impression Creep of Sn-3.5Ag Microelectronic Solder Balls and Associated Mechanics-Related Effects: *Deng Pan*¹; Robert A. Marks¹; Indranath Dutta¹; ¹Naval Postgraduate School, Mech. Engrg., 700 Dyer Rd., Monterey, CA 93943 USA

Impression creep, in which a flat-ended cylindrical indenter is used to load a small area of the specimen surface under a constant compressive stress, has been used to study the creep behavior of a wide range of materials. One of the attractive features of the impression creep test is its ability to test specimens of very small material volumes and miniaturized components with minimal sample preparation. In this paper, we report the development of an apparatus and approach for impression creep testing of microelectronic solder balls of 0.75mm diameter attached to a ball grid array (BGA) substrate, using a 0.1-mm diameter indenter. This approach enables direct on-substrate or on-chip testing of solder balls. Details of apparatus design, experimental

methodology, and experimental creep results based on lead-free solders (Sn-Ag and Sn-Ag-Cu) will be presented. A mechanics-induced complication of impression creep, particularly under conditions of slow deformation, which can potentially cause anomalous interpretation of the resultant creep data, is also discussed. A methodological remedy of this problem is proposed, and validated via experiments.

4:30 PM

A Technique for Measuring Compressive Properties of Single Microballoons: *Kipp B. Carlisle¹*; Mark C. Koopman¹; Krishan K. Chawla¹; Gary M. Gladysz²; ¹University of Alabama, 1150 10th Ave. S., BEC 254, Birmingham, AL 35294 USA; ²Los Alamos National Laboratory, Engrg. Scis. & Applications Div., Weapon Matls. & Mfg., MS C930, Los Alamos, NM 87545 USA

A technique has been developed to obtain mechanical properties of individual hollow microspheres, or microballoons. This technique utilizes a nanoindentation instrument equipped with a cylindrical sapphire tip, thereby replicating a conventional mechanical compression test on a nanometer scale. The procedure has thus been termed nanocompression, since the extreme sensitivity of the nanoindentation instrument provided a load resolution of 50 nN and a displacement resolution better than 0.02 nm. The load-displacement curves resulting from this test provided mechanical properties including maximum load and strain to failure. Materials tested included polymer, glass, and carbon microspheres, with the primary focus being carbon microballoons. Characterization of the microballoons, in terms of wall thickness and diameter, was undertaken through quantitative microscopy in an effort to correlate morphology to mechanical properties. A trend has been observed between strain to failure and carbon microballoon diameter. This work was supported by DOE/LANL sub-contract 44277-SOL-02 4X, LA-UR-03-5700.

4:50 PM

High Temperature Tensile and Creep of 7034 Aluminum Alloy: *K. Xu¹*; R. F. Alessi¹; D. S. Kmietek¹; R. Zawierucha¹; ¹Praxair, Inc., 175 E. Park Dr., Tonawanda, NY 14051 USA

Conventional 7xxx aluminum alloys have excellent mechanical properties at room temperature. However, their strength degrades rapidly at elevated temperatures due to the coarsening of the precipitates. Spray forming is a relatively new technology in material fabrication which produces near net shape preforms by rapid solidification of atomized droplets in a single step. In this investigation, the tensile and creep properties of spray formed 7034 aluminum alloy (Al-Zn-Mg-Cu-Zr) were studied in the temperature range of 90 to 150°C. It was found that the new alloy not only had a superior strength at room temperature, its creep resistance was also greatly improved compared with 7075-T6. The high strength of the alloy was achieved by the high Zn content, which resulted in a high percentage of precipitates. The enhancement in creep resistance was attributed to the addition of Zr which formed finely dispersed stable intermetallic compound Al₃Zr. The spray forming process made it possible to produce the high Zn aluminum alloy without macro segregation and cracking.

Solidification of Aluminum Alloys: Microstructural Evolution II

Sponsored by: Materials Processing & Manufacturing Division, MPMD-Solidification Committee

Program Organizers: Men Glenn Chu, Alcoa Inc., Alcoa Technical Center, Alcoa Center, PA 15069 USA; Douglas A. Granger, GRAS, Inc., Murrysville, PA 15668-1332 USA; Qingyou Han, Oak Ridge National Laboratory, Oak Ridge, TN 37831-6083 USA

Tuesday PM

Room: 207B/C

March 16, 2004

Location: Charlotte Convention Center

Session Chairs: Douglas A. Granger, GRAS Inc., Murrysville, PA 15668-1332 USA; David E.J. Talbot, Consultant, Ruislip HA 47TG, Middlesex UK

2:00 PM

Recent Progress in Understanding Eutectic Solidification in Aluminum-Silicon Foundry Alloys: *Arne K. Dahle¹*; Stuart D. McDonald²; Kazuhiro Nogita²; Liming Lu¹; ¹University of Queensland, CRC for Cast Metals Mfg., Div of Matls. Engrg., Brisbane, Qld 4072 Australia; ²University of Queensland, Div. of Matls. Engrg., Brisbane, Qld 4072 Australia

It is now well established that three different eutectic solidification mechanisms may occur in Al-Si foundry alloys. The operation of each

mechanism can be controlled by altering chemical composition and casting conditions. Recent research has focussed on the understanding of the mechanisms determining the eutectic solidification mode by investigating the growth mechanisms in ultra-high purity and commercial purity alloys, the effect of a wide range of different potential modifier elements and investigating the eutectic nucleation mode. It is concluded that nucleation of eutectic grains is prolific in unmodified commercial purity alloys. In contrast, high-purity alloys have relatively few nuclei and only a few grains nucleate. Nuclei can also be removed, or rendered inactive, by the addition of modifying elements to commercial purity alloys. Nucleation frequency has an effect on the morphology, as does also some modifier elements. The practical implications of the eutectic nucleation and growth modes are discussed.

2:20 PM

The Role of Iron in the Nucleation of Eutectic Silicon in Aluminum-Silicon Hypoeutectic Alloys: *Sumanth Shankar¹*; Yancy W. Riddle¹; Makhlof M. Makhlof¹; ¹Worcester Polytechnic Institute (WPI), Advd. Casting Rsch. Ctr., Metal Proc. Inst. (MPI), Dept. of Mech. Engrg., 100 Inst. Rd., Worcester, MA 01609 USA

Understanding the mechanism of evolution and modification of the eutectic phases in the hypoeutectic Al-Si alloys greatly enhances our understanding and predictive capabilities of casting properties such as feedability, porosity distributions, heat treatment responses, etc. For the past eighty years there has been various contradicting hypotheses proposed to understand the evolution and modification of the eutectic phases in hypoeutectic Al-Si alloy. One of the main reasons for the lack in understanding is due to the lack of technology to critically analyze the microstructures and support a working mechanism. Novel emerging technologies such as Focused Ion Beam (FIB) milling, advanced Transmission Electron Microscopy (TEM) and Electron Back Scatter Diffraction patterns (EBSD) aided an in-depth understanding of the evolution of the eutectic phases in Al-Si cast alloys. A theory has been proposed in this paper to explain the nucleation of the eutectic phases: Si and Al during solidification. It was observed that iron is a critical impurity in Aluminum-Silicon alloys that affects the nucleation of the eutectic phases in the alloy. Results show that the eutectic Si nucleates on a (Al₃Si₂Fe) phase in the solute field ahead of the primary aluminum dendrites and the eutectic aluminum grains nucleate on the eutectic Si. Another theory is also presented in this paper to explain the modification of the eutectic phases in the alloy. A working mechanism has been proposed wherein the drastic change in the fluid properties of the interdendritic eutectic liquid upon adding modifiers such as Sr, Na, etc. plays a critical role in modification of the eutectic phases. The change in wetting characteristics of the eutectic liquid delays the nucleation event of the eutectic silicon phase and results in considerable undercooling of the melt at the eutectic transformation temperature. Addition of modifiers to the alloy melt results in refinement of the silicon morphology from flaky to fibrous structure and in refinement of the eutectic aluminum grains by at least an order of magnitude.

2:40 PM

Effects of Simultaneous Na and Sr Additions in a Eutectic Al-Si Casting Alloy: *Hamish R. McIntyre¹*; *Milo V. Kral¹*; Jason Looij²; ¹University of Canterbury, Mech. Engrg., PO Box 4800, Christchurch New Zealand; ²CWF Hamilton, PO Box 709, Christchurch New Zealand

The eutectic modification of Al-Si casting alloys through additions of modifying elements has been studied extensively in previous work. Sodium has a rapid modification effect with short duration while strontium is associated with a slower acting but longer lasting effect. It is also known that simultaneous additions of Na and Sr can be beneficial but this phenomenon is not particularly well-documented or understood. The purpose of this work was to characterise the effects of combined Na and Sr additions to a commercial eutectic Al-Si alloy in comparison with the separate additions of Na and Sr. The influence of modification on the morphology and size of iron-rich intermetallics was also of interest. Eutectic and intermetallic particle morphology, tensile strength and compositional data were obtained from samples taken at intervals during extended melt holding periods. A predictive model for the diminishing effect of modifiers over time is proposed.

3:00 PM

High-Rate Growth Transitions in Al-Si Eutectic: *Luke G. Englund¹*; Ralph E. Napolitano¹; ¹Iowa State University, MSE, 104 Wilhelm Hall, Ames, IA 50011 USA

The high-rate growth-mode transition (i.e. quench modification) observed in the eutectic solidification of Al-Si alloys was studied using directional solidification over a wide range of growth velocities. Measurements of interface undercooling, phase spacing, particle morphol-

ogy, and crystallographic orientation were performed to understand the role of interfacial properties and crystallographic anisotropy on mechanisms of spacing adjustment, texturing, and morphological selection through the quench modification transition.

3:20 PM Break

3:40 PM Keynote

Grain Refinement of Aluminum Alloys: *A. Lindsay Greer*¹; ¹University of Cambridge, Matls. Sci. & Metall., Pembroke St., Cambridge CB2 3QZ UK

This review describes recent studies of the mechanisms by which inoculation refines the as-cast grain structure of aluminum alloys. The emphasis is on where fundamental understanding can improve industrial practice with existing refiners and also can assist the development of new refiners. The problems of relating fundamental studies to industrial practice are also addressed. The nucleation of new grains is difficult to analyze because many parameters are not known with precision; nevertheless in favorable cases grain size can be predicted quantitatively as a function of alloy composition and processing conditions. Topics to be covered include: nucleation mechanisms, growth restriction by solute, fade of refiner performance, the various mechanisms of poisoning and ways to avoid it, design of refiners, comparison of different refiners from both main types Al-Ti-B and Al-Ti-C, prediction of grain size, and prediction of the columnar-to-equiaxed transition.

4:10 PM

Factors Affecting the Development of a Fine Grained Solidification Microstructure in Aluminum Alloys: *Mark Easton*¹; David StJohn²; ¹Monash University, CRC for Cast Metals Mfg. (CAST), Sch. of Physics & Matls. Engrg., PO Box 69, Melbourne, Victoria Australia; ²University of Queensland, CRC for Cast Metals Mfg. (CAST), Div. of Matls., Brisbane, Queensland Australia

In addition to the need for potent heterogeneous particles to activate nucleation, the alloy content, described by the growth restriction factor, and the solidification conditions, in particular the cooling rate and the amount of undercooling produced when pouring metal into a chill mold, also affect the final grain size achieved. This paper overviews recent work that investigates these factors for the addition of Al-Ti-B type grain refiners in a variety of wrought aluminum alloys. It was found that relatively simple relationships can be developed between the potency and number of nucleant particles and the cooling rate, that allow the determination of the most effective means of achieving a particular grain size. The influence of using thermal undercooling to generate wall crystals and its effect on the grain size is also discussed. The findings are then applied to the problem of achieving lowest cost grain refiner additions in VDC casting.

4:30 PM

An Investigative Study of Si Poisoning in Al-Si Alloys Using the Metallic Glass Technique: *Brian John McKay*¹; P. Schumacher¹; ¹University of Leoben, Inst. of Gießereikunde, Franz-Josef Str. 18, Leoben A-8700 Austria

An Al80Cu10Ni8Si2 (at. %) alloy was selected for a metallic glass study. Melt-spinning the alloy and a Al-5Ti-1B grain refiner rod resulted in heterogeneous boride particles being embedded within a glass matrix. The degree of nucleation and crystallization of the glass on borides within the matrix was controlled by the quench rate. Results indicate that Al nucleates on the borides with the close packed planes and directions being parallel: $\{111\}Al//\{001\}TiB_2$, $\langle 110 \rangle Al//\langle 100 \rangle TiB_2$. However, with a high Ti content (0.09 at. %) and with long holding times (30 minutes) a silicide phase was found nucleating on the borides: the borides displaying no evidence of nucleating Al. This silicide phase observed was not present under the previous conditions. It is proposed that the silicides consume heterogeneous nucleation sites thus preventing a-Al from nucleating. This mechanism is suggested to be the one that is commonly referred to in the literature as 'Si poisoning'. Other intermetallics were also found to nucleate on the borides.

4:50 PM

Columnar-to-Equiaxed Transition Studies in Al-2wt%Cu, Al-4wt%Cu, Al-10wt%Cu, Al-20wt%Cu and Al-33.2wt%Cu Alloys: Alicia Esther Ares²; Rubens Caram³; *Carlos Enrique Schvezov*¹; ¹University of Misiones, 1552 Azara St., Posadas-Misiones 3300 Argentina; ²CONICET, 1552 Azara St., Posadas-Misiones Argentina; ³State University of Campinas, CP 6122, Campinas-Sao Paulo CP 6122 Brazil

The columnar to equiaxed transition (CET) was studied in Al-2wt%Cu, Al-4wt%Cu, Al-10wt%Cu, Al-20wt%Cu and Al-33.2wt%Cu alloys, which were solidified directionally from a chill face. The main parameters analyzed include the temperature gradients, solidification velocities of the liquidus and solidus fronts, and grain size. The transi-

tion does not occur in an abrupt form in the samples and is present when the gradient in the liquid ahead of the columnar dendrites reaches critical and minimum values, being negative in most of cases. In addition, there is an increase in the velocity of the liquidus front faster than the solidus front, which increases the size of the mushy zone. The size of the equiaxed grains increase with distance from the transition, an observation that was independent of alloy composition. The results are compared with those obtained by other authors.

Solidification Processes and Microstructures: A Symposium in Honor of Prof. W. Kurz: Rapid Solidification

Sponsored by: Materials Processing & Manufacturing Division, MPMD-Solidification Committee

Program Organizers: Michel Rappaz, Ecole Polytechnique Fédérale de Lausanne, MXG, Lausanne Switzerland; Christoph Beckermann, University of Iowa, Department of Mechanical Engineering, Iowa City, IA 52242 USA; R. K. Trivedi, Iowa State University, Ames, IA 50011 USA

Tuesday PM
March 16, 2004

Room: 207D
Location: Charlotte Convention Center

Session Chair: W. J. Boettinger, National Institute for Standards and Technology, Gaithersburg, MD 20879 USA

2:00 PM Invited

Rapid Dendrite Growth in Undercooled Melts: Experiments and Modeling: *Dieter M. Herlach*¹; ¹German Aerospace Center, Inst. of Space Simulation, Linder Hoehe, Cologne, NRW D-51170 Germany

Essential progress of modeling of rapid dendrite growth in undercooled melts was achieved by the "classic" work of Wilfried Kurz et al. [1]. At the same time new experimental techniques were developed to measure rapid dendrite growth velocities as a function of undercooling in metallic melts. In the present work, non-equilibrium phenomena are reviewed occurring during rapid growth of dendrites in undercooled melts. Experimental results and their analysis within dendrite growth models are presented for the solidification of segregation-free microstructures and disordered superlattice structures of intermetallics. It will be shown that the short range order in the undercooled melt and its similarity/dissimilarity to the short range order of the solidifying phase has an essential impact on the atomic attachment kinetics and thus the kinetic interface undercooling of the solidification front. J. Lipton, W. Kurz, and R. Trivedi, *Acta Metall.* 35 (1987) 957-964.

2:30 PM Invited

Tests of Theories for Nonplanar Growth During Rapid Alloy Solidification: *Michael J. Aziz*¹; ¹Harvard University, Div. of Engrg. Appl. Scis., 29 Oxford St., Cambridge, MA 02138 USA

During rapid solidification, kinetically suppressed solute partitioning at the crystal/melt interface, as well as kinetic interfacial undercooling, become important. Both of these effects are expected to have significant stabilizing influences on a planar interface during rapid solidification. We will present experimental tests of models for the transition from planar to cellular growth, and for the velocity-undercooling function of the dendrite tip, in the velocity regime where nonequilibrium interface kinetics are important.

3:00 PM Invited

Phase Selection Transitions During Undercooled Melt Solidification: *John H. Perepezko*¹; ¹University of Wisconsin, Dept. Matls. Sci. & Engrg., 1509 Univ. Ave., Madison, WI 53706 USA

Alloy phase selection is often controlled by nucleation during solidification of undercooled melts. The structure options are defined by thermodynamics, but the selection process is determined by a nucleation kinetics competition. During product phase transitions that develop with changing undercooling level or alloy composition, competitive nucleation can yield mixed phase microstructures as shown for rapid solidification of eutectics and glass forming alloys. Alternatively, at increasing rates, an initial solidification reaction can be superseded by a new nucleation controlled phase selection transition due to growth kinetic limitations that can develop during resolidification following surface melting or due to modification of heterogeneous nucleants. The complete analysis of solidification microstructure evolution during phase selection transitions also requires the consideration of solid-state reactions. The support of ARO (DAAD 19-01-1-0486) and NASA (NAG8-1672) are gratefully acknowledged.

3:30 PM Break

4:00 PM Invited

Rapid Solidification Microstructures: Rohit K. Trivedi¹; ¹Iowa State University, Matls. Sci. & Engrg., 100 Wilhelm Hall, Ames, IA 50011 USA

During the past 20 years, significant theoretical and experimental contributions have been made by Wilfried Kurz that have advanced our understanding of microstructure evolution under rapid solidification conditions. These contributions are presented with specific emphasis on the application of the models to the data obtained by laser processing and by the solidification of fine droplets. Key concepts in the microstructure evolution under rapid solidifications that still remain to be addressed quantitatively will be discussed.

4:30 PM

Diffuse Solid-Liquid Interfaces and Solute Trapping: Reza Abbaschian¹; Wilfried Kurz²; ¹University of Florida, Matls. Sci. & Engrg., PO Box 116400, Gainesville, FL 32611 USA; ²EPFL, Metallurgie Physics, MXG-Ecublens, CH 1015 Lausanne Switzerland

A phenomenological model is presented for partitioning of solute atoms across solid-liquid interface during solidification. The model treats the interface as being "diffuse", for which the transition from one phase to another takes place gradually when time-averaged over the entire layer of atoms parallel to the interface. For such an interface, the chemical potential of species also changes continuously from those in the liquid side of the interface to those in the solid. Moreover, the solute redistribution coefficient during solidification will depend on the diffuseness of the interface, which in turn is related to the interfacial Peclet number. The latter is related to the interface velocity, its thickness and the overall migration rate of species across the interface. The influence of solidification rate on the solute trapping will be discussed and compared to other solute trapping models.

4:45 PM

Glass Forming Ability and Type of Eutectic-Coupled Zone: Yong Zhang¹; Hao Tan¹; Dong Ma¹; Yi Li¹; ¹National University of Singapore, Dept. of Matls. Sci., Lower Kent Ridge Rd., Singapore 119260 Singapore

As the critical cooling rate for metallic glass formation has been reduced dramatically over the last ten years, e.g. 0.1 K/s for Pd based alloys, the microstructure control, particularly the primary dendrite plus amorphous matrix becomes possible by conventional solidification processing techniques, e.g. copper mould casting and directional solidification technique. Many crystalline reinforced metallic glass matrix in-situ composites by have been reported with improved mechanical properties. We report our experimental results on the formation of crystalline phase reinforced amorphous matrix in-situ composite and the microstructural changes in several novel bulk glass forming alloys, processed by Bridgman technique. The emphasis will be on the dendritic spacing, and volume fraction of the crystalline phases and their effect on the mechanical properties of these composites in Pd, La and Zr based amorphous forming alloys. We will also attempt to correlate glass forming ability and the microstructure changes with the types of the eutectic-coupled zone of these alloys.

5:00 PM

Optimum Stability in Rapidly Solidified Nickel-Based Alloys: Paul R. Algosio¹; William H. Hofmeister¹; Robert J. Bayuzick¹; ¹Vanderbilt University, Chem. Engrg., VU Sta. B 351604, Nashville, TN 37235-1604 USA

Solidification velocities of various nickel-based alloys were measured as a function of undercooling. A leveling in the solidification velocity (or 'plateau') was observed at intermediate undercoolings due to the presence of solute. This result does not agree with the IMS model (Ivantsov solution with marginal stability arguments), which relates dendrite growth velocity to total undercooling. The IMS model does not predict a velocity plateau at intermediate undercoolings for alloys with a sufficiently high equilibrium partition coefficient, $k_E > 0.1$, although a plateau exists for a wide range of alloys regardless of the value of k_E . The disagreement between the IMS model and experiment is due to the restriction of the marginal stability parameter to a constant, $\sigma^* = 0.025$. Another interfacial stability model, the optimum stability conjecture (OSC), allows for σ^* to vary as a function of Peclet number, $\sigma^* = \sigma^*(Pe)$. The OSC exhibits excellent agreement with experimental results.

5:15 PM

Nonequilibrium Phase Selection During Weld Solidification of Fe-C-Mn-Al Steels: Sudarsanam Suresh Babu¹; John M. Vitek¹; John W. Elmer²; Stan A. David¹; ¹Oak Ridge National Laboratory, M&C Div., 1 Bethel Valley Rd., Bldg. 4508; MS 6096, Oak Ridge, TN

37831-6096 USA; ²Lawrence Livermore National Laboratory, Livermore, CA USA

The phase selection phenomena as a function of composition and interface growth velocity were investigated in Fe-0.2C-0.5Mn-Al (wt.%) self-shielded flux cored arc weld metal deposits. Two aluminum concentrations (1.8 and 3.7 wt.%) were investigated to observe different δ -ferrite stabilizing effects on the microstructure. Under normal weld cooling conditions, the primary solidification in these steels occurs by δ -ferrite formation, however, solidification morphology changes at high cooling rates. The changes in weld cooling rates were produced by changes in the arc welding conditions, and it was shown that, above a critical interface velocity, a shift was induced in the primary solidification mode to nonequilibrium austenite. Moreover, the change in primary solidification mode occurred irrespective of aluminum concentration. The above phase selection phenomenon was tracked in-situ using a time-resolved X-ray diffraction technique employing Synchrotron radiation. Using the theoretical treatment of dendritic solidification and phase selection maps advanced by Kurz and his co-workers, the microstructure evolution at high weld solidification rates was evaluated. The dendrite growth theories for multicomponent solidification suggest that phase selection in this alloy system may be closely related to high carbon concentrations in these steels that cannot be trapped in the δ -ferrite phase at high solid-liquid interface velocities. This in-turn leads to enrichment of carbon in the liquid phase and the subsequent change in primary solidification mode from primary δ -ferrite to nonequilibrium austenite. Research sponsored by the U.S. Department of Energy, Division of Materials Sciences and Engineering under contract Number DE-AC05-00OR22725 with UT-Battelle, LLC. A portion of this work was performed under the auspices of the U. S. Department of Energy, Lawrence Livermore National Laboratory, under Contract No. W-7405-ENG-48.

5:30 PM

Femtosecond Laser Micromachining of Superalloy Single Crystals: Q. Feng¹; Y. N. Picard¹; H. Liu²; S. M. Yalisove¹; G. Mourou²; T. M. Pollock¹; ¹University of Michigan, Dept. of Matls. Sci. & Engrg., 2300 Hayward St., Ann Arbor, MI 48109 USA; ²University of Michigan, Ctr. for Ultrafast Optical Sci., 2200 Bonisteel Blvd., Ann Arbor, MI 48109 USA

Femtosecond laser micromachining with ultrafast laser pulses is attractive for a range of applications in manufacturing and life sciences, where minimal collateral damage, a limited heat affected zone and high precision processing are required. One potential application is the drilling of cooling holes in aircraft engine components, such as turbine blades and vanes. Femtosecond laser micromachining of Ni-based superalloy single crystals and thermal barrier coated (TBC) superalloys have been carried out on a laser system using a series of 780nm wavelength, 150fs pulse-length laser shots. Microstructural analyses of regions machined with multiple pulses revealed no indication of negative effects such as microcracking and remelting layers in the vicinity of the laser-machined holes. Further, the studies were conducted using transmission electron microscopy (TEM). The damaged region near 5 μ m diameter laser-machined holes drilled in pre-thinned TEM foils was less than 2 μ m and 0.5 μ m with the laser power intensity at 10 times ablation threshold and near the threshold, respectively. A high density of dislocations and dislocation networks were found inside the channels of the γ matrix within 4 μ m from the edge of holes. The deformation substructures of the samples will be compared to those observed in high temperature creep and high strain rate deformation.

5:45 PM

Microstructure Selection During Rapid Solidification of Al-Si Powder: Amber L. Genau¹; Iver E. Anderson²; Rohit Trivedi²; ¹Iowa State University, 223 Metals Dvlp., Ames, IA 50011 USA; ²Ames Laboratory, Ames, IA 50011 USA

Gas atomization techniques provide access to regions of extreme undercooling in metal alloys. The rapid solidification which occurs at such extremes often produces unique and desirable microstructures, while also presenting an opportunity to study the fundamental processes of nucleation and growth. Aluminum-silicon was chosen as a model for simple eutectic systems displaying a faceted/unfaceted interface. Fine droplets of Si-15Al and Si-18Al (wt. %) were produced using high-pressure gas (He) atomization. Quantitative measurements of eutectic spacing were made using SEM and TEM images of cross-sectioned particles. The spacings were compared to those predicted by theoretical solidification models and a maximum undercooling was estimated for the particles. A variation in the selection of nucleation sites as a function of particle size was also observed. These results are analyzed to predict microstructure selection as a function of both

Surfaces and Interfaces in Nanostructured Materials: Grain & Phase Boundaries

Sponsored by: Materials Processing and Manufacturing Division, MPMD-Surface Engineering Committee

Program Organizers: Sharmila M. Mukhopadhyay, Wright State University, Department of Mechanical and Materials Engineering, Dayton, OH 45435 USA; Arvind Agarwal, Florida International University, Department of Mechanical and Materials Engineering, Miami, FL 33174 USA; Narendra B. Dahotre, University of Tennessee, Department of Materials Science & Engineering, Knoxville, TN 37932 USA; Sudipta Seal, University of Central Florida, Advanced Materials Processing and Analysis Center and Mechanical, Materials and Aerospace Engineering, Oviedo, FL 32765-7962 USA

Tuesday PM Room: 217A
March 16, 2004 Location: Charlotte Convention Center

Session Chairs: Sharmila M. Mukhopadhyay, Wright State University, Dept. of Mech. & Matls. Engrg., Dayton, OH 45435 USA; Sudipta Seal, University of Central Florida, Advd. Matls. Procg. & Analysis Ctr., Oviedo, FL 32765-7962 USA

2:00 PM Invited

Nanoanalysis of Advanced Materials: *Manfred Rühle*¹; ¹MPI für Metallforschung, Heisenbergstr. 3, Stuttgart 70569 Germany

Advanced materials are mostly designed so that they possess specific properties for specific applications. Quite often it is also important that the overall dimensions of a component made out of advanced materials is small since for many applications, e. g. in telecommunication systems and microelectronics, only restricted space is available. In addition, often nanomaterials are also used as advanced materials. For nanomaterials at least one dimension of the component is in the nanometer scale. By advanced TEM techniques the structure and composition of specific areas of nanomaterials can be analyzed to the atomic level. The most interesting areas are concentrated around crystal lattice defects, such as interfaces, dislocations, etc. In the presentation recent results, opportunities and limitations of advanced TEM techniques will be described.

2:25 PM Invited

Dislocations, Dislocation Boundaries and High Angle Boundaries in Nanocrystalline Copper Deformed by Sliding: *Darcy A. Hughes*¹; Niels Hansen²; ¹Sandia National Laboratories, PO Box 969, MS 9405, Livermore, CA 94551-0969 USA; ²Riso National Laboratory, Ctr. for Fundamental Rsch., Metal Structures in Four Dimensions, PO Box 49, Roskilde Denmark

Quantitative measurement and analysis of structural parameters have shown that the microstructural evolution follows a universal path of grain subdivision down to the nanoscale. This behavior has allowed an analysis of the formation and evolution of graded nanoscale structures produced by sliding. Transmission electron microscopy studies and scaling analyses of such these structures show the dominating role of dislocations in the development of deformation microstructures at multiple length scales. The crucial role of dislocations has been documented by high resolution electron microscope (HREM) analysis which has revealed the presence of a large number of glide dislocations in layers between boundaries with individual spacing as fine as 5 nm. HREM has also been used to survey the structure of dislocation and high angle boundaries including grain orientation, boundary misorientation angle and boundary width. This work was supported by the Office of Basic Energy Sciences, the U.S. D.O. E. under contract no. DE-AC04-94AL85000.

2:50 PM

Atomistic Modeling of Point Defects and Diffusion in Grain Boundaries: *Akira Suzuki*¹; Yuri Mishin¹; ¹George Mason University, Sch. of Computational Scis., 4400 Univ. Dr., MS 5C3, Fairfax, VA 22030-4444 USA

A variety of atomistic simulation techniques have been applied to study point defects and diffusion in metallic grain boundaries and the impact of grain-boundary kinetics on the materials behavior. The simulations have been performed for Al, Cu, and the Cu-Ag system. Atomic interactions are modeled by embedded-atom potentials fit to both experimental and first-principles data. Atomic mechanisms of

vacancy and interstitial formation and migration in a large set of grain boundaries have been studied by molecular dynamics and other methods. New structural forms of point defects have been found, such as unstable vacancies and delocalized vacancies and interstitials. Besides the standard vacancy mechanism, grain boundary diffusion is often mediated by collective processes involving 2-4 atoms. The diffusion coefficients in grain boundaries calculated by molecular dynamics and kinetic Monte Carlo simulations compare well with experimental data. Possible mechanisms of defect formation and migration in non-equilibrium grain boundaries are discussed.

3:10 PM Break

3:30 PM

Differences in Lattice Constant Between the <100> and <111> Oriented Grains in Nanocrystalline Ni and Ni-20 % Fe Electrodeposits: *Dong Nyung Lee*¹; ¹Seoul National University, Rsch. Inst. of Advd. Matls., Seoul 151-742 Korea

Park et al. (2002) measured the deposition and annealing textures of nanocrystalline 30 mm thick Ni and 20 mm thick Ni-20 % Fe electrodeposits obtained from Watts-type solutions (nickel chloride, iron sulfate, boric acid, saccharine and other additives) using an x-ray diffraction method. They found that the deposition texture of major <100> + minor <111> changed to the texture characterized by major <111> + minor <100> after annealing. They also found that the lattice constants of the <100> oriented grains in the as-deposited state are larger than those of the <111> oriented grains, which were measured by a Synchrotron x-ray diffraction of 8C1 POSCO beam line. In this paper, a model has been advanced to explain the unusual results of lattice constants and the texture transition after annealing has been discussed based on differences in grain boundary energy and mobility between the <100> and <111> oriented grains.

3:50 PM Invited

Lattice Microstrain and Grain Boundary Structure in a Nanocrystalline Al Alloy Prepared Via Mechanical Alloying: *Alexandre L. Vasiliev*¹; Angel L. Ortiz²; *Leon L. Shaw*¹; ¹University of Connecticut, Metall. & Matls. Engrg., Storrs, CT 06269 USA; ²Universidad de Extremadura, Depto. de Electrónica e Ingeniería Electromecánica, Badajoz 06071 Spain

Lattice microstrains in a nanocrystalline Al₉₃Fe₃Cr₂Ti₂ alloy prepared via mechanical alloying (MA) starting from elemental powders have been investigated through the X-ray diffraction (XRD) Rietveld method coupled with the line-broadening analysis. The microstrains so-determined are related to the structure in the interiors and at the grain boundaries of the nanograins determined via transmission electron microscopy (TEM) and high-resolution electron microscopy (HREM). Although the nanograins are produced via severe plastic deformation, the interiors of the nanograins are free of dislocations. The high lattice microstrains produced in these nanograins are attributed to lattice bending induced by the stresses imposed by the non-equilibrium grain boundaries. Annealing at intermediate temperatures results in more stable grain boundary structure and thus lower lattice microstrains.

4:15 PM

Interface-Controlled Nanocrystal Phase Transformations: *Gerhard Wilde*¹; Peter Bunzel¹; Harald Roesner¹; Ruslan Z. Valiev²; Jörg Weissmueller¹; ¹Forschungszentrum Karlsruhe, Inst. of Nanotech., PO Box 3640, Karlsruhe 76021 Germany; ²Ufa State Aviation University, Inst. of Physics of Advd. Matls., Ufa 450 000 Russia

The impact of interface properties and - more specifically - of the morphology of the interface of matrix-encased metallic nanoparticles on macroscopic properties such as the melting behavior has been investigated experimentally by a combination of microscopic, microanalytical and calorimetric measurement methods. In order to elucidate the interface contribution clearly, material of identical chemical composition has been synthesized by mechanical attrition or, alternatively, by rapid melt quenching. Additionally, thermal annealing and high-pressure torsion straining have been applied to modify the interface morphology for the differently pre-treated material in order to investigate the reversibility of the relation between interface morphology and macroscopic materials properties. As one result, the measurements clearly indicate that the shift of the melting temperature at small system size is thermodynamic in nature, as opposed to explanations based on nucleation kinetics. In addition, internal interfaces become important if multiphase alloy nanoparticles are concerned. Here, first results on the constitutive behavior of nanoscaled binary alloy systems will be discussed. This work is supported by the DFG under contract no. WI 1899/2-2.

4:35 PM

Grain Boundary Dissociation in Nanocrystalline Gold: Douglas L. Medlin¹; G. A. Lucadamo¹; D. Cohen¹; S. M. Foiles²; ¹Sandia National Laboratories, Thin Film & Interface Sci. Dept., MS 9161, 7011 East Ave., Livermore, CA 94551 USA; ²Sandia National Laboratories, Matls. & Proc. Modlg. Dept., MS 1411, Albuquerque, NM 87185 USA

A common structural relaxation at grain boundaries in low stacking-fault-energy metals is the dissociation of the interface into dense arrays of stacking faults. This phenomenon is of particular importance in nanocrystalline materials because it increases the volume fraction of material associated with interfacial sites and because the constraints of geometric compatibility in such small-grained systems can locally promote the dissociation. Here, using HRTEM observations and atomistic simulations, we consider the structure of dissociated boundaries in nanocrystalline, [110]-textured Au films. We discuss how the specific interfacial stacking in dissociated layers is connected to the intergranular misorientation via the geometric properties of Shockley partial dislocations. To illustrate, we examine the specific orientations that lead to 9R and HCP stacking. This work is supported by the U.S. Department of Energy under contract No. DE-AC04-94AL85000 by the Office of Basic Energy Science, Division of Materials Science.

Symposium on Microstructural Stability in Honor of Prof. Roger D. Doherty: Microstructural Stability: Precipitation and Other Topics

Sponsored by: Aluminum Association, Materials Processing and Manufacturing Division, Structural Materials Division, MPMD-Solidification Committee, SMD-Physical Metallurgy Committee
Program Organizer: Anthony D. Rollett, Carnegie Mellon University, Department of Materials Science & Engineering, Pittsburgh, PA 15213-3918 USA

Tuesday PM

Room: 216A

March 16, 2004

Location: Charlotte Convention Center

Session Chair: A. K. Vasudevan, Office of Naval Research, Arlington, VA USA

2:00 PM

Modeling the Dispersoid Effect on Recrystallization in Hot Deformed Aluminum Alloys: Jaakko P. Suni¹; ¹Alcoa, Inc., Alcoa Techn. Ctr., 100 Techn. Dr., Alcoa Ctr., PA 15069 USA

A model framework, involving evolutionary size distributions of subgrains and recrystallized grains is described, including the effect of fine particle drag. The model is applied to a well characterized data set, consisting of different dispersion levels for commercially hot rolled aluminum alloy 3004. In this case, the normal Zener drag term is inadequate, in that substantially more drag is required to fit recrystallization kinetic data than is provided by the standard equation. Similarly, fitting recovery data using an evolved mean subgrain size also requires greater dispersoid drag than is normally obtained. By simply increasing the Zener drag by a factor 3-4, improvement can be obtained in the fit to this particular kinetic data. However, the effect of dispersion on recrystallized grain size is not well fit in this case. These results, in addition to other work in the literature, suggest that the drag provided by dispersoids on recovery, recrystallization and even normal grain growth is not well understood. Specifically, it appears that different mathematical treatment may be required for the drag situation pertaining to differences in grain size, misorientation and stored energy. An attempt is made to illustrate these requirements, within the context of an evolutionary model comprising recovery, recrystallization and normal grain growth.

2:40 PM

High Temperature Control of Recrystallization in Wrought Al Alloys Using Sc and Zr: Yancy W. Riddle¹; ¹Worcester Polytechnic Institute, MPI/Advd. Casting Rsch. Ctr., 100 Inst. Rd., Worcester, MA 01609-2280 USA

Addition of dispersoid-forming elements to aluminum alloys has long been recognized as a route leading to successful retention of strain-hardened microstructure and restricted grain growth. Potency of resultant dispersoids depends largely on volume fraction, spatial dispersion, and coarsening rate. In practice it is also important to understand the effect of the dispersoid-forming elements on processing and, of course, economics. To date addition of Zr, which can form

metastable Al₃Zr with L12 structure, has proven itself as one of the most effective dispersoids currently in use. Recent research established Sc addition and its Al₃Sc dispersoid, also with L12 structure, as a powerful recrystallization inhibitor. However both Zr and Sc also have undesirable characteristics. The current research seeks to enhance effectiveness of dispersoids by leveraging the benefits from combined addition of both Zr and Sc. Ironically one way this benefit is realized is by demoting detrimental properties associated with Zr and/or Sc in Al using synergistic effects. Alloys with significantly higher recrystallization resistance in both temperature and time have been created using this alloy development approach. This paper will discuss how increased recrystallization resistance and restricted grain growth resulting from the Al₃(Sc,Zr) dispersoids is more effective than either Al₃Zr or Al₃Sc dispersoids acting alone. Discussion will include effects in basic alloy systems of Al-(Zr)-(Sc) as well as practical implications in many of the wrought alloy systems.

3:20 PM

Influence of Predeformation on Precipitation Kinetics and Ageing Behavior of the AA6022 Alloy: Reza Shahbazian Yassar¹; David Paul Field¹; ¹Washington State University, Sch. of Mech. & Matls. Engrg., Spokane St., Pullman, WA 99163-2920 USA

During the industrial hot deformation of heat treatable aluminum alloys, both precipitation reactions and development of dislocation structure occur simultaneously. These processes are coupled which makes it difficult to define a physically based model for the microstructure evolution. The aim of this paper is to investigate the effect of dislocation structure on precipitate morphology and mechanical properties of an Al-Mg-Si alloy (AA6022) by using DSC, TEM and hardness measurements. Selected samples were subjected to different level of deformation before ageing treatment. The evolution of precipitates morphology and ageing characteristics of the predeformed samples in comparison to undeformed samples has been investigated. It is found that pre-deformation has a significant effect on precipitation sequences and volume fraction of precipitates. Also in the case of predeformed samples, a decrease in peak hardness has been seen.

3:50 PM

Improvements in Modeling Quench Sensitivity of Aluminum Alloys Via C-Curves and Their Application to 2090-T8 Plate: Murat Tiryakioglu¹; James T. Staley²; Ralph T. Shuey³; ¹Robert Morris University, Dept. of Engrg., John Jay Engrg. Lab., Moon Twp., PA 15108 USA; ²Retired, Durham, NC USA; ³Alcoa, Inc., Alloy Tech., Alcoa Ctr., PA 15069 USA

We discuss the recent progress we have made in modeling quench sensitivity of heat-treatable aluminum alloys by using C-curves. Instead of allowing all the coefficients in the critical time, Ct, equation, we propose the use of independent thermodynamic data for two of the constants. In addition, we introduce a physically-based ϕ_{min} equation to represent the growth limit. Following this new approach, we reanalyze the data for 2090-T8 plate, used by Staley, Doherty and Jaworski in their 1993 publication. We highlight the additional insight about the physical metallurgy of the alloy gained by the improved model. We also discuss extrapolations into modeling fracture toughness by C-curves.

4:20 PM

Orientation Imaging Microscopy of Deformation in Extruded Al₃Mg and 6063 Aluminum Alloys: Raja K. Mishra¹; Anil K. Sachdev¹; Clyde L. Briant²; ¹General Motors, R&D Ctr., MC 480-106-212, 30500 Mound Rd., Warren, MI 48090 USA; ²Brown University, Div. of Engrg., Providence, RI 02912 USA

In this paper we use orientation imaging to examine the differences in deformation in 6063 and Al₃Mg aluminum alloys. We show that in the 6063 material the deformation proceeds by dislocation rearrangement into subgrains and ultimately to localization in planar arrays. These arrays are precursors to shear band formation and failure. In the Al₃Mg alloy, deformation leads to grain break up, grain rotation and grain elongation that, in combination, alter the microtexture and texture and determines the failure mechanism. These results compare well with previous TEM studies while providing important insight into deformation mechanisms and initiation of instability. We demonstrate that much of the information obtained by TEM can be deduced from these OIM studies that examine a much larger volume of material.

4:50 PM

Microstructure Design Employing 2-Point Correlation Functions: Brent Larsen Adams¹; ¹Brigham Young University, Mech. Engrg., 435 CTB, Provo, UT 84602 USA

Continua with microstructure can be described by (spatial) correlation functions of the local state variables (order parameters). Advances in a spectral representation of the 2-point correlation func-

TUESDAY PM

tions are described, including application to the problem of microstructure design. A conservation relationship is obtained as a necessary condition on the physical realizability of 2-point correlations in representative volumes of finite size. The implications of the conservation relationship are explored in terms of solutions for optimal elastic/plastic properties obtained by sequential quadratic programming.

5:20 PM

Environmental Effects on the Resistance of Long Fatigue Cracks: *A. K. Vasudevan*¹; K. Sadananda²; ¹Office of Naval Research, Arlington, VA USA; ²Naval Research Labs., Washington, DC USA

Environment affects the kinetics of fatigue crack growth through the time and stress dependent processes. This is reflected in the reduction the K_{max} component of the cycle compared to the DK. It is observed that the environmental effects on crack resistance falls broadly into four types of behavior, kinetics of each depending on the combination of time and stress. These four types of mechanisms seem to be common to most commercial materials. Examples of experimental results from Al- alloys and AERMET-100 steels will be presented to show these four processes on a DK-K_{max} fatigue map. Such a map provides a tool to the basic understanding of the overall fatigue behavior of the alloys.

The Didier de Fontaine Symposium on the Thermodynamics of Alloys: Interatomic Potentials and Cluster Expansion Techniques

Sponsored by: Materials Processing and Manufacturing Division, MPMD-Computational Materials Science & Engineering (Jt. ASM-MSCTS)

Program Organizers: Diana Farkas, Virginia Polytechnic Institute and State University, Department of Materials Science and Engineering, Blacksburg, VA 24061 USA; Mark D. Asta, Northwestern University, Department of Materials Science and Engineering, Evanston, IL 60208-3108 USA; Gerbrand Ceder, Massachusetts Institute of Technology, Department of Materials Science and Engineering, Cambridge, MA 02139 USA; Christopher Mark Wolverton, Ford Motor Company, Scientific Research Laboratory, Dearborn, MI 48121-2053 USA

Tuesday PM Room: 216B
March 16, 2004 Location: Charlotte Convention Center

Session Chair: TBA

2:00 PM

Interatomic Bond-Order Potentials and Cluster Expansions: *David G. Pettifor*¹; ¹University of Oxford, Dept. of Matls., Parks Rd., Oxford OX1 3PH UK

This talk will outline recent developments in the application of interatomic bond-order potentials (BOPS) to modelling the growth of semiconductor films and the defect properties of bcc transition metals and high temperature intermetallics. The link between BOPs and the cluster expansions at the heart of Didier de Fontaine's research will be explored.

2:30 PM

Atomistic Modeling of Extended Crystal Defects in Alloys: *Vaclav Vitek*¹; ¹University of Pennsylvania, Dept. of Matls. Sci. & Engrg., 3231 Walnut St., Philadelphia, PA 19104 USA

Extended crystal defects, in particular grain boundaries and dislocations, govern mechanical properties of crystalline materials. This is particularly pronounced in alloys, where segregation to grain boundaries controls their propensity to fracture while dislocation glide often differs significantly from that in elemental solids even if their crystal structure is the same or very similar. This is the reason why atomistic modeling of extended defects has always been striving to tackle alloys although the majority of such calculations were invariably done for elemental solids as the first step. In this paper we shall reflect on the development of the atomistic modeling in metallic alloys in the last twenty years. In the first place we shall discuss the impact of the advancement of central-force many-body potentials, i. e. EAM and Finnis-Sinclair potentials, on such studies. As a specific example we present investigation of bismuth segregation to grain boundaries in copper and studies of segregation to grain boundaries in Ni₃Al. The next important step in the development of the methods of description of interatomic forces is a more appropriate incorporation of the electronic structure effects, i. e. the chemistry of alloys. Obviously, this is

done most completely in DFT based calculations. However, those are rarely feasible for extended defects and the best alternative is at present methods based on the tight-binding approach. Specifically, bond-order potentials (BOPs) that are an order N method usable in real space. As examples we shall present recently developed BOPs for Ti-Al alloys, their application in studies of dislocations in TiAl with the L10 structure, as well as the development of BOPs for molybdenum silicides. In this context we shall discuss how essential is inclusion of directional bonds into the modeling of defects in alloys with mixed metallic and covalent bonding.

3:00 PM

Thermodynamics Emerging from Embedded Atom Models of Alloys: *Alfredo Caro*¹; Patrice E.A. Turchi¹; Edmundo Lopasso²; Magdalena Caro²; ¹Lawrence Livermore National Laboratory, Chmst. & Matls. Sci. Direct., PO Box 808 - L-371, Livermore, CA 94551 USA; ²Centro Atomico Bariloche, Bariloche 8400 Argentina

Most of the large body of research using empirical potentials for MD simulations addresses properties of pure elements. Alloys have been difficult to model with the present degree of complexity of the potentials used. Basic thermodynamic properties, as the equilibrium crystal structure, are absent from the formalism and can only be incorporated in an indirect way. In most cases the thermodynamics that emerges from these empirical models is unknown. Here we present recent results on the computational calculation of the exact phase diagram of several binary alloys as described by widely used EAM potentials. These results clearly show the power and limitations of empirical potentials, as well as the need of more involved descriptions of cohesion in transition metals. We also discuss the possibility of using this information to help develop new potentials with known thermodynamic properties. Some applications to ultra fast solidification occurring in radiation-damaged materials are also presented.

3:20 PM

Configurational Thermodynamics of the Sigma Phase in the Ru-W System: *Chris C. Fischer*¹; Gerbrand Ceder¹; Eric Wu¹; ¹Massachusetts Institute of Technology, Dept. of Matls. Sci. & Engrg., 77 Mass. Ave., Rm. 13-4061, Cambridge, MA 02139 USA

Using a cluster expansion parameterization of configurational energetics obtained from ab initio calculations, thermodynamic stability in the Ru-W system is investigated. Finite temperature equilibration is performed with the Monte Carlo method. The Ru-W system, a phase separating system, displays finite temperature stability of the sigma phase. The sigma structure, a topologically close packed structure with space group P4_{sub}2/mnm, presents a challenge with regard to the structure inversion method due to a large unit cell and/or lack of symmetry. While the structure of the sigma phase contains a large number of symmetrically distinct clusters, giving rise to challenges in the implementation of the cluster expansion, configurational energetics are likely dominated by short range interactions due to the topologically close packed character of the structure. Sources of error in the structure inversion method are discussed in the context of cross-validation score, and effective cluster interaction variance. An algorithm for interaction selection is presented whose purpose is to minimize cross-validation, as implemented in the Alloy Theoretic Automated Toolkit, while maximizing robustness of fit.

3:40 PM Break

3:50 PM

Cluster Expansion Techniques to Describe Size Calibration of Nanostructures: *Hugues C. Dreyssé*¹; Vasyi Tokar²; ¹IPCMS, GEMME, 23 rue du Loess, Strasbourg 67034 France; ²National Academy of Sciences, Inst. of Magnetism, 36-b Vernadsky str., Kiev-142 03142 Ukraine

In heteroepitaxy, a lattice size mismatch between substrate and adlayer is common. In this contribution, we propose an atomistic model for the growth of submonolayer. By assuming a coherent deposition, the systems is projected on a lattice gas model in a way similar to cluster expansion in the theory of alloy.¹ The 1D case has been solved exactly.² It is possible to show, that if the nearest-neighbors interaction is attractive and if the lattice size mismatch is large enough, at low temperature the atoms self assemble into size calibrated clusters. Moreover under certain conditions, the clusters display self-organisation. It is even possible to have self-assembly at finite temperature which vanishes at T = 0K. ¹V. Tokar et H. Dreyssé, Comp. Mat. Sci. 24 (2002) 72. ²V. Tokar et H. Dreyssé, Phys. Rev. E (2003) under press.

4:20 PM

Origin of the Complex Wetting Behavior in Co-Pt Alloys: *Yann M. Le Bouar*¹; Annick Loiseau¹; Alphonse Finel¹; ¹CNRS-ONERA, LEM, 29, av de la Division Leclerc, BP 72, Chatillon 92322 France

In the Co-Pt system, a simple cooling experiment can drive a sample ordered in the tetragonal $L1_0$ structure (CuAu type) close to the two-phase region involving $L1_0$ and the cubic $L1_2$ (Cu₃Au type) structure. Using transmission electron microscopy observations, we show that interfaces in the $L1_0$ structure are decorated: orientational domain walls are wetted by a single layer of $L1_2$ structure whereas three macroscopic layers ($L1_2/L1_0/L1_2$) appear at the antiphase boundaries. We then analyse this complex behavior in the framework of the Ising model with interactions limited to first and second nearest neighbors. The finite temperature properties of the various $L1_0/L1_0$ interfaces are computed with a Low Temperature Expansion and Cluster Variation Method simulations in the inhomogeneous Tetrahedron-Octahedron approximation. The results are in full agreement with our experimental observations concerning the wetting of interfaces.

4:40 PM

Cluster Expansion-Based Precipitate Modeling for Magnesium Alloys: *Gus Hart*¹; ¹Northern Arizona University, Physics & Astron., PO Box 6010, Flagstaff, AZ 86011-6010 USA

We have generalized the reciprocal-space formulation of the cluster expansion approach to treat the long range strain effects in alloys of any crystal structure (not just cubic alloys as has been done previously). We use this improved approach to study precipitate formation (precipitate size vs. shape vs. temperature) in several common magnesium-based alloys.

5:00 PM

Cluster Expansion of bcc Al-Cu: The Role of Mechanical Instabilities: *Chao Jiang*¹; Christopher Wolverton²; Zi-Kui Liu¹; Long-Qing Chen¹; ¹Pennsylvania State University, Matls. Sci. & Engrg., Univ. Park, PA 16802 USA; ²Ford Research Laboratory, MD3028/SRL, Dearborn, MI 48121 USA

First-Principles total energy calculations have shown that the bcc structure of both Al and Cu are mechanically unstable with respect to tetragonal deformations. Consequently, many bcc-based superstructures actually become fcc after full relaxation. This poses a serious problem for the cluster expansion of the Al-Cu bcc structure, which is stable in the Al-Cu system at high temperatures. In the present work, the total energies of all bcc-based superstructures are calculated by relaxing only the volume and cell-internal degrees of freedom. In this way, all structures still remain bcc. Using the obtained cluster expansions, Monte-Carlo simulations are performed to obtain the enthalpy of mixing of the bcc solution at various compositions and temperatures. The results are compared with direct calculations using Special Quasirandom Structures (SQS). The presence of SRO and the role of vibrational entropy is discussed.

Third International Symposium on Ultrafine Grained Materials: Microstructure and Properties

Sponsored by: Materials Processing & Manufacturing Division, MPMD-Shaping and Forming Committee

Program Organizers: Yuntian Ted Zhu, Los Alamos National Laboratory, Materials Science and Technology Division, Los Alamos, NM 87545 USA; Terence G. Langdon, University of Southern California, Departments of Aerospace & Mechanical Engineering and Materials Engineering, Los Angeles, CA 90089-1453 USA; Terry C. Lowe, Metallum, Santa Fe, NM 87501 USA; S. Lee Semiatin, Air Force Research Laboratory, Materials & Manufacturing Directorate, Wright Patterson AFB, OH 45433 USA; Dong H. Shin, Hanyang University, Department of Metallurgy and Material Science, Ansan, Kyunggi-Do 425-791 Korea; Ruslan Z. Valiev, Institute of Physics of Advanced Material, Ufa State Aviation Technology University, Ufa 450000 Russia

Tuesday PM

March 16, 2004

Room: 207A

Location: Charlotte Convention Center

Session Chairs: S. Lee Semiatin, Air Force Research Laboratory, Matls. & Mfg. Direct., Wright Patterson AFB, OH 45433 USA; Zhe Jin, Alcoa Technical Center, Alcoa Ctr., PA 15069 USA; Terry R. McNelley, Naval Postgraduate School, Dept. Mech. Engrg., Monterey, CA 93943-5146 USA

2:00 PM Invited

Structural and Mechanical Fatigue Properties of Nanostructured Cu Subjected to Severe Plastic Deformation: *Kai Zhang*¹; Julia R. Weertman¹; ¹Northwestern University, Matls. Sci. & Engrg., 2220 N. Campus Dr., Evanston, IL 60208 USA

Comparatively little is known and reported about the fatigue properties of nanocrystalline materials, in particular, effect of cyclic deformation on their internal microstructure. In the present work, an initial set of fatigue testing has been carried out on nanocrystalline Cu subjected to cryogenic cold-rolling and further thermal treatment. The primary goal is to study cyclic deformation and fatigue lifetimes in comparison with time-independent uniaxial tensile experiments. Results regarding microstructural stability and deformation mechanism during cycling are reported. This research was supported under US DoE grant DE-FG02-02ER46002.

2:20 PM

New Observations of High Strength and Ductility in SPD-Produced Nanostructured Materials: *Ruslan Z. Valiev*¹; ¹Ufa State Aviation Technical University, Inst. of Physics of Advd. Matls., 12 K. Marx St., Ufa 450000 Russia

Bulk nanostructured metals with a mean grain size of about 50 - 100 nm very often demonstrate high hardness but poor ductility. However, recent works demonstrate that very high strength and quite high ductility can be observed in nanostructured metals produced by severe plastic deformation (SPD). In this paper we show that the combination of high strength and ductility is originated not only from the presence of fine grains, but a structure of grain boundaries and internal stresses, as well as disperse precipitations of second phases. The origin of this phenomenon is considered and discussed in this work based on analysis of performed mechanical tests and thorough microstructural studies. High strength and ductility are of great engineering importance, in particular for attaining high fatigue properties and fracture toughness.

2:35 PM

The Microstructure-Mechanical Properties Relationship of Ultrafine Grained Structural Materials Processed by Equal Channel Angular Pressing: *Dong Hyuk Shin*¹; Byung Du Ahn¹; Hyun Soo Cho¹; Kyung Tae Park²; ¹Hanyang University, Dept. of Metall. & Matls. Sci., Ansan, Kyunggi-Do 425-791 Korea; ²Hanbat National University, Div. of Advd. Matls. Sci. & Engrg., Taejon 305-719 Korea

During the past decade, the characterization of bulk ultrafine grained (UFG) structural materials processed by equal channel angular pressing (ECAP) has been one of the hottest subjects in the materials research field. However, UFG materials fabricated by ECAP exhibit both superior and inferior mechanical properties, as the prominent structural materials, compared to coarse grained ones. For instance, the superior mechanical properties are ultrahigh strength and exceptional high temperature ductility (i.e. superplasticity) and the inferior mechanical properties are a degraded strain hardening capability and low room

temperature ductility. In this study, the microstructure-mechanical properties relationship of UFG structural materials fabricated by ECAP will be reviewed in order to provide insight broadening their future applicability. In addition, recent effort overcoming their mechanical inferiorities will be addressed by referring various sources.

2:50 PM

TEM Observation of Strain Rate Dependent Dynamic Recrystallization of Ferrite in Low Carbon Steel: *Seung Chan Hong*¹; Seung Ki Seo¹; Chong Seung Yoon¹; Kyung Jong Lee¹; Dong Hyuk Shin¹; Kyung Sub Lee¹; ¹Hanyang University, Matls. Sci. & Engrg., 17 Haeng dang dong, Seong dong gu, Seoul 133-791 Korea

The dynamic recrystallization (DRX) of ferrite was investigated under different strain rates and initial grain sizes in low carbon steel. Hot compression tests were carried out at 735C ($\alpha + \gamma$ region) by Gleeble 1500. The dislocation movement during the DRX was observed using a heating strain holder in TEM. The DRX of ferrite occurred by two different mechanisms depending on the strain rate. Below the strain rate of 0.1/s ($Z = 3.29E13/s$, $Q: 280$ kJ/mol), dynamic discontinuous recrystallization occurred via bulging of grain boundaries resulting in dislocation-free grains with a size of 5 μm . As the strain rate increased to 5/s ($Z = 1.64E15/s$), dynamic continuous recrystallization took place by clustering of dense dislocation walls which led to the progressive increase of the misorientation angles between sub-grains. As a result of the dynamic continuous recrystallization, much smaller ferrite grains with a size of 1 μm were obtained.

3:05 PM

Reciprocating Sliding Wear of Ultra-Fine Grained Ti-6Al-4V: Eliana K.Y. Fu¹; H. Chandana Bellam²; *H. J. Rack*²; Vladimir Stolyarov³; Ruslan Z. Valiev³; ¹Allvac, 2020 Ashcraft Ave., Monroe, NC 28110 USA; ²Clemson University, Sch. of Matls. Sci. & Engrg., Clemson, SC 29634 USA; ³Ufa State Aviation Technical University, Inst. of Physics of Advd. Matls., 12 K. Marx St., Ufa 450000 Russia

The reciprocating dry sliding wear performance of ultra-fine grained (UFG) Ti-6Al-4V (Ti-64) and annealed medical grade Ti-6Al-4V ELI against hardened steel have been investigated. Equal channel angular extrusion (ECAE) of Ti-64 to a true strain of 6.5 resulted in primary • grain refinement and increased microstructure homogeneity. This microstructure enhancement was found to result at a contact stress of 5 MPa, in a reduction of the dynamic friction coefficient. However little difference between the steady-state dry reciprocating sliding wear rate of UFG Ti-64 and medical grade Ti-64 was observed under high stress steady-state conditions. Indeed at low apparent stresses, 1.5 MPa, the dry reciprocating-sliding wear resistance of UFG Ti-64 was lower than annealed Ti-64. This difference in wear performance is consistent with the expected evolution of the surface and sub-surface microstructure in these two materials with increasing reciprocating sliding distance.

3:20 PM

The Effect of Mn on Microstructure and Mechanical Properties After Heavy Warm Deformation of C-Mn Steel: *Rongjie Song*¹; Radko Kaspar¹; Dirk Pongel¹; Dierk Raabe¹; ¹Max Planck Institute for Iron Research, Microstruct. Physics & Metal Forming, Max-Planck-St. 1, Duesseldorf, Nordrhein-Westfalen D-40237 Germany

The effect of Mn on the ferrite grain refinement has been investigated in plain 0.2%C-Mn steels after heavy warm deformation processed by plane strain compression. The final microstructure consists of spheroidized cementite within ultrafine grained ferrite matrix. It was observed that an increase in the Mn content from 0.7mass.% to 1.5 mass.% leads to a drop in the average ferrite grain size and to a change in grain shape from an elongated to a more equiaxed morphology. The fraction of high-angle grain boundaries changed from 55% to 74%. The ultimate tensile strength increased from 590MPa to 680MPa, while the total elongation of 18% was the same for both materials. EDS analysis revealed an enrichment of Mn in the fine cementite particles.

3:35 PM

Microstructure of Austenitic and Ferritic Steels Produced by Severe Plastic Deformation and Subsequent Annealing: *Andreas Vorhauer*¹; Reinhard Pippan¹; Siegfried Kleber²; ¹Austrian Academy of Sciences, Erich Schmid Inst. of Matls. Sci., Jahnstrasse 12, Leoben A-8700 Austria; ²Böhler Edelstahl GmbH & Co KG, Kapfenberg A-8605 Austria

In this paper an austenitic and a ferritic steel are subjected to SPD at room temperature ($\sim 0.16T_m$) followed by subsequent annealing. The aim of this materials processing is the refinement of the initially coarse microstructure. The microstructural change during SPD as a function of applied plastic strain (maximum 32) is analyzed for both steels by Back Scattered Electrons micrographs captured in a SEM.

The same microstructural analysis is performed for samples, which are annealed at different annealing parameters. A correlation between microstructure and mechanical properties at different states of materials processing is realized by subsize tensile tests. Additionally the microtexture of selected samples is measured by the automated Electron Back Scattering Diffraction method within a SEM. The size of the structural elements in the SPD state is clearly below 100nm. Appropriate thermal treatments transform these metastable deformation microstructures into more stable grained microstructures with grain sizes smaller than 500nm.

3:50 PM Break

4:00 PM Invited

Characterization of Nanocrystalline Materials by X-Ray Peak Profile Analysis: *Tamás Ungár*¹; ¹Eötvös University Budapest, Dept. of Gen. Physics, H-1518, POB 32, Budapest Hungary

During the past couple of years several research groups have spent extended efforts to improve the method of X-ray diffraction peak profile analysis (XDPPA) in order to characterize the microstructure of crystalline materials in terms of size and size-distribution and strain. As a result, a variety of different procedures are now available which enable this. The prerequisite for all different approaches is to start with best quality experimental data. These are either provided by high resolution synchrotron experiments, or by special high resolution laboratory diffractometers, possibly equipped by incident beam monochromators, or by well aligned Bregg-Brentano diffractometers using long enough counting periods. Model based evaluation approaches provide crystallite size distribution in terms of log-normal or gamma distributions and strain in terms of dislocations, stacking- or twin faults and in special cases disclinations. If large enough number of peaks are available, strain anisotropy enables the determination of slip systems or Burgers vector populations. In textured samples the dislocation structure in the individual texture components can also be evaluated.

4:20 PM Invited

Deformation and Recrystallization Textures of Shear Deformed 1050 Aluminum Alloy: *Dong Nyung Lee*¹; ¹Seoul National University, Rsch. Inst. of Advd. Matls., Seoul 151-742 Korea

A study has been made of the deformation and recrystallization textures of aluminum alloy sheets deformed by ECAP. The ECAP was performed under varied shear deformation histories. The deformation textures of the sheets showed an inhomogeneous distribution through the thickness, even though they were mainly the shear deformation textures which can be approximated by the ND $\{111\}$ and $\{001\} <110>$ components. The recrystallization textures of sheets ranged from weakened deformation textures to the cube texture depending on the density of cube component in the deformation texture. The deformation and recrystallization textures were discussed based on a texture simulation and the strain energy release maximization model, respectively.

4:40 PM

Structure and Property Evolutions of ECAP Processed 7075 Al Alloy During Annealing: *Yonghao Zhao*¹; Xiaozhou Liao¹; Zhe Jin²; Ruslan Z. Valiev³; Yuntian T. Zhu¹; ¹Los Alamos National Laboratory, Matl. Sci. & Tech. Div., MS G755, Los Alamos, NM 87545 USA; ²Alcoa Technical Center, Alcoa Ctr., PA 15069 USA; ³Ufa State Aviation Technical University, Inst. of Phys. of Advd. Matls., 12 K. Marx St., 450000 Ufa Russia

Microstructure and microhardness evolutions of ECAP-processed and coarse grained (CG) 7075 Al alloy during differential scanning calorimeter (DSC) annealing were investigated by x-ray diffraction (XRD), transmission electron microscopy (TEM) and microhardness measurements. Upon annealing, the microhardness of the ECAP processed sample decreases gradually, while there exists a hardening peak for the CG sample. XRD and TEM show that the hardening peak of the CG sample is mainly caused by the second phase precipitation hardening. For the ECAP processed sample, upon annealing the microstrain (dislocation density) decreases and the crystallites grow, which decrease the overall hardness in spite of precipitation strengthening. DSC analysis indicates that the ECAP process does not change the sequence of phase precipitation. It only changes the aging kinetics.

4:55 PM

Microstructure and Mechanical Properties of Severely Deformed Ti-6Al-4V and Ti-6Al-4V+10%TiC Metal Matrix Composite: *Guney Guven Yapici*¹; Ibrahim Karaman¹; Zhiping Luo²; ¹Texas A&M University, Dept. of Mech. Engrg., MS 3123, College Sta., TX 77843 USA; ²Texas A&M University, Microscopy & Imaging Ctr., College Sta., TX 77843 USA

The present work focuses on the severe plastic deformation of Ti-6Al-4V and Ti-6Al-4V reinforced with 10% TiC metal matrix composites using equal channel angular extrusion (ECAE). The initial materials that were manufactured by hot isostatic pressing of the alloy powders were canned in stainless steel and extruded non-isothermally through two channels of equal cross section intersecting at an angle of 90°. Microstructure and mechanical properties of successfully extruded billets were reported using light microscopy, transmission electron microscopy (TEM), tension and compression experiments and hardness measurements. The effects of extrusion conditions (temperature and processing route) on the microstructure and mechanical properties are investigated. ECAE shear deformation causes refinement in α plates, elimination of prior β boundaries without forming bimodal microstructures and thus possibly without alloy partitioning effect. Decreasing extrusion temperature and increasing number of passes decreases α plate size and grain size, leading to significant increase in tensile and compressive flow stresses at room temperature. Tension/compression asymmetry in flow strengths and strain hardening coefficients is because of the activation of different deformation systems along tension and compression axis of the test samples.

5:10 PM

Synthesis of Ultrafine-Grained Alloys by Repeated Cold-Rolling: Guru Prasad Dinda¹; Harald Roesner¹; *Gerhard Wilde*¹; ¹Forschungszentrum Karlsruhe, Inst. of Nanotech., PO Box 3640, Karlsruhe 76021 Germany

Repeated cold-rolling with intermediate folding represents a technique to obtain severe plastic deformation that avoids excessive heating at the internal interfaces and that proceeds without the simultaneous action of a high pressure in the range of several GPa. Aside from the opportunity to obtain amorphous bulk samples, the processing pathway also allows for synthesizing dense, bulk nanocrystalline materials. In the present work, massive Ni₅₀Ti₅₀ samples with average grain sizes below 10 nm have been synthesized at ambient temperature using two different processing pathways that start from individual elemental sheets and, alternatively, from a pre-alloyed NiTi intermetallic compound. The development of the microstructure in dependence of deformation was investigated by X-ray diffraction and scanning and transmission electron microscopy. As one result, a cyclic cross-over between grain-size refinement and coarsening as a function of continuous strain energy input has been observed for Ni-Ti. The development of the nanoscale microstructure during intense deformation- including the early and the late stages of deformation-induced nanocrystal formation - is analyzed in terms of the major thermodynamic and mechanical properties that govern grain refinement and intermixing. This work is supported by the DFG under contract no. WI 1899/1-2.

5:25 PM

Microstructure Evolution to Nanometer Scale of 1200 and 3103 Aluminum Alloys Processed Via Equal Channel Angular Pressing: Marcello Cabibbo¹; *Enrico Evangelista*¹; Erik Nes²; ¹Polytechnic University of Marche, Dept. of Mech., Via Brecce Bianche, Ancona I-60131 Italy; ²NTNU, Inst. of Matls. Tech., Alfred Guess GIT7, Trondheim VEI-2B Norway

The deformation processes occurring in two aluminum alloys (1200 and 3103) after Equal Channel Angular Pressing (ECAP) have been studied by means of TEM and EBSD techniques. Grains and subgrains spacing and misorientation evolution upon increasing ECAP passes were studied by EBSD on a FEGSEM, whilst the ultrafine and low-misorientation subgrain structure was studied by TEM. A nano-structure was achieved after 6 ECAP passes for both the materials and the High Angle Grain Boundary misorientation constantly increased reaching a 58% fraction among the total amount of boundaries. The mean subgrain misorientation was of 4-5° and the mechanism of transformation from Low-Angle Boundary subgrain to High-Angle Boundary grain, i.e. those higher than 15°, was documented via TEM inspections. Finally, the grain refining results attained through ECA pressing were compared to the published results in the Cold-Rolling of the same 1000 and 3000 aluminum alloy series.

5:40 PM

Structure of Martensite Transformed from Severely Deformed Austenite in Fe-28.5at.%Ni Alloy: *Hiromoto Kitahara*¹; Takashi Kimura¹; Nobuhiro Tsuji¹; Yuichiro Koizumi¹; Yoritoshi Minamino¹; ¹Osaka University, Dept. of Adaptive Machine Sys., 2-1, Yamadaoka, Suita, Osaka 565-0871 Japan

Grain refinement of bulk materials by the SPD process followed by martensite transformation was investigated. Fe-28.5at.%Ni alloy sheets were severely deformed in austenite structure by the ARB process, and then cooled down to 77 K to cause martensite transformation. The

ARB processed sheets deformed to 4.0 of total equivalent strain were filled with the ultra-fine lamellar boundary structure having about 200 nm of average lamellar spacing. Martensite transformation starting temperature decreased with increasing the total equivalent strain. Martensite having characteristic morphologies appeared from the ultra-fine lamellar austenite in the sheet ARB processed by 5 cycles, although martensite transformed from conventionally recrystallized specimens with several tens micrometers of grain sizes showed typical plate (lenticular) morphology. It was concluded that the grain refinement by martensite transformation from ultrafine grained austenite is possible but low-angle boundaries in the austenite are not effective for refinement by martensite transformation.

Index

A

Aaronson, H I 186, 228,
..... 282, 327, 370, 415
Abadias, G 429
Abbaschian, R 345, 377, 420
Abe, E 295
Abe, T 420
Abedrabbo, S 180, 321
Abiko, T 366
Abinandanan, T A 181
Ablitzer, D 219
Abraham, T 209
Abu-Dheir, N M 450
Abu-Farha, F K 398
Acharjee, S 237
Ackland, G J 222
Acoff, V L 190, 237, 255,
..... 259, 362, 441, 456
Adachi, H 314
Adam, G 323, 406
Adamini, P 329
Adams, A N 217
Adams, B L 347, 390,
..... 391, 431, 451
Adams, D P 394
Adams, M 329
Adams, T M 321
Addressio, L B 233, 453, 454
Afshar, S 177
Agarwal, A 301, 346,
..... 388, 428, 450
Agarwal, S 264
Aghion, E 333, 375
Agia, M 331
Agnew, S R 233, 256, 287,
..... 339, 392, 410
Agrapetian, A 173
Ahmed, F M 437
Ahn, B D 349
Ahn, J 214
Ahn, J 426, 448
Ahn, J 221
Ahn, S 453, 454
Ai, X 276
Aindow, M 228
Ajayan, P M 381
Akarapu, R 380, 441
Akhnokh, A 437
Akhtar, R J 360
Akiba, E 210, 353
Akinc, M 175, 215
Akogwu, O 180
Al Ali, M T 317
Al Maharbi, M 342
Albers, R C 431
Albright, D 191, 375, 444
Albuquerque, M A 230
Alcorn, T 171, 212, 267,
..... 312, 356, 398, 399, 437
Alessi, R F 343

Alex, T C 171
Alexander, D J 207, 253,
..... 255, 434
Alexandrov, I V 252, 256,
..... 258, 306
Alfantazi, A M 280, 325,
..... 366, 409, 444
Algozo, P R 345
Ali, M T 360
Allaire, C 177, 178
Allaire, J 177
Allameh, S 308
Allen, S M 420
Allison, J E 191, 375
Allocca, C M 414
Alman, D E 440
Almer, J D 272, 283
Alonso, F 218
Alpas, A T 254, 413
Alpay, S P 426
Alsem, D 309
Altendorf, W 313
Altorfer, F 250
Alur, A P 316
Alven, D A 174, 215,
..... 269, 315, 357, 400
Aly, I H 403
Amaranti, J 329
Amweg, M L 447
An, K 247
Anand, S 336
Andersen, F B 400
Anderson, A J 341
Anderson, I E 287, 295,
..... 296, 345, 377, 420
Anderson, P M 408
Anderson, R P 364
Ando, T 411
Andrade, G J 213
Andrews, E 212
Angelini, P 436
Anglin, P 271
Angove, J E 329
Anilkumar, A V 247
Aning, A O 295, 296
Ankem, S 379, 422, 445
Antipov, N I 427, 449
Antolín, R 361
Antonioni, A 317
Anyalebechi, P N 194, 236,
..... 289, 335, 378, 420
Aoki, K 397
Aoki, M 359
Apel, M 222
Apelian, D 369, 414
Apostolescu, I 290
Apps, P 258
Aquino, A M 317
Arafah, D 180, 321
Arai, H 453
Araujo, E D 243
Aravamudhan, S 274
Arbegas, W J 314
Ardell, A J 250, 322
Arenas, M 190, 362
Ares, A E 195, 344, 440
Argon, A S 283

Argyropoulos, S A 379, 423,
..... 446, 447
Arif, M 210
Ariza, M P 365
Arjunan, V 397
Arkhipov, G V 438
Arlyuk, B 313
Arroyave, R 363
Artemev, A 334, 384
Arvanitis, A 216
Arya, A 274
Arzt, E 188
Arzt, E 229, 383
Asaro, R 259
Ashida, T 265, 399
Asta, M D 205, 250, 304,
..... 305, 348, 358, 389, 430
Athreya, B 386
Atkins, G J 192
Atzmon, M 316
AuBuchon, B 172
Auciello, O H 429
Audet, D 361
Augustyn, B 403
Aurrecoechea, J M 411
Avraham, S 444
Aydiner, C C 176
Azari, H N 269
Aziz, M J 301, 344

B

Babu, S S 203, 223, 345
Bacchi, D P 319
Backerud, L 403
Backhouse, N 172
Bacon, D J 183, 184,
..... 224, 226, 425
Bacon, W G 188
Bae, B 246
Bae, D H 287, 438
Bae, J 382
Baek, C 352
Baerhold, F 329
Baghbanan, M 308
Bahr, D 224, 262, 275, 394, 435
Bai, G R 238
Bai, J G 428
Baik, S 252
Bailey, C 232, 362, 416
Bailey, R 376
Bainbridge, I 272, 281, 439
Baker, I 204, 238, 281
Baker, J D 436
Bakhtiyarov, S I 375, 450
Bakke, P 444
Balancin, O 237
Balascuta, S 337
Balema, V P 263
Balk, T J 229
Balogh, M P 264
Balooch, M 310
Balsone, S J 204
Bamberger, M 444
Ban, Z 426
Banerjee, D K 178, 319
Bang, J J 395

Bang, W	283, 383	Bhansali, S	178, 219, 273,	Boutorabi, S M	439
Bannuru, T	352 274, 319, 362, 404,	455	Bowden, D M	419
Banovic, S W	418	Bhattacharya, A K	411	Bowles, A L	445
Barabash, R	279, 324, 394	Bhattacharya, P	291	Bowman, B	286
Barajas, A	214	Bhethanabotla, V R	455	Bowman, R C	210
Barber, M	312	Bi, S	265	Boyapati, K	431
Barber, R E	259	Bian, Z	217	Boyce, B L	261, 308, 342
Barbour, J C	352	Biancaniello, F S	372	Boydon, J F	264
Barca, B J	399	Bickert, C	177	Boylstein, R E	318
Bark, C	441	Bieler, T R	188, 190, 229, 286,	Bradley, J R	264, 265
Barmak, K	455 303, 324, 390, 431, 451		Bradshaw, R C	438
Barnes, A J	264	Bilello, J C	176	Brady, M P	215
Barnett, M R	340	Bilodeau, J	361	Brady, S	263
Barnett, R S	385	Biloni, H	300, 450	Braginsky, M V	452
Barnett, S	188, 231,	Biner, S B	317, 365	Brandstaetter, W	404
..... 330, 415, 443		Bing, X	289	Bratkovsky, A M	425
Baró, M	254	Bingert, J F	234, 235, 445	Braun, M J	178
Barrabes, S A	433	Birdsell, S A	353	Braun, M W	228, 327
Barrie, R L	340	Birol, Y	173	Bravman, J C	394
Barron, M F	266	Bisen, K B	362	Bray, G	410
Barseghyan, S A	236	Bittencourt, E	377	Brechet, Y	307, 438
Bartelo, J	416	Bizios, R	381	Bretz, G T	287
Bartos, S C	333	Bjerke, W	399	Briant, C L	264, 347, 418, 419
Basak, D	247	Blakely, K A	209	Brill, M	395
Baskes, M I	279, 282, 306, 324	Blanchard, D	353	Brinks, H W	353
Bastaweesy, A	403	Blanchard, P J	287	Brokmeier, H	252
Bastawros, A	317	Blander, A J	356	Bronchart, Q	390
Bates, C E	428	Blandin, J	417, 438	Bronfin, B	333
Battaile, C C	181, 452	Blasques, J	M 172	Brooks, C R	271
Battle, T	185, 368	Blawert, C	445	Brown, D W	207, 255, 283, 296,
Bautista, R G ...	169, 210, 262, 309,	Bletry, M	438 297, 328, 339, 372, 434	
..... 353, 354, 395, 396, 435, 436		Blinov, V V	212	Brown, J A	222
Bayuzick, R J	345	Bliznyukov, S	440	Brown, T L	207, 259
Beals, R S	191	Blobaum, K J	431	Brown, W L	352
Beckermann, C	202, 247, 299,	Bloch, J	395	Browning, J	172, 399
..... 344, 379, 386, 423, 446		Bloomfield, M O	423	Browning, P F	411
Behrani, V	175, 215	Blue, C A	287, 411	Brubaker, C	417
Bei, H	357, 372, 401	Blum, V	304	Brueck, S R	394
Beleggia, M	196	Blum, W	383	Bruggeman, J	212, 267, 312,
Bell, B F	381, 451	Blust, J W	411 356, 398, 399, 437	
Bellam, H C	350	Boehlert, C J	391, 445	Bruggink, P R	244
Bellet, M	178, 203, 404	Boender, W	219	Buarzaiga, M	284
Belt, C K	177	Boening, M	358	Buchanan, R A	175, 216, 270,
Ben-Eliah, Y	395	Boettcher, H	403 271, 297, 316, 359, 402, 438	
Benedikt, B	371	Boettinger, W J	247, 276,	Buchheit, T E	261, 308,
Benedyk, J C	237 322, 344	 342, 352, 452	
Bennett, B V	225	Boger, R	214, 314	Budilov, I N	256
Benson, M L	271, 297, 411	Bogicevic, A	193	Buelow, N	296
Benum, S	385	Boileau, J	328	Buffière, J	411
Benzio, M	417	Bojarevics, V	437	Bugge, M	172
Berberoglu, H	173	Boland, M	415	Bujalski, W	318
Berczik, D	215	Bonacuse, P J	340	Bulatov, V V	225
Berezin, A I	212, 267	Bonsager, M C	198	Bunton, J H	198
Berezowsky, R M	284, 443	Bontha, S	281	Bunzel, P	346
Bergman, C	414	Borge, G	361	Burchett, S N	230
Bergoint, D	365	Borjas, N M	230	Burda, C	170
Bernard, D	273, 361	Bossuyt, S	316	Burghardt, A	219
Berrueta, L D	213	Bottani, C E	429	Burhan, N	433
Besser, A D	200	Bouchet, J	431	Burton, B P	304
Besterci, M	296, 311	Boulianne, R	171	Bushby, A	262
Bewlay, B	358	Bounds, W M	212	Butu, M	290
Beyerlein, I J	207, 255, 256, 434	Bourham, M	197		
Beygelzimer, Y	208, 255, 260	Bourgeois, L	295		
Bezençon, C	203	Bourke, M A ...	187, 207, 229, 255,		
Bhaduri, S	445 272, 283, 284, 296,			
Bhaduri, S B	445 297, 327, 328, 371, 434			
Bhambri, Y	227, 281	Bourret, R H	370		

C

Cabibbo, M	351
Cady, C M	233
Cahn, J W	205, 384

Calata, J N	428	Chang, T	285	Chin, J	443
Cale, T S	423	Chang, Y A	198, 216	Chin, L A	311
Callahan, P	339	Chani, V	342	Chinnappan, R	181
Calonne, O	225	Chapelle, P	404	Chipara, M	337
Campbell, F	188	Charette, A	423	Chisholm, M F	225
Candy, I	330	Charit, I	207, 311	Chiti, F	318
Cantor, B	386	Chase, R	399	Chitre, K	275, 321
Cao, F	270	Chashchin, O A	212	Cho, G	376
Cao, G	196	Chatterjee, A	175, 400	Cho, H S	349
Cao, X	207	Chaubal, M V	265	Cho, J	221
Cao, Y	257	Chaudhari, G	237, 255, 259	Cho, J	448
Cao, Y	257	Chaudhury, P	281	Cho, J	339
Capps, J	450	Chawla, K K	293, 343	Cho, J	275, 321
Caram, R	195, 344, 440	Chawla, N	286, 293, 331, 341, 342, 416, 446	Cho, K H	362
Caraveo, V	356	Chen, C	332, 374, 382	Cho, S	453
Carbonneau, A	177	Chen, G	260, 439	Cho, S	189
Carlberg, T	218, 298	Chen, G S	242	Cho, W D	226, 368
Carleton, E	354	Chen, G Z	182, 199, 280	Choate, W T	245, 313
Carlisle, J A	429	Chen, H	269	Choe, H	356
Carlisle, K B	343	Chen, H	409	Choi, B	413
Carmo, O A	329	Chen, J	243	Choi, D	381
Caro, A	348	Chen, J	407	Choi, G	453, 454
Caro, M	348	Chen, J J	184, 225, 226, 281, 326, 368, 399, 411, 412, 441	Choi, W K	189
Caron, Y	273	Chen, L	332	Choi, Y	334
Carpenter, D A	256	Chen, L	181, 277, 294, 305, 322, 349, 363, 364, 406, 408, 426	Choi, Y	455
Carper, T	339	Chen, L J	294	Choksi, R	425
Carsley, J E	211, 265	Chen, L J	392	Choo, H	202, 296, 297, 372
Carte, S	399	Chen, L J	411	Choudhury, S	426
Carter, E A	274	Chen, L Q	277	Chown, L H	270
Carter, J T	386, 450	Chen, M	374	Choy, K	322
Carter, W T	219, 414	Chen, P	409	Chrisey, D B	197, 239
Castro, M	273	Chen, Q	410, 411	Christakis, N	404
Castro-Cedeno, M H	273	Chen, Q	312	Christie, M A	197
Caswell, K K	395	Chen, S	198, 240, 293, 338, 382	Christodoulou, J	182
Catalina, A V	178, 179, 219, 273, 319, 362, 404	Chen, S	213	Christodoulou, L	182, 422
Cathey, W K	210	Chen, S	298	Christopher, W	181
Ceder, G	205, 250, 289, 304, 305, 348, 389, 430	Chen, S	330	Chromik, R R	232, 352
Cefalu, S A	219	Chen, S	233, 367	Chrzan, D	183, 225
Celanovic, I	179	Chen, T	374	Chu, J P	241, 326, 438
Cerreta, E K	233, 303, 453, 454	Chen, T T	186, 230	Chu, M G	298, 343, 385, 427, 449
Cha, P	353	Chen, W	383	Chumbley, L S	455, 456
Chada, S	189, 231, 285, 331, 373, 416	Chen, X	292	Chumlyakov, Y I	302, 442
Chadha, G	375	Chen, X G	439	Chung, K	314
Chan, H W	355	Chen, Y	304, 389	Chung, K H	433
Chan, K S	365, 376	Chen, Y	326	Chung, Y	422
Chan, W	241	Chen, Z	238	Church, B C	296
Chandler, R C	397	Cheng, C Y	443	Cieciwa, B T	321
Chandra, D	169, 210, 262, 309, 353, 354, 395, 396, 397, 435, 436	Cheng, L	182	Cirincione, R	271
Chandrasekar, S	207, 259	Cheng, Y	413	Civelekoglu, S	391, 445
Chang, A	298	Chenming, X	455	Claiborn, C R	456
Chang, C	382	Cheong, Y M	412, 454	Clapham, M	244
Chang, C	442	Cherukuri, B	184	Clarke, D R	283
Chang, C W	199, 374	Chesonis, C	177, 218, 272, 318, 319, 361, 403, 439	Claude, G	171
Chang, H	281	Chiang, C	438	Clausen, B	271, 272, 284, 296, 297, 328, 360, 371, 434
Chang, H	324	Chiang, F	377	Cleary, P J	218
Chang, H J	217	Chiang, H	374	Clemens, B	210
Chang, I T	341	Chiang, H	232	Clerin, P	170
Chang, J	173	Chien, W	436	Cleveland, R	310
Chang, K	221	Chiew, H T	294	Cochran, J K	236
Chang, L J	439	Childs, R A	377	Cockayne, E	304
Chang, M S	375	Chin, B A	410	Cockcroft, S	214, 218, 219, 386
Chang, S	232, 377			Cockeram, B V	184, 315

Coleman, M A 436
 Colley, L J 386
 Collins, P C 358
 Collins, T L 319
 Collins, T 418
 Colton, F 329
 Colvin, J 406, 431
 Combeau, H 248
 Compton, C C 303
 Compton, W D 207, 259
 Conard, B R 244
 Conlon, K T 371
 Conrad, H 380, 392
 Conradi, M 263
 Conway-Mortimer, J 230
 Cook, B A 287
 Cook, R 341
 Cooley, J C 253
 Cooper, K G 242
 Cooper, K P 394, 435
 Cooper, R P 191
 Copeland, B J 245
 Corby, C P 376
 Cordes, R 369
 Cordill, M J 262
 Coriell, S R 247
 Cormier, D 197
 Cornish, L 270
 Correa, O V 429
 Corson, R P 396, 397
 Costa, M L 329
 Cotts, E J 382, 416
 Counts, W A 452
 Couper, M J 299
 Coupeze, T 178
 Courtenay, J 361, 403
 Couturier, G 250
 Covert, C 266
 Cramb, A W 248
 Crimp, M A 324, 431
 Crist, E M 220
 Cristol, B 170, 171, 212
 Cross, M 404
 Cruz, E S 272
 Csontos, A A 199, 200, 226
 Cuitino, A M 365
 Cunningham, J M 226
 Curlook, W 285, 443
 Curran, M 316
 Curry, M 262
 Curtarolo, S 205, 289
 Czerny, C 329

D

da Cruz, V F 320
 Dahle, A 272, 299,
 343, 403, 411
 Dahotre, N B 301, 346,
 388, 428, 429, 450
 Dai, K 208
 Daigle, E O 185
 Daimer, J 177
 Dalmijn, W L 173, 245
 Dalton, R 172
 Dalvi, A D 188, 231
 Dammers, A J 248

Dando, N R 267, 399
 Dan'ko, V A 180
 Dantzig, J A 386
 Dariavach, N 339
 Darmawan, F 448
 Das, R P 336
 Das, R R 195, 237,
 290, 291, 336
 Das, S K 172, 213,
 268, 313, 385
 Dasari, A 302
 Dasgupta, A 192
 Dashwood, R J 223, 323
 Date, M 294
 Dattelbaum, A M 447
 Dauskardt, R H 229, 240, 270
 David, S A 203, 223, 345
 Davies, R W 268
 Davis, B R 357
 Davis, L J 218
 Daw, M 183, 222, 225
 Dawson, P R 235
 Dax, B 379, 423, 446
 Dax, R F 319
 Daya, Z A 417
 Dayan, D 287
 Dayananda, M A 215, 315
 Daymond, M R 297, 328, 372
 De Angelis, R J 257
 de Campos, M F 204
 De Fontaine, D R 205
 De Graef, M 196, 422
 de Groot, J D 273
 De Hosson, J T 275
 de Jong, R A 362
 de Jong, T P 173, 245
 de Lima, N B 429
 De Messemaeker, J 392
 de Napole Gregolin, E 440
 de Vasconcelos, P D 172
 de Vries, A J 360
 Decker, R F 418
 Deevi, S C 413
 Defendi, G A 320
 Dehm, G 229
 Dehoff, R R 358
 Dejmek, M 387
 Del Corso, G 414
 Delaire, O 405
 Delos-Reyes, M A 279
 Demopoulos, G P 378, 426
 Deneys, A C 184, 225, 226, 281,
 326, 368, 411, 412, 441
 Deng, X 286, 293, 331, 341, 416
 Denning, J W 276, 332
 Dennis, K 296
 Derev'yanko, O V 381
 Derin, B C 185
 Derlet, P M 305
 Dervede, E 398
 DeRosset, W S 182
 Deryagin, A 255
 Desai, V 246, 410
 Deshmukh, P V 398
 Desilets, M 213
 Deslippe, J 183
 Desmulliez, M 232

Detavernier, C 370
 Deveaux, E 415
 Deveaux, M 361
 Devincre, B 278
 DeYoung, D H 273, 361
 Dias, H P 213
 Diaz, L 199, 321
 Díaz, R J 171
 Dickerson, M B 291
 Dickerson, R 342, 411
 Dickmann, D 391
 Diepers, H 386
 Dijkstra, W O 248
 Dimiduk, D M 309, 357
 Dinda, G 351
 Ding, J 243
 Ding, R 280
 Ding, W 325
 Ding, W 288
 Dinh, L N 310
 Diplas, S 216
 Ditenberg, I A 256
 Dixon, T W 217
 Djambazov, G S 362
 Dobatkin, S V 253, 432, 433
 Dogan, N 273
 Dogan, O N 401
 Doherty, R 204, 250, 302, 303
 Dolan, D S 189
 Donaldson, A 369
 Donaldson, D J 285
 Dong, H 278, 406
 Dong, S 234
 Dong, Y 200
 Dong, Z F 241
 Dorsam, G 400
 Dou, S X 354
 Douglas, E 377
 Doumanidis, H 209
 Dow, J D 276
 Downes, S 232, 339
 Doyle, C 415
 Doyle, F M 280, 448
 Drawin, S 358
 Drchal, V 192, 304
 Dregia, S A 249
 Dresler, W 444
 Dresselhaus, M S 193, 209
 Dreyfus, J 177
 Dreyse, H C 348
 Drezet, J 203, 218, 385, 450
 Dring, K F 223, 323
 Driver, J 250
 Droste, W E 219
 Drouet, M G 245
 Drummond, B G 173
 Druschitz, A P 442
 Druschitz, E A 442
 Du, Q 323, 387, 406
 Du, T 410, 448
 Du, Z 207, 257
 Duda, S 373
 Dudley, E 230
 Dudo, T 259
 Dufour, G 171
 Dugger, M T 309

Duh, J G	190, 293, 332,
.....	339, 355, 409, 447
Dulikravich, G S	193, 288
Dunand, D C	327, 328, 340, 356
Dündar, M	273, 450
Dunham, S N	381
Dunn, J	365
Dunstan, D	262
Duomo, Z	378
Dupuis, M	437
Duquette, D J	413
Durairaj, R	232, 416
Duterque, J	329
Dutrizac, J E	186, 230, 231
Dutta, I	187, 188, 229, 283,
.....	286, 327, 342, 371
Duval, H	319
Duxbury, P M	391
Duygulu, O	233
Duz, V A	278, 364, 365, 440
Dybkov, V I	455
Dyck, C	394
Dye, D	371
Dyer, T	370

E

Earthman, J C	326
Eastman, J A	238
Easton, M	344, 403
Eaton, S	263
Eberl, C	188
Eckert, C E	370
Edelstein, A S	241
Edrisky, A	413
Edwards, B J	317
Edwards, L	217
Efros, B M	255, 260
Efros, N	255
Egami, T	216
Ege, E S	286
Egry, I	380
Eidet, T	272
Eisinger, N	391, 445
Eizenberg, M	198
Ekenes, J M	272
Ekere, N	232, 416
El-Kaddah, N	362, 428
Elder, K R	322
Eliezer, D	192
Elliott, A J	195
Elliott, A L	281, 282
Elmadagli, M	254
Elmer, J W	345
Embury, D	339, 408
Embury, J D	261, 302, 303
Emelander, D	417
Emerson, J A	394
Emura, S	337
Engh, T A	266
England, L G	300, 343
Enikeev, N A	252, 258
Enomoto, M	186
Erasmus, L	330
Erb, A	276
Erb, U	308
Erickson, K L	338

Erlebacher, J D	379
Ernst, W	364
Erol, A	290
Esaka, H	184, 301
Escobedo, J	361
Escudero, R	378
Eskin, D	203
Espinoza-Nava, L	399
Esquivel, E V	279, 395, 441
Essadiqi, E	233
Estey, C M	214
Estrin, Y	251, 252, 260
Evangelista, E	351
Evans, G A	292
Evans, J W	280, 319,
.....	354, 366, 448
Evans, K J	246
Evelin, S S	329
Ewing, W	448

F

Fabina, L	436
Fachinotti, V D	203
Fagerlund, K	186
Faivre, G P	300
Faizan, M	374
Fallahi, A	303, 431
Falleiros, I G	204, 228
Faller, K	278
Falticeanu, L C	341
Fan, J	380
Fan, P	368
Fan, W	394
Fang, J S	242
Fang, Q T	318
Farkas, D	205, 224, 250, 282,
.....	301, 304, 348, 389, 430, 451
Favet, S	265
Fazeli, F	405
Fecht, H	307
Feigl, K	317
Feng, F	313
Feng, G	204
Feng, J C	392
Feng, Q	270, 345
Feng, Z	191
Fenton, C	271
Fergus, J W	325
Fernandes, F	320
Fernandes, S M	429
Fernandez, F E	199, 321
Fernandez, J	218
Fernández-Flores, R	408
Fernández-Serrano, R	361
Ferreira, I	368
Ferreira, M A	230
Ferres, L	265
Ferron, C J	284
Ferry, M	433
Field, D P	220, 221,
.....	279, 320, 347, 431
Field, R D	283
Fielden, D E	202, 234, 392
Fields, R J	418
Finel, A	349, 390
Fiory, A	180, 276, 321

Fiot, L	172
Fischer, B	270
Fischer, C C	348
Fischer, F D	405
Fischer, W K	360
Fishman, S G	315
Fiske, M	242
Fiterman, M J	267
Fittock, J E	373, 443
Fitz-Gerald, J	321
Fjaer, H	218, 385
Fjeld, A	319
Fleay, J	230
Fleming, C A	284
Flemings, M C	202, 296, 369
Fleury, D R	230
Flisakowski, P J	361
Florando, J N	309
Flores, A	361
Flores, K H	316
Flores, K M	316
Floro, J A	394
Flower, H M	173, 223, 323
Foecke, T J	268
Foiles, S M	347
Fok, I	285
Folch, R	387
Foley, J C	242, 295, 340
Folz, H	442
Fonseca, M B	230
Foosnaes, T	218
Forbes Jones, R M	219, 414
Fornaro, O	300
Forrest, S	180
Forslund, K G	176
Forté, G	170, 311
Fortier, M	439
Fortunier, R	250
Fox, S P	278, 406
Fraczkiewicz, A	225
Franetovic, V	386, 450
Frank, R A	361
Frankel, J I	298, 421
Franklin, J S	296
Frary, M	451
Fraser, H L	309, 358
Fray, D J	182, 199, 223, 278,
.....	280, 323, 364, 406, 440
Frazier, W E	419, 420
Frear, D R	187, 229,
.....	283, 327, 371
Frederick, M J	422
Free, M L	226, 369, 413
Freels, M	271
Freeman, A J	270, 430
Freibergs, J	437
Frias, J	415
Friedman, L H	408
Friedman, P A	211, 264,
.....	310, 355, 397, 398
Friedrich, H	365
Fries, S G	206
Frisk, K	363
Froes, F H	182, 223, 278,
.....	323, 364, 365, 406, 440
Frost, H J	204
Frost, M T	417

Fu, E K	350
Fu, X	390
Fuentes-Cabrera, M	431
Fujii, H	323
Fujii, H	354
Fujikura, M	315
Fujita, A	396
Fujiyoshi, M	294
Fukamichi, K	396
Fuller, C	226
Fultz, B	206, 354, 405
Furrer, D U	174, 215, 269, 315, 357, 400
Furu, E	172
Furuhara, T	282, 327
Furukawa, M	206, 251, 258, 311, 433
Furuno, K	433
Furuya, K	301
Fushen, L	325

G

Gabb, T P	340
Gable, B M	199, 376
Gabrielyan, T N	312
Gaddis, C S	291
Gagne, J	171
Galarraaga, R A	171
Gali, A	185
Galloway, T	170, 212, 265, 311
Gamsjäger, E	405
Ganapathysubramanian, S	235
Gandin, C	202, 248
Ganesan, P G	422
Gang, F	261
Gangloff, R P	410
Gangopadhyay, A K	438
Gao, B	400
Gao, H	395
Gao, J	177
Gao, M C	363, 442
Gao, W	413
Gao, W	241
Gao, X	445
Gao, Y	173
Gararia, S N	312
Garbellini, O B	450
Garcia, A J	240, 291
Gariepy, B	266
Garmestani, H	237
Garner, C M	209
Garratt, M	410
Garud, C	237
Garvin, J W	249
Gatty, D G	399
Gazder, A A	254
Geerapuram, D N	196
Geiss, E	451
Geltmacher, A B	234, 235
Gemeinböck, G	392
Genau, A L	345
Geng, J	359
Gentz, M	371
George, E P	185, 269, 372, 401
George, S	261
Gerberich, W W	261

Gerdemann, S J	440
Gerogiorgis, D I	356
Gerritsen, T	330, 331
Gesing, A J	172, 173
Geveci, A	185
Geyrhofer, W	336
Ghomashchi, M R	423
Ghomashchi, R	439
Ghoniem, N M	224
Ghorbani, H R	331
Ghosh, A K	211, 264, 310, 355, 397, 418, 419
Ghosh, G	294, 304, 358
Ghosh, S	229
Ghosh, S	328
Giannuzzi, L A	432
Gibala, R	379, 430
Gibson, R	399
Gigliotti, M F	195
Gillaspie, J	443
Gilmer, G	431
Giordani, E J	237
Girgin, S	426
Girin, O B	280, 447
Gjestland, H	191
Gladysz, G M	343
Glaner, L	270
Glatzel, U	270
Glavicic, M G	324
Gleeson, B	295, 455, 456
Glicksman, M E	181, 248, 299, 409
Gnäupel-Herold, T	268, 372
Go, J	268
Goddard, III, W A	192
Godfrey, A B	407
Goff, A	295
Goldsmith, C	416
Gole, J L	170, 435
Golovashchenko, S F	213, 214
Golumbskie, W J	243
Gomes, A S	272
Gomez-Cordobes, J	412
Gong, J	237
Gonzalez, C	449
Gonzalez Crespo, P A	207, 258
González, M A	361
González-Doncel, G	361
Goods, S H	209, 261, 308, 352, 394, 418
Gordon, R B	244
Goren-Muginstein, G R	444
Gorman, W C	288
Gornostyrev, Y N	270
Gorsse, S	175, 425
Gosselin, T A	189, 416
Gou, L	395
Goutière, V	266
Gouttebroze, S	203
Graedel, T E	244
Graetz, J	354
Graeve, O A	354
Granada, D G	442
Granasy, L	386
Grandfield, J F	218, 219
Granger, D A	298, 343, 385, 427, 449

Grant, G J	268, 314
Grasso, P	385, 450
Gratias, D	206
Gray, G T	233, 303, 326, 367, 453, 454
Grazier, J M	331
Green, B	359
Green, J A	245
Green, W P	264
Greer, A J	276
Greer, A L	298, 316, 344, 403
Greer, J R	261
Gregori, F	366
Gremaud, M	203
Gribb, T T	198
Griese, R	276, 332
Griffin, J V	273
Griffith, M	370
Grimm, T L	303
Grindstaff, Q G	396
Grosjean, E	417
Gross, K J	262, 310
Groza, J R	242
Gruen, G	219
Grugel, R N	247
Grund, G	330
Gschneidner, K A	396
Gu, S	171
Gu, Y	269, 270
Guangjun, Z	455
Guclu, M	365
Guduru, R	393
Guertsman, V	355
Guillemot, G	248
Guillot, J	319
Guinta, R K	394
Guldhav, A	272
Gundakaram, R C	391
Gunderov, D V	260
Gungor, M N	223, 323
Gunnewick, L	362, 424
Guo, D	447
Guo, F	217
Guo, G	323
Guo, H	282
Guo, T	178, 387
Guo, X	288
Guo, Z X	215
Guozhi, Z	325
Gupta, A K	399
Gupta, M	262
Gupta, P	185
Gurupira, T Z	414
Guruswamy, S	396, 397
Gusev, A	437
Gustafson, T W	173
Guthrie, R I	417
Guven, I	229
Guyer, J E	276
Guyot, P	438

H

Ha, D	453
Ha, J	260
Haataja, M	276
Haberling, C	383

Hackenberg, R E	442	Hashimoto, S	338	Holloway, P H	377
Haeffner, D R	250, 272	Haskel, D	250	Holm, E A	181, 182, 224, 278, 324, 365, 391, 407
Haggett, R	420	Hasnaoui, A	305	Holmsen, A	398
Hagiwara, M	337	Hassan, H	372	Holtkamp, D B	303
Hagman, A	436	Hassan, M I	385	Homentcovschi, D	417
Hagni, A M	295	Hata, S	390	Hon, M	374
Hahn, H W	306	Hatch, C	323	Hong, D	377
Hakik, M	342	Hatsuda, K	206	Hong, F	417
Hakonsen, A	318	Hauback, B C	353	Hong, J	321
Halali, M	369	Haugen, T	318	Hong, K	293
Halas, N	240	Hawk, J A	401	Hong, S	214, 350
Haldenwanger, H	383	Hayashi, T	215, 315, 401	Hongming, G	455
Halikia, I	330	Hayashi, Y	435	Hoo, N	416
Hall, M G	282	Hayes, P C	330	Hopkins, P L	338
Hallbom, D J	443	Haywood, R	362	Horita, Z	206, 251, 258, 311, 340, 433
Hamadou, H	203	Hazzledine, P M	225	Horstemeyer, M	356
Hamawi, D	395	He, G	337	Hort, N	445
Hamipikian, J	381	He, M	373	Horton, D J	297
Hammar, R H	211	Heamot, N	426	Horton, J A	184, 287, 359
Hammon, D L	261	Hearne, S J	209, 261, 308, 352, 394, 418	Horton, W S	286
Hampikian, J	381, 388	Heason, C P	253	Hosford, W F	257
Han, B Q	256, 352, 391, 392	Hebert, R J	253	Hosking, F M	368
Han, C	448	Hedjazi, J	439	Houchin, M	443
Han, E	288, 412	Heilmaier, M	315, 355	House, J W	257
Han, G	226	Hellmig, R	252	Houston, D Q	191
Han, J	301, 326, 388	Hemker, K J	283	Howard, D W	395
Han, J	454	Henager, C H	355	Howard, S M	214, 314
Han, K	407	Henderson, D W	189, 286, 416, 417	Howe, J M	371, 384
Han, K	392	Hendriksen, M	232, 416	Howell, S W	441
Han, K	448	Henein, H	379, 423, 446	Hoyt, J J	180, 222, 276, 322, 363, 405
Han, L	311	Hennig, R G	183, 431	Hryn, J	199, 244, 357, 417, 429
Han, M K	247	Henrie, B L	233, 303, 326, 451, 453	Hsieh, K	242
Han, Q	227, 266, 281, 298, 299, 318, 343, 383, 385, 427, 449	Henry, D M	428	Hsieh, Y Y	241
Han, S	222	Henry, P J	441	Hsiung, L L	225
Han, S Y	433	Herlach, D M	344, 380	Hsu, E	201
Hanada, S	175, 315	Herman, G	252	Hsu, S C	294
Hanagan, M J	319	Hermesmann, C	214	Hsu, Y	332, 382
Handtrack, D	315	Hernández-Morales, J B	408, 409	Hsueh, J	225
Hanna, M D	211	Hesch, V B	353	Hu, H	311, 313, 376, 447
Hanrahan, R J	396	Hess, P A	270	Hu, S	277, 408
Hansen, B L	451, 453	Higashi, K	340, 356	Hu, Y C	332, 338
Hansen, J	436	Higuchi, K	390	Hua, F	294, 331
Hansen, N	251, 252, 302, 346	Hildebrand, M M	291	Huang, C	269
Hanson, R	404	Hildebrand, Z C	417	Huang, C	242
Hao, Y	195	Hile, J T	324	Huang, C S	332, 339
Haouaoui, M	257, 341	Hill, D J	287	Huang, J	224
Harada, H	174, 269, 270	Hiltmann, F	177	Huang, J	257
Hardwick, D A	174, 215, 269, 315, 357, 400	Hines, J A	191, 225	Huang, J G	234, 247
Hardy, J S	235	Hirai, H	175	Huang, J Y	234, 247
Hariharaputran, R	181	Hirai, M	194	Huang, J Y	306
Harringa, J L	287	Hirata, T	323	Huang, L	271
Harris, B	230	Hiroshi, A	214, 404, 453	Huang, M	271
Harris, G B	329	Hiroshi, H	269	Huang, S	242
Harris, R	333	Hirth, J P	261, 408	Huang, T F	439
Harris, S J	328	Hixson, R S	453	Huang, X	251, 252, 302
Harrison, N R	397	Hoagland, R	355	Huang, Y	261
Harrysson, O	197	Hoagland, R	261, 302, 394, 408	Huang, Y	261
Harshman, D R	276	Hoc, T	278	Huang, Y	258
Hart, G	349	Hodnett, B K	171, 311	Huang, Y	374
Hart, M D	295	Hoeht, J W	261	Hufnagel, T C	271, 402
Hartley, C S	288, 324	Hofmeister, W	345, 370	Huggins, D A	189
Hartwig, K T ...	216, 259, 341, 435	Hogenboom, M	178	Hughes, D A	251, 346
Hasan, S A	413	Hohl, B	177, 272	Huh, J	293, 384
Hashi, K	397	Hohlov, P Y	212	Hull, B A	198
Hashimoto, H	420				

Hultman, L 429
Hults, W L 283
Hung, C M 375
Hünsche, I 401
Hunt, M 217
Huo, Y 380
Hur, B 214, 404, 453
Hurysh, K M 236
Hutchinson, C R 425
Huzmezan, M 195
Hwang, C 190, 338
Hwang, S 254
Hwang, W 285
Hwang, Y J 197
Hyde, B 224, 301
Hyde, J R 441
Hyers, R W 289, 299, 438
Hyland, M 218, 265, 399, 412

I

Ice, G E 279, 324, 394
Ichikawa, T 354
Ichimura, S 220
Ignatenko, L N 258
Ikeda, M 324
Ilegbusi, O J 448
Ilyoukha, N 369
Im, J 259, 341, 435
Im, Y H 423
Imai, T 234
Imam, A 278
Imam, M 182, 223, 278,
..... 323, 364, 406, 440
Imbert, C A 201, 441
Imrie, W P 188, 230, 231, 284,
..... 328, 330, 372, 415, 443
Indrakanti, S K 227, 281
Indutnyy, I Z 180
Inel, C 173
Inman, D 323
Inoue, A 216, 271
Inoue, H 401
Inspektor, A 421
Ionescu, A 173
Iosub, V 210
Ipser, H 231, 382
Irvine, S 441
Isac, M 417
Ishida, K 191, 242
Ishikawa, K 397
Islam, Z 250
Itakura, M 390
Itharaju, R R 258
Ito, K 215, 315, 357, 401
Ivan, J 296
Ivanisenko, Y 307
Ivanov, Y F 255
Iwata, S 304
Iyer, M K 241
Izumi, K 220

J

Jablokov, V R 173
Jackson, G 416
Jackson, M 223, 323

Jackson, M R 358
Jackson, S M 413
Jacobsen, L 364
Jacobson, D L 210
Jacot, A 203, 385, 387
Jäger, S 234
Jahnsen, E J 330
Jak, E 330
Jakobsson, A 409
Jalkanen, H 186
Jamey, C 172
Jang, G Y 293, 332
Jang, S J 439
Jankowski, A 406
Janousek, M 174, 215,
..... 269, 315, 357, 400
Janzen, J 330, 331
Jaouen, O 178
Jaradeh, M 298
Jardy, A 219, 404
Jarry, P P 298
Jayakumar, T 227
Jayaraj, B 410
Jayasekera, S 329
Jeannette, J 417
Jéhanno, P 315, 358
Jensen, C M 263, 353
Jeong, H 438
Jeong, S 286
Jerman, G 419
Jha, G 214
Jha, M K 171
Jian, X 299, 318
Jiang, C 349, 364
Jiang, F 379, 446
Jiang, H 303
Jiang, W 194
Jiang, W 316
Jiang, Y T 439
Jiao, H 228
Jiao, W L 290
Jin, C 291
Jin, M 275
Jin, S 196, 197, 337
Jin, Y M 183, 277, 384
Jin, Z 349, 350
Jo, H 376
Jog, J 302
Johnson, C 442
Johnson, D D 205
Johnson, D R 215, 269,
..... 270, 315, 387
Johnson, G L 212
Johnson, J A 284, 318
Johnson, J R 353
Johnson, W C 277, 384
Johnson, W L 316, 369
Jolly, M R 318
Jonas, J J 201, 205
Jonas, R K 212
Jones, C L 414
Jones, H 298, 301
Jones, H N 392, 435
Jones, J W 375, 418
Jones, K S 420
Jones, R H 170
Joo, H 441

Joo, Y 241, 293
Jörgl, H P 336
Josell, D 220, 229,
..... 247, 280, 409
Joubert, J 210
Juarez, J A 449
Jung, C 300
Jung, J 383
Jung, J 241
Jung, K 380, 392
Jung, S 198, 338, 374, 455
Jung, Y 362
Jungk, J 261, 308
Juul Jensen, D 204, 390

K

Kabansky, A E 169
Kabra, S 185
Kaczorowski, J 266
Kad, B 366, 371, 383
Kadolkar, P B 411
Kai, H 378
Kaibyshev, R O 311
Kaikake, A 415
Kainer, K U 418, 445
Kainuma, R 191, 242
Kakegawa, K 296
Kakihira, T 366
Kalantar, D H 366
Kalidindi, S R 303
Kaligotla, A 214
Kalu, P 205, 407
Kamachi, M 206
Kamavaram, V 325
Kammer, D 248
Kamp, N 411
Kampe, S L 223, 295, 296
Kane, J 413
Kaneno, Y 174, 401
Kanert, O 297
Kang, S 258
Kang, S H 179, 198,
..... 220, 274, 320
Kang, S K 189, 231,
..... 285, 331, 373, 416
Kang, T 382
Kang, Y 309
Kantzoz, P T 340
Kao, C R 198, 199, 240, 293,
..... 332, 338, 373, 374, 382
Kao, H R 375
Kao, S T 190
Kao, V 233
Kaplan, D I 364
Kaplan, H 332
Kapusta, C 321
Kapusta, J 184
Karabasevic, D 180
Karabelchtchikova, O P 421
Karaca, H 442
Karaman, I 207, 216, 257,
..... 302, 341, 350, 442
Karanjai, M 224
Karma, A S 386
Karner, W 329
Karney, G B 195

Kasapoglu, Z	315	Kim, D	374	Kiss, L I	213, 447
Kaschner, G C	451	Kim, D H	217, 438	Kissane, J	360
Kashani-Nejad, S	333	Kim, D S	287	Kitahara, H	351
Kashyap, B	224	Kim, H	442	Kiyobayashi, T	263
Kashyap, S C	239	Kim, H	453, 454	Klarstion, D L	202
Kaspar, R	259, 350	Kim, H	448	Klarstrom, D L	226, 297, 411
Kassner, M E	279, 433	Kim, H	339	Kleber, S	350
Kastebo, J	218	Kim, H	389	Klein, B	443
Katgerman, L ...	203, 220, 248, 385	Kim, H	448	Kleinschrodt, H	437
Katiyar, R S	291	Kim, H	258	Kletskey, S V	275
Katsman, A	444	Kim, H J	411	Klingbeil, D	367
Kaufman, L	192	Kim, H S	252	Klingbeil, N W	281
Kawagoishi, N	410, 411	Kim, H Y	254	Klingensmith, M A	318
Kawakami, A	323	Kim, I J	287	Klinger, C	367
Kawamura, Y	295, 438	Kim, I S	412	Klug, K L	223, 323
Kawano, Y	449	Kim, J	246	Klushin, S D	335
Kawasaki, M	258	Kim, J	175	Kluthe, C	353
Kawazoe, Y	390	Kim, J	389	Kmiotek, D S	343
Kay, N R	229	Kim, J	352	Knabl, W	401
Kay, R	232	Kim, J	455	Knapp, J A	261
Ke, L	294	Kim, J	416	Knott, S	190
Ke, W	288	Kim, J	453, 454, 455	Ko, Y G	433
Kear, B H	209	Kim, J H	433	Kobade, R	339
Kecskes, L J	254	Kim, J H	286, 294	Kobayashi, K	326
Keen, L	377	Kim, J S	417	Kobayashi, T	270
Keist, J	414	Kim, K	190	Kobbeltvedt, O	172
Keles, Ö	273, 450	Kim, K	281	Koch, C C	256, 391, 420
Kelkar, K	219, 362	Kim, K	309	Kogut, D	364
Keller, J	396	Kim, N	382	Kohlbrecher, J	250
Keller, R	399	Kim, N J	287	Kohn, A	198
Kelly, J J	308	Kim, S	198, 338	Kohn, R V	425
Kelly, P M	228	Kim, S	214, 453	Kohyama, A	184
Kelly, S M	223	Kim, S	451	Koike, J	199, 340, 384, 425
Kelly, T F	198	Kim, S	455	Koike, K	220
Kelton, K F	289, 438	Kim, S	264	Koike, M	407
Kemp, D J	189, 231	Kim, S	454	Koizumi, Y	259, 351, 388
Kempshall, B W	432	Kim, S	215, 241	Kolbe, M	380
Kendig, K	175	Kim, S G	387	Kolobov, Y R	306
Kennedy, M S	275	Kim, S H	454	Koltun, P	333
Kenney, M	378, 420	Kim, S K	376	Komandur, K	411
Kepes, A	330	Kim, S S	412	Komatsu, S	324
Kerdouss, F	361	Kim, S W	199, 435	Kommel, L	258
Kerns, R	441	Kim, T	374	Kompan, Y Y	223
Kerr, M	331	Kim, W	321, 358	Kondoh, K	418
Kerstiens, B	330	Kim, W T	217, 387, 438	Kondoh, M	440
Kertý, B	273, 450	Kim, Y	287	Koneva, N A	255, 258
Kertz Yurko, J E	299	Kim, Y	352	Kongoli, F	185
Keskinkilic, E	185	Kim, Y	260	Konopnicki, M G	212
Kestler, H	315	Kim, Y	455	Konstantinov, K K	354
Khachaturyan, A	183, 277, 353, 384	Kim, Y	309	Kontsevoi, O Y	270
Khan, Z H	171	Kim, Y H	374	Koo, H	325
Khemelevskaya, I Y	253	Kim, Y S	412, 454	Koo, J	455
Khor, K	411	Kimura, T	351	Koo, Y	441
Khraisheh, M K	258, 398, 450	Kimura, T	384	Kooistra, G W	326
Khraishi, T	221, 356, 451	Kimura, Y	199, 358, 435	Kool, P	385
Kiese, J	365	Kinaka, M	191	Koopman, M C	293, 343
Kift, J R	415	Kinder, J	367	Kopf, S R	414
Kikuchi, E	449	King, A H	259	Kopka, L	191
Kikuchi, K	314	King, D E	416	Korb, G	392
Kikuchi, M	407	King, W	406	Korhonen, M A	286, 416
Kilmametov, A R	306	King, W T	195	Korhonen, T K	286
Kim, C	180	Kinyanjui, R	382, 416	Korhonen, T M	416
Kim, C	212	Kirby, J L	272	Korotaev, A D	254
Kim, C	179, 220, 221, 274, 320, 339	Kirchheim, R	309, 353	Korshunov, A I	254
Kim, C	442	Kirkland, S	268	Korzekwa, D A	255
		Kirkpatrick, D ...	170, 212, 265, 311	Kosaka, Y	278, 406
		Kiso, M	338	Koslowski, M	365

Kossler, W J	276
Koster, E	276
Kostika, I	330
Kostorz, G	250
Kourov, N I	260
Kovar, D	356
Kovgan, P A	186
Kozeschnik, E	405
Kozlov, E V	255, 258
Kraft, E H	182
Kraft, O	188, 383
Krajewski, P E	211, 264, 310, 355, 397, 398
Kral, M V	327, 343
Krallics, G	256
Kramer, M J	175, 215, 238, 296
Kramer-White, J	419
Krane, M J	195, 219, 387, 408
Krasilnikov, N A	256, 433
Krause, A R	214
Krause, E	230, 231
Krill, C E	181
Krioukovsky, V	437
Kripesh, V	241
Krishnamurthy, R K	233
Krishnan, A	366
Kroupa, A	382
Kruger, G A	212
Krumdick, G K	200, 244, 357
Krupakara, P V	226
Kruzic, J J	315, 316
Krylov, L	437
Kuba, M	263
Kubat, F	188
Kubin, L	278
Kudrnovsky, J	192, 304
Kulas, M	264
Kulkarni, A V	207
Kumar, A	227
Kumar, A	222
Kumar, D	336
Kumar, M	390, 406, 431
Kumar, R	171
Kumar, S	225, 316, 360
Kumosa, M	371
Kumta, P	424
Kumta, P N	381
Kunioshi, C T	429
Kuo, C	201, 227, 280
Kuo, R C	234, 247
Kuriyama, N	263
Kurokawa, A	220
Kurtz, R J	355
Kurz, G	233
Kurz, W	203, 345
Kushida, A	426
Kushnarev, B	242
Kusui, J	314
Kutty, M G	445
Kutty, T N	239
Kuwana, K	218
Kuwano, N	390
Kvande, H	356
Kvithyld, A	266
Kyu, T	387

L

Laberge, C	213
LaCombe, J	395
Lacroix, S	177
Ladeuille, L	202
Ladwig, P F	198
Laha, T	388
Lai, Y	357
Lakshmanan, V I	199, 244, 329
LaLonde, A	417
Lamb, J H	397
Lamérant, J	265
Lamperti, A	429
Landgraf, F J	204
Landis, C	328
Lane, J F	410
Lang, J C	250
Langdon, T G ..	206, 251, 253, 254, 256, 258, 305, 311, 340, 349, 391, 392, 432, 433
Langer, S A	406
Langlais, J	273
Lapovok, R	252, 260, 269, 333
Larocque, J E	311
Larouche, A	273
Larson, C	417
Larson, D J	198
Larson, E J	436
Lashkari, O	423
Latapie, A	301
Latour, R A	240
Latroche, M	210
Latysh, V V	259
Laughlin, D E	371
Lauridsen, E M	204
Lauro, P	416
Laux, H	179, 423
Lavernia, E J	256, 306, 352, 391, 392, 433, 449
Lavoie, C	370
Laxminarayana, P	412
Lazarz, K A	287
Le Bouar, Y M	349, 390
Le Brun, P	318, 361
Lech-Grega, M	403
Lechevalier, B	252
Lee, C	374
Lee, C P	247
Lee, C S	368, 411
Lee, C S	433
Lee, D	221, 346, 350
Lee, D L	368
Lee, D R	250
Lee, F G	212
Lee, G W	438
Lee, H	325, 442
Lee, H	389
Lee, H	454
Lee, H C	287
Lee, H M	198, 240, 286, 293, 294, 338, 382
Lee, I	382
Lee, J	382, 416
Lee, J	383
Lee, J	262, 309, 389
Lee, J	300

Lee, J	339
Lee, J	247
Lee, J	301
Lee, J	454
Lee, J	293, 409, 447
Lee, J C	374
Lee, J G	188, 285, 286, 293
Lee, J G	287
Lee, J K	277
Lee, J W	293
Lee, K	309
Lee, K	455
Lee, K	453
Lee, K	376
Lee, K J	350
Lee, K S	214, 350
Lee, M	438
Lee, M G	314
Lee, P D	173
Lee, S	309
Lee, S	271, 272, 360
Lee, S	293
Lee, S	442
Lee, W	455
Lee, W	453, 454
Lee, Y	309
Lee, Y	236, 438
Lee, Y B	208
Legault-Seguin, E N	444
Lehman, L P	286, 382, 416
Lei, Y	232
Leidl, A	188
LeMay, J D	310
Lenosky, T J	183
Leo, P H	277
Leon Iriarte, J	207
Leonard, D	189
Leonard, F	276
LeSar, R A	182, 224, 278, 324, 365, 407
Lesoult, G	202
Levanyuk, A P	425
Levi-Setti, R	429
Levine, L E	279
Lewandowski, J J	359, 360, 371, 372
Lewis, A C	234, 235
Lewis, C	443
Lewis, M	371
Lherbier, L	414
Li, B	276, 289, 379, 380, 423, 441, 446
Li, B	265
Li, C	432
Li, C	203
Li, D	312
Li, D	336
Li, D	237
Li, F	243
Li, H	178
Li, H	238
Li, H	452
Li, J	204
Li, J	319
Li, J	357
Li, J	384
Li, J	410

Li, J	334	Liu, C T	175, 269, 271, 402	Lubarda, V A	366
Li, J C	283, 327, 342	Liu, C Y	294, 332, 375	Lubecka, M	321
Li, L	200, 368	Liu, H	345	Lucadamo, G A	308, 347
Li, M	288	Liu, H	284	Lucas, J P	188, 285,
Li, N	191, 313, 376, 447	Liu, H	443	286, 308, 394
Li, P	371	Liu, H	199, 321	Luckey, S G	397, 398
Li, Q	357	Liu, H J	195	Ludwig, A	178, 247, 386, 423
Li, S	207, 434	Liu, H K	354	Ludwig, L	395
Li, S	374	Liu, J	374	Ludwig, O	218
Li, S X	247	Liu, J	292	Ludwig, W	411
Li, W	312	Liu, N	416	Lue, M	242
Li, W	424	Liu, S	446	Lui, T	332, 337
Li, X	352, 395	Liu, S	299, 300	Luis Pérez, C J	207, 258
Li, X	262	Liu, S	379	Lukac, P D	425
Li, Y	345, 402	Liu, S	319	Lukashchuk, Y V	256
Li, Y	383	Liu, T	374	Lukyanov, I V	312
Li, Y L	324, 426	Liu, W	279, 324	Lund, A C	234, 236, 317
Li, Z	268	Liu, W J	233	Luo, A A	191, 233, 287,
Liang, B	332	Liu, X J	191	332, 375, 417, 444
Liang, C C	232	Liu, Y	428	Luo, W C	199, 374
Liang, J	232, 339	Liu, Y	268	Luo, Z	207, 257, 350
Liang, J	323, 413	Liu, Y	357	Lupulescu, A	248, 409
Liang, R	449	Liu, Y H	421	Lynch, F E	210
Liang, Y	332	Liu, Z	181, 192, 194, 221, 269,	Lynn, K	380
Liang, Z	319	277, 294, 305, 322, 349,	Lyon, P	445
Liao, C	382, 383	363, 364, 406, 417, 426, 445	Lysczek, E M	198
Liao, X	306, 350	Liu, Z	304		
Liaaw, P K	175, 184, 201, 202,	Liu, Z	313		
.....	208, 216, 226, 234, 246,	Liu, Z	421		
.....	247, 256, 270, 271, 296,	Livneh, T	395		
.....	297, 316, 317, 342, 359,	Lloyd, D J	303		
.....	372, 392, 402, 411, 438	Llubani, S	185		
Liedl, G L	377	Lo, C	438		
Liedtke, A	447	Lo, C C	317		
Lienert, U	272, 328, 372	Lo, T	337		
Lifen, L	325	Loan, M	171, 311		
Lightle, C	172, 399	Lofland, S E	291		
Lilleodden, E T	261, 275	Loiseau, A	349		
Lim, C	201	Lokshin, R G	267		
Lim, K	454	Lomas, R	323		
Lim, S	321, 358	Longo, F G	415		
Limata, L	232	Looij, J	343		
Lin, A	291	Loomis, E	201		
Lin, C	280	Lopasso, E	348		
Lin, C C	326	Lopez, M F	233		
Lin, C H	241	Lorimer, G W	294, 295		
Lin, C H	326	Lou, J	261, 308, 377		
Lin, C	382	Louchet, F H	225		
Lin, D C	190	Loutfy, R O	224, 278		
Lin, H	256	Love, R	267, 399		
Lin, K	189, 231, 285,	Lowe, T C	206, 251, 253, 257,		
.....	331, 338, 373, 416	259, 260, 305, 349, 391, 432		
Lin, Q	425	Lowrie, S	441		
Lin, T	326, 337	Lu, C	288		
Lin, W	455	Lu, C C	294		
Lin, Y	449	Lu, G	428		
Lin, Y H	332, 338	Lu, H	416		
Lin, Y L	332, 338	Lu, H	411		
Lincoln, J D	326	Lu, H	313, 332		
Lindley, T C	173	Lu, L	299, 343		
Ling, Y	378	Lu, T B	232		
Lisovskyy, I P	180	Lu, W	440		
Litovchenko, I	257	Lu, X	325, 409		
Little, A L	297	Lu, Y L	411		
Littleton, H E	320, 428	Lu, Z	265		
Liu, B	319	Lu, Z P	175		
Liu, C	372	Luangvaranaunt, T	418		

M

Ma, B M	238
Ma, D	345
Ma, E	176, 305, 391
Ma, H	176
Ma, N	249
Ma, P X	292
Ma, R	313, 332
Ma, S	279, 283
Ma, T	331
Ma, Y	195
Ma, Y	250
Ma, Z Y	311
MacDonald, B	446
MacKay, R A	322, 364
Mackenzie, J M	444
Mackowiak, V	447
MacLaren, I	307
Madenci, E	229
Madshus, S	218
Maeland, A J	353
Magadi, G	248
Magee, T J	230, 329
Magnusson, J H	361
Mahajan, S	193
Mahalingam, T	241
Mahapatra, S P	171, 368
Mahato, C	428
Mahoney, M	226
Maier, H J	257, 302, 341
Maijer, D M	173, 195, 386
Majetich, S	336
Majkrzak, C F	210
Majumdar, B S	187, 188, 229,
.....	279, 283, 286, 327, 328, 371
Majzoub, E H	263, 430, 436
Makhlouf, M M	343, 376, 409
Maki, T	282
Maksymowicz, L J	321

Maksyutov, A F	270	McBow, I	185	Michael, N L	221
Maland, G	318	McCabe, R J	306, 324	Middleton, W J	189
Malgin, D	256	McCall, L	441	Migchielsen, J	273
Mallick, P K	288	McCallum, W	296	Mihalkovic, M	431
Mandal, P	215	McClellan, K J	201	Mikula, A	190
Mani, A S	196	McClung, M	213, 399	Miles, M P	226
Manias, E	424	McComas, E	370	Militzer, M	268, 405
Manickam, K	236	McConaghy, E	188	Miller, G	443
Maniruzzaman, M	404, 423	McCord, M G	197, 447	Miller, G	329, 230
Mann, A B	197	McCoy, R A	374	Miller, M	329
Mann, V C	267	McCrabb, L C	443	Miller, M K	402, 408
Manning, C	366	McCune, R C	191, 288	Miller, M P	235
Mannweiler, U	360	McDanel, S	418	Mills, M J	183, 309,
Manohar, P A	180	McDanice, R	202	352, 358, 407
Mantese, J V	426	McDaniels, R L	226	Minamino, Y	259, 351, 388
Mara, N A	317, 432	McDonald, M	420	Mineta, K	449
Marcus, H L	451	McDonald, N J	300	Minisandram, R S	219, 220
Margulies, L	302, 372	McDonald, R G	284	Minor, A	275, 352
Marian, J	183	McDonald, S D	343	Minor, A M	275
Marks, J	399	McDougall, J L	367	Mintz, M H	395
Marks, R A	229, 342	McDowell, D L	289	Miodownik, M A	181
Marshall, D	284	McFadden, G B	276, 322	Miracle, D	175, 402
Martchek, K	244, 398	McGarrity, E	391	Mirchi, A A	176, 217,
Martens, R L	198	McIntyre, H R	343	272, 317, 360
Martin, C	218	McKamey, C G	269	Mirpuri, K	221
Martin, C	437	McKay, B J	344	Mishima, Y	174, 199, 215, 269,
Martin, E S	266	McKay, J	378	315, 357, 358, 359, 400, 435
Martin, G	389	McKean, B	231	Mishin, Y	222, 346, 377
Martin, J	177, 218, 272,	McKenzie, P	252	Mishra, B	193, 199,
.....	318, 361, 403, 439	McKillip, J L	381	210, 235, 244
Martin, J J	338	McLean, A	417	Mishra, C R	171
Martin, P L	182, 357	McLean, W	310	Mishra, N C	336
Martinent, V	265	McNelley, T R	252, 264, 349	Mishra, R K	347
Martinez, H	326	McNerny, C	421	Mishra, R S	207, 211, 264,
Martinez, J V	435	McQueen, H J	201, 302	310, 311, 355, 397
Martinez, R A	202	Meade, D	195	Misra, A	261, 302, 324, 408
Martocci, A	436	Meco, H	300	Misra, D K	302
Maruyama, K	384	Medlin, D L	308, 347	Mistree, F	289
Marvin, J	328	Meek, T T	299, 318	Mitchell, T E	324, 408
Marzari, N	304	Meeks, H S	341	Mitlin, D	408
Mason, D E	431	Megahed, M M	437	Miura, S	359
Mason, P G	328, 443	Mehl, M J	377	Miura, Y	424
Mason, T A	303, 451	Mehrotra, P	421	Miyahara, Y	340
Massalski, T B	371	Meier, M	176, 217,	Miyamoto, H	253
Mast, D	238	272, 317, 360	Mizutani, Y	300
Masuda, C	255, 393	Meinke, J H	391	Mo, A	385
Masumura, R A	302	Melcher, S	239	Mobasher, A	242
Mathaudhu, S N	216, 259, 341	Melissari, B	447	Moffat, T P	220, 280
Mathier, V	385	Mello, J M	317	Mohamed, F A	391, 392
Mathis, A	361	Mendelev, M I	222, 223	Mohamed, S A	437
Mathisen, S T	172	Mendiratta, M G	174, 357	Mohanty, P S	288
Matson, D M	246, 289, 299	Mendoza, R	248, 322	Mohney, S E	198, 240,
Matsuda, T	397	Meng, D	221	293, 338, 382
Matsumoto, A	326	Meng, Y	203	Mohri, T	304, 359, 389, 431
Matsuoka, R	449	Mengel, J	436	Mokadem, S	203
Matthews, S R	197	Menon, S K	174, 357	Moldovan, P	290
Matyas, A	330	Menzel, B	270	Monig, R	188
Maurice, C	250	Mercer, C	271	Monlevade, E F	228
Maxey, E	297	Merfeld, D	180	Monteiro-Riviere, N	197
Mayer, R	411	Meschter, S J	191	Montejano, S	454
Mayer, T M	261	Mesina, M	245	Montgomery, G P	397, 398
Mayeaux, B	419	Messersmith, P B	424	Montgomery, J S	278, 364,
Maziarz, W	321	Metson, J B	265, 399	365, 440
Mazuelas, A	250	Metzger, H	250	Montheillet, F	252
Mazumder, J	192	Meyers, M	291, 366, 381	Moody, N R	209, 261, 262,
Mazunov, D O	180	M'Hamdi, M	218, 385	308, 352, 394, 418
Mazzei, A C	368	Michael, J R	308	Moore, A R	418

Moore, J F 429
 Morales, A T 211
 Morando, C N 450
 Moraru, A 173, 437
 Mordike, B 383
 More, K L 215
 Morgan, D 205, 289
 Morgan, J K 441
 Mori, H 301
 Mori, T 297
 Morin, G 375
 Morishita, M 427
 Moriyama, K 415
 Morral, J E 174, 322
 Morris, J G 249, 314
 Morris, J R 222, 316, 317, 365
 Morris, J W 275, 283, 331
 Morrison, M L 271, 359
 Morrow, A 415
 Morsi, K B 242, 295, 340
 Mortensen, D 385
 Mosher, J 329
 Moss, S C 250
 Mostovoy, S 237
 Mota, G E 172, 213
 Motahari, S 328
 Motoyasu, G 417
 Moura, R R 317
 Mourou, G 345
 Moxson, V 278, 364, 365, 440
 Mucciardi, F 380
 Muddle, B 371, 415
 Mueller-Krumbhaar, H 386
 Muhlstein, C L 309
 Muir, D M 284
 Mukherjee, A 317, 355, 432
 Mukhopadhyay, A 362, 404
 Mukhopadhyay, G 194
 Mukhopadhyay, P 194
 Mukhopadhyay, S M 301, 346,
 388, 428, 429, 450
 Mulholland, M 356
 Muller, K 239
 Müller, S 181
 Muncy, M 172
 Mungsantisuk, P 396, 397
 Munitz, A 287, 418
 Murali, K 397
 Murayama, N 426, 427
 Murphy, C J 395
 Murphy, K 263
 Murr, L E 192, 279, 395, 441
 Murray, J 277
 Murray, J A 188
 Murti, V S 413
 Murty, K L 201, 246, 256,
 296, 297, 342, 379
 Musin, F 311
 Myrbostad, E 318

N

Na, K 236
 Nafisi, S 423, 439
 Nagano, T 186
 Nagasawa, Y 390
 Nah, J 294

Naik, R R 291
 Nakagawa, Y 401
 Nakamori, Y 263
 Nakamura, H 401
 Nakamura, N 384
 Nakamura, Y 210
 Nakano, T 390
 Nakano, T 300
 Nakayama, K 427
 Nam, S 281
 Nam, W J 208
 Nandy, T 270
 Napolitano, R 300, 343, 427
 Narayan, J 291, 334, 336
 Narayan, R J 197, 239, 291, 337,
 381, 424, 447, 450, 451
 Nardi, P 352
 Narita, H 449
 Narvekar, R N 217
 Nash, P 237, 314
 Nastac, L 178, 219, 220,
 273, 319, 362, 404
 Nastasi, M 302, 408
 Navarra, P 380
 Nayak, S 334
 Nazarov, A A 252
 Necker, C T 249
 Nedkova, T 184
 Needleman, A 377
 Neelameggham, R 332
 Neilsen, M K 230
 Neitzel, G P 404
 Nendick, R M 189
 Nenkov, K 239
 Nerikar, P 302
 Nes, E 205, 351
 Neudorf, D A 189, 443
 Neuschütz, D 404
 Ng, K W 333
 Ngoh, S L 339
 Nguyen, V 218
 Ni, H 254
 Nibur, K A 224
 Nicholson, B K 406
 Nicholson, D 359, 431
 Nicol, M J 443
 Nie, J 187, 228, 294, 295,
 339, 371, 383, 425, 445
 Nieh, T G 438
 Nielsen, M C 179
 Niemczura, W 263
 Nienow, A W 318
 Nieves, J 291
 Nigam, A K 196
 Nikandrov, K P 267
 Nikoloski, A N 443
 Nishimura, T 182
 Nishio, T 326
 Nishiyama, K 227
 Nix, W D 261, 309
 Nizovtsev, P N 259
 Noakes, R 276
 Nobile, A 253
 Noebe, R D 251
 Nogita, K 343
 Noguez, M E 454
 Norfleet, D M 352

Noronha, S 224
 Northwood, D 311
 Notis, M R 189, 198, 231, 232,
 240, 285, 293, 331,
 338, 373, 382, 416
 Novichkov, S B 245
 Novotnak, D 414
 Nowak, R 177
 Noyan, I C 416
 Ntakaburimvo, N 178
 Nunomura, Y 174
 Nurminen, E 186
 Nyberg, E 287

O

O'Brien, J M 257
 O'Callaghan, J F 373
 Ochoa, F A 331
 Oda, T 323
 Oda, Y 407
 Oertel, C 401
 Ogata, S 194
 Oh, B 337
 Oh, K 383
 Oh, K H 283
 Oh, S 382
 Oh-ishi, K 252, 264, 433
 Ohkubo, C 407
 Ohkubo, K 359
 Ohmori, T 242
 Ohnaka, I 300
 Ohno, M 389, 431
 Ohnuma, I 191
 Okabe, T 366, 407, 449
 Okamura, Y 206
 Okane, T 299
 Okazaki, K 434
 Okuno, O 407
 Olevsky, E A 242
 Olivares, R 440
 Oliveira, T 252
 Oliver, E C 297
 Oliver, S R 275, 321
 Oliver, W C 308
 Olson, D L 192, 210
 Olson, G B 192, 358,
 369, 384, 425
 Olson, J D 198
 Olsvik, A 272
 Oltman, E 198
 Omanovic, S 280
 Omran, A M 403
 Onderka, B 240
 Ooij, W V 238
 Oona, H 436
 Oosterkamp, L D 191
 Oppenheimer, S M 340
 Opsahl, T 398
 Orimo, S 263, 396
 Orlov, D 208, 255, 260
 Orlova, T S 252, 258
 Orth, A 330
 Ortiz, A L 346
 Ortiz, M 365
 Osada, K 211
 Osamura, K 314

Osborne, G E 421
 Osborne, R C 188, 230, 231
 Osetsky, Y N 183, 184, 224, 226
 Oshinowo, L 285, 362, 424
 Ossi, P M 429
 Österle, W 367
 Oswald, K 218
 Otto, F 425
 Ou, S 231
 Ouimet, L J 191
 Ovcharenko, V I 280
 Overfelt, R A 375, 450
 Oyama, Y 200
 Øye, H 176, 218
 Oygard, A 318
 Ozaki, K 226, 326
 Ozcan, A 370
 Ozolins, V 263, 305, 430

P

Padhi, B 368
 Paglieri, S N 353, 436
 Paik, J 241
 Paik, K 294, 339
 Pal, U B 280, 325, 366, 409
 Palacio, H A 300, 450
 Palenik, B P 291
 Palumbo, G 308
 Pan, D 232
 Pan, D 229, 286, 342
 Pan, M X 217
 Pan, T 191
 Panaitescu, A 173, 437
 Panaitescu, I 173, 437
 Pande, C S 246, 302, 435
 Pandya, D K 239
 Pang, J H 286, 338, 339
 Pang, J W 279, 324
 Pang, Y 278, 406
 Panov, A V 312
 Pant, B B 198
 Pao, P S 392
 Papaconstantopoulos, D A 377
 Papadimitrakopoulos, F 451
 Papangelakis, V G 284
 Parent, L 361
 Paretsky, V M 185, 186,
 200, 335, 427, 449
 Parikh, A N 447
 Parish, C 395
 Parisi, A 387
 Park, C 455
 Park, C 229
 Park, E S 217
 Park, H 236
 Park, H 241
 Park, J 339
 Park, J 203
 Park, J 452
 Park, J I 442
 Park, J S 453, 454
 Park, J S 411
 Park, K S 368
 Park, K T 349
 Park, S 386
 Park, S 442

Park, S 453
 Park, S 455
 Park, S S 287
 Park, Y 339
 Parkes, R C 286
 Parkin, S 290
 Paromova, I V 312
 Parrish, E 238
 Parsell, D E 359
 Parsey, J M 193, 235
 Parthasarathy, T A 174, 357
 Paserin, V 355
 Pasturel, A 390
 Patankar, S V 219
 Patel, A D 219, 220
 Patel, J 394
 Patel, M K 362, 404
 Patino, E 378
 Pattabiraman, R 236
 Pattanaik, G R 239, 291
 Patterson, E 399
 Patti, A 380
 Patzelt, N 330
 Paulsen, K 172
 Pavo, J 235
 Pawaskar, D N 406
 Pawlek, R P 313
 Paxton, D M 235
 Payzant, E A 176, 256, 392
 Pecharsky, V K 263, 396
 Pedersen, R 272
 Peker, A 271, 359
 Pekguleryuz, M O 444
 Pelletier, J 438
 Pellin, M J 429
 Pena, J S 320
 Peng, H 238
 Peng, L 434
 Peralta, P D 201, 342, 411
 Percheron-Guégan, A 210, 262
 Pereloma, E V 254
 Perepezko, J H .. 215, 241, 253, 344
 Perez-Prado, M 433
 Perruchoud, R C 360
 Perry, T 413
 Peter, W 271, 359
 Peterson, L 204
 Peterson, R 244, 266
 Petit, P 358
 Petraroli, M 190
 Petricca, S 381
 Petrova, R S 275
 Pettengill, E C 264
 Pettersen, K 444
 Pettifor, D G 348
 Pharr, G M 372, 401
 Phillion, A 219
 Phillips, E C 171
 Phillpot, S R 222
 Piascik, R 418
 Picard, Y N 345
 Pickens, J R 223, 365
 Pickering, H W 409
 Pillai, V C 399
 Pillis, M F 243
 Pilon, L 173
 Pilyugin, V 255

Pineault, J 177
 Pinoncelly, A 272, 399
 Pint, B A 174
 Piotrowski, G B 341
 Pippan, R 252, 254, 350
 Pisarkiewicz, T 321
 Piskajova, T V 267
 Pitchure, D 287
 Plapp, M 387
 Platek, P 268
 Platonov, V 437
 Plikas, T 362, 424
 Pluth, M J 301, 388
 Podey, L 318
 Pohar, P 378
 Poirier, D R 385, 428
 Polasik, S J 309
 Poliakov, P V 267
 Pollock, T M 195, 270, 345
 Pomrenke, G S 179
 Pomykala, J A 357
 Poncsák, S 447
 Pond, R C 228, 425
 Ponge, D 259, 350
 Pongsaksawad, W 367
 Poole, W J 268, 303, 307
 Poon, J 216, 217
 Popescu, G 290
 Popov, V P 381
 Popova, N A 258
 Portella, P D 367
 Porter, W 176, 298, 421
 Portmann, M J 250
 Posada, T 361
 Potens, B 388
 Potluri, K 274
 Potocnik, V 437
 Potzies, C 418
 Poulsen, H 302, 372
 Pourboghrat, F 431
 Powell, A C 194, 236, 280, 289,
 323, 325, 335, 366,
 367, 378, 408, 409, 420
 Powell, B R 191, 444
 Powell, G 395, 396
 Prabhakaran, R 226
 Prado, F G 372
 Prado, F L 372
 Prakash, M 218
 Prangnell, P B 253, 258
 Prask, H J 268, 372
 Predecki, P 371
 Prevey, P 340
 Price, A 436
 Pridgeon, J 378
 Prins, S N 269
 Proffen, T E 360
 Prokoshkin, S D 253
 Protokovilov, I V 223
 Proulx, P 177, 361
 Provenzano, V 195
 Pruski, M 263
 Puertas Arbizu, I 207, 258
 Puligandla, V 339
 Pundt, A 353
 Purdy, G R 186, 187, 282
 Pushin, V G 260

Puttlitz, K J 286, 416

Q

Qi, G 373
Qi, Y 331
Qian, M 294, 376, 417
Qin, Q 357
Qiu, Z 357, 400
Quan, Z 214
Quatravaux, T 219
Quested, T E 298
Quiroga, A S 300

R

Raab, G I 255, 256, 257
Raabe, D 259, 350
Rabba, S A 360
Rabeeh, R 308
Rabenberg, J 219
Rabiei, A 381, 447
Rabkin, E 260
Rack, H 446
Rack, H J 350
Rackaitis, M 424
Radmilovic, V 408
Raghavan, P 406
Raghavan, S 387
Rahman, M M 274
Raj, B 227
Raj, I A 236
Rajagopalan, B 288
Rajagopalan, S 342
Rajan, K 192, 234, 288,
..... 289, 334, 376, 419
Rajeev, K P 196, 239
Rama Mohan, T R 224
Ramachandran, V 199, 244
Ramakrishnan, S 333
Ramanath, G 389, 422
Ramanathan, L V 243, 429
Ramanujan, R V 238, 424
Ramaswamy, K 256
Ramchandran, R 244
Ramesh, N N 412
Ramesh, R 195, 237, 290, 336
Ramirez, A G 453
Ramirez, J 386
Ramírez, J 454
Ramovic, R 180
Ramsey, L 172
Rangaswamy, P 283, 371
Ranieri, S 188
Ranki-Kilpinen, T 186
Rao, S 183
Rao, V N 412
Rapkoch, J M 200
Rappaz, M 202, 247, 299,
..... 300, 344, 385, 386, 450
Ratchev, I 440
Rath, B B 169, 334, 446
Rath, C 336
Rathod, C R 297
Rathz, T J 438
Ratke, L 380
Ratner, B D 197, 239

Raty, M 171, 311
Ravinder Reddy, N 355
Ravindra, N M 179, 180,
..... 220, 274, 320, 321
Rawn, C J 400
Ray, K K 227
Ray, L D 318
Raychenko, O I 381
Readey, D W 193
Ready, J 179, 220, 274, 320
Rebak, R B 246
Reck, B 244
Reddy, M R 413
Reddy, R G 185, 243, 268,
..... 325, 354, 355, 357
Redl, C 404
Reed, B 406, 431
Reichert, H 251
Reichman, S H 278
Reid, J G 372, 373
Reilly, E K 354
Reilly, J J 353
Rejaee, M 333
Rejent, J A 331
Remhof, A 395
Remington, B A 366
Renaudier, S 437
Reny, P 177
Reshetov, A 208
Reuter, M A 200, 232, 245, 362
Reutzel, S 380
Reynier, Y 354
Reynolds, T 270
Reynolds, W T 282, 371
Rez, P 354
Reznik, I D 185
Rhee, H 188, 285, 286
Rhee, K H 269
Richards, C D 275, 435
Richards, R F 275, 435
Richardson, J W 184, 297, 372
Ricker, R 287
Ricketts, N J 376
Rickkets, M S 288
Riddle, R K 330
Riddle, Y W 343, 347, 376
Ried, P P 191
Rieger, L E 326
Riehl, W 230
Rietz, W 417
Rigg, P A 453
Rigopoulos, E 330
Rigsbee, J M 197, 239, 291, 326,
..... 337, 381, 413, 420, 424, 447
Rijssenbeek, J 263
Riman, R E 197
Ritchie, R O 309, 315, 418, 419
Ritchie, R R 316
Rivard, J D 341
Riverin, G 266
Rivéro, I V 421
Rivière, C 319
Rivoaland, L 177
Ro, Y 270
Ro, Y J 410
Robach, J 183
Robbins, J 221

Robertson, I M 183
Robinson, J A 198
Robinson, M C 275
Robinson, T P 313
Rocha, M S 230
Rodnov, O O 212, 267
Rodrigues, R L 329
Rodriguez Gan, R 373
Rodriguez, P 415
Roesner, H 346, 351
Rogan, R 328, 372
Rogers, J R 289, 438
Rohrer, G 390, 391
Rolander, N 246
Rolland, K 172
Rollett, A D 180, 204, 249,
..... 282, 302, 347, 451
Romanov, A E 252, 258
Rong, Z 224
Rosales, I 326
Rosales, P I 175
Rösner, H 307
Ross, C A 420
Rossler, U K 239
Rousseaux, J 171
Roven, H J 208
Roy, A 357
Roy, A K 226
Roytburd, A L 322, 334, 384, 425
Roizin, A V 318
Ruban, A V 405
Rubinovich, Z 333
Rubisov, D 284
Ruckebusch, H 173
Ruda, M 451
Rudd, T J 301
Rudin, S P 183, 282
Rudko, G Y 180
Rugg, D 182, 323
Rühle, M 346
Ruile, W 188
Runt, J P 424
Russell, R 436
Russell, R 418, 419
Ruuskanen, P R 412
Ruzylo, J 221
Ryan, L 415
Ryu, D 413
Ryu, H 453, 454
Ryu, J 442

S

Saatci, A 265
Sabau, A S 218, 298, 362,
..... 379, 421, 423, 446
Sachdev, A K 233, 347
Sachenko, P 432
Sadananda, K 348, 366
Sadigh, B 406, 431
Sadler, B A 360
Sadoway, D R 223, 325, 366, 420
Saeki, Y 359
Saez, E 178
Safi, M 203
Sahling, M 398
Saito, K 218, 450

Saito, N	234	Schönfeld, B	250	Shaw, B A	409
Saito, T	440	Schroth, J G	211, 212,	Shaw, L L	202, 208, 346
Saito, Y	206	264, 310, 355, 397	Shcherbakov, A V	256
Sakaguchi, T	227	Schuh, C A	234, 236,	She, H	213
Sakai, T	206	317, 438, 451	Sheen, S R	355
Sakamoto, H	449	Schultz, A	191	Shen, C	183
Sakamoto, M	175	Schultz, A E	198	Shen, F	290
Sakasagawa, H	184	Schulz, M	238	Shen, H	201
Sakidja, R	215, 400	Schulze, R K	302	Shen, J	176
Salami, T O	275, 321	Schumacher, P	344	Shen, Y	408
Salas, G	454	Schvezov, C E	195, 344, 440	Shen, Y	221, 286, 356, 451
Saleh, T A	297	Schwandt, C	280	Shepelyavyj, P E	180
Salem, A A	252, 303	Schwartz, C L	368	Sheretz, R J	448
Salimgareyev, H	208	Schwarz, R B	353	Shevade, S S	274
Samanta, D	319	Schwarz, S M	432	Shi, D	238, 448
Sambandam, S N	455	Sciammarella, F M	314	Shi, X	179
Sampson, D	230	Seal, S	301, 346,	Shi, X Q	339
Samson, S	274	388, 395, 428, 450	Shi, Y	232
Sanchez, J E	187, 229,	Searles, M	189	Shi, Z	357
.....	283, 327, 371	Sears, J	341, 406, 440	Shian, S	291
Sanders, D G	211	Sedighy, M	331	Shibata, J	426, 427, 448
Sanders, R E	249	Seekely, M J	309	Shieh, Y C	199, 374
Sanders, T H	296, 404	Seel, S C	394	Shield, J E	388
Sanders, W S	175, 227, 402	Seeley, L	284, 328, 443	Shields, J A	174, 215,
Sandhage, K H	291, 337	Seetharaman, S	280, 409	269, 315, 357, 400
Sandoz, D	415	Seetharaman, S	248, 300	Shiflet, G J	216, 217,
Sandrock, G	170	Segal, A	441	228, 327, 363, 376, 442
Sankar, J	337	Sehitoglu, H	302	Shigemastu, I	234
Sankaran, K K	192, 234,	Seidman, D N	250, 251	Shih, D	189, 416
.....	288, 334, 376, 419	Sekhar, J A	248, 301, 388	Shih, M	179
Santella, M	191, 436	Sekido, N	358	Shih, P	338
Santiago, V R	199, 321	Semenova, I P	257	Shiina, S	358
Sardesai, A S	217	Semiatin, S L ...	206, 251, 252, 253,	Shim, J	455
Sarihan, V	187	303, 305, 349, 391, 432, 433	Shima, M	234, 334
Sarikaya, M	292, 337	Sémoroz, A	300	Shimizu, T	358
Sastry, D H	432	Sen, S	366	Shin, D	221
Sato, K	294	Sen, S	179	Shin, D H	455
Sato, M	388	Senft, D C	320	Shin, D H	254, 260, 350
Saunders, T	172	Senk, D	203	Shin, D H	206, 208, 251, 253,
Sauter, L	229	Senkov, O	175, 402	305, 349, 391, 432, 433
Sauvage, X	306	Senkova, S V	402	Shin, E	276
Savage, M F	352	Seo, S	350	Shin, K S	287
Savin, I	322	Seok, C	246	Shinozuka, K	184, 301
Saxena, S	193, 288	Seol, D J	277	Shiomori, K	449
Sayed, H S	437	Sergueeva, A V	317, 432	Shizuo, N	269
Saylor, D M	391	Serin, K	237, 255	Shobu, K	175
Saytaeva, K	311	Serra, A	183, 425	Shoji, T	294
Scarber, P	320	Sethiaraj, S	180	Shreve, A	424, 447
Scattergood, R O	256, 393	Sfeir, C	381	Shrimpton, J	362
Schadler, L S	381	Sha, G	412	Shu, Y	380
Schaeffer, J C	204	Shafer, K E	275	Shuey, M S	364
Schaffer, P L	403	Shah, R P	312	Shuey, R T	347
Schaper, M	315	Shah, S	419	Shukla, S	395
Schildbach, M A	310	Shaheen, M A	403	Shulan, W	367
Schlapbach, L	169, 210, 262, 309,	Shalcross, S	405	Shull, R D	195
.....	353, 354, 395, 396, 435, 436	Shamsuzzoha, M	428	Shyam, A	418
Schmid-Fetzer, R	240	Shan, D	288	Sichen, D	409
Schmidt, H W	265	Shang, R	313	Sidhu, R	331, 416
Schmidt, S	204, 390	Shangguan, D	232	Sieck, L V	364
Schmidt, T	229	Shankar, S	343	Siegel, R W	381
Schmitz, T	330	Shao, G	359, 401	Siegert, K	234, 398
Schneibel, J H	174, 215, 269,	Shao, R	195	Siegfried, R M	365
.....	315, 316, 357, 400, 401, 432	Shao, T	374	Siekhaus, W J	310
Schneider, M S	366	Sharma, A	210	Sikder, A K	222
Schobert, H H	217	Sharma, P	454	Sikka, V	436
Schofield, J G	330, 415	Sharp, J	435	Sikora, M	321
Scholvin, D	381	Shashishekar, B	238	Siljan, O	312, 400

Sim, G	214	Spadafora, F	220, 278, 406	Street, S C	262
Simak, S I	405	Spaldin, N	291, 422	Stroeder, M	265
Sinclair, C S	307	Spanos, G	234, 327	Stroganov, A G	245
Sinclair, I	411	Sparks, C J	185	Stronach, C E	276
Sinclair, K	360	Speakman, S	176	Stuczynski, T	403
Singh, A K	429	Spelt, J K	331	Stulíková, I	383
Singh, P	235, 236	Spencer, D B	370	Sturm, E	398
Singh, R J	312	Spencer, R	323	Sturm, P	265
Singler, T J	191, 417	Speyer, R F	296	Styrov, V V	169
Sinha, S K	250	Spolenak, R	188, 394	Su, Y J	241
Sinnott, M	218	Spreij, M	178	Subbanna, G N	239
Sinnott, S B	428	Spuskanyuk, A V	253	Subramanian, K N	187, 188, 190, 285, 286, 293, 373
Sisneros, T	296, 297	Srajer, G	250	Suda, S	262
Sisson, R	404, 423	Sridhar, R	244, 329	Sudakar, C	239
Sisson, R D	409	Srinivasan, R	184, 227, 281	Sudbrack, C K	251
Skar, J I	191	Srinivasan, S G	279, 282, 306, 324, 431	Sudhakar, K	413
Skepper, I G	284, 372	Srinivasan, S S	263	Sudhakar, N	196, 239
Skibin, A P	318	Srinivasan, V	439	Suematsu, H	194
Sklenicka, V	434	Srivatsan, T S	190	Suery, M	417
Skoptsov, A M	212	Srolovitz, D J ...	182, 222, 223, 353	Suganuma, K	190, 338
Skripnyuk, V	260	Stach, E A	275, 309	Sugiyama, A	300
Skriver, H L	405	Staley, J T	347	Sui, Z	200
Skrotzki, W	401	Stanbery, B J	321	Suk, M	299
Skyllas-Kazacos, M	267	Stanciu, L A	242	Suleiman, M	353
Sleboda, T	413	Stanton, K T	171, 311	Sullivan, T M	435
Sluiter, M H	390	Starke, E A	199, 200, 376	Sun, D	263
Slutsker, J	322, 334, 384, 425	Staudenmann, J	369, 414	Sun, F	278, 364, 440
Smith, D	273	Staudhammer, K P ...	242, 295, 340	Sun, H	437
Smith, F M	353	Stauffer, E	367	Sun, W	320, 428
Smith, S	418	Stefanescu, D M	179	Sun, Y	202
Smola, B	383	Steinbach, I	222	Sun, Y	176
Smugeresky, J E	209, 261, 308, 352, 394, 418	Steiner, C	250	Sun, Y	423
Snow, R C	353	Steiner, J	404	Sun, Z	232
Snugovsky, P	331	Steingart, D A	354	Sun, Z	420
Snurnitsyna, S S	312	Stellacci, F	388	Sundaresan, R	224
Snyder, A J	424	Stencel, J M	414	Sung, P K	428
Snyder, G J	169, 435	Stephens, C	202	Sung, Y	186
Snyder, J	435	Stephens, J J	230	Suni, J P	347
So, C	214	Stevens McFadden, F	267	Sunkara, M K	334, 419
Sobkow, Z S	321	Stevenson, J W	235, 236	Supatarawanich, V	215
Soboyejo, W	180, 261, 270, 271, 308, 377	Stevenson, M E	367, 410, 441	Surek, T	169
Soda, H	417	Steverson, W B	266	Suresh, S	334, 420
Soer, W A	275	Stewart, D L	266	Suryawanshi, A	450
Soffa, W A	371	Stierman, R	293	Suss, A G	312
Sofo, J	364, 406, 445	StJohn, D H	294, 344, 385, 403, 417	Süss, R	270
Sohn, Y	246, 275, 281, 282, 410	Stober, F	330, 331	Sutou, Y	242
Sohn, Y C	382	Stock, R	254	Suyitno	220
Somasekharan, A C	192, 441	Stockhausen, W	265	Suyitno, X	203
Somerday, B P	224	Stoica, A D	184, 297	Suzuki, A	324
Song, H	175, 400	Stoica, G M	256, 392	Suzuki, A	346
Song, H	331	Stoker, G	230	Suzuki, M	384
Song, H G	283	Stölken, J S	431	Suzuki, S	194
Song, J	332, 416	Stoloff, N S	413	Suzuki, T	387
Song, J L	318	Stolyarov, V	208, 350	Suzuki, T	194
Song, J Y	382	Stone, G A	314	Suzuki, Y	291
Song, R	259, 350	Stone, I C	386	Svoboda, J	405
Song, W	380	Stone, M O	291	Swaminathan, S	207, 259
Song, Y	215	Stone, Z	208	Swan-Wood, T	354, 405
Sopori, B	320, 321	Stont, P D	212, 267	Sweet, E	403
Sordelet, D J	438	Storm, D R	278	Swenson, D J	198, 240, 241, 293, 338, 382, 417
Sørli, M	176, 272	Stoudt, M R	418	Swift, D	201
Soshnikova, E P	208	Stout, J	170	Swift, G A	283, 284
Soubeyroux, J	438	Stoyanov, S	232	Swisher, D L	252
Soucy, G	311	Straatsma, E N	220	Swygenhoven, H V	305
Southwick, L M	373, 427	Stratton, M	404	Synkov, S	208

Szpunar, J A 221, 249, 254,
 280, 281, 356, 452
 Szymczak, R 321

T

Tabaru, T 175
 Tabereaux, A T 170, 171, 176,
 177, 199, 212, 217, 218,
 244, 265, 267, 272, 311,
 312, 317, 318, 356, 360,
 361, 398, 399, 403, 437, 439
 Tada, S 420
 Taghavi, S M 369
 Takahashi, K 323
 Takaku, Y 191
 Takami, Y 426
 Takamiya, H 440
 Takano, H 415
 Takashi, S 449
 Takasugi, T 174, 401
 Takeshita, H T 309, 310, 436
 Takeuchi, I 289
 Talas, S 290
 Talbot, D E 343, 427, 428
 Taleff, E M 184, 211, 225, 226,
 264, 281, 310, 326, 355,
 356, 368, 397, 411, 412, 441
 Talin, A 308
 Tallant, D R 263, 430
 Tamura, M 184, 301
 Tamura, N 372, 394, 441
 Tan, H 345
 Tan, L 428
 Tan, P 335, 404
 Tanabe, M 427
 Tanaka, M 426, 449
 Tandon, S 196
 Tandon, S C 317
 Tang, J 380
 Tang, W 296
 Tarasov, A V 185, 186,
 200, 335, 427, 449
 Tatalovich, J 352
 Tatyannin, E V 253
 Taub, M 240
 Tavares, R P 320
 Tavera, F J 378
 Tawfic, S N 200
 Taya, M 201
 Taylor, C 212
 Taylor, J A 272, 385
 Taylor, M P 212
 Taylor, P R 426
 Tedstrom, R 222
 Teigs, T N 372
 Telang, A U 188, 190, 229
 Telesman, J 340
 Téllez-Martínez, J S 408, 409
 Tenhundfeld, G 185
 Teramoto, S 401
 Teranishi, K 406
 Terpstra, R L 295
 Teter, D F 233, 283, 396
 Tewari, R 175, 400
 Tewari, S N 248
 Thibault, M 171

Thiel, G H 286
 Thirumalai, N 183
 Thom, A J 175, 215
 Thoma, D J 253, 283
 Thomas, B G 203, 218,
 379, 423, 446
 Thomas, J 272
 Thompson, L J 238
 Thompson, S A 411
 Thompson, S R 407
 Thomson, P F 269, 333
 Thonstad, J 437
 Thuramalla, N V 398
 Thurston, A K 360
 Tian, B 254
 Tian, H 184, 202, 226, 297
 Tian, Z 357
 Tikare, V 242
 Tilly, D J 278
 Timofeeva, V 369
 Tin, S 174
 Tiryakioglu, M 347
 Tiwari, A 195, 237,
 290, 291, 336
 Tiwari, R 248
 Tizon, E 170
 Toda, H 411
 Todaka, Y 253
 Tokar, V 348
 Tokarz, M L 176
 Tokimatsu, R C 368
 Tomala, J 177
 Tomasino, T 437
 Tome, C N 207, 255, 339
 Tommey, C 172
 Tomokiyo, Y 390
 Tong, L 243
 Tonheim, J 172
 Tonti, R T 217
 Toppo, B 368
 Torbet, C J 418
 Torek, P 172
 Torosyan, A R 236
 Torres, V 230, 231, 329, 443
 Torsiello, S 171
 Tortorelli, P F 174, 215, 269,
 315, 316, 357, 400
 Tran, S 416
 Tratteberg, O 172
 Trebuh, O A 267
 Trichy, G R 256
 Triessnig, A 404
 Trinkle, D R 183, 431
 Trivedi, P B 279
 Trivedi, R 202, 247, 299,
 300, 344, 345, 386
 Trojanova, Z 425
 Trubitsyna, I B 253
 Trumble, K P 195, 207, 259
 Tryon, B 270
 Tsai, C M 332, 338
 Tsai, D 332
 Tsai, J Y 199, 374
 Tsai, Y 285
 Tsakiroopoulos, P 175, 216,
 359, 401, 421
 Tsau, C H 176

Tso, C 227
 Tsuchida, N 328
 Tsuchiya, K 253
 Tsuchiyama, A 300
 Tsui, F 238
 Tsuji, N 207, 259, 351, 388
 Tsunekane, M 315
 Tsuzuki, R 418
 Tszeng, C 314
 Tu, K 187, 231, 294
 Tuominen, M T 336
 Turbini, L J 189, 231,
 285, 331, 373, 416
 Turchi, P E 192, 304, 348
 Turner, J 329
 Turpeinen, P 286
 Tyagi, S A 268
 Tyumentsev, A N 254, 256, 257

U

Ubhi, H S 411
 Uchic, M D 309, 352
 Ucok, I 223, 323, 365
 Udaykumar, H S 249
 Udovic, T J 210
 Ueda, M 324
 Ueji, R 259
 Uekawa, N 296
 Ueshima, M 190
 Uesugi, K 300
 Uhrig, J R 318
 Ulfig, R M 198
 Umakoshi, Y 390
 Umantsev, A 196
 Umeda, T 299
 Umemoto, M 253, 305
 Ungár, T 350
 Unland, J 240
 Unlu, N 363
 Upadhaya, C 336
 Upadhyay, V 274
 Urbani, M D 443
 Ustundag, E 176, 271, 272, 283,
 284, 328, 360, 372
 Utigard, T A 313
 Utsunomiya, H 206
 Utyashev, F Z 255

V

Vabishchevich, P 437
 Vahed, A 329
 Vaidyanathan, R 201, 246,
 296, 297, 342
 Vainik, R 403
 Valek, B C 394
 Valiev, R Z 206, 251, 252, 253,
 255, 256, 257, 258,
 259, 260, 305, 306, 307,
 346, 349, 350, 391, 432
 Valls, R A 230
 van de Walle, A 304, 358, 430
 Van Den Avyle, J J 342
 van den Broek, B 312
 Van der Giesen, E 377
 van der Merwe, J H 228, 327

van der Meulen, D 329
 Van der Ven, A 305
 Van Haaften, W 385
 Van Humbeek, J 392
 van Klaveren, E P 219
 Van Schaik, A 200
 Van Vliet, K J 334
 Van Weert, G 333
 Van Wert, J 370
 Vandermeer, R A 204
 Vanderson, E 261
 VanEvery, K J 219
 Vanvoren, C 172
 Vardill, W 188
 Varyukhin, V 208, 260
 Vashishth, D 418, 419
 Vasiliev, A L 346
 Vasquez, O 199, 321
 Vasudevan, A K 347, 348
 Vasudevan, V K 175, 238, 301,
 326, 327, 388, 400
 Vaudreuil, S 361
 Vega, S 215
 Velgosova, O 296, 311
 Vella, J B 229
 Venkatesh, R 289
 Venkatesh, V 407
 Venkateswaran, S 422
 Venskutonis, A 315, 358
 Verlinden, B 392
 Verma, H C 336
 Verma, R 265
 Verma, V 233
 Vetrano, J S 355
 Vetrone, J M 238
 Vetter, R 195
 Vianco, P T 331, 338
 Vidal, E E 426, 448
 Vidvei, T 272
 Viehland, D 384
 Villegas, D 361
 Villegas, J C 202, 208
 Vinci, R P 232, 352, 422
 Vinogradov, A Y 391, 392
 Virnig, M J 444
 Vishweswaraiah, S 410
 Viswanathan, S 218, 219, 299,
 379, 383, 385, 423, 446, 449
 Vitek, J M 203, 345
 Vitek, V 348
 Vlassak, J J 445
 Vlassov, A V 213
 Voermann, N 330, 331
 Vogel, M 383
 Vogel, S C 207, 255, 296, 434
 Voglauer, B 336
 Vogt, F 217
 Vogt, H 437
 Vogt, S A 176
 Volkert, C A 188
 Völkl, R 270
 Voller, V R 248
 von Grossmann, B 383
 Voorhees, P W 248, 322
 Vorberg, S 270
 Vorhauer, A 252, 350
 Vrestal, J 382

Vuik, C 248
 Vulcan, M 398

W

Wadley, H N 326, 352
 Waghmare, U 304
 Wagner, G J 279
 Wagnière, J 203, 450
 Wagoner, R H 214, 314
 WaKimoto, Y 200
 Waku, Y 300
 Waldo, R A 264
 Waldron, D J 268
 Walker, C A 230
 Walker, M S 235, 236
 Wall, J J 372
 Wallace, J P 365
 Walters, R T 353
 Walukas, D M 418
 Wan, X 276
 Wang, C 278, 406
 Wang, D 232
 Wang, G 178, 190, 387
 Wang, G 202, 226, 271
 Wang, G Y 271, 411
 Wang, H 379, 446
 Wang, H 302
 Wang, H 424
 Wang, J 214
 Wang, J 181
 Wang, J 242
 Wang, J ... 207, 251, 257, 258, 260
 Wang, J 356
 Wang, J C 210
 Wang, L 219
 Wang, M 374
 Wang, N 200
 Wang, P 316, 360
 Wang, P T 412
 Wang, Q 438
 Wang, Q 312
 Wang, Q 410, 411
 Wang, R 440
 Wang, R J 217
 Wang, S 326
 Wang, S 243
 Wang, S 233
 Wang, S F 241
 Wang, S H 198
 Wang, S J 375
 Wang, T 322
 Wang, T 363, 364
 Wang, W 426
 Wang, W H 217, 402
 Wang, X 410
 Wang, X 184, 297, 402
 Wang, Y 197
 Wang, Y 291
 Wang, Y 184, 297
 Wang, Y 431
 Wang, Y 421
 Wang, Y 305, 322, 363, 364
 Wang, Y 391
 Wang, Y 174, 182, 183, 224,
 249, 278, 322, 324, 365, 407
 Wang, Y U 183, 277, 384

Wang, Z 400
 Wang, Z 286
 Wang, Z 417
 Wang, Z X 188
 Wanjale, M 302
 Wannasin, J 296
 Ward, W G 337
 Ward-Close, C M 407
 Warren, J A 276, 322, 386
 Waryoba, D R 205
 Watanabe, M 432
 Watanabe, T 390
 Waterstrat, R M 304
 Watkins, T R 400
 Watson, T J 419
 Watts, J 401
 Waz, E 437
 Weaver, M L 262, 367,
 410, 422, 441
 Webb, D A 220
 Webster, T J 197
 Wedde, G 398
 Weertman, J 201
 Weertman, J R 349
 Wegryzn, J 353
 Wei, C 382
 Wei, C C 332
 Wei, J 232
 Wei, J H 290
 Wei, L 421
 Wei, M 243
 Wei, W 260
 Weil, K 235
 Weil, K G 409
 Weiland, H 277
 Weinan, E 182
 Weirauch, Jr., D A 273
 Weissmueller, J 346
 Welch, B 267
 Welch, B J 212, 399
 Wellnitz, R 214
 Wells, M A 268, 386
 Welp, U 238, 250
 Welsh, G S 271, 272
 Wen, S 280, 281
 Wen, W 314
 Wenderoth, M 270
 Weninger, J A 251
 Wenner, M 233
 Wermer, J R 210, 262, 395, 436
 Werner, J 215
 Werner, J H 447
 Wetscher, F 254
 Wetteland, C J 302
 Wezyk, W 403
 Wheeler, D 220, 280
 White, B 244
 White, D 329
 White, P 267
 Whitfield, D S 267
 Whiting, M 216
 Whittington, B I 284
 Widjaja, A 377
 Widom, M 431
 Wiench, J 263
 Wiezorek, J M 379
 Wilde, G 346, 351

Wilkening, S 177
 Wilkins, J W 183, 431
 Wilkinson, D S 268, 269,
 342, 355
 Willander, M 180
 Williams, D B 432
 Williams, F S 170
 Williams, G A 242
 Williams, R K 185
 Wilson, O C 446
 Winkelman, G 371
 Winterscheidt, D L 278, 406
 Winther, G 252, 302
 Wirth, B D 183
 Wiseman, M 189
 Withers, A 244
 Withers, J C 224, 278
 Withers, P J 297
 Wittig, J E 327
 Wochner, P 250
 Wolanski, R 172, 173
 Wolf, A 266
 Wolf, D 305
 Wolfe, R C 409
 Wolverton, C 181, 205, 250, 277,
 304, 305, 348, 349, 389, 430
 Wolverton, C C 406
 Wong, C K 232
 Wong, G C 239
 Wong, L L 246
 Wong, P W 439
 Woo, W 297
 Wood, J R 173
 Woodard, S 215
 Woodman, R H 254
 Woods, J J 416
 Woodward, C 322
 Woodward, C 183, 430
 Wright, I G 174
 Wright, J 416
 Wright, P K 354
 Wright, R D 338
 Wright, R N 413
 Wright, W 286
 Wu, B 313
 Wu, D T 181, 225, 226, 281
 Wu, E 348
 Wu, J 375
 Wu, K 322
 Wu, K 240
 Wu, L L 421
 Wu, M 178, 247, 423
 Wu, W 326
 Wu, X 287
 Wu, X 233
 Wu, Y Q 238
 Wuttig, M 379, 422, 445

X

Xi, J H 421
 Xia, G 235, 236
 Xia, X 276, 332
 Xia, Z 232
 Xia, Z C 397, 398
 Xiang, X 290
 Xiang, Y 182

Xiao, H 439
 Xiao, J Q 290
 Xiao, X 295
 Xie, F 298
 Xie, S 202
 Xie, Y 265
 Xihong, Y 269
 Xing, Q 302
 Xu, C 256, 258, 311, 392, 433
 Xu, G 231
 Xu, H 387
 Xu, H 299, 318
 Xu, J 176
 Xu, J 357
 Xu, K 343
 Xu, Q 319
 Xu, R 424
 Xu, W 399
 Xu, Y 412
 Xu, Y 231
 Xu, Y B 412
 Xue, L 243
 Xue, Q 326, 367
 Xueyi, G 378

Y

Ya Ping, Y 325
 Yablinsky, C A 233, 303, 453
 Yalisove, S M 345
 Yamabe-Mitarai, Y 269
 Yamagiwa, M 415
 Yamaguchi, M 215, 315, 401
 Yamaguchi, S 200
 Yamamoto, H 426, 427, 448
 Yamaoka, H 358
 Yamashita, Y 323
 Yamauchi, A 315
 Yan, F Y 195
 Yan, X 298
 Yang, B 234, 247, 271
 Yang, B 430
 Yang, C 382
 Yang, D 261
 Yang, F 434
 Yang, H 410
 Yang, H 223
 Yang, J 357
 Yang, J 442
 Yang, M 194
 Yang, N Y 308
 Yang, Q 312
 Yang, Q 275, 321
 Yang, W 328
 Yang, W 233
 Yang, X 187
 Yang, Y 249
 Yang, Y 265
 Yang, Y 216
 Yang, Y 245, 362
 Yang, Y 332
 Yang, Z 193
 Yang, Z G 235, 236
 Yanushkevich, K I 433
 Yao, G C 290, 421
 Yapici, G G 257, 341, 350
 Yarrapareddy, E R 341

Yassar, R S 347
 Yasskin, P B 259
 Yasuda, H 300
 Yatsui, K 194
 Yazami, R 354
 Ydstie, B 356
 Ye, F 295
 Yee, C E 447
 Yeh, A 174
 Yeh, H 440
 Yeh, H H 440
 Yeo, I 358
 Yi, J 173
 Yi, J 283
 Yildirim, T 210
 Yin, L 191, 417
 Yin, Z 171
 Yinbiao, Y 234
 Ying, J Y 197, 291
 Yingjun, L 367
 Yoko, Y 269
 Yokobayashi, M 215
 Yokoyama, Y 271, 359
 Yonamine, T 204
 Yoon, C 350
 Yoon, J 198, 338
 Yoon, K E 251
 Yoon, M 293
 Yoon, S 438
 Yoon, S W 241
 Yoon, Y B 412
 Yoon, Y S 275
 Yoshida, S 296
 Yoshimi, K 215, 315
 Yost, F G 368
 Young, J A 183
 Youssef, K M 391
 Yu, A 376, 447
 Yu, J 189, 231, 285,
 331, 373, 382, 416
 Yu, K 278, 406
 Yu, L 332
 Yu, O 182
 Yu, S 254
 Yuan, H 319
 Yuan, L 354
 Yuan, W 202, 226, 271
 Yuan, Z 401
 Yuanchi, D 368
 Yücel, O 185
 Yue, S 233
 Yunyou, Z 325
 Yurchenko, L I 260
 Yurievich, B E 194
 Yurko, J 202
 Yurkov, V V 267
 Yuzyuk, Y I 291
 Yvon, K 309

Z

Zabaras, N 235, 237, 319, 428
 Zacharia, T 223
 Zaitsev, A 342
 Zakharov, A E 245
 Zakharov, I D 280
 Zamiri, A 431

Zamkotowicz, Z	403	Zhou, B	245, 323
Zangari, G	237	Zhou, F	306
Zantye, P	222	Zhou, G	325
Zarembo, S	321	Zhou, H	336
Zavalij, L	382, 416	Zhou, N	383
Zawierucha, R	343	Zhou, S	322, 363, 364
Zeh, J	266	Zhou, W	339
Zehetbauer, M ...	252, 392, 391, 393	Zhou, W	288
Zeipper, L	392	Zhou, X	352
Zelenitsas, K	175	Zhou, Y	451
Zelin, M	355	Zhou, Y	449
Zender, G A	338	Zhu, A	217, 376
Zeng, K	293	Zhu, J	322
Zeng, X	383	Zhu, J	422
Zerkle, R	213, 399	Zhu, J	294, 364
Zevgolis, E N	330, 373	Zhu, J	312
Zhai, C	288	Zhu, S	445
Zhai, T	410	Zhu, T	290
Zhang, D	323, 413	Zhu, W	323
Zhang, D L	406	Zhu, X	404
Zhang, F	407	Zhu, Y	196
Zhang, G	357	Zhu, Y T	206, 251, 253, 257,
Zhang, G P	188	259, 260, 305, 306,
Zhang, H	223	349, 350, 391, 432
Zhang, J	213	Zhuo, L	281
Zhang, J H	412, 421	Zi, A	252
Zhang, K	349, 413	Ziegler, D P	437
Zhang, L	290	Zikanov, O	437
Zhang, M	295	Zindel, J W	403
Zhang, M	357	Zinovev, A V	429
Zhang, M	228	Zoeller, T	404
Zhang, Q A	210	Zong, Z	261, 377
Zhang, R	259	Zribi, A ...	179, 220, 274, 320, 326
Zhang, S	290, 445	Zunger, A	304, 389
Zhang, W	432		
Zhang, W	187, 295, 370		
Zhang, X	197, 239, 261, 291,		
.....	302, 337, 381, 424, 447		
Zhang, X M	421		
Zhang, Y	313		
Zhang, Y	345		
Zhang, Z	290		
Zhang, Z	375		
Zhang, Z	207, 257		
Zhang, Z	451		
Zhang, Z	428		
Zhao, D Q	217		
Zhao, H	380		
Zhao, J	322		
Zhao, J K	402		
Zhao, Q	173		
Zhao, Q	312, 454		
Zhao, Q	265		
Zhao, X	207, 257		
Zhao, Y	451		
Zhao, Y	306, 350		
Zhao, Y	249		
Zhao, Y Q	324		
Zhao, Z W	354		
Zhdanov, A N	255, 258		
Zheng, Q	268		
Zhernakov, V S	256		
Zhilina, M	256		
Zhilyaev, A P	251, 254		
Zhitong, S	368		
Zholnin, A G	245		
Zhong, Y	364, 445		